

CONTROL MODEL DEVELOPMENT
FOR PACKED BED CHEMICAL REACTORS

Thesis by

Rohit Khanna

In Partial Fulfillment of the Requirements

for the Degree of

Doctor of Philosophy

California Institute of Technology

Pasadena, California

1984

(Submitted May 16, 1984)

• 1984

Rohit Khanna

All Rights Reserved

To my parents for their support and encouragement
throughout my education and to my wife for her love
and understanding throughout the past six years.

ACKNOWLEDGEMENT

This thesis would clearly not be possible without the guidance of my advisor, Dr. Seinfeld. I am grateful that he was able to allow me to conduct research in the areas of my interest without significant restrictions. His assistance is greatly appreciated. I would also like to thank the National Science Foundation for their graduate fellowship that provided much of the assistance for this research.

Much of the real credit for this thesis should go to my family. Without the visions and foresight of my parents and without their high expectations this would never have been possible. Most of all I would like to thank Debbie for her love and support throughout the time at Caltech and especially on all those nights when she wished that I could be home but understood that I had to work.

Finally, I would like to thank Dave and Barry for helping provide the outside interests necessary to keep life stimulating and enjoyable and to retain enthusiasm in the research.

ABSTRACT

Although control algorithms have been conceived for industrial chemical systems, their acceptance by industry has been slow due to a lack of direct experimental evidence of their effectiveness and to volumes of conflicting, or at least incompatible, recommendations on control structure design. This thesis provides the basis for a concerted theoretical and experimental program in multivariable process control structure design for packed bed chemical reactors by presenting an in-depth control analysis of a practical, multivariable, distributed parameter system—the heat conduction problem defined by the simple diffusion equation—using both frequency-domain and time-domain analyses and the formulation, numerical solution, and analysis of a detailed model for packed bed reactors, along with reduction to a low-order state-space representation suitable for on-line process control.

The study of the heat conduction system allowed for consideration of various control design techniques and the relation between measurement structure and control system design. This study shows that the choice of measurements and their locations significantly affects the optimal control design and the usefulness of the different design techniques and the importance of an accurate process model and the necessity of model reduction to a low-order state-space representation for control structure design and implementation.

The second portion of this study provides a detailed mathematical modeling analysis of packed bed catalytic reactors that significantly extends previous studies in the detail of the model and in the consideration of all aspects of the model development and reduction to a state-space control representation. The

general view that modeling simplifications are desired since they lead to a reduction in numerical solution effort is contested, and it is shown that many simplifications are no longer necessary with today's advanced computational capabilities. A unified approach to dynamic reactor modeling is developed and its importance in the accurate description of dynamic and steady state reactor behavior, in the investigation of reactor start-up or the effects of process disturbances, and in the development of an accurate reduced state-space model for the design of control structures to stabilize the reactor under various disturbances or to provide optimal system recovery from input changes is shown.

TABLE OF CONTENTS

Acknowledgement	vi
Abstract	v
Notation	xii
1. Introduction	1
1. Objectives of the Current Work	2
2. Industrial Control Considerations	5
3. Review of Experimental Control Studies	8
2. Multivariable Control Structure Design for a Heat Conduction System	13
1. Introduction	14
2. Preliminary Analysis	18
1. <i>Model Reduction</i>	18
2. <i>Controllability</i>	26
3. <i>Root-Locus</i>	27
3. Time-Domain Analysis	35
1. <i>Optimal Control</i>	36
2. <i>Modal Control</i>	40
4. Non-Interacting Control	46
1. <i>Perfect Dynamic Compensation</i>	46
2. <i>Steady State Decoupling</i>	49
3. <i>Set Point Compensation</i>	49
4. <i>Inner-Loop Decoupling</i>	50

5. Inverse Nyquist Array	58
6. Characteristic Locus Method	78
1. <i>Basic System Analysis</i>	84
1. <i>Case I: Measurements $z_1=0.3, z_2=0.7$</i>	84
2. <i>Case II: Measurements $z_1=0.4, z_2=0.6$</i>	86
3. <i>Case III: Measurements $z_1=0.4, z_2=0.8$</i>	87
2. <i>Inner Loop Analysis</i>	89
1. <i>Case I: Measurements $z_1=0.3, z_2=0.7$</i>	92
2. <i>Case II: Measurements $z_1=0.4, z_2=0.6$</i>	94
3. <i>Case III: Measurements $z_1=0.4, z_2=0.8$</i>	95
3. <i>Modified Inner-Loop Analysis</i>	95
7. Control System Performance	119
1. <i>Case I: Measurements $z_1=0.2, z_2=0.8$</i>	124
2. <i>Case II: Measurements $z_1=0.3, z_2=0.7$</i>	125
3. <i>Case III: Measurements $z_1=0.4, z_2=0.6$</i>	126
4. <i>Case IV: Measurements $z_1=0.4, z_2=0.8$</i>	128
8. Discussion of Control Analysis	161
3. Mathematical Model of a Packed Bed Catalytic Reactor	166
1. <i>Introduction</i>	167
2. <i>Review of Packed Bed Reactor Modeling</i>	172
3. <i>Model Development for Packed Bed Catalytic Reactors</i>	179
1. <i>Reactor System</i>	179
2. <i>Reaction Kinetics</i>	182
3. <i>Formation of Complete Mathematical Model</i>	187
4. <i>Mathematical Relationships</i>	192

5. Numerical Solution	199
1. Solution Techniques	200
2. Orthogonal Collocation	204
3. Model Reduction	206
4. Numerical Simulation	216
4. Model Analysis	223
1. Modeling Parameters	224
2. Steady-State Behavior	229
3. Dynamic Simulations	230
4. Effects of Reactor Operating Conditions	232
5. Radial Concentration Analysis	234
6. Adiabatic Analysis	238
7. Importance of Thermal Well	239
8. Dispersion Effects	241
5. OCFE Model Analysis	271
1. Formulation of OCFE Technique	272
2. Model Comparisons	279
6. Control Model Development	293
1. State-Space Representation	293
2. Model Linearization	296
1. Linearization of the Reaction Rates	297
2. Linearization of the Algebraic Equations	298
3. Linearization of the Differential Equations	300
4. Numerical Solution of the Linearized Model	302
3. State-Space Simulations	304
7. Model Dimensionality	317

1. <i>Model Discretization</i>	317
2. <i>Physical Modeling Simplifications</i>	320
1. <i>Homogeneous Analysis</i>	321
2. <i>Quasi Steady State Approximation</i>	326
3. <i>Negligible Energy Accumulation in Gas</i>	328
3. <i>Model Reduction</i>	329
1. <i>Davison's Method</i>	331
2. <i>Marshall's Method</i>	334
4. <i>Discussion of Reduced Model</i>	336
4. Results and Discussion of Future Experimental Studies	351
1. Conclusions of Current Analysis	352
2. Parameter Estimation and Model Verification	361
3. Control Model Configuration	367
4. Control System Design	374
5. Appendices	378
1. Computer Programs for Heat Conduction Problem	379
2. Normalized Packed Bed Reactor Model	385
3. Radial Collocation of Packed Bed Reactor Model	391
4. Computer Model of the Packed Bed Reactor	398
5. Orthogonal Collocation on Finite Elements Model	452
6. Linear Packed Bed Reactor Model	466
6. References	485

NOTATION

A	state matrix
A_{ij}, B_{ij}	collocation weights for first and second derivative
B	control matrix
c	concentration, g-moles/cm ³
c_{ij}	element ij of measurement matrix C
c_p	heat capacity, cal/g °K
C	measurement matrix
d	disturbance vector
d_i	radial collocation weights
D	bulk molecular diffusivity, cm ² /sec
E_a	activation energy, cal/g-mole
f_1, f_2	pressure dependence constants for steam-shift reaction rate
f_{ij}	element ij of inner-loop compensator F
F	inner-loop compensator
g_i	element of process transfer function G_p
G_c	controller transfer function
G_i	interaction compensator transfer function
G_p	process transfer function
G_s	set point compensator transfer function
h_{ij}	heat transfer coefficient between phase i and j, cal/sec cm °K
ΔH	heat of reaction, cal/g-mole

J^*	molar flux relative to molar average velocity
k	thermal conductivity
k_0	reaction rate constant
k_b	Blake-Kozeny constant
k_i	diagonal gain element of \mathbf{K}
k_r, k_z	radial (axial) thermal conductivity, cal/sec cm °K
\mathbf{K}	diagonal proportional gain matrix
K_1, K_2	methanation reaction rate constants, atm ⁻¹
$\mathbf{K}_L, \mathbf{K}_H$	low and high frequency compensators
K_p	equilibrium constants, atm ⁻² for methanation
l_i	Lagrangian polynomials
L	reactor length, cm
\mathbf{L}_e	controllability matrix
M_g	molecular weight of gas, g/g-mole
N_i	molar flux with respect to stationary coordinates
P	pressure, atm
\hat{P}	total pressure neglecting mole change, atm
P_c	closed-loop characteristic polynomial
P_i	partial pressure of species i , atm
P_o	open-loop characteristic polynomial
Pe	dimensionless Peclet number

Q	open-loop transfer function
r	radial coordinate, cm
r	normalized radial coordinate, r/R_1
r_c	radial collocation point
R	reaction rate, g-mole/sec cm ³
R	closed-loop transfer function
R₀, R₁	radius of thermal well and outer wall, respectively, cm
R'	normalized reaction rate
R_g	universal gas constant, 1.987 cal/g-mole °K
t	time, sec
t	normalized time for heat conduction problem
T	absolute temperature, °K
u	control vector
u₁, u₂	control inputs to heat conduction system
u_g	interstitial velocity of gas, cm/sec
U	internal energy
U_{ij}	overall heat transfer coefficient between phase i and j, cal/sec °K
v_g	normalized fluid velocity, u_g/\bar{u}_g
V	volume, cm ³
w_j	weighting functions
x	state vector

x_i	mole fraction of species i, g-mole i / g-mole total
y	normalized temperature distribution for heat conduction problem
\mathbf{y}	output vector
\mathbf{y}_0	normalized temperature distribution at $t=0$
\mathbf{y}_d	desired normalized temperature distribution
y_i	normalized mole fraction, \hat{x}_i/\bar{x}_{00}^0
z	axial coordinate, cm
z	normalized space coordinate for heat conduction problem
z_1, z_2	outputs for heat conduction system

Greek Letters

α	dimensionless axial dispersion, $\propto Pe_z^{-1}$
β	dimensionless radial dispersion, $\propto Pe_r^{-1}$
δ	moles CO reacted in methanation per total inlet moles
ϵ	void fraction of bed
η	dimensionless heat capacity
γ	dimensionless heat transfer coefficient, $\propto St$
κ	dimensionless heat generation parameters
λ	eigenvalues
λ_{ijk}	Biot numbers
Λ	diagonal matrix of eigenvalues
μ	viscosity
ω	constants from radial collocation
φ_0	normalized radius of thermal well, R_0/R_1
φ_1, φ_2	dimensionless heats of reaction
ρ	density, g/cm ³
σ	dimensionless reaction coefficients
τ	dimensionless pressure drop, $\hat{P}_{z=L}/\hat{P}_{z=0} - 1$
ϑ	normalized time, $(t \cdot \bar{u}_{g_0})/L$
Θ	normalized temperature, T/\bar{T}_0
ζ	normalized axial coordinate, z/L

Subscripts and Superscripts

0	value at inlet
b	reactor bed
f	value at outlet
g	gas
h	heat
m	mass
M	methanation reaction
r	radial
s	solid catalyst
S	steam-shift reaction
t	thermal well
w	cooling wall
z	axial
\sim	based on inlet conditions
-	steady state
'	deviation variable

Chapter 1

INTRODUCTION

1.1 OBJECTIVES OF CURRENT WORK

One of the major difficulties in the application of advanced process control theories to industrial chemical processes is the lack of complete understanding of the chemical process and the inability to predict system behavior in the presence of unknown and uncharacterized disturbances. This difficulty is compounded by physical and chemical interactions or nonlinear coupling of the process variables. Although complex control algorithms have been conceived for industrial chemical systems, their acceptance by industry has been slow due to a lack of direct experimental evidence of their effectiveness and to volumes of conflicting, or at least incompatible, recommendations on control structure design. Significant research efforts are necessary in duplicating industrial processes in a research setting and providing a unified approach to the mathematical modeling and control structure design.

This thesis provides the basis for a concerted theoretical and experimental program in multivariable process control structure design for packed bed reactor systems. Along with the detailed design and construction of both a kinetics and pilot-scale control reactor (Strand, 1984), this work presents the necessary prerequisites to a substantial effort in the study of the applicability of process control theory to a laboratory- or pilot-scale industrial chemical process. In view of these objectives, this thesis is divided into two major sections:

- an in-depth analysis of a practical, multivariable, distributed parameter system—the well-defined heat conduction process defined by the simple diffusion equation—using both frequency-domain and time-domain analyses and
- the formulation, numerical solution, and analysis of a detailed dynamic model for packed bed reactors, along with reduction to a low-

order state-space representation suitable for on-line process control.

The first section of this work, the analysis of the heat conduction problem, is presented in Chapter 2 and is a self-contained presentation of many of the control aspects of a multivariable, distributed parameter system (Khanna and Seinfeld, 1982). Although this heat conduction system is much simpler than the packed bed reactor, a considerable amount of insight into control structure design can be obtained from this process since the control aspects are not lost in the complexity of the mathematical system as they may be in an initial detailed control study of the experimental packed bed reactor. In particular, an analysis of a number of multivariable process control strategies, including non-interacting control, optimal control, inverse Nyquist array, and characteristic locus techniques, is carried out theoretically on a one-dimensional, two-input heat conduction system. The potential improvements in control performance through the use of extra measurements and through the appropriate selection of measurement locations is assessed and a new non-interacting control strategy, termed inner-loop decoupling, is developed.

The remainder of this thesis centers on the complete dynamic modeling analysis of a packed bed reactor, along with reduction to an accurate low-order state-space representation suitable for control studies. According to Jutan et al. (1977), this is

"one of the more complicated processes to model in chemical engineering. Because of this, it is essential when deriving a process model to keep in mind the purpose for which the model is to be used. If, for example, the model is to be used as the basis for on-line regulatory control of the reactor, large simplifications to most of the models proposed in the literature must be made. Although most of the models tend to be somewhat complex and, in general, unsuitable for control, by examining the formulation of these models some insight into the important effects occurring within a reactor may be gained, and ideas for simplifying the models for the purpose of the control may be found."

In view of these comments, this study allows accurate description of dynamic and steady state reactor behavior for process optimization and design, for the investigation of reactor start-up or the effects of process disturbances, and for the analysis and design of control structures. Various common assumptions and model structures are considered, and the appropriate numerical solution techniques are discussed. This analysis is not intended to be specific to any particular packed bed reactor system but rather to present a detailed study of modeling techniques, assumptions, and solutions and to develop a unified approach to dynamic reactor modeling and control model development. The work significantly extends previous studies in the detail of the mathematical model and in the systematic consideration of all aspects of the model development and the reduction to a state-space control representation.

1.2 INDUSTRIAL CONTROL CONSIDERATIONS

Until only recently, the process control industry has been dominated by applications to mechanical or electrical processes where systems are generally well-defined and numerically simple due to minimal nonlinearities and relatively simple physical characteristics. Even so-called 'modern' control theories developed in the 1960's have only played an important role in fields such as robotics and the space program. Their applicability to complex industrial chemical processes which are inherently burdened by nonlinearities, large time delays, and distributed parameter behavior has been extremely limited in spite of an enormous effort by researchers. Although significant theoretical efforts have been made by many research groups in the development of control algorithms for ill-defined distributed parameter systems as are common in the chemical industry, these efforts have not found wide application in actual industrial problems. Thus during the past twenty years, a significant control 'gap' has developed between process control theory and practice (Foss, 1973; Seborg and Edgar, 1982).

Due largely to increased costs for energy, increased governmental safety and environmental restrictions, and increased foreign competition, significant efforts are now being made by industry to modernize and automate production facilities with a major emphasis on integrating energy requirements and improving throughputs and system performance (Ray, 1981). Additionally with the major improvements and general acceptance of computers suitable for on-line control, attempts at applying sophisticated control theories are only now beginning. One of the conclusions of the discussion on the problem of the control 'gap' between academic theories and practice is that there exists a pressing need for careful, systematic studies of the design and implementation of control systems for pilot-scale industrial processes, thus providing the prime motivation

behind the current theoretical and experimental program for which this thesis provides a basis.

Several steps are necessary prior to developing and testing control strategies. These include the design and construction of a pilot-scale system possessing much of the modeling characteristics and control difficulties of the actual industrial process, the development of an accurate mathematical model for process design and analysis, and the reduction of the full model to one suitable for control structure design and on-line control. The first of these steps was performed by Strand (1984), and the latter two steps are the concern of this current work. A packed bed nonadiabatic chemical reactor was selected as the chemical process to be studied due to its complexity and inherent control difficulties and its extensive industrial importance for carrying out exothermic, gas phase reactions.

Upon completion of these preliminary research efforts, the elements of the control structure:

- the measured variables,
- the manipulated variables,
- the control configuration connecting the measured and manipulated variables, and
- the control logic governing the behavior of the manipulated variables

can be considered. In particular, it is important to determine control structures that make optimal use of the available measurements in the chemical process. Although in general there may be quite a few measured variables available, they may not be the variables of most concern, and these variables may need to be reconstructed using the process model. An example of this is the measurement of the outlet gas temperature in the packed bed reactor from which the

outlet concentrations may need to be estimated. Further problems with measurements result from various random and systematic errors or noise in the measurements and long delays due to the complexity of the chemical or physical analyses.¹ The use of an accurate process model can in many cases minimize these difficulties by allowing prediction of some unavailable measurements, by improving the knowledge of the system performance through simulations, and by allowing design improvements to the process.

Thus the central role played by dynamic and steady state models in the design and optimization of chemical processes and in the development and application of control strategies justifies considerable effort in their development. The philosophy of this modeling work is presented by Foss (1973),

'Forms of the models range from sets of nonlinear differential equations to empirically or experimentally derived transfer functions. The forms of the models may not be selected arbitrarily; they are determined in part by the control objectives and the type of control analysis to be pursued. In short, process modeling is a substantial and crucial task, and by no means routine. ... The operation of control systems of modern design also requires estimates of the process states used for control. This requires a process model, perhaps different than that used for design calculations, and a means of rapid solution of the model equations.'

The work presented in this thesis is intended to minimize the difficulties associated with process modeling by providing an accurate unified approach to the model development for packed bed chemical reactors.

1. Such as using a chromatograph to measure outlet concentrations from a reactor.

1.3 REVIEW OF EXPERIMENTAL CONTROL STUDIES

Several experimental laboratory-scale packed bed reactor systems have been studied in terms of control considerations. Table 1.2-1 outlines some of the work done by several groups that have made significant contributions in this area. Their work is by no means the extent of control applications for chemical processes (there is much published work on the control of separation processes and other reactor configurations) but is the major extent of published experimental application of control techniques to packed bed reactors.

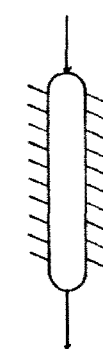
The Denmark group (Clement and Jorgensen, 1981; Clement et al., 1980; Hallager and Jorgensen, 1981; Sorensen, 1977; Sorensen et al., 1980) considered an adiabatic pilot-plant chemical reactor with the reaction between oxygen and hydrogen over an alumina supported platinum catalyst. Initial dynamic modeling and experimental studies were carried out by Hansen and Jorgensen (1974, 1976ab) and by Sorensen (1976). The group considered various reactor and control models and investigated control strategies based on optimal control, direct Nyquist arrays, and the self-tuning regulator.

The Berkeley group (Foss et al., 1980; Michelsen et al., 1973; Silva et al., 1979; Vakil et al., 1973; Wallman et al., 1979) studied the same hydrogen/oxygen system but used a two-bed reactor structure with an interstage quench stream. Again the beds were taken as adiabatic, and various control strategies were devised. The first control studies by Silva et al. (1979) and Wallman et al. (1979) considered the control of the quench flowrate and temperature using temperature measurements and a product concentration estimator using the stochastic linear quadratic regulator and multivariable integral control. The latter work by Foss et al. (1980) uses the flowrate and temperature of the quench stream and the feed temperature to regulate the product concentration and tempera-

ture using the characteristic locus method of control system analysis. A major significance of their work was the consideration of the large number of available measurements and the appropriate choice of control configurations.

The McMaster group (Jutan et al., 1977; MacGregor and Wong, 1978; Wright and Schryer, 1978) considered the hydrogenolysis of butane carried out over a nickel on silica gel catalyst in a nonadiabatic packed bed reactor. The work by Jutan et al. (1977) provides an excellent foundation for packed bed reactor modeling and control studies for multiple reaction systems by specifically considering the state-space model development, the parameter estimation and stochastic disturbance identification, and on-line linear quadratic control. The earlier work by MacGregor and Wong (1978) and Wright and Schryer (1978) deviated from the mechanistic approach to reactor modeling taken by most studies where models are developed by careful consideration of the important chemical and physical phenomena occurring within the process. They considered the use of statistical methods to identify process transfer functions from empirical input/output process data. They then applied a model reference adaptive controller and a state-space stochastic linear quadratic regulator.

Finally, the dynamic behavior of an autothermal reactor with internal countercurrent heat exchange using the steam-shift reaction was modeled by Bonvin (1980) and Bonvin et al. (1979, 1980). Modal control using state feedback was found appropriate for stabilizing the reactor around an unstable steady state.



Adiabatic

Denmark Group					
System	References	Original Model	Control Model	Control Variables	Control Strategy
$H_2 + O_2 \rightarrow 2H_2O$	Sorensen (1977)	$-\frac{\partial X}{\partial Z} + \frac{1}{PeM_2n} \frac{\partial^2 X}{\partial Z^2} - \frac{R_0}{C_o} = 0$	- Collocation (4-8 points)	Measured	Stochastic linear quadratic
	Clement, Jorgensen, Sorensen (1980)	$-\frac{\partial Y}{\partial Z} + \frac{1}{PeTZn} \frac{\partial^2 Y}{\partial Z^2} - \frac{2Nu}{PeTR} (Y - Y_W)$ $-\frac{\alpha}{C_{T_o}} \Delta H_R = \frac{\partial Y}{\partial T}$	- Linearized	- LI temperature - O_2 concentration - Total flowrate Manipulated - Feed temperature - O_2 feed concentration - Total flowrate	regulator
	Clement, Jorgensen (1981)	Same as above	Same as above	Same as above	Direct Nyquist array
	Hallager, Jorgensen (1981)	$x(t) = A(q^{-1})x(t-1) + B(q^{-1})u(t-d) + e(t) + c$ or $x_1(t) = \phi_1^T(t)\theta_1 + e_1(t)$	- Least squares identification - Time series model	Same as above	MIMO self-tuning regulator (LQR)

Table 1.2-1
Summary of Published Research on Packed Bed Reactor Control

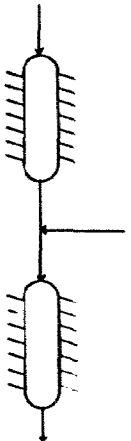
Berkeley Group					
System	Reference	Original Model	Control Model	Control Variables	Control Strategy
$\text{H}_2 + \text{O}_2 \rightarrow 2\text{H}_2\text{O}$ 	Silva, Wallman, Foss (1979)	$\frac{\partial X}{\partial Z} - \frac{R_0}{C_0} = 0$ $-\frac{\partial Y}{\partial Z} = \frac{2\text{Nu}_S}{Pe_{TR}} (Y_S - Y) + \frac{2\text{Nu}_S}{Pe_{TR}} (Y_W - Y)$ $\frac{2\text{Nu}_S}{Pe_{TR}} (Y_S - Y) + \frac{\theta}{CT_0} \Delta H_R = \frac{\partial Y_S}{\partial T}$ $\frac{2\text{Nu}_W}{Pe} (Y_W - Y) - \gamma U (Y_W - Y_E) = \frac{\partial Y_W}{\partial T}$	-Linearization -Collcication - 14 points -Order reduction - 7 points - Method of Divison	Measured - 14 temperatures Manipulated - Quench flowrate - Temperature at quench mixing point	Stochastic linear quadratic regulator
	Wallman, Silva, Foss (1974)	Same as above	Same as above	Measured - 5 temps in Bed II Manipulated - Same as above	Stochastic linear quadratic regulator with integral action
	Foss, Edmunds, Kouvaritakis (1980)	Same as above	Same as above	Measured - 7 temperatures - Exit concentration Manipulated - Feed temperature - Quench temperature - Quench flowrate	Characteristic locus method

Table 1.2-1 Continued

McMaster Group					
System	References	Original Model	Control Model	Control Variables	Control Strategy
Butane Hydrogenolysis (3 Independent Reactions)	Jutan, Tremblay, MacGregor, Wright (1977)	$\frac{\partial x^1}{\partial Z} + \frac{k}{Pe_{HR}} \frac{\partial}{\partial R} \left(\frac{1}{R} \frac{\partial x^1}{\partial R} \right) - \frac{R \dot{u}}{C} = \frac{\partial x^1}{\partial t}$ $- \frac{\partial y}{\partial Z} + \frac{k}{Pe_{TR}} \frac{\partial}{\partial R} \left(\frac{1}{R} \frac{\partial y}{\partial R} \right)$ $+ \frac{0}{\bar{C} T_0} \sum_{i=1}^3 \Delta H_i \dot{u}^i = \frac{\partial y}{\partial t}$	<ul style="list-style-type: none"> -Quasi ss approximation -Collocation -Linearized 	<ul style="list-style-type: none"> Measured - 11 axial temperature - Exit concentrations Manipulated - Inlet H_2 flowrate - Inlet C_4H_{10} flowrate 	Stochastic linear quadratic regulator
	MacGregor, Wong (1978)	$w_t^i = \beta^i z_t + e_t^i \quad i = 1, 2, 3$	<ul style="list-style-type: none"> -Linear regression of conc, temp. measurements -Time series analysis (ARIMA) 	Same as above	State space stochastic linear quadratic regulator
	Wright, Schryer (1978)	$x_m^{(k+1)} = A_m x_m^{(k)} + B_m u_m^{(k)}$ $y_m^{(k)} = H_m x_m^{(k)}$ $u_m^{(k)} = K_{FB} x_m^{(k)} + K_{SP} y_{SP}^{(k)}$	<ul style="list-style-type: none"> -Form reference model (2x2) -Time-series analysis to estimate transfer function 	Same as above	Model reference Adaptive control

Nonadiabatic

1
20
1

Table 1.2-1 Continued

Chapter 2

MULTIVARIABLE CONTROL STRUCTURE DESIGN FOR A HEAT CONDUCTION SYSTEM

2.1 INTRODUCTION

Classical process control techniques were largely developed on a trial and error basis, with the theoretical concepts developed later to substantiate the empirical results. The classical controller was based on a single-input, single-output (SISO) system with three types of possible control action--proportional, integral, and derivative--based on the feedback error. Although design techniques such as root-loci, Bode diagrams, and Nyquist plots led to empirical rules for setting the appropriate amounts of control action, these methods were limited to SISO systems. Since most processes have multiple inputs and outputs, additional considerations became necessary, due to the failure of single-loop analysis for interacting loops. Since frequency-domain methods dominated control system design in the scalar case and led to relatively simple controllers, it is not surprising that considerable effort went into extending these methods to the multivariable case. However, direct extension of scalar frequency-domain procedures was not possible, and major modifications of the existing theories were necessary to meet the design objectives. Furthermore, design complexities were often enhanced due to the additional objective of noninteraction. Nevertheless, several excellent frequency response procedures were developed in the late 60's and 70's, led by the work of Rosenbrock, MacFarlane, and Kouvaritakis.

At the same time, "modern" control techniques were developed. These methods rely on an exact knowledge of the system state, which is reconstructed from a finite number of measurements using current theories in optimal filtering, smoothing, and estimation. The ideas have been extended to account for modeling and measurement uncertainties and inaccuracies. Although these "modern" methods, which rely heavily on variational calculus and dynamic programming, generally lead to a more complex control structure, they are less heuristic than the frequency-domain methods and allow for more precise

control objectives, such as the minimization of the variance in the state vector.

This chapter describes an in-depth analysis of a practical, multivariable, distributed parameter system using both frequency-domain and time-domain analysis. As a typical distributed system, a one-dimensional, heat conduction problem is considered. The process is described by the diffusion equation

$$\frac{\partial^2 y(z,t)}{\partial z^2} = \frac{\partial y(z,t)}{\partial t} , \quad (2.1-1)$$

where the temperature distribution, $y(z,t)$, is dependent on the space coordinate z , which is normalized ($0.0 < z < 1.0$) with respect to the thickness of the system, and on time, which is normalized so that the coefficient corresponding to the thermal diffusivity is unity. For simplicity, the controls $u_1(t)$ and $u_2(t)$ are taken to be the heat fluxes at $z = 0$ and $z = 1$. Thus the initial and boundary conditions are

$$y(z,0) = y_0(z) \quad (2.1-2)$$

$$\left. \frac{\partial y(z,t)}{\partial z} \right|_{z=0} = -u_1(t) , \quad \left. \frac{\partial y(z,t)}{\partial z} \right|_{z=1} = u_2(t) . \quad (2.1-3)$$

Although this heat conduction process is a relatively simple control problem due to the simplicity of the model and ease of obtaining measurements, the analysis leads to conclusions that can be extended to general, multivariable control theory. Actually the system is an excellent choice, since Equations (2.1-1) - (2.1-3) can be solved analytically to give the temperature distribution for any control action. Thus model reduction and control design techniques can be applied to the reduced system and compared with the actual process model. Additionally, the heat conduction system is a highly interacting process with implicit transportation lags.

Due to the simplicity of the model, both distributed and lumped analyses

can be performed. Since most frequency-response techniques require a low-order, lumped, state-space representation, model reduction is an important step in the analysis. Section 2.2 discusses the model lumping and reduction using exact techniques. Additionally, an analysis of output and system controllability, along with a multivariable root-loci analysis, is presented. Much insight can be obtained from these preliminary considerations.

Section 2.3 discusses the time-domain analysis of both the lumped and distributed models of the system. Both optimal feedback control and modal techniques are discussed in detail, along with derivations of the control schemes. Since much work has been published on the application of optimal control theory to the single-input, one-dimensional heat conduction problem and since little additional complexity is introduced in the optimal analysis by adding another control, this aspect is not dealt with in detail.

Section 2.4 considers non-interacting control. Since a major difficulty in multivariable, feedback control design arises from the steady state and dynamic interactions that occur between the various input and output variables, it is usually desirable to reduce these interactions. If they can be reduced sufficiently, single-loop control theories can be applied directly to each of the non-interacting loops. The technique of perfect, non-interacting compensation is attempted for this purpose. However since such compensation is in many cases impractical or excessively complicated, other methods that only eliminate steady state interactions are also considered. Finally, a new method, that uses a relatively simple control structure to eliminate all steady state and dynamic interactions, is considered. This procedure, called inner-loop decoupling, makes use of extra available measurements through an inner-loop structure.

Several methods at the forefront of current multivariable frequency-

response analysis are also studied. Section 2.5 discusses the application of Rosenbrock's (1962) inverse Nyquist array technique, which is an extension of the classical Nyquist stability criterion. Section 2.6 analyzes the heat conduction system using the characteristic locus method. The analysis is based on the latest refinements of the technique originally introduced by Belletrutti and MacFarlane (1971). The current work provides a systematic approach for designing a proportional-integral controller with the best compromise of system stability, interaction, integrity, and accuracy.

Section 2.7 presents an overall analysis of the control system performance. Using computer simulations of the responses of both the lumped model and the actual system to step input changes, the effectiveness of the various control designs are compared. This analysis leads to conclusions about the model reduction and design techniques that can be extended to general, multivariable feedback control.

2.2 PRELIMINARY ANALYSIS

Difficulties arise in the control system design of distributed parameter systems because of state variations in both time and space. The thrust of many of the feedback control design techniques for distributed systems is to reduce the system to a lumped one and then to take advantage of the many theories available for lumped parameter control design. However, problems arise in that all of the analysis performed on the lumped system is dependent on the method and accuracy of the reduction. Although considerable model reduction is necessary to reduce computational complexities in the design procedures, excessive or inaccurate reduction can lead to a system whose behavior is quite different from that of the original process.

2.2.1 Model Reduction

To obtain the lumped parameter model for a system described by partial differential equations, many efficient techniques are described in the literature. In particular, much work has been published on various lumping strategies for linear diffusion equations. A particularly useful means of treating both linear and nonlinear partial differential equation systems is the method of weighted residuals along with other pseudo-modal techniques, such as finite element methods (Norrie and DeVries, 1973) or the use of spline functions (Finlayson, 1972). The method of weighted residuals is comprised of the following basic techniques, depending on the choice of the weighting function (Prabhu and McCausland, 1970; Ray, 1981):

- a. Galerkin's Method (Lynn and Zahradnik, 1970; Newman and Sen, 1972; Prabhu and McCausland, 1970)

- b. Method of Subdivisions
- c. Method of Moments
- d. Method of Collocation (Finlayson, 1972)
- e. Least Squares Method.

Although these techniques are quite powerful, Mahapatra (1977) points out that solutions using the method of weighted residuals often require considerable effort to determine the set of orthogonal coordinate functions and a high-order lumped model for accurate results. To eliminate these difficulties, spatial discretization techniques (Leden, 1976; Mahapatra, 1977) are often quite useful for linear diffusion systems, since they retain the physical characteristics of the system. However, they too often lead to high-order lumped models.

Thus to improve the accuracy and reduce the order of the model, it may be best to use an exact reduction technique. Since the heat equation is governed by a parabolic equation, exact lumping can be performed using a Laplace transform in time or through a modal analysis. The latter, which is simply an application of the separation of variable solution procedure, is quite attractive for systems which can be made self-adjoint, since the technique leads directly to the eigenvalues and eigenfunctions (modes) of the system. If the eigenvalues are real, discrete and well spaced, the modal representation is a convenient method to reduce the order of the system, since only the dominant modes need be retained for design purposes.

Both the Laplace transform and modal analysis techniques were applied to the one-dimensional heat conduction problem. Other techniques have been discussed in detail in the literature. Although the methods can be shown to lead to equivalent results, the modal analysis leads directly to a lumped, state-space representation. Disadvantages of the separation of variable technique were

cited by Prabhu and McCausland (1970), but the technique is well suited to the linear diffusion problem because time and space variables are easily separated and an analytic solution is possible.

Consider the system described by Equation (2.1-1), scaled so that $y_0(z)=0$. Taking the Laplace transform with respect to time gives:

$$sy(z,s) = \frac{d^2y(z,s)}{dz^2} , \quad (2.2-1)$$

which has the solution

$$y(z,s) = A \sinh \sqrt{s}z + \cosh \sqrt{s}z . \quad (2.2-2)$$

After application of the boundary conditions

$$\frac{dy(0,s)}{dz} = -u_1(s) \quad \frac{dy(1,s)}{dz} = u_2(s) . \quad (2.2-3)$$

the solution in the Laplace domain is

$$y(z,s) = \mathbf{G}_p^T(z,s) \mathbf{u}(s) , \quad (2.2-4)$$

where

$$\mathbf{u}^T(s) = [u_1(s) , u_2(s)] \quad (2.2-5)$$

$$\mathbf{G}_p^T = [g_1(z,s) , g_2(z,s)] = \left[\frac{\cosh(1-z)\sqrt{s}}{\sqrt{s} \sinh \sqrt{s}} , \frac{\cosh z \sqrt{s}}{\sqrt{s} \sinh \sqrt{s}} \right] . \quad (2.2-6)$$

Thus a distributed transfer function representation is obtained, from which a simple feedback control strategy can be envisioned (Figure 2.2-1). The closed-loop distributed transfer function is

$$\frac{y(z,s)}{y_d(z,s)} = [I + \mathbf{G}_p(z,s) \mathbf{G}_c(s)]^{-1} \mathbf{G}_p(z,s) \mathbf{G}_c(s) . \quad (2.2-7)$$

However in general, measurements will only be available as discrete points. If these points are z_1, \dots, z_N , the appropriate block diagram structure is shown in

Figures 2.2-2 and 2.2-3 with

$$\mathbf{A}^T = \left[\delta(z-z_1), \delta(z-z_2), \dots, \delta(z-z_N) \right] . \quad (2.2-8)$$

Note that Figure 2.2-3 is equivalent to Figure 2.2-1 with $\mathbf{G}_c(z,s) = \mathbf{G}_c(s)\mathbf{A}$

Using contour integration to invert Equations (2.2-4)-(2.2-6), the time-domain representation of the solution can be obtained. The inverse of $g_i(z,s)$ is the sum of the residues of $e^{st}g_i(z,s)$. Each $g_i(z,s)$ has an infinite number of simple poles at $s_n = -n^2\pi^2$, $n = 1, 2, 3, \dots$ and a pole at $s_0 = 0.0$. Simple expansions of the numerator and denominator of $e^{st}g_i(z,s)$ about $s_0 = 0.0$ lead to a residue of 1.0 at s_0 . The residues at s_n are obtained by Taylor expanding $\sinh \sqrt{s}$ about s_n and applying residue theory. This results in

$$\begin{aligned} g_1(z,t) &= 1.0 + \sum_{n=1}^{\infty} 2.0(-1)^n \cos n\pi(1-z) e^{-n^2\pi^2 t} \\ g_2(z,t) &= 1.0 + \sum_{n=1}^{\infty} 2.0(-1)^n \cos n\pi z e^{-n^2\pi^2 t} \end{aligned} . \quad (2.2-9)$$

Then using convolution theory, the time-domain behavior is directly related to the control action:

$$y(z,t) = \int_0^t \mathbf{G}(z,t-\tau) \mathbf{u}(\tau) d\tau \quad \mathbf{G}^T(z,t) = [g_1(z,t), g_2(z,t)] . \quad (2.2-10)$$

Since the time-domain results are obtained as an infinite series of exponentials with eigenvalues $\lambda_n = n^2\pi^2$, the Laplace-domain behavior can also be represented as an infinite series with $y(z,s)$ being described by Equation (2.2-4) along with the following:

$$\mathbf{G}_p^T(z,s) = \left[\frac{1}{s} + \sum_{n=1}^{\infty} \frac{2(-1)^n \cos n\pi(1-z)}{s-\lambda_n}, \quad \frac{1}{s} + \sum_{n=1}^{\infty} \frac{2(-1)^n \cos n\pi z}{s-\lambda_n} \right] . \quad (2.2-11)$$

Then if the series can be truncated after the first few terms without excessive inaccuracy, normal multivariable design techniques can be applied directly.

However since separation of variables for the one-dimensional heat conduction system leads to a self-adjoint operator with real, discrete eigenvalues, modal decomposition is attractive for this system. The problem can be redefined using the Dirac delta function:

$$\frac{\partial y(z,t)}{\partial t} = \frac{\partial^2 y(z,t)}{\partial z^2} + \delta(z-0)u_1(t) + \delta(z-1)u_2(t) \quad (2.2-12)$$

$$z = 0^-, \quad z = 1^+ \quad \frac{\partial y(z,t)}{\partial z} = 0 .$$

It can be proven that this change is rigorous by integrating Equation (2.2-12) across the infinitesimal intervals $1^- < z < 1^+$ and $0^- < z < 0^+$. For example:

$$\int_{0^-}^{0^+} \frac{\partial y}{\partial t} dz = \int_{0^-}^{0^+} \frac{\partial}{\partial z} \left(\frac{\partial y}{\partial z} \right) dz + \int_{0^-}^{0^+} \delta(z-0)u_1(t) dz + \int_{0^-}^{0^+} \delta(z-1)u_2(t) dz \quad (2.2-13)$$

Thus

$$0 = \left. \frac{\partial y}{\partial z} \right|_{0^-}^{0^+} + u_1(t)$$

But $\frac{\partial y}{\partial z} = 0$ at $z = 0^-$; therefore $\frac{\partial y}{\partial z} = -u_1(t)$ at $z = 0^+$. Thus formulation (2.2-12) is equivalent to that described by Equations (2.1-1) - (2.1-3).

The space and time variables can then be separated by assuming a solution of the form

$$y(z,t) = \sum_{n=0}^{\infty} a_n(t) \varphi_n(z) \quad (2.2-14)$$

$$\delta(z-0)u_1(t) + \delta(z-1)u_2(t) = \sum_{n=0}^{\infty} b_n(t) \varphi_n(z) .$$

After substituting into (2.2-12) and simplifying, the equations become

$$\left. \begin{aligned} \frac{1}{a_n(t)} \frac{da_n(t)}{dt} - \frac{b_n(t)}{a_n(t)} &= \frac{1}{\varphi_n(z)} \frac{d^2 \varphi_n(z)}{dz^2} \\ z=0 \quad \frac{d\varphi_n(z)}{dz} &= 0, \quad z=1 \quad \frac{d\varphi_n(z)}{dz} = 0 \end{aligned} \right\} n=0, 1, 2, \dots \quad (2.2-15)$$

By choosing the separation constant as $-\lambda_n$,

$$\left. \begin{aligned} \frac{d^2 \varphi_n(z)}{dz^2} + \lambda_n \varphi_n &= 0 \\ \frac{da_n(t)}{dt} + \lambda_n a_n(t) &= b_n(t) \end{aligned} \right\} n=0, 1, 2, \dots \quad (2.2-16)$$

Clearly (2.2-16a) is a self-adjoint differential equation that can be solved to yield

$$\varphi_n(z) = A_n \cos \sqrt{\lambda_n} z \quad \lambda_n = n^2 \pi^2, \quad n=0, 1, 2, \dots \quad (2.2-17)$$

after application of the boundary conditions from (2.2-15). Because (2.2-16a) is a homogeneous, self-adjoint differential equation with homogeneous boundary conditions, the eigenfunctions, Equation (2.2-17), are orthogonal. It is convenient to choose the arbitrary constant A_n so as to make the eigenfunctions orthonormal, i.e.,

$$\int_0^1 \varphi_n^2(z) dz = 1.0 \quad (2.2-18)$$

The appropriate choice of A_n leads to

$$\varphi_n(z) = \begin{cases} 1.0 & n=0 \\ \sqrt{2} \cos n\pi z & n=1, 2, \dots \end{cases} \quad (2.2-19)$$

Then by application of the orthogonality of the eigenfunctions

$$a_n(t) = \int_0^1 \varphi_n(z) y(z, t) dz, \quad (2.2-20)$$

or in particular for $y_0(z) = 0$, $a_n(0) = 0$. Similarly the coefficients $b_n(t)$ are given by

$$\begin{aligned} b_n(t) &= \int_0^1 \varphi_n(z) [\delta(z-0)u_1(t) + \delta(z-1)u_2(t)] dz \\ &= \varphi_n(0)u_1(t) + \varphi_n(1)u_2(t). \end{aligned} \quad (2.2-21)$$

Thus

$$b_n(t) = \begin{cases} u_1(t) + u_2(t) & n=0 \\ \sqrt{2}u_1(t) + (-1)^n \sqrt{2}u_2(t) & n=1, 2, \dots \end{cases} \quad (2.2-22)$$

Since the eigenvalues, $\lambda_n = n^2\pi^2$, increase rapidly with increasing n , the system can be accurately represented by the first few eigenfunctions, $n = 0, 1, \dots, N$. The process model can then be obtained as an N th-order lumped state-space representation with the $N+1$ states a_0, \dots, a_N .

$$\dot{\mathbf{x}}(t) = \mathbf{A}\mathbf{x}(t) + \mathbf{B}u(t), \quad y(z,t) = \mathbf{C}\mathbf{x}(t), \quad (2.2-23)$$

where

$$\mathbf{x}^T(t) = [a_0(t), \dots, a_N(t)]$$

$$\mathbf{A} = \text{diag}(-n^2\pi^2), \quad \mathbf{B} = \begin{bmatrix} 1 & 1 \\ \sqrt{2} & -\sqrt{2} \\ \vdots & \vdots \\ \sqrt{2} & (-1)^N \sqrt{2} \end{bmatrix},$$

$$\mathbf{C} = [\varphi_0(z), \varphi_1(z), \dots, \varphi_N(z)]$$

The resulting feedback control system can be drawn in block diagram form (Figure 2.2-4)

In theory, the control scheme of Figure 2.2-4 (and of Figure 2.2-1) requires the complete temperature profile, $y(z,t)$, of the system. However, Ray (1981) points out several means of circumventing this problem. He suggests:

- i. measuring $y(z_i, t)$ at many points $i = 1, 2, \dots, M$ and using an optimal smoothing technique to approximate $y(z, t)$,
- ii. measuring $y(z_i, t)$ at a few points and using a state estimator to estimate $y(z, t)$,
- iii. or measuring $y(z_i, t)$ at $N+1$ spatial points and letting

$$\mathbf{y}^T(t) = [y(z_1, t), y(z_2, t), \dots, y(z_{N+1}, t)]$$

$$\mathbf{C} = \begin{bmatrix} \varphi_0(z_1) & \dots & \varphi_N(z_1) \\ \vdots & & \vdots \\ \varphi_0(z_{N+1}) & \dots & \varphi_N(z_{N+1}) \end{bmatrix} \quad (2.2-24)$$

Then $\mathbf{y}(t) = \mathbf{C}\mathbf{x}(t)$ or $\mathbf{x}(t) = \mathbf{C}^{-1}\mathbf{y}(t)$ as long as z_1, \dots, z_{N+1} are selected to keep \mathbf{C} nonsingular.

Actually it is possible to control the system by taking measurements at M points, where $M < N+1$. For this case, the system should be controlled by using set points on the outputs rather than on the states, since the $N+1$ th-order state vector $\mathbf{x}(t)$ cannot be obtained uniquely with $M < N+1$ measurements.

Regardless of the technique for estimating $y(z, t)$, the appropriate transfer function representation can be obtained by converting to the Laplace domain. With $y_0(z) = 0$,

$$\mathbf{x}(s) = (sI - \mathbf{A})^{-1} \mathbf{B}u(s), \quad \mathbf{y}(z, s) = \mathbf{C}\mathbf{x}(s), \quad (2.2-25)$$

or with measurements at M distinct points:

$$\mathbf{y}(s) = \mathbf{C}\mathbf{x}(s), \quad \mathbf{C} = \begin{bmatrix} \varphi_0(z_1) & \dots & \varphi_N(z_1) \\ \vdots & & \vdots \\ \varphi_0(z_M) & \dots & \varphi_N(z_M) \end{bmatrix} \quad (2.2-26)$$

Thus the lumped parameter system process transfer function is given by

$$G_p(s) = C(sI - A)^{-1}B \quad (2.2-27)$$

2.2.2 Controllability

The distributed system has been lumped through an N eigenfunction decomposition. Before attempting to design a control strategy for the lumped system, an analysis of system and output controllability is necessary.

Although the concept of controllability is formally defined in many references (Brockett, 1970; Douglas, 1972; Lee and Marcus, 1967; Ray, 1981), it is convenient to consider a system completely controllable if some control action exists that will take the system from any given initial state to any specified final state in finite time. The necessary and sufficient condition for complete controllability of the system described by (2.2-23) with $N-1$ states and two controls is that the controllability matrix L_c

$$L_c = [B | AB | A^2B | \dots | A^{N-1}B] \quad (2.2-28)$$

$$L_c = \begin{bmatrix} 1 & 1 & \dots & 0 & 0 \\ \sqrt{2} & -\sqrt{2} & \dots & (-\pi^2)^N \sqrt{2} & -(-\pi^2)^N \sqrt{2} \\ \vdots & \vdots & & \vdots & \vdots \\ \vdots & \vdots & & \vdots & \vdots \\ \sqrt{2} & (-1)^N \sqrt{2} & \dots & (-N^2 \pi^2)^N \sqrt{2} & (-1)^N (-N^2 \pi^2)^N \sqrt{2} \end{bmatrix}$$

has rank $N-1$. Since L_c has full rank for all N , the system is completely controllable. Thus the two controls u_1 and u_2 are capable of influencing all of the states.

However, the lumped analysis will be based on k measurements. Thus a more important concept is that of output controllability, i.e., the controls must be able to influence all k outputs. The output controllability matrix

$$L_e' = [CB \mid CAB \mid \dots \mid CA^{N-1}B] \quad (2.2-29)$$

must have rank k for the system to be output controllable. It can easily be shown that, for the heat conduction system, output controllability is assured if no two measurements are taken at the same point.

It can be concluded that, for k distinct measurements, the lumped, one-dimensional heat conduction system is completely controllable with heat flux control at $z = 0$ and $z = 1$. Thus multivariable lumped parameter control theory can be applied to the state-space representation of the system. However, it should be recalled that this analysis of controllability is dependent on the accuracy of the model reduction and lumping. Although the approximate lumped parameter system has been shown to be completely controllable, the actual distributed system may indeed be only partially controllable. Additionally, care must be taken in making conclusions from this type of analysis, since no consideration of the physical constraints of the system have been made.

2.2.3 Root-Locus

The concept of root-locus analysis is basic to classical control system design for single-input, single-output processes. The root-locus diagram is advantageous since it describes the character of the response as the gain of the controller is continuously changed, by allowing rapid determination of the roots of the characteristic equation. Although scalar root-locus techniques are well-known, the multivariable root-locus problem is relatively new. Kouvaritakis (1978), Kouvaritakis and MacFarlane (1976ab), and Kouvaritakis and Shaked (1976) describe the technique and discuss the analysis of system zeros.

The objective of the root-locus method is to investigate the behavior of the closed-loop characteristic frequencies when the feedback gain matrix has the

form $\mathbf{G}_c = k\mathbf{I}$. For the modal-lumped representation of the heat conduction system, the process transfer function was shown to be $\mathbf{G}_p = \mathbf{C}(\mathbf{sI} - \mathbf{A})^{-1}\mathbf{B}$. The characteristic equation is then (Hsu and Chen, 1968)

$$|\mathbf{I} + k\mathbf{G}_p| = \frac{P_c(s)}{P_o(s)} . \quad (2.2-30)$$

where $P_o(s)$ is the open-loop characteristic polynomial and $P_c(s)$ is the closed-loop characteristic polynomial. Then if we define

$$z(s) = \begin{bmatrix} \mathbf{sI} - \mathbf{A} & -\mathbf{B} \\ \mathbf{C} & \mathbf{0}_{m,m} \end{bmatrix} , \quad (2.2-31)$$

the $n-m-d$ closed-loop characteristic frequencies¹ will tend toward the roots of $z(s) = 0$ as k increases. These roots are the finite zeros of the process. For the two-control, 3rd-order, heat conduction system, there is one finite zero and two infinite zeros if \mathbf{CB} has full rank. If \mathbf{CB} has lost rank, all three zeros will be infinite. This occurs for the following choices of measurement locations:

$$\begin{array}{lllllll} z_1 & 0.20 & 0.33 & 0.40 & 0.60 & 0.67 & 0.80 \\ z_2 & 0.60 & 0.67 & 0.80 & 0.20 & 0.33 & 0.40 \end{array}$$

Thus for any combination of outputs other than these, there will be one finite zero given by $z(s) = 0$. The solution to this is

$$s = \frac{4\pi^2(c-a)}{\sqrt{2(ad-bc)+(a-c)}} , \quad (2.2-32)$$

1. where n is the order of the lumped model, m is the number of inputs, and d is the rank deficiency of \mathbf{CB}

$$a = \varphi_1(z_1) \quad b = \varphi_2(z_1) \quad c = \varphi_1(z_2) \quad d = \varphi_2(z_2) \quad .$$

This root is finite for all z_1 and z_2 other than those listed above, since the denominator of Equation (2.2-32) is then nonzero.

The root-loci for the system are the loci of the roots of the characteristic equation

$$0 = |I + kG_p| = |sI - A| |I + kG_p| = s(s + \pi^2)(s + 4\pi^2) + k[(2 + \sqrt{2}(a - c) + \sqrt{2}(b + d))s^2 + [10\pi^2 + 4\sqrt{2}\pi^2(a - c) + \pi^2\sqrt{2}(b + d) + 2\sqrt{2}k(a - c) + 4k(ad - bc)]s + 8\pi^2\sqrt{2}k(a - c) + 8\pi^4] \quad (2.2-33)$$

as k varies from 0 to ∞ . Obviously, the poles ($k = 0$) of the system are at $s = 0$, $-\pi^2$ and $-4\pi^2$ independent of the measurements. As k approaches infinity, (2.2-33) reduces to

$$\sqrt{2}(ad - bc)s + (a - c)s + 4\pi^2(a - c) = 0 \quad (2.2-34)$$

which is equivalent to (2.2-32) above.

Figure 2.2-5 shows the root-loci for various measurement locations. Both symmetric and unsymmetric cases were studied. For the symmetric cases, the root-loci remain stable (in the left-half plane) at high gains for $z_1 \leq 0.33$; whereas, the loci become unstable at high gains for $0.33 < z_1 < 0.50$. This is expected due to the large lag time between the control action at $z_1 = 0$ and its effect on the output. The symmetric cases with z_1 and z_2 reversed, i.e., $z_1 > 0.50$ and $z_2 < 0.50$ (not shown), lead to root-loci identical to those in Figure 2.2-5 except that the locus beginning at $-\pi^2$ approaches $+\infty$ rather than $-\infty$. Thus such a system is less stable.² Additionally from the root-loci analysis, the

2. This is also a result of the large lag times.

responses for the (0.2,0.8) case are expected to be non-oscillatory; whereas, for all other cases, oscillations are expected at moderate to high gains.

It can be concluded that, for symmetric measurements with $z_1 < 0.33$ or for the unsymmetric case (0.4,0.8), system stability is insured even for high gains. Thus a proportional controller may provide adequate control action. Since the other cases lead to instability at high gains, more complicated control schemes should be considered.

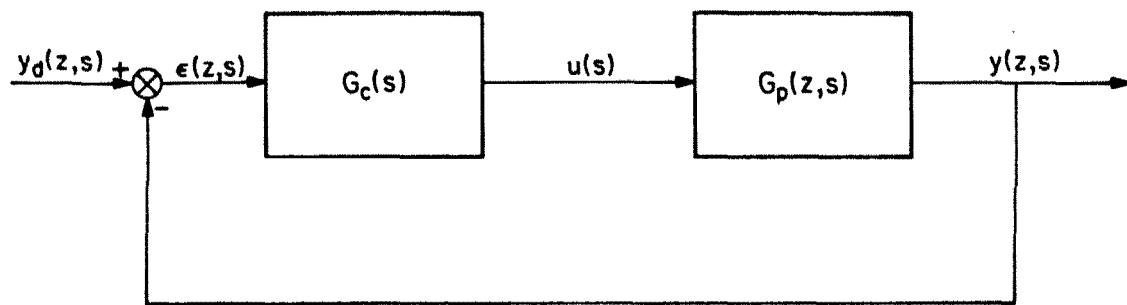


Figure 2.2-1
Distributed Feedback Control Design

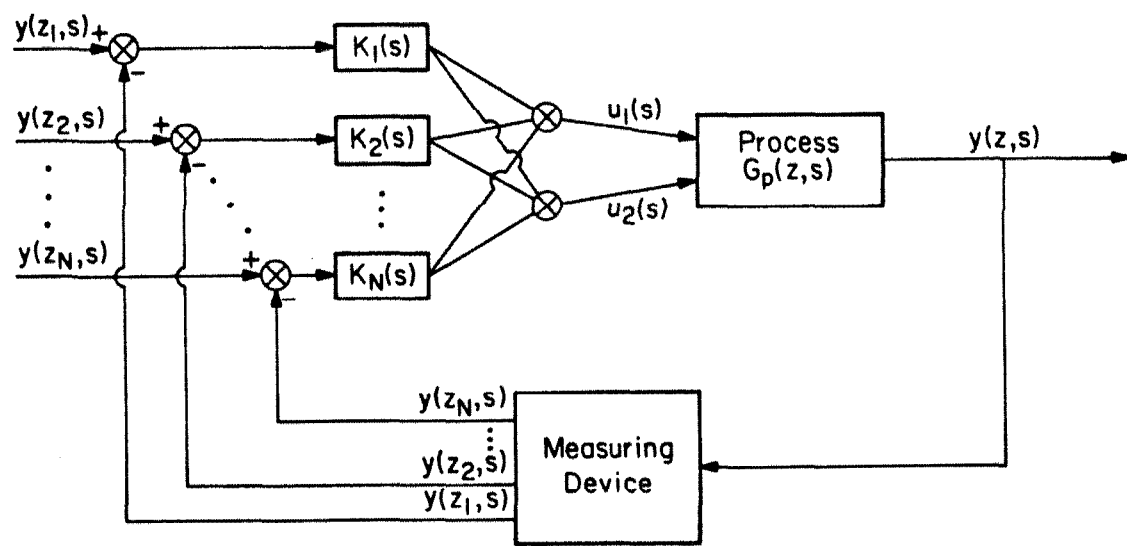


Figure 2.2-2
Feedback Control Strategy with N Discrete Measurements

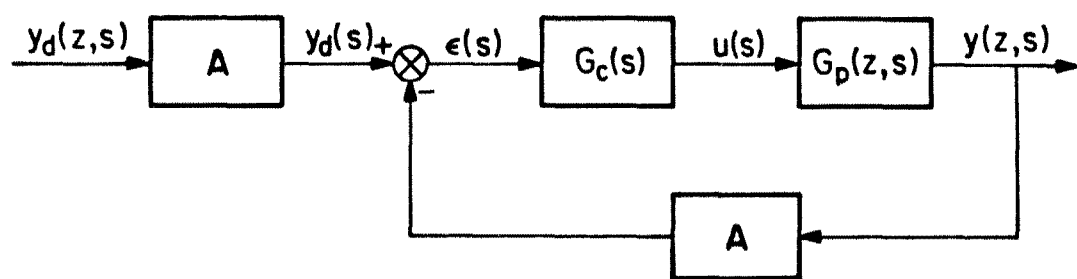


Figure 2.2-3
Modified Feedback Control Strategy with N Discrete Measurements

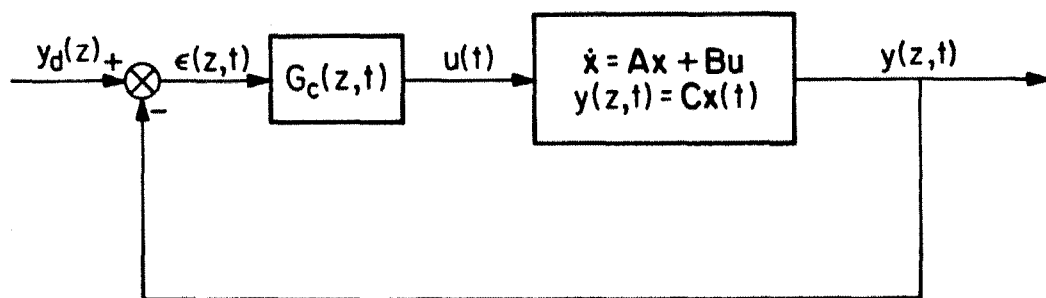
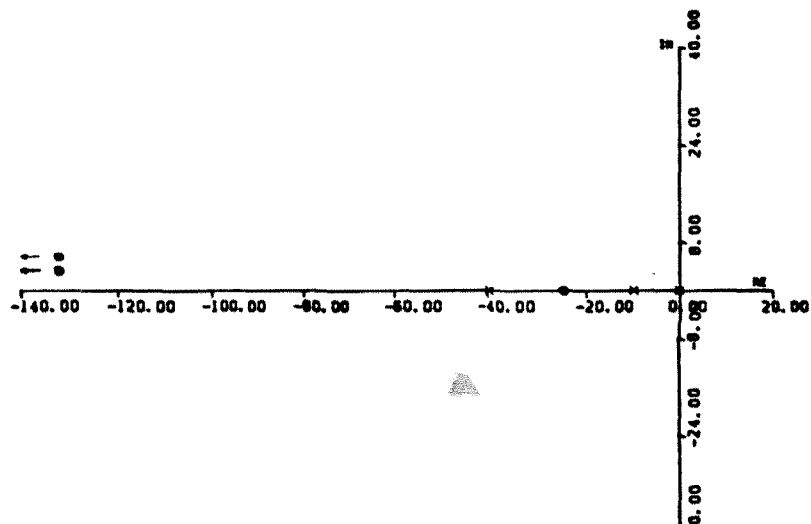
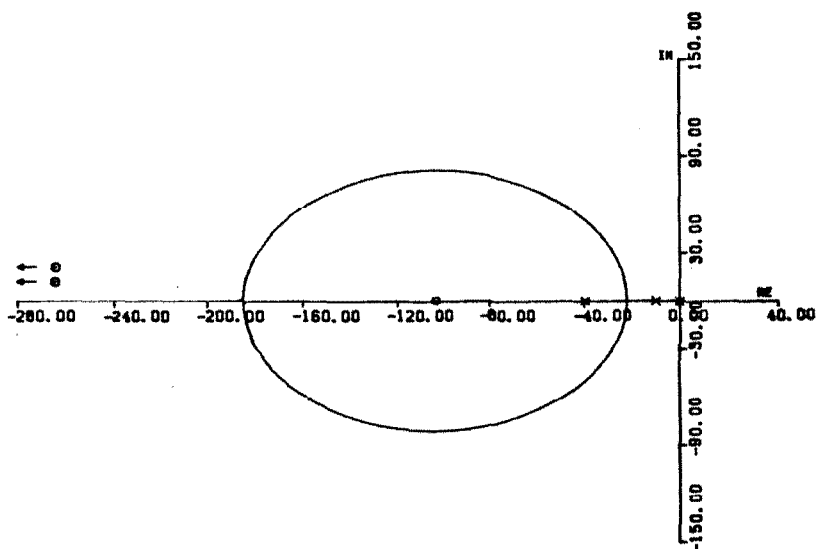


Figure 2.2-4
Nth-Order Lumped Feedback Control Design



(a)

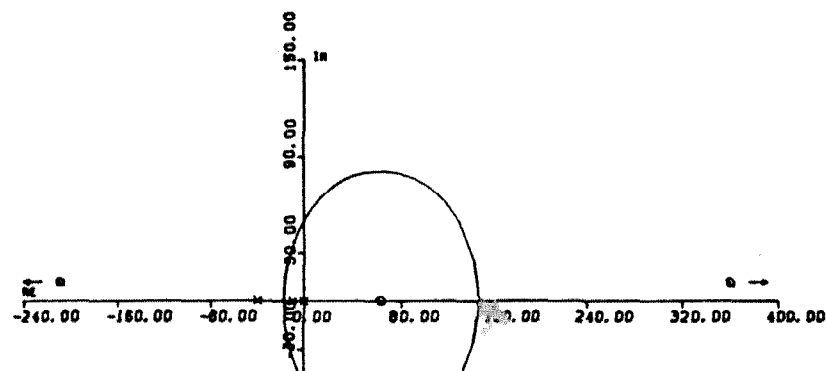


(b)

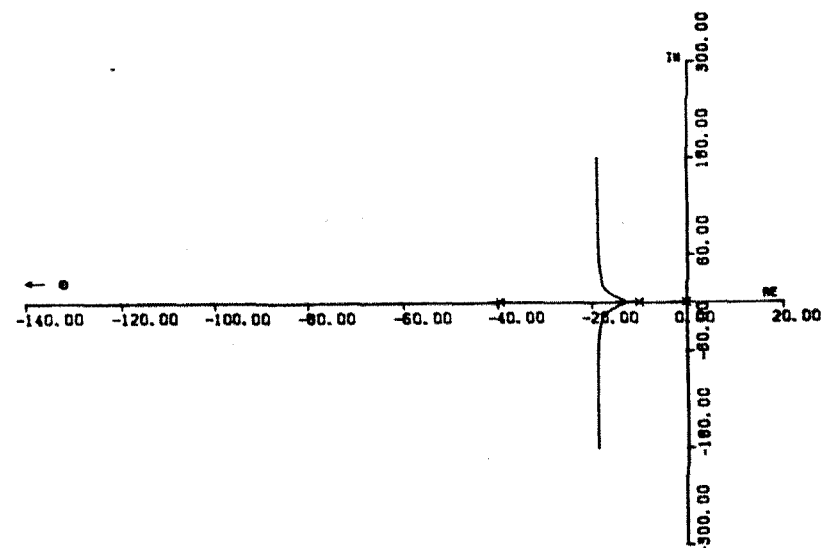
Figure 2.2-5
Root-Loci Diagrams for Various Outputs

a. (0.2,0.8) b. (0.3,0.7) c. (0.4,0.6) d. (0.4,0.8)

x - Poles o - Zeros



(c)



(d)

Figure 2.2-5 Continued

2.3 TIME-DOMAIN ANALYSIS

The time-domain approach for control system analysis utilizes the differential or difference equations directly rather than using transfer functions, as in the frequency-domain analysis. Although the time-domain technique is actually older than frequency response techniques, its development was slow due to the difficulty of making calculations in the differential domain. The emergence of digital computation as a widely accepted tool led to a resurgence of interest in time-domain analysis. In particular, the techniques of state estimation, optimal control, modal control, and adaptive control rose to the forefront of research. Although these methods have a strong theoretical basis, they only became practical with the development of small and reliable digital computers capable of high-speed information processing. Consideration of ideas for which frequency-domain techniques were inappropriate, such as simultaneous control of several interacting variables, and the application of different types of controller objectives, such as the minimization of energy consumption, became practical.

Of the many time-domain procedures, optimal control and modal control are the most common techniques and thus have been studied extensively for both lumped and distributed parameter systems. The one-dimensional diffusion equation has often been used to illustrate the application of these methods. Due to the many studies of these theories and on their application to heat conduction systems, only a cursory examination of the techniques will be presented. Additionally, other methods such as adaptive control and state estimation will not be considered in this theoretical analysis of the heat conduction process, although they may be quite useful in practical applications.

2.3.1 Optimal Control

Optimal control methods can be divided into two schemes--open- and closed-loop. When an excellent mathematical model of the system is available in terms of differential equations, open-loop control schemes can be useful for start-up, shut down, and other transient conditions. However in practice, most models contain some error; therefore, closed-loop schemes are often necessary for satisfactory controller performance, since they involve feedback of process measurements. Regardless of whether open or closed-loop control is to be used, the technique involves the selection of an index which measures the performance of the system, from which the optimal control strategy is selected as that which minimizes this index. A major difficulty in the design of an optimal control system is the establishment of the criteria for optimality. The optimal control procedure is in contrast to the other techniques that try to obtain satisfactory responses in terms of offset, gain margin or decay ratios, since once the criteria is selected a unique solution is obtained.

As previously mentioned, much work has been published concerning optimal control of parabolic systems such as that described by the heat equation. McCausland (1970), Prabhu and McCausland (1970), and Mahapatra (1977) studied time-optimal control of the linear diffusion process. For such control, the objective is to force the system to reach the desired design conditions in minimum time. Others (Betts and Citron, 1972; Sakawa, 1964; Sheirah and Hamza, 1974) treated the problem of optimal control of the heat conduction problem by minimizing the deviation of the temperature distribution from the desired distribution throughout time. Additionally much literature is available on the general problem of optimal control of distributed parameter systems.

An important special case of the optimal control problem is linear-

quadratic control, which leads to an optimal, state-feedback control law. Numerous papers have been written on this problem, including several on its application to parabolic systems (Ahmed and Teo, 1981; Matsumoto and Ito, 1970; Wang, 1975). This technique uses a quadratic penalty function to control a system at a set point without excessive control action and not exceeding acceptable levels of state. The method is readily applicable to either a lumped model of the system or to the original distributed model.

For the heat conduction system, the lumped parameter model is described by the linear differential equation

$$\dot{\mathbf{x}} = \mathbf{Ax} + \mathbf{Bu}, \quad \mathbf{y} = \mathbf{Cx}, \quad (2.3-1)$$

with \mathbf{A} , \mathbf{B} , and \mathbf{C} defined by Equations (2.2-23) and (2.2-26). The objective of this technique is to obtain the feedback law which minimizes the performance index

$$J = \frac{1}{2} \mathbf{x}^T \mathbf{S}_F \mathbf{x} \Big|_{t_0}^{t_F} + \frac{1}{2} \int_{t_0}^{t_F} [\mathbf{x}^T \mathbf{F} \mathbf{x} + \mathbf{u}^T \mathbf{E} \mathbf{u}] dt, \quad (2.3-2)$$

where \mathbf{S}_F , $\mathbf{F}(t)$, and $\mathbf{E}(t)$ are symmetric, positive definite weighting matrices which describe the relative importance of reaching the desired set point $\mathbf{x}_d = 0$, using small levels of the state and using little control action. If the desired set point is nonzero, then deviation variables can be used to convert the problem to the above form. Thus let \mathbf{x}_d and \mathbf{u}_d be the desired steady state values. Then letting

$$\mathbf{x}' = \mathbf{x} - \mathbf{x}_d, \quad \mathbf{u}' = \mathbf{u} - \mathbf{u}_d \quad (2.3-3)$$

and recognizing that at steady state $\mathbf{Ax}_d + \mathbf{Bu}_d = 0$, Equation (2.3-1) becomes

$$\dot{\mathbf{x}}' = \mathbf{Ax}' + \mathbf{Bu}' \quad (2.3-4)$$

with the performance index:

$$J = \frac{1}{2}(\mathbf{x} - \mathbf{x}_d)^T \mathbf{S}_F (\mathbf{x} - \mathbf{x}_d) \Big|_{t_F} + \frac{1}{2} \int_{t_0}^{t_F} [(\mathbf{x} - \mathbf{x}_d)^T \mathbf{F} (\mathbf{x} - \mathbf{x}_d) + (\mathbf{u} - \mathbf{u}_d)^T \mathbf{E} (\mathbf{u} - \mathbf{u}_d)] dt \quad (2.3-5)$$

Then from quadratic feedback control theory (Bryson and Ho, 1969; Ray, 1981), the feedback control law is

$$\mathbf{u}(t) = \mathbf{u}_d - \mathbf{K}(t)(\mathbf{x} - \mathbf{x}_d) \quad (2.3-6)$$

where $\mathbf{K}(t)$ is given by

$$\mathbf{K}(t) = \mathbf{E}^{-1} \mathbf{B}^T \mathbf{S}(t) \quad (2.3-7)$$

and $\mathbf{S}(t)$ is found by solving the Riccati equation backward from t_F :

$$\dot{\mathbf{S}}(t) = -\mathbf{S}\mathbf{A} - \mathbf{A}^T \mathbf{S} + \mathbf{S}\mathbf{B}\mathbf{E}^{-1}\mathbf{B}^T \mathbf{S} - \mathbf{F}, \quad \mathbf{S}(t_F) = \mathbf{S}_F. \quad (2.3-8)$$

Thus a proportional feedback controller with time-varying gain has been designed to control the system while minimizing the index given by Equation (2.3-5). This control structure is quite useful because the time-varying gain $\mathbf{K}(t)$ can be determined off-line since it does not depend on $\mathbf{x}(t)$ or $\mathbf{u}(t)$. Then if $t_F \rightarrow \infty$ and \mathbf{A} , \mathbf{B} , \mathbf{F} , and \mathbf{E} are constant, $\mathbf{S}(t)$ becomes constant. It is the solution to

$$\mathbf{S}\mathbf{B}\mathbf{E}^{-1}\mathbf{B}^T \mathbf{S} - \mathbf{S}\mathbf{A} - \mathbf{A}^T \mathbf{S} - \mathbf{F} = 0 \quad (2.3-9)$$

In this case, the controller is simply a constant gain proportional controller.

The linear-quadratic problem can also be applied to the distributed parameter system described by Equations (2.1-1) - (2.1-3). The objective is then to minimize the index

$$\begin{aligned} J = & \frac{1}{2} \int_0^1 [y'(z, t_F)]^2 \mathbf{S}_F dz + \frac{1}{2} \int_0^{t_F} \int_0^1 F[y'(z, t)]^2 dz dt \\ & + \frac{1}{2} \int_0^{t_F} [E_0[u'_1(t)]^2 + E_1[u'_2(t)]^2] dt \end{aligned} \quad (2.3-10)$$

where y' and u' are deviation variables with $y_d(z)$ being the desired temperature

profile. The derivation of the optimal control law is carried out using the procedure described by Ray (1981). The results are:

$$\begin{aligned} u_1(t) &= -E_0^{-1} \int_0^1 S(0,s,t) y(s,t) ds \\ u_2(t) &= -E_1^{-1} \int_0^1 S(1,s,t) y(s,t) ds \end{aligned} \quad (2.3-11)$$

where $S(r,s,t)$ can be computed off-line from

$$\begin{aligned} S_r(r,s,t) &= -S_{ss} - S_{rr} + S(r,0,t) E_0^{-1} S(0,s,t) \\ &\quad + S(r,1,t) E_1^{-1} S(1,s,t) - F \delta(r-s) \end{aligned} \quad (2.3-12)$$

with the boundary conditions

$$S_s(r,1,t) = S_s(r,0,t) = S_r(0,s,t) = S_r(1,s,t) = 0 \quad (2.3-13)$$

and terminal condition

$$S(r,s,t_F) = S_F(r,s) = S_F \delta(r-s) \quad (2.3-14)$$

Thus linear-quadratic optimal control can readily be applied to the heat conduction system to obtain the feedback control law using either the lumped or distributed parameter model. However several problems exist with the optimal control technique. MacFarlane (1972) points out that optimal controllers provide gain margins far in excess of those required for stability, are often difficult to tune on-line and may be of low integrity to transducer failures. Additionally there are several other major concerns:

- i. Optimal control design requires an accurate model of the system. This can lead to difficulties in the lumped parameter design due to errors introduced by model reduction. Even in the distributed parameter design, model inaccuracies could be quite large due to heat losses or inefficiencies in the controls.

ii. Optimal control design requires all of the system states to be accessible. Thus for the lumped model, the technique is restricted to the case where the number of measurements equals the order of the model and the measurement matrix is nonsingular. Only then are the states accessible from the measurements:

$$\mathbf{x} = \mathbf{C}^{-1}\mathbf{y} \quad (2.3-15)$$

For the distributed parameter design, the entire temperature profile $y(z,t)$ is needed. Considerable effort has been directed at overcoming this difficulty by using observers or Kalman-Bucy filters to recover the inaccessible states. Much literature has been published on combining such techniques with optimal linear quadratic control.

iii. Optimal control design requires a selection of the weighting matrices \mathbf{S}_F , \mathbf{F} , and \mathbf{E} . Unfortunately, in many chemical engineering applications, the choice of the weighting matrices may be quite difficult. For the heat conduction system, no easy criterion is available for selecting the weights. Consequently, much of the literature dealing with optimal control of diffusion systems considers simple minimization of the time needed to reach the desired state or the deviation of the system from the desired state.

2.3.2 Modal Control

Early work in modal control was dominated by Rosenbrock (1962) and Gould and Murray-Lasso (1966), with many others (Bradshaw and Porter, 1972; Davison, 1970; Ellis and White, 1965abc; Fisher and Denn, 1978; Porter and Bradshaw, 1972) extending the basic theories. Much work has also been published on the application of modal techniques to various systems ranging from linear diffusion problems (Balas, 1979; McGlothin, 1974; Porter and Bradshaw,

1972; Wang, 1972) to large chemical plants (Davison and Chadha, 1972). Although many texts discuss the concepts of modal analysis, Gould (1969) provides a detailed discussion of the use of the method for distributed systems and for lumped systems with an arbitrary number of states, controls, and measurements. This latter situation is of great interest for the heat conduction problem, since the order of the model may be much larger than the number of controls and measurements.

Modal analysis is based on the postulate that the transient behavior of a process is primarily governed by the modes associated with the smallest eigenvalues and that the response of the system can be improved by using a control design to increase these eigenvalues. Additionally, the method suggests that it is possible to approximate a complicated, high-order system by a lower-order system whose slow modes are the same as the original system. This technique was used in the modal lumping of the previous section to obtain the Nth-order lumped model for the heat conduction system. However several references (Douglas, 1972; Gould, 1969; Ray, 1981) point out that disturbances affect the different modes differently; therefore, the reduced model may not be satisfactory if the disturbances have their greatest effect on the neglected faster modes. Additionally, although Rosenbrock's (1962) approach implied the possibility of altering each eigenvalue separately without limit, this is often impractical owing to limitations on the number of controls and measurements and their locations.

The ideal case for lumped modal analysis is when the number of controls and number of measurements equal the order of the model. For the system described in Equation (2.2-23):

$$\dot{\mathbf{x}} = \mathbf{Ax} + \mathbf{Bu}, \quad \mathbf{y} = \mathbf{Cx} \quad (2.3-16)$$

the modal technique calls for the selection of $\mathbf{C} = \mathbf{L}$, where \mathbf{L} is the matrix of left

eigenvectors of matrix \mathbf{A} . The controller is then designed as a simple proportional controller with

$$\mathbf{G}_c = \mathbf{B}^{-1} \mathbf{R} \mathbf{K} \quad (2.3-17)$$

where \mathbf{R} is the matrix of right eigenvectors of \mathbf{A} and \mathbf{K} is a diagonal proportional gain matrix with diagonal elements k_i . With these selections,

$$\dot{\mathbf{x}} = \mathbf{R}(\Lambda - \mathbf{K})\mathbf{L}\mathbf{x}, \quad \dot{\mathbf{y}} = (\Lambda - \mathbf{K})\mathbf{y} \quad (2.3-18)$$

where Λ is a diagonal matrix of the eigenvalues. Thus the outputs have no interaction, and the eigenvalues have been shifted by k_i . Since \mathbf{A} is a diagonal matrix for the heat conduction system, $\Lambda = \mathbf{A}$ and the matrices \mathbf{R} and \mathbf{L} can be simply taken as identity matrices. Thus the technique calls for the selection of the measurement matrix as an identity matrix. Therefore, an appropriate combination of the temperatures should be used so that the system states are actually measured.¹

However in most practical systems, the number of states will exceed the number of controls. Consider the heat conduction process with two controls and N states and measurements. Gould (1969) shows that, if \mathbf{B} and \mathbf{C} can be chosen arbitrarily, the two lowest eigenvalues can be made as large and negative as desired while leaving the others and all the eigenvectors unchanged. As shown above, the restrictions on \mathbf{C} can be accommodated by measuring a combination of the temperatures. However for the heat conduction system, \mathbf{B} is fixed due to the *a priori* selection of the controls. By slight modification of the analysis, modal control is still applicable. Consider adding both a compensator \mathbf{G}_c to adjust for the fixed \mathbf{B} and a diagonal proportional control matrix \mathbf{K} :

1. Thus the compensator \mathbf{C}^{-1} should be included after the process and set points or after the difference junction.

$$\mathbf{u} = -\mathbf{G}_c \mathbf{K} \mathbf{y} \quad \text{with set point } \mathbf{y}_d = 0. \quad (2.3-19)$$

Note that previously when \mathbf{B} had dimension N ,² \mathbf{G}_c was selected as $\mathbf{G}_c = \mathbf{B}^{-1} \mathbf{R}$. However in this case, \mathbf{B} can not be inverted. Thus

$$\dot{\mathbf{x}} = (\mathbf{A} - \mathbf{B}\mathbf{G}_c \mathbf{K})\mathbf{x} \quad (2.3-20)$$

with $\mathbf{A} = \mathbf{A}$ and \mathbf{C} selected as $\mathbf{C} = \mathbf{L}$.³ Then the choice of

$$\mathbf{G}_c = \begin{bmatrix} -\frac{1}{2} & -\frac{1}{2\sqrt{2}} & 0 & \dots & 0 \\ -\frac{1}{2} & -\frac{1}{2\sqrt{2}} & 0 & \dots & 0 \end{bmatrix} \quad (2.3-21)$$

leads to

$$\mathbf{B}\mathbf{G}_c \mathbf{K} = \begin{bmatrix} -k_1 & 0 & 0 & \dots & \\ 0 & -k_2 & 0 & \dots & \\ -\sqrt{2}k_1 & 0 & 0 & \dots & \\ 0 & -\sqrt{2}k_2 & 0 & \dots & \\ -\sqrt{2}k_1 & 0 & 0 & \dots & \\ \vdots & \vdots & \ddots & & \\ \vdots & \vdots & \ddots & & \\ \vdots & \vdots & \ddots & & \end{bmatrix} \quad (2.3-22)$$

Thus the first two eigenvalues can be altered by arbitrary selection of k_1 and k_2 without affecting the higher $N-2$ eigenvalues; however, the first two eigenvectors have also been altered slightly. Thus a disturbance in either of the first two modes will cause a disturbance in the higher modes. Since they decay rapidly, little difficulty should result. The appropriate block diagram is shown in Figure 2.3-1.

Gould (1969) also presents a detailed discussion of the situation where the number of measurements is less than the dimension of the process. This would

2. \mathbf{B} was invertible.

3. Note that \mathbf{L} is taken as the identity matrix.

obviously lead to difficulties in the modal analysis since the system state cannot be obtained from the measurements. An appropriate control scheme can be designed but will lead to considerable interaction between the control loops. Because of the complexity of the resulting control scheme and the ease of obtaining temperature measurements for a heat conduction process, it is recommended that sufficient measurements be taken so that the state vector can be constructed. Balas (1979) discusses the introduction of a Luenberger observer for this purpose.

Additionally, modal control can be applied directly to the distributed parameter system. Gould and Murray-Lasso (1966) and Gould (1969) present a detailed discussion of modal control for linear, distributed systems. However, using these techniques and considering the limitations imposed by taking only a finite number of discrete measurements and by manipulating only two controls, the analysis becomes equivalent to using modal lumping and applying lumped modal analysis.

Although modal analysis leads to exact placing of the poles, the procedure leads to a simple proportional controller and can not give any guidance as to the selection of additional control action. More importantly, the technique uses no information concerning the zeros of the transfer functions. Problems can easily arise if the zeros of the closed-loop transmittances move into the right-half plane. Furthermore, the method gives the best results only if all the states of the system are accessible. Although this does not cause any difficulty for the heat conduction process, it is not practical for most systems.

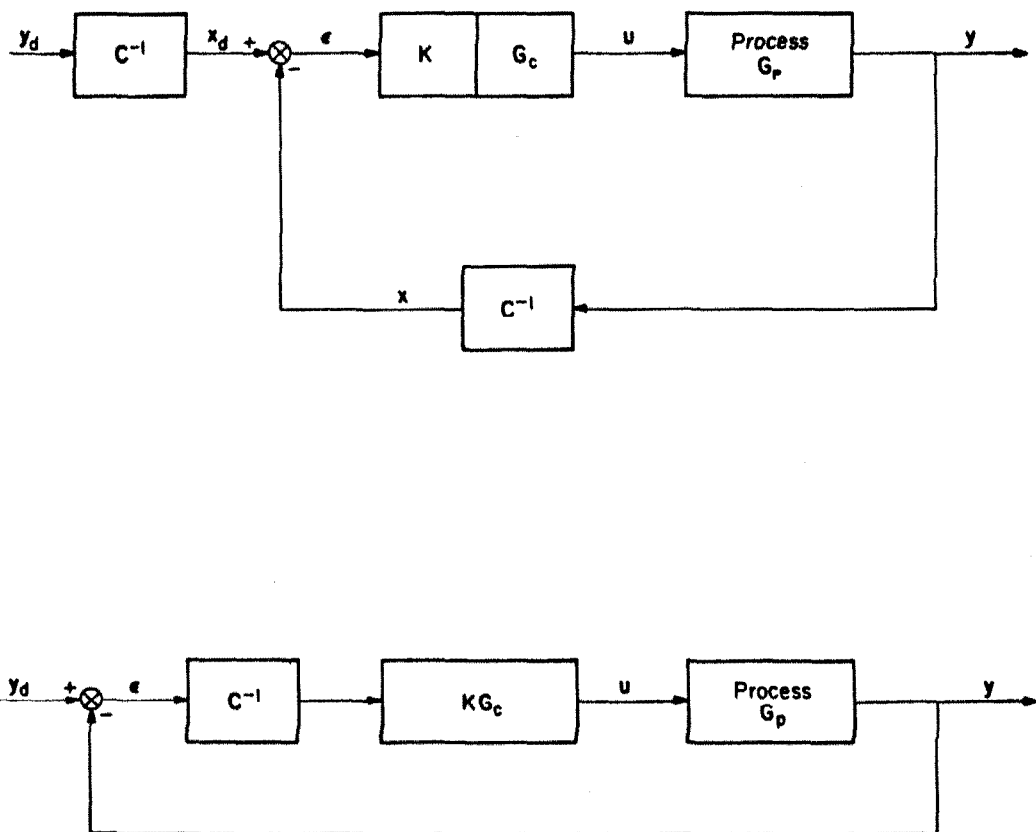


Figure 2.3-1
Lumped Modal Feedback Control Design

2.4 NON-INTERACTING CONTROL

A major difficulty in multivariable, feedback control design arises from the steady state and dynamic interactions which occur between the various input and output variables. In most systems, it is desired that one specific output $y_i(s)$ responds to input $u_i(s)$, while all other outputs remain unchanged. The term interaction can then be used to refer to the effects that a particular input $u_i(s)$ has on the output $y_j(s)$, $j \neq i$. Thus low interaction is usually desirable. In fact if it is possible to eliminate all the coupling between variables, and if the number of controllable inputs and outputs is equal, the multivariable system can be treated as a combination of single-loop systems, and classical techniques can be used to tune each loop. Unfortunately, most multivariable systems have considerable interaction; thus, several techniques have been devised to eliminate or at least reduce the interaction to an acceptable level.

For the heat conduction process, analysis of the system transfer function $G_p = C(sI - A)^{-1}B$ shows that interaction is high and cannot be eliminated by simple selection of the measurement locations. Thus compensators that reduce or eliminate interaction may be useful. Several design techniques including perfect non-interacting compensation, steady state decoupling, and set point compensation are available for this purpose. The application of these methods to the heat conduction problem is discussed. Additionally, a new technique is presented that eliminates interaction by using extra measurements within an inner loop, leading to a relatively simple control strategy.

2.4.1 Perfect Dynamic Compensation

Consider the third-order model for the heat conduction system with two controls and measurements. The Laplace-domain representation of the system

is

$$\mathbf{y} = \mathbf{G}_p \mathbf{u} \quad \mathbf{G}_p = \mathbf{C}(\mathbf{sI} - \mathbf{A})^{-1} \mathbf{B} \quad (2.4-1)$$

with

$$\mathbf{A} = \begin{bmatrix} 0 & & \\ & -\pi^2 & \\ & & -4\pi^2 \end{bmatrix} \quad (2.4-2)$$

$$\mathbf{B} = \begin{bmatrix} 1 & 1 \\ \sqrt{2} & -\sqrt{2} \\ \sqrt{2} & \sqrt{2} \end{bmatrix} \quad (2.4-3)$$

$$\mathbf{C} = \begin{bmatrix} 1 & c_{12} & c_{13} \\ 1 & c_{22} & c_{23} \end{bmatrix} = \begin{bmatrix} 1 & \sqrt{2}\cos\pi z_1 & \sqrt{2}\cos 2\pi z_1 \\ 1 & \sqrt{2}\cos\pi z_2 & \sqrt{2}\cos 2\pi z_2 \end{bmatrix} \quad (2.4-4)$$

The process transfer function \mathbf{G}_p is

$$\mathbf{G}_p = \begin{bmatrix} \frac{1}{s} + \frac{\sqrt{2}c_{12}}{s + \pi^2} + \frac{\sqrt{2}c_{13}}{s + 4\pi^2} & \frac{1}{s} - \frac{\sqrt{2}c_{12}}{s + \pi^2} + \frac{\sqrt{2}c_{13}}{s + 4\pi^2} \\ \frac{1}{s} + \frac{\sqrt{2}c_{22}}{s + \pi^2} + \frac{\sqrt{2}c_{23}}{s + 4\pi^2} & \frac{1}{s} - \frac{\sqrt{2}c_{22}}{s + \pi^2} + \frac{\sqrt{2}c_{23}}{s + 4\pi^2} \end{bmatrix} \quad (2.4-5)$$

As mentioned earlier, the off-diagonal terms are significant and cannot be eliminated with the selection of the measurement locations z_1 and z_2 .

Consider the feedback control system (Figure 2.4-1) consisting of single-loop controllers, represented by a diagonal transfer function matrix \mathbf{G}_c , and a non-interaction compensator \mathbf{G}_l proceeding the process. The closed-loop response for this scheme is

$$\mathbf{y} = (\mathbf{I} + \mathbf{G}_p \mathbf{G}_l \mathbf{G}_c)^{-1} \mathbf{G}_p \mathbf{G}_l \mathbf{G}_c \mathbf{y}_d = \mathbf{G}_{cl} \mathbf{y}_d. \quad (2.4-6)$$

The compensator \mathbf{G}_l should be designed to eliminate as much interaction as possible. Ideally \mathbf{G}_l should be selected to make \mathbf{G}_{cl} diagonal and to drive $\mathbf{G}_{cl} \rightarrow \mathbf{I}$ for $s=0(t \rightarrow \infty)$. Note that such analysis is only applicable to systems with square transfer function matrices. If there are more controls than outputs, then a subset of controls may be chosen for decoupling, while if there are more outputs

than controls, only partial decoupling is possible (Ray, 1981).

If \mathbf{G}_c is diagonal, a sufficient criterion for \mathbf{G}_{cl} to be diagonal and $\mathbf{G}_{cl}(0) \rightarrow \mathbf{I}$ as the controller gains increase is to select

$$\mathbf{G}_I = \mathbf{G}_p^{-1} \text{diag } \mathbf{G}_p(s) \quad , \quad (2.4-7)$$

where $\text{diag } \mathbf{G}_p(s)$ is a diagonal matrix of the diagonal elements of $\mathbf{G}_p(s)$. If this decoupling is performed perfectly, the closed-loop response will obey

$$y_i(s) = \frac{g_{c_{ii}}(s)g_{p_{ii}}(s)}{1+g_{c_{ii}}(s)g_{p_{ii}}(s)} y_{d_i}(s) + \frac{1}{1+g_{c_{ii}}(s)g_{p_{ii}}(s)} \sum_{j=1}^k g_{d_{ij}}(s)d_j(s) \quad , \quad (2.4-8)$$

where $d_j(s)$ are the disturbances and $g_{d_{ij}}(s)$, $g_{c_{ii}}(s)$, and $g_{p_{ii}}(s)$ are the elements of the disturbance, controller, and process transfer function matrices, respectively. This selection of \mathbf{G}_I leads to a total decoupling for set point changes and, even though each disturbance can influence all the outputs, its effect on output y_i is damped by a single controller $g_{c_{ii}}(s)$ (Ray, 1981).

Although this method is simple and seemingly eliminates all the complications inherent in multivariable, feedback control design, it has several major disadvantages. Perfect compensation requires a perfect transfer function model. Though the model is well-known for the heat conduction process, approximations such as finite lumping can lead to badly behaving or even unstable control schemes. Furthermore, MacFarlane (1972) and Ray (1981) point out that another potential disadvantage is that a great deal of control flexibility is used up in making $\mathbf{G}_p\mathbf{G}_I\mathbf{G}_c$ diagonal, often by sacrificing closed-loop dynamic performance. In many cases some interaction may actually improve dynamic performance. Finally, the technique possibly leads to an unnecessarily complicated compensator and fails if the determinant of \mathbf{G}_p has right-half plane zeros or if the transfer functions are not square. Thus other techniques may lead to a simpler control scheme which is easier to tune on-line and less

sensitive to model inaccuracies.

2.4.2 Steady State Decoupling

Although perfect compensation may be impossible or merely impractical, steady state decoupling is usually quite useful and can be implemented before applying other design techniques such as inverse Nyquist array or the characteristic locus method. Steady state decoupling uses a compensator

$$G_I = \lim_{s \rightarrow 0} [G_p^{-1}(s) \text{ diag } G_p(s)] \quad (2.4-9)$$

to eliminate steady state interaction. However, it cannot improve dynamic behavior. Unfortunately, due to the perfect symmetry of the heat conduction system, even this method leads to difficulty. For the third-order heat conduction system, the appropriate compensator is singular:

$$G_I = \begin{bmatrix} \frac{\pi^2}{2\sqrt{2}(c_{12}-c_{22})} & \frac{-\pi^2}{2\sqrt{2}(c_{12}-c_{22})} \\ \frac{-\pi^2}{2\sqrt{2}(c_{12}-c_{22})} & \frac{\pi^2}{2\sqrt{2}(c_{12}-c_{22})} \end{bmatrix} \quad (2.4-10)$$

Introduction of this compensator into the control loop leads to dependent control action and is therefore not advisable, since it will lead to excessive dynamic interaction and poor closed-loop performance.

2.4.3 Set Point Compensation

Steady state interaction arises because a change in the set point of one controlled variable affects all the system outputs. A means of eliminating steady state interaction could be to simultaneously alter all the other set points in such a way as to cancel the effect of the original change. This idea is the basis for set point compensation, which is used to eliminate or minimize steady state

offset due to set point adjustments.

Consider the control scheme of Figure 2.4-2, where \mathbf{y}_d is the actual set point desired, \mathbf{G}_c is a diagonal controller matrix, and \mathbf{G}_s is the set point compensation matrix. The overall closed-loop transfer function is

$$\mathbf{G}_{cl} = (\mathbf{I} + \mathbf{G}_p \mathbf{G}_c)^{-1} \mathbf{G}_p \mathbf{G}_c \mathbf{G}_s. \quad (2.4-11)$$

The objective is to select \mathbf{G}_s so that \mathbf{G}_{cl} is diagonal at steady state. Using the theory of Laplace transforms,

$$\mathbf{G}_s = \lim_{s \rightarrow 0} [(\mathbf{I} + \mathbf{G}_p \mathbf{G}_c)^{-1} \mathbf{G}_p \mathbf{G}_c]^{-1} = (\mathbf{G}_{ss} \mathbf{G}_c)^{-1} + \mathbf{I} \quad (2.4-12)$$

where

$$\mathbf{G}_{ss} = \lim_{s \rightarrow 0} \mathbf{G}_p \quad (2.4-13)$$

For the heat conduction system,

$$\mathbf{G}_s = \begin{bmatrix} 1 + \frac{\pi^2}{2\sqrt{2}(c_{12}-c_{22})g_{c_{11}}} & -\frac{\pi^2}{2\sqrt{2}(c_{12}-c_{22})g_{c_{11}}} \\ -\frac{\pi^2}{2\sqrt{2}(c_{12}-c_{22})g_{c_{22}}} & 1 + \frac{\pi^2}{2\sqrt{2}(c_{12}-c_{22})g_{c_{22}}} \end{bmatrix} \quad (2.4-14)$$

Note that $c_{12} \neq c_{22}$ if $z_1 \neq z_2$. Although this compensator is realizable and does not lead to dependent control, it cannot improve the response to a disturbance in the system since it does not appear in the feedback loop.

2.4.4 Inner-Loop Decoupling

Several recent studies (Foss et al., 1980; Kouvaritakis et al., 1979) discuss squaring down extra measurements in an inner loop to obtain a system that shows better control properties from the viewpoint of the outer loop. Usually the inner loop is used to adjust the poles of the system, and then other frequency response techniques are used to design the outer-loop control for the

improved process. However, the method presented here uses the additional degrees of freedom inherent in adding an inner loop to eliminate or minimize the interaction, with only simple proportional gain compensators and without severely limiting the design freedom available for the outer loop.

Consider the process shown in Figure 2.4-3, with an outer loop consisting of two outputs and two controls. This is identical to the system used by the previous methods. Using the third-order model for the process, a third independent measurement can be made. The three measurements are denoted by \mathbf{y}_M . The following relationships describe the control scheme.

$$\mathbf{y} = \bar{\mathbf{L}}\bar{\mathbf{C}}\mathbf{x} = \mathbf{C}\mathbf{x}, \quad \mathbf{y}_F = \bar{\mathbf{F}}\bar{\mathbf{C}}\mathbf{x} = \mathbf{F}\mathbf{x} \quad (2.4-15a)$$

$$\bar{\mathbf{L}} = \begin{bmatrix} 1 & 0 & 0 \\ 0 & 1 & 0 \end{bmatrix}, \quad \bar{\mathbf{C}} = \begin{bmatrix} 1 & \varphi_1(z_1) & \varphi_2(z_1) \\ 1 & \varphi_1(z_2) & \varphi_2(z_2) \\ 1 & \varphi_1(z_3) & \varphi_2(z_3) \end{bmatrix} \quad (2.4-15b)$$

Let $\bar{\mathbf{G}}_p$ be the transfer function from \mathbf{w} to \mathbf{y} , or essentially the transfer function of the process seen by the outer loop. The objective of the technique is to select the elements of \mathbf{F} to reduce or eliminate interactions, i.e., select \mathbf{F} so that $\bar{\mathbf{G}}_p$ has small off-diagonal elements.

The overall closed-loop transfer function for the inner loop is

$$\bar{\mathbf{G}}_p = \mathbf{C}(\mathbf{sI} - \bar{\mathbf{A}})^{-1}\mathbf{B}[\mathbf{I} + \mathbf{F}(\mathbf{sI} - \bar{\mathbf{A}})^{-1}\mathbf{B}]^{-1} \quad (2.4-16)$$

If \mathbf{F} is taken as

$$\mathbf{F} = \begin{bmatrix} f_{11} & f_{12} & f_{13} \\ f_{21} & f_{22} & f_{23} \end{bmatrix}, \quad (2.4-17)$$

then

$$\bar{\mathbf{G}}_p = \begin{bmatrix} g_1(z_1, z_2, f_{21}, f_{22}, f_{23}) & g_2(z_1, z_2, f_{11}, f_{12}, f_{13}) \\ g_3(z_1, z_2, f_{21}, f_{22}, f_{23}) & g_4(z_1, z_2, f_{11}, f_{12}, f_{13}) \end{bmatrix} \quad (2.4-18)$$

To eliminate interaction, there are eight degrees of freedom available—the

locations of the two major measurements and the six elements of the squaring down compensator \mathbf{F} . The location of the final measurement can be left to the discretion of the designer since it will only affect the components of $\bar{\mathbf{F}}$ once \mathbf{F} is specified. Obviously, z_3 must be selected different from z_1 and z_2 so that $\bar{\mathbf{C}}$ is nonsingular. For the third-order model of the heat conduction system, the measurement locations and the elements of \mathbf{F} should be selected so that the (1,2) and (2,1) terms of $\bar{\mathbf{G}}_p$ are identically zero. Since the model is third order, it takes three degrees of freedom to make each term identically zero. Thus of the eight available degrees of freedom, six are used to eliminate interaction, and the remaining two can be used to improve the performance (move the poles) of each non-interacting loop. Further analysis shows that

To eliminate term (1,2):

$$\begin{aligned} c_{13} &= c_{12} - \frac{1}{\sqrt{2}} \\ f_{12} &= c_{12}f_{11} - \frac{\pi^2}{2\sqrt{2}} \\ f_{13} &= c_{12}f_{11} - \sqrt{2}\pi^2 + \frac{\sqrt{2}\pi^2 - c_{12}f_{11}}{\sqrt{2}c_{12}} \end{aligned}$$

To eliminate term (2,1):

$$\begin{aligned} c_{23} &= -c_{22} - \frac{1}{\sqrt{2}} \\ f_{22} &= c_{22}f_{21} + \frac{\pi^2}{2\sqrt{2}} \\ f_{23} &= -c_{22}f_{21} - \sqrt{2}\pi^2 - \frac{\sqrt{2}\pi^2 + c_{22}f_{21}}{\sqrt{2}c_{22}} \end{aligned}$$

The additional relations:

$$\begin{aligned} c_{12} &= \sqrt{2}\cos\pi z_1 & c_{13} &= \sqrt{2}\cos 2\pi z_1 \\ c_{22} &= \sqrt{2}\cos\pi z_2 & c_{23} &= \sqrt{2}\cos 2\pi z_2 \end{aligned} \tag{2.4-19}$$

lead to the requirements that $z_1 = 0.2$ or 0.6 and $z_2 = 0.4$ or 0.8 . Note that the elements of \mathbf{F} are all simply constants. Thus the following situations are allowable for decoupling of the loops

z_1	z_2	
0.2	0.4	Case I: $c_{12} = -c_{23}$, $c_{13} = c_{22}$
0.6	0.8	
0.6	0.4	Case II: $c_{12} = -c_{22}$, $c_{13} = c_{23}$
0.2	0.8	

(2.4-20)

These rules lead to considerable simplification in the transfer functions:

$$\text{Case I: } \bar{\mathbf{G}}_p = \begin{bmatrix} \frac{2\sqrt{2}c_{12}}{s+2\sqrt{2}c_{12}f_{11}} & 0 \\ 0 & \frac{2\sqrt{2}c_{12}}{s+2\sqrt{2}c_{12}f_{21}} \end{bmatrix} \quad (2.4-21)$$

$$\text{Case II: } \bar{\mathbf{G}}_p = \begin{bmatrix} \frac{2\sqrt{2}c_{12}}{s+2\sqrt{2}c_{12}f_{11}} & 0 \\ 0 & \frac{2\sqrt{2}c_{12}}{s+2\sqrt{2}f_{21}(2-2\sqrt{2}c_{12})} \end{bmatrix} \quad (2.4-22)$$

Thus, not only has interaction been eliminated by using simple gain in an inner loop, the new process is quite simple, and two degrees of freedom, along with the location of z_3 , remain at the disposal of the designer. The selection of f_{11} and f_{21} can easily be used to move the poles of each decoupled loop.

The final design then involves a squaring down compensator $\bar{\mathbf{F}}$ which together with the measurement matrix $\bar{\mathbf{C}}$ leads to the desired \mathbf{F} :

$$\mathbf{F} = \begin{bmatrix} f_{11} & c_{12}f_{11} - \frac{\pi^2}{2\sqrt{2}} & c_{12}f_{11} - \sqrt{2}\pi^2 + \frac{\sqrt{2}\pi^2 - c_{12}f_{11}}{\sqrt{2}c_{12}} \\ f_{21} & c_{22}f_{21} + \frac{\pi^2}{2\sqrt{2}} & -c_{22}f_{21} - \sqrt{2}\pi^2 - \frac{\sqrt{2}\pi^2 + c_{22}f_{21}}{\sqrt{2}c_{22}} \end{bmatrix} \quad (2.4-23)$$

The fact that $\bar{\mathbf{F}}$ is a constant matrix is of great importance. If more degrees of freedom are desired than the two available with this technique, \mathbf{F} can be designed as a function of s . For instance, term (1,2) could also be eliminated by letting

$$f_{19} = \frac{1}{4c_{12}s} [(1 - \sqrt{2}c_{12} + \sqrt{2}c_{13})s^2 + (2\sqrt{2}f_{12} - 2\sqrt{2}c_{12}f_{11} + 4c_{13}f_{12} + 5\pi^2 - 4\pi^2\sqrt{2}c_{12} + \pi^2\sqrt{2}c_{13})s + 4\pi^2 + 8\pi^2\sqrt{2}f_{12} - 8\pi^2\sqrt{2}c_{12}f_{11}] \quad (2.4-24)$$

with no restriction on f_{12} or z_1 . However, this leads to an unnecessarily complicated feedback compensator for the third-order heat conduction system.

Inner-loop decoupling is an improvement over the perfect, non-interacting control scheme for the heat conduction system. Although all of the techniques can be easily applied, the inner-loop decoupling strategy may lead to a very simple control structure for processes where extra measurements can readily be obtained while leaving considerable design freedom available for tuning the dynamic behavior of the overall system. The only restriction on the extra measurements is that all outputs must be linearly independent. Additionally, the method still suffers from the apparent necessity of an accurate process model. However, as we will show in Section 2.7, although the design is conducted on the approximate, third-order model for the heat conduction process, interaction is still nearly eliminated for the actual system. In fact, simulations also show low sensitivity to the measurement locations. Thus the inner-loop scheme may be superior to conventional non-interacting control methods.

Further analysis shows that an inner loop with constant feedback gains cannot be designed to decouple the heat conduction system in the absence of

extra measurements. However for such a case, a feedback compensator that is a function of s can decouple the system but is of the same complicated complicated form as that designed by the perfect, non-interacting control scheme. Thus without extra measurements, inner-loop decoupling has no advantage over conventional techniques.

Inner-loop decoupling still suffers from some of the inherent problems associated with the field of non-interacting control. A non-interacting system may not be desirable for chemical processes, since the major objective in such processes is often the reduction of the effects of disturbances on the system. Although non-interacting analyses can lead to simplifications that allow completion of the design using single-loop approaches, there is no intrinsic reason for non-interaction to improve control. Actually, exploitation of the interaction among the variables may be useful. Furthermore, the determinant of the process transfer function matrix for multivariable chemical processes often has right half plane zeros, which lead to poor or unstable control performance with the non-interacting techniques.

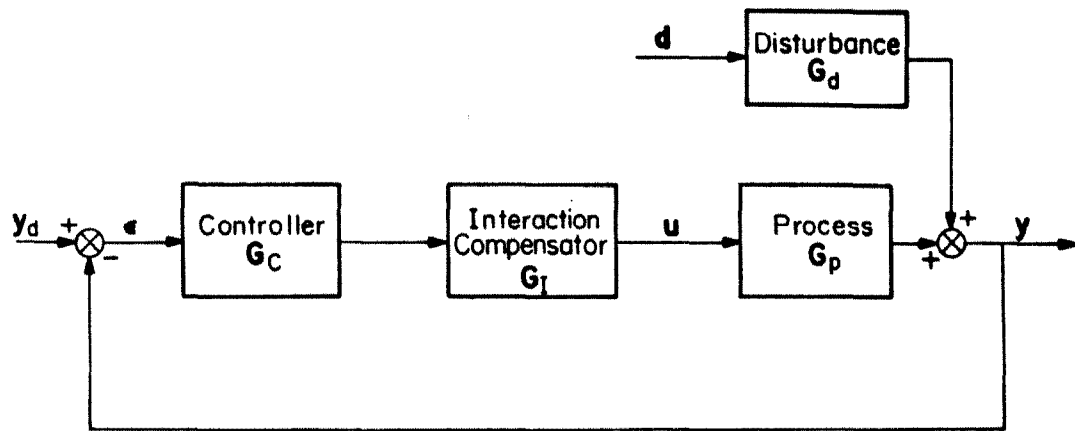


Figure 2.4-1
Perfect Non-Interacting Control Strategy

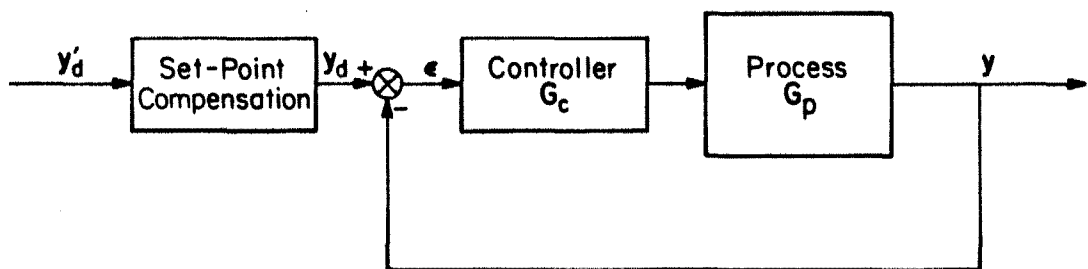


Figure 2.4-2
Set Point Compensation

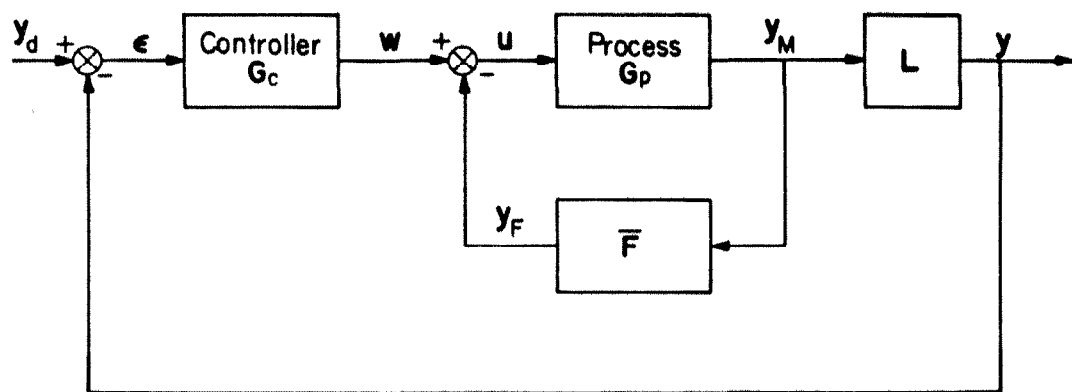


Figure 2.4-3
Inner-Loop Decoupling

2.5 INVERSE NYQUIST ARRAY

Since classical frequency methods have proven extremely useful for designing single-loop control systems, much work has been devoted to extending these techniques to multivariable systems. The Nyquist diagram, which is a polar plot of the information presented in a Bode diagram, is an excellent classical method for determining system stability criteria for single-loop processes, since both the magnitude and phase information appear in a single curve. Using the Nyquist representation, it is fairly simple to determine the process stability characteristics and the closed-loop dynamics from the graph for the open-loop process.

The inverse Nyquist array (I.N.A.) technique, introduced by Rosenbrock (1969), is a useful extension of scalar Nyquist array methods to the design of multivariable control systems. It allows for considerable flexibility, is insensitive to model inaccuracies, and reduces to traditional methods in the single-loop case. Also, the technique is able to handle models specified only in terms of a limited amount of directly obtained experimental data (MacFarlane, 1972) and can be easily incorporated into a computer-aided design package.

Assuming that the open-loop transfer function $\mathbf{Q}(s) = \mathbf{G}_p(s)\mathbf{G}_c(s)$ is nonsingular, which is necessary for output controllability, the inverse of the closed-loop transfer function is

$$\mathbf{R}^{-1} = \hat{\mathbf{R}} = \mathbf{I} + \hat{\mathbf{Q}} \quad (2.5-1)$$

The notation $\hat{\mathbf{Q}} = \mathbf{Q}^{-1}$ has been used for convenience, since in general $q_{ij}^{-1}(s) \neq \hat{q}_{ij}(s)$, where q_{ij} and \hat{q}_{ij} denote the elements of matrices \mathbf{Q} and $\hat{\mathbf{Q}}$, respectively. Thus the elements of $\hat{\mathbf{R}}$ can easily be found from the elements of

$$\left. \begin{array}{l} f_{ii}(s) = \hat{q}_{ii}(s) + 1.0 \\ f_{ij}(s) = \hat{q}_{ij}(s) \end{array} \right\} \quad i, j = 1, 2, \dots, m. \quad (2.5-2)$$

where m is the number of controls and outputs. Furthermore if the k th feedback loop is opened, $\hat{r}_{kk}(s) = \hat{q}_{kk}(s)$. Then the I.N.A. is the set of m^2 diagrams representing the loci in the complex plane corresponding to the elements of $\hat{Q}(j\omega)$. In terms of frequency-response plots, the I.N.A. allows easy determination of the elements of $\hat{R}(j\omega)$, whether the feedback loops are open or closed.

The basis of the I.N.A. design technique is Rosenbrock's stability theorem (Rosenbrock, 1969):

Let D be a contour in the complex plane consisting of the imaginary axis from $-j\alpha$ to $+j\alpha$ and a semicircle of radius α in the right-half plane, where α is sufficiently large to insure that all finite poles and zeros of $|Q|$, $|R|$, q_{ij} , \hat{q}_{ij} , r_{ij} , and \hat{r}_{ij} lying in the open right-half plane are within D and those on the imaginary axis lie on D . Then a feedback system will be closed-loop stable if the system is open-loop stable and if $G_c(s)$ is designed such that

- i) the inverse Nyquist mapping, Γ_i , of each diagonal element $\hat{q}_{ii}(j\omega)$ of the I.N.A. for $Q(j\omega)$ encircles the point $(-1.0, 0.0)$ the same number of times in the same direction as it encircles the origin.
- ii) for $i = 1, 2, \dots, m$ and for all s on D

$$|\hat{q}_{ii}(s)| > \sum_{j=1, j \neq i}^m |\hat{q}_{ij}(s)| \quad (2.5-3)$$

- iii) for each loop j which is closed and for all s on D

$$|f_{ii}(s)| > \sum_{j=1, j \neq i}^m |f_{ij}(s)| \quad (2.5-4)$$

The conditions (ii) and (iii) lead to diagonal dominance and thus insure that

interactions are sufficiently small to allow stability (condition (i)) to be deduced from the diagonal elements of \hat{Q}_{ii} alone.

For the lumped model of the two-control, heat conduction process, the criteria for diagonal dominance are that

$$\begin{aligned} |\hat{q}_{11}| &> |\hat{q}_{12}| & |\hat{q}_{11} + 1| &> |\hat{q}_{12}| \\ |\hat{q}_{22}| &> |\hat{q}_{21}| & |\hat{q}_{22} + 1| &> |\hat{q}_{21}| \end{aligned} \quad (2.5-5)$$

for all s on D . These conditions can be represented graphically (MacFarlane, 1972) as in Figure 2.5-1. Thus diagonal dominance is insured if the origin and the point $(-1.0, 0.0)$ are not within or on any of the circles. Closed-loop stability can then be checked from the two diagonal entries of $\hat{Q}(j\omega)$. The system is stable if Γ_1 and Γ_2 satisfy the encirclement criteria.

The I.N.A. design method involves adding controllers to make the system's open-loop transfer functions diagonally dominant. The remainder of the design is completed on the basis of a set of individual single loops using conventional single-loop inverse Nyquist techniques. The I.N.A. method thus leads to a stable system which has high integrity and low interaction, when diagonal dominance is imposed.

The third-order model of the heat conduction process was analyzed using the I.N.A. procedure with various measurement locations (Table 2.5-1). Both the symmetric (Group I) and the unsymmetric (Group II) cases were considered with $z_1 < 0.50$. For the situation where $z_1 > 0.50$, a permutation matrix should be used to interchange the inputs and outputs.

Due to the symmetry of the system for Group I, only the $\hat{q}_{11}(s)$ and $\hat{q}_{12}(s)$ elements of the I.N.A. are needed since $\hat{q}_{22}(s)$ and $\hat{q}_{21}(s)$ are identical. Additionally to aid in the design procedure, logarithmic plots of $|\hat{q}_{11}|$, $|1 + \hat{q}_{11}|$, and $|\hat{q}_{12}|$ versus the frequency were also used. These are easier to use to check for

Group I		Group II	
z_1	z_2	z_1	z_2
0.10	0.90	0.40	0.70
0.20	0.80	0.30	0.80
0.25	0.75	0.40	0.80
0.30	0.70		
0.33	0.67		
0.40	0.60		

Table 2.5-1
Measurement Locations

diagonal dominance than the type shown in Figure 2.5-1. Although all of the cases in Group I were analyzed, only two need to be considered in detail since the others are similar. Figures 2.5-2 and 2.5-3 show the I.N.A. plots for measurement locations (0.3,0.7) and (0.4,0.6). These cases were considered since the root-locus analysis showed that the (0.3,0.7) case is stable while the (0.4,0.6) case becomes unstable for gains above about 33.0. The I.N.A. analysis for the cases in Group I verify the root-locus results that stability is insured at high gains for the symmetric case if $z_1 < 0.33$. Note that the I.N.A. plots are only drawn for $s = \omega j$ with $\omega = 0 \rightarrow \infty$, since $s = -\omega j$ simply gives the reflection.

For the cases with $z_1 < 0.33$ ($z_1 = 0.3$ in particular), the conditions for diagonal dominance are satisfied for all s on D except at $s = 0$. At this point, $\hat{q}_{11} = \hat{q}_{12} = \hat{q}_{21} = \hat{q}_{22}$. Further analysis shows that the problem that arises at $s = 0$ is due to the pole which is at the origin in our process model. With these problems at $s = 0$ eliminated, the cases for $z_1 < 0.33$ would be diagonally dominant, and the system would be stable since the encirclement criterion is satisfied.

One method of analysis is suggested by MacFarlane and Postlethwaite (1977). They show that when a pole occurs on the imaginary axis, the modified

Nyquist contour, D' , shown in Figure 2.5-4 should be used. Then the conditions for diagonal dominance must be examined in the regions:

$$\left. \begin{array}{ll} a) s = \omega j & \omega = -\infty \rightarrow -\varepsilon \\ b) s = \varepsilon e^{j\theta} & \theta = -\frac{\pi}{2} \rightarrow \frac{\pi}{2} \\ c) s = Re^{j\theta} & \theta = \frac{\pi}{2} \rightarrow -\frac{\pi}{2} \end{array} \right\} \text{ where } R \rightarrow \infty \text{ and } \varepsilon \rightarrow 0.$$

Mathematical calculations for these regions indicate that the conditions for diagonal dominance are satisfied for $z_1 < 0.33$ with $z_2 = 1.0 - z_1$. Then since the encirclement criterion is also satisfied, stability is assured. The I.N.A. technique then concludes that elimination of interaction is unnecessary since arbitrary high gains can be applied to each of the two principal loops without instability and will lead to a system with little interaction.

Figure 2.5-3 shows that the (0.4,0.6) case does not satisfy conditions (ii) and (iii) of Rosenbrock's theorem (1962), since $|\hat{q}_{12}|$ is larger than $|\hat{q}_{11}|$ and $|\hat{q}_{11} + 1|$ for some values of ω . Although condition (i) seems to show closed-loop instability for this process, no conclusion can be drawn since the stability criterion is a sufficient condition and only becomes necessary if (ii) and (iii) are satisfied.

The problem then is to design a compensator, $G_c(s)$, so that the system's open-loop transfer function $Q(s)$ is diagonally dominant when $0.33 < z_1 < 0.50$. Using a general 2×2 compensator, the restrictions on the elements of $G_c(s)$ can be derived. Specifically consider the case (0.4,0.6). Using the modified Nyquist contour, it can be shown that $s = 0$ presents no difficulty. Figure 2.5-3 then shows that conditions (ii) and (iii) are satisfied at low ω but fail at high ω . Using the restrictions on the elements of $G_c(s)$, it can be shown that, owing to the symmetry of the system, it is not possible to design a nonsingular constant matrix $G_c(s)$ to make the system diagonally dominant for all s on the modified Nyquist

contour. However, the analysis also shows that a compensator with the following properties will lead to diagonal dominance:

$$\text{As } \omega \rightarrow 0 \quad G_c(s) \rightarrow \begin{bmatrix} 1 & 0 \\ 0 & 1 \end{bmatrix}, \quad (2.5-6)$$

$$\text{As } \omega \rightarrow \infty \quad G_c(s) \rightarrow \begin{bmatrix} 0 & 1 \\ 1 & 0 \end{bmatrix}.$$

After many controllers were tried, the best results were obtained with

$$G_c(s) = \begin{bmatrix} \frac{5.0}{s+5.0} & \frac{s}{s+5.0} \\ \frac{s}{s+5.0} & \frac{5.0}{s+5.0} \end{bmatrix}. \quad (2.5-7)$$

Figure 2.5-5 shows the I.N.A. plots with this compensator. The controller has indeed made the system diagonally dominant for all s on D' ; however, the encirclement criterion shows that the system becomes unstable for moderate gains. This was verified using root-locus and characteristic locus analyses for the system with this compensator. Attempts at eliminating the instability were futile, and further analysis showed that the stability problems arise from an unstable finite zero. Unfortunately, it can be shown that dependent control action is necessary to move this zero to the left-half plane. I.N.A. analysis using the dependent controllers¹

$$G_c(s) = \begin{bmatrix} 1 & -1 \\ -1 & 1 \end{bmatrix} \text{ or } \begin{bmatrix} \frac{1}{s} & -\frac{1}{s} \\ -\frac{1}{s} & \frac{1}{s} \end{bmatrix} \text{ or } \begin{bmatrix} \frac{1+s}{s} & \frac{-1-s}{s} \\ \frac{-1-s}{s} & \frac{1+s}{s} \end{bmatrix} \quad (2.5-8)$$

verifies system stability. However dependent control leads to very bad closed-loop response and is thus not desirable. Therefore the best that can be obtained is a simple control scheme designed to ensure a diagonally dominant system for which single-loop theory can be applied to two loops that remain

1. Dependent control results from a singular compensator matrix.

stable only for moderate gains.

Table 2.5-2 summarizes the results for assuring diagonal dominance with symmetric measurement placement. Since the conditions for stability and diagonal dominance are satisfied for $z_1 < 0.33$, arbitrarily high gains can be applied in each of the two principal loops without instability. This is equivalent to the results found in analyzing the multivariable root-loci. There it was shown that for $z_1 < 0.33$ high gains would not lead to instability; however, using the I.N.A. method it is also shown that no attempt to eliminate interaction is necessary, since large gains will lead to a system with little interaction. This can be seen by considering the transfer functions of the process with a diagonal gain controller, $\mathbf{G}_c(s) = \text{diag}(k_i)$. The effect of applying a gain k_i is to multiply \hat{q}_{i1} and \hat{q}_{i2} by k_i^{-1} . As k_1 and k_2 are increased, the system approximates over an increasingly wide band to a diagonal system. The transfer function between y_{it} and y_i when the j th ($j \neq i$) loop is closed with gain k_i and the i th loop is open leads to

$$r_{ii}^{-1}(s) = \hat{q}_{ii} - \frac{\hat{q}_{i2}\hat{q}_{21}}{k_j + \hat{q}_{jj}} \quad (2.5-9)$$

As k_1 and k_2 become large, the interaction effect is small and

$$r_{11}^{-1}(s) = \hat{q}_{11} \quad r_{22}^{-1}(s) = \hat{q}_{22} \quad (2.5-10)$$

The design can then be carried out using the $f_w(s)$ as though they were inverse Nyquist diagrams for separate loops.

Finally it is instructive to consider the case where the measurements are not placed symmetrically, i.e., $z_2 \neq 1 - z_1$. The I.N.A. then consists of the four diagrams representing $\hat{q}_w(j\omega)$. Several cases were considered using the modified Nyquist contour. Figure 2.5-6 shows the I.N.A. diagrams for the case (0.4,0.8), which is diagonally dominant and stable. Thus arbitrarily high gains can be applied, leading to a system with small interaction. Other cases that were

$0.00 < z_1 < 0.33$	diagonal dominance and stability assured without compensation
$0.33 < z_1 < 0.50$	add compensator to get diagonal dominance and attempt to control unstable single loops
$0.50 < z_1 < 1.00$	add permutation compensator $G_c = \begin{vmatrix} 0 & 1 \\ 1 & 0 \end{vmatrix}$ to interchange the measurements and design as above

Table 2.5-2
I.N.A. Results for Symmetric Measurement Placement

considered are (0.4,0.7) and (0.3,0.8). Only the first of these requires compensation.

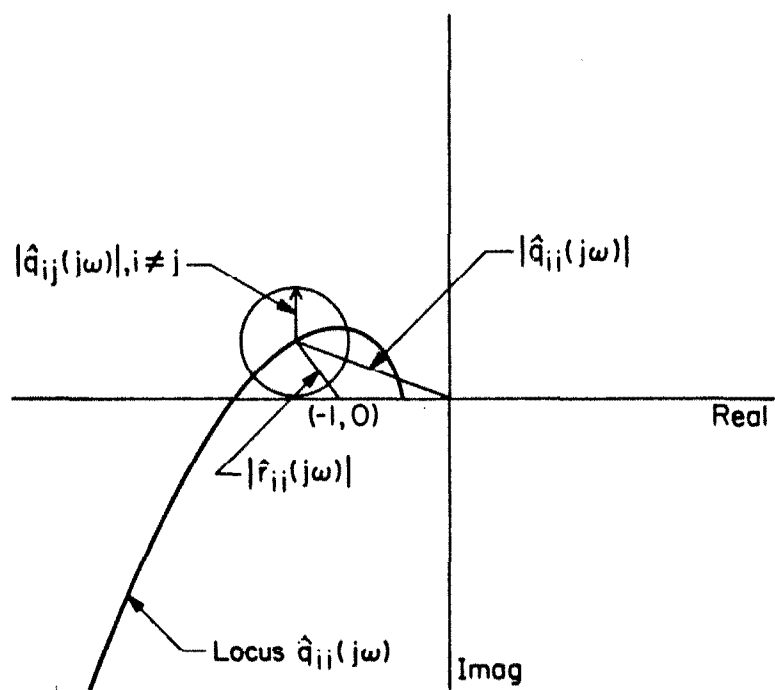
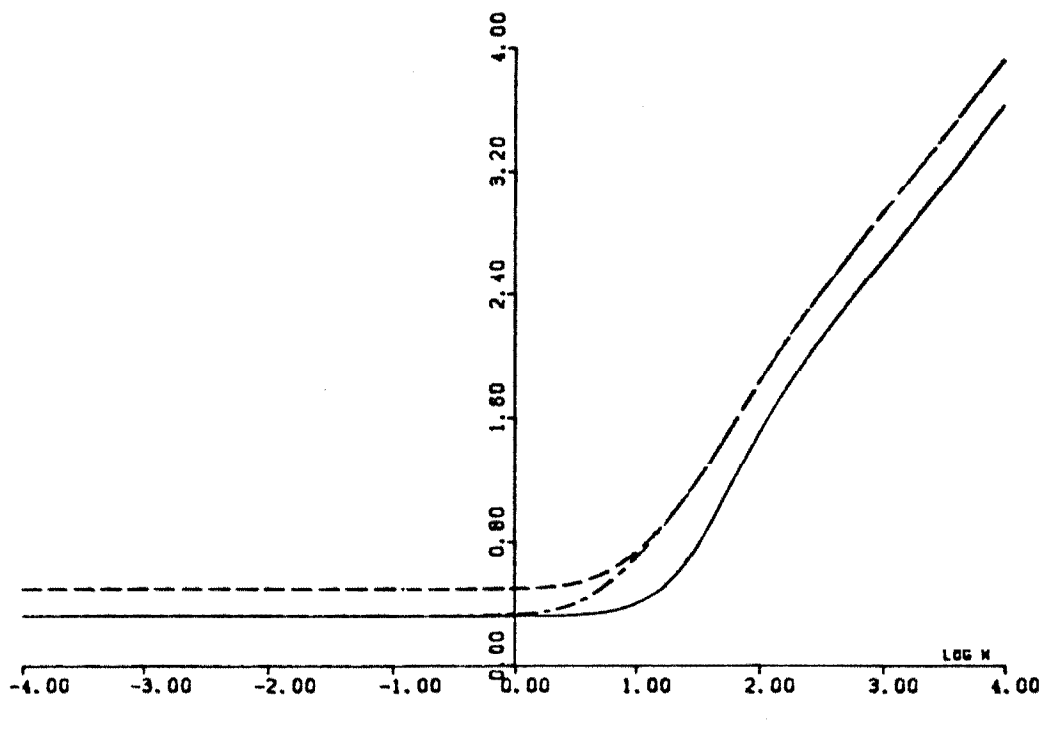


Figure 2.5-1
Diagonal Dominance Criteria



(a)

Figure 2.5-2
Inverse Nyquist Plots for Outputs $z_1=0.3, z_2=0.7$

a. Logarithmic Plots

----- $|\hat{q}_{11}|$ - - - $|1+\hat{q}_{11}|$ — $|\hat{q}_{12}|$

b. Element $\hat{q}_{11}(s)$ c. Element $\hat{q}_{12}(s)$

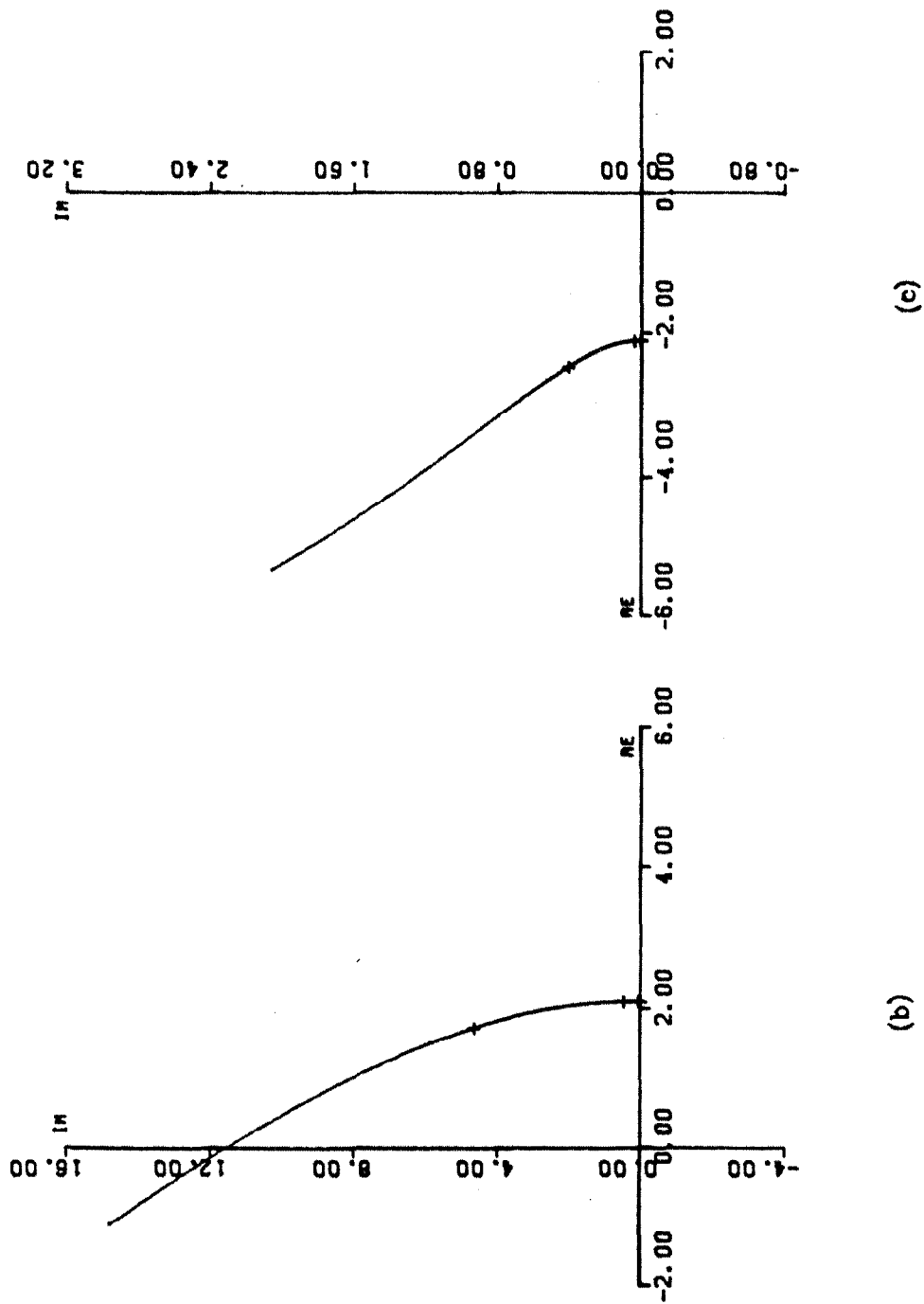
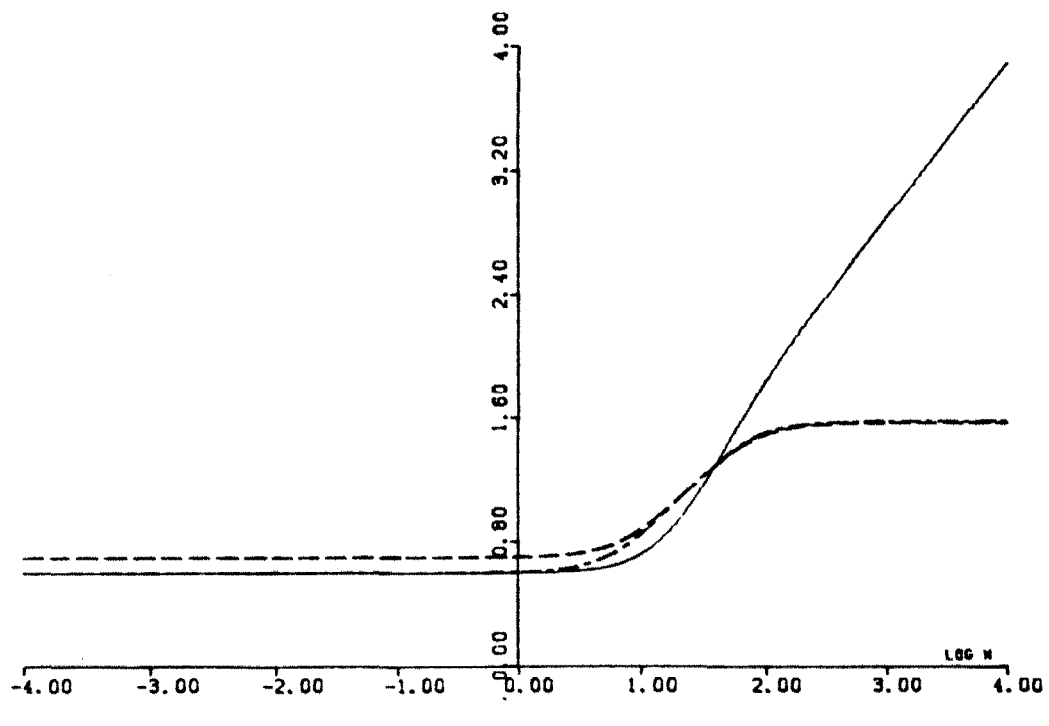


Figure 2.5-2 Continued



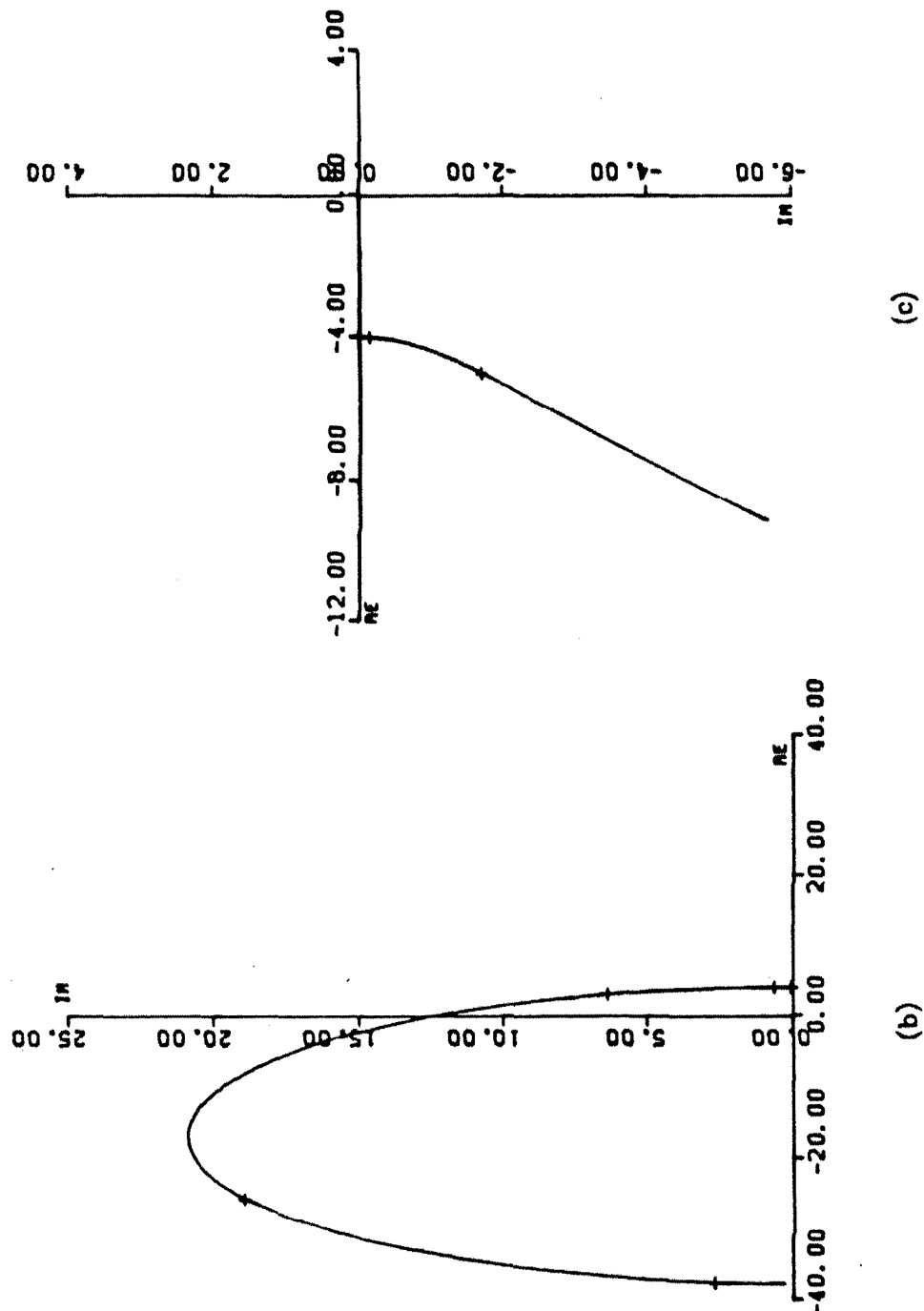
(a)

Figure 2.5-3
Inverse Nyquist Plots for Outputs $z_1=0.4, z_2=0.6$

a. Logarithmic Plots

----- $|\hat{q}_{11}|$ - - - $|1+\hat{q}_{11}|$ — $|\hat{q}_{12}|$

b. Element $\hat{q}_{11}(s)$ c. Element $\hat{q}_{12}(s)$



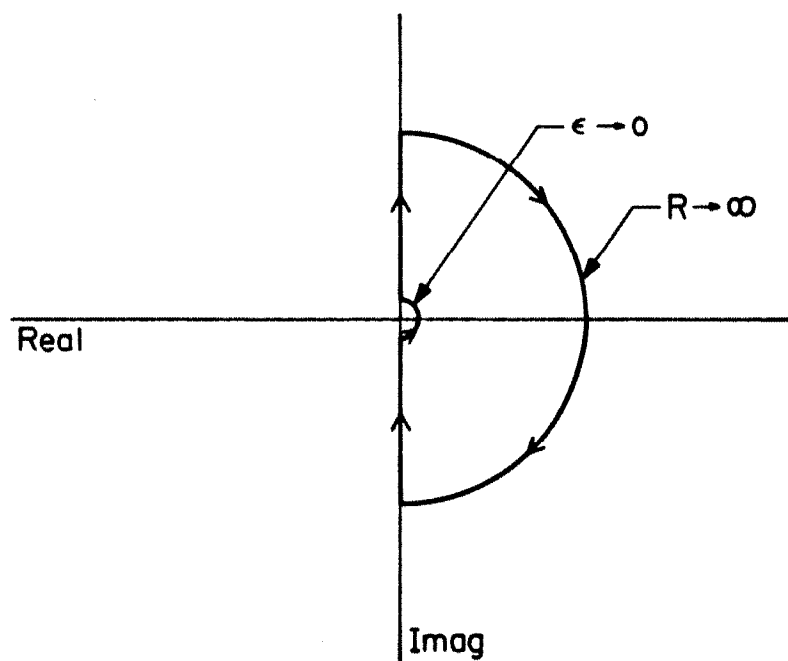
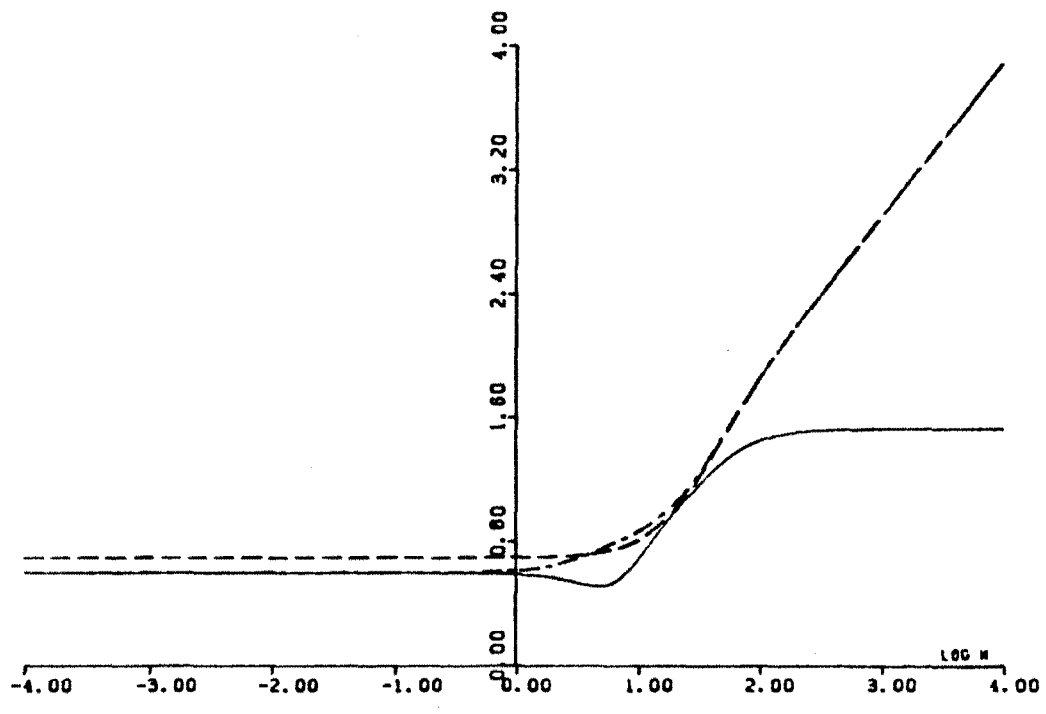


Figure 2.5-4
Modified Nyquist Contour
System with a Pole at the Origin



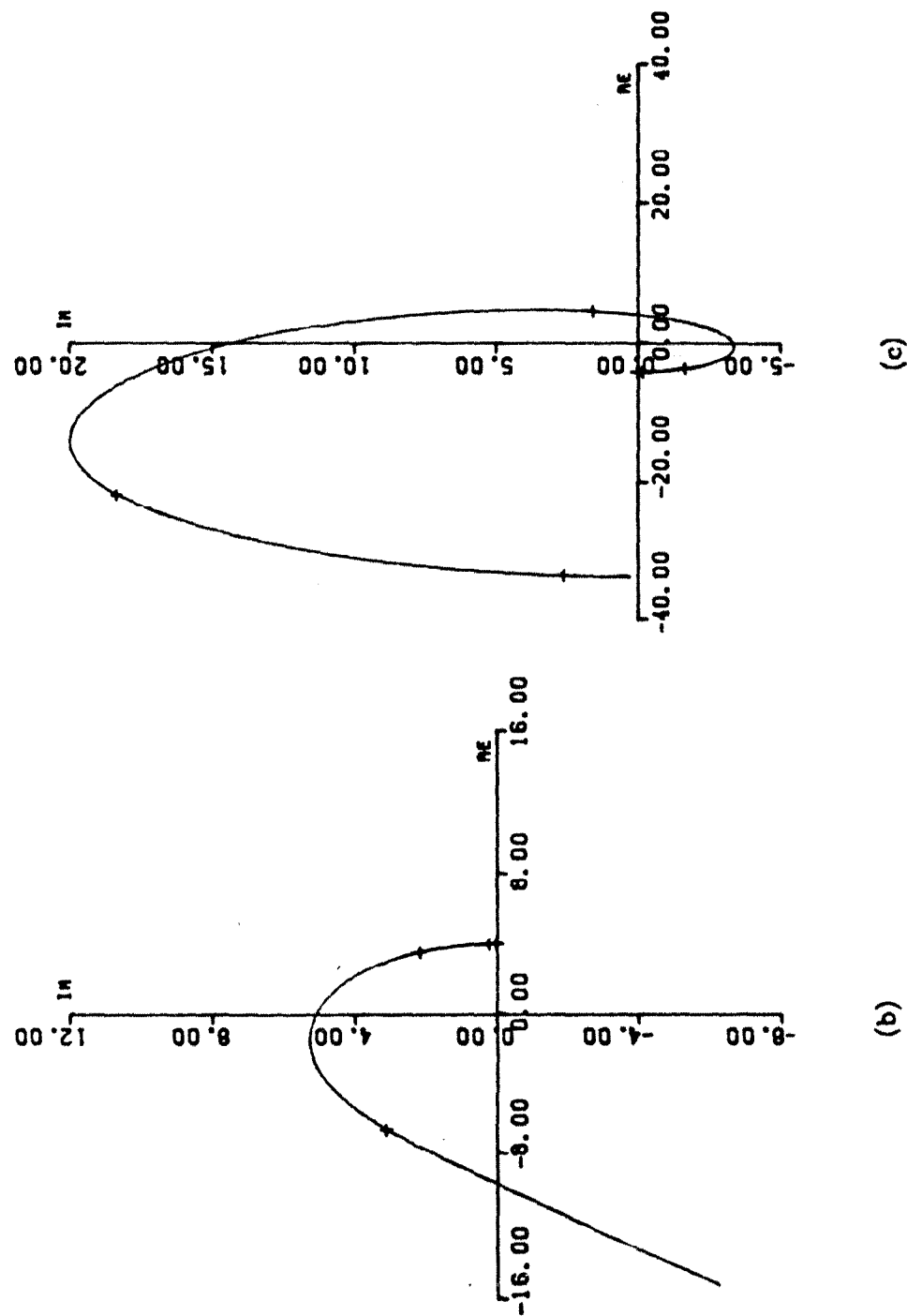
(a)

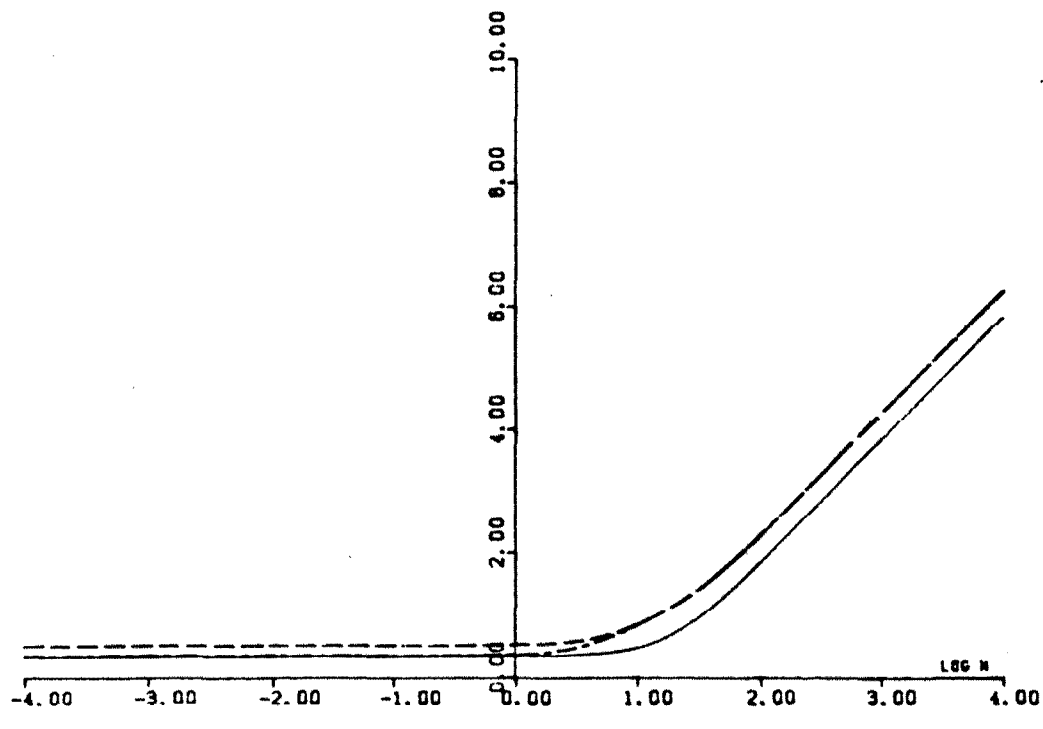
Figure 2.5-5
Inverse Nyquist Plots for Outputs $z_1=0.4$, $z_2=0.6$

a. Logarithmic Plots

--- $|\hat{q}_{11}|$ - - - $|1+\hat{q}_{11}|$ — $|\hat{q}_{12}|$

b. Element $\hat{q}_{11}(s)$ c. Element $\hat{q}_{12}(s)$





(a)

Figure 2.5-6
Inverse Nyquist Plots for Outputs $z_1=0.4$, $z_2=0.8$

a. Logarithmic Plots

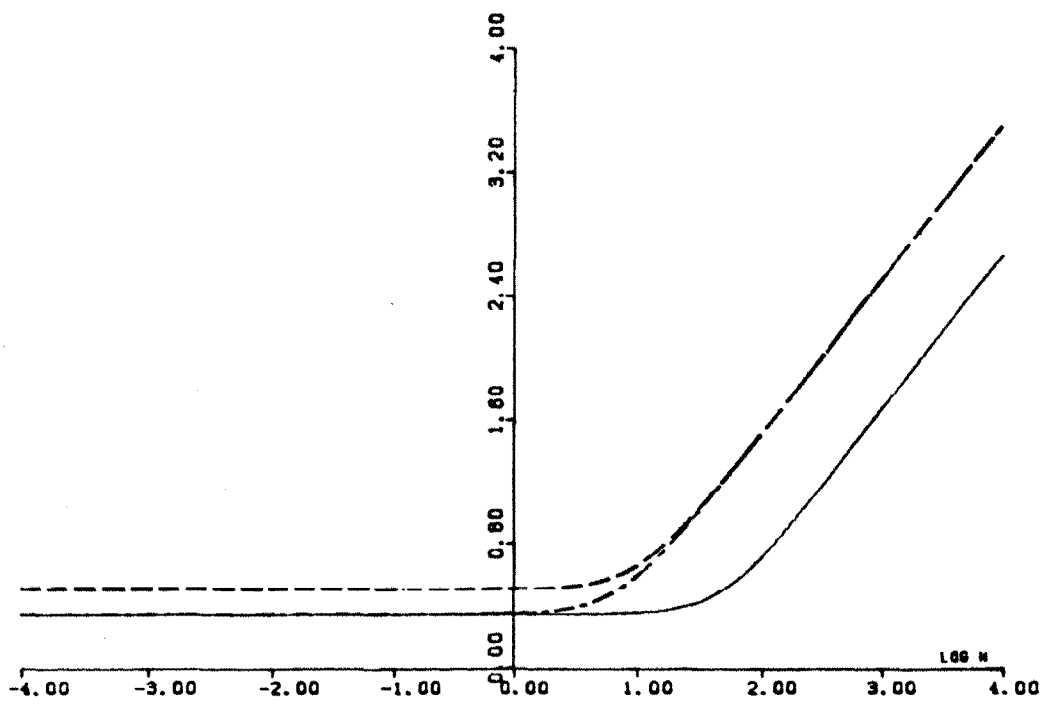
----- $|\hat{q}_{11}|$ - - - $|1 + \hat{q}_{11}|$ — $|\hat{q}_{12}|$

b. Logarithmic Plots

----- $|\hat{q}_{22}|$ - - - $|1 + \hat{q}_{22}|$ — $|\hat{q}_{21}|$

c. Element $\hat{q}_{11}(s)$ d. Element $\hat{q}_{12}(s)$

e. Element $\hat{q}_{21}(s)$ f. Element $\hat{q}_{22}(s)$



(b)

Figure 2.5-6 Continued

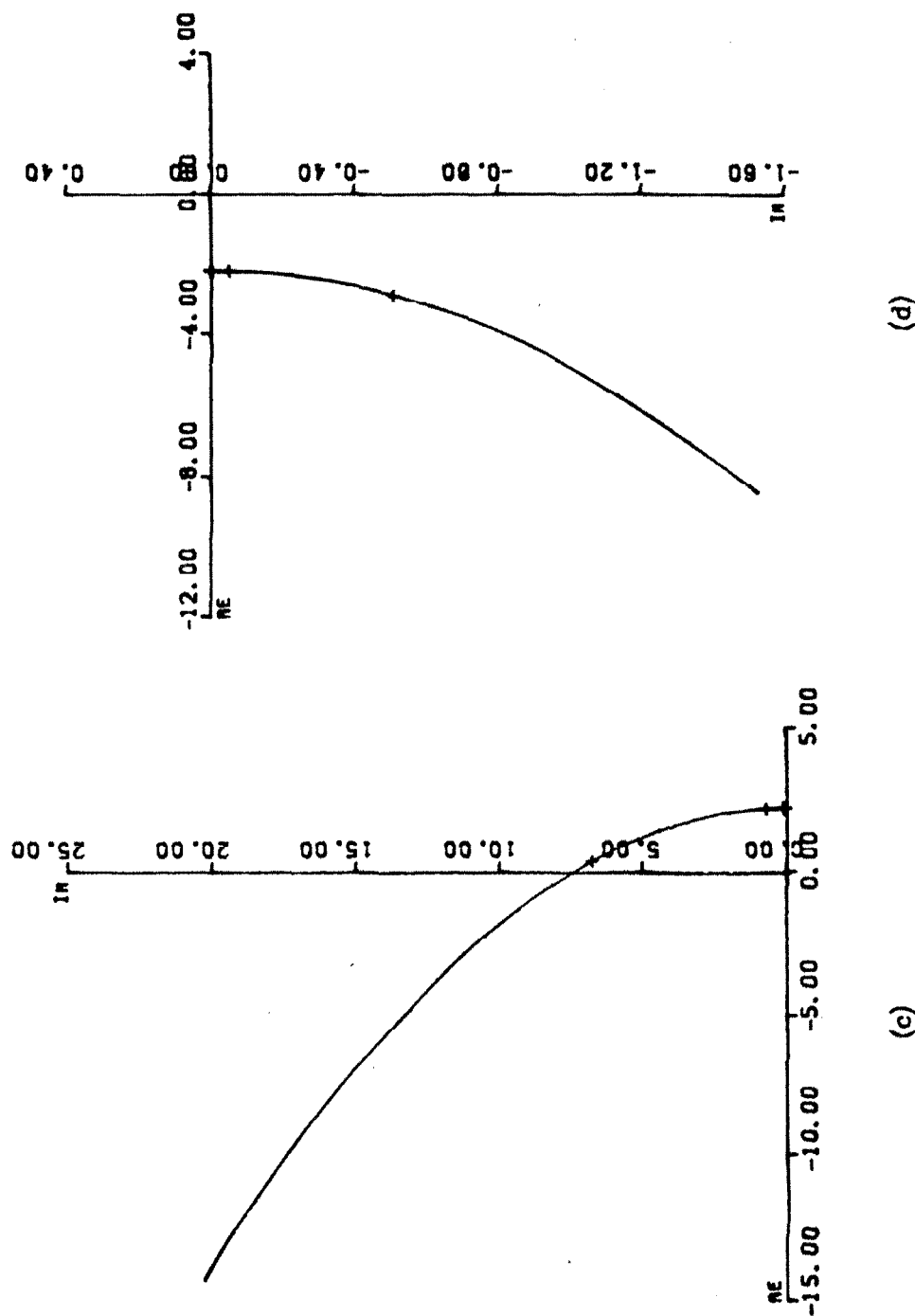


Figure 2.5-6 Continued

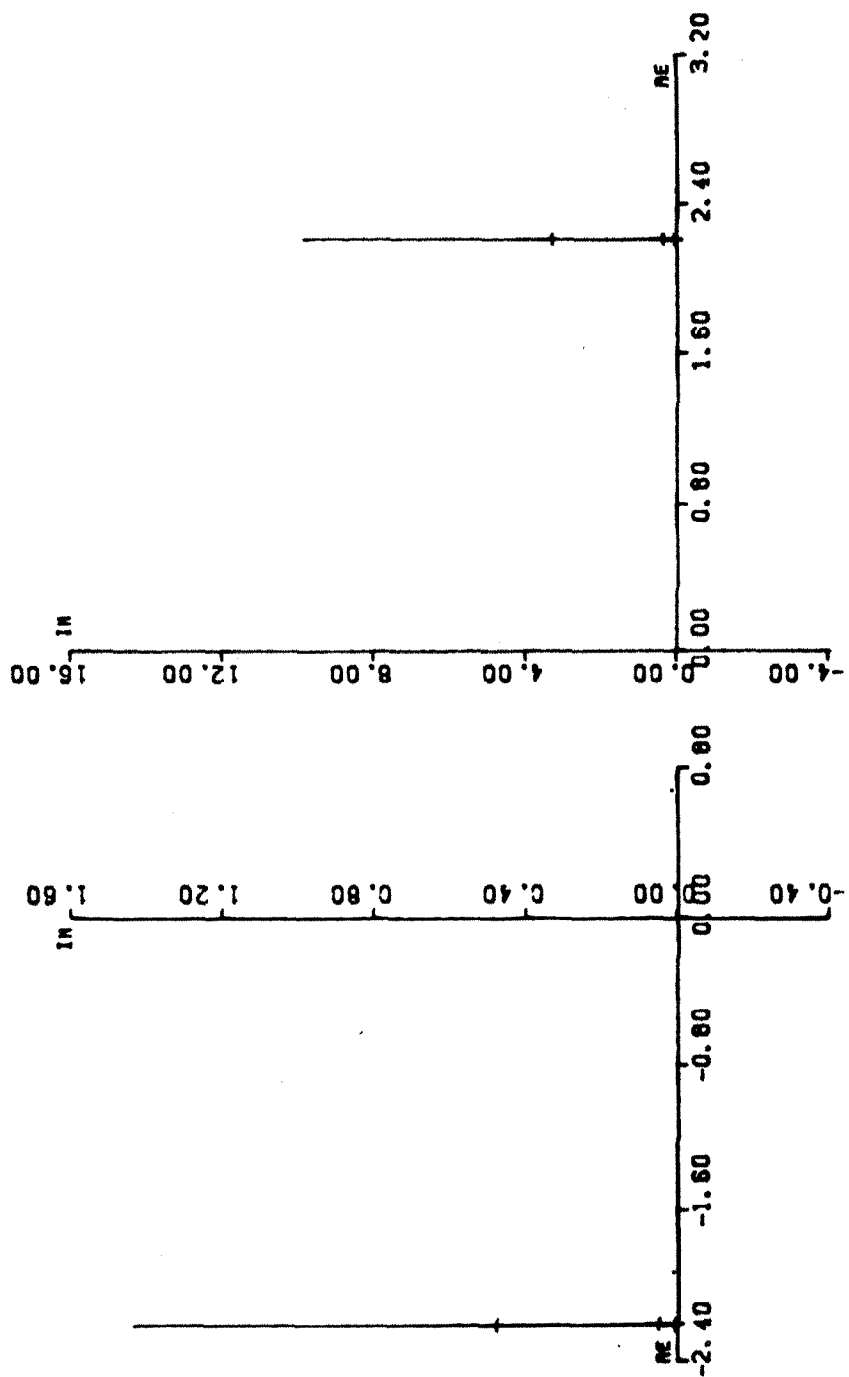


Figure 2.5-8 Continued

(f)

(e)

2.6 CHARACTERISTIC LOCUS METHOD

The characteristic locus method (C.L.M.) is an extension of classical Bode-Nyquist frequency-response theories and state-space techniques for the design of general, multivariable feedback control schemes. The method combines the essential features of both approaches by using the properties of linear vector spaces defined over base fields of complex functions. As in the I.N.A. technique, the C.L.M. requires the use of a computer-aided graphic display and can be incorporated into a computer-aided design package. Although the I.N.A. technique defines approximate conditions for stability using bands on inverse Nyquist plots, the C.L.M. gives an exact indication of stability and a systematic technique for choosing the best controller matrix in terms of system stability, integrity, interaction, and accuracy, rather than simply stressing diagonal dominance and single-loop design. The original method, developed by MacFarlane and Bellettratti (Bellettratti and MacFarlane, 1971; MacFarlane and Bellettratti, 1973), has been refined and systematized through the late 70's (Edmunds and Kouvaritakis, 1979; MacFarlane and Kouvaritakis, 1977) and has been experimentally tested on an automatic flight control system (Kouvaritakis et al., 1979) and a two-bed reactor process (Foss et al., 1980).

The C.L.M. uses the frequency dependent properties of the eigenvalues and eigenvectors of the open-loop transfer function $Q(s) = G_p(s)G_c(s)$ to assess the closed-loop properties of the system. The design technique attempts to compensate and modify the system's response by adjusting the eigenproperties of $Q(s)$. The basis for this use of the open-loop transfer function in the analysis of the feedback system is the congruence of the closed- and open-loop eigenframes. This relation can easily be seen from the dyadic expansions of $Q(s)$ and $R(s)$ for unity feedback systems (MacFarlane and Bellettratti, 1973):

$$\mathbf{Q}(s) = \sum_{i=1}^m q_i(s) \mathbf{w}_i(s) \mathbf{v}_i^T(s) \quad (2.6-1a)$$

$$\mathbf{R}(s) = [\mathbf{I} + \mathbf{Q}(s)]^{-1} \mathbf{Q}(s) = \sum_{i=1}^m \frac{q_i(s)}{1+q_i(s)} \mathbf{w}_i(s) \mathbf{v}_i^T(s) \quad (2.6-1b)$$

where $q_i(s)$ are the eigenvalues of $\mathbf{Q}(s)$ and $\mathbf{w}_i(s)$ and \mathbf{v}_i^T are the corresponding eigenvectors and dual eigenvectors. Obviously, the characteristic functions are the same for both the closed- and open-loop systems and the eigenvalues are directly related.

The analysis for multivariable systems leads to the following criteria for achieving a compromise between the basic objectives of stability, integrity, interaction, and accuracy (MacFarlane and Belletrutti, 1973). The basis of the technique is the use of the characteristic loci, which are the paths in the complex plane drawn by the eigenvalues of $\mathbf{Q}(s)$ as s traverses the standard Nyquist contour.

Stability

Closed-loop stability can be assured by selecting the compensator $\mathbf{G}_c(s)$ such that the net sum of the counterclockwise encirclements of the critical point $(-1.0, 0.0)$ by the characteristic loci is equal to the number of open-loop unstable poles p_0

$$\sum_{i=1}^m n_i = -p_0 \quad (2.6-2)$$

where m is the number of inputs and outputs of the system and is thus the number of loci needed for complete description of the system's eigenproperties. It should be noted that the direction along the characteristic loci is taken as that which corresponds to a clockwise traversal of the Nyquist contour. For the third-order, lumped model of the heat conduction process, the open-loop characteristic

equation is $s(s + \pi^2)(s + 4\pi^2)$. Since the poles are at 0, $-\pi^2$, and $-4\pi^2$, $p_0 = 0$, and the encirclement criterion reduces to

$$\sum_{i=1}^2 n_{k_i} = 0 . \quad (2.6-3)$$

Integrity

A multivariable feedback system is of high integrity if it remains stable under all types of failure conditions. The major probable difficulties include output transducer, error-monitoring channel, and actuator failures. For practical systems, the control design must obviously take into consideration such component breakdowns. Integrity against transducer and error-monitoring channel failures in all possible combinations of the loops can be assured if the characteristic loci of all the principal submatrices of $Q(s)$ satisfy the encirclement criterion. For integrity against actuator failures, similar considerations apply to the matrix $G_c(s)G_p(s)$.

Interaction

Reduction of interaction in a multivariable system is usually desired to improve closed-loop dynamic response and is often necessary to assure stability. At low frequencies, interaction can be suppressed by imposing high gains, i.e., $|q_i(j\omega)| >> 1.0$. Then the dyadic expansion of $R(s)$,

$$R(j\omega) \rightarrow \sum_{i=1}^m w_i(j\omega) v_i^T(j\omega) = I , \quad (2.6-4)$$

shows that the closed-loop system becomes essentially non-interacting. However, this restriction cannot always be achieved because stability conditions usually require that the characteristic

gains have small moduli at high frequency. Since the eigenvalues of $\mathbf{G}(s)$ satisfy $|q_i(j\omega)| << 1.0$ at high frequency,

$$\mathbf{R}(j\omega) \rightarrow \sum_{i=1}^m q_i(j\omega) \mathbf{w}_i(j\omega) \mathbf{v}_i^T(j\omega) = \mathbf{Q}(j\omega) \quad (2.6-5)$$

and therefore the cross-couplings in $\mathbf{R}(j\omega)$ are carried over from $\mathbf{Q}(j\omega)$. Thus to suppress interaction at high frequency, $\mathbf{G}_c(s)$ should be selected so that the eigenvectors of $\mathbf{Q}(s)$ are nearly as possible aligned with the standard base set. If the measure of alignment is taken as the angles between the eigenvectors $\mathbf{w}_i(j\omega)$ and the base vectors \mathbf{e}_i for $i = 1, 2$ (since $m = 2$ for the heat conduction system), the objective is to reduce the misalignment angles. MacFarlane and Bellettrutti (1973) show that, although these criteria lead to a reduction in interaction, they do not necessarily result in a $\mathbf{Q}(s)$ which is nearly diagonal or diagonally dominant, and thus a feedback system can be made nearly non-interacting without imposing diagonal dominance.

Accuracy

A system has high accuracy if the actual system output closely follows the desired output. In general, system accuracy will be high provided that the characteristic loci have large moduli at low frequency.

The objective of the characteristic locus method is then to select a controller $\mathbf{G}_c(s)$ so that the characteristic loci of $\mathbf{Q}(s)$ satisfy the stability criterion and have high gains at low frequencies and low misalignment angles at high frequencies. Additionally, $\mathbf{G}_c(s)$ should be selected so that its elements are rational functions of s , so that $|\mathbf{G}_c(s)|$ is nonsingular and has no right half plane zeros, and so that all the poles of $\mathbf{G}_c(s)$ are in the open left half complex plane.

MacFarlane and Kouvaritakis (1977) present a systematic approach for using the C.L.M.. In particular, a means of manipulating the characteristic loci and characteristic directions is developed so that the phase of the loci can be adjusted to achieve acceptable stability and integrity and so that the directions can be aligned and the gains balanced to reduce interaction. As outlined in several publications, a procedure for optimal alignment of a given complex plane with a real frame according to a misalignment measure can be incorporated into a computer algorithm.¹ The design procedure can then be split into two distinct parts:

i. High-Frequency Controller Performance

At high frequencies, it is desirable to reduce the misalignment angles between the compensated system's characteristic direction set and the standard basis vectors. This can be accomplished by designing a real compensator K_H that approximates the complex frame of $G_p^{-1}(j\omega)$ at some high frequency ω_h . A program ALIH which was written for this purpose uses the routine ALIGN to perform the actual alignment. A listing of the program is presented in Appendix 1. The signs of the columns of K_H are arbitrary and are selected so that the eigenvalues of CBK_H are positive, real. The compensated system then has infinite zeros with asymptotes on the negative real axis.

ii. Low-Frequency Controller Performance

At low frequencies, the encirclement criterion should be satisfied and the moduli of the characteristic loci should be large. This can be accomplished by manipulating the loci with an appropriate approxi-

1. This algorithm (ALIGN), which is a basis for high frequency alignment and low frequency manipulations, was written specifically for this project and is included in the programs ALIH and ALIL discussed below and listed in Appendix 1. It should not to be confused with the program ALIGN referred to by other authors, although their structures should be similar.

mately commutative controller \mathbf{K}_L , where $\mathbf{K}_L = \mathbf{A}\Gamma_k(s)\mathbf{B}$ with \mathbf{A} and \mathbf{B} being the real frame matrices that approximate the complex frame of the eigenvector matrix $\mathbf{W}(j\omega)$ and dual eigenvector matrix $\mathbf{V}(j\omega)$. Again the routine ALIGN is incorporated into a program ALIL for this purpose. This program is also listed in Appendix 1. The elements of the diagonal matrix $\Gamma_k(s)$ are then chosen on the assumption that $q_i = g_i k_i$ where q_i and g_i are the eigenvalues of the compensated and uncompensated system and k_i are the elements of $\Gamma_k(s)$. The compensator \mathbf{K}_L is thus used to insure stability and integrity and to adjust the gains at low frequency to reduce interaction.

The effect of \mathbf{K}_H and \mathbf{K}_L must be combined in such a manner so that each operates in the appropriate frequency range without significantly altering the effect of the other in its appropriate range. This is achieved by using the low-frequency controller as matrix-integral control:

$$\mathbf{G}_c(s) = \frac{\alpha}{s} \mathbf{K}_L + \mathbf{K}_H \quad (2.6-6)$$

where α is a constant chosen to achieve a suitable transition from the low-frequency to high-frequency behavior of $\mathbf{G}_c(s)$.

Although the C.L.M. is seemingly complicated, it is actually a simple design technique once the appropriate computer facilities and programs are available. The major programs are ALIH and ALIL, while other programs were used to calculate and graphically display the characteristic loci and misalignment angles. All programs were tested on the automatic flight control system (Kouvaritakis et al., 1979) and gave results equivalent to those published. Then for the heat conduction process, the design was performed using the third-order, lumped model with two controls and outputs and then with an extra measurement, which was squared down in an inner loop.

2.6.1 Basic System Analysis

For the uncompensated system, characteristic locus plots were drawn for the cases that were considered in the I.N.A. design (Table 2.5-1). Figures 2.6-1 - 2.6-3 show the loci with the measurement locations (0.3,0.7), (0.4,0.6) and (0.4,0.8).² For the symmetric cases with $z_1 < 0.33$, the encirclement criterion is satisfied for all gains. As was also shown using root-loci and I.N.A. analyses, these cases will remain stable with increasing gain. Also as expected, high gains lead to instability for $0.33 < z_1 < 0.50$. In particular, a maximum gain of 32.0 would be allowed before the critical point is encircled for $z_1 = 0.4$. Thus, for the symmetric cases, compensation is required for stability of the system at high gains when $0.33 < z_1 < 0.50$. Additionally, regardless of the measurement location, one eigenvalue has large magnitude at low frequencies while the second has very small magnitude, and the misalignment angles are both 45° at high frequencies. Thus some compensation is desired for all the cases to improve integrity, interaction, and accuracy of the system. Although the unsymmetric case (0.4,0.8) is also stable for all gains, compensation is desired to improve its closed-loop response. Since the cases (0.3,0.7), (0.4,0.6), and (0.4,0.8) are representative of the problem, they will be analyzed in detail using the C.L.M..

2.6.1.1 Case I: Measurements $z_1 = 0.3$, $z_2 = 0.7$

As discussed above, this case satisfies the stability criterion for all gains. The objective of the control action is thus to improve dynamic system performance by aligning the characteristic directions at high frequency, balancing the gains of the characteristic loci at low frequency, and injecting gain into the overall system, while maintaining stability. An analysis of the integrity against

2. Note that the vertical axis in the figures of $|q_t|$ versus frequency are defined in terms of $dB = 20 \log |q_t(j\omega)|$.

all types of failures leads to the conclusion that the system is of high integrity, since the characteristic loci of the principal submatrices of $G(s)$ also satisfy the encirclement criterion.

Preliminary analysis shows that the compensator

$$G_c(s) = \begin{bmatrix} 1 & 0 \\ 0 & -1 \end{bmatrix} \quad (2.6-7)$$

balances the gains perfectly and significantly reduces misalignment, but further analysis shows that such a compensator leads to system instability. Therefore rather than trying to guess the appropriate control structure, it is best to perform the systematic alignment procedure discussed previously.

The first step involves designing K_H to reduce the misalignment angles. For the third-order model of the heat conduction with symmetric measurements, the matrix of eigenvectors is approximately³

$$W = \begin{bmatrix} 1.0 + 0i & -1.0 + 0i \\ 1.0 + 0i & 1.0 + 0i \end{bmatrix} \quad (2.6-8)$$

throughout the frequency range 10^{-4} to 10^4 . Figures 2.6-1 and 2.6-2 show that as expected the angles between the standard base vectors and the characteristic direction set are about 45° . The alignment is attempted using ALIH at several frequencies in the range $\omega_h = 1 \rightarrow 100$, but unfortunately the analysis of many possible compensators K_h leads to the conclusion that no real matrix can adequately reduce misalignment angles at high frequencies for symmetric measurements without leading to system instability. This problem results from the eigenvector matrix W being nearly real and having off-diagonal terms identical in magnitude to the diagonal terms. Although it seems plausible to select a complex compensator $K_H = G^{-1}(j\omega_h)$, the resulting controller is not physically realiz-

3. The imaginary parts are of $O(10^{-10})$ at $\omega = 10^{-4}$ and $O(10^{-4})$ at $\omega = 10^4$.

able. Thus K_H should merely be selected as the identity matrix. If instead K_H is selected as the zero matrix, $G_c = \frac{\alpha}{s} K_L$ and as s approaches infinity, G_c approaches zero. This could lead to problems.

At low frequencies, ALL is designed to calculate real matrices A and B which approximate the eigenvector and dual eigenvector matrices; however, this leads to numerical difficulties with symmetric measurement placement. The problem is actually trivial since W is approximately real at all frequencies (especially at low frequencies). Thus with the selection of $A = W$ and $B = V$, $K_L = WA_kV$. The gains were then balanced at the frequencies $\omega_L = 1.0, 0.1, 0.01$, and 0.001 by selecting

$$\Lambda = \begin{bmatrix} 1 & 0 \\ 0 & \gamma \end{bmatrix}, \quad \text{where } \gamma = \frac{|q_1(j\omega_L)|}{|q_2(j\omega_L)|}. \quad (2.6-9)$$

Furthermore since $G_c(s) = \frac{\alpha}{s} K_L + I$, the values of α can be adjusted to give the best response. After consideration of many combinations of α and ω_L , the best balance at low and moderate gains was obtained with

$$G_c(s) = \frac{1.0}{s} \begin{bmatrix} 6.4 & -5.4 \\ -5.4 & 6.4 \end{bmatrix} + \begin{bmatrix} 1 & 0 \\ 0 & 1 \end{bmatrix}. \quad (2.6-10)$$

Figure 2.6-4 shows that this compensator leads to a stable system with nearly identical gains at $\omega = 1.0$ and high gains throughout the range $\omega < 1.0$. However, the misalignment angles have not been reduced. The final step in the design is to increase the moduli by injecting gain into the compensated system.

2.6.1.2 Case II: Measurements $z_1 = 0.4, z_2 = 0.6$

Since this case is stable only for gains less than 32.0, the major concern of the compensator should be to insure stability for higher gains. Attempts are

made to design such a high frequency compensator. However even by using ALIH and selecting the compensators so that the eigenvalues of CBK_H are positive, the overall system remains unstable. This is explainable since the condition that the eigenvalues of CBK_H are positive is necessary for stability but is not sufficient. In addition to the two infinite zeros, there is a finite zero at approximately +63.0, according to the root-loci analysis. In designing K_H , there are only two degrees of freedom available for selecting the appropriate signs, so only the two infinite zeros can be placed. Further analysis shows that dependent control action is necessary to move the finite zero into the left half plane.⁴ The problem essentially reduces to a single-input, double-output system. However since dependent control leads to very bad closed-loop response,⁵ the best that can be accomplished is to reduce interaction and increase accuracy without eliminating the instability for high gains.

Using ALIH and ALIL, the best design for balancing gains and reducing misalignment angles is

$$G_c(s) = \frac{1.0}{s} \begin{bmatrix} 11.8 & -10.8 \\ -10.8 & 11.8 \end{bmatrix} + \begin{bmatrix} 0 & -1 \\ -1 & 0 \end{bmatrix} \quad (2.6-11)$$

The characteristic loci for the system with this compensator is shown in Figure 2.6-5. Unfortunately, this system is unstable for all gains and is therefore not desirable. Thus a better control strategy is necessary for the heat conduction system with measurement locations (0.4,0.6).

2.6.1.3 Case III: Measurements $z_1 = 0.4, z_2 = 0.8$

Though this case is stable for all gains without compensation, Figure 2.6-3 shows that a compensator may be quite useful to balance the magnitudes of the

4. The same conclusion was reached using the I.N.A. design procedure.

5. This is shown in the simulations in Section 2.7.

loci at low frequency and to reduce misalignment angles at high frequency. Whereas the misalignment angles were always 45° and could not be reduced in the symmetric cases without causing instability, high frequency compensation is useful for this unsymmetric case. Considerable analysis using ALIH and ALIL at various frequencies along with adjusting α leads to an excellent C.L.M. design. With the compensator

$$G_c(s) = \frac{0.8}{s} \begin{pmatrix} 4.348 & -4.348 \\ -4.348 & 4.348 \end{pmatrix} + \begin{pmatrix} 1.0 & -0.371 \\ 0 & 0.929 \end{pmatrix} \quad (2.6-12)$$

the characteristic loci (Figure 2.6-6) have nearly identical moduli at low frequency, and the misalignment angles are quite small at high frequency. Thus the C.L.M. seemingly leads to a stable system with high integrity, low interaction and high accuracy. Furthermore, the method concludes that this design has the best compromise between these qualities, since the compensators were designed using approximately commutative theories. The final step in the design is to inject gain into the compensated system.

Thus the C.L.M. provides a systematic approach for designing a system which best satisfies the criteria of stability, large moduli of the characteristic loci at low frequencies and small misalignment angles at high frequency. Simulations are necessary to show the actual extent of the improvement obtained by using this design technique, but it is apparent that the designs for the symmetric cases do not adequately satisfy the C.L.M. criteria. Only for the (0.4,0.8) case is an excellent design obtained. Thus it may be advantageous to use extra temperature measurements within an inner loop to improve the system, for which the C.L.M. will be used to design the outer-loop controller.

2.6.2 Inner-Loop Analysis

The use of easily available measurements in excess of the commanded outputs⁶ is considered, so as to make more efficient use of the gain. The procedure involves squaring down the extra measurements within an inner loop, in order to form a new set of outputs equal in number to the number of inputs. Instead of using the extra degrees of freedom to reduce interaction as was done in Section 2.4, the objective is to use the inner loop to suitably place the poles of the outer loop so that the C.L.M. (or I.N.A. method) can be applied to a 'better' system as seen from a control point of view. The inner-loop design is based on the placement of the finite zeros and the manipulation of the root-loci asymptotes for the inner loop so that by finally setting the inner-loop gain at a suitable value, the poles of the outer loop are pulled into better locations in the complex frequency plane.

Consider the process shown in Figure 2.6-7. The outer loop consists of two measurements and two controls. However, three measurements are actually taken and squared down in an inner loop using the compensator \bar{F} . The system is described by the following relationships, where L and \bar{C} were defined in Section 2.4.

$$\begin{aligned} \mathbf{y} &= L\bar{C}\mathbf{x} = C\mathbf{x} & \mathbf{y}_F &= F\mathbf{x} = \bar{F}\bar{C}\mathbf{x} \\ \mathbf{x} &= (sI - A)^{-1}Bu & \alpha &= G_c[\mathbf{y}_d - \mathbf{y}] \\ \mathbf{u} &= K_l(\alpha - \mathbf{y}_F) \end{aligned} \quad (2.6-13)$$

The method involves designing F , from which \bar{F} can be calculated if \bar{C} is non-singular. Using the above description of the process, the inner-loop closed-loop response is

$$\mathbf{y}_F = (I + G_l K_l)^{-1} G_l K_l \alpha \quad \text{where } G_l = F(sI - A)^{-1} B. \quad (2.6-14)$$

6. The commanded outputs are those directly needed for comparison with the set points.

The characteristic equation for the inner loop is

$$|sI - A| \cdot |I + G_I K_I| = 0 \quad (2.6-15)$$

from which the root loci are obtained by letting $K_I = kI$. Then the overall closed-loop response is given by

$$y = [I + G_p K_I (I + G_I K_I)^{-1} G_c]^{-1} G_p K_I (I + G_I K_I)^{-1} G_c y_d \quad (2.6-16)$$

with G_p given by Equation (2.2-27), and the characteristic equation for the overall system is

$$|sI - A| \cdot |I + G_I K_I| \cdot |I + G_p K_I (I + G_I K_I)^{-1} G_c| = 0 \quad (2.6-17)$$

Using $G_c(s) = k' I$, the poles of the outer system are given by $k' = 0$ and are thus described by the solutions to

$$|sI - A| \cdot |I + G_I K_I| = 0 \quad (2.6-18)$$

Since Equations (2.6-15) and (2.6-18) are equivalent, the poles of the outer system are described by the root-loci of the inner system. Thus the inner-loop design can be used to place the outer-loop poles by selecting k .

Consider the case with $F = C$.⁷ Then since $G_I = G_p$, the root-loci for the inner loop are identical to those obtained in Section 2.2 for the outer loop. Thus if the root-loci of the original system without an inner loop show good characteristics--zeros well into the left half plane and little oscillation--then extra measurements may not be needed. The outer-loop poles can be shifted simply by imbedding an inner loop with sufficient gain. This is similar to the ideas of modal control.

The desired characteristics of the inner root-loci are that the infinite zeros are along the negative real axis and that the finite zeros are well into the left half plane. Obviously, many possible F matrices can lead to such root-loci. In

7. One possibility would be to take no additional measurements.

the following analysis, we consider only four such matrices.

Remembering that the root-loci of the original system with $z_1 < 0.33$ and $z_2 = 1.0 - z_1$ satisfy the desired criteria, the inner-loop compensator can be taken as $\mathbf{F} = \mathbf{C}(z_1, z_2)$, where $\mathbf{C}(z_1, z_2)$ is the \mathbf{C} matrix obtained with the points z_1 and z_2 .⁸

The cases that were considered are \mathbf{F}_A , \mathbf{F}_B , and \mathbf{F}_C shown in Table 2.6-1.

$$\mathbf{F}_A = \begin{pmatrix} 1.000 & 0.831 & -0.437 \\ 1.000 & -1.144 & 0.437 \end{pmatrix} = \mathbf{C}(.3, .8) \quad k = 8.0$$

$$\mathbf{F}_B = \begin{pmatrix} 1.000 & 0.831 & -0.437 \\ 1.000 & -0.831 & -0.437 \end{pmatrix} = \mathbf{C}(.3, .7) \quad k = 6.0$$

$$\mathbf{F}_C = \begin{pmatrix} 1.000 & 1.144 & 0.437 \\ 1.000 & -1.144 & 0.437 \end{pmatrix} = \mathbf{C}(.2, .8) \quad k = 10.0$$

$$\mathbf{F}_D = \begin{pmatrix} 2.000 & 1.000 & -0.414 \\ 2.000 & -1.000 & -0.414 \end{pmatrix} \quad k = 4.0$$

Table 2.6-1
Inner-Loop Compensators

For $\mathbf{F} \neq \mathbf{C}$, the criteria necessary to have infinite zeros along the negative real axis (i.e., $\mathbf{F}\mathbf{B}$ has all positive, real eigenvalues) and the finite zero well into the left half plane are

8. Note that the z_1 and z_2 have no relation to the actual measurement locations for this inner-loop problem. This structure of \mathbf{F} is only used for convenience since we know that the \mathbf{C} matrices with $z_1 < 0.33$ and $z_2 = 1.0 - z_1$ have root-loci with the desired features. The actual measurements define \mathbf{C} , from which \mathbf{F} is determined.

- a) $f_{11} + \sqrt{2}f_{12} + \sqrt{2}f_{13} > 0$
- b) $(f_{12}f_{21} - f_{11}f_{22}) + \sqrt{2}(f_{23}f_{12} - f_{22}f_{13}) > 0$
- c) $f_{21}f_{12} - f_{11}f_{22} \gg 0$

Although the elements of \mathbf{F} should be selected to satisfy these conditions, there are still an infinite number of possibilities available. However, consider

$$\bar{\mathbf{B}} = \begin{bmatrix} 1 & 1 \\ \sqrt{2} & -\sqrt{2} \end{bmatrix} \quad \bar{\mathbf{F}} = \begin{bmatrix} \alpha & f_{12} \\ \beta & f_{22} \end{bmatrix} \quad \begin{aligned} \alpha &= f_{11} + \sqrt{2}f_{13} \\ \beta &= f_{21} + \sqrt{2}f_{23} \end{aligned} \quad (2.6-19)$$

and specify that $\mathbf{Q} = \mathbf{FB} = \bar{\mathbf{F}}\bar{\mathbf{B}}$ should have all real, positive eigenvalues. Then with the further restriction that the rate of divergence to the infinite zeros is the same for all corresponding root-loci, \mathbf{F} must be of the form $\mathbf{F} = \gamma\bar{\mathbf{B}}^{-1}$. After trying various values of γ , f_{11} , and f_{21} , the best inner-loop design using this technique was found to be \mathbf{F}_D shown in Table 2.6-1.

The second stage of the design procedure, the outer-loop design, consists of the application of the C.L.M. to the system with the inner loop in place. Again the design is considered for commanded outputs (0.3,0.7), (0.4,0.6), and (0.4,0.8). Since the inner loop has been designed and since only z_1 and z_2 are needed for the outer loop, z_3 can be selected arbitrarily as long as $\bar{\mathbf{C}}$ remains nonsingular. This restriction is satisfied if z_3 is not equal to z_1 or z_2 . Then although the best C.L.M. design for the system without an inner loop was unable to reduce misalignment angles, it may be possible to improve on that design.

2.6.2.1 Case I: Measurements $z_1 = 0.3$, $z_2 = 0.7$

Although the outer-loop design was performed using all the inner-loop compensators shown in Table 2.6-1, only the analysis with \mathbf{F}_A will be discussed since all the cases lead to similar loci and since \mathbf{F}_A leads to the best overall design. A

preliminary examination of the characteristic loci for this case without outer-loop compensation (Figure 2.6-8) establishes the need for such compensation due to the disparity of the characteristic gains and the high misalignment between the characteristic directions of $Q(j\omega)$ and the basis vectors.

The C.L.M. is then performed using slightly modified versions of the programs previously discussed. Although ALIH can be used to calculate K_H , unfortunately it cannot be used to solve the inherent sign ambiguity. Previously this was possible since the infinite zeros were along the negative real axis if CBK_H had positive, real eigenvalues. However, the analysis with the inner loop in place shows a much more complicated result. If F , C , and B were square matrices, the simpler result could be derived.

With the inner-loop structure, it is possible to change the misalignment angles by designing an appropriate K_I . However whenever one of the misalignment angles is reduced at high frequency, the other is increased by about the same amount. Thus $K_H = I$ still provides the best compromise. Low-frequency compensation is then designed using ALIL at several frequencies, and α is adjusted to give the best balance between the low and high effects. The final overall design is

$$K_I = \text{diag}(8.0) \quad F = \begin{bmatrix} 1.0 & 0.831 & -0.437 \\ 1.0 & -1.144 & 0.437 \end{bmatrix} \quad (2.6-20)$$
$$G_c(s) = \frac{10.0}{s} \begin{pmatrix} 1.267 & -0.267 \\ -0.457 & 1.457 \end{pmatrix} + \begin{pmatrix} 1 & 0 \\ 0 & 1 \end{pmatrix}.$$

The characteristic loci with this design are shown in Figure 2.6-9. They obviously indicate that this design is better than that without an inner loop. In particular, the loci are much better balanced, and although the misalignment angles were immobile without an inner loop, they are greatly reduced for moderate frequencies.

cies with this design. Unfortunately, they are still 45° at very high frequency ($\omega > 100$).

2.6.2.2 Case II: Measurements $z_1 = 0.4$, $z_2 = 0.6$

Previously this case was found to be unstable for high gains due to an unstable finite zero, and it was shown that only dependent control would lead to stability since such control action was necessary to move the finite zero. Unfortunately, simple algebraic calculations show that an inner loop has no effect on the finite zeros of the system, and therefore the stability arguments are unchanged. Nevertheless, a compensator can be designed to improve the system by reducing interaction and increasing accuracy, if the values of the gain are restricted so as to assure stability.

Figure 2.6-10 shows characteristic loci for the best overall design that was obtained using the C.L.M.. The design consists of

$$K_L = \text{diag}(8.0) \quad F = \begin{bmatrix} 1.0 & 0.831 & -0.437 \\ 1.0 & -1.144 & 0.437 \end{bmatrix} \quad (2.6-21)$$
$$G_c(s) = \frac{1.0}{s} \begin{bmatrix} 1 & 0 \\ 0 & 1 \end{bmatrix} + \begin{bmatrix} 0 & 1 \\ -1 & 0 \end{bmatrix}$$

This system has a good balance of gains at low frequencies and low misalignment angles at high frequencies but will be unstable for outer-loop gains greater than 3.1. Since this is an overall gain of 24.8,⁹ it is not much lower than the stability limit for the uncompensated system.

⁹. The overall gain is the product of the outer-loop gain and the inner-loop gain.

2.6.2.3 Case III: Measurements $z_1 = 0.4, z_2 = 0.8$

Since the C.L.M. design for this case without an inner loop led to a compensator that perfectly balanced the gain at low frequency and significantly reduced the misalignment angles at high frequency, there seems to be little or no need to add an inner loop. Nevertheless, such an analysis was performed leading to the following design.

$$K_t = \text{diag}(8.0) \quad F = \begin{bmatrix} 1.0 & 0.831 & -0.437 \\ 1.0 & -1.144 & 0.437 \end{bmatrix} \quad (2.6-22)$$
$$G_c(s) = \frac{10.0}{s} \begin{bmatrix} 1.080 & -0.212 \\ 0.091 & 0.747 \end{bmatrix} + \begin{bmatrix} 1 & 0 \\ 0 & 1 \end{bmatrix}$$

The corresponding root-loci are shown in Figure 2.6-11. This design does not appear to be as good as that without an inner loop. Further refinement could lead to a slightly better system.

2.6.3 Modified Inner Loop Analysis

Finally, another outer-loop design suggested by Kouvaritakis et al. (1979) was considered (Figure 2.6-12). Since the purpose of the inner loop is to improve system dynamics by making use of all available measurements, while the overall objective is to exercise control over two of the measured variables, some minor modifications are made so that the inner loop operates only on the extra measurement. The new configuration makes more efficient use of gain since it closes the loops around z_1 and z_2 only once.

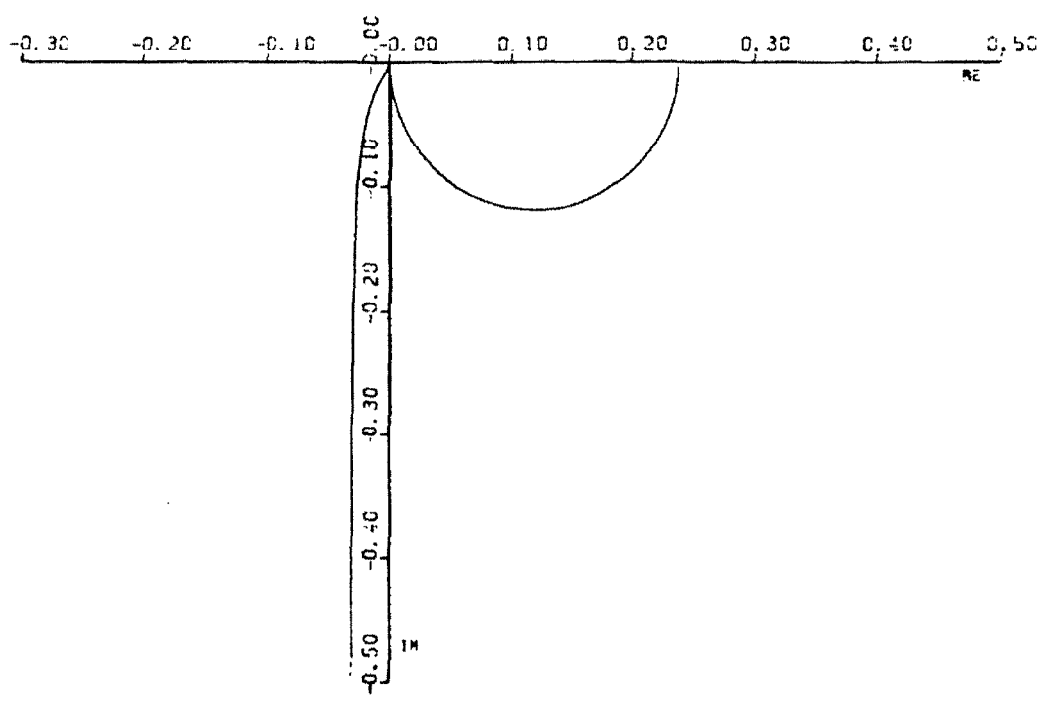
The design consists of

$$I_1 = \begin{bmatrix} 1 & 0 & 0 \\ 0 & 1 & 0 \end{bmatrix} \quad I_2 = (0 \ 0 \ 1) \quad (2.6-23)$$

while F_2 is 2×1 and F_1 is 2×2 . However using this design, the inner-loop root-

loci for the previous system (Figure 2.6-8) do not describe the behavior of the poles for the outer loop of the new system. Only with $G_c = I$ are the resulting root-loci for varying k identical to those obtained before rearrangement. Applying the C.L.M. to the new inner-loop system results in similar characteristic loci to those obtained previously, but the new configuration makes more efficient use of the gain.

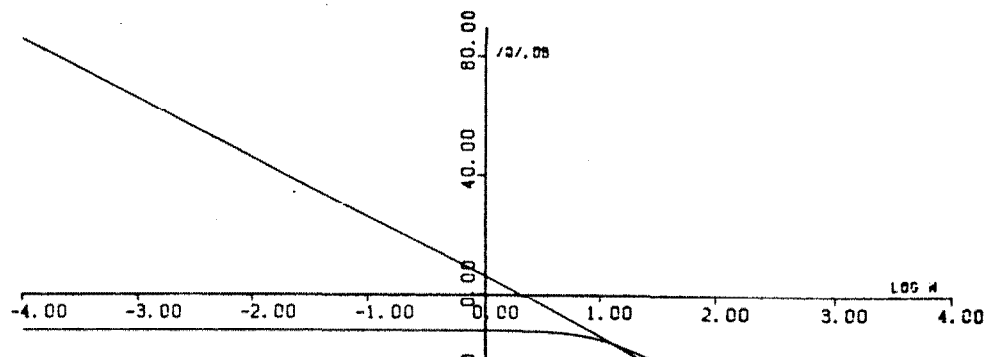
Finally it can be concluded that, although the inner loop is often beneficial, it does not always improve the overall design. If the criteria for a good C.L.M. design can be satisfied without an inner loop, then further analysis may not be necessary. However, if the misalignment angles cannot be reduced or the gains balanced without an inner loop, the inner loop may be useful.



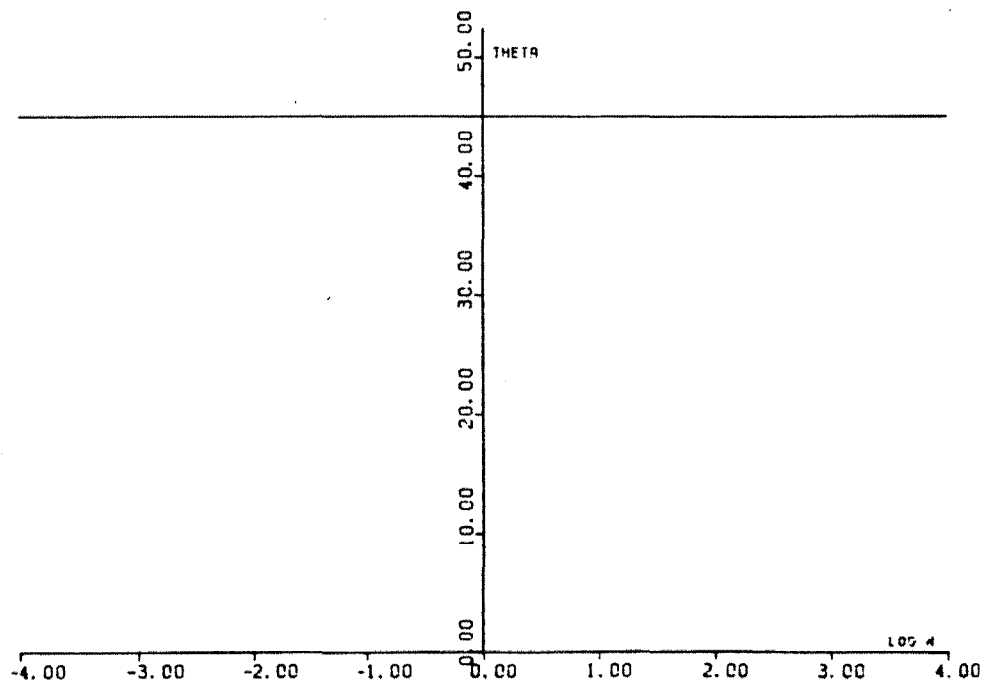
(a)

Figure 2.6-1
Characteristic Loci Diagrams for Outputs $z_1=0.3, z_2=0.7$

- a. C.L.M. Plots
- b. Magnitude vs. Log Frequency
- c. Misalignment Angles vs. Log Frequency

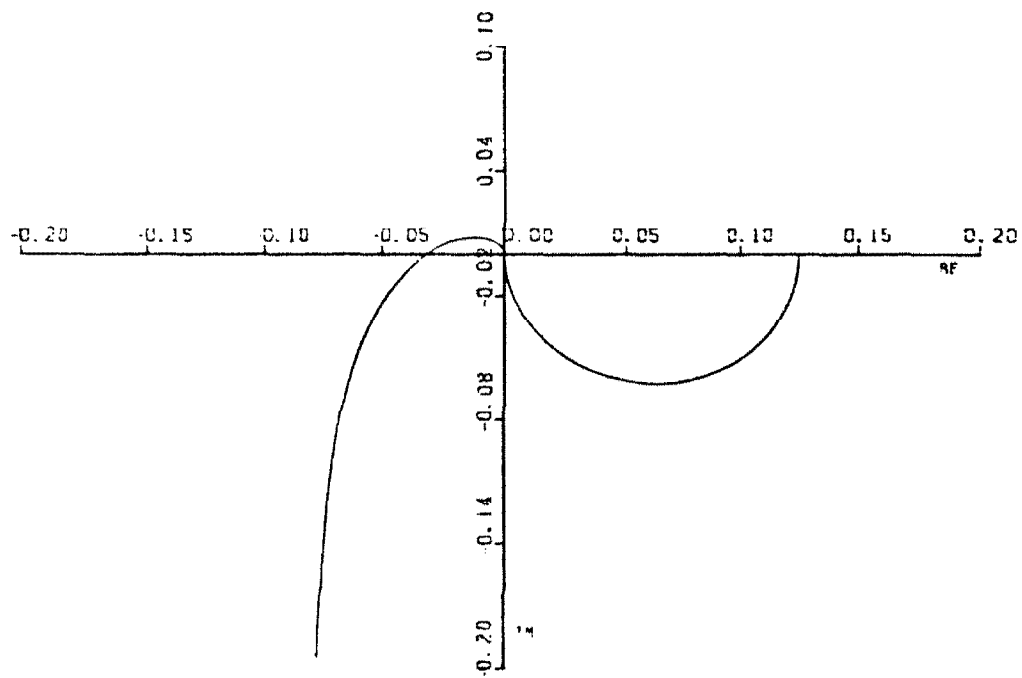


(b)



(c)

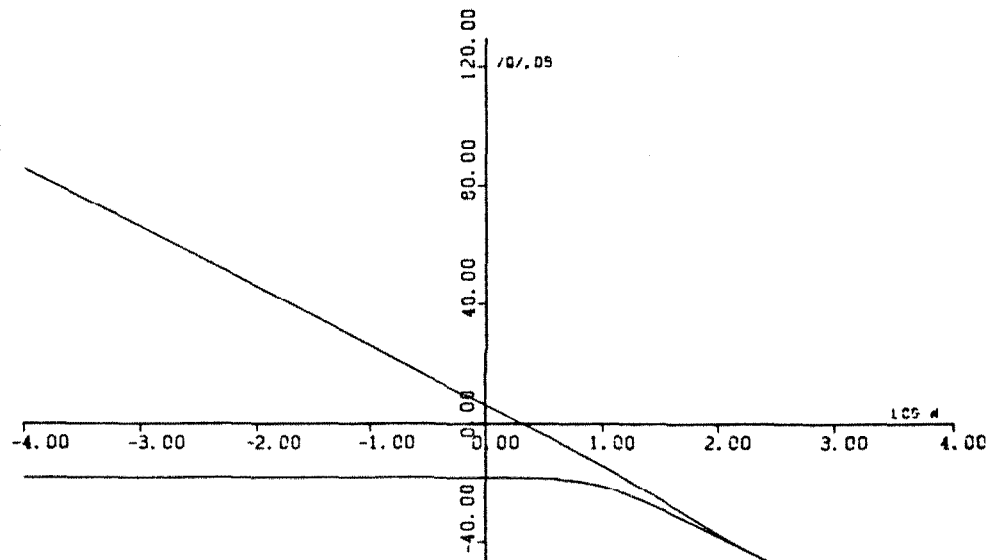
Figure 2.6-1 Continued



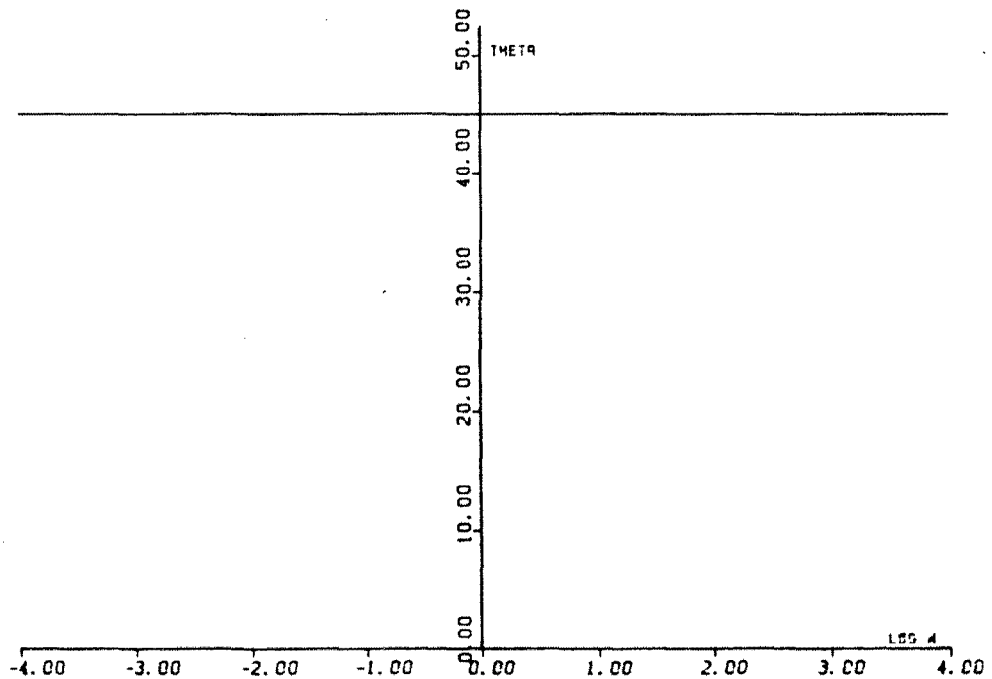
(a)

Figure 2.6-2
Characteristic Loci Diagrams for Outputs $z_1=0.4$, $z_2=0.6$

- a. C.L.M. Plots
- b. Magnitude vs. Log Frequency
- c. Misalignment Angles vs. Log Frequency

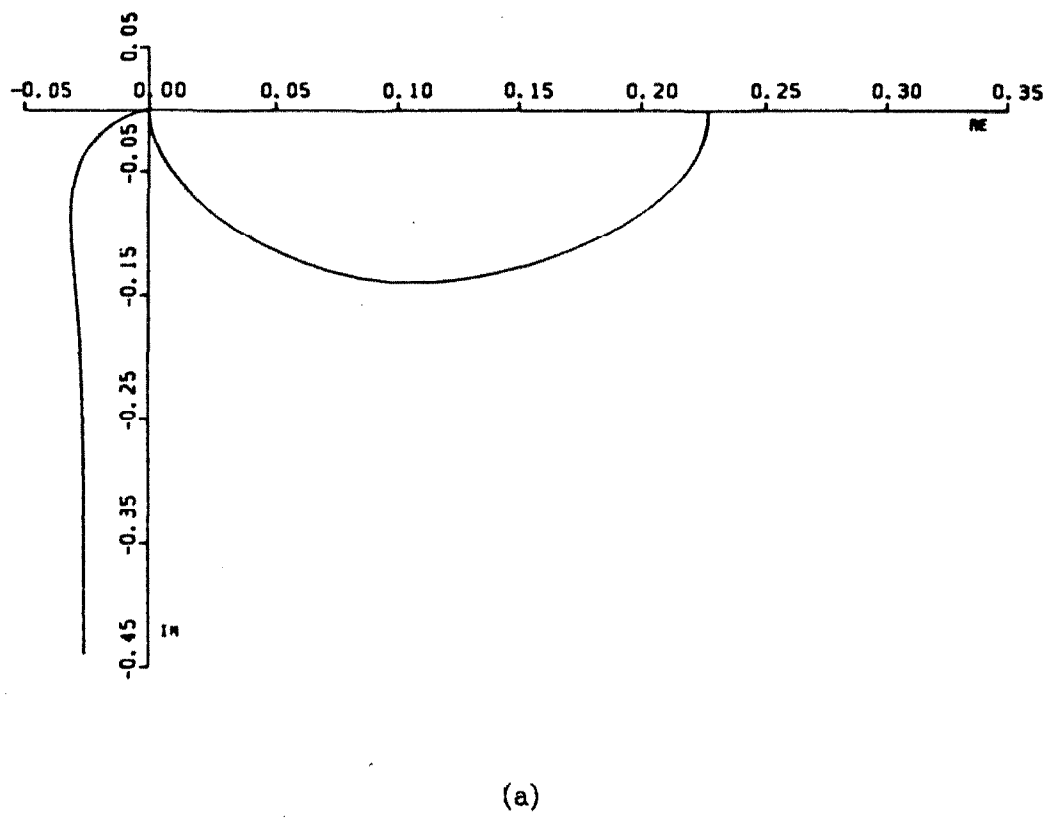


(b)



(c)

Figure 2.6-2 Continued



(a)

Figure 2.6-3
Characteristic Loci Diagrams for Outputs $z_1=0.4$, $z_2=0.8$

- a. C.L.M. Plots
- b. Magnitude vs. Log Frequency
- c. Misalignment Angles vs. Log Frequency

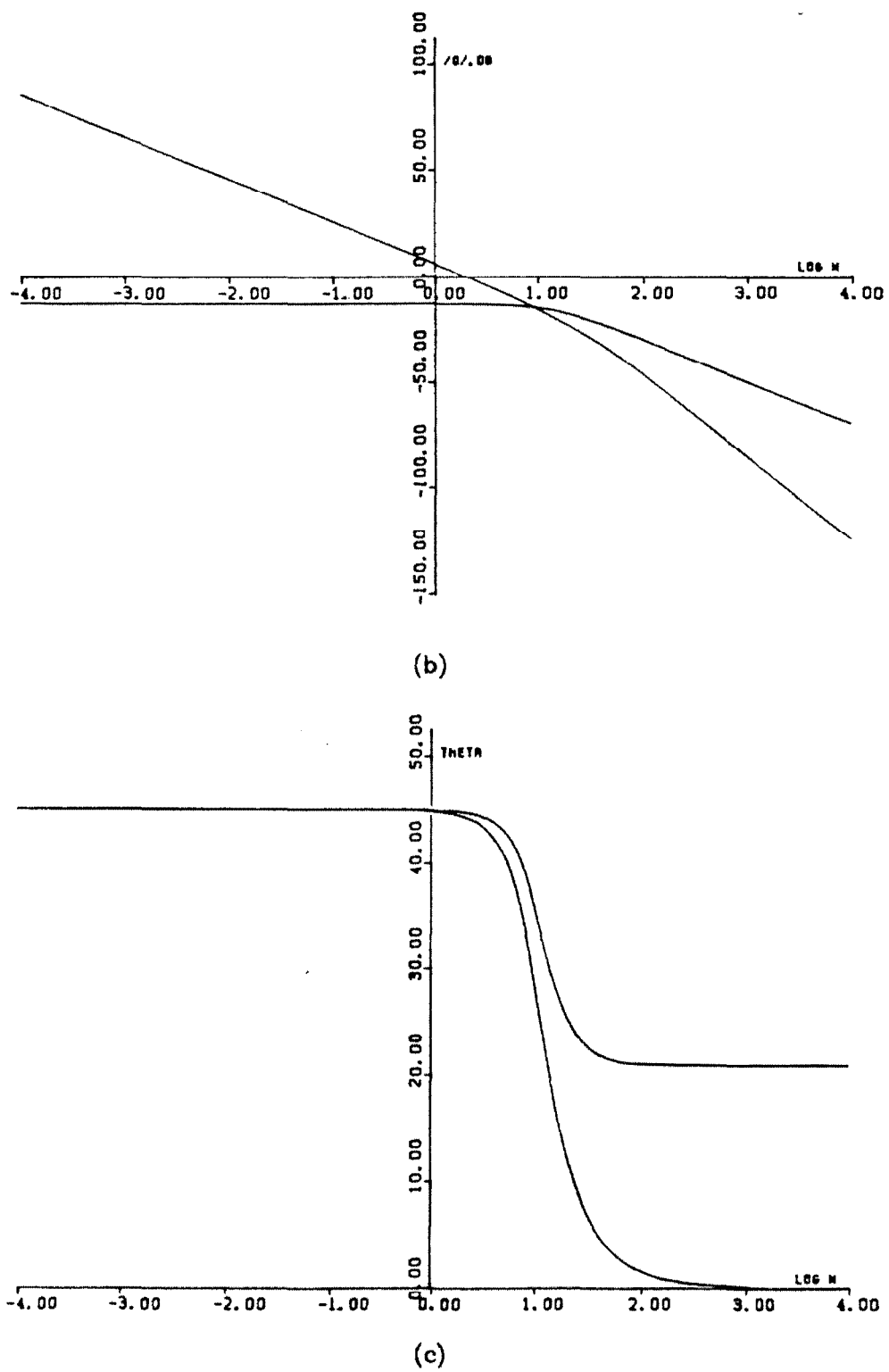
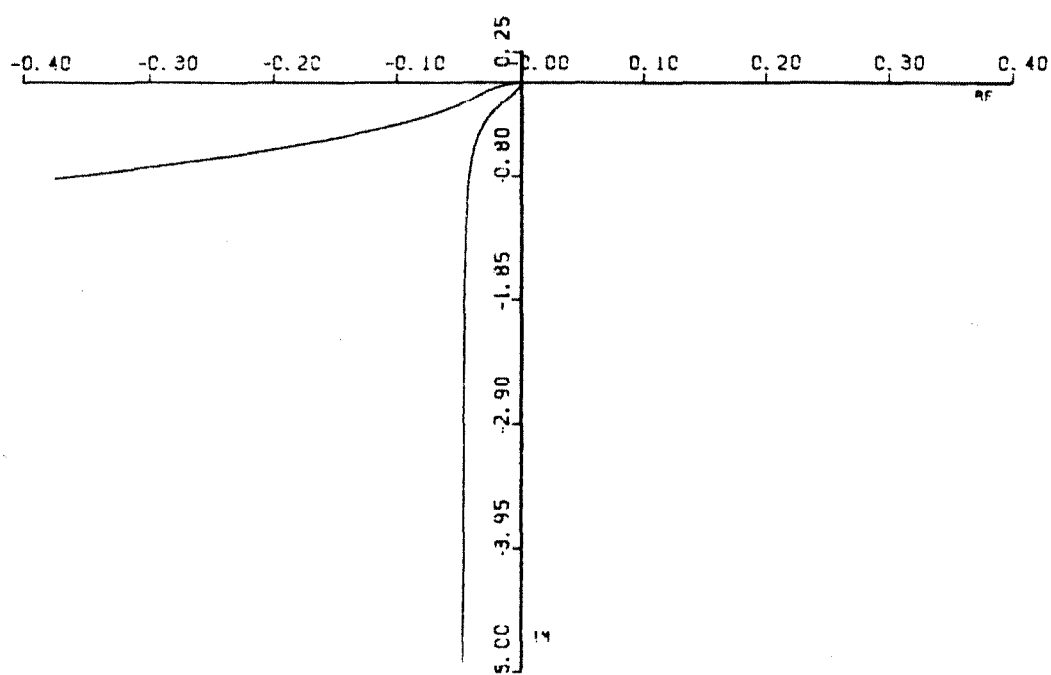


Figure 2.6-3 Continued



(a)

Figure 2.6-4
Characteristic Loci Diagrams for Outputs $z_1=0.3$, $z_2=0.7$
Compensator Given by Equation (2.6-10)

- a. C.L.M. Plots
- b. Magnitude vs. Log Frequency
- c. Misalignment Angles vs. Log Frequency

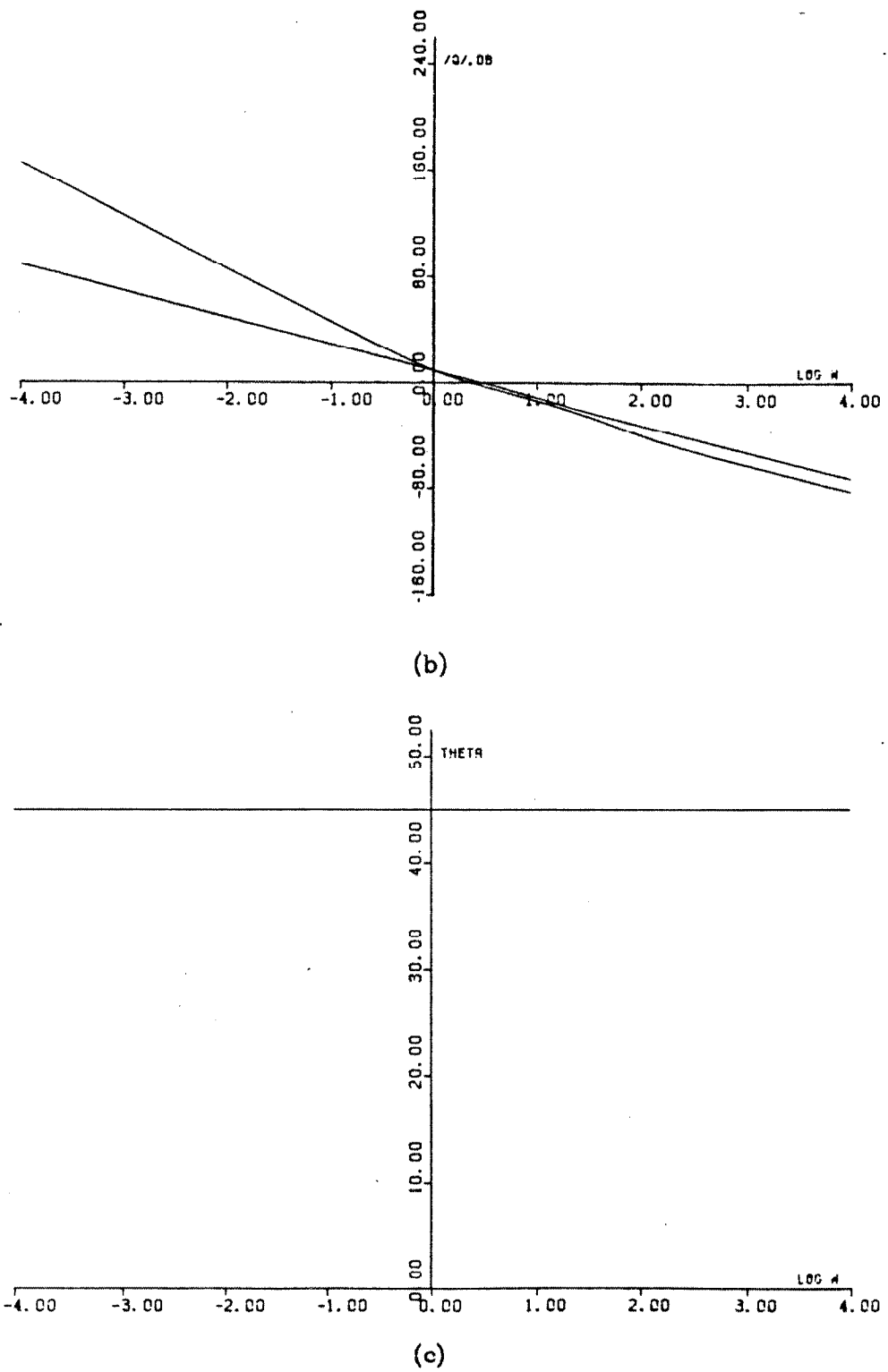
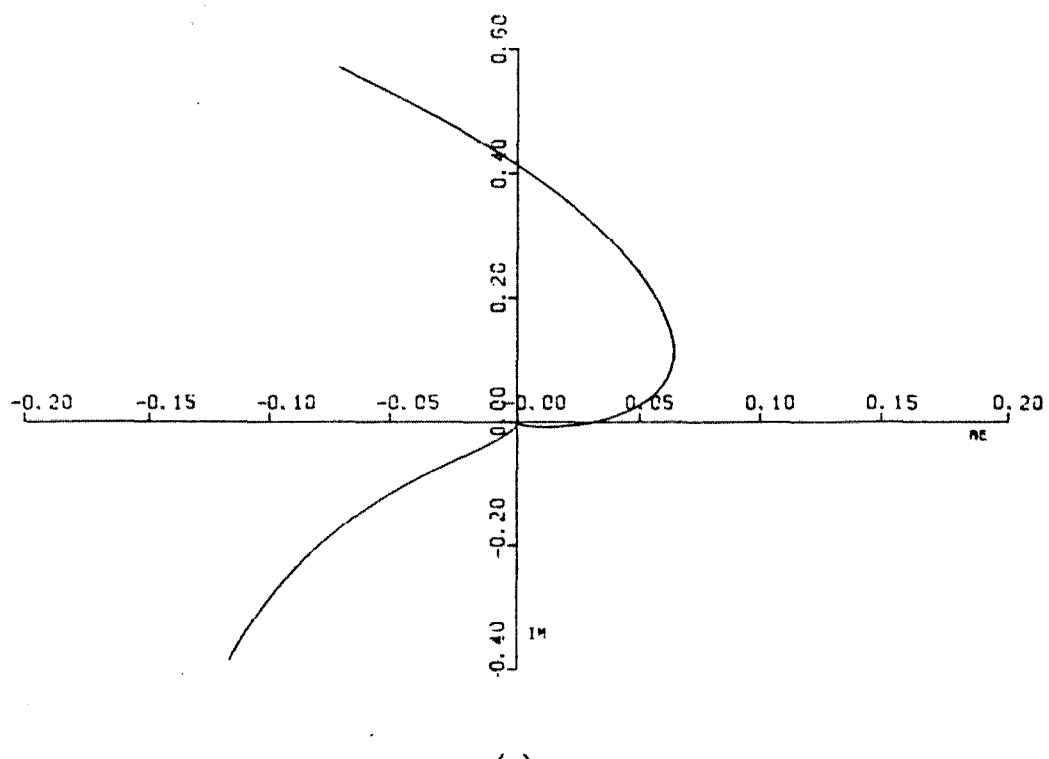


Figure 2.6-4 Continued



(a)

Figure 2.6-5
Characteristic Loci Diagrams for Outputs $z_1=0.4$, $z_2=0.6$
Compensator Given by Equation (2.6-11)

- a. C.L.M. Plots
- b. Magnitude vs. Log Frequency
- c. Misalignment Angles vs. Log Frequency

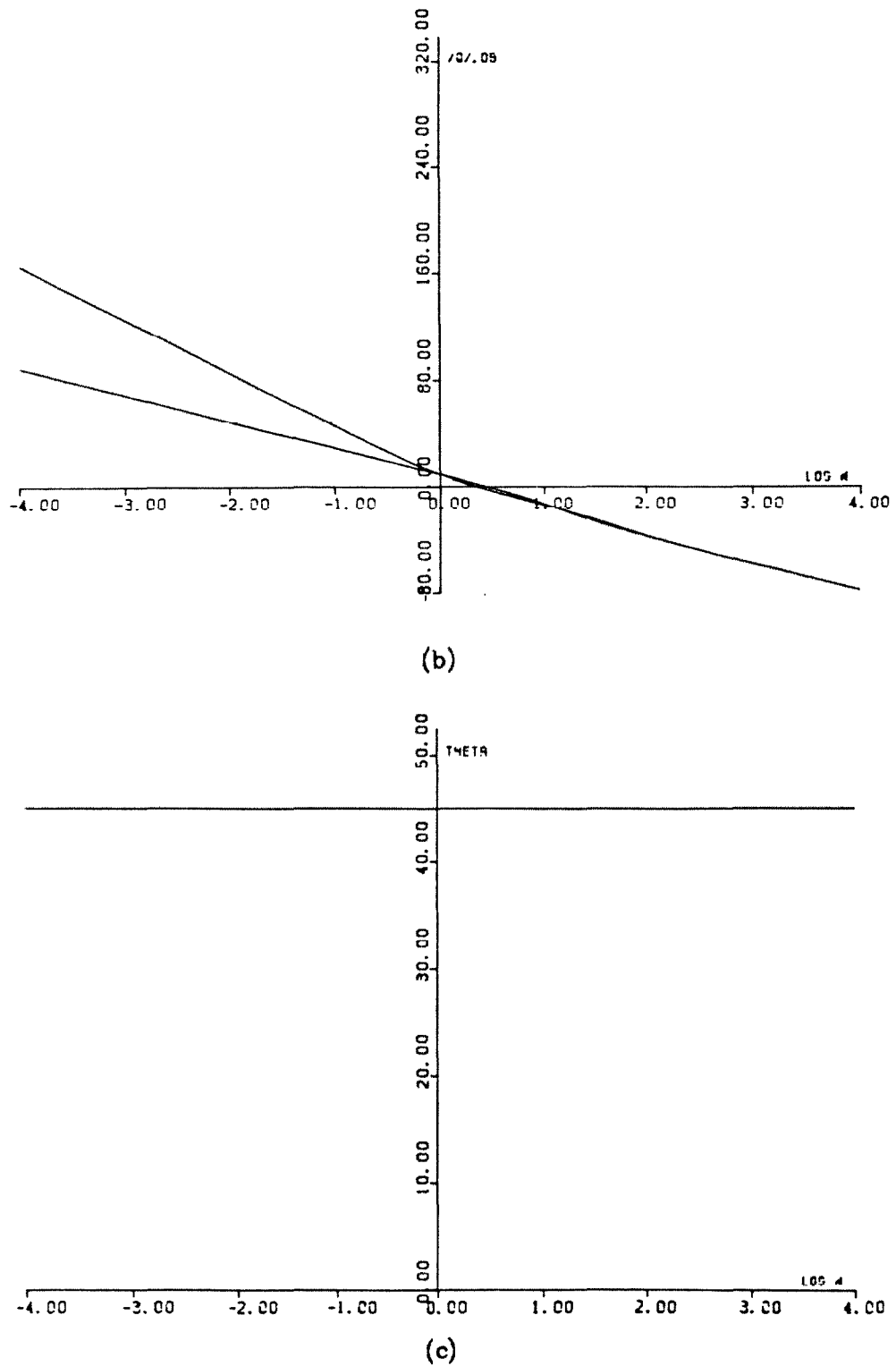


Figure 2.6-5 Continued

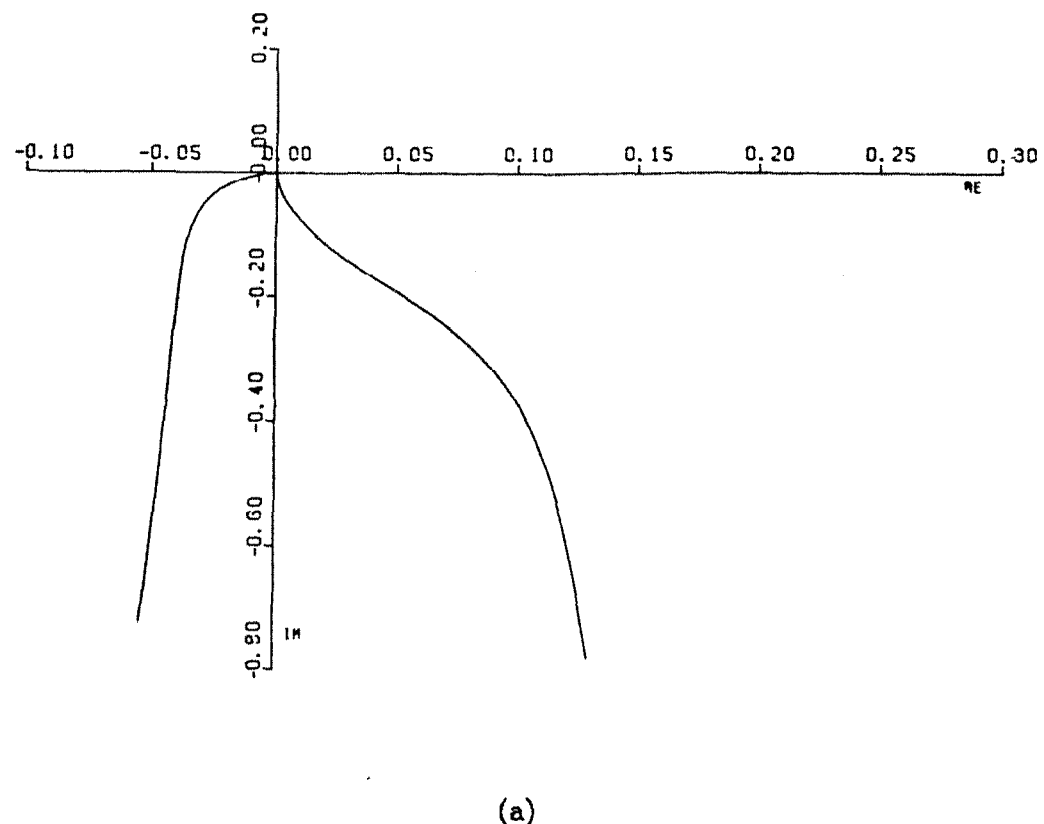
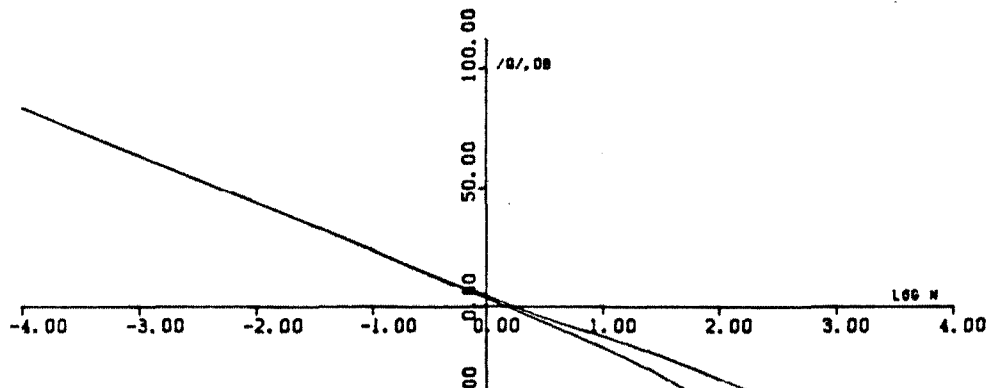
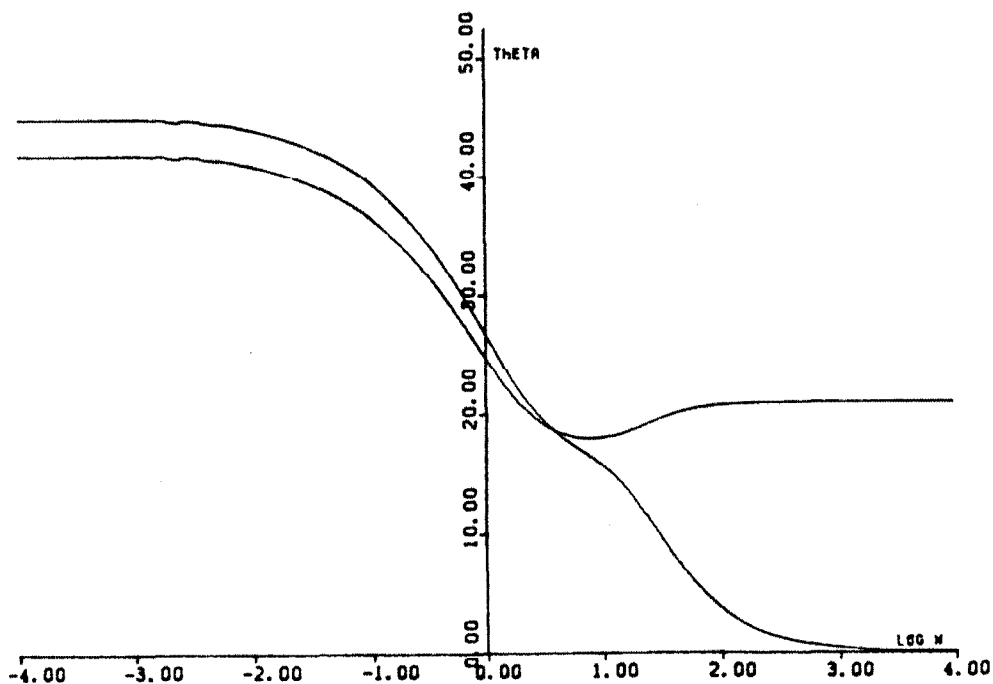


Figure 2.6-6
Characteristic Loci Diagrams for Outputs $z_1=0.4$, $z_2=0.8$
Compensator Given by Equation (2.6-12)

- a. C.L.M. Plots
- b. Magnitude vs. Log Frequency
- c. Misalignment Angles vs. Log Frequency



(b)



(c)

Figure 2.6-6 Continued

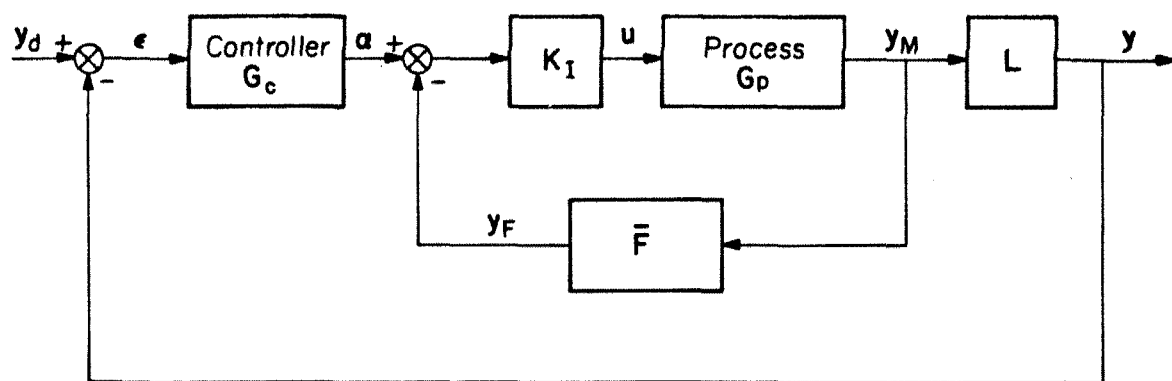
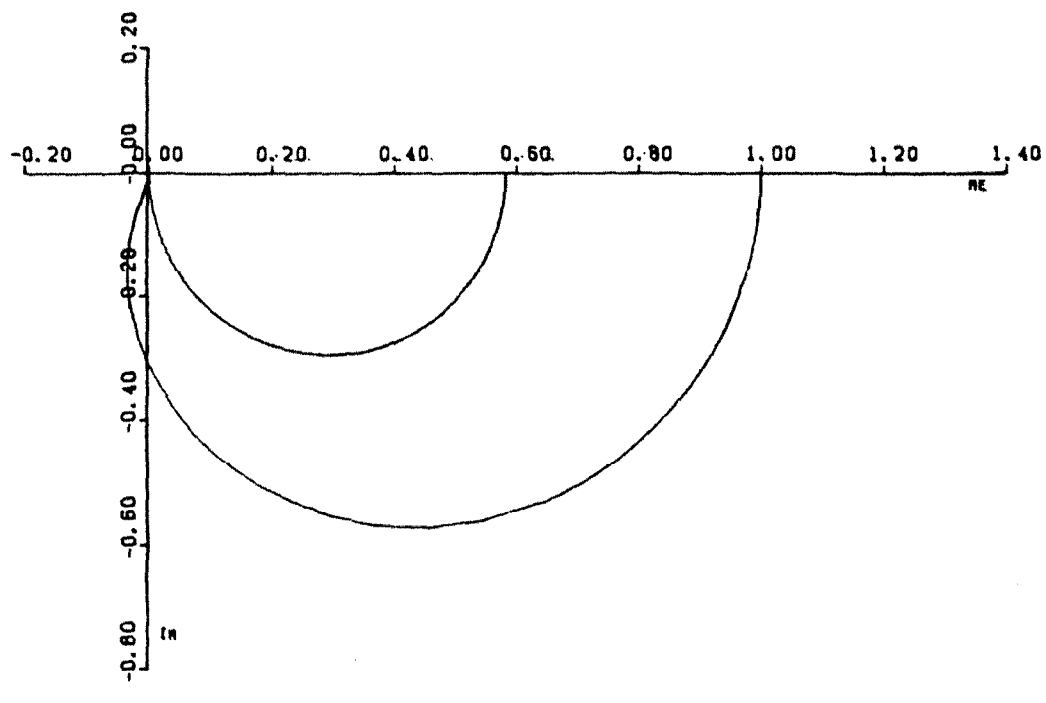


Figure 2.6-7
Inner-Loop Control Design Strategy



(a)

Figure 2.6-8
Characteristic Loci Diagrams for Outputs $z_1=0.3, z_2=0.7$
Inner-Loop Compensator F_A
No Outer-Loop Compensation

- a. C.L.M. Plots
- b. Magnitude vs. Log Frequency
- c. Misalignment Angles vs. Log Frequency

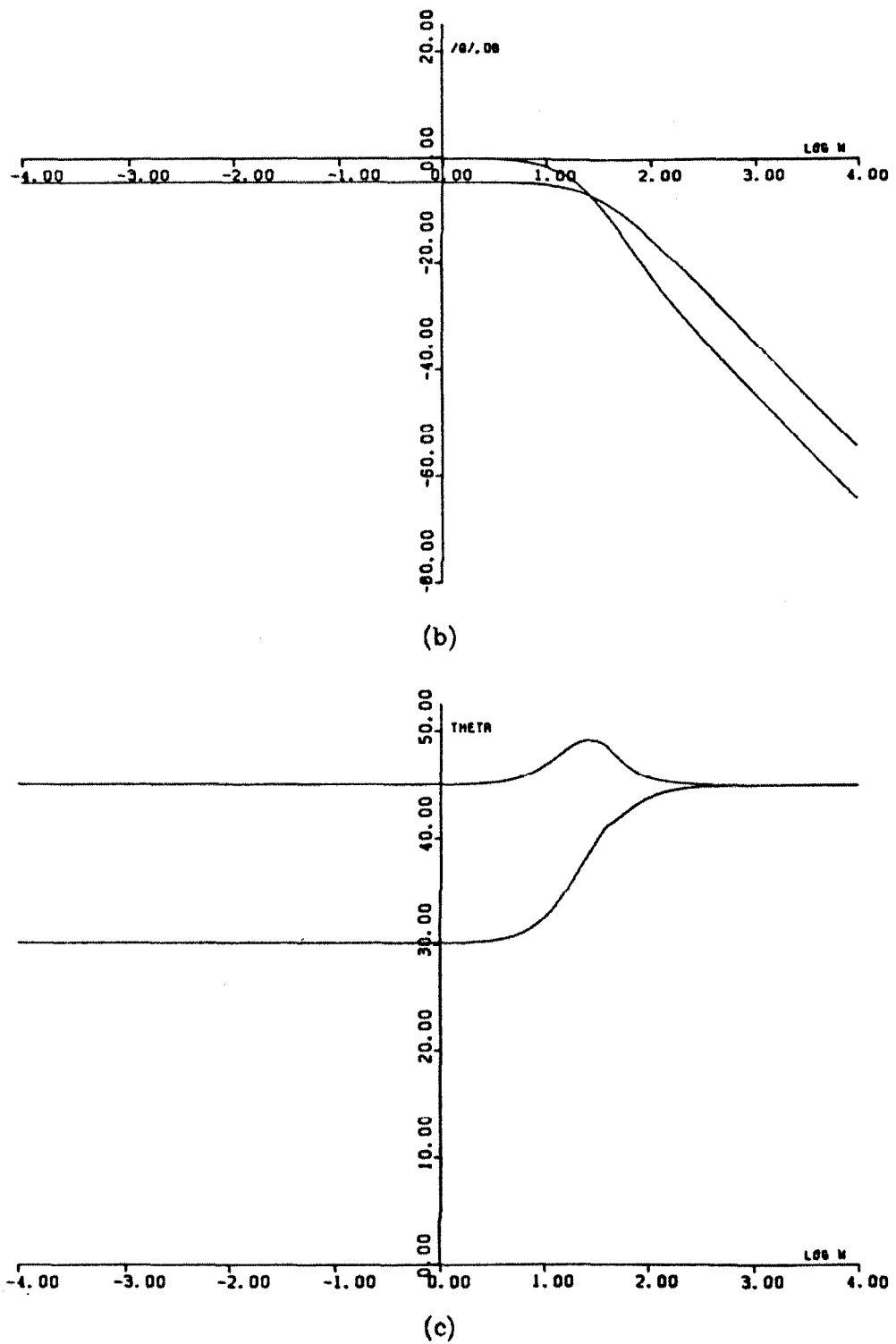
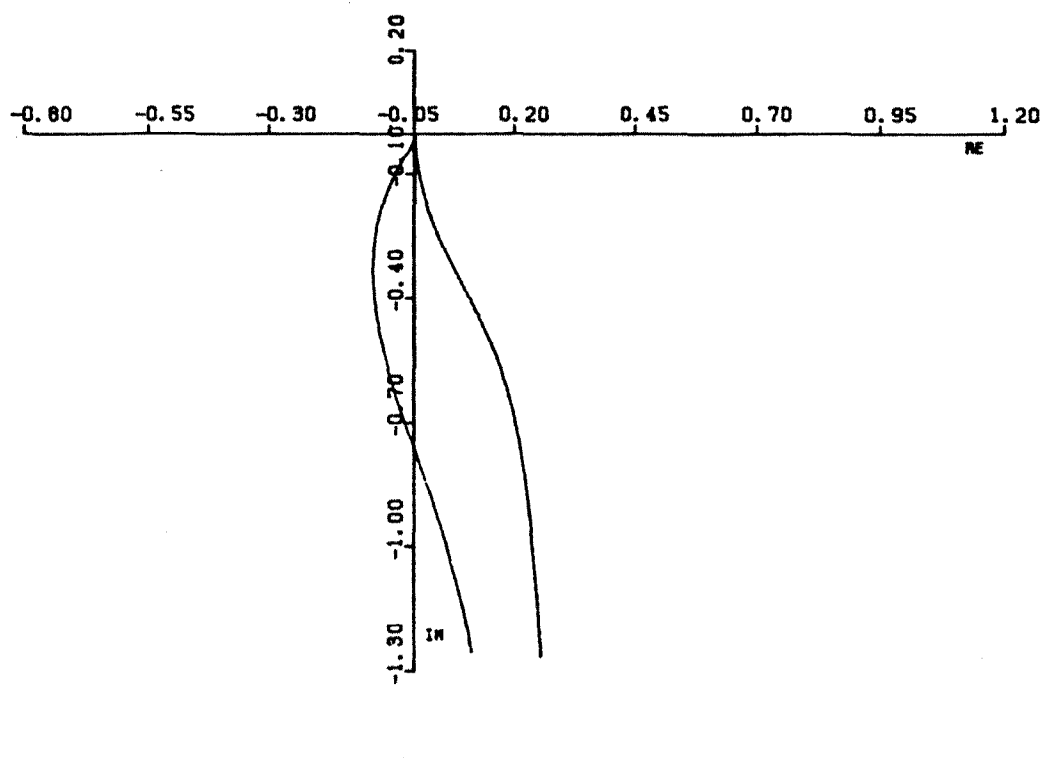


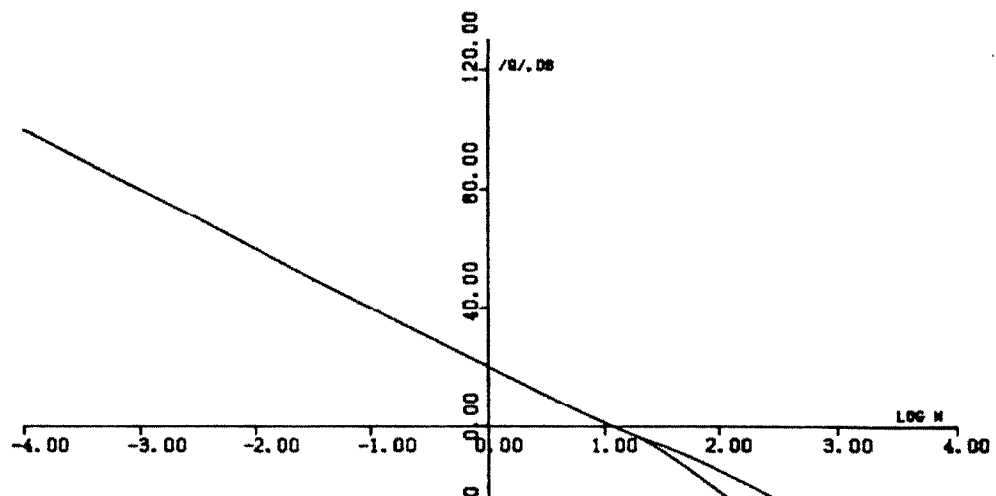
Figure 2.6-8 Continued



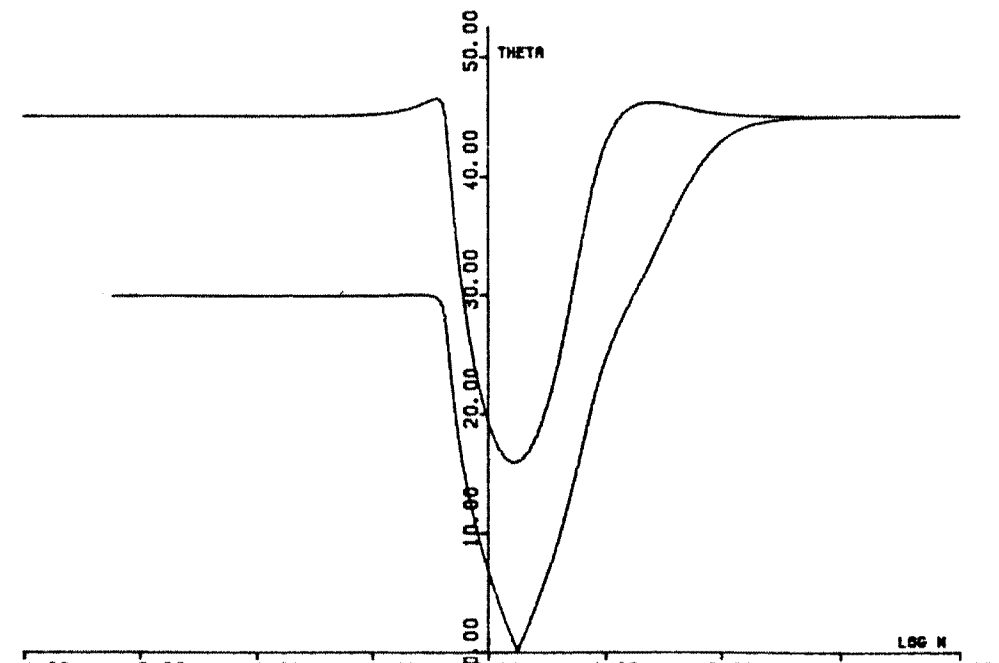
(a)

Figure 2.6-9
Characteristic Loci Diagrams for Outputs $z_1=0.3$, $z_2=0.7$
Inner-Loop Compensator F_A
Outer-Loop Compensator Given by Equation (2.6-20)

- a. C.L.M. Plots
- b. Magnitude vs. Log Frequency
- c. Misalignment Angles vs. Log Frequency



(b)



(c)

Figure 2.6-9 Continued

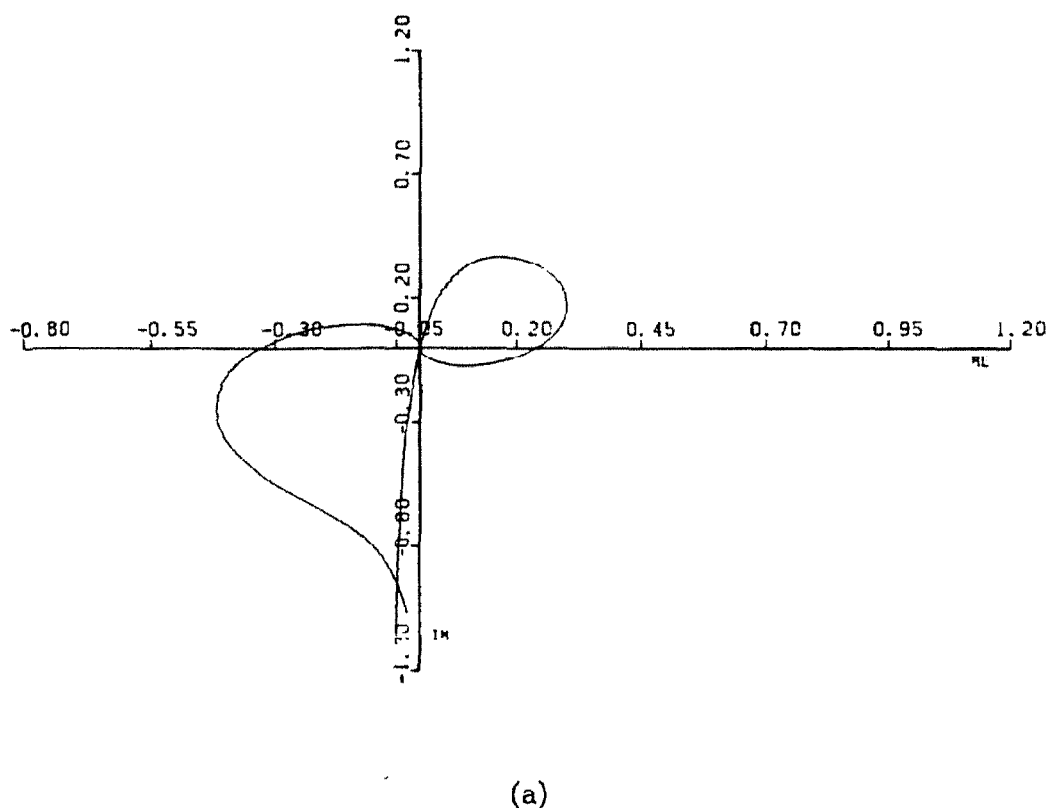


Figure 2.6-10
Characteristic Loci Diagrams for Outputs $z_1=0.4$, $z_2=0.6$
Inner-Loop Compensator \mathbf{F}_A
Outer-Loop Compensator Given by Equation (2.6-21)

- a. C.L.M. Plots
- b. Magnitude vs. Log Frequency
- c. Misalignment Angles vs. Log Frequency

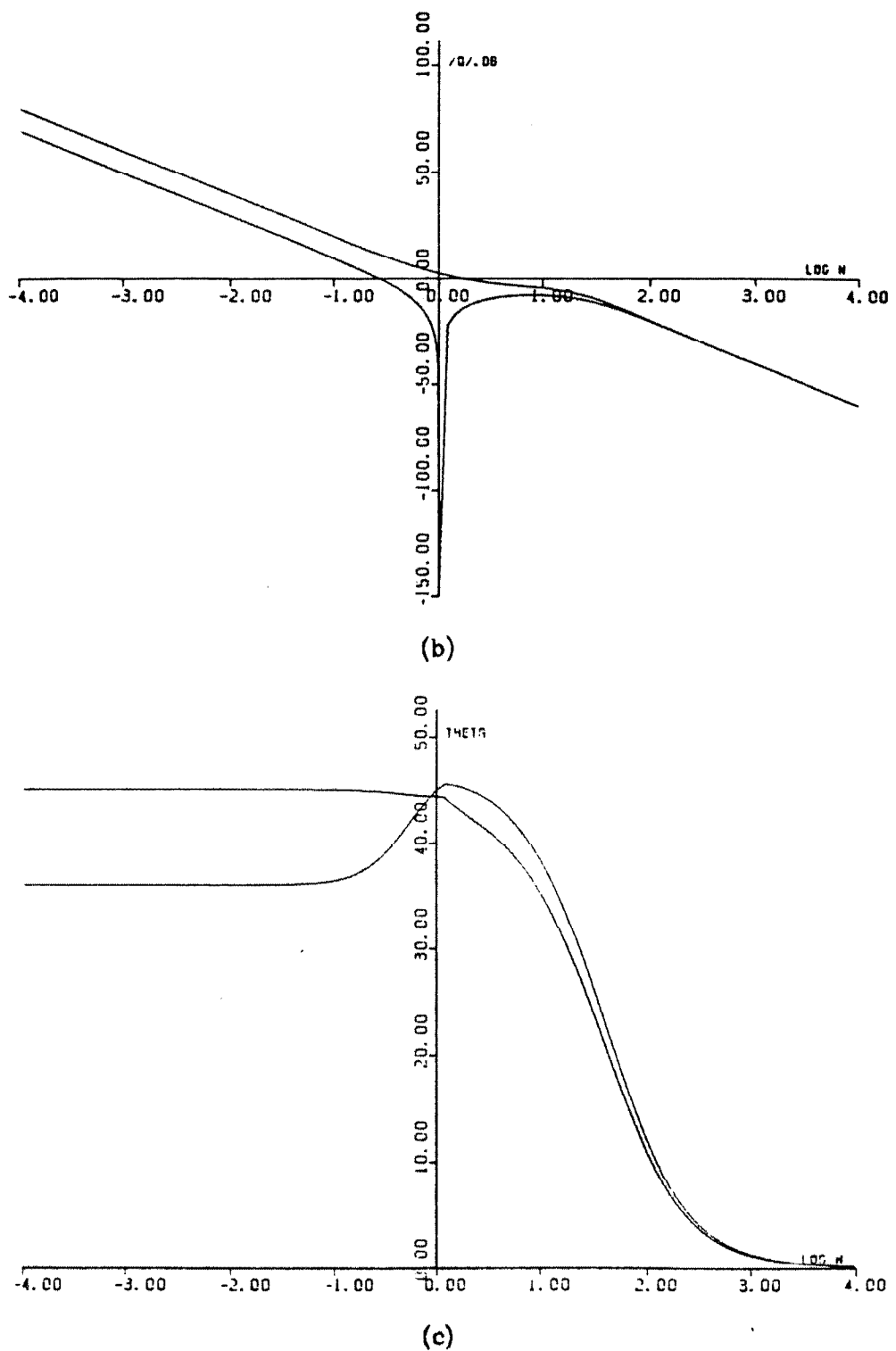


Figure 2.6-10 Continued

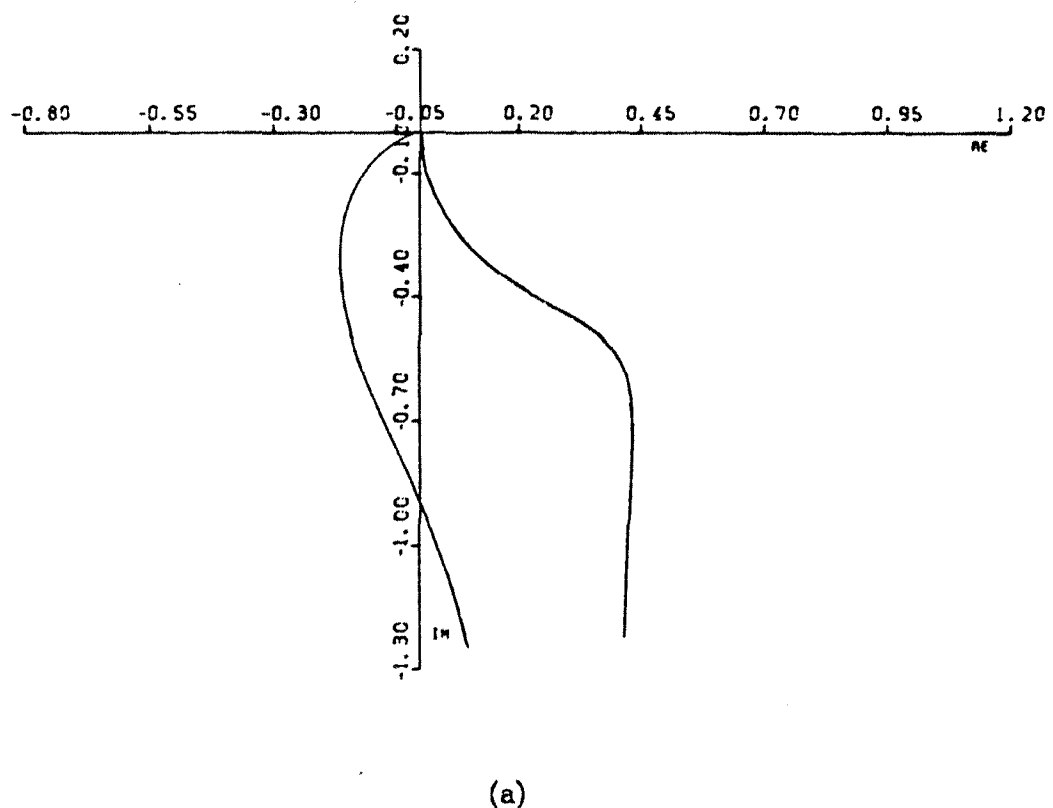


Figure 2.6-11
Characteristic Loci Diagrams for Outputs $z_1=0.4$, $z_2=0.8$
Inner-Loop Compensator \mathbf{F}_A
Outer-Loop Compensator Given by Equation (2.6-22)

- a. C.L.M. Plots
- b. Magnitude vs. Log Frequency
- c. Misalignment Angles vs. Log Frequency

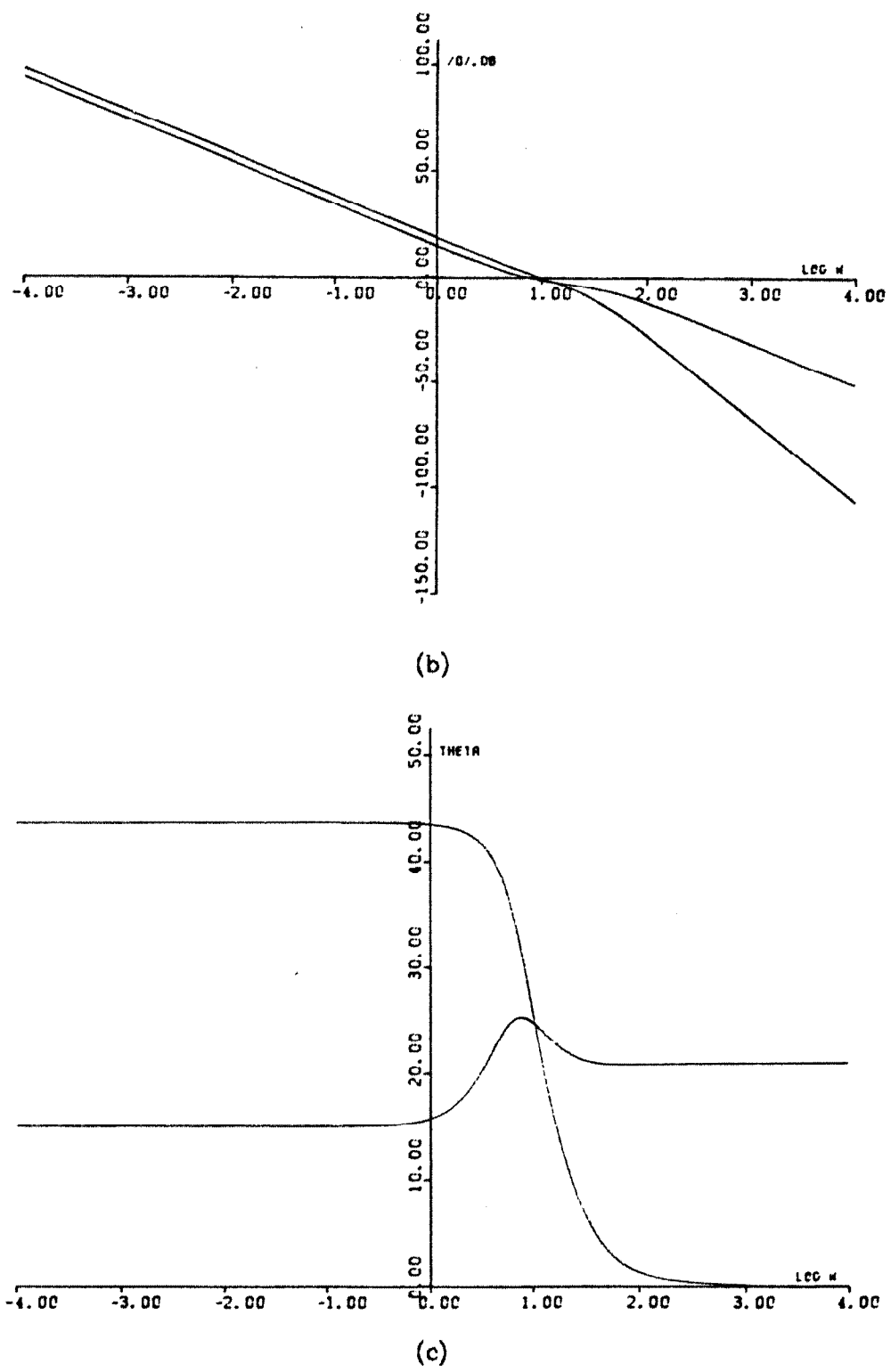


Figure 2.6-11 Continued

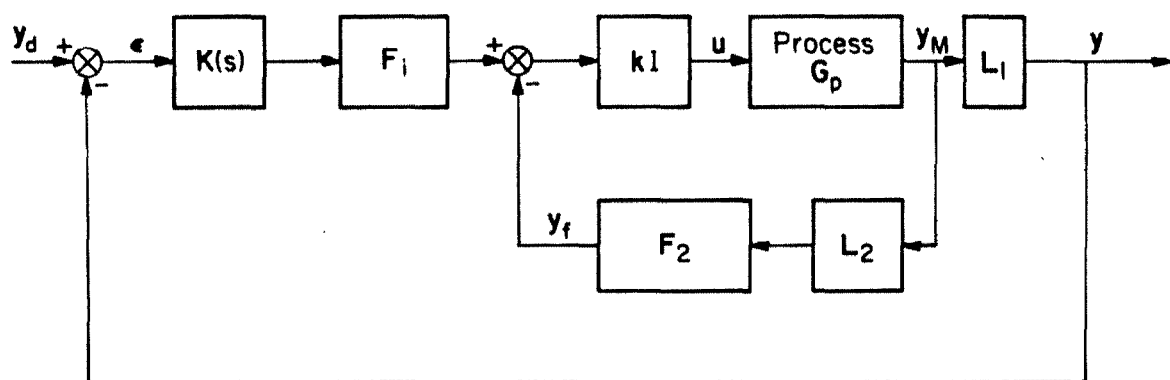


Figure 2.6-12
Alternate Inner-Loop Control Strategy

2.7 CONTROL SYSTEM PERFORMANCE

The control structure analysis for the heat conduction system was performed on the third-order, lumped model using various frequency-response techniques. These include non-interacting control methods, root-loci analysis, inverse Nyquist array, and the characteristic locus method. Additionally, the time-domain techniques of optimal and modal control were applied to both the lumped and distributed models. Since all of the schemes provide a design for the control structure, a comparison among the system responses is needed to determine the extent of improvement in the closed-loop behavior of the overall process. Additionally since most of the designs were performed using the third-order lumped model, simulations of the actual system are necessary to assess the effectiveness of the designed controllers. Computer simulations of the system responses to various set point changes were performed for the different control system structures. Simulations of the optimal control strategies were not performed, since such simulations could not easily be compared to those using frequency-response designs due to the necessity of defining the conditions of optimality. In practice, these conditions are usually selected to minimize energy costs or to increase profit margins, rather than simply to reduce response times or interaction. Responses of the heat conduction system with an optimal controller to set point changes and system disturbances are shown in literature (Betts and Citron, 1972; Sakawa, 1964).

Simulations of the heat conduction process can easily be performed using the modal or Laplace models derived in Section 2.2. Since both of these were shown to be equivalent, either model can be used; however, since the frequency-response designs were performed on the lumped, state-space representation obtained from the modal-lumping procedure, the simulations used the following results:

$$y(z,t) = \sum_{n=0}^{\infty} a_n(t) \varphi_n(z) \quad (2.7-1)$$

$$\varphi_n(z) = \begin{cases} 1.0 & n = 0 \\ \sqrt{2} \cos n\pi z & n = 1, 2, \dots \end{cases} \quad (2.7-2)$$

with $a_n(t)$ given by

$$\frac{da_n(t)}{dt} + \lambda_n a_n(t) = b_n(t) \quad (2.7-3)$$

$$a_n(0) = \int_0^1 \varphi_n(z) y_0(z) dz .$$

where $\lambda_n = n^2\pi^2$ and

$$b_n(t) = \begin{cases} u_1(t) + u_2(t) & n = 0 \\ \sqrt{2}u_1(t) + (-1)^n \sqrt{2}u_2(t) & n = 1, 2, \dots \end{cases} \quad (2.7-4)$$

Then if $y_0(z) = 0$,

$$a_n(t) = e^{-\pi_n t} \int_0^t b_n(t) e^{\pi_n t} dt . \quad (2.7-5)$$

The closed-loop response $y(z,t)$ can then be obtained by applying a discrete time analysis to the control structure and feedback information. Although the actual distributed system is described by the infinite-order model (Equation 2.7-1), simulations show that a tenth-order analysis accurately describes the actual process. Thus system responses for the various control strategies were calculated using both third- and tenth-order lumped process models.

The first control structure to be considered is proportional feedback control. Although such control may seem excessively elementary, it has the advantage of simple implementation and is the method of control recommended by several of the design techniques. For stable, diagonally dominant systems, the conclusion of an I.N.A. analysis is that no attempt should be made to reduce interactions by using more complicated compensation. Instead, large gains should be used in each feedback loop, leading to a stable system with little

interaction. The root-locus analysis, C.L.M., and I.N.A. methods show that the symmetric cases with $z_1 < 0.33$ and the unsymmetric cases (0.3,0.8) and (0.4,0.8) are diagonally dominant and stable. However since these conclusions were based on the third-order lumped model, proportional control should be attempted on the actual system.

In general, the simulations show that the exact process behaves qualitatively similarly to the third-order model and that high gain significantly reduces interaction for certain cases. However, proportional control leads to considerable offset. Even if only one of the two set points is changed, there is offset in both outputs. This is obviously a result of the steady state interactions in the system. Although steady state decoupling would seem beneficial, previous analysis showed that such compensation leads to a dependent control system. Thus although the root-loci and I.N.A. analyses showed that arbitrarily high gains would reduce interaction without leading to instability in certain cases, very high gains are often needed to sufficiently reduce the offset and interaction. Such high gains may be impractical or may lead to large overshoot, and even when steady state interactions are reduced by high gains, considerable dynamic interaction may still be present.

Thus although simple introduction of high gain into both control loops may be adequate, the control structure can often be improved by a slightly more complicated compensator. From classical theory, it is obvious that some form of integral action should be introduced to eliminate the offset. The C.L.M. determined the best compensator of the proportional-integral (PI) form to reduce interaction, to increase system integrity and accuracy, and to insure stability. However, simple analysis shows that, due to the integral action, the closed-loop responses become oscillatory. Simulations were performed using the C.L.M. designs with and without the inner loop. They show that system responses can

be improved with integral action and that appropriate design of the inner loop can eliminate the oscillations.

Obviously in a heat conduction problem, another difficulty in designing a control scheme is the lag time between a control action and the response of the outputs. For the heat conduction process, this lag leads to large overshoot when the feedback loop has high gains but will not lead to instability as long as the measurements are placed within the first and last third of the system. If the measurements are very near the edges of the system, even high gains will not lead to overshoot; whereas, high gains leads to system instability if the measurements are within the center third of the system. Thus it would seem appropriate to add some sort of anticipatory control, i.e., add some derivative action. This should reduce oscillations and keep the system stable up to higher gain. None of the common multivariable control design techniques incorporates the use of derivative action, since it is often difficult to physically incorporate into the process and can lead to difficulties for step input changes and for noisy systems. Nevertheless, the application of derivative action is considered for the (0.4,0.6) case.

Additionally, the inner-loop decoupling control strategy was considered. Theoretically, it led to a perfectly non-interacting system for several measurement locations, but the design was based on the third-order model and could be useless for the exact system. However, simulations show that it is an excellent control scheme for the heat conduction process, even when the measurement locations are not those specified by the technique. With inner-loop decoupling, it was shown that

$$\bar{G}_p = \begin{bmatrix} \frac{2\sqrt{2}c_{12}}{s+2\sqrt{2}c_{12}f_{11}} & 0 \\ 0 & \frac{2\sqrt{2}c_{12}}{s+2\sqrt{2}f_{21}(2-2\sqrt{2}c_{12})} \end{bmatrix} \quad (2.7-6)$$

with the measurement locations (0.2,0.8) or (0.6,0.4) and arbitrary f_{11} and f_{21} . Using additional proportional control with gain k_i in the i th loop, the response to a set point change is

$$y_i(t) = C_i(1 - e^{-t/\tau_i}) \quad t \geq 0 \quad (2.7-7)$$

where

$$\begin{aligned} C_i &= \frac{k_i A_i}{1+k_i A_i} & \tau_i &= \frac{\gamma_i}{1+k_i A_i} \\ A_1 &= c_{12} \frac{1}{f_{11}} & \gamma_1 &= \frac{1}{2\sqrt{2}c_{12}f_{11}} \\ A_2 &= \frac{1}{f_{21}(2-2\sqrt{2}c_{12})} & \gamma_2 &= \frac{1}{2\sqrt{2}f_{21}(2-2\sqrt{2}c_{12})} \end{aligned} \quad (2.7-8)$$

Consider the first loop. The offset is obviously $1.0 - C_1 = \frac{f_{11}}{f_{11} + k_1}$. Thus no offset occurs if $f_{11} = 0$ or as $k_1 \rightarrow \infty$. However if f_{11} is negative, $y(t)$ is unstable.¹ The simulations verify these results. The application of integral action to eliminate the offset is also considered.

Finally, perfect non-interacting compensation and steady state decoupling are considered. The latter is obviously undesirable since it leads to dependent control. Additionally, perfect compensation sacrifices closed-loop performance to non-interaction and thus leads to poor dynamic behavior. Simulations using the perfect, non-interacting compensator led to numerical difficulties.

Simulations of the closed-loop responses were performed for step changes with various measurement locations. For the system with symmetric outputs

1. Note that c_{12} is positive for the cases of interest.

and control action, both outputs respond identically to a set point change of (1,1),² and the responses for (0,1) are reversed from that for (1,0). Simulations were performed using both the third- and tenth-order process models.³

2.7.1 Case I: Measurements $z_1 = 0.2, z_2 = 0.8$

Previous analysis showed that this case is stable and diagonally dominant. Thus high gains should reduce offset, interaction, and response time. Figure 2.7-1 shows the third-order response to a step change (0,1) with feedback gains 1.0 and 50.0. Although interaction is small at a gain of 50.0, such gain is quite high, and steady state offset is still about 5%.⁴

This case was one shown to be applicable to inner-loop decoupling. Using extra measurements and an appropriate inner-loop compensator, the third-order model was shown to reduce to a completely non-interacting system for which classical methods could be used to complete the design. Third-order simulations (Figure 2.7-2) verify the results predicted from the model. Interaction is completely eliminated and the response is non-oscillatory. Additionally with $f_{11} = f_{21} = 0$, proportional control does not result in steady state offset. As f_{11} and f_{21} increase, offset increases, and as the gain increases, offset decreases. Negative values for f_{11} and f_{21} lead to instability.

Even the tenth-order model acts qualitatively as expected. Simulations (Figure 2.7-3) show that high gain leads to overshoot and eventually to instability. Nevertheless for moderate gain, there is only a very small amount of interaction. Thus even though the gain is somewhat limited, offset can be eliminated and interactions greatly reduced while still having excellent response

2. This notation means that the set points are $y_{d_1} = 1.0$ and $y_{d_2} = 1.0$ for $t \geq 0$ with $y_{d_1} = y_{d_2} = 0.0$ for $t < 0$.

3. Note that the tenth-order model is taken to represent the exact process.

4. In comparing the simulations, note that the time axes vary significantly.

time. For example, with a gain of 20.0, the response time is about 0.08 and there is negligible interaction. With simple proportional control, even with a gain of 50.0, the response time is 50% more, while interaction and offset are significant. Finally, integral action can be added but is not necessary since $f_{11} = f_{21} = 0$ leads to a response with no offset. Also as shown in Figure 2.7-3, offset increases if f_{11} and f_{21} are greater than zero.

2.7.2 Case II: Measurements $z_1 = 0.3, z_2 = 0.7$

This case is similar to the previous in that high gains should reduce response times, offset, and interaction, without leading to instability. The simulations (Figures 2.7-4 and 2.7-5) for proportional control behave as expected. For low gains, considerable interaction and offset are present along with long response times. For high gains, interaction is reduced and the system becomes oscillatory. However even for very high gains, the overshoot is only about 10% with a large decay ratio, and thus the response times are short. Additionally, the simulations show that the qualitative behavior of the responses for the tenth-order system are identical to those for the third-order model, though some qualitative differences are apparent at high gains.

Figure 2.7-6 shows the responses of the system with the addition of the compensator that was designed using the characteristic locus method. At a gain of 1.0, the third- and tenth-order responses are similar (only the tenth-order responses are shown). The addition of the compensator has eliminated offset and steady state interactions while adding some overshoot. However dynamic interactions are still significant for $t < 3.2$. Increasing the gain reduces the response times and interaction but increases the overshoot. At the extremely high gain of 200.0, the tenth-order model (not shown) shows that the system is

unstable, although the third-order model shows a good response. Nevertheless, short response times and little interaction can be obtained at much lower gain.

The C.L.M. procedure predicted a dramatic improvement with the addition of an inner loop. Third- and tenth-order simulations were performed using the design obtained in Section 2.4. The responses for the system with an inner loop and with only proportional control in the outer loop showed considerable offset even for step changes of (1,1). However, the responses (Figure 2.7-7) for the system with the inner-loop compensator F_A and the designed outer-loop compensator G_c given by Equation 2.6-20 show tremendous improvement. Although the (0,1) and (1,0) step changes no longer give identical results, the responses are so similar that only one is shown. For gains below 8.0, both the third- and tenth-order models show no oscillation (again only the tenth-order responses are shown). The third-order model also shows an elimination of not only the offset but almost all the interaction. Even though the actual system is unstable for very high gain, the inner-loop design is excellent, since even at a relatively low overall gain of 20.0,⁵ oscillations and interaction are minor and response times are short.

2.7.3 Case III: Measurements $z_1 = 0.4$, $z_2 = 0.6$

All of the design techniques showed that this case becomes unstable at high gain (above ~ 32.0). The responses (Figure 2.7-8) verify these expectations. For low gain, the system has high interaction, large offset and long response times. As the gain increases, the oscillations increase while the response times and offset decrease. Nevertheless, interactions remain high at short times— $t < 0.5$. Slight differences between the third- and tenth-order models are apparent at

5. The overall gain equals outer-loop gain—2.5—times the inner-loop gain—8.0.

higher gain. Although the third-order system is unstable at a gain of 35.0, the actual system remains stable up to a higher gain (~45.0).

Both the I.N.A. technique and C.L.M. showed that the only compensator capable of insuring system stability at high gain is a dependent controller. However as previously discussed, the use of such a controller has serious disadvantages. For a set point change of (0,1) or for unsymmetric dependent control with (1,1), the closed-loop behavior shows very high offset (Figure 2.7-9), and for symmetric dependent control, a set point change of (1,1) has no effect on the system--the output remains unchanged.

Even by squaring down extra measurements through an inner loop, stability cannot be assured at high gain. However with the inner- and outer-loop controllers that were designed using the C.L.M., the responses (Figure 2.7-10) at moderate gain have no offset, but at the expense of increased oscillation and response time. High overall gain (> 40.0) does indeed lead to instability.

Thus a good design has not been found for the heat conduction system with measurements at (0.4,0.6). Obviously good feedback information is not available due to excessive transportation lag. Thus a PD or PID controller may be useful. If a slight amount of derivative action is added, both the third-order model at a gain of 35.0 and the actual system at a gain of 50.0 are stable (Figure 2.7-11). The system has a very short response time but shows some slight offset. By further introduction of some integral action (PID control), the offset can be eliminated. At higher gains, it becomes necessary to increase the derivative action to insure stability; however, high gains and increased derivative action cause numerical difficulties due to a small downward oscillation in the initial response ($t < 0.2$). Since such a downward 'blip' is not physically explainable, it must be a consequence of the model reduction. This is proven in Figure 2.7-

12. The region $t < 0.064$ is enlarged, and it is obvious that the "blip" gets smaller as the order of the model is increased. Finally, Figure 2.7-12 shows the response with derivative action with the "blip" artificially removed. This response is physically reasonable due to the transportation lag between the inputs and the outputs. However, although this technique allows higher gain, derivative action is still not advisable due to problems with implementation and process disturbances.

Finally the case (0.6,0.4) was shown to be applicable to inner-loop decoupling. Thus with the measurements at (0.4,0.6), a permutation matrix could be used to convert the system to that necessary for use of this technique. However, the tenth-order response for the system with the permutation matrix and inner-loop decoupling shows instability at moderate gain due to the excessive transportation lag with the outputs at a distance of 0.6 from the inputs. The inner-loop structure designed for the (0.6,0.4) case is applied directly to the (0.4,0.6) case. Surprisingly the results (Figure 2.7-13) are excellent! Although the interactions are not completely eliminated, they are small and may be reduced further by improving the outer-loop design with the C.L.M.. The choice $f_{11} = f_{21} = 0$ eliminates offset, and even moderate gain leads to little interaction and small response time. Unfortunately, the system is still unstable at high gains.

2.7.4 Case IV: Measurements $z_1 = 0.4, z_2 = 0.8$

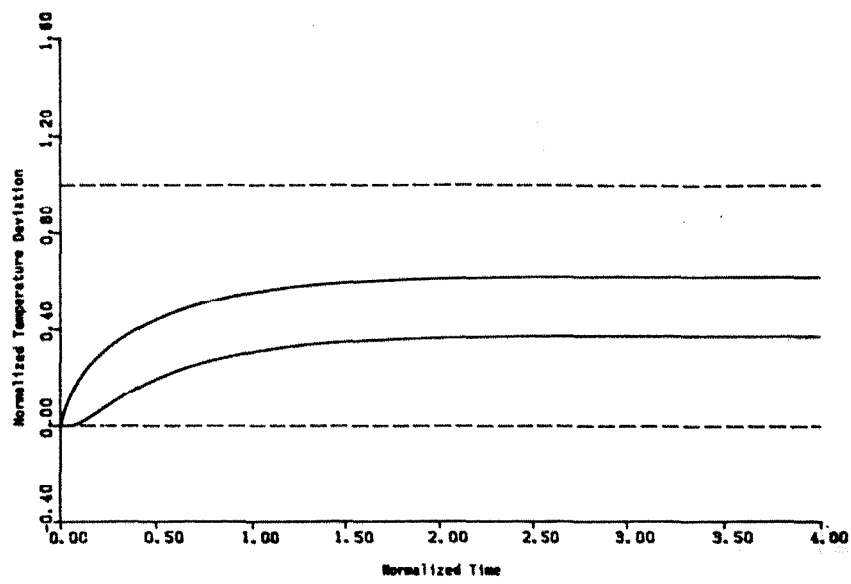
This case gives further insight into the system since the outputs are not symmetric and since the root-loci have vertical asymptotes for the third-order model. Due to the lack of symmetry, simulations are considered for the set point changes (1,1), (1,0), and (0,1). As expected, the responses of the two out-

puts are not identical, and the measurement at $z_2 = 0.8$ responds faster than that at $z_1 = 0.4$. Although the third- and tenth-order models show similar responses for low gain, they differ considerably at higher gains. The actual case shows much worse behavior than the third-order model predicts. For proportional control (Figure 2.7-14), the offset is reduced as the gain increases. However even at a gain of 50.0, the responses are quite bad. The actual system shows a high degree of oscillation and a long response time. The output at $z_2 = 0.8$ has an overshoot of 30%, while the other has an overshoot of 80% for a set point change (1,1). The effects of interaction are clearly illustrated by the set point change (0,1). The measurement at z_2 , whose set point was changed, has a fast response while the other output, whose set point remained unchanged shows significant oscillation and long response time. If instead the set point change (1,0) is considered, the measurement at z_2 is only slightly affected. Obviously the output at $z_2 = 0.8$ is much more stable than that at z_1 .

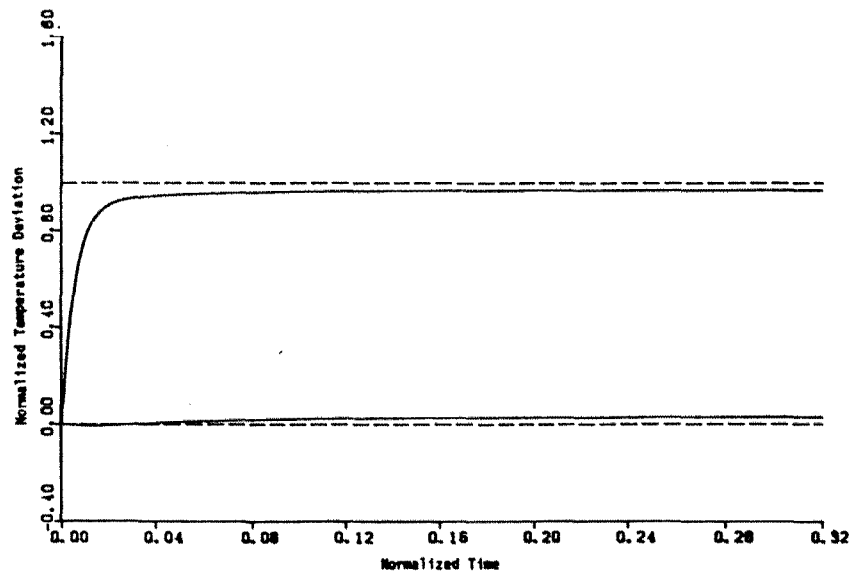
For a gain of 100.0, the third-order response is stable and shows shorter response times. However for all of the set point changes, the response of the output at z_1 is unstable while that at z_2 remains stable. Even when only the set point at z_2 is changed, the interactions cause the other output to become unstable. The instability of the tenth-order model can be explained through a root-locus analysis, since the tenth-order model has additional poles and zeros which can cause the vertical asymptotes to curve into the right half plane.

Since high gains are desired to reduce offset and interaction and since very high gains lead to an unstable response at z_1 , it seems best to impose high gains in the feedback loop on z_2 and moderate gains on the output at z_1 . Figure 2.7-15 shows the responses with gains 25.0 and 100.0 imposed on the two outputs. The output at z_2 responds quickly and is only slightly affected by interaction, while the other responds more slowly.

The precompensator that was designed using the C.L.M. is then added to the system. The C.L.M. showed that the compensator should reduce interaction and lead to a stable system with high accuracy and integrity. The responses (Figure 2.7-16) show that though offset has been eliminated, dynamic interaction is only slightly reduced. Again it is evident that the output at z_1 has too much transportation lag. Its response is highly oscillatory and becomes unstable at very high gains, even though the third-order model predicts stability. Thus although the C.L.M. leads to a compensator that reduces interaction, the instability problem is still present. As in the (0.4,0.6) case, some derivative action may be useful if very high gains are desirable. Finally even if an inner loop is added, the C.L.M. showed that little improvement is obtainable. This is verified using system simulations.



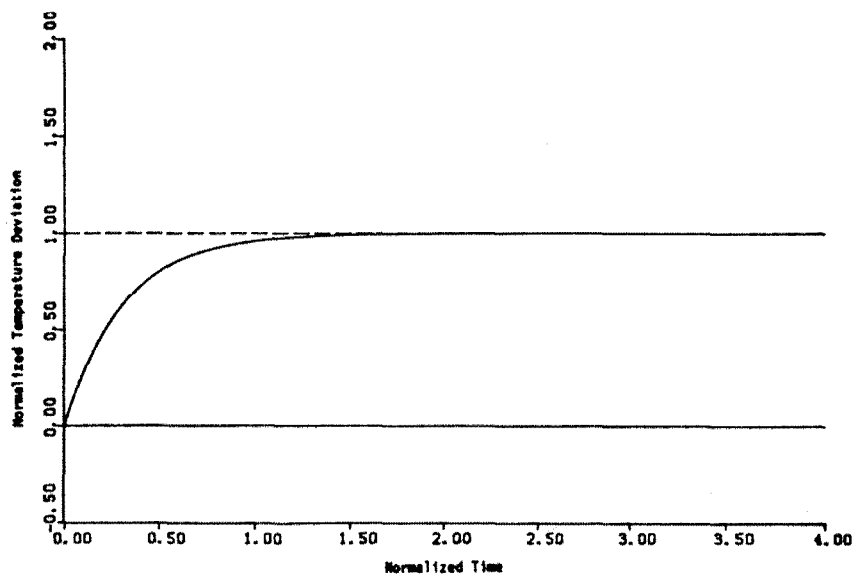
(a)



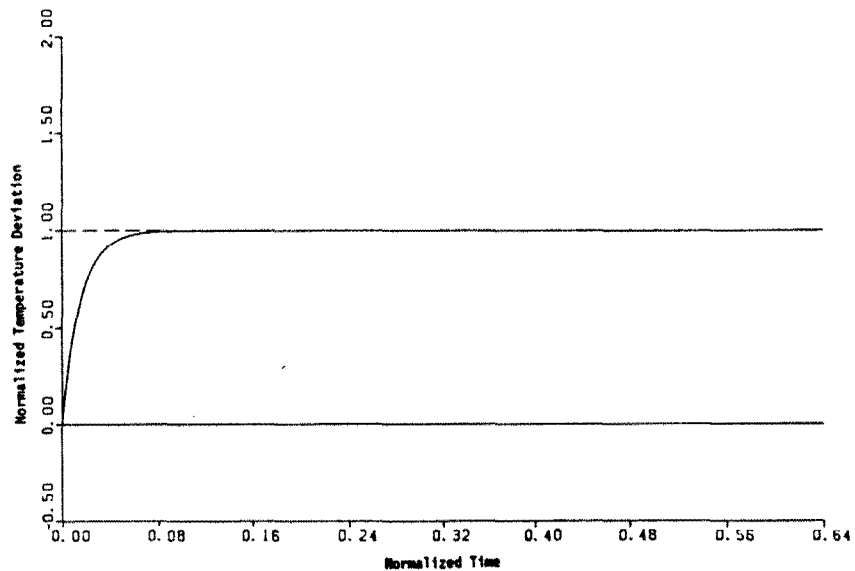
(b)

Figure 2.7-1
Third-Order Simulations with Outputs $z_1=0.2$, $z_2=0.8$
Set Point Change (0,1)

a. Gain = 1.0 b. Gain = 50.0



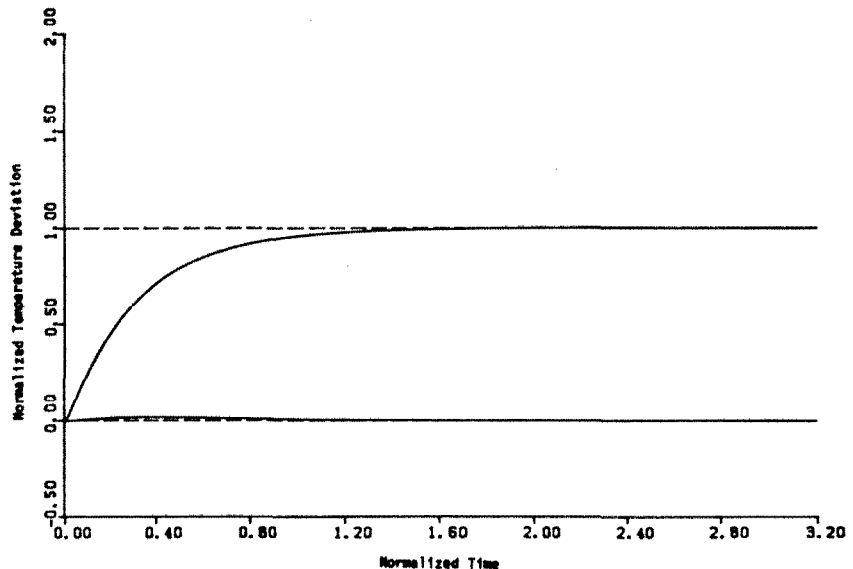
(a)



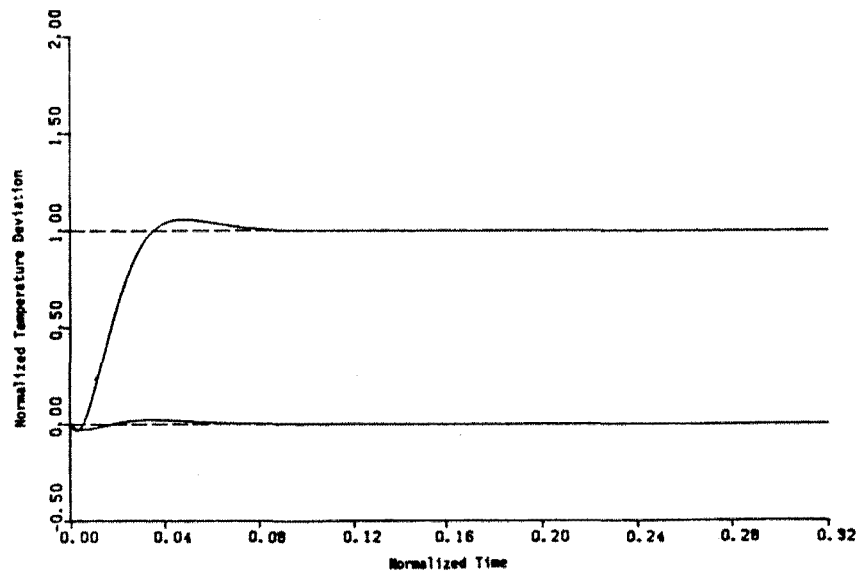
(b)

Figure 2.7-2
Third-Order Simulations with Outputs $z_1=0.2$, $z_2=0.8$
Inner-Loop Decoupling with $f_{11} = f_{21} = 0$
Set Point Change (0,1)

a. Feedback Gain = 1.0 b. Feedback Gain = 20.0



(a)

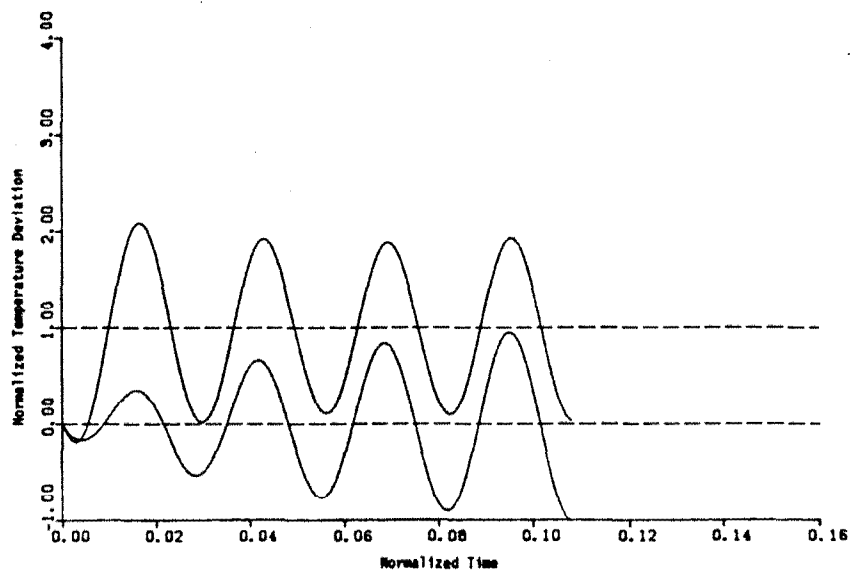


(b)

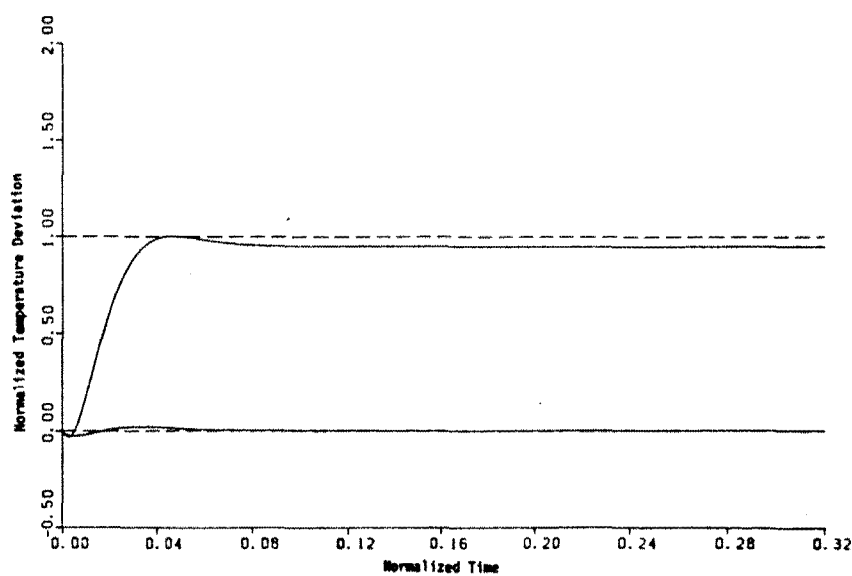
Figure 2.7-3
Tenth-Order Simulations with Outputs $z_1=0.2$, $z_2=0.8$
Inner-Loop Decoupling
Set Point Change (0,1)

$f_{11}=f_{21}=0$: a. Gain = 1.0 b. Gain = 20.0 c. Gain = 100.0

$f_{11}=f_{21}=1$: d. Gain = 20.0

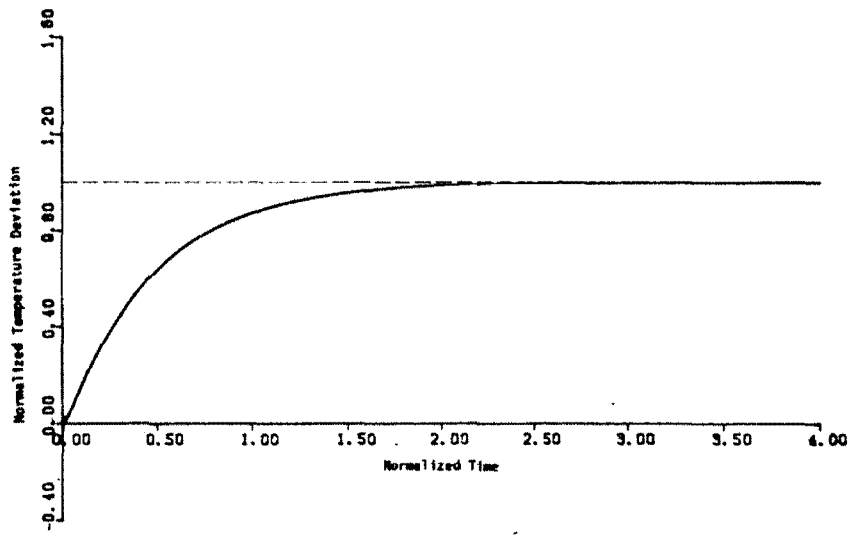


(c)

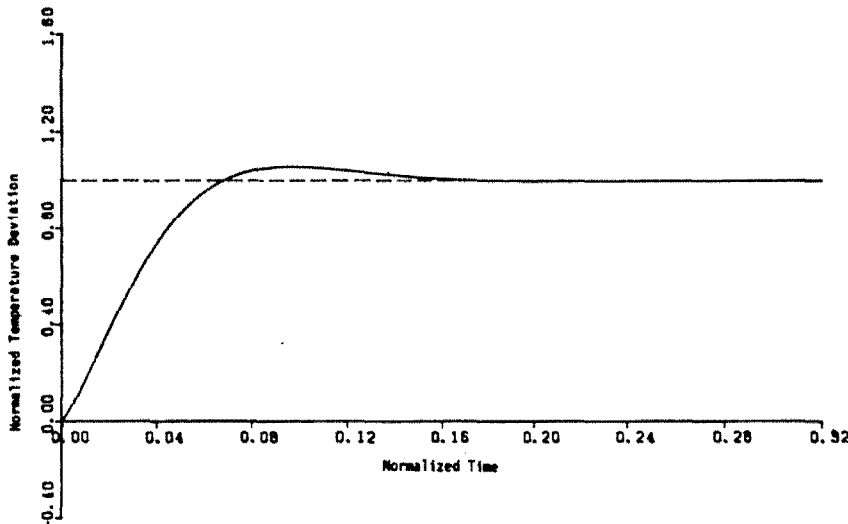


(d)

Figure 2.7-3 Continued



(a)

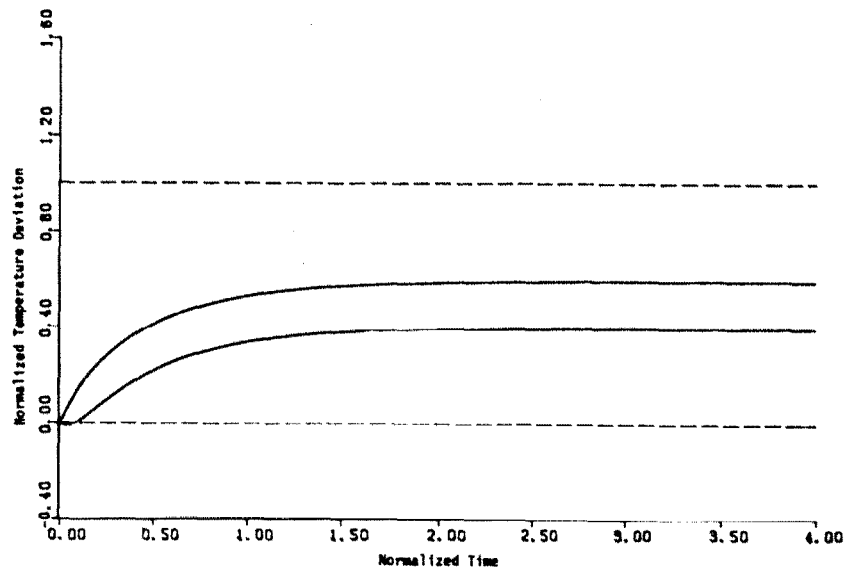


(b)

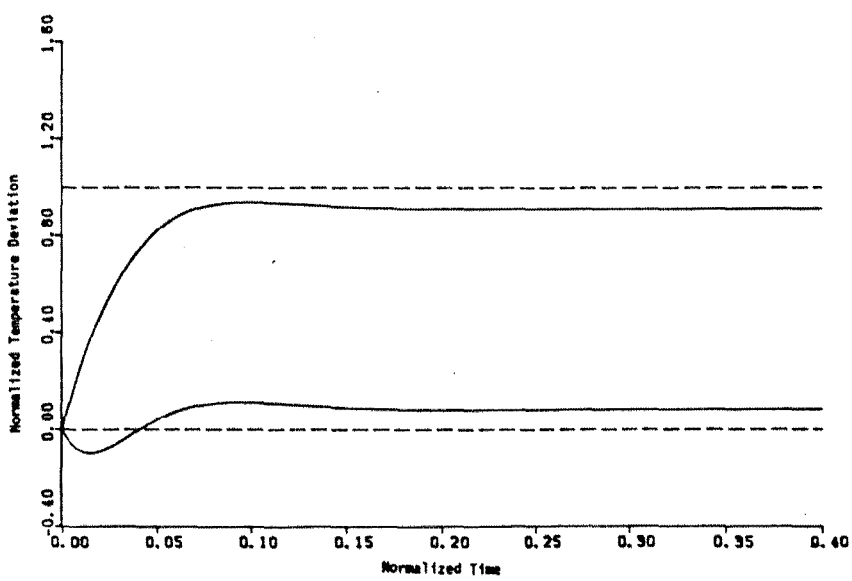
Figure 2.7-4
Third-Order Simulations with Outputs $z_1=0.3$, $z_2=0.7$

Set Point Change (1,1): a. Gain = 1.0 b. Gain = 20.0

Set Point Change (0,1): c. Gain = 1.0 d. Gain = 20.0

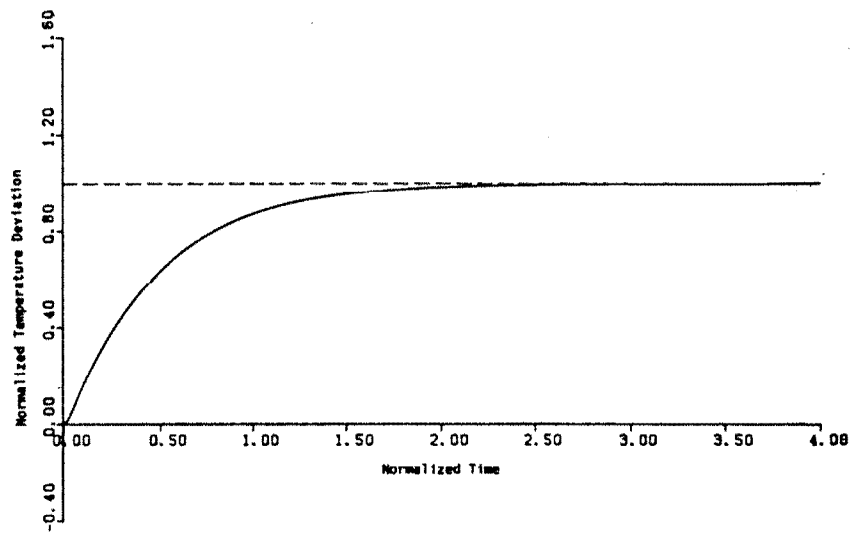


(c)

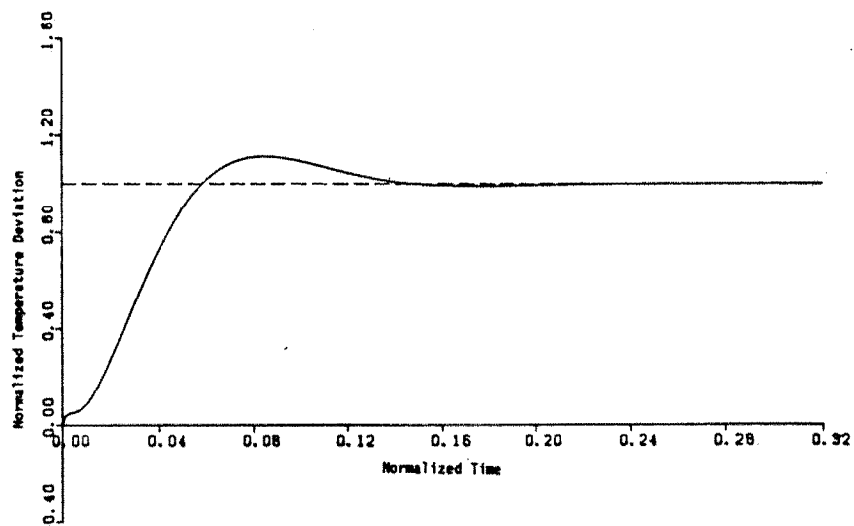


(d)

Figure 2.7-4 Continued



(a)

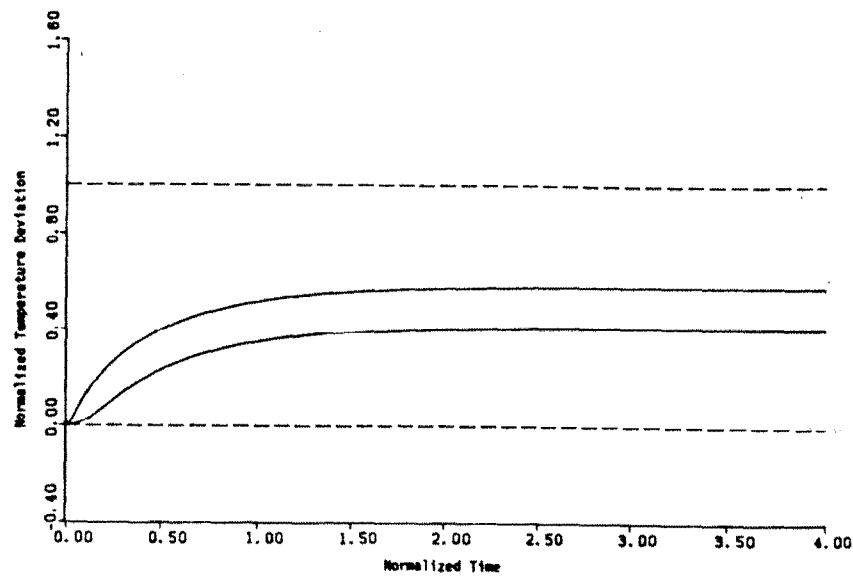


(b)

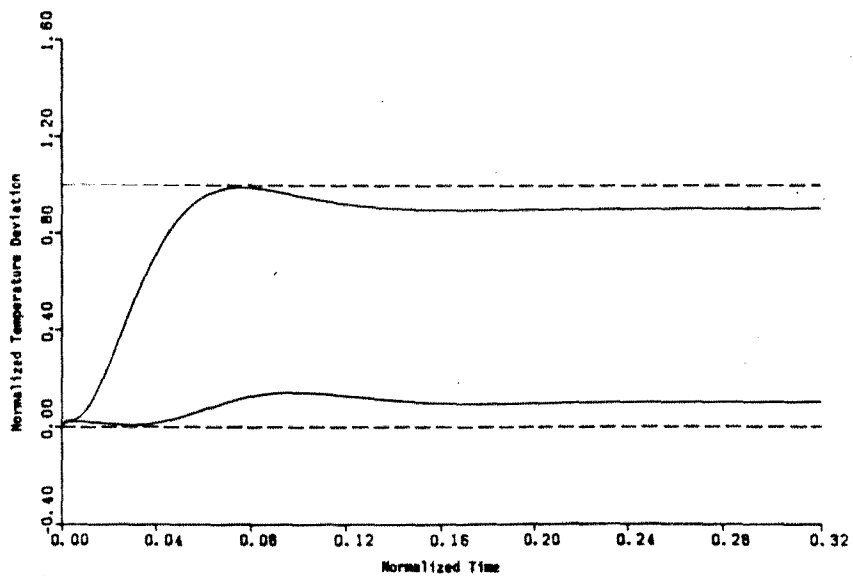
Figure 2.7-5
Tenth-Order Simulations with Outputs $z_1=0.3$, $z_2=0.7$

Set Point Change (1,1): a. Gain = 1.0 b. Gain = 20.0

Set Point Change (0,1): c. Gain = 1.0 d. Gain = 20.0

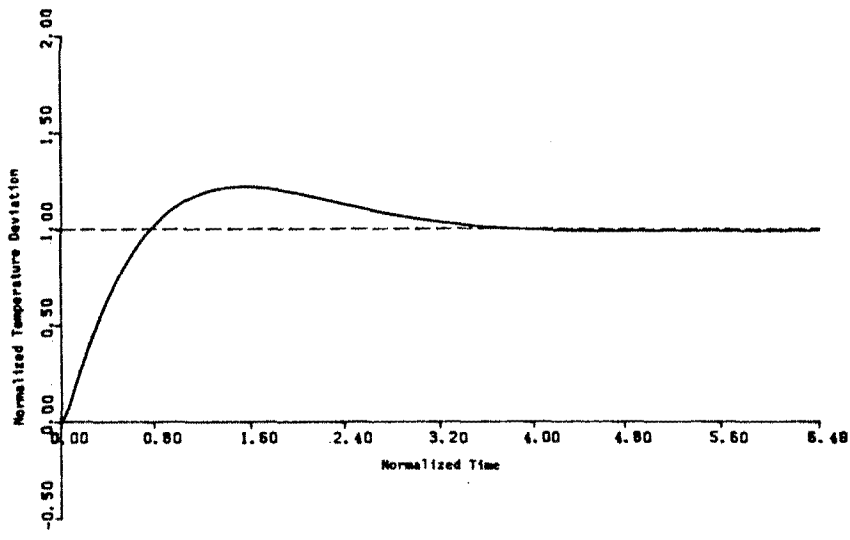


(c)

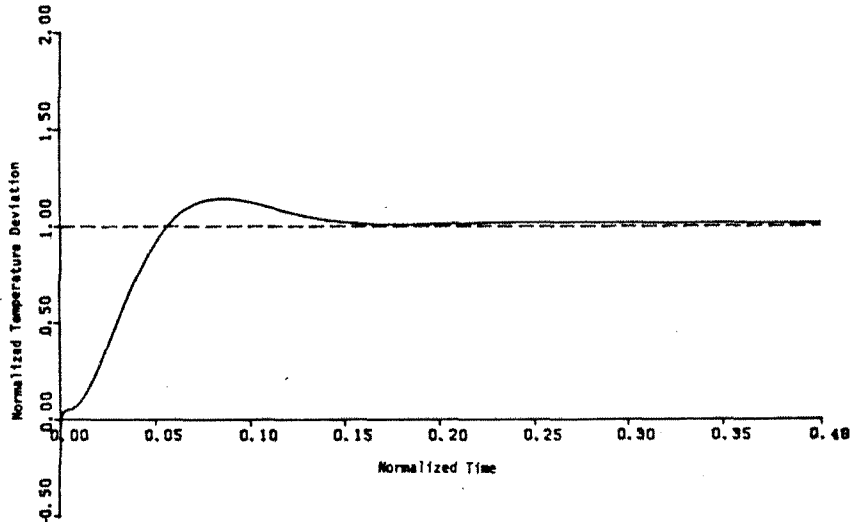


(d)

Figure 2.7-5 Continued



(a)

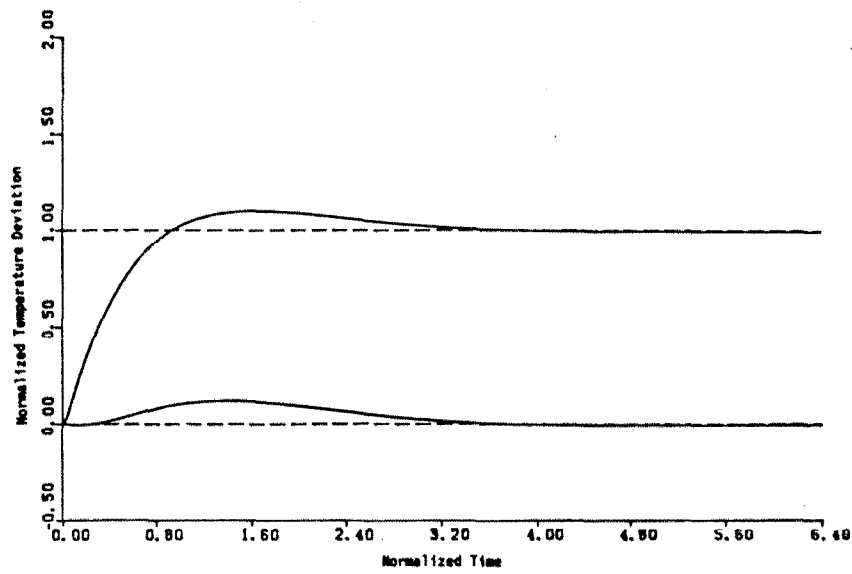


(b)

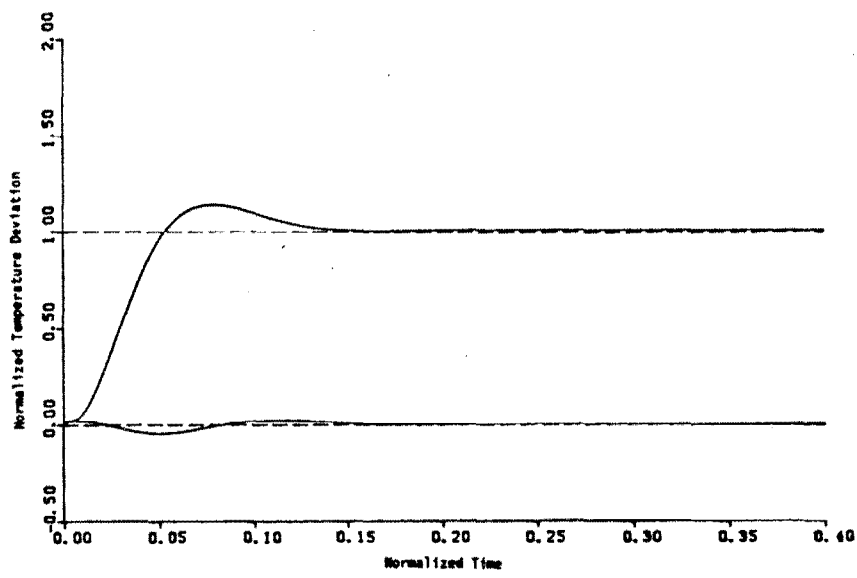
Figure 2.7-6
Tenth-Order Simulations with Outputs $z_1=0.3$, $z_2=0.7$
C.L.M. Compensation Defined by Equation (2.6-10)

Set Point Change (1,1): a. Gain = 1.0 b. Gain = 20.0

Set Point Change (0,1): c. Gain = 1.0 d. Gain = 20.0

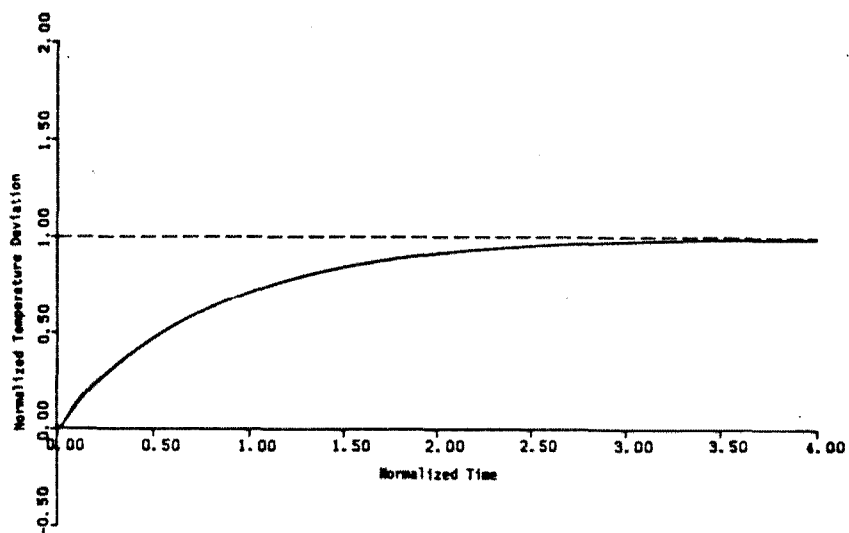


(c)

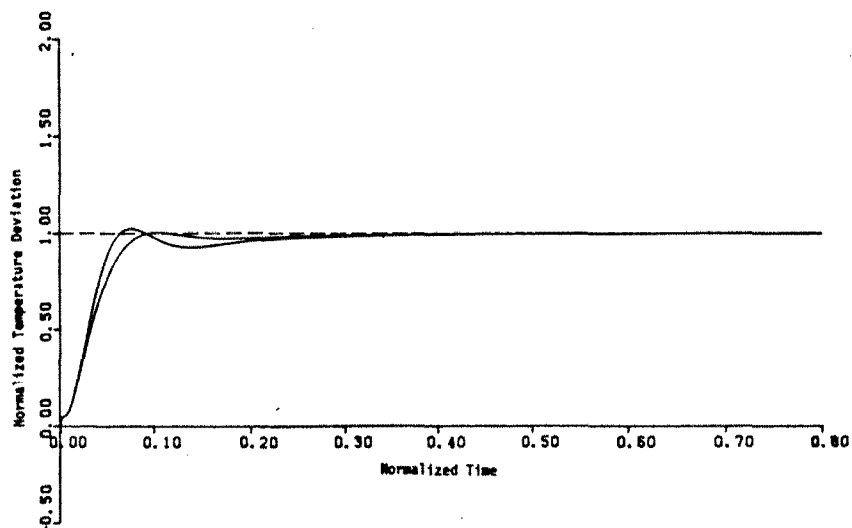


(d)

Figure 2.7-6 Continued



(a)

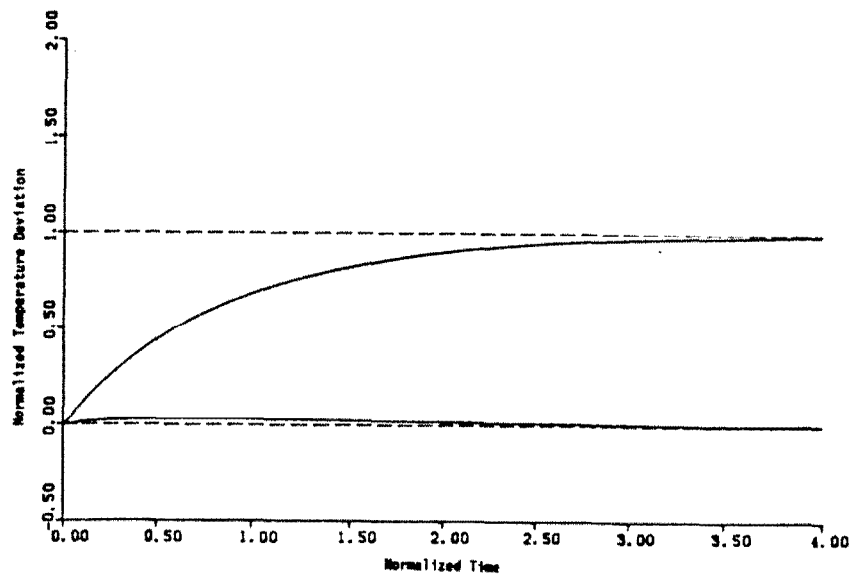


(b)

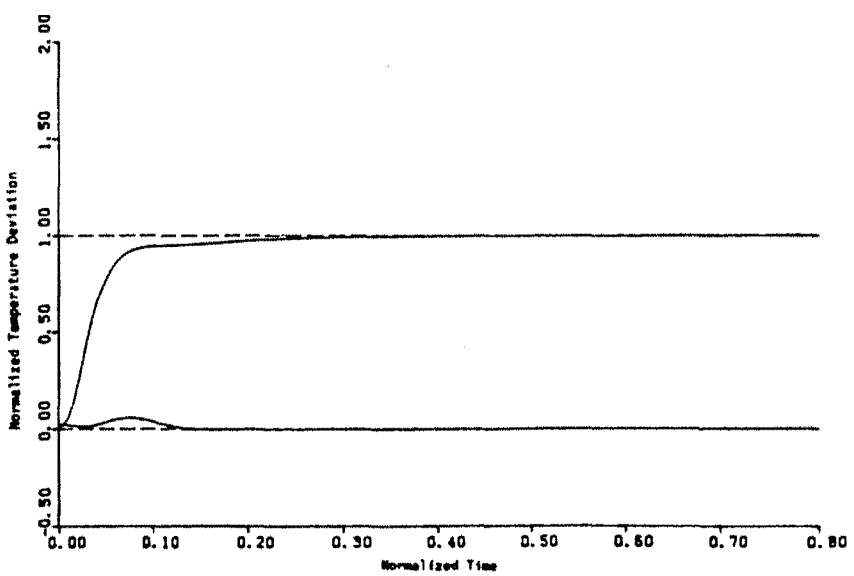
Figure 2.7-7
Tenth-Order Simulations with Outputs $z_1=0.3$, $z_2=0.7$
Outer-Loop C.L.M. Compensator Defined by Equation (2.6-20)
Inner-Loop Compensator F_A

Set Point Change (1,1): a. Overall Gain = 1.0 b. Overall Gain = 20.0

Set Point Change (0,1): c. Overall Gain = 1.0 d. Overall Gain = 20.0

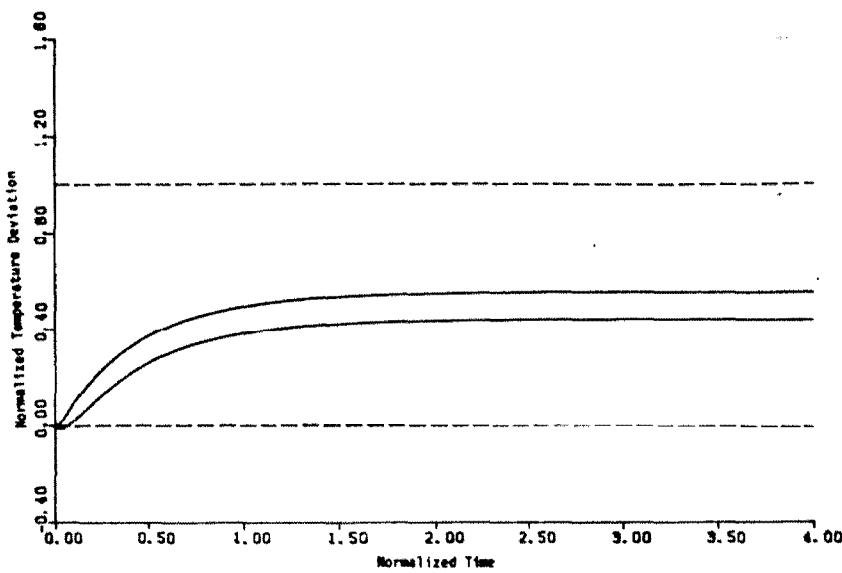


(c)

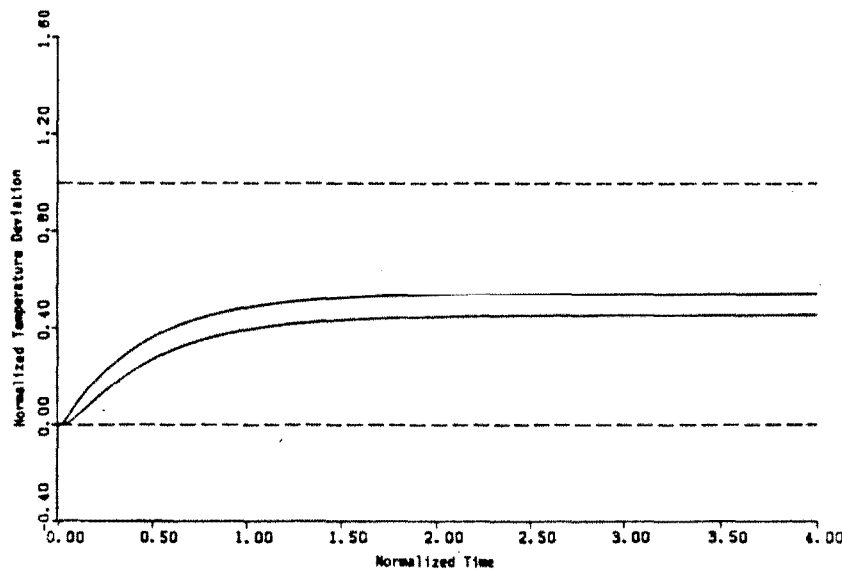


(d)

Figure 2.7-7 Continued



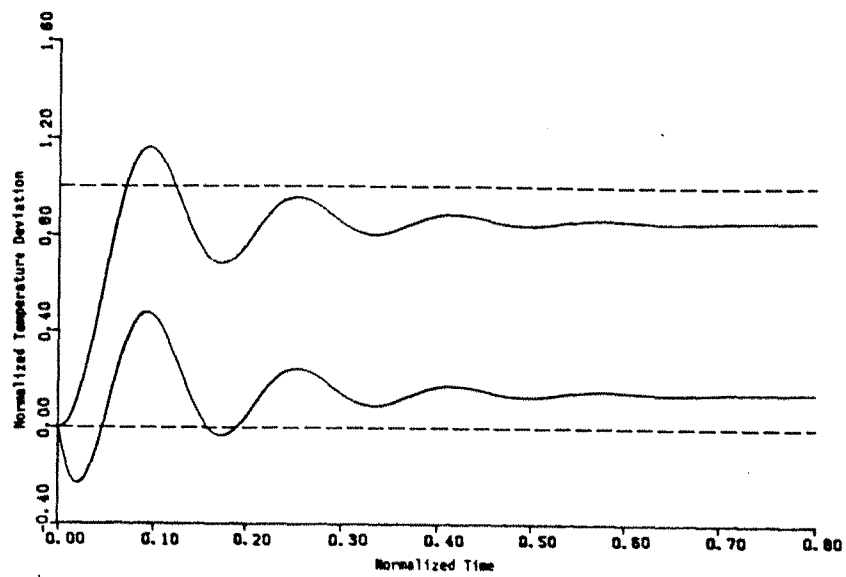
(a)



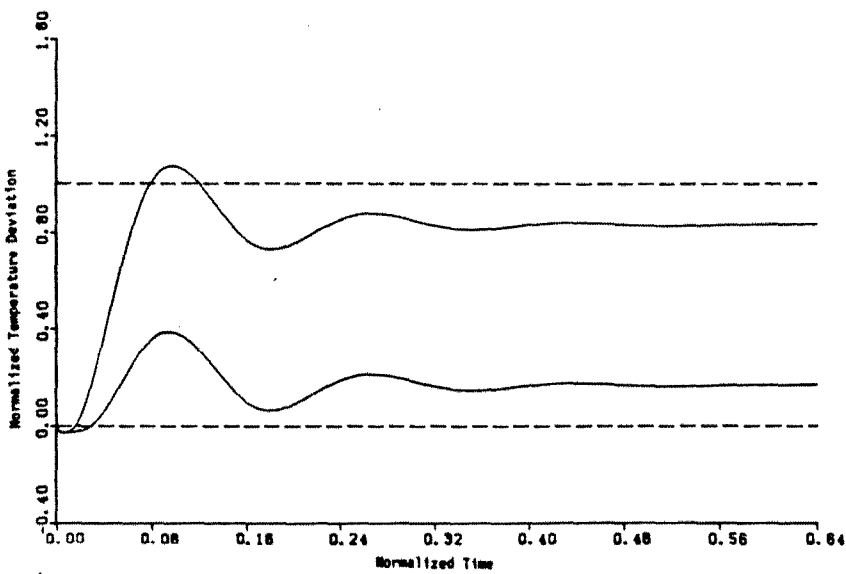
(b)

Figure 2.7-8
Simulations with Outputs $z_1=0.4, z_2=0.6$
Set Point Change (0.1)

Gain = 1.00:	a. Third-Order	b. Tenth-Order
Gain = 20.0:	c. Third-Order	d. Tenth-Order
Gain = 35.0:	e. Third-Order	f. Tenth-Order

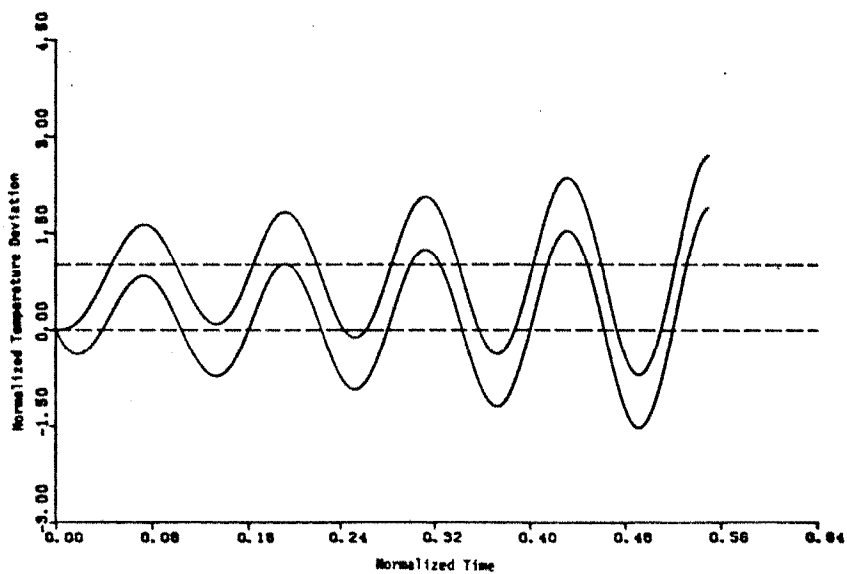


(c)

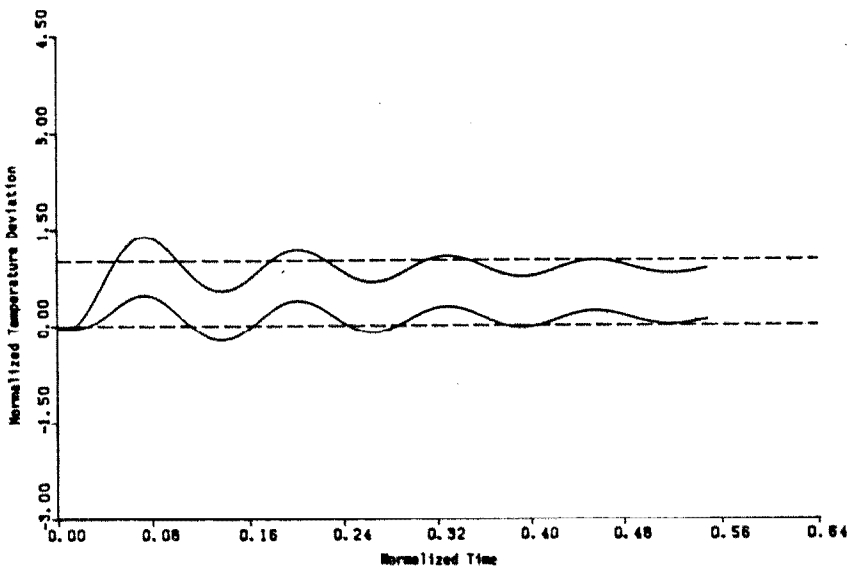


(d)

Figure 2.7-8 Continued



(e)



(f)

Figure 2.7-8 Continued

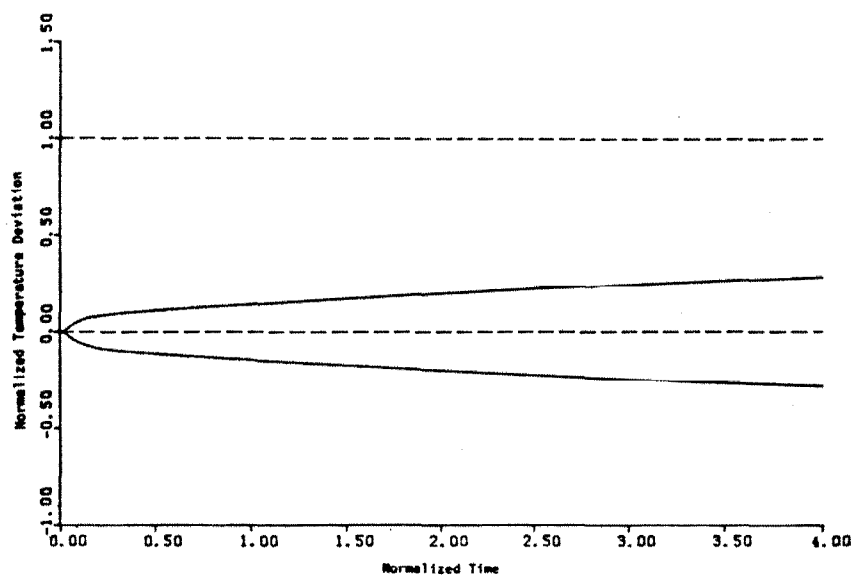
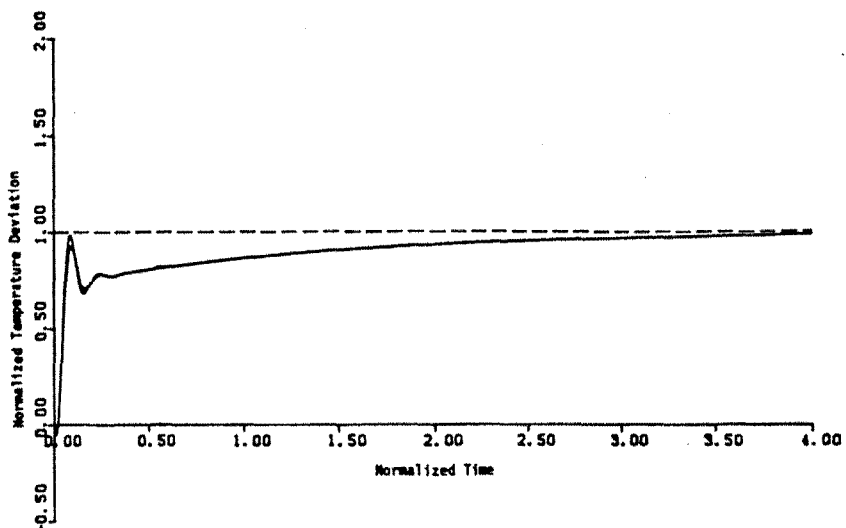
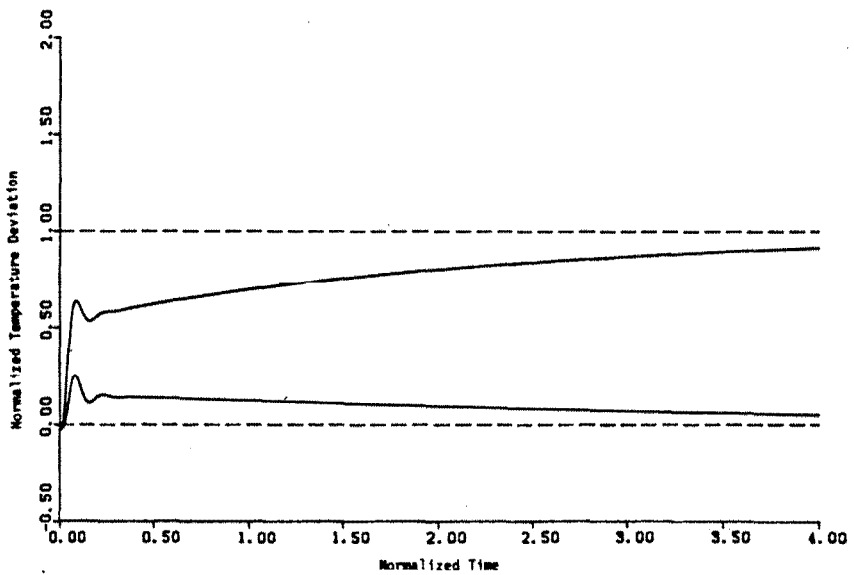


Figure 2.7-9
Tenth-Order Simulations with Outputs $z_1=0.4$, $z_2=0.6$
Dependent Control Action Defined by Equation (2.5-8c)
Set Point Change (0,1)



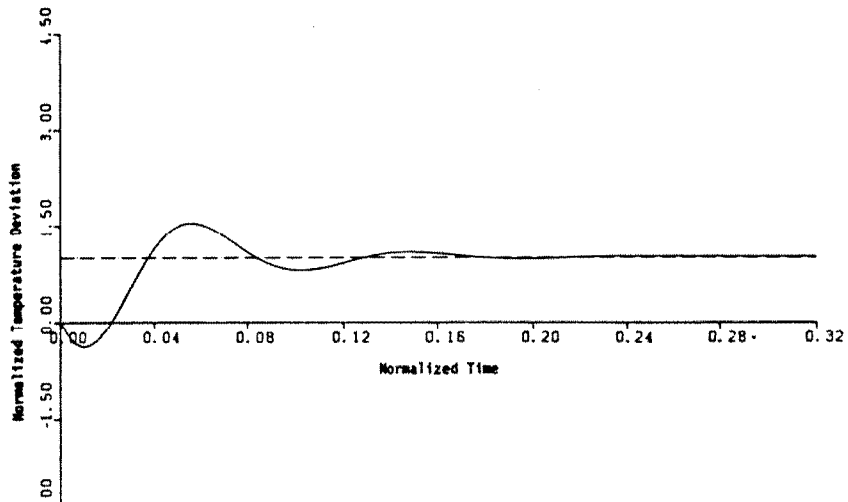
(a)



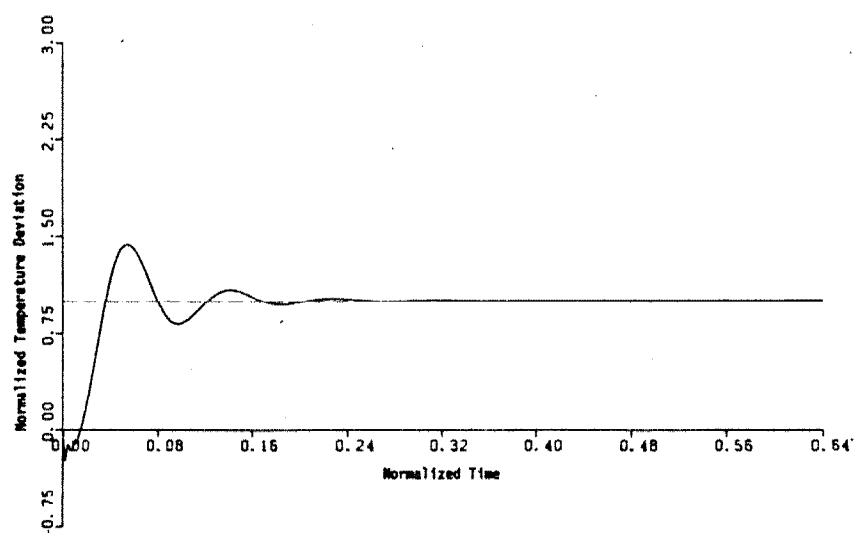
(b)

Figure 2.7-10
Tenth-Order Simulations with Outputs $z_1=0.4, z_2=0.6$
Outer-Loop C.L.M. Compensation Defined by Equation (2.6-21)
Inner-Loop Compensator F_A
Overall Gain = 20.0

a. Set Point Change (1,1) b. Set Point Change (0,1)



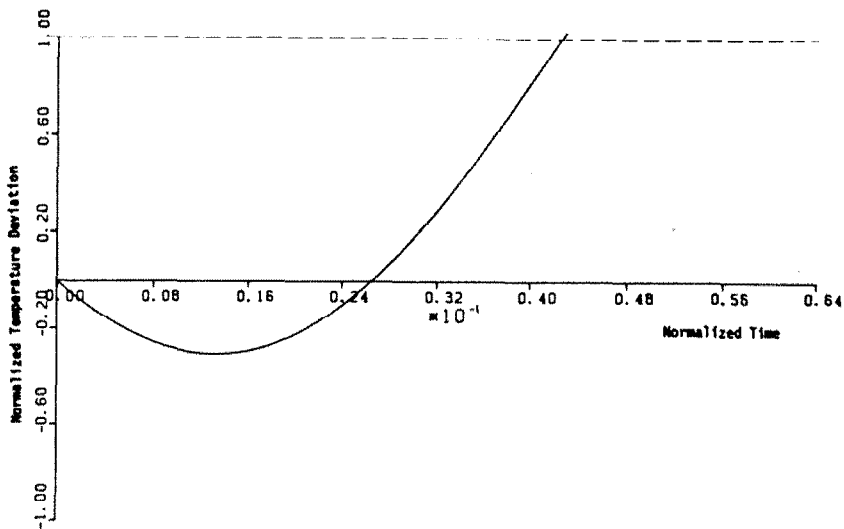
(a)



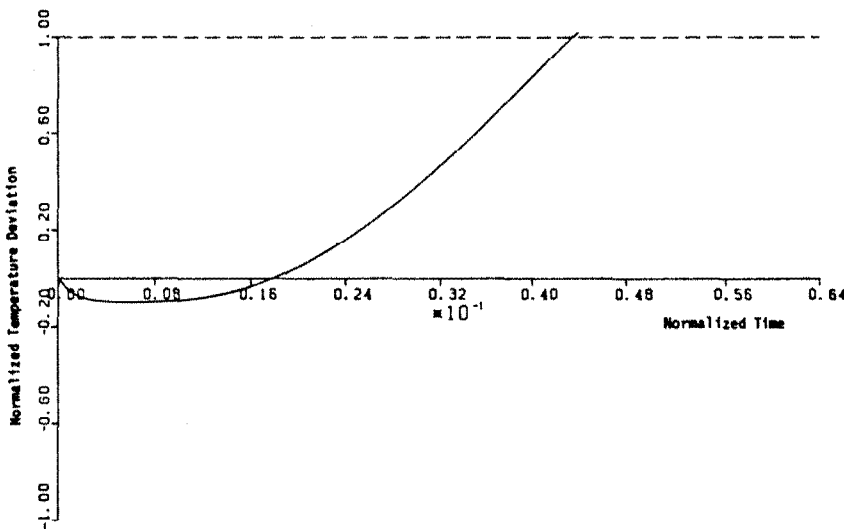
(b)

Figure 2.7-11
Simulations with Outputs $z_1=0.4$, $z_2=0.6$
PD Control Action ($\tau_D = 0.01$)

a. Third-Order, Gain = 35.0 b. Tenth-Order, Gain = 50.0



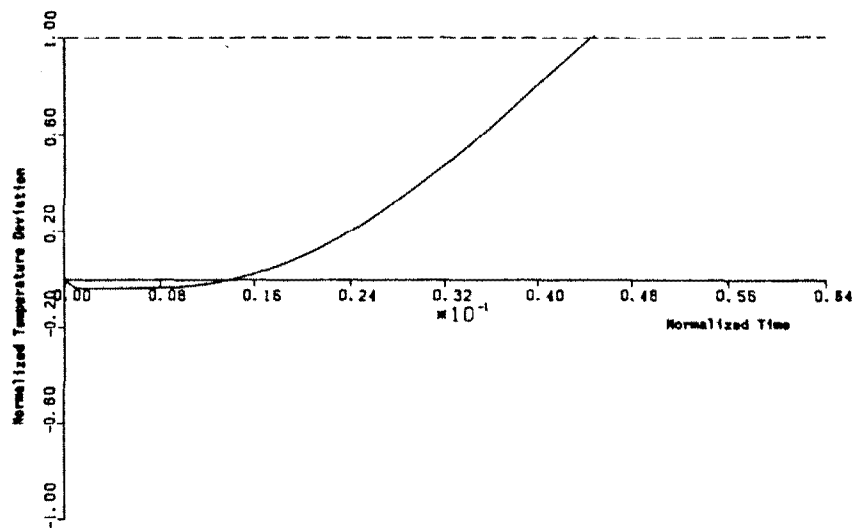
(a)



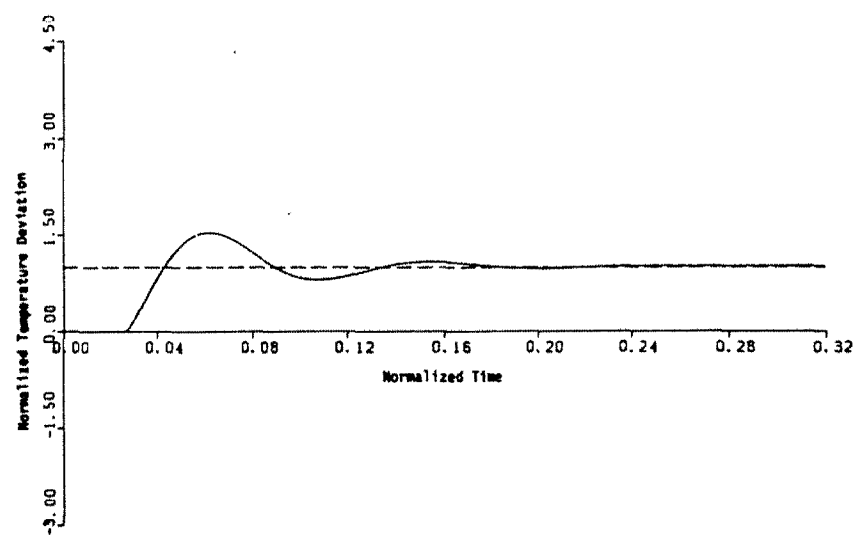
(b)

Figure 2.7-12
Initial Response Characteristics with Outputs $z_1=0.4$, $z_2=0.6$
PD Control Action ($\tau_D = 0.01$)
Set Point Change (1,1), Gain = 35.0

- a. 3rd-Order
- b. 10th-Order
- c. 50th-Order
- d. 3rd-Order Simulation with Initial Negative Response Removed

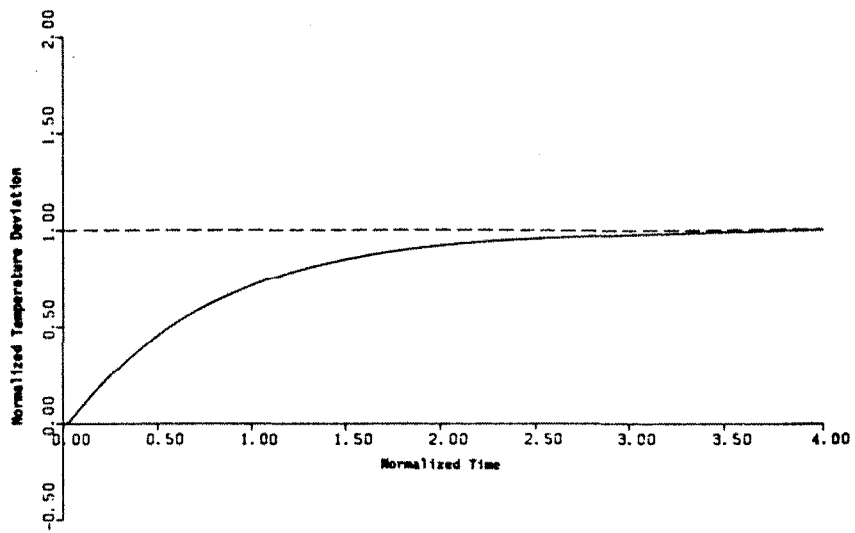


(c)

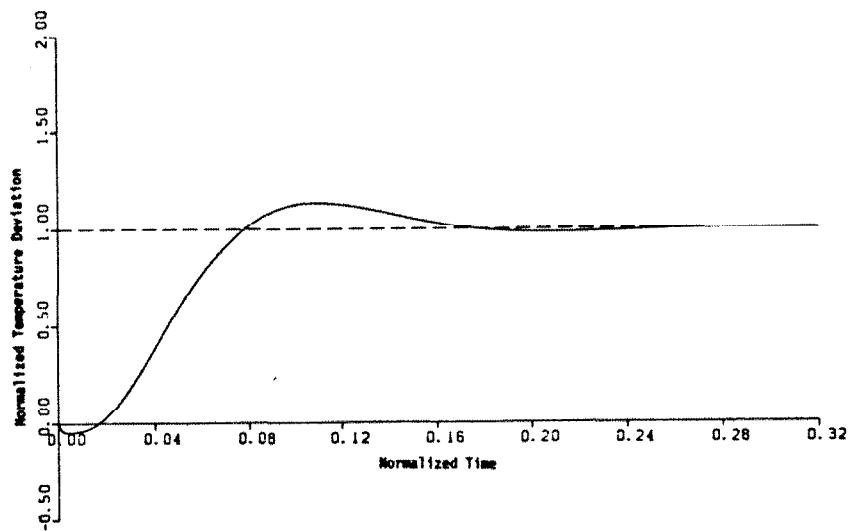


(d)

Figure 2.7-12 Continued



(a)

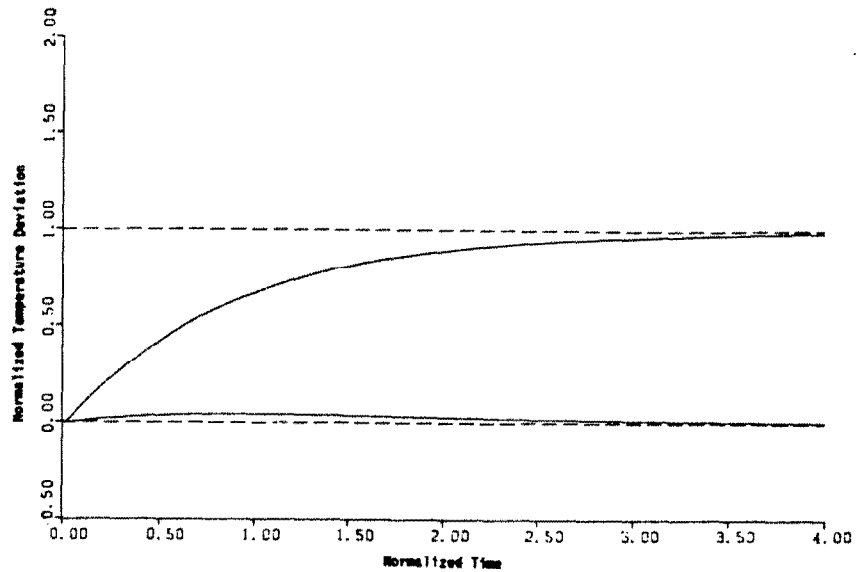


(b)

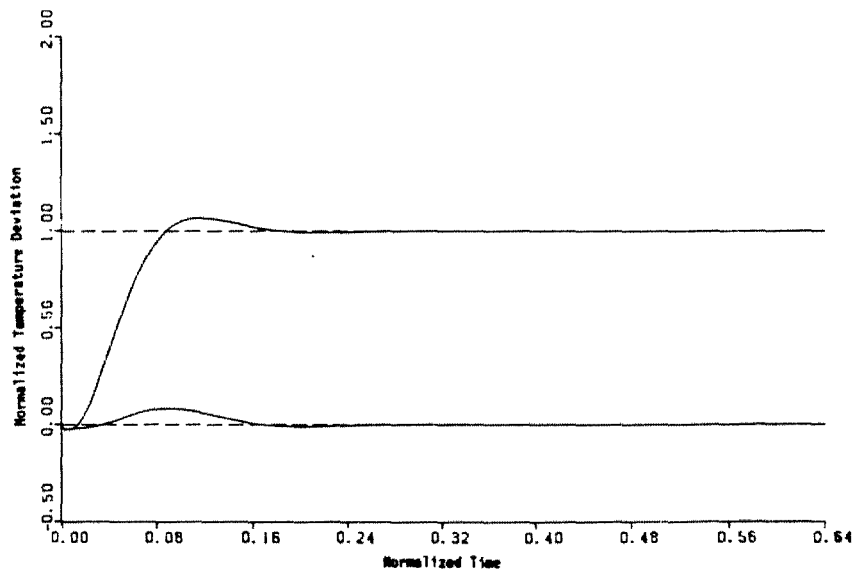
Figure 2.7-13
Tenth-Order Simulations with Outputs $z_1=0.4$, $z_2=0.6$
Inner-Loop Decoupling with $f_{11}=f_{21}=0$

Set Point Change (1,1): a. Gain = 1.0 b. Gain = 20.0

Set Point Change (0,1): c. Gain = 1.0 d. Gain = 20.0

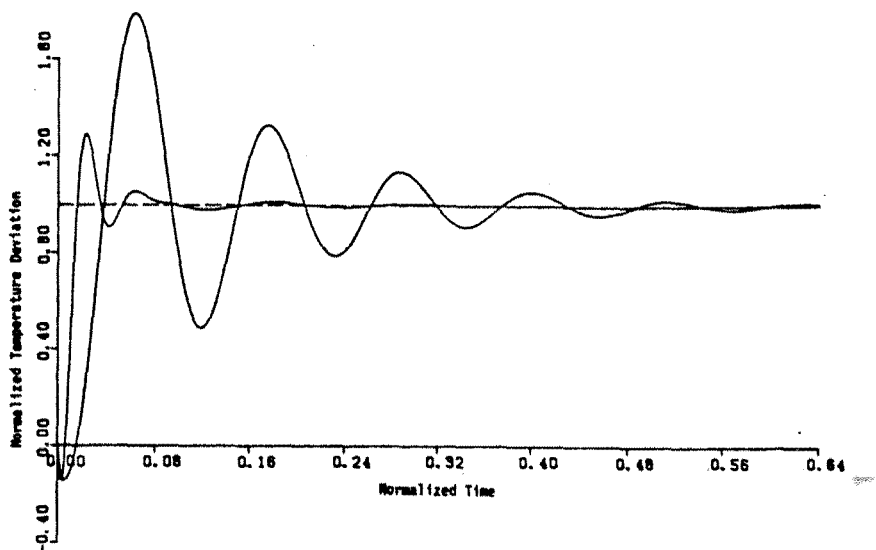


(c)

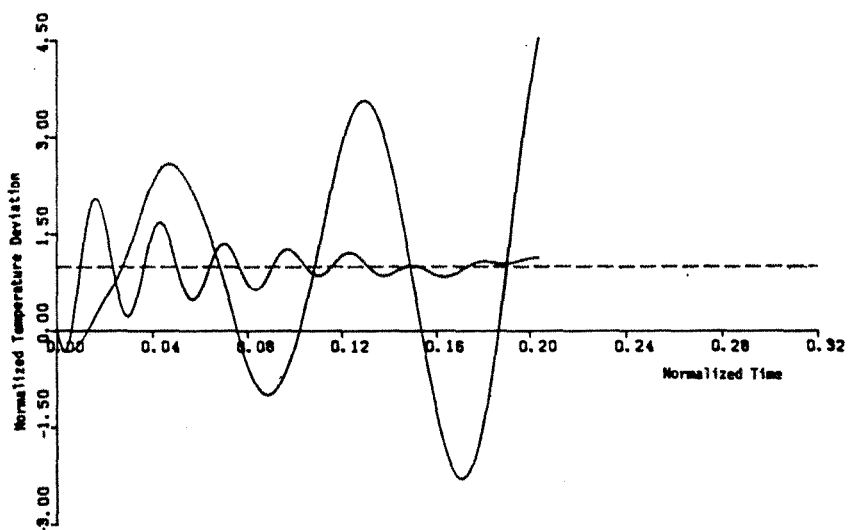


(d)

Figure 2.7-13 Continued



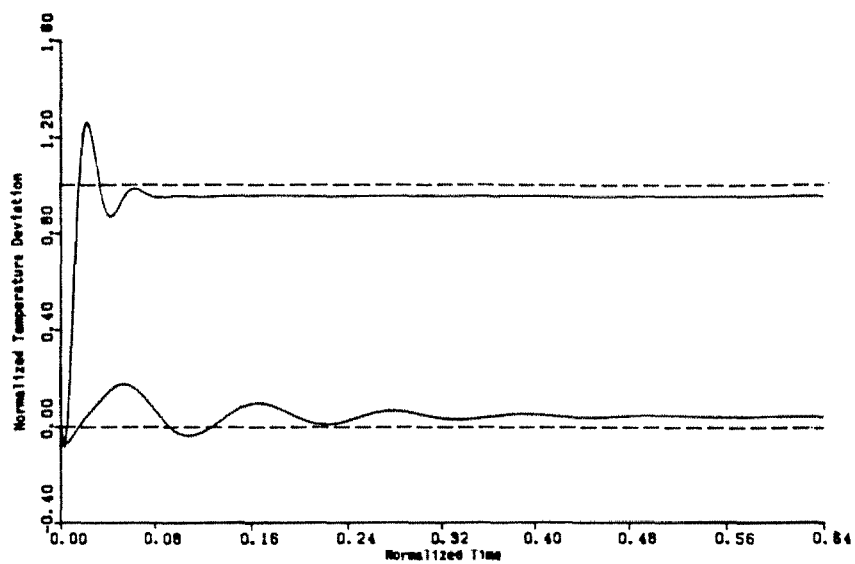
(a)



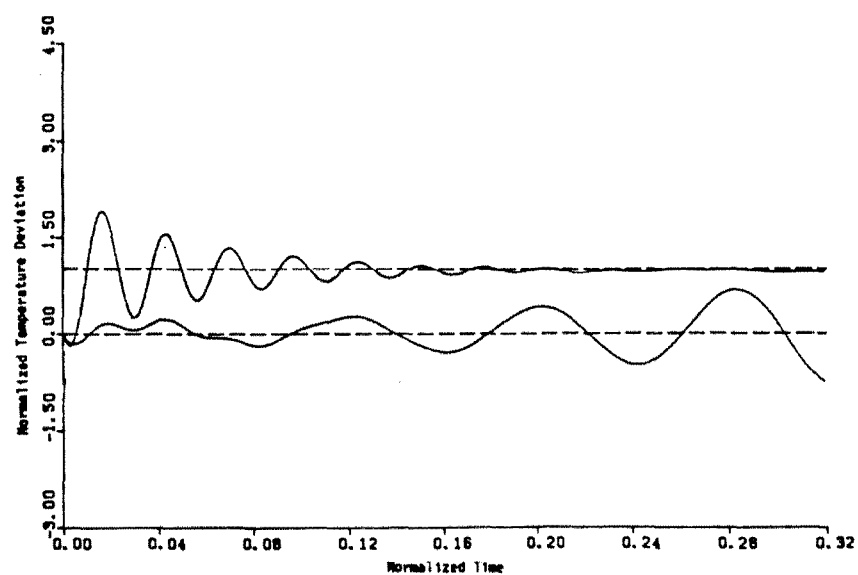
(b)

Figure 2.7-14
Tenth-Order Simulations with Outputs $z_1=0.4$, $z_2=0.8$

Set Point Change (1,1): a. Gain = 50.0 b. Gain = 100.0
Set Point Change (0,1): c. Gain = 50.0 d. Gain = 100.0
Set Point Change (1,0): e. Gain = 50.0 f. Gain = 100.0

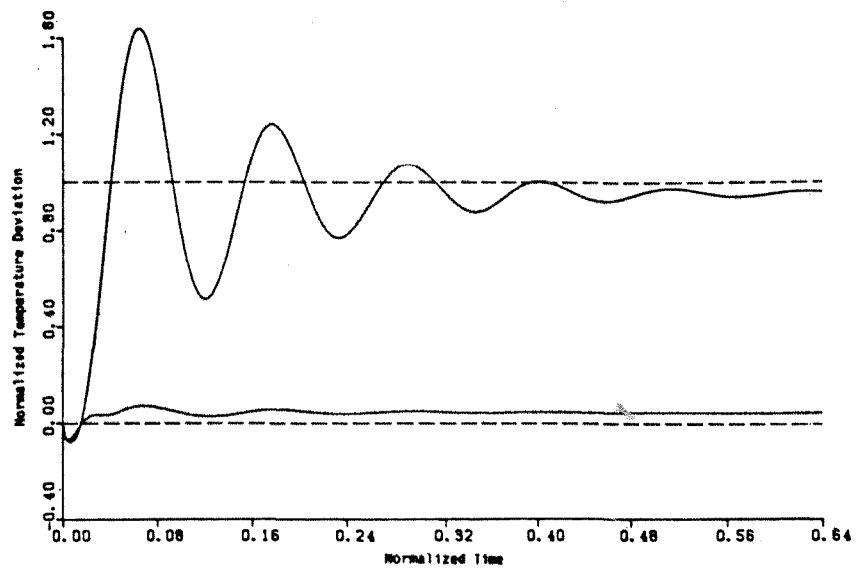


(c)

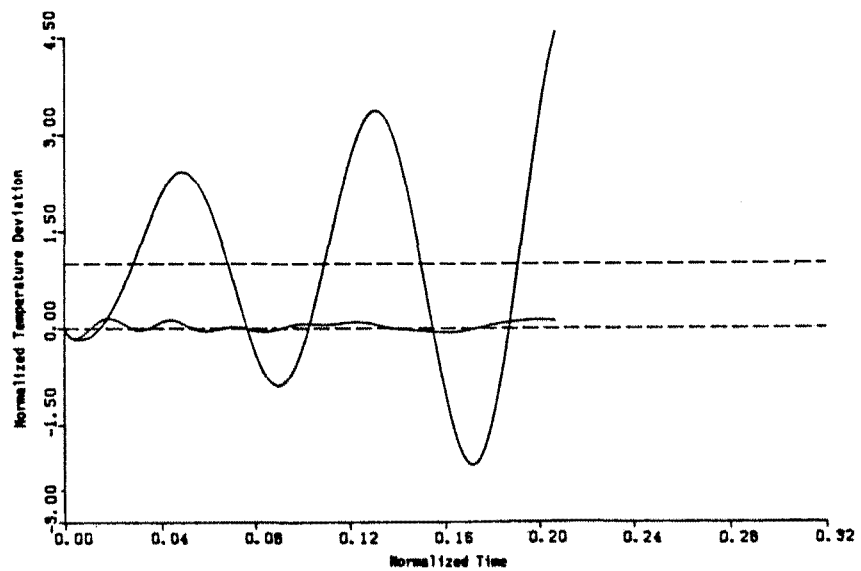


(d)

Figure 2.7-14 Continued

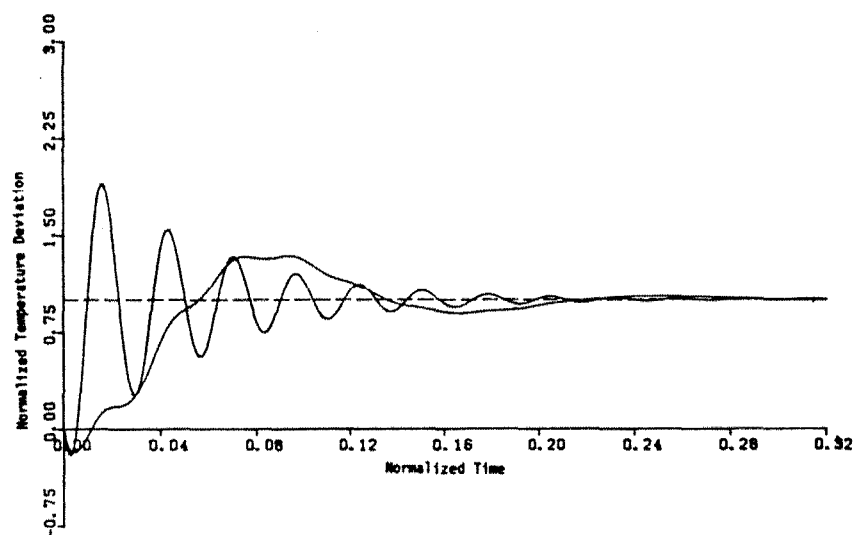


(e)



(f)

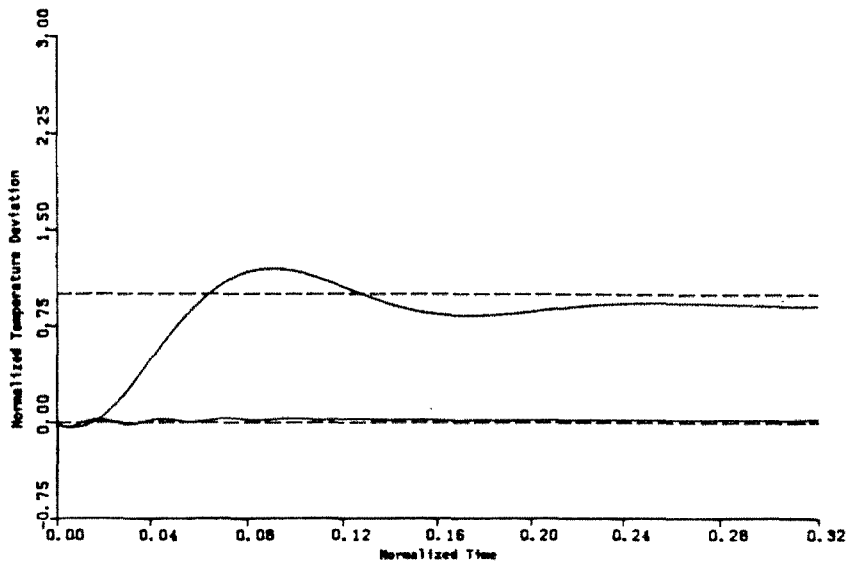
Figure 2.7-14 Continued



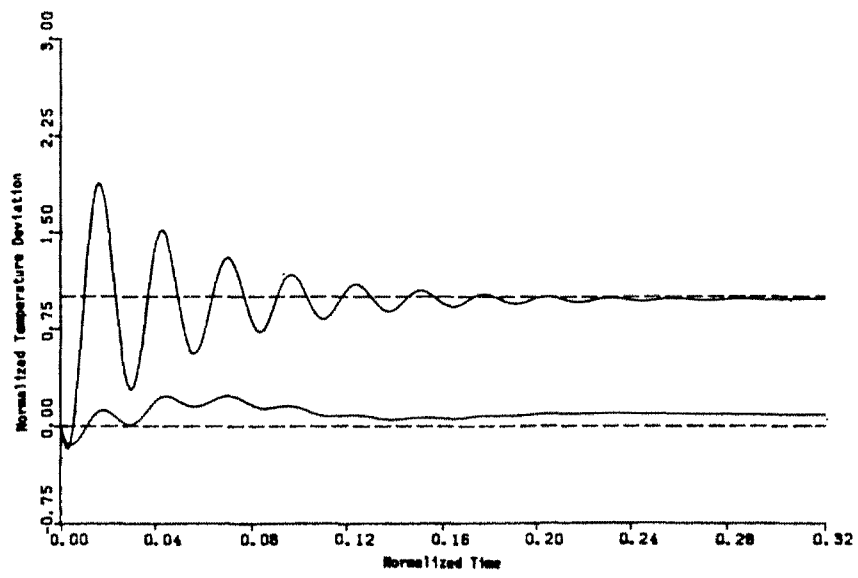
(a)

Figure 2.7-15
Tenth-Order Simulations with Outputs $z_1=0.4$, $z_2=0.8$
Gains 25.0 and 100.0 Imposed on the Outputs z_1 and z_2 , Respectively

a. Set Point Change (1,1)
b. Set Point Change (0,1) c. Set Point Change (1,0)

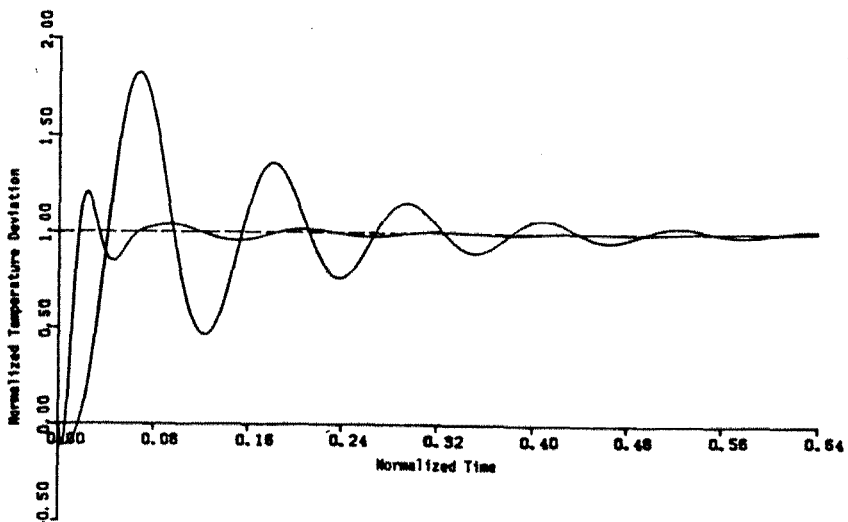


(b)

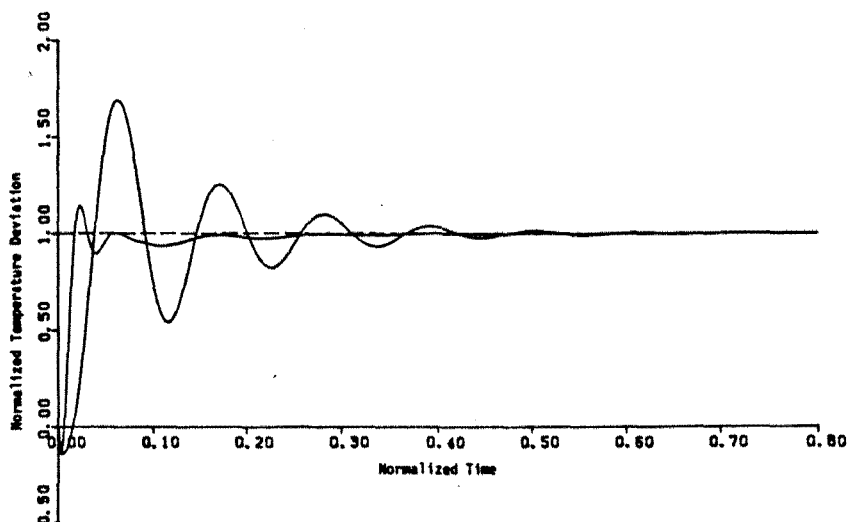


(c)

Figure 2.7-15 Continued



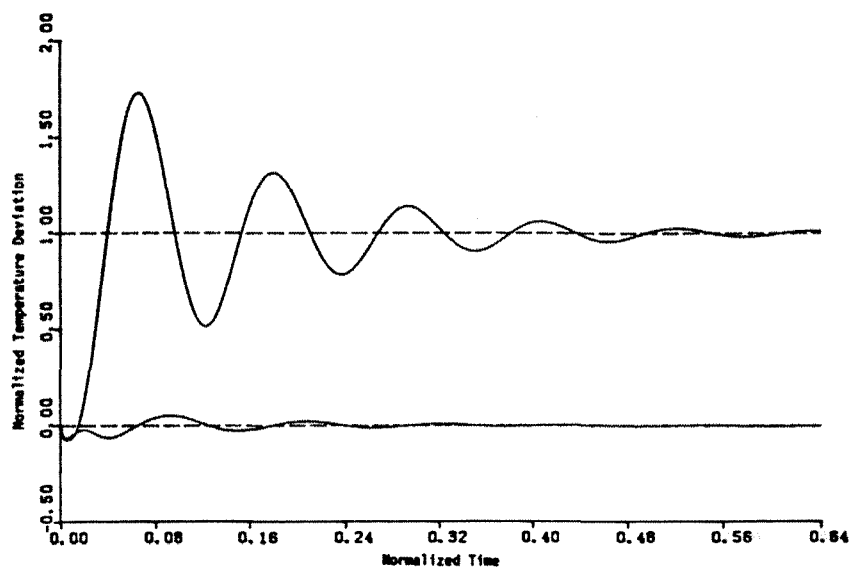
(a)



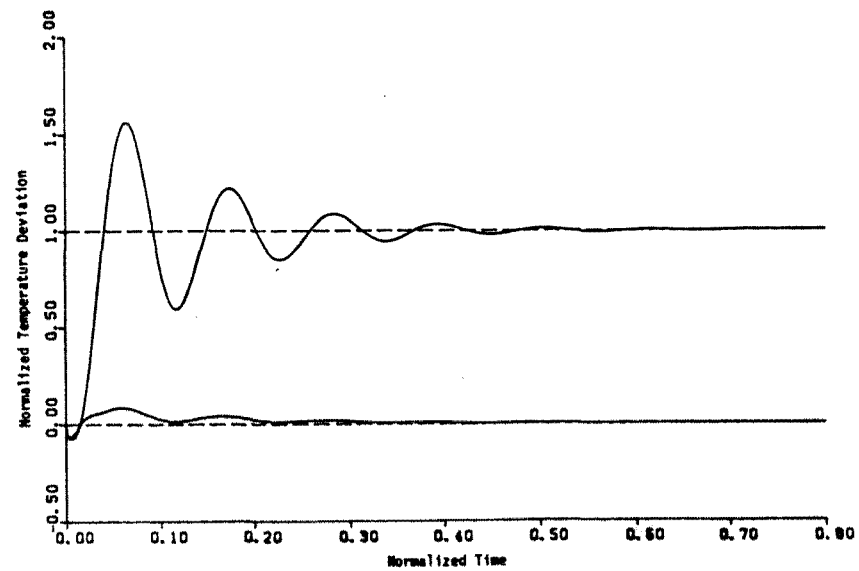
(b)

Figure 2.7-16
Tenth-Order Simulations with Outputs $z_1=0.4$, $z_2=0.8$
C.L.M. Compensation in Outer Loop, Overall Gain = 50.0

Set Point Change (1,1): a. No Inner Loop b. Inner Loop F_A
Set Point Change (1,0): c. No Inner Loop d. Inner Loop F_A
Set Point Change (0,1): e. No Inner Loop f. Inner Loop F_A

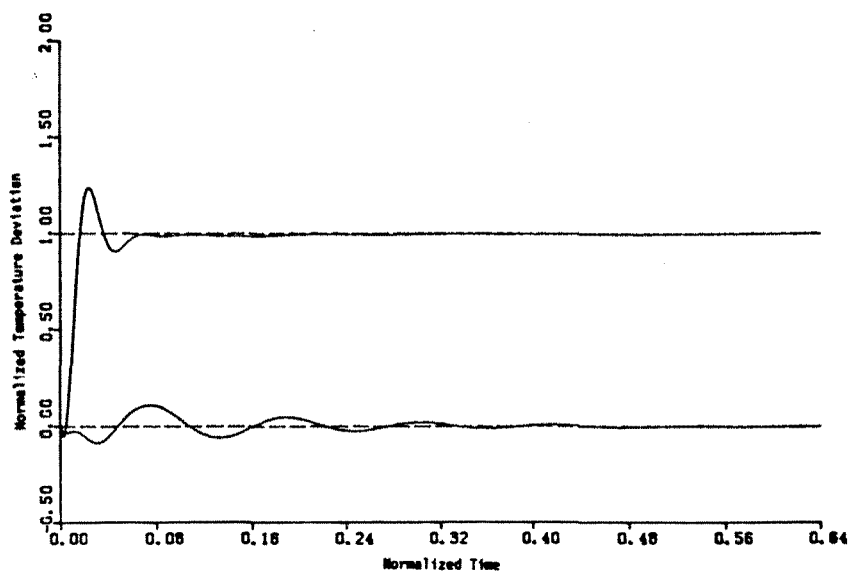


(c)

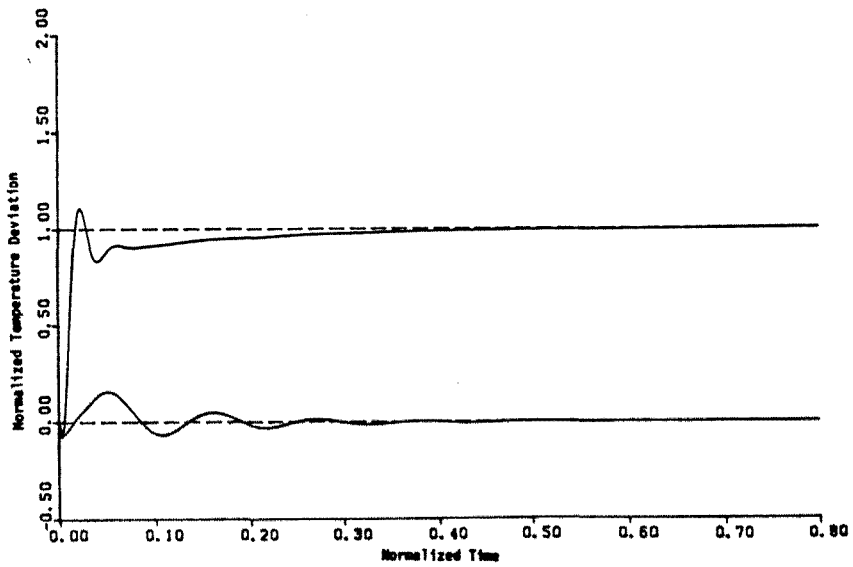


(d)

Figure 2.7-16 Continued



(e)



(f)

Figure 2.7-16 Continued

2.8 DISCUSSION OF CONTROL ANALYSIS

Although much of the analysis and design in this project is an application of published results, the work provides an insight into the current state of multivariable, feedback control theory. Unlike a review paper that compares the theoretical bases of the design techniques, this project performed a complete analysis of a distributed control problem using various currently available methods. In particular, an extensive study of time-domain analysis, frequency-domain design, and non-interacting control has been conducted for a two-input, heat conduction system. Although heat conduction systems have previously been studied in relation to optimal and modal control, the multiple-input problem has been relatively neglected.

Additionally, the role of the number of measurements and their location was studied. Due to the ease of taking temperature measurements for the heat conduction problem, outputs can be obtained as needed by the control system. Thus the complete system state could easily be approximated using many measurements and optimal smoothing or fewer measurements and state estimation. However, since such flexibility is not available in many practical, distributed systems, the control scheme must work on a limited amount of output information. Thus the analysis of the heat conduction system was performed with a finite number of measurements, leading to the problems of measurement placement and feedback loop interaction and instability. Since most design techniques require feedback of outputs equal in number to the inputs, analysis of the use of 'extra' measurements for improving system response, by reducing interaction or moving system poles, was performed. This work led to the new technique of inner-loop decoupling, which shows excellent results for the highly-interacting, highly-symmetric, heat conduction system.

Although the problem that was studied is a relatively simple heat conduction process with two heat-flux controls, the results lead to conclusions that can be extended to general, multivariable control theory. The choice of the particular system is actually quite good since many difficulties arise in the feedback design, due to excessive transportation lags and high interaction between the outputs. In particular, the classical means of steady state decoupling and perfect, non-interacting control are not useful for this system, and thus more complicated design methods are necessary. Therefore, though this project leads to results specific to the heat conduction problem, the major contribution of the work is in the general area of feedback control theory.

The study clearly showed that, although excessive model lumping and reduction can lead to significant inaccuracies, a high degree of model reduction is usually needed so that the various techniques of control design can be considered. Most methods require a low-order, state-space representation of the process for practical and efficient control structure design. Although the exact lumping techniques of modal analysis and Laplace transform were easily applicable to the heat conduction system, many other efficient techniques are available and are necessary for processes described by more complicated differential equations. These methods include space discretization techniques and the method of weighted residuals, along with other pseudo-modal procedures. Before attempting any control design strategy, an accurate system model is required. However regardless of the accuracy of the model, its usefulness is limited unless accurate model reduction can be performed. For the heat conduction process, modal lumping led to simple model reduction by directly specifying the system eigenvalues. Since they were shown to increase rapidly, only the first few dominant modes needed to be retained to accurately represent the system. The simulations showed that the qualitative behavior of the third-order model is

similar to that of the actual system, but the differences are magnified at high gain and often lead to quite different behavior.

The project also allows for an excellent comparison of the currently available design techniques. Overall, the best technique that was studied in this project is the characteristic locus method. Both with and without an inner loop, this scheme provides a systematic, computer-aided design strategy in terms of high and low frequency compensation that leads to an excellent, proportional-integral controller. Actually at the specific frequencies used in the design, the technique determines the best possible controller to insure stability, reduce interaction, and increase integrity and accuracy, by calculating the compensator that best aligns the real and complex frames. The method is based on manipulating the characteristic loci and characteristic directions of the system to meet the necessary objectives. Once the appropriate computer programs and plotting facilities are available, the final design can readily be obtained by considering various high and low frequencies at which the alignment is applied.

The inverse Nyquist array analysis can also easily be performed with the appropriate computer facilities but does not lead to as good a control design. The procedure involves making the system stable and diagonally dominant. Then a high amount of proportional gain can be used to reduce interactions. However such high gain is often impractical and leads to excessive oscillations. Additionally due to the lack of integral action, offset is a significant problem at low gain and can only be reduced by increasing the gain substantially. The major advantage of this technique over simple multivariable root-loci analysis is that, although both can be used to check stability, the inverse Nyquist method also insures diagonal dominance. However, the characteristic locus analysis shows that diagonal dominance is not a necessary condition¹ for reduction of

¹. However it is sufficient.

interaction at high gain.

Non-interaction control methods were also considered for the heat conduction system. Although perfect, non-interacting control and steady state decoupling have little use for this particular system, they may in general be applicable. Whereas non-interacting control usually leads to an excessively complicated controller and requires an accurate system model, steady state decoupling is usually very simple and an excellent technique to perform in conjunction with other control schemes. Furthermore, the inner-loop decoupling strategy, that uses extra measurements to eliminate or reduce the interactions, seems to be quite promising. Though further analysis of the method for a more complicated system is necessary, it seems to be quite insensitive to model inaccuracies and leads to a very simple feedback system with little interaction.

Other conclusions pertaining to general multivariable, feedback control can be made. In particular, it was shown that none of the currently available design techniques allow for derivative action. Though such control action may be useful in many processes where transportation lags are significant, it is impractical to physically incorporate into the system and leads to problems with step changes and noisy processes by requiring excessive control action.

Additionally, the project showed that the use of extra measurements may drastically improve the control design or may have little or no effect, depending on the placement of the commanded outputs. The extra outputs can be used for inner-loop decoupling or for adjusting the poles of the process so that an improved characteristic locus design can be obtained. In cases where extra outputs are available or easily accessible, they should be considered and may simplify the control structure significantly. However, since a simple inner loop cannot move system zeros, stability problems due to unstable finite zeros cannot

easily be eliminated with extra measurements. Unfortunately, no good technique is currently available to insure stability of such systems.

Finally the role of measurement location has been considered. Each choice of measurement location leads to a completely different optimal design and significantly affects the usefulness of each design technique, since the locations determine the extent of interaction and system symmetry. As expected, problems are minimized with measurements near the edges of the system, since interaction and transportation lags are reduced.

Thus though the two-control, heat conduction process has been analyzed in detail, further analysis could lead to additional insight. In particular, the transportation lag problem should be further studied, especially in regard to current work on computer-aided, multivariable control design for systems with time delays (Ogunnaike and Ray, 1979). More importantly, an analysis of the stochastic problem needs to be performed, along with an analysis of heat losses and other disturbances. Finally, several computer-aided design packages should be tried to further verify the results and spatial-discretization lumping procedures and adaptive control techniques should be considered.

Chapter 3

MATHEMATICAL MODEL OF A PACKED BED CATALYTIC REACTOR

3.1 INTRODUCTION

The central role played by dynamic and steady state models in the design and optimization of chemical processes and in the development and application of control strategies justifies considerable effort in their development. The area of packed bed reactor modeling has been the emphasis of a considerable amount of research effort during the past twenty years and has really been at the forefront of modeling research since the early 1970's with the acceptance of new mathematical techniques for the solution of the systems of partial differential equations encountered throughout the chemical industry. Still one of the most challenging problems is that of packed bed catalytic reactor modeling.

Packed bed catalytic reactors are extensively used for carrying out exothermic, gas-phase reactions. The complexities of the simultaneous heat and mass transfer processes in such reactors have led to considerable effort in their mathematical modeling. A major concern has been in the amount of detail necessary for accurate description of the dynamic and steady state behavior of these reactors (Hoiberg et al., 1971). Although it is obvious that insufficient detail can lead to a model incapable of accurately representing the physical system, model complexity has often been limited by computational considerations. Many authors have concluded that, although the mathematical treatment of every aspect of the reactor system may be intellectually fulfilling, a model based on such detail could be impractical since the resulting system of partial differential equations would be computationally intractable. For these reasons, much work has been directed at determining the processes that are of minor importance and can safely be neglected in the models.

Such work has led to the extensive use of pseudo-homogeneous models--

those that do not distinguish between the conditions within the fluid and those on the solid catalyst. For highly exothermic reactions, a pseudo-homogeneous description is often inaccurate due to the large temperature gradients that exist between the solid and fluid phases. A more detailed two-phase model, in which the exchange of energy and mass between the two phases is explicitly described, is then necessary. Furthermore, in order to limit the complexity of the heterogeneous model, radial concentration and temperature gradients, axial dispersion and the variation of physical properties are frequently neglected (Carberry, 1976; Finlayson, 1971; Hoiberg et al., 1971; Jutan et al., 1977).

Advances over the past decade in computational techniques for the solution of partial differential equations—the orthogonal collocation method, in particular—have made extensive simplifications of packed bed reactor models unnecessary. Thus the formulation and solution of accurate dynamic models of chemical packed bed reactors is now possible, allowing

- accurate description of dynamic and steady state reactor behavior for process optimization, design and safety considerations.
- investigation of reactor start-up or the effects of system disturbances, and
- the analysis and design of control structures to stabilize the reactor under various disturbances or to provide optimal system recovery from input changes.

As a basis for a concerted effort in multivariable control system design, the present study provides a mathematical modeling analysis of packed bed catalytic reactors that significantly extends previous studies in the detail of the mathematical model and systematic consideration of all aspects of the model development and the reduction to a state-space control representation. This

analysis is not intended to be specific to any particular packed bed system, although our experimental methanation reactor is used throughout most of the discussions, but rather to present a detailed study of modeling techniques, assumptions, and solutions and to develop a unified approach to dynamic reactor modeling. We feel that the modeling approach and the conclusions concerning the model development and the importance of model simplifications presented in this thesis should carry over to other similar catalytic packed bed systems.¹

In particular, this thesis provides a complete modeling analysis of a packed bed chemical reactor based on currently available computational procedures. Various common assumptions, model structures, and numerical solution techniques are discussed. Although some simplifying model assumptions are considered, their necessity and effect on the resulting system simulations are rigorously analyzed.

After providing a cursory review of packed bed reactor modeling, the formulation and numerical solution of a dynamic model, incorporating all of the mechanisms necessary for an accurate description of the physical and chemical phenomena occurring in industrial reactors, is presented for a packed bed reactor in Section 3.3. The model accounts for axial and radial dispersion of mass and energy, for mole changes that occur along the bed due to reaction, and for temperature, pressure and mole dependencies of gas velocity, density, average molecular weight, heat capacity, reaction rate constants, and heats of reaction. Additionally, a central axial thermal well is included in the study to provide an accurate representation of many industrial reactors, where the well is often

1. In line with this reasoning, all computer programs developed in this work for the reactor model are modular and allow for simple modification to study various packed bed reactors with varying degrees of model complexity. Furthermore, the analysis presented is for the general packed bed system with a cooling jacket and axial thermal well. The model and computer programs are set up for consideration of simpler systems, such as adiabatic reactors and those without a thermal well. These are merely subsets of the more general case.

used to obtain the temperature measurements necessary for process control. Finally, the model is based on a three-dimensional--time, axial, and radial--heterogeneous analysis and incorporates the effects of axial pressure gradients.

The model can then be used to study the steady state and dynamic behavior of the methanation reactor, the effects of reactor operating conditions, and the overall effects of various common modeling simplifications. The generality of the analysis also allows for studies of similar systems under adiabatic operation and without axial thermal wells. These extended analyses are presented in Section 3.4.

Unfortunately, the numerical solution procedures used throughout the early portions of the analysis may be inappropriate for reactors with very steep axial concentration or temperature gradients due to numerical difficulties inherent in the model discretization. Section 3.5 considers such conditions and presents an extended numerical solution procedure using orthogonal collocation on finite elements that remains stable even under the worst of these simulations.

The analysis of the mathematical relationships describing the chemical and physical processes within the reactor and the numerical approximation methods leads to a computational technique for simulating the steady state and dynamic behavior of the packed bed reactor. However, computing facilities generally available for on-line control cannot perform the necessary calculations rapidly enough for practical control applications with the full, nonlinear model. Furthermore, solution times for dynamic simulations with this model even make detailed parameter studies and process optimization impractical. Thus a simplified lower-order model is desired for on-line multivariable control and for process studies and is developed in Section 3.6.

Finally, a major difficulty in accurate packed bed modeling is that of excessive model dimensionality. Incorporation of all of the physical information available into an accurate description of the reactor can lead to numerical models of very high dimensionality. An analysis of the effect of the model discretization on model dimensionality and techniques for accurate reduction of the size of the model are presented in Section 3.7.

Before control studies can be performed using the model developed in this work and even before extensive simulations are used for system design and optimization, parameter estimation for the system of interest is necessary. Although many of the parameters needed for the mathematical description of the reactor system can be calculated directly from physical considerations, the reaction and heat transfer parameters must be measured directly for the experimental system. This step, outlined in Section 4.2, is by no means trivial and may require considerable experimentation to obtain kinetic data, including consideration of transient kinetics, and to obtain heat transfer and energy and mass dispersion parameters.

3.2 REVIEW OF PACKED BED REACTOR MODELING

The area of packed bed reactor modeling was the emphasis of considerable amount of research effort into the early 1970's. Many specific aspects of the models were investigated, and well defined techniques for packed bed reactor models were developed (Carberry, 1976; Froment, 1972; Hlavacek, 1970; Karanth and Hughes, 1974a; Paris and Stevens, 1970; Smith, 1970).

Conclusions based on careful analyses of each specific aspect of the reactor design led to modeling simplifications that were necessary due to limitations of the available numerical solution techniques and computational equipment. The use of pseudo-homogeneous models, the elimination of dispersion effects, and the assumption of constant physical properties were often necessary and became standard modeling practice. Steady state analyses dominated the modeling efforts, since computational techniques for dynamic simulations were not well-developed. However, these steady state models were able to provide fairly accurate results for most investigations.

Advances over the past decade in computational techniques for the solution of partial differential equations such as those describing a packed bed catalytic reactor have made extensive simplifications of the analysis unnecessary. In particular, a drastic reduction in computer time has been achieved by application of the orthogonal collocation method, which is ideally suited to boundary value problems of the type encountered in catalytic reactor modeling. In the collocation procedure, the solution is approximated by a series of known functions with unknown coefficients, which are then determined by satisfying the differential equations at a number of collocation points. As developed by Villadsen and Stewart (1967), the technique uses orthogonal polynomials as the expansion functions and the roots of these polynomials as the collocation points. The

method has been applied to various problems including the non-symmetric axial diffusion for a tubular reactor (Fan et al., 1971), the steady state solution for a nonadiabatic packed bed reactor (Finlayson, 1971), the simulation of a simplified adiabatic packed bed reactor (Karanth and Hughes, 1974b), and the modeling of a nonadiabatic packed bed reactor using a pseudo-homogeneous approach (Jutan et al., 1977).

Obviously, we cannot attempt to provide a detailed review of packed bed reactor modeling in this thesis since entire books or major portions of reaction engineering textbooks (Carberry, 1976; Karanth and Hughes, 1974a; Smith, 1970) are devoted to this subject. Instead, we wish simply to outline some of the major advances in this area and to show the wide disparity in modeling techniques and thus the importance of a unifying study such as that presented here. Table 3.2-1 shows a brief summary of several published nonisothermal, nonadiabatic packed bed reactor models developed during the past twenty years. This table is not intended to present all of the models used throughout this period or even present the major modeling techniques, but instead to describe representative models that exemplify the progress of this field during the period. The table shows the continuous increase in model complexity due to computational improvements and the generality of the present work in comparison to previous studies.

Reference	System	Solution Technique	Heterogeneous	Dynamic	Dispersion Thermal	Mass
Current	Methanation	Orthogonal Collocation	Yes	Yes	Axial Radial	Axial Radial
Jutan et al. (1977)	Butane Hydrogenolysis	Orthogonal Collocation	No	Yes	Radial	Radial
Valstar et al. (1975)	Vinyl Acetate Synthesis	Finite Differences	No	No	Radial	Radial
Hoiberg et al. (1971)	$H_2 + O_2$		No (s.s.) Yes (dynamic)	Yes	Radial	Radial
De Wasch and Froment (1971)	$A+B \rightarrow C$	Finite Differences	Yes	No	Radial	Radial
Finlayson (1971)		Orthogonal Collocation	No	No	Radial	Radial
Hlavacek (1970)	$A \rightarrow B$	Finite Differences	No	No	Radial	Radial
Carberry and White (1969)	Naphthalene Oxidation	Finite Differences	No	No	Radial	Radial
Carberry and Wendel (1963)	$A \rightarrow B \rightarrow C$ Quasi-Adiabatic	Finite Differences	No	No	Axial	Axial

Table 3.2-1
Summary of Nonisothermal, Nonadiabatic Packed Bed Modeling

Carberry and Wendel (1963) considered the influence of inter-intraphase transport phenomena yield for consecutive reactions in an adiabatic packed bed catalytic reactor. A simple digital computer model was developed with simple extensions to the nonisothermal, nonadiabatic case in the absence of radial gradients (quasi-adiabatic analysis). This study was extended by Carberry and White (1969) to the steady state modeling of a packed bed catalytic reactor for the highly exothermic oxidation of naphthalene over V_2O_5 . Their numerical simulations demonstrate the necessity of a two-dimensional, axial and radial, description of the temperature distribution and the adequacy of a one-dimensional mass continuity description. Detailed computations further showed the existence of significant interphase concentration and temperature differences, even at steady state, for the highly exothermic reaction.

Hlavacek (1970) provided a unified review of the design of packed catalytic reactors, including the formulation of modeling equations governing heat and mass transfer in packed bed reactors and considerations of heat transfer simplifications in packed beds and numerical solution methods for the resulting set of nonlinear partial differential equations. Hlavacek describes both one- and two-dimensional modeling of a packed bed reactor for a simple $A \rightarrow B$ reaction. As with most packed bed analyses, he assumes a homogeneous reaction system, in contradiction to the real heterogeneous structure of the packed bed. His resulting system of nonlinear elliptic partial differential equations is reduced to a set of parabolic equations by omitting the effects of axial mixing. Finally, steady state solution of the equations is performed using finite differences. The major contribution of his work is really in unifying the approach to packed bed reactor design by showing the necessity and use of accurate reactor models in studying design considerations.

Major advancements in packed bed reactor modeling were published in 1971. Finlayson (1971) presented the first orthogonal collocation solution for packed bed reactor analysis. Although he showed the method to be much faster and more accurate than finite difference calculations and easily applicable to two-dimensional models with both radial temperature and concentration gradients, the finite difference technique remained the generally accepted procedure for packed bed reactor model solution until about 1977 when the analysis by Jutan et al. (1977) of a complex butane hydrogenolysis reactor showed the real potential of the collocation procedure.

Also in 1971, De Wasch and Froment (1971) and Hoiberg et al. (1971) published the first two-dimensional packed bed reactor models that distinguished between conditions in the fluid and on the solid. The basic emphasis of the work by De Wasch and Froment (1971) was the comparison of simple homogeneous and heterogeneous solutions and the relationships between 'lumped' heat transfer parameters (wall heat transfer coefficient and thermal conductivity) and the 'effective' parameters in the gas and solid phases. Hoiberg et al. (1971) presented the first detailed, two-dimensional, heterogeneous dynamic modeling analysis (a homogeneous analysis was used for steady state calculations). This work considered the amount of detail necessary in dynamic models through a comparison of experimental and calculated results for a packed bed reactor in which the highly exothermic reaction between hydrogen and oxygen occurred on a platinum catalyst. The major limitation of this work was the amount of detail possible for numerical solution using the finite difference solution scheme.

The work by Valstar et al. (1975) provided the first real experimental comparisons between two-dimensional packed bed calculations and radial measurements. Although their model was somewhat simple, especially for as late as 1975 (four years after the detailed modeling work by Hoiberg et al. (1971) was

published), their experimental radial temperature measurements provided the basis for the generally used assumption of quadratic radial temperature profiles.

Finally, a significant advance in packed bed reactor modeling and control model development was published by Jutan et al. (1977). They used the orthogonal collocation discretization technique to reduce an accurate dynamic three-dimensional--time, axial, and radial--partial differential equation model for the multiple butane hydrogenolysis reactions in a packed bed catalytic reactor to a state-space representation suitable for on-line control studies.

Other recent work by MacGregor and Wong (1978) and Wright and Schryer (1978) deviated from the mechanistic approach taken by most studies where models are developed by properly including the major phenomena occurring within the system through the application of the basic physical and chemical laws governing such systems. They considered the use of statistical methods to identify process transfer functions from empirical input/output process data. The advantages of this statistical approach include rapid implementation without the necessity of any specific knowledge of the process. However, these empirical models are only valid within a very narrow region about the operating conditions for which they have been derived and are only practical in cases where very low-order models will suffice. With such complex systems as packed bed reactors, such low-order models may be insufficient to accurately describe the dynamic behavior of the process. Thus, these models cannot in general be safely used for process optimization and design or the investigation of start-up procedures and the effects of major system disturbances.

The current work presented in this thesis uses these past studies as a basis to develop a unified general approach to packed bed reactor modeling and con-

trol model development. This approach includes detailed heterogeneous dynamic modeling with complete axial and radial, mass and temperature considerations and gas and solid property variations with minimum *a priori* simplifications.

3.3 MODEL DEVELOPMENT FOR PACKED BED CATALYTIC REACTORS

3.3.1 Reactor System

Due to the need for careful, systematic studies of the model development and the design and implementation of control processes, a fully automated, completely instrumented, non-adiabatic, tubular, catalytic reactor was designed and built (Strand, 1984). The reactor system was constructed, not specifically for any particular reaction mechanism, but rather to include various heat and mass transfer mechanisms of interest in control studies and is versatile enough for multivariable computer control studies of a variety of catalytic reactions. Figure 3.3-1 shows a detailed schematic of the experimental system. The primary reaction process chosen for the initial studies is the methanation reaction, discussed in Section 3.3.2.

Because of the difficulties in heat removal from a packed bed, exothermic, catalytic reactor and the subsequent problems with temperature and concentration control, various reactor designs have been used to permit easier heat removal. A common approach is that of using multiple adiabatic reactor beds with interstage quench cooling. In such systems, careful control of the temperature and concentration is necessary to assure that the adiabatic temperature rise across the bed is not too large. Control of such a system was studied by Foss et al. (1980), Silva (1978), Silva et al. (1979), and Wallman et al. (1979).

Another approach is to remove the heat of reaction through the reactor walls into an outer jacket filled with a cooling fluid. This approach is especially useful for highly exothermic systems, since heat is removed continuously along the reactor bed, but requires small reactor diameters due to radial heat transfer limitations. Nonadiabatic reactors for highly exothermic systems are

then typically built with a large number of tubes in a cooling oil shell. Our reactor is designed to simulate one of these tubes. Due to the high radial thermal gradients in such tubes, detailed radial modeling is necessary.

The cooling system for the experimental reactor consists of a high temperature oil (Dowtherm) circulating between the reactor jacket and condenser by natural convection. Continuous temperature measurements of the oil are available, and its boiling temperature can be controlled by adjusting the pressure of nitrogen within the condenser. At normal operating conditions, the cooling fluid will boil¹ in the jacket leading to a countercurrent flow of the oil through the outer jacket, and the reactor wall temperature will be nearly independent of length along the reactor. The coolant system was sized based on expected heat loads of the reactor. A computer-controlled immersion heater is located in the Dowtherm reservoir so that the Dowtherm can also be used to heat up the reactor during start-up, since low operating temperatures can lead to undesired side reactions.

The experimental system is designed for both feed-effluent heat exchange and cold gas recycle that can lead to steady state multiplicities and instabilities and are of great interest in control system design. The cold gas recycle can actually be used to damp the highly exothermic methanation reaction by diluting the feed concentration, inhibiting the forward reaction by the introduction of methane and by increasing the heat capacity of the feed mixture due to the large specific heat of the methane product. A double-acting, reciprocating piston-type compressor is used for the recycle, requiring an upstream water knockout drum to remove the condensing water in the reactor effluent.

In addition to the feed-effluent heat exchanger, an electric preheater is

1. The normal boiling point of Dowtherm is 257° C.

available for controlling the inlet gas temperature to the reactor. Thus the control configuration can consider the complete control of the inlet feed temperature or simply feed-effluent heat exchange.

The actual reactor bed consists of a 1.194 cm radius stainless steel tube, through the center of which runs a 0.159 cm radius thermal well containing thermocouples at various axial positions². The reactor chamber is about 30 cm long and packed with finely ground³ nickel on alumina catalyst particles. Because of the cooling jacket, radially mounted thermal wells are impractical, so all internal temperature measurements are made within the thermal well, as is common in many industrial reactors.

All feed gases to the reactor are supplied by standard gas cylinders. Each stream is controlled by a mass flow controller and is equipped with a regulator, an oxygen absorber/catalyst, a filter/drier, a moisture indicator and a solenoid shutoff valve. Under normal operations for the methanation process, nitrogen, hydrogen and carbon monoxide are used as the inlet streams.

The computer system used for measurements and control is a Digital Equipment (DEC) LSI 11/23 to which all control valves, thermocouples, heaters, and solenoid valves are connected. Concentration measurements are obtained periodically using a gas chromatograph with a thermal conductivity detector. An on-line CO/CO₂ detector will be installed for future control studies.

This experimental system is advantageous for multivariable computer control studies due to its flexibility, the large number of available of measurements, feed-effluent heat exchange, the possibility of product recycle, and the inherent time delays. The reactor can actually be used to study a large number of processes simply by changing the inlet gases and the catalyst.

- 2. The thermal well is designed to contain up to 24 thermocouples.
- 3. 0.8 - 1.0 mm average diameter

3.3.2 Reaction Kinetics

Although a large variety of reaction processes could be studied in this experimental packed bed reactor, the methanation reaction was chosen for the initial studies since methanation is highly exothermic and the temperature and concentration control of exothermic packed bed systems has traditionally been difficult, since methanation is a reaction of great industrial importance and since methanation has been well-characterized in the literature. Methanation is one of a more general class of Fischer-Tropsch processes where carbon monoxide and carbon dioxide are hydrogenated to form various light hydrocarbons and water. When using specific selective catalysts, the resulting product is primarily methane. The catalyst used in our studies is Girdler catalyst G-65, a nickel on alumina catalyst used industrially to specifically promote methanation without the excessive formation of other hydrocarbons. Another advantage in using methanation for the initial control studies is that by simply replacing the catalyst, higher-order Fischer-Tropsch processes with additional control difficulties can be studied.

Although the primary reaction on this catalyst is the methanation of carbon monoxide, appreciable side reactions can occur in the methanation system. These are shown in Table 3.3-1 and include carbon dioxide methanation, steam-shift, carbon deposition, nickel carbonyl formation and other Fischer-Tropsch processes. By operating at $H_2:CO$ ratios of about 3:1 and temperatures above 200° C. most side reactions are suppressed and only the CO methanation, CO_2 methanation, and steam-shift reactions should be significant. Of these three reactions, only two are independent. In light of the discussion below on CO_2 methanation, the CO methanation and steam-shift reactions are taken as the independent reactions. These reactions have been studied extensively and kinetic information is available.

CO Methanation:	$CO + 3H_2 = CH_4 + H_2O$
CO ₂ Methanation:	$CO_2 + 4H_2 = CH_4 + 2H_2O$
Steam-Shift:	$CO + H_2O = CO_2 + H_2$
Carbon Deposition:	$2CO \rightarrow CO_2 + C$
Nickel Carbonyl Formation:	$Ni + 4CO \rightarrow Ni(CO)_4$
Fischer-Tropsche:	$nCO + 2nH_2 = (CH_2)_n + nH_2O$

Table 3.3-1
Reactions in Methanation Systems
(Source: Strand, 1984)

A general rate expression for CO methanation over a nickel catalyst is given by Lee (1973) and Vatcha (1976). They report that a Langmuir-Hinshelwood equation of the form

$$R_M = \frac{k_{0M} e^{-E_{aM}/RT} P_{CO}(P_{H_2})^{0.5}(1-v)}{1 + K_1 P_{H_2} + K_2 P_{CH_4}} \quad (3.3-1)$$

$$\text{where } v = \frac{P_{CH_4} P_{H_2O}}{P_{CO}(P_{H_2})^3} \frac{1}{K_{PM}} \quad (3.3-2)$$

is superior to simple power law relationships. These reaction kinetics (Equations 3.3-1 and 3.3-2) are based on experimental data taken by Lee (1973) in a catalytic CSTR under conditions of ideal mixing for CO methanation over a Harshaw Ni-0104T nickel-Kieselguhr catalyst and extensions by Vatcha (1976) to include the factor (1-v) to reduce the rate to zero at equilibrium. The range of validity for this expression is given in Table 3.3-2, and empirical values for the rate constants are given in Table 3.3-3. Vatcha reports that the low activation energy indicates that the above rate expression describes the global rate, thus incorporating any mass transfer limitations. Gas phase concentrations can then be used in the reaction analysis. This use of gas phase concentrations in the

analysis does not limit the generality of the model, since the mass transfer effects are simply included in the rate expressions and since the interparticle mass transfer limitations are often minimal for packed bed reactors where the gases flow rapidly over solid catalyst particles (Jutan et al., 1977).

As far as side reactions, Vatcha (1976) concludes that

"the presence of CO strongly inhibits the methanation of CO_2 , but CO_2 barely influences the methanation of CO in their mixtures. Thus, in a reactor CO_2 would remain unconverted until the CO became depleted to a very low concentration (typically 200 ppm on nickel) and only then would the CO_2 begin to get methanated."

Total Pressure	1 - 69 atm
Temperature	547 - 755° K
Feed Gas Composition	
$\text{H}_2:\text{CO}$	> 2.85
H_2O	< 5%
CO_2	< 20%
N_2	< 50%
H_2S	< 0.5 ppm

Table 3.3-2
Validity Range of Methanation Rate Expression
(Source: Vatcha, 1976)

Methanation		Steam-Shift	
k_{0M}	$0.075 \frac{\text{mole CO}}{\text{sec g cat atm}^{1.5}}$	k_{0S}	$17.816 \frac{\text{mole CO}_2}{\text{atm}^2 \text{g cat sec}}$
E_{aM}	$6944. \frac{\text{cal}}{\text{g-mole}}$	E_{aS}	$18900. \frac{\text{cal}}{\text{g-mole}}$
K_1	1.47 atm^{-1}	f_1	0.83 atm
K_2	0.73 atm^{-1}	f_2	0.17

Table 3.3-3
Empirical Constants for Equations (3.3-1) and (3.3-3)

Although Vatcha also shows that literature surveys on the steam-shift reaction are inconclusive, we have included this side reaction in our modeling

analysis. This allows consideration of multiple reactions in the control model development. A complete analysis of the steam-shift reaction is provided by Moe (1962). Based on correlations of experimental data, he reports a rate expression of the form

$$R_S = k_{D_S} e^{-E_{AS}/R_T} \left[x_{CO_2} x_{H_2} - \frac{x_{CO} x_{H_2} O}{K_{P_S}} \right] \quad (3.3-3)$$

which should be appropriate over a wide range of operating conditions. The pressure dependence of the steam-shift reaction rate

$$R_{S(P)} = R_{S(1atm)} (f_1 + f_2 P) \quad (3.3-4)$$

is also derived from empirical results (Moe, 1962).

Finally, the equilibrium constants K_{P_M} and K_{P_S} are taken as functions of temperature as given by van't Hoff's equation:

$$\begin{aligned} \ln K_{P_M} &= K_{P_{M1}} + \frac{K_{P_{M2}}}{T} \\ \ln K_{P_S} &= K_{P_{S1}} + \frac{K_{P_{S2}}}{T} \end{aligned} \quad (3.3-5)$$

The necessity of these relationships and values for the parameters in these expressions are presented in Section 3.4.

The empirical rate expressions given in Equations (3.3-1) and (3.3-3) were used for initial simulations. Actual rate expressions for our specific catalyst, reactor bed and expected operating conditions were determined in preliminary experiments using a kinetics reactor (Strand, 1984) built specifically for these studies. Preliminary results show that the kinetics for our catalyst are actually much different than those predicted by the above expressions. The dependence of the rate on the specific concentrations of carbon monoxide, hydrogen, and methane are significantly different, and the activation energy is much higher. In

particular, the reaction was much more sensitive to operating conditions and especially to the temperature, leading to much steeper gradients in the axial concentration and temperature profiles. These new methanation kinetics are of the form (Strand, 1984)

$$R_M = \frac{k_{0M} e^{-E_{aM}/RT} P_{CO} P_{H_2}}{(1 + K_1 P_{CO} + K_2 P_{H_2})^2} e^{-\alpha t} \quad (3.3-6)$$

with the rate constants shown in Table 3.3-4. The final term, $e^{-\alpha t}$, in the rate expression is an empirical catalyst deactivation term. The steam-shift reaction was found to be negligible with the nickel on alumina catalyst under the preliminary experimental conditions.

k_{0M}	1.26×10^{14}	$\frac{\text{mole CO}}{\text{sec gr cat atm}^2}$
E_{aM}	37000.	$\frac{\text{cal}}{\text{mole}}$
K_1	110.	atm^{-1}
K_2	2.32	atm^{-1}
α	0.3	hr^{-1}

Table 3.3-4
Rate Constants for Methanation Reaction
Kinetics Given By Equation (3.3-6)

This rate expression differs significantly from that proposed by Vatcha (1976). The new expression does not include any terms explicitly for the equilibrium (i.e., a term like $1-v$ in Vatcha's expression). This term was not found to be needed under the limited planned operating conditions (relatively low temperatures and concentrations), since at these conditions the equilibrium constant K_{pM} is approximately 10^8 and the reaction therefore goes to nearly 100% completion. Furthermore, experimental results showed a very high activation energy and rapid deactivation of the catalyst. The rate expression includes an empirical deactivation term, although the activity remains nearly constant dur-

ing most control experiments of reasonable duration (3-5 hours) after an initial deactivation period of about 100 hours.

Significant insight into the mathematical modeling of packed bed reactors can then be obtained by completely modeling the experimental reactor using both reaction rate expressions for methanation. Because of the preliminary nature of the new kinetic expression (Equation 3.3-6), much of the analysis presented in this thesis is performed using the methanation kinetics expression given by Equation (3.3-1). Conclusions in this modeling work were verified with the new reaction kinetics, thus allowing consideration of various kinetic models in the modeling analysis. The only major effect of the new kinetics on the modeling work is discussed in Section 3.5.

As pointed out in this section, global reaction kinetics are used in this analysis. These kinetics must then account for the adsorption/desorption on the catalyst surface and the intraparticle diffusion. However, most available kinetic information is based on steady state data. A major concern is then the importance of the transient behavior of the adsorption/desorption processes and the characteristic times for the intraparticle diffusion dynamics. Although the intraparticle diffusion can be shown to be generally insignificant in the reactor dynamics,⁴ experimental efforts are needed to gain further information on the dynamics of the adsorption/desorption processes.

3.3.3 Formation of Complete Mathematical Model

A two-dimensional, two-phase mathematical representation of the experimental packed bed reactor is developed in this section. This mathematical

4. The time constants for the temperature and concentration profiles in the pellet to change are at least an order of magnitude faster than the time constants for the temperature and concentration profiles in the reactor bed.

model significantly extends previous packed bed modeling studies through a reduction in *a priori* simplifications. Detailed consideration of the common simplifications is then possible, and the validity of certain assumptions can be assessed in light of the combined effect of multiple assumptions and of the overall benefits of the assumptions. The general view that modeling simplifications will lead to a reduction in numerical solution effort and are therefore desirable or in many cases necessary is shown to not be universally correct with today's new computational capabilities. Furthermore, most previous modeling studies have been restricted to specific systems due to the applicability of the chosen assumptions for each individual case. The approach taken in this work was to minimize these assumptions so as to develop a general packed bed reactor model that could be transported to other systems with minimal effort.⁵

The heterogeneous packed bed reactor consisting of solid, nonspherical catalyst particles and reacting gas is treated as two phases with the assumption that the packed bed may be treated as a continuum insofar as changes occur smoothly and continuously within each phase throughout the bed. This assumption is generally valid for most industrial reactors and should be valid under the conditions of this analysis (Carberry and Wendel, 1963; Hlavacek, 1970; Stewart, 1967), since the ratio of bed diameter to particle diameter for the experimental reactor is about 25 and the axial aspect ratio is very large (200 - 300). The heat and mass fluxes can then be treated in a form analogous to Fourier and Fick laws, respectively.

Previous investigations have often assumed that the difference between the catalyst and gas temperatures are negligible in tubular reactors for fast flowing

5. Although this current modeling is for a general, nonadiabatic packed bed reactor with an axial thermal well, the analysis easily extends to the consideration of adiabatic reactors and those without a thermal well. These are merely subsets of the more general case.

gas-solid systems. Industrial experience and experimental studies (Froment, 1974; Gould, 1969; Hoiberg et al., 1971; Jutan et al., 1977) have verified that there is essentially no temperature difference ($< 5^\circ \text{ K}$) between the catalyst and gas at steady state. Furthermore, this assumption has also often been defended by the argument that it is difficult in practice to measure separately the gas and solid temperatures. However, for control studies, the two-phase representation is necessary since considerable ($> 10^\circ \text{ K}$) differences can exist between gas and solid temperatures during dynamic conditions, and for control applications, the dynamic situation is of major importance. The measurement problems can and often are in practice reduced by measuring temperatures within an internal thermal well rather than in either the gas or catalyst. Modeling of the thermal well in the system is then necessary to perform accurate dynamic control.

A variety of assumptions is often made concerning the axial and radial dispersion of mass and energy. These assumptions are based on a significant amount of supporting literature and for most systems involve neglecting axial and radial mass diffusion and axial energy diffusion, depending on the aspect ratios of the reactor bed. Although these assumptions have often been necessary in the past due to limitations of the computational techniques available for numerical solutions of the model and in particular the second derivative diffusion terms, current techniques do not require such assumptions and may indeed be hindered by them.

The present analysis begins by incorporating all axial and radial dispersion effects, including axial conduction within the thermal well. Axial conduction in the outer wall is neglected based on the first assumption presented below and on Bonvin's (1980) results that the conduction in the outer wall is most likely insignificant and can be neglected from the model if axial dispersion in the bed is retained. Although many dynamic analyses of packed bed reactors have

neglected radial gradients to limit the complexity of the resulting model, this work considers a packed bed system with extensive cooling at the reactor wall and thus must account for the radial profiles within the bed (Jutan et al., 1977). Radial temperature gradients are neglected within the thermal well due to its comparatively small radius and high thermal conductivity.

Also accounted for by the model are density, heat capacity, and molecular weight variations due to temperature, pressure, and mole changes, along with temperature induced variations in equilibrium constants, reaction rate constants, and heats of reaction. Axial variations of the fluid velocity are accounted for in the mathematical description using the overall mass conservation or continuity equation. These variations are the result of axial temperature changes and the change in the number of moles due to the methanation reaction.

The major assumptions underlying the original model are:

1. The reactor wall temperature is equal to the cooling fluid temperature and is independent of length along the reactor (Carberry and Wendel, 1963; Jutan et al., 1977; Smith, 1970). The validity of this assumption is generally based on the very high thermal conductivity of the reactor wall and on the use of boiling fluids or high convection in the outer cooling shell. The experimental reactor is designed to have boiling fluid in the cooling jacket, as is common in highly exothermic industrial reactors.
2. Gas properties are functions of temperature, pressure, and total moles as dictated by the ideal gas law. The assumption of ideal gas behavior will be accurate as long as the operating temperatures of the reactor are much higher than the critical temperatures of the component species and the pressures are relatively low. These conditions should be met at the

expected operating conditions of the experimental methanation reactor and are in general valid for most gaseous reaction systems.

3. There is no radial velocity, and the axial velocity across the radius of the packed bed is uniform. Schwartz and Smith (1953) found that the velocity across the diameter of a packed bed is not uniform for radial aspect ratios (tube-to-particle diameter) less than about 30, due to the significant effect of the increased void space near the wall where the particles are locally ordered. This result has been verified by Hoiberg et al. (1971) for a packed bed reactor with radial aspect ratio about 50. They considered a radial velocity function suggested by experimental observations with a sharp peak about 15% greater than the mean fluid velocity situated close to the wall. Simulations using their model showed results virtually identical to those obtained with a uniform velocity profile. Although the radial aspect ratio for our experimental reactor is under 30,⁶ a uniform velocity profile was assumed. Preliminary residence time distribution studies should be conducted on the experimental packed bed reactor to test this assumption. Although in many cases it may be desired to increase the radial aspect ratio (possibly by crushing the catalyst), this may be difficult in our system due to the highly exothermic solid-catalyzed reaction that can lead to excessive temperature rises near the center of the bed. Carberry (1976) recommends reducing the radial aspect ratio to minimize these temperature gradients. If the velocity profile in the experimental reactor is significantly nonuniform, the mathematical model developed here allows predictive equations such as those by Fahien and Stankovic (1979) to be easily incorporated.

6. Actually there are only about 12 particle diameters between the thermal well and outer wall.

4. The physical properties of the solid catalyst and thermal well are taken as constant, since the conditions within the reactor introduce only minor variations in these parameters, and the heats of reaction and gas heat capacities are taken as linear functions of temperature.
5. Hlavacek (1970) has shown that radiation between the solid catalyst and gas can significantly affect the temperature dynamics in packed bed systems operating in excess of 673° K. Since the system considered in this work usually operates well below these conditions, radiation terms are not explicitly included in the model. However, their effect can to some degree be accounted for in the overall heat transfer coefficients.⁷

It should be noted that the model developed in this analysis may be much more complex than that necessary for accurate description of the experimental methanation reactor. The increased complexity and generality allow simple extensions of the model to other systems and to include additional physical and chemical processes such as radial velocity variations and the dependence of heat transfer coefficients on physical properties as defined by heat transfer correlations.

3.3.4 Mathematical Relationships

The analysis in this thesis centers around the actual reactor bed. Combining these results with a simple analysis of the external processes, such as the product recycle and feed-effluent heat exchanger, allows overall system analysis. Figure 3.3-2 shows an expanded section of the reactor bed and defines the coordinate system for the mathematical modeling.

A complete mathematical description of the reactor bed results using the

7. But not entirely since radiation effects are nonlinearly related to temperature.

six differential equations that describe the catalyst, gas, and thermal well temperatures, CO and CO₂ concentrations, and gas velocity. These are the continuity equation, three energy balances, and two component mass balances. The following equations are written in dimensional quantities and are general for packed bed analyses. Systems without a thermal well can be modeled simply by letting h_{ws}, h_{tg}, and R₀ equal zero and by eliminating the thermal well energy equation. Adiabatic analysis simply involves setting h_{ws} and h_{wg} equal to zero.

Total mass conservation (continuity):

$$\frac{\partial \rho_g}{\partial t} + \frac{\partial(\rho_g u_g)}{\partial z} = 0 \quad (3.3-7)$$

$$z=0 \quad \rho_g u_g = \rho_{g0} u_{g0}$$

Energy balance for the gas:

$$\rho_g c_{p_g} \frac{DT}{Dt} = \nabla \cdot k \nabla T + Q \quad (3.3-8)$$

Then for the reactor bed after assuming k_{zg} and k_{rg} constant,

$$\varepsilon \rho_g c_{p_g} \frac{\partial T_g}{\partial t} = -\varepsilon \rho_g u_g c_{p_g} \frac{\partial T_g}{\partial z} + k_{zg} \frac{\partial^2 T_g}{\partial z^2} - \frac{U_{sg}(T_g - T_s)}{V_b} + \frac{k_{rg}}{r} \frac{\partial}{\partial r} \left[r \frac{\partial T_g}{\partial r} \right] \quad (3.3-9)$$

$$r=R_0 \quad k_{rg} \frac{\partial T_g}{\partial r} = h_{tg}(T_g - T_t)$$

$$r=R_1 \quad -k_{rg} \frac{\partial T_g}{\partial r} = h_{wg}(T_g - T_w)$$

$$z=0 \quad k_{zg} \frac{\partial T_g}{\partial z} = h_{sg}(T_g - T_s) - u_g c_{p_g} \rho_g \varepsilon (T_0 - T_g)$$

$$z=L \quad -k_{zg} \frac{\partial T_g}{\partial z} = h_{sg}(T_g - T_s)$$

Note that the convective term in the outlet boundary condition is generally assumed negligible (Hoiberg et al., 1971). This assumption is used throughout the ensuing analysis. Also note that the gas heat capacity, c_{p_g} , gas density, ρ_g , and gas velocity, u_g , are functions of position and time due to their dependence on mole changes, pressure, and temperature. Original calculations considered the gas heat capacity and thermal conductivity as linear functions of temperature since expected changes in molar composition throughout the bed had minimal effects (< 1%) on these properties. However, later analysis replaced the thermal conductivities and heat transfer coefficients with dimensionless Peclet and Biot numbers which were taken as constant throughout the bed.

Energy balance for the catalyst:

Using a similar analysis to that for the energy balance of the gas and after assuming constant physical properties of the solid phase,

$$(1-\varepsilon)\rho_s c_{p_s} \frac{\partial T_s}{\partial t} = k_{zs} \frac{\partial^2 T_s}{\partial z^2} + (-\Delta H_M)R_M + (-\Delta H_S)R_S - \frac{U_{sg}(T_s - T_g)}{V_b} + \frac{k_{rs}}{r} \frac{\partial}{\partial r} \left[r \frac{\partial T_s}{\partial r} \right] \quad (3.3-10)$$

$$r=R_0 \quad k_{rs} \frac{\partial T_s}{\partial r} = h_{ts}(T_s - T_t)$$

$$r=R_1 \quad -k_{rs} \frac{\partial T_s}{\partial r} = h_{ws}(T_s - T_w)$$

$$z=0 \quad k_{zs} \frac{\partial T_s}{\partial z} = h_{sg}(T_s - T_g)$$

$$z=L \quad -k_{zs} \frac{\partial T_s}{\partial z} = h_{ag}(T_s - T_g)$$

The heats of reaction for the methanation and steam-shift reactions are

taken as linear functions of temperature:

$$\Delta H_i = \Delta H_{i_1} T + \Delta H_{i_2} \quad i = S, M \quad (3.3-11)$$

based on literature data and standard temperature dependence of the heat capacities of the gas components. A verification of the necessity and applicability of this relationship along with the specific parameters for methanation and steam-shift is given in Section 3.4.

Energy balance for the thermal well:

Assuming constant physical properties in the thermal well,

$$\rho_t c_{p_t} \frac{\partial T_t}{\partial t} = k_{zt} \frac{\partial^2 T_t}{\partial z^2} + \frac{U_{ts}}{V_t} (T_{s_{z=R_0}} - T_t) + \frac{U_{tg}}{V_t} (T_{g_{z=R_0}} - T_t) \quad (3.3-12)$$

$$z=0 \quad T_t = T_{t_0}$$

$$z=L \quad \frac{\partial T_t}{\partial z} = 0$$

De Wasch and Froment (1971) discuss the calculation of the wall heat transfer coefficients for the fluid and gas phases based on a lumped wall heat transfer coefficient. Furthermore, radial heat conduction in the thermal well is neglected since it should be of minor importance for a thin solid well.

Mass balance in the reactor section:

Since two independent reactions are expected to be important within the reactor, a mass balance must be written for each of two independent species. Due to the sensitivity of the concentrations of the gaseous species in the reactor under the planned operating conditions and to difficulties in accurate concentration measurements, these two are taken as CO and CO₂ in this analysis. Both of these species can accurately be detected using a

chromatograph with a simple thermal conductivity detector or with a continuous CO/CO₂ analyzer. Note that $i = 1$ refers to CO and $i = 2$ refers to CO₂ in the following analyses.

The equation of continuity in cylindrical coordinates is (Bird et al., 1960)

$$\frac{\partial c_i}{\partial t} + \left[\frac{1}{r} \frac{\partial (r N_{ir})}{\partial r} + \frac{1}{r} \frac{\partial N_{i\theta}}{\partial \theta} + \frac{\partial N_{iz}}{\partial z} \right] = R_i \quad (3.3-13)$$

But

$$1. \quad \frac{\partial N_{i\theta}}{\partial \theta} = 0$$

$$2. \quad N_i = J_i + c_i u_g = -c D \nabla x_i + c_i u_g$$

thus

$$N_{iz} = c_i u_g - c D_z \frac{\partial x_i}{\partial z}$$

$$N_{ir} = -c D_r \frac{\partial x_i}{\partial r}$$

If we then incorporate the void fraction and apply the continuity equation for species i along with Fick's law of diffusion and the assumption of constant diffusivity and no radial velocity

$$\frac{\partial c_i}{\partial t} = -\frac{\partial (c_i u_g)}{\partial z} + D_z \frac{\partial}{\partial z} \left(c \frac{\partial x_i}{\partial z} \right) + \frac{D_r}{r} \frac{\partial}{\partial r} \left(r c \frac{\partial x_i}{\partial r} \right) - \bar{R}_i \quad (3.3-14)$$

where $\bar{R}_1 = R_M - R_S$, $\bar{R}_2 = R_S$.

$$r=R_0, R_1 \quad \frac{\partial x_i}{\partial r} = 0$$

$$z=0 \quad u_g(c_{i_0} - c_i) = -c D_z \frac{\partial x_i}{\partial z}$$

$$z=L \quad \frac{\partial x_i}{\partial z} = 0$$

The rate terms R_M and R_S are taken to be global rates, incorporating all mass transfer limitations. This allows bulk phase concentrations to be used throughout the analysis. Although species concentration is proportional to mole fraction, $c_i = cx_i$, complications arise since the total number of moles decreases as the methanation reaction progresses. Therefore to simplify the analysis technique, the mass balances are written using molecular weights and mole fractions based on inlet conditions. Letting δ be the moles of CO reacted in the methanation reaction per total inlet moles,

$$\delta = \frac{x_{1_0} + x_{2_0} - x_1 - x_2}{1 + 2x_1 + 2x_2} \quad (3.3-15)$$

the following relations hold

$$\hat{M}_g = M_g(1-2\delta), \quad \hat{x}_i = x_i(1-2\delta). \quad (3.3-16)$$

The advantage of this formulation is that the molecular weight based on inlet conditions, \hat{M}_g , is constant. Thus

$$c_i = \frac{x_i \rho_g}{M_g} = \frac{\hat{x}_i \rho_g}{\hat{M}_g}, \quad c = \frac{\rho_g}{M_g} = \frac{\rho_g(1-2\delta)}{\hat{M}_g}. \quad (3.3-17)$$

Then after application of the overall continuity, Equation (3.3-15) becomes

$$\begin{aligned} \rho_g \frac{\partial \hat{x}_i}{\partial t} &= -u_g \rho_g \frac{\partial \hat{x}_i}{\partial z} + D_z \frac{\partial}{\partial z} \left[\rho_g \frac{\partial \hat{x}_i}{\partial z} + \frac{2\rho_g \hat{x}_i}{1-2\delta} \frac{\partial \delta}{\partial z} \right] \\ &+ \frac{D_r}{r} \frac{\partial}{\partial r} \left[r \rho_g \frac{\partial \hat{x}_i}{\partial r} + \frac{2\rho_g \hat{x}_i r}{1-2\delta} \frac{\partial \delta}{\partial r} \right] - \frac{\bar{R}_i M_g}{\varepsilon} \end{aligned} \quad (3.3-18)$$

$$r=R_0, R_1 \quad \frac{\partial \hat{x}_i}{\partial r} + \frac{2\hat{x}_i}{1-2\delta} \frac{\partial \delta}{\partial r} = 0$$

$$z=0 \quad u_g(\hat{x}_{i_0} - \hat{x}_i) = -D_z \left[\frac{\partial \hat{x}_i}{\partial z} + \frac{2\hat{x}_i}{1-2\delta} \frac{\partial \delta}{\partial z} \right]$$

$$z=L \quad \frac{\partial \hat{x}_i}{\partial z} + \frac{2\hat{x}_i}{1-2\delta} \frac{\partial \delta}{\partial z} = 0$$

Furthermore, algebraic manipulation of the boundary conditions using the reaction relationship $\delta = \hat{x}_{1_0} + \hat{x}_{2_0} - \hat{x}_1 - \hat{x}_2$ leads to⁸

$$\begin{array}{ll} r=R_0, R_1 & \frac{\partial \hat{x}_i}{\partial r} = 0 \\ z=0 & u_g(\hat{x}_{i_0} - \hat{x}_i) = -D_z \frac{\partial \hat{x}_i}{\partial z} \\ z=L & \frac{\partial \hat{x}_i}{\partial z} = 0 \end{array}$$

Additional relations:

Finally, relationships for density and pressure changes are necessary. The ideal gas law leads to

$$\rho_g = \frac{M_g P}{R_g T} . \quad (3.3-19)$$

The changes in the pressure along the bed are taken as linear by assuming uniform packing and negligible wall effects. The overall pressure drop across the bed is simply defined by the Ergun equation (Perry and Chilton, 1973)

$$\Delta P = L \left[\frac{150(1-\varepsilon)\mu_g}{D_p} + 1.75 \rho_{g_0} u_{g_0} \right] \frac{1-\varepsilon}{\varepsilon} \frac{u_{g_0}}{D_p} \quad (3.3-20)$$

where $D_p = \frac{6(\text{volume of particle})}{\text{external surface area of particle}}$

This could easily be replaced with a Blake-Kozeny type relationship

$$\frac{\partial P}{\partial z} = -k_b \mu_g u_g \quad P = P_0 \text{ at } z=0 \quad (3.3-21)$$

if the original assumption is inadequate.

8. The stipulation $\hat{x}_{1_0} + \hat{x}_{2_0} \neq \frac{1}{2}$ is needed for rigorous mathematical derivation of the reduced boundary conditions.

It should be noted that the importance of the continuity equation in the general modeling presented throughout this thesis may be questionable since its only use is in evaluating actual velocities within the reactor bed as influenced by the mole, temperature, and pressure changes. Because of the use of mass velocities ($\rho_g u_g$) throughout much of the analyses, the importance of the actual velocities is really restricted to analyses where pressure relationships such as the Blake-Kozeny equation or velocity effects on heat transfer parameters are considered. Since our analysis is set up to be general and allow the inclusion of these effects, the continuity equation is necessary. As seen later, very little increased computational effort is introduced by retaining this equation, since it is solved as a set of algebraic equations.

3.3.5 Numerical Solution

Before attempting to solve the system of partial differential equations, they are reduced to dimensionless form. The axial parameters are normalized with respect to the reactor length, L , radial parameters with respect to the outer radius, R_1 , time with respect to the characteristic time L/\bar{u}_{g0} , and the remaining parameters with respect to the steady state inlet conditions. The concentrations are actually normalized with respect to the inlet steady state concentration of CO rather than with respect to each individual component, since some inlet concentrations (except CO) may be zero during normal experimental conditions.

The resulting mathematical system consists of six coupled, three-dimensional, nonlinear partial differential equations along with nonlinear algebraic boundary conditions, which must be solved to obtain the temperature profiles in the gas, catalyst, and thermal well, the concentration profiles, and

the velocity profile. These equations are presented in Appendix 2. In their present form, direct solution is not possible. However, approximation techniques are available to reduce the equations to a set of first-order ordinary differential equations in the time domain. The resulting system can then be solved numerically using a variety of standard techniques. In this work, the method of orthogonal collocation is used for this reduction, since it has proven to be an extremely powerful technique in reactor modeling (Bonvin, 1980; Finlayson, 1971; Jutan et al., 1977).

3.3.5.1 Solution Techniques

Considerable emphasis has been placed during the past twenty years on numerical solution techniques for complex nonlinear systems of the types common in chemical reactors. Traditional finite difference schemes are being replaced by applications of the methods of weighted residuals. Finlayson (1972, 1980) has presented and compared the application of these various techniques for the nonlinear analysis of problems in chemical engineering.

The finite difference method involves dividing the domain up into intervals with the boundary points between intervals being called the grid or mesh points. Then for a continuous function across the interval, a Taylor series expansion can be used to deduce difference formulas for first and second derivatives. If the differential equations are written at each grid point using the difference formulas and the values at the first and last grid point solve the boundary conditions, enough equations are available to solve for the value of the function at each grid point and thus provide a representation of the solution. For most chemical systems, the resulting equations are nonlinear, and accurate solution requires a large number of grid points. Solution of the system is not trivial but

can usually be obtained quite rapidly using various standard numerical procedures (Dahlquist and Björke, 1974; Davis, 1984; Finlayson, 1980).

The finite difference method can easily be extended to multidimensional systems by applying the same techniques in each of the dimensions. However, the scale of the numerical problem increases dramatically with the number of dimensions. Since nonadiabatic packed bed reactors consist of two important spatial dimensions, radial and axial, along with the time dimension and usually require a large number of grid points, accurate solution using the finite difference scheme is often computationally prohibitive and may limit the complexity of the mathematical model.

The method of weighted residuals presented in detail by Finlayson (1972, 1980) is a general method of obtaining solutions to both linear and nonlinear systems of partial differential equations and is often used in one of its forms to reduce the computation time from that of the finite difference technique. In the method of weighted residuals, the unknown exact solutions are expanded in a series of specified trial functions, that are chosen to satisfy the boundary conditions, with unknown coefficients that are chosen to give the 'best' solution to the differential equations:

$$y(x) = \varphi_0(x) + \sum_{k=0}^N c_k \varphi_k(x) \quad (3.3-22)$$

These trial functions are substituted into the differential equations, and the result is the residual (R). This residual is weighted by functions characteristic of the particular method, and the weighted residuals are minimized over the domain of the independent variable (V). In particular, the weighted integrals of the residuals are set to zero:

$$(w_j, R) = 0 \quad j = 1, 2, \dots, N \quad (3.3-23a)$$

where the inner product is defined by

$$(w_j, R) = \int_V w_j R dV \quad (3.3-23b)$$

The method of weighted residuals is comprised of the following basic techniques, depending on the choice of the weighting function (Finlayson, 1972):

Subdomain Method

The domain is divided up into N subdomains, V_j , and the weights are chosen as

$$w_j = \begin{cases} 1 & x \text{ in } V_j \\ 0 & x \text{ not in } V_j \end{cases} \quad (3.3-24)$$

The differential equation, integrated over the subdomain, is then zero. As N increases, the differential equation is satisfied on the average in smaller and smaller subdomains and approaches the exact solution everywhere.

Collocation Method

The weighting functions are chosen to be the Dirac delta function

$$w_j = \delta(x - x_j) \quad (3.3-25)$$

Thus

$$\int_V w_j R dV = R \Big|_{x_j} \quad (3.3-26)$$

This technique then forces the residual to be zero at N specified collocation points. As N increases, the residual is zero at more and more points and presumably approaches zero everywhere.

Least Squares Method

The least squares method uses the weighting functions

$$w_j = \frac{\partial R}{\partial c_j} \quad (3.3-27)$$

so that the mean square residual $\int_V R^2(c_i, x) dV$ is being minimized.

The mean square residual is zero for the exact solution, so that, as the number of parameters is increased, the mean square residual gets smaller and the approximate solution approaches the exact solution.

Galerkin's Method

In this method, the weighting functions are chosen to be the trial functions, which must be selected as members of a complete set of functions. (A set of functions is complete if any function of a given class can be expanded in terms of the set.) Also according to Finlayson (1972),

"a continuous function is zero if it is orthogonal to every member of a complete set. Thus the Galerkin method forces the residual to be zero by making it orthogonal to each member of a complete set of functions (in the limit as $N \rightarrow \infty$)."

Method of Moments

In the Method of Moments, the weighting functions are chosen as

$$w_j = x^{j-1} \quad (3.3-28)$$

Thus successively higher moments of the residual are required to be zero.

All of these methods of weighted residuals have proven to be quite powerful and have been shown by Finlayson (1972, 1980) to be accurate numerical techniques

superior to finite difference schemes for the solution of complex differential equation systems.

Another potential solution technique appropriate for simulations of the packed bed reactor is the method of characteristics. This procedure is suitable for hyperbolic partial differential equations of the form obtained from the energy balance for the gas and catalyst and the mass balances if axial dispersion is neglected and if the radial dimension is first discretized by a technique such as orthogonal collocation. The thermal well energy balance would still require a numerical technique that is not limited to hyperbolic systems since axial conduction in the well should be significant.

3.2.0.1 Orthogonal Collocation

Of the various methods of weighted residuals presented in the previous section, the collocation method and in particular the orthogonal collocation technique described in this section has proven to be quite effective in the solution of complex, nonlinear problems of the type typically encountered in chemical reactors. The basic procedure was used by Stewart and Villadsen (1969) for the prediction of multiple steady states in catalyst particles, by Ferguson and Finlayson (1970) for studying the transient heat and mass transfer in a catalyst pellet, and by McGowin and Perlmutter (1971) for local stability analysis of a nonadiabatic tubular reactor with axial mixing. Finlayson (1971, 1972, 1974) showed the importance of the orthogonal collocation technique for packed bed reactors.

The orthogonal collocation method has several important differences from other reduction procedures. With other techniques, difficulties are often encountered in deriving the values of the integrals involving complex nonlinear

terms. In collocation, it is only necessary to evaluate the residual at the collocation points. The orthogonal collocation scheme developed by Villadsen and Stewart (1967) for boundary value problems has the further advantage that the collocation points are picked optimally and automatically so that the error decreases much faster as the number of terms increases. The trial functions are taken as a series of orthogonal polynomials which satisfy the boundary conditions and the roots of the polynomials are taken as the collocation points. Thus the choice of the trial functions and collocation points is no longer arbitrary, and further analysis (Finlayson, 1972) shows that with this choice, low-order collocation results are more dependable. A major simplification that arises with this method is that the solution can be derived in terms of its value at the collocation points, instead of in terms of the coefficients in the trial functions, and that at these points the solution is exact.

A rigorous description of the technique requires appropriate definitions of the orthogonal polynomials $P_m(x)$ as

$$P_m(x) = \sum_{j=0}^m c_j x^j \quad (3.3-29)$$

with degree m and order $m+1$. The coefficients are defined so as to require the orthogonality condition

$$\int_a^b w(x) P_n(x) P_m(x) dx \quad n = 0, 1, 2, \dots, m-1 \quad (3.3-30)$$

to be satisfied for weighting functions $w(x) \geq 0$. For boundary value problems, the solution is expanded in terms of orthogonal polynomials with the first term satisfying the boundary conditions followed by a series that has unknown coefficients, with each term satisfying the homogeneous boundary conditions. Various expansions are then possible. The most common and useful are:

$$\begin{aligned}y_N(x) &= \sum_{i=1}^{N+1} a_i x^{i-1} \\y_N(x) &= \sum_{i=1}^{N+1} b_i P_{i-1}(x) \\y_N(x) &= \sum_{i=1}^{N+1} y(x_i) L_i(x)\end{aligned}\quad (3.3-31)$$

Since derivatives are actually expressed in terms of the solution at all of the grid points in the collocation scheme rather than simply in terms of the neighboring grid points as in finite difference schemes, the orthogonal collocation technique then leads to computer programs that are relatively simple and to numerical solutions that require a very few number of collocation points in comparison to the number of grid points necessary for a similar finite difference solution.

3.3.5.3 Model Reduction

Finite difference methods have traditionally been used for reduction of partial differential equation systems to ordinary differential equations or even to systems of algebraic equations that can readily be solved using simple numerical techniques. However in chemical reactors, this method has a major drawback. For the system of six coupled, three-dimensional, nonlinear partial differential equations describing the methanation reactor, if we assume that even 5 grid points are adequate for discretizing the radial direction and 30 grid points for the axial direction,⁹ we have a mesh of 150 grid points. At each grid point, there are six ordinary differential equations in time. Hence the total number of ordinary differential equations necessary to describe the system would be 900! Much too large for extensive simulations or for control.

The method of orthogonal collocation on the other hand has been very suc-

⁹. Other studies have used up to 20 radial grid points and 10000 axial grid points!

cessfully applied to chemical reactors and provides an accurate means of transforming partial differential equations into a reasonably small set of ordinary differential equations. This procedure is applied to the reactor model to discretize both the radial and axial dimensions, leaving a manageable set of ordinary differential equations in time.

3.3.5.3.1 Radial Collocation

The first step in the solution procedure is discretization in the radial direction. This involves writing the three-dimensional differential equations as a possibly enlarged set of two-dimensional equations at the radial collocation points with the assumed profile identically satisfying the radial boundary conditions. An examination of experimental measurements (Valstar et al., 1975) and typical radial profiles (Finlayson, 1971) indicates that radial temperature profiles can adequately be represented by a quadratic function of radial position. The quadratic representation is preferable to one of higher order since only one interior collocation point is then necessary,¹⁰ thus not increasing the dimensionality of the system. The assumed profile is of the form:

$$\Theta^{(n)}(\vartheta, \zeta, r) = \sum_{i=1}^{n+2} d_i(\vartheta, \zeta) r^{i-1} \quad (3.3-32)$$

with the number n of interior radial collocation points taken as one. This profile must satisfy the boundary conditions and must be exact at the collocation points $r = \varphi_0$, r_c , and 1.0, where the interior collocation point r_c is selected as the zero of the appropriate orthogonal polynomial. This formulation is equivalent to the trial function

$$y(x) = b + cx + x(1-x) \sum_{i=1}^N a_i P_{i-1}(x)$$

10. Along with two boundary points, there are three collocation points.

(3.3-33)

given by Villadsen and Stewart (1967) for nonsymmetric profiles.¹¹

Rigorous application of the procedure as presented by Finlayson (1972) or the equivalent procedure presented below of satisfying the boundary conditions with the assumed profile, leads to the coefficients $d_i(\vartheta, \zeta)$ for the gas and temperature profiles in terms of the temperatures at the collocation point, within the well, and at the outer wall. Since the objective of radial collocation is to eliminate the radial derivatives, Equation (3.3-32) is then substituted into the partial differential equations.

For example, consider the radial temperature profile in the gas. At the three radial collocation points $r = \varphi_0$, r_c , and 1.0, let the gas temperatures be Θ_{g_0} , Θ_{g_r} , and Θ_{g_1} and assume that the radial profile is quadratic:

$$\Theta_g(\vartheta, \zeta, r) = d_0(\vartheta, \zeta) + d_1(\vartheta, \zeta)r + d_2(\vartheta, \zeta)r^2 \quad (3.3-34)$$

This profile must satisfy the boundary conditions

$$\begin{aligned} \frac{\partial \Theta_g}{\partial r} \Big|_{r=\varphi_0} &= \lambda_{trg}(\Theta_{g_{r=\varphi_0}} - \Theta_t) \\ \frac{\partial \Theta_g}{\partial r} \Big|_{r=1} &= -\lambda_{wrg}(\Theta_{g_{r=1}} - \Theta_w) \end{aligned} \quad (3.3-35)$$

where λ_{trg} and λ_{wrg} are the dimensionless radial Biot numbers at the thermal well and cooling wall, respectively. The profile must also be exact at the three collocation points:

$$\begin{aligned} \Theta_{g_0} &= d_0 + d_1\varphi_0 + d_2\varphi_0^2 \\ \Theta_{g_r} &= d_0 + d_1r_c + d_2r_c^2 \\ \Theta_{g_1} &= d_0 + d_1 + d_2 \end{aligned} \quad (3.3-36)$$

After rearranging and eliminating Θ_{g_0} and Θ_{g_1} ,

11. Due to the presence of the thermal well, a nonsymmetric function is necessary to describe the profile between $r = \varphi_0$ and $r = 1.0$.

$$\begin{bmatrix} 1 & r_c & r_c^2 \\ \lambda_{trg} & \varphi_0 \lambda_{trg} - 1 & \varphi_0^2 \lambda_{trg} - 2\varphi_0 \\ \lambda_{wrg} & \lambda_{wrg} + 1 & \lambda_{wrg} + 2 \end{bmatrix} \begin{bmatrix} d_0 \\ d_1 \\ d_2 \end{bmatrix} = \begin{bmatrix} \Theta_{g_r} \\ \lambda_{trg} \Theta_t \\ \lambda_{wrg} \Theta_w \end{bmatrix} \quad (3.3-37)$$

The expressions for $d_i(\vartheta, \xi)$ in terms of Θ_{g_r} , Θ_t and Θ_w can be simply obtained by applying Cramer's Rule. These solutions are shown in Appendix 3.

Since

$$\begin{aligned} \frac{\partial \Theta_g}{\partial r} &= d_1 + 2d_2 r \\ \frac{\partial^2 \Theta_g}{\partial r^2} &= 2d_2 \end{aligned} \quad (3.3-38)$$

the dimensionless form of Equation (3.3-10) becomes

$$\rho_g c_{p_g} \frac{\partial \Theta_g}{\partial \vartheta} = -\rho_g v_g c_{p_g} \frac{\partial \Theta_g}{\partial \xi} + \alpha_g \frac{\partial^2 \Theta_g}{\partial \xi^2} + \beta_g \left[4d_2 + \frac{d_1}{r_c} \right] + \gamma_g (\Theta_s - \Theta_g) \quad (3.3-39)$$

where Θ_g and Θ_s are now the temperatures at the radial collocation point r_c , and ρ_g and c_{p_g} are now dimensionless parameters, normalized with respect to the inlet steady state values. Similar results are obtained for the energy balance of the catalyst. Although the solutions of the differential equations are then obtained for the temperatures at the radial collocation point, the temperature at any radial point can easily be determined using the radial profile given by Equation (3.3-34) along with the solutions to Equation (3.3-37) for $d_i(\vartheta, \xi)$ presented in Appendix 3.

The radial collocation point is then selected as the zero of the orthogonal polynomial for cylindrical geometry between $r = \varphi_0$ and $r = 1.0$. To be rigorous, the entire analysis could be based on the shifted variable

$$r' = \frac{r - \varphi_0}{1 - \varphi_0} \quad 0 \leq r' \leq 1 \quad (3.3-40)$$

However, lengthy algebraic manipulations show that the results are identical.

Nevertheless, it is convenient to use r' to find the radial collocation point, which is then the zero of the Jacobi polynomial for a nonsymmetric system between zero and one.¹²

For radial concentration profiles, a quadratic representation may not be adequate since application of the zero flux boundary conditions at $r = \varphi_0$ and $r = 1.0$ leads to $d_2 = d_3 = 0$. Thus a quadratic representation for the concentration profiles reduces to the assumption of uniform radial concentrations, which for a highly exothermic system may be significantly inaccurate. Although additional radial collocation points greatly increase the dimensionality of the resulting model, they may be necessary to accurately express the radial concentration profiles. Preliminary analysis in this section considers only one interior radial concentration collocation point, although a detailed analysis of this assumption is presented in Section 3.4.5. In that analysis, an assumed concentration profile of the same form as Equation (3.3-32) is solved with several interior radial collocation points to determine the radial concentration coefficients. The mass balances are then satisfied at each collocation point.

Thus, the original differential equations have been reduced from three-dimensional in variables ξ , r , and ϑ to two-dimensional in variables ξ and ϑ by orthogonal collocation in the radial variable r . The reduced temperature equations are a function of the dependent variables at the radial collocation point r_c , but incorporate radial information via the well and wall temperatures. Radial profiles can be generated from the collocation equation using the expressions for the coefficients $d_i(\vartheta, \xi)$ presented in Appendix 3. Similarly, the continuity equations are functions of the concentrations at each collocation point for multipoint radial collocation. With one interior collocation point for the concentration analysis, the system consists of six differential equations describing the

¹² The single radial collocation point is taken as $r' = 0.5$ for the methanation system.

overall continuity, energy balance for the thermal well, energy balance for the gas and catalyst in terms of conditions at r_c , and mass balances for CO and CO₂. This shows the incentive for using only one radial collocation point, since the number of two-dimensional partial differential equations is the same as the original number of three-dimensional equations.

3.3.5.3.2 Axial Collocation

Since the resulting system after radial collocation is still too complex for direct mathematical solution, the next step in the solution process is discretization of the two-dimensional system by orthogonal collocation in the axial direction. Although elimination of the spatial derivatives by axial collocation greatly increases the number of equations,¹³ they become ordinary differential equations and are easily solved using traditional techniques. Since the position and number of points are the only factors affecting the solution obtained by collocation, any set of linearly independent polynomials may be used as trial functions.

The Lagrangian polynomials of degree N based on the collocation points ζ_j

$$L_i(\xi) = \prod_{j=0, j \neq i}^{N+1} \left(\frac{\xi - \zeta_j}{\zeta_i - \zeta_j} \right) \quad i=0, 1, \dots, N+1 \quad (3.3-41)$$

are used here. The differential equations are then collocated at the N zeros, ζ_k , $k = 1, 2, \dots, N$, of a Legendre polynomial. Since only one Lagrangian is non-zero at a collocation point and since the residual is set equal to zero at this point, the coefficient of the Lagrangian term is equal to the solution at that point.

Following the development of Villadsen and Michelsen (1978), the assumed axial profiles are:

13. Since more than one axial collocation point is generally necessary.

$$\begin{aligned}
 \Theta_s(\xi, \vartheta) &= \sum_{i=0}^{N+1} \Theta_{s,i}(\vartheta) L_i(\xi) & y_j(\xi, \vartheta) &= \sum_{i=0}^{N+1} y_{j,i}(\vartheta) L_i(\xi) & j = 1, 2 \\
 \Theta_g(\xi, \vartheta) &= \sum_{i=0}^{N+1} \Theta_{g,i}(\vartheta) L_i(\xi) & v_g(\xi, \vartheta) &= \sum_{i=0}^{N+1} v_{g,i}(\vartheta) L_i(\xi) \\
 \Theta_t(\xi, \vartheta) &= \sum_{i=0}^{N+1} \Theta_{t,i}(\vartheta) L_i(\xi)
 \end{aligned} \tag{3.3-42}$$

Since the $L_i(\xi)$ are known functions based solely on the collocation points, the differential operators can be applied *a priori*:

$$A_{ji} = \left. \frac{dL_i(\xi)}{d\xi} \right|_{\xi_j}, \quad B_{ji} = \left. \frac{d^2L_i(\xi)}{d\xi^2} \right|_{\xi_j} \tag{3.3-43}$$

Then after operating on the assumed solutions with the differential operators and substituting into the partial differential equations, the residuals are set equal to zero at the collocation points.

The collocation points are calculated using programs given by Villadsen and Michelsen (1978) for calculating the zeros of an arbitrary Jacobi polynomial $P_N^{(\alpha, \beta)}(x)$ that satisfies the orthogonality relationship

$$\int_0^1 u^\beta (1-u)^\alpha P_i(u) P_j(u) du = C_i \delta_{ij} \tag{3.3-44}$$

where C_i is a constant, δ_{ij} is the delta function and α and β are chosen based on the geometry of the system. For the methanation reactor, zeros of $P_N^{(0,0)}(z)$ are used as collocation points.

The resulting equations in terms of conditions at the collocation points z_i are:

Catalyst Energy Balance

$$\begin{aligned}
 \frac{d\Theta_{s_i}}{d\vartheta} &= \alpha_s \sum_{j=0}^{N+1} B_{ij} \Theta_{s_j} + \omega_1 \Theta_{s_i} + \omega_2 \Theta_{t_i} + \gamma_s \Theta_{g_i} \\
 &\quad + \kappa_1 (1 + \varphi_1 \Theta_{s_i}) R'_M + \kappa_2 (1 + \varphi_2 \Theta_{s_i}) R'_S + \omega_3
 \end{aligned} \tag{3.3-45}$$

$$\begin{aligned}\sum_{j=0}^{N+1} A_{0,j} \Theta_{g_j} &= \lambda_{g_{00}} (\Theta_{g_0} - \Theta_{g_0}) \\ \sum_{j=0}^{N+1} A_{N+1,j} \Theta_{g_j} &= \lambda_{g_{N+1}} (\Theta_{g_{N+1}} - \Theta_{g_{N+1}})\end{aligned}$$

Gas Energy Balance

$$\begin{aligned}\frac{(\tau\zeta_i + 1) \hat{M}_g c_{p_g}}{\Theta_{g_i}} \frac{d\Theta_{g_i}}{d\vartheta} &= \frac{-(\tau\zeta_i + 1) v_{g_i} \hat{M}_g c_{p_g}}{\Theta_{g_i}} \sum_{j=0}^{N+1} A_{ij} \Theta_{g_j} \\ &+ \alpha_g \sum_{j=0}^{N+1} B_{ij} \Theta_{g_j} + \omega_4 \Theta_{g_i} + \omega_5 \Theta_{t_i} + \gamma_g \Theta_{s_i} + \omega_6\end{aligned}\quad .(3.3-46)$$

$$\begin{aligned}\sum_{j=0}^{N+1} A_{0,j} \Theta_{g_j} &= -\lambda_{g_{00}} (\Theta_{g_0} - \Theta_{g_0}) + \frac{v_{g_0} \hat{M}_{g_0} c_{p_{g_0}}}{\alpha_g \Theta_{g_0}} (\Theta_{g_0} - \Theta_0) \\ \sum_{j=0}^{N+1} A_{N+1,j} \Theta_{g_j} &= \lambda_{g_{N+1}} (\Theta_{g_{N+1}} - \Theta_{g_{N+1}})\end{aligned}$$

Mass Balances

$$\begin{aligned}\frac{dy_{k_i}}{d\vartheta} &= -v_{g_i} \sum_{j=0}^{N+1} A_{ij} y_{k_j} + \alpha_m \left\{ \sum_{j=0}^{N+1} B_{ij} y_{k_j} + \left[\sum_{j=0}^{N+1} A_{ij} y_{k_i} \right] \left[\frac{\tau}{\tau\zeta_i + 1} - \frac{1}{\Theta_{g_i}} \sum_{j=0}^{N+1} A_{ij} \Theta_{g_j} \right] \right\} \\ &- \frac{2y_{k_i}}{1-2\delta} \frac{\partial^2 \delta}{\partial \zeta^2} - \frac{2}{1-2\delta} \left[\sum_{j=0}^{N+1} A_{ij} y_{k_j} \right] \frac{\partial \delta}{\partial \zeta} - \frac{2y_{k_i}}{1-2\delta} \left[\frac{\tau}{\tau\zeta_i + 1} - \frac{1}{\Theta_{g_i}} \sum_{j=0}^{N+1} A_{ij} \Theta_{g_j} \right] \frac{\partial \delta}{\partial \zeta} \\ &+ \frac{4y_{k_i}}{(1-2\delta)^2} \left(\frac{\partial \delta}{\partial \zeta} \right)^2 + \begin{cases} -\sigma_1 \frac{\Theta_{g_i}}{\hat{P}} R'_M + \sigma_2 \frac{\Theta_{g_i}}{\hat{P}} R'_S & k = 1 \\ -\sigma_3 \frac{\Theta_{g_i}}{\hat{P}} R'_S & k = 2 \end{cases}\end{aligned}\quad .(3.3-47)$$

where

$$\frac{\partial^2 \delta}{\partial \xi^2} = - \left[\bar{x}_1^0 \sum_{j=0}^{N+1} B_{ij} y_{1j} + \bar{x}_2^0 \sum_{j=0}^{N+1} B_{ij} y_{2j} \right]$$

$$\frac{\partial \delta}{\partial \xi} = - \left[\bar{x}_1^0 \sum_{j=0}^{N+1} A_{ij} y_{1j} + \bar{x}_2^0 \sum_{j=0}^{N+1} A_{ij} y_{2j} \right]$$

$$\sum_{j=0}^{N+1} A_{0j} y_{kj} = \frac{v_{g_0}}{\alpha_m} (y_{k0} - y_k^0)$$

$$\sum_{j=0}^{N+1} A_{N+1,j} y_{kj} = 0$$

Thermal Well Energy Balance

$$\frac{d\Theta_{t_k}}{d\vartheta} = \alpha_t \sum_{j=0}^{N+1} B_{ij} \Theta_{t_j} + \omega_7 \Theta_{g_1} + \omega_8 \Theta_{g_2} + \omega_9 \Theta_{g_3} + \omega_{10} \quad (3.3-48)$$

$$\sum_{j=0}^{N+1} A_{N+1,j} \Theta_{t_j} = 0$$

Overall Continuity

$$\Theta_{g_i} \sum_{j=0}^{N+1} A_{ij} v_{g_i} - \frac{d\Theta_{g_i}}{d\vartheta} + \frac{v_{g_i} \Theta_{g_i} \tau}{\tau \xi_i + 1} - v_{g_i} \sum_{j=0}^{N+1} A_{ij} \Theta_{g_i} = 0 \quad (3.3-49)$$

Note that $i = 1, 2, \dots, N$ for all of the equations except the last where $i = 1, 2, \dots, N+1$, that the ω_i coefficients are the result of radial collocation and are presented in Appendix 3, and that all other dimensionless parameters are

defined in Appendix 2. Furthermore, the reaction terms R'_M and R 's are calculated at the conditions at the collocation points.

The resulting equations are a set of $6N+1$ ordinary differential equations along with algebraic boundary conditions. The solution procedure is further simplified by solving the last equation for v_g as a set of algebraic equations, using the gas temperatures and derivatives of the gas temperatures from the solutions of the remaining differential equations.¹⁴ Additionally, simple algebraic manipulation allows for explicit solution of v_{g0} , Θ_{t_0} , $\Theta_{t_{N+1}}$, y_{i_0} and $y_{i_{N+1}}$, while solution for Θ_{s_0} , $\Theta_{s_{N+1}}$, Θ_{g_0} , and $\Theta_{g_{N+1}}$ requires the simultaneous solution of four coupled algebraic equations. The resulting dynamic model is then a set of $5N$ coupled, nonlinear ordinary differential equations and $N+5$ coupled, nonlinear algebraic equations, where N is the number of interior axial collocation points.

Typical steady state profiles along a reactor obtained by other authors (Jutan et al., 1977; Hoiberg et al., 1971) indicate that these profiles can be represented by relatively low-order polynomials. However, temperature profiles with steep gradients, as may be likely in a highly exothermic system such as methanation, may require higher-order polynomials. Although approximation error is reduced by increasing the number of collocation points, numerical problems with fitting higher-order polynomials to process curves may result. Section 3.7 discusses the model dimensionality in detail. Presently, let it suffice to say that 6 - 8 axial collocation points are generally sufficient, leading to a system of 30 - 40 coupled, nonlinear ordinary differential equations and 11 - 13 coupled, nonlinear algebraic equations.

14. i.e., effectively substituting Equation (3.3-48) into Equation (3.3-49) for $\frac{d\Theta_g}{d\vartheta}$.

3.3.5.4 Numerical Simulation

Steady state solutions can be obtained by carrying a dynamic simulation to steady state or by setting the time derivatives equal to zero in the ordinary differential equations and then solving the resulting system of $6N+5$ algebraic equations. In the latter technique, solutions for very steep axial profiles often show numerical convergence problems. These can be reduced by using better initial guesses or by varying the actual solution algorithm. In extreme cases, it may be necessary to carry the dynamic solution part way to steady state and then use its results as an initial guess of the steady state solution.

Due to the large size of the mathematical problem and the complexity of the nonlinear equations, both dynamic and steady state solutions require powerful algorithms for the solution of nonlinear algebraic equations and for the solution of initial value problems in ordinary differential equations. Considerable analysis of various solution algorithms led to the final selection of the techniques described in this section due to their robustness under a great variety of conditions and their relative speed of solution in comparison to other techniques. Most other procedures exhibited convergence problems. Even the selected techniques fail to converge under certain conditions, but in general are flexible enough to allow solution with the adjustment of several convergence parameters.

Although the solution of the algebraic equations is relatively simple for the dynamic simulations, it is extremely difficult for steady state solutions with poor initial estimates of the solution profiles. Two methods are used in the computer simulation programs developed in this work for the solution of the systems of nonlinear algebraic equations. These are based on algorithms by Powell (Rabinowitz, 1970) and Brown (1967). Although Brown's algorithm is in most cases

more powerful than that of Powell, it is in general significantly slower. Thus although the computer programs are written to use either technique, Brown's algorithm is only used in those cases where Powell's algorithm fails to converge to an appropriate solution.

Consider the system of nonlinear equations

$$f_k(\mathbf{x}) = 0 \quad k = 1, 2, \dots, n \quad (3.3-50)$$

where \mathbf{x} is the vector of unknowns (x_1, x_2, \dots, x_n) . $F(\mathbf{x})$ is the sum of squares of the residuals

$$F(\mathbf{x}) = \sum_{k=1}^n [f_k(\mathbf{x})]^2 \quad (3.3-51)$$

Powell's technique for the solution of nonlinear equations is a hybrid of the classical Newton-Raphson procedure and the Levenberg/Marquardt steepest descent method. The new algorithm retains the fast convergence of the Newton method but is modified to take steps along the steepest descent direction of $F(\mathbf{x})$, if it seems that the classical Newton iteration diverges.

The major difference between this hybrid algorithm and the standard Levenberg/Marquardt iteration is that Powell's procedure does not require explicit expressions for the derivatives of the functions, but instead uses successive values of $f_i(\mathbf{x}^{(j)})$ ($i = 1, 2, \dots, n$; $j = 1, 2, \dots$) to build up a numerical approximation to the Jacobian matrix. Note that $\mathbf{x}^{(j)}$ is the j th estimate of the solution. The technique further includes several parameters that can be adjusted to improve convergence for each particular system. One common difficulty with this algorithm is that the method may converge to a stationary point of $F(\mathbf{x})$, although this may not be a global minimum. The theory underlying this procedure, along with examples and a sample Fortran program are given by Powell (Rabinowitz, 1970).

In the event that Powell's algorithm fails to obtain a solution to the equations, a different initial estimate of \mathbf{x} can be attempted or Brown's (1967) quadratically convergent algorithm can be used. Basically, Brown's procedure consists of

"expanding the first equation in a Taylor series about the starting guess, retaining only linear terms, equating to zero and solving for only one variable, say x_k , as a linear combination of the remaining $n-1$ variables. In the second equation, x_k is eliminated by replacing it with its linear representation found above, and again the process of expanding through linear terms, equating to zero and solving for one variable in terms of the now remaining $n-2$ variables is performed. One continues in this fashion, eliminating one variable per equation, until for the n th equation, we are left with one equation and one unknown. A single Newton step is now performed, followed by back-substitution in the triangularized linear system generated for the x_i 's. A pivoting effect is achieved by choosing for elimination at any step that variable having a partial derivative of largest absolute value." (Brown, 1967)

Dynamic solutions of the mathematical model for the packed bed reactor also require a powerful method for initial value problems in ordinary differential equations. The procedure selected in this work is a standard Adams-Moulton predictor-corrector technique. This procedure is based on the formula

$$\mathbf{y}(x_{n+1}) - \mathbf{y}(x_n) = \int_{x_n}^{x_n + \delta x} \frac{dy}{dx} dx = \int_{x_n}^{x_n + \delta x} \mathbf{f}(\mathbf{x}, \mathbf{y}(\mathbf{x})) dx \quad (3.3-52)$$

where the differential equations are defined as

$$\frac{dy}{dx} = \mathbf{f}(\mathbf{x}, \mathbf{y}(\mathbf{x})) \quad (3.3-53)$$

In the Adams-Moulton case, $\mathbf{f}(\mathbf{x}, \mathbf{y}(\mathbf{x}))$ is approximated by an interpolation polynomial determined by the values at each iteration, $f_{n+1}, f_n, \dots, f_{n-k+1}$. In the particular routines used in this work, k is taken as three and the predictor-corrector formulas are

$$\begin{aligned} \mathbf{y}_{n+1}^{(pred)} - \mathbf{y}_n &= \frac{\Delta x}{24} (55\mathbf{f}_n - 59\mathbf{f}_{n-1} - 37\mathbf{f}_{n-2} - 9\mathbf{f}_{n-3}) \\ \mathbf{y}_{n+1}^{(corr)} &= \mathbf{y}_n + \frac{\Delta x}{24} (9\mathbf{f}_{n+1} + 19\mathbf{f}_n - 5\mathbf{f}_{n-1} + \mathbf{f}_{n-2}) \end{aligned} \quad (3.3-54)$$

This method is combined with an automatic control of the step size and uses the method of Runge-Kutta-Gill to start the integration process and to restart the integration any time the interval size has been changed.

Thus the system of ordinary differential equations describing the reactor is solved using an Adams-Moulton predictor-corrector technique with the method of Runge-Kutta-Gill being used to start the integration process, and the non-linear system of algebraic equations is solved using Powell's hybrid algorithm (Rabinowitz, 1970) or Brown's (1967) quadratically convergent algorithm.

The computer simulation programs developed for this system use modified, double precision versions of the Caltech Library routines MODDEQ, NSES1, and NSES2 for these algorithms. Combining these techniques with a variable time-step analysis, based on increasing the time-steps as the derivatives decrease during the approach to steady state, leads to an efficient solution procedure for obtaining dynamic reactor responses. All programs are written in double precision and are modular so as to allow for easy modification or use with other reactor systems by simple subroutine replacement. These computer programs and complete operating instructions are included in Appendix 4.

Although the technique described above is useful for simulating the full, nonlinear ordinary differential equation model, solution times can often be quite long, even up to several hours of computation time on a Digital Equipment (DEC) Vax 11/780 for a fifteen minute simulation due to the size and nonlinearity of the system. These can be reduced significantly by linearizing the set of ordinary differential equations around the steady state solution.¹⁵ The linearization is not

¹⁵ This of course requires the ability to directly solve for the steady state solution.

limited to only the rate expressions but is performed on the entire differential equations and is complicated by the dependence of the velocities, densities, heat capacities, and other gas properties on the temperatures and compositions throughout the bed. A linearization around steady state conditions leads directly to a model of the form

$$\dot{\mathbf{x}}(t) = \mathbf{A}\mathbf{x}(t) + \mathbf{B}\mathbf{u}(t) + \mathbf{D} \quad (3.3-55)$$

where the state vector \mathbf{x} includes the solid, gas, and thermal well temperatures, and CO and CO₂ concentrations at the collocation points. The control vector \mathbf{u} consists of the expected disturbance and control variables, including cooling wall temperature, inlet velocities, inlet gas temperatures, and inlet concentrations of all species.

This linearized model can be solved explicitly in terms of matrix exponentiation for time periods t_0 to t_i where \mathbf{u} remains fixed:

$$\mathbf{x}(t_i) = e^{\mathbf{A}(t_i - t_0)} \mathbf{x}(t_0) + \mathbf{A}^{-1} [e^{\mathbf{A}(t_i - t_0)} - \mathbf{I}] [\mathbf{B}\mathbf{u} + \mathbf{D}] \quad (3.3-56)$$

This analytic solution can then be simulated using eigenfunction evaluation of the matrix exponential. Further explanation of this analysis is presented in Sections 3.6 and 3.7.

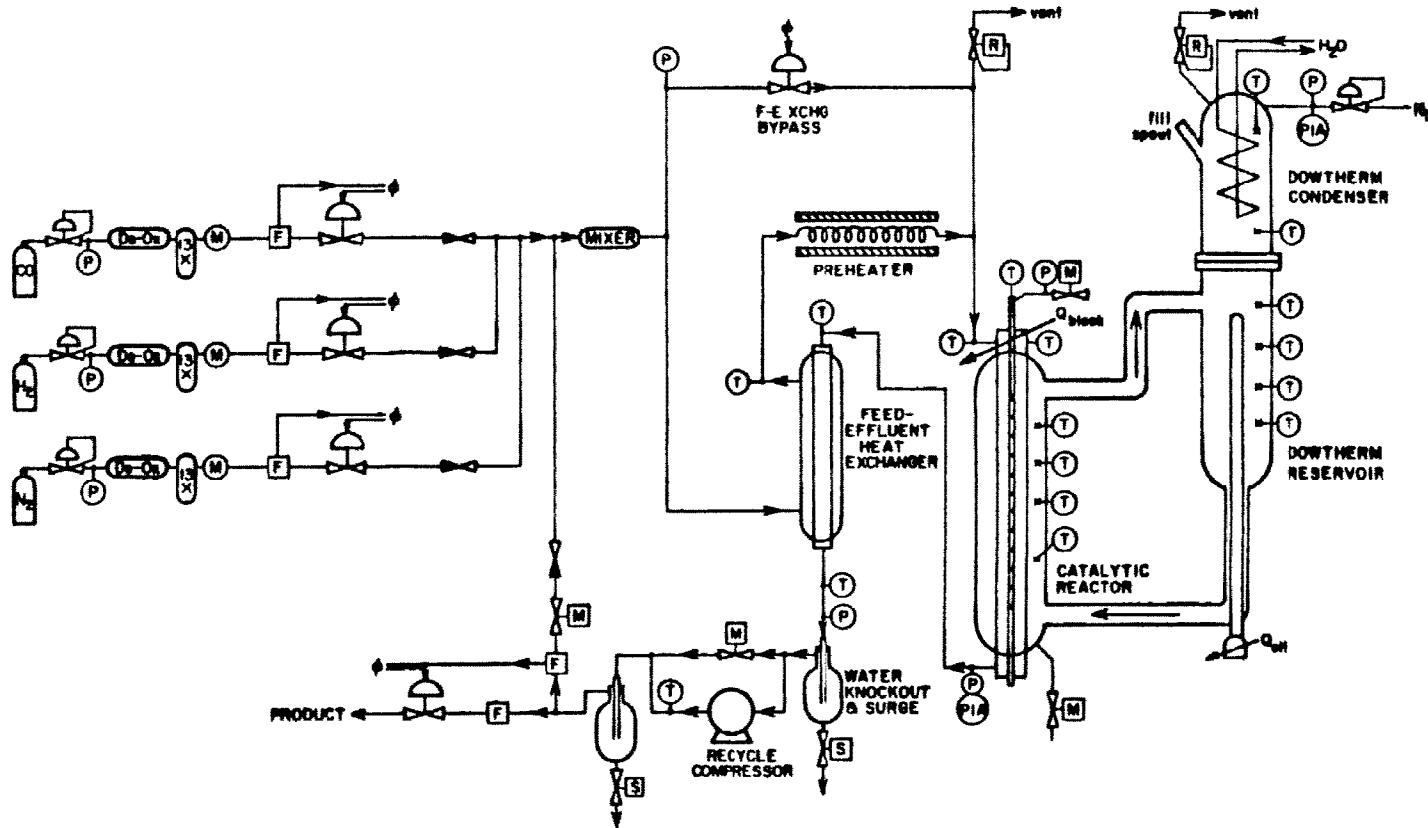


Figure 3.3-1
 Process Diagram for Experimental Catalytic Reactor
 (Source: Strand, 1984)

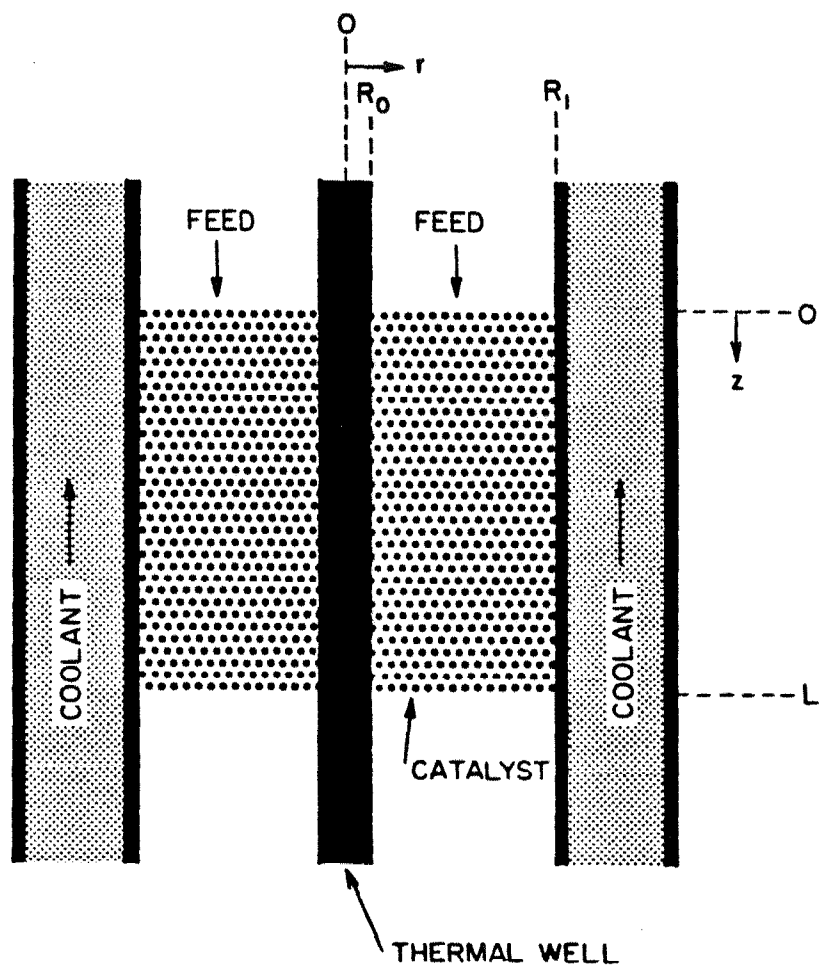


Figure 3.3-2
Expanded Section of Reactor Bed

3.4 MODEL ANALYSIS

The objective of developing a complete mathematical description of an experimental reactor is not simply intellectual fulfillment, but rather to study the steady state and transient effects of various parameters, operating conditions, and modeling assumptions on the behavior, or actually the predicted behavior, of the experimental process. This allows gaining significant insight into the operation of the system without unnecessary lengthy and often hazardous experiments. Using the fully developed model, specific experiments can be planned, and the experimental design can be optimized to minimize potential hazards and to focus on the areas of concern.

The steady state and transient effects of various parameters and assumptions on the mathematical simulations of the packed bed catalytic reactor are now examined using the complete mathematical model developed in the last section. These studies lead to conclusions concerning the importance of various physical and chemical phenomena and to the importance of a generalized overall model structure. Note that the importance of this study is not simply in defining our experimental system, but rather in its general applicability to packed bed reactor modeling. All of the analyses presented in this thesis are based on numerical solutions of the full, nonlinear model using the methanation kinetics of Vatcha (1976), although many analytic solutions using the reduced linear model developed in Section 3.6 and solutions with the methanation kinetics proposed by Strand (1984) were used as verification of the important conclusions.

Unless otherwise stated, all figures presented throughout this and the following sections are based on the reversible methanation kinetics of Vatcha (1976), all axial gas and catalyst temperature profiles are at the radial colloca-

tion point, and all concentration profiles are mole fractions based on the total inlet moles as defined by Equation (3.3-17). Furthermore, all simulations are based on the kinetic parameters in Table 3.3-3, along with the modeling parameters and operating conditions presented in the next section. The purpose of this is to retain consistency throughout this thesis so that the various simulations can easily be compared.

3.4.1 Modeling Parameters

The numerical values of the parameters used for this analysis are based on published results of other packed bed analyses. Typical values of the major parameters are shown in Table 3.4-1. The kinetic parameters are given in Table 3.3-3. Unless stated otherwise, these are the parameters used in the preliminary simulations.

Catalyst Parameters		Thermal Well Parameters	
c_{p_s}	0.23	c_{p_t}	0.12
ρ_s	1.04	ρ_t	8.02
k_{zs}, k_{rs}	0.0005	k_{zt}	0.039
Heat Transfer Parameters		Reactor Parameters	
U_{sg}	17.02	L	30.00
U_{ts}	0.02	R_0	0.159
U_{tg}	0.14	R_1	1.194
λ_{gss}	600.00	Pe_{mz}	10.00
λ_{ezg}	13.00	Pe_{mr}	2.00
$\lambda_{trs} = \lambda_{wrs}$	7.16	Pe_{hz}	2.00
$\lambda_{trg} = \lambda_{wrg}$	1.25	Pe_{hr}	8.00

Table 3.4-1
Typical Reactor Parameters

The physical reactor parameters were measured for the experimental methanation reactor. The void fraction must be empirically determined for the specific catalyst used in the experiments due to differences in catalyst crushing. The catalyst used for the preliminary experiments is standard Girdler G-65 methanation catalyst. Its physical properties are shown in Table 3.4-2, which is reproduced from the specification sheet from United Catalysts Inc. Although the density of the catalyst is given in the specification sheet, the overall density should be measured for the specific experimental conditions since the catalyst is actually crushed substantially for our use. The heat capacity of the catalyst is calculated over the expected temperature range of operation based on the heat capacities of the individual components of the catalyst and the catalyst composition. Results of this analysis are shown in Table 3.4-3. Since the temperatures within the reactor bed should generally remain within 100° K, a constant heat capacity can be used.

The thermal well properties are calculated using data for stainless steel (type 304) from CRC Handbook of Chemistry and Physics (Weast, 1976) and Chemical Engineers' Handbook (Perry and Chilton, 1973). The heats of reaction and equilibrium constants for the methanation and steam-shift reactions are also readily available. Linear regression of data provided by United Catalysts Inc. is shown in Figures 3.4-1 and 3.4-2 over the expected temperature range of operation and is used to determine linear temperature relationships for the heats of reaction and relationships for the equilibrium constants based on van't Hoff's equations (Equation 3.3-5). Notice that the heats of reaction and the equilibrium constants for both the methanation and steam-shift reactions vary greatly over the temperature range of interest. Although the use of constant values for these parameters would be highly inaccurate, relationships based on van't Hoff's equation for the equilibrium constants and linear equations of the

Methanation Catalyst		Typical Chemical and Physical Properties	
Catalyst Type, Form and Size	Catalyst Type G-65 Form Tablets Size $\frac{1}{4}$ " x $\frac{1}{4}$ "	Effective: January 25, 1960 Supersedes: January 31, 1978	
Chemical Composition	Weight Percent Ni* 24-27 Al ₂ O ₃ 55-65 CaO 4-6 SiO ₂ <0.30 C (As Graphite) 3-5 S* (Maximum) 0.05 Na* (Maximum) 0.30	Weight Percent Fe ₂ O ₃ <0.15 MgO <0.10	Weight Percent LOI to Constant Weight at: 1000°F* 10.0 Max.
Physical Properties	A. Bulk Density, lbs./cu. ft. 65 \pm 5 B. Surface Area, m ² /g. 35-65 The surface area is obtained by a modified BET method which consists of nitrogen adsorption by the sample. The sample is ground to a fine powder (60-100 mesh) and purged with nitrogen at 200°C to a constant weight. C. Pore Volume, cc/g. 0.15-0.25 The pore volume is obtained with a mercury porosimeter at 60,000 psig which corresponds to the total pore volume or pores greater than 29.2 Angstroms diameter. D. Crush Strength, Minimum Average* 90.0 lbs. No More Than 5% Less Than 40.0 lbs. Apparatus — Hydraulic press with horizontal plates of which the bottom plate moves vertically. In series with the bottom plate is a pressure gauge which records the pressure exerted on the tablet. Procedure — The tablet is placed on its side and the lower plate is raised to the tablet with zero pounds pressure on the gauge. The pressure is then increased on the bottom plate until the tablet crushes and the pressure at breakage is recorded. The crush on a minimum of twenty-five tablets is obtained and the average is taken arithmetically. To pretreat the sample, dry the catalyst at 400°F for three hours and allow to cool. Crush Strength Range on Individual Tablets. 40-150		
*Properties normally measured by Quality Control.			

Table 3.4-2
Girdler G-65 Catalyst Specifications

form given in Equation (3.3-12) should be very accurate. As discussed in Section 3.3, these equations were incorporated in the original model. The coefficients for our experimental conditions calculated using linear regression of the data presented in Figures 3.4-1 and 3.4-2 are given in Table 3.4-4.

The remaining parameters for the mathematical description of the experimental system are the heat transfer variables and the reaction kinetics.

Temperature (° K)	c_p (cal/g ° K)
550.	0.225
575.	0.228
600.	0.230
625.	0.231
650.	0.232
675.	0.233
700.	0.235
725.	0.237

Table 3.4-3
Temperature Dependence of Catalyst Heat Capacity

Although these need to be estimated from initial experiments for our specific catalyst and reactor bed (described in Section 4.2), preliminary values from literature are used. Effective thermal conductivities and heat transfer coefficients are given by De Wasch and Froment (1971) for the solid and gas phases in a heterogeneous packed bed model. Representative values for Peclet numbers in a packed bed reactor are given by Carberry (1976) and Mears (1976). Values for Peclet numbers from 0.5 to 200 were used throughout the simulations.

For consistency, several sets of typical operating conditions are used for the simulations presented in this thesis. These are shown in Table 3.4-5 and will be referred to as standard Type I, II, or III conditions. These three significantly different sets of conditions were chosen to cover a wide range of potential operating conditions. Type I corresponds to operation at moderate to high temperatures, pressures, and flowrates with relatively low inlet CO and H₂ concentrations and small amounts of inlet CH₄, CO₂, and H₂O either from recycle or from the upstream process when the methanator is being used to cleanup the process stream prior to ammonia synthesis. Type II corresponds to realistic conditions for the industrial use of methanation in synthetic natural gas pro-

Methanation	Steam-Shift
K_{PM_1}	-29.44
K_{PM_2}	26341.
ΔH_{M_1}	-6.14
ΔH_{M_2}	-48350
K_{PS_1}	4.39
K_{PS_2}	-4615.
ΔH_{S_1}	-2.44
ΔH_{S_2}	10760.

Table 3.4-4
Coefficients for Equations (3.3-5) and (3.3-12)

duction. Note that the inlet methane concentration is much higher than in Type I. This large amount of methane significantly reduces the reaction rate. Finally, Type III corresponds to single-pass laboratory experimental conditions where only CO and H₂ are fed to the reactor. Flowrates and temperatures are relatively low.

Type I Conditions			
Parameters:	$\varepsilon = 0.40$ $u_{g_0} = 75.0 \text{ cm/sec}$	$T_0 = 573^\circ \text{ K}$ $P = 20 \text{ atm}$	$T_w = 573^\circ \text{ K}$
Inlet Mole Fractions:	$x_{CH_4} = 0.02$ $x_{CO} = 0.03$	$x_{CO_2} = 0.03$ $x_{H_2} = 0.20$	$x_{H_2O} = 0.024$
Type II Conditions			
Parameters:	$\varepsilon = 0.57$ $u_{g_0} = 75.0 \text{ cm/sec}$	$T_0 = 573^\circ \text{ K}$ $P = 10 \text{ atm}$	$T_w = 573^\circ \text{ K}$
Inlet Mole Fractions:	$x_{CH_4} = 0.60$ $x_{CO} = 0.06$	$x_{CO_2} = 0.015$ $x_{H_2} = 0.19$	$x_{H_2O} = 0.02$
Type III Conditions			
Parameters:	$\varepsilon = 0.57$ $u_{g_0} = 14.0 \text{ cm/sec}$	$T_0 = 510^\circ \text{ K}$ $P = 20 \text{ atm}$	$T_w = 530^\circ \text{ K}$
Inlet Mole Fractions:	$x_{CH_4} = 0.00$ $x_{CO} = 0.04$	$x_{CO_2} = 0.00$ $x_{H_2} = 0.12$	$x_{H_2O} = 0.00$

Table 3.4-5
Typical Operating Conditions

3.3.1 Steady-State Behavior

Steady state axial gas and solid temperature profiles at various radial positions and concentration profiles for the standard Type I operating conditions are displayed in Figure 3.4-3, and the corresponding radial temperature profiles are displayed in Figure 3.4-4. As mentioned previously, the concentration profiles show the mole fractions of CO and CO₂ based on the total inlet moles. The definition of these values is the moles of CO or CO₂ divided by the total inlet number of moles. This definition is used rather than standard mole fractions in most situations since the total number of moles decreases rapidly in the bed.

At the conditions chosen for Type I operation, the methanation reaction is quite rapid and approaches completion. The steam-shift reaction, which is much slower, leads to a slight formation of CO₂. Note that the overall conversion of the CO₂ is actually quite small (less than 1%).

The steady state temperature profiles (Figures 3.4-3b and 3.4-4) show that a 'hot spot' is present about half way through the reactor bed and is predominant near the center of the bed. The presence of such a hot spot is a result of the cooling jacket and is common in nonadiabatic packed bed reactors. The steady state temperature profiles show a difference of up to 10° K between the solid and gas temperatures, and later transient results show differences up to 20° K (leading to differences of over 20% in the reaction rates), thus providing initial verification of the necessity of the heterogeneous analysis.

In the small region near the cooling wall, even the steady state temperature differences between the solid and gas are significant due to the higher heat transfer between the solid and cooling wall than that between the gas and the cooling wall. The radial temperature profiles (Figure 3.4-4) also verify the necessity of the radial temperature analysis, since the radial gradients are significant

throughout the bed. Notice that except near the cooling wall the catalyst temperature is greater than the gas temperature due to the exothermic reaction occurring on the catalyst surface.

The standard Type II operating conditions are much milder and result in only about 40% CO conversion and much lower reactor temperatures due to the lower pressure, the larger void fraction, and the large amount of methane in the feed. Steady state axial temperature and concentration profiles for these conditions are shown in Figure 3.4-5, and the steady state radial temperature profiles are shown in Figure 3.4-6. Again the temperature differences between the solid and gas are significant.

3.3.2 Dynamic Simulations

The real power of the model developed in this work is not in steady state analyses, since this is relatively simple and has been investigated in detail in the past, but rather in the transient or dynamic simulations necessary for control design. This model has been used to simulate the effects of various process disturbances and input changes. Under normal reactor operating conditions, step or pulse changes in inlet gas temperatures, concentrations, or velocity or changes in cooling rates can significantly affect the behavior of the process. These disturbances must be understood for optimal system operation and control.

Figure 3.4-7 shows the effect of a 10% drop in the inlet gas temperature (from 573° K to 515.7° K) on the axial temperature profiles within the reactor for standard Type I operating conditions. Since such a disturbance would, in general, not occur instantaneously, the inlet temperature was actually changed from its initial to final value in a 0.5 second ramp. The complexities of the

resulting reactor profiles are enhanced by the behavior of the cooling system. Although the inlet gas temperature is reduced, the cooling jacket temperature remains unchanged ($T_w = 573^\circ \text{ K}$). Thus the cooling jacket acts as a heating system in the early part of the reactor and as a cooling system in the later part, thus in effect transferring heat from the later stage to the early stage of the reactor. Figure 3.4-7 also shows that although the inlet gas temperature is reduced, the steady state outlet temperature actually increases by about 8° K , since the hot spot shifts further down the reactor, effectively reducing the cooling region. As expected, the responses of the concentration profiles (not shown) are much faster than that of the thermal profiles, indicating the possible applicability of the quasi steady state approximation for the concentrations (this will be discussed in detail in Section 3.7).

Figure 3.4-8 shows the axial gas and solid temperature profiles during start-up operation. Notice that the 'hot spot' in the reactor moves down the bed as the heat generated from reaction heats up the catalyst particles. Also note the significant temperature difference between the catalyst and gas in the early part of the reactor where conversion is rapid. These differences are even more pronounced (over 20° K) near the center of the bed and near the outer wall.¹

Figure 3.4-9 shows the temporal behavior of the catalyst, gas, and thermal well temperatures at $\zeta = 0.38$ and $\zeta = 1.0$ for a step change in the cooling fluid temperature from 573° K to 593° K as would occur through increasing the nitrogen pressure in the Dowtherm condenser. This figure exemplifies the slow response of the catalyst and thermal well temperatures due to their high thermal capacitance. As discussed later, the gas temperature merely follows the behavior of the solid due to the negligible accumulation of energy in the gas and the high heat transfer coefficient between the gas and solid. This figure along

1. The profiles shown in Figure 3.4-8 are at the radial collocation point r_c .

with further evidence presented later in this thesis shows that the dynamic behavior of the reactor is dominated by the catalyst and thermal well thermal behavior.

Many other disturbances have been simulated, leading to an understanding of the control complexities of the system. Many of these simulations are shown in Sections 3.6 and 3.7 and are therefore not reproduced here. Axial temperature measurements have been found to be essential in determining and controlling the behavior of the process. Outlet temperatures alone cannot provide adequate information for control of the reactor.

3.3.3 Effects of Reactor Operating Conditions

One of the major purposes of accurate mathematical modeling of the reactor bed is to study the effects of various operating conditions on the behavior of the reactor, thus allowing process optimization and insight into the performance of the system under changes in various input parameters. This enables careful design of control structures for the experimental system without significant *a priori* experimentation.

Figure 3.4-10 shows the effect of the inlet gas temperature on both the outlet gas temperature and CO conversion for the reversible kinetics given by Equations (3.3-1) and (3.3-3), and Figure 3.4-11 shows the effects on the steady state axial gas temperature profiles. As expected, the conversion and the 'hot spot' temperature increase with increasing inlet gas temperature. However under many conditions, the outlet gas temperature is inversely related to inlet gas temperature. An increase in the inlet gas temperature produces a decrease in the outlet gas temperature² as a result of the shifting of the 'hot spot' down

2. The so-called 'wrong-way' behavior.

the bed (see Figure 3.4-7 also). However as shown in Figure 3.4-10, this is not true throughout the possible operating regimes. Obviously, this behavior can lead to significant control difficulties if the control design is based on the outlet gas temperature as is often the case.

The steady state axial concentration profiles for an inlet gas temperature of 623° K are shown in Figure 3.4-12. As before, the steam-shift reaction leads to a slight formation of CO₂ in the early part of the reactor due to the presence of a large amount of CO. However as the CO is rapidly depleted in methane formation, the steam-shift reaction reverses. Due to the higher temperatures within the reactor, the rates for both reactions are much higher than for the standard Type I conditions.

Figure 3.4-10 also shows the tremendous effect that the inlet velocity or flowrate has on conversion and temperatures. Figure 3.4-13 shows the steady state axial gas temperature profiles at various inlet gas velocities. A sudden drop in the inlet flowrate would cause the 'hot spot' to become much more pronounced and to shift towards the entrance of the bed. The lower flowrates also lead to higher conversions (not shown).

Finally, the effects of the inlet CO concentration and cooling fluid temperature on the CO conversion and outlet gas temperature are shown in Figures 3.4-14 and 3.4-15. An increase in either the inlet CO concentration or the Dowtherm temperature³ increases the conversion and the outlet gas temperature. Not too surprisingly, the relationship between the outlet gas temperature and cooling fluid temperature is nearly linear since for these conditions the reaction is nearly complete in the first half of the reactor and the second half acts as a heat exchanger to cool the gas.

3. This would be the result of increasing the nitrogen pressure in the Dowtherm condenser.

3.3.4 Radial Concentration Analysis

Radial gradients are generally ignored in dynamic analyses of packed bed reactors, mainly due to the increased complexity of the resulting model. As pointed out by Jutan et al. (1977), in the only other major dynamic packed bed reactor study that incorporates radial profiles, radial gradients are important in industrial processes where wall cooling is required for safety or control. The original mathematical model developed in the proceeding section includes complete radial analysis of both the temperature and concentration profiles. However, explicit solution of the resulting partial differential equation model is not feasible, and discretization is needed to reduce the model to a form suitable for numerical solution. This reduction used the method of orthogonal collocation in both the radial and axial dimensions.

The radial discretization must then account for the projected radial profiles. In the analysis performed in the last section, one interior radial collocation point was used. This along with the two radial boundary values at the thermal well and cooling wall resulted in an inherent assumption of quadratic radial gradients. An examination of experimental measurements (Valstar et al., 1975) and typical radial profiles (Finlayson, 1971) for similar reactors indicates that radial temperature profiles can adequately be represented by a quadratic function of radial position. This quadratic representation is preferable to one of higher order since the dimensionality of the system is minimized through the use of only one interior collocation point.

However, a quadratic representation of the radial concentration profile may not be adequate since application of zero flux conditions at the inner thermal well and outer cooling wall with a quadratic profile reduces to an assumption of constant radial concentrations. Although additional radial collocation points

greatly increase the dimensionality of the resulting model, they may be necessary to accurately express the radial concentration profiles. This section considers the problem in detail by comparing simulations with additional radial collocation.

The original model is discretized in the radial dimension using orthogonal collocation with multiple interior collocation points for the concentration profiles and a single radial collocation point for the gas and catalyst temperatures. For example, with two interior collocation points, the assumed radial concentration profile is

$$y_i(\vartheta, \xi, r) = d_0(\vartheta, \xi) + d_1(\vartheta, \xi)r + d_2(\vartheta, \xi)r^2 + d_3(\vartheta, \xi)r^3 \quad (3.4-1)$$

This profile must satisfy the boundary conditions

$$\begin{aligned} \frac{\partial y_i}{\partial r} \Big|_{r=r_0} &= 0 \\ \frac{\partial y_i}{\partial r} \Big|_{r=r_1} &= 0 \end{aligned} \quad (3.4-2)$$

The profile must also be exact at the collocation points, $r = \varphi_0$, r_{c_1} , r_{c_2} , and 1.0:

$$\begin{aligned} y_{i_0} &= d_0 + d_1\varphi_0 + d_2\varphi_0^2 + d_3\varphi_0^3 \\ y_{i_{c_1}} &= d_0 + d_1r_{c_1} + d_2r_{c_1}^2 + d_3r_{c_1}^3 \\ y_{i_{c_2}} &= d_0 + d_1r_{c_2} + d_2r_{c_2}^2 + d_3r_{c_2}^3 \\ y_{i_1} &= d_0 + d_1 + d_2 + d_3 \end{aligned} \quad (3.4-3)$$

After rearranging and eliminating y_{i_0} and y_{i_1} ,

$$\begin{bmatrix} 0 & 1 & 2 & 3 \\ 0 & 1 & 2\varphi_0 & 3\varphi_0^2 \\ 1 & r_{c_1} & r_{c_1}^2 & r_{c_1}^3 \\ 1 & r_{c_2} & r_{c_2}^2 & r_{c_2}^3 \end{bmatrix} \begin{bmatrix} d_0 \\ d_1 \\ d_2 \\ d_3 \end{bmatrix} = \begin{bmatrix} 0 \\ 0 \\ y_{i_{r_{c_1}}} \\ y_{i_{r_{c_2}}} \end{bmatrix} \quad (3.4-4)$$

The expressions for $d_i(\vartheta, \xi)$ can be obtained as:

$$d_{0i} = \alpha \left[r_{c_2}^3 - \frac{3}{2} r_{c_2}^2 (\varphi_0 + 1) + 3r_{c_2} \varphi_0 \right] y_{i_{r_{c_2}}} \\ - \alpha \left[r_{c_1}^3 - \frac{3}{2} r_{c_1}^2 (\varphi_0 + 1) + 3r_{c_1} \varphi_0 \right] y_{i_{r_{c_1}}} \quad (3.4-5)$$

$$d_{1i} = 3\varphi_0 \alpha \left[y_{i_{r_{c_2}}} - y_{i_{r_{c_1}}} \right] \quad (3.4-6)$$

$$d_{2i} = -\frac{3}{2} (1 + \varphi_0) \alpha \left[y_{i_{r_{c_2}}} - y_{i_{r_{c_1}}} \right] \quad (3.4-7)$$

$$d_{3i} = \alpha \left[y_{i_{r_{c_2}}} - y_{i_{r_{c_1}}} \right] \quad (3.4-8)$$

$$\text{where } \alpha = \left[(r_{c_2}^3 - r_{c_1}^3) - \frac{3}{2} (r_{c_2}^2 - r_{c_1}^2) (1 + \varphi_0) + 3\varphi_0 (r_{c_2} - r_{c_1}) \right]^{-1} \quad (3.4-9)$$

These radial collocation solutions are then substituted into the partial differential equations, using the relationships

$$\frac{\partial y_i}{\partial r} = d_{1i} + 2d_{2i}r + 3d_{3i}r^2 \\ \frac{\partial^2 y_i}{\partial r^2} = 2d_{2i} + 6d_{3i}r \\ \frac{\partial \theta_g}{\partial r} = -\frac{M_g P_t}{\Theta_g^2} \frac{\partial \Theta_g}{\partial r} \quad (3.4-10) \\ \frac{\partial \delta}{\partial r} = -\bar{x}_{CO}^o \frac{\partial y_1}{\partial r} - \bar{x}_{CO_2^o} \frac{\partial y_2}{\partial r} \\ \frac{\partial^2 \delta}{\partial r^2} = -\bar{x}_{CO}^o \frac{\partial^2 y_1}{\partial r^2} - \bar{x}_{CO_2^o} \frac{\partial^2 y_2}{\partial r^2}$$

where $\frac{\partial \Theta_g}{\partial r}$ is obtained from the one point radial collocation of the gas temperatures. The concentration equations are then valid at both radial collocation points r_{c_1} and r_{c_2} since the residuals will be zero at these points. The full radial

concentration profile can be reconstructed from Equations (3.4-1) and (3.4-5) through (3.4-9). The energy balances for the gas, catalyst, and thermal well and the continuity equation are unchanged.

Axial collocation and numerical solution is performed in an identical manner as before with this larger system of equations. The size of the differential equation model has been increased by $2N$ nonlinear ordinary differential equations, where N is the number of axial collocation points. Note that for each additional radial collocation point for the concentrations, the model will be increased by $2N$ nonlinear ordinary differential equations.

Simulations were then performed with this model and compared to those using the earlier model. In the simulations, the bulk concentration can then be obtained by integrating the radial profiles:

$$\text{Bulk Concentration} = \frac{\int_{R_0}^{R_1} 2\pi r y_i(r) dr}{\int_{R_0}^{R_1} 2\pi r dr} \quad (3.4-11)$$

This allows direct comparison with previous simulations. Figure 3.4-16 shows a comparison of the axial gas temperature and bulk concentration profiles for the reactor with standard Type I operating conditions using the original model with no radial concentration gradient (i.e., infinite radial diffusion) and using the new model with a representative radial mass Peclet number of 2.0 and with a radial mass Peclet number of ∞ (i.e., no radial diffusion). Figure 3.4-17 shows a similar comparison with Type II operating conditions.

Figure 3.4-18 shows the radial temperature profiles at the reactor outlet. The radial and axial temperature and bulk concentration profiles are effectively not influenced by these modeling differences. Figure 3.4-19 shows the radial concentration profiles at $\zeta = 0.38$ and at the reactor outlet. Even with very high Peclet numbers, the differences between the radial concentration profile across

the relatively small bed and the assumed uniform profile are minimal. Definitely under planned operating conditions with small Peclet numbers, there is no benefit to increasing the number of radial collocation points, especially in light of the increased dimensionality of the resulting system.

3.3.5 Adiabatic Analysis

Modeling of the packed bed catalytic reactor under adiabatic operation simply involves a slight modification of the boundary conditions for the catalyst and gas energy balances. A zero flux condition should be used at the outer reactor wall. This can be accomplished using the programs developed in this work simply by setting the outer wall heat transfer coefficients, h_{ws} and h_{wg} (or corresponding Biot numbers), equal to zero. Simulations under adiabatic operation do not significantly alter any of the conclusions presented throughout this work and are often used for verification of worst-case nonadiabatic operation. Figure 3.4-20 shows the adiabatic steady state temperature and concentration profiles for standard Type I operating conditions. As expected, the temperature rise through the bed is more dramatic than in the non-adiabatic case, leading to much higher conversions through the bed. Due to the lack of any cooling, no 'hot spot' develops and all heat generated by the reaction is removed from the bed by the product gas, resulting in a very high temperature rise (200° K) within the bed. Such high temperatures are undesirable since they can significantly increase catalyst deactivation. Also note that in the adiabatic analysis the temperature difference between the gas and catalyst is negligible. Although the heat transfer coefficient between the gas and solid are as large as in the nonadiabatic analysis, major differences exist during nonadiabatic operation between the radial heat transfer through each phase.⁴ The results shown in 3.4-20a along

⁴. The heat transfer coefficient from the solid to the outer wall and the radial conduction in the

with other simulations indicates that a homogeneous analysis of the bed may be adequate for adiabatic analyses.

Figure 3.4-20b shows that CO conversion is much higher under adiabatic operation due to the higher bed temperatures. Note that the conversion of the CO₂ becomes important as soon as CO is nearly depleted. The 'rippling' in the CO₂ curve is a result of the axial orthogonal collocation.⁵ Numerical solution problems such as this will be discussed in Section 3.5.

3.3.6 Importance of Thermal Well

The mathematical model developed in this work allows for an analysis of the effects of a central axial thermal well. Although the presence of the well was found to have little effect on the concentration profiles, it significantly alters the transient temperature response of the reactor bed, since its large thermal capacitance increases the thermal time constant of the bed. Figure 3.4-21 shows the radial gas and solid temperature profiles at the reactor exit ($z = L$) during reactor start-up. As shown, the steady state profiles are similar, although conduction along the thermal well slightly alters the surrounding gas temperature. The transient behavior exemplifies the slow response of the thermal well. It can be seen that the response of the exit temperature profile is rapid without the well, with steady state being approached in under one minute; whereas, the presence of the well introduces a finite heat sink into the reactor center that slowly absorbs some of the heat produced. Over ten minutes are necessary to approach steady state with an eighth-inch diameter well. This is further seen in Figure 3.4-22 where the temporal behavior of the catalyst and gas temperature

solid is greater than the corresponding parameters in the gas phase.

5. Although only 6 axial collocation points are used in most simulations, 12 points were necessary here and even then the results are less than optimum.

at the reactor exit are compared with and without the presence of the thermal well. These figures also show that the temperatures in the reactor center are higher without the thermal well as would be expected. However, Figure 3.4-23 shows that the well has very little effect on the axial concentration profiles, and overall conversion is only slightly affected.

Although the thermal well increases the thermal capacitance of the reactor bed and reduces the reaction volume, these effects alone cannot account for the dramatic increase in the thermal time constants of the bed with a thermal well.⁶ Whereas the dynamics of the catalyst particle temperatures are very fast due to the heat generation on the particles from the exothermic reactions, the dynamics of the thermal well temperatures are much slower since the heat is generated on the surrounding particles. Much of this energy is transferred to the outer cooling jacket or out of the bed with the gas phase. Only a small portion is transferred to the thermal well and even this through relatively slow mechanisms, thus resulting in the slow dynamic behavior of the well.

Since a thermal well is sometimes used in industry to obtain temperature measurements for process monitoring or control, we note the importance of incorporating even a relatively small well into the modeling and control analysis. Basing decisions on measured temperatures within an axial thermal well and a model without a thermal well (i.e., assuming that the measured temperatures are the predicted temperatures at the center of the bed) can be dangerous.

Simple modifications to the model development presented in this work allow for simulating systems that do not include central thermal wells. In such cases, the dimensionality of the mathematical system is reduced by N, since one partial differential equation is eliminated. The modeling programs developed in

6. Due to the relatively small radius of the well, the thermal capacitance ($V\rho c_p$) of the bed with the thermal well (16 cal/ $^{\circ}$ K) is only slightly higher than that without (14 cal/ $^{\circ}$ K) and the loss in reaction volume is only about 2%.

this work can be used directly for systems without thermal wells simply by setting the parameters for the well diameter and the thermal well heat transfer coefficients, h_{ts} and h_{tg} (or corresponding Biot numbers), equal to zero.

3.3.7 Dispersion Effects

Much work has been focused on the significance of dispersion terms in the transient material and energy equations for packed bed reactors. In general, axial diffusion of mass and energy and radial diffusion of mass have been neglected in comparison with convective terms in most packed bed reactor studies (Carberry and Wendel, 1963; De Wasch and Froment, 1971; Hlavacek, 1970; Hoiberg et al., 1971; Jutan et al., 1977; Valstar et al., 1975).

For packed bed reactors, Carberry and Wendel (1963), Hlavacek and Marek (1966), and Carberry and Butt (1975) report that axial dispersion effects are negligible if the reactor length is sufficient. These and other researchers (Mears, 1976; Young and Finlayson, 1973) have developed criteria based on the reactor length for conditions where the axial dispersion can safely be neglected. Since the tube length/pellet diameter for the experimental methanation reactor is about 150, just at the limit of most of the published criteria for neglecting axial heat dispersion, careful analysis of these dispersion effects is needed. However, neglecting axial mass dispersion should be a safe assumption since the tube length/pellet diameter for the experimental system is well above the value of 50 generally recommended. Radial mass dispersion can also be neglected and is inherently eliminated from our model since the one point radial collocation results in a constant radial concentration profile. However, the radial diffusion of energy must be retained since it is one of the most important physical processes influencing the dynamic and steady state behavior of the system by

governing the radial flow of energy through the bed to the cooling wall.

Simulations using the full model were then used to study the necessity of these dispersion effects and to verify some of the common assumptions. A wide range of Peclet numbers were used in the simulations. The actual values for the methanation reactor will have to be estimated from preliminary heat transfer experiments in the reactor (Section 4.2). Based on extensive previous studies, the radial gas Peclet number should range from 5 to 10 and the axial gas Peclet numbers from 0.5 to 2.0 (Carberry, 1976). For completeness, our simulations used Peclet numbers over a much wider range.

Comparison of steady state profiles for Type I conditions (Figure 3.4-24) shows that neglecting axial mass diffusion has very little effect on the temperature and concentration profiles even though the axial gradients are significant. However, Figure 3.4-25 shows that neglecting the axial thermal dispersion in the gas does affect the solution profiles. The axial temperature profiles are offset and the concentration profiles are shifted slightly. Further simulations show minimal effect of neglecting the axial conduction of energy in the solid.

Figure 3.4-26 shows that, for standard Type II operating conditions, neglecting the axial thermal dispersion leads to instabilities in the orthogonal collocation solution with six collocation points. Although the solutions at the collocation points are similar, neglecting axial dispersion of heat leads to some 'rippling' in the axial temperature profiles. However, the concentration profiles are nearly unaffected. This 'rippling' is a result of the axial orthogonal collocation and can be reduced by increasing the number of collocation points. However, this leads to a substantial increase in model dimensionality and thus solution time. Obviously, the axial thermal diffusion has a stabilizing effect on the numerical solution using orthogonal collocation and actually damps the behavior of

the solution polynomial.

Finally, Figure 3.4-27 shows the effect of neglecting axial diffusion on the dynamic simulations of the reactor under start-up operation with Type II conditions. Significant differences are apparent.

The reduction in solution time for these simulations is minimal and in some cases the elimination of the axial diffusion terms actually increases the solution time. Simulations show that neglecting the axial dispersion of mass has little effect on numerical computation time; whereas, eliminating axial dispersion of energy may significantly increase computation time and only rarely decreases it substantially.

Thus our analysis of the effects of dispersion on the simulated behavior of the reactor along with the work by Bonvin (1980) shows the necessity of including the thermal diffusion terms. Simulations here verify that the numerical stability of the model is greatly enhanced by retaining these dispersive effects and that, although minor additional effort may be necessary in the model development, the numerical solution time may actually be reduced by retaining some of these terms. Furthermore, simulations verify that the axial dispersion of mass can usually be neglected, although the inclusion of these terms in the model introduces little complication in the collocation solution; whereas, other solution procedures are often significantly hindered by these second derivative terms. The radial dispersion of mass seemingly has little effect on either the simulated results or solution times and can safely be neglected. This conclusion is based on the radial concentration analysis presented in Section 3.4.5, since the standard mathematical solution that uses one point radial collocation in this work effectively assumes no radial concentration gradient.

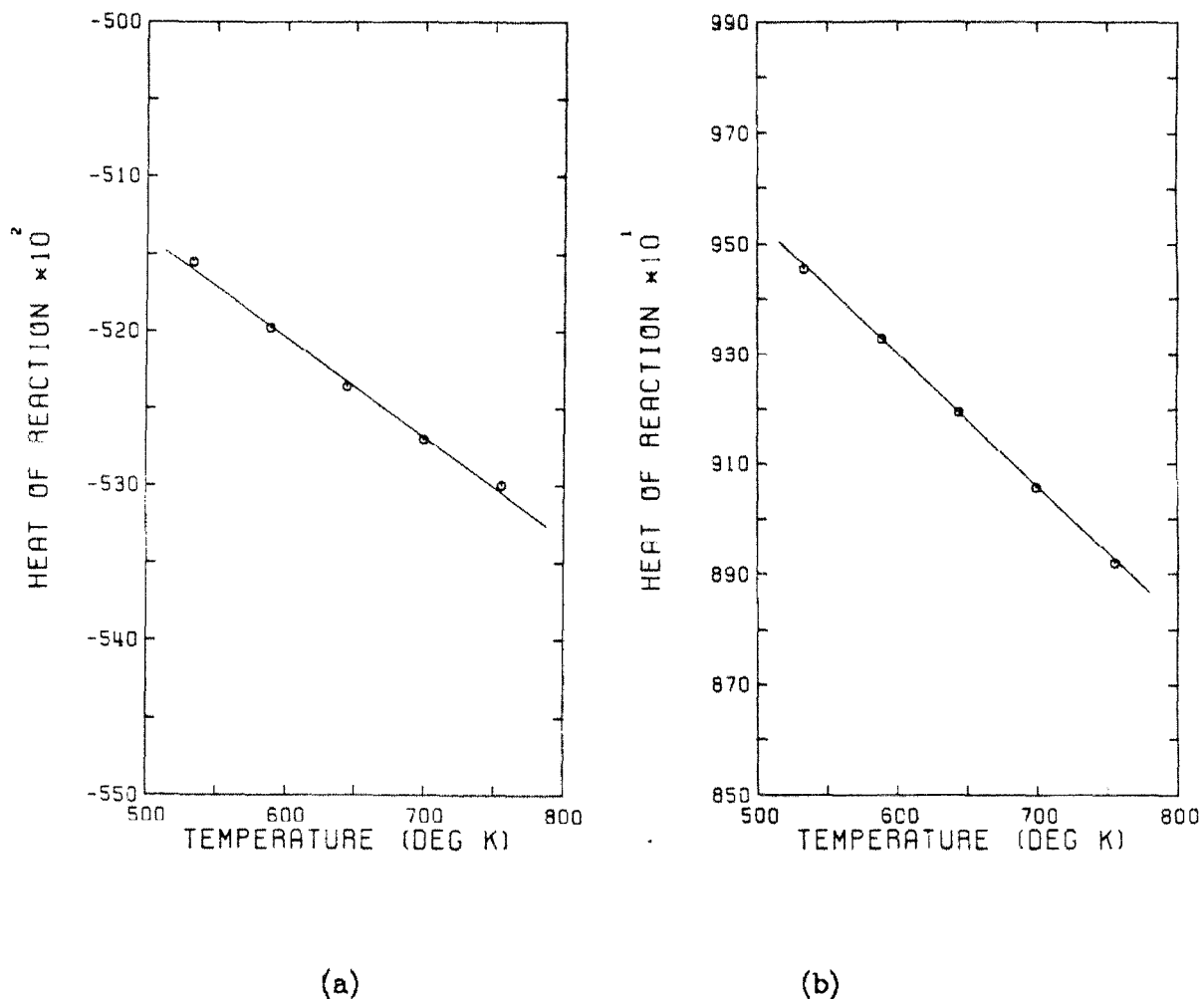


Figure 3.4-1
Temperature Dependence of Heats of Reaction
(a. Methanation, b. Steam-Shift)
(Source: United Catalysts Inc.)

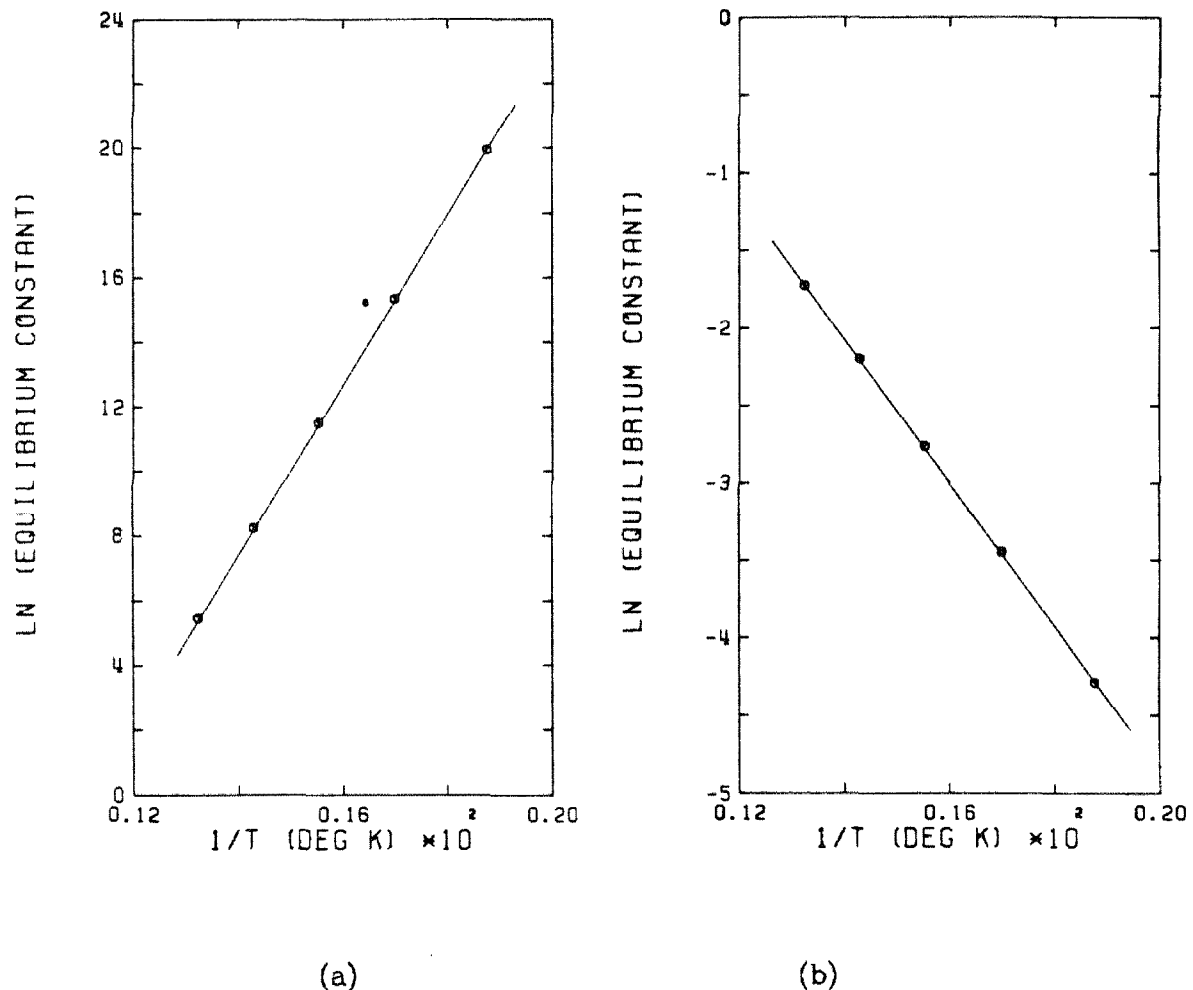
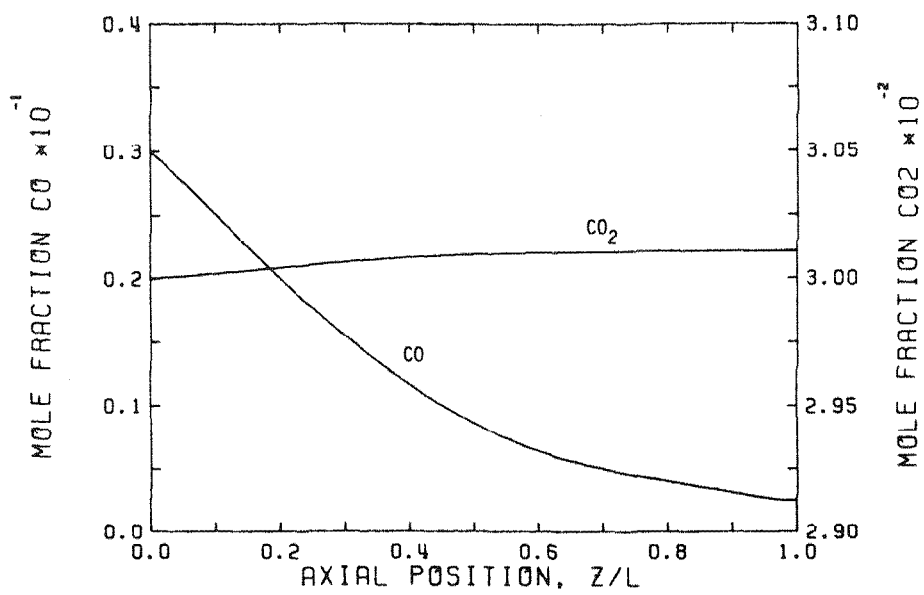
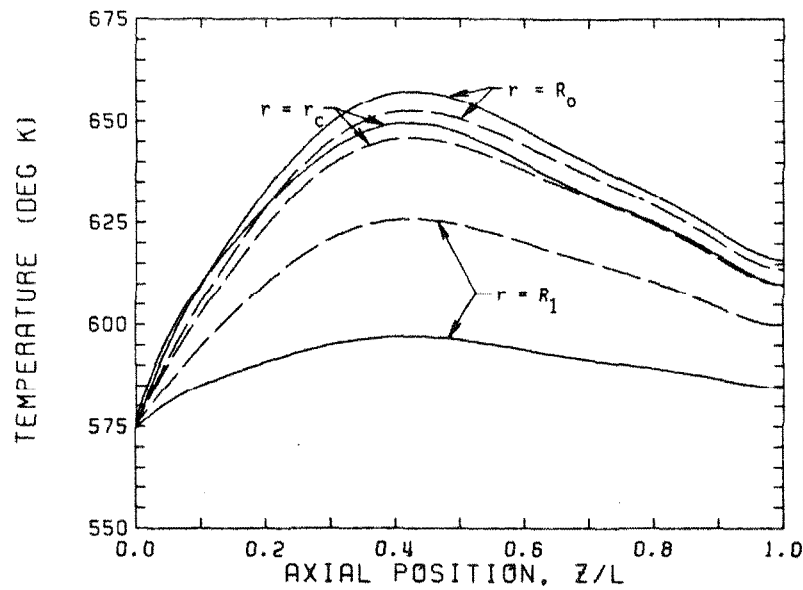


Figure 3.4-2
Temperature Dependence of Equilibrium Constants
(a. Methanation, b. Steam-Shift)
(Source: United Catalysts Inc.)



(a)



(b)

Figure 3.4-3
Steady State Axial Profiles
Standard Type I Operating Conditions

a) Concentration Profiles Based on Inlet Total Moles
b) Temperature Profiles at $r = R_0, r_c, R_1$

— Solid Phase - - - Gas Phase

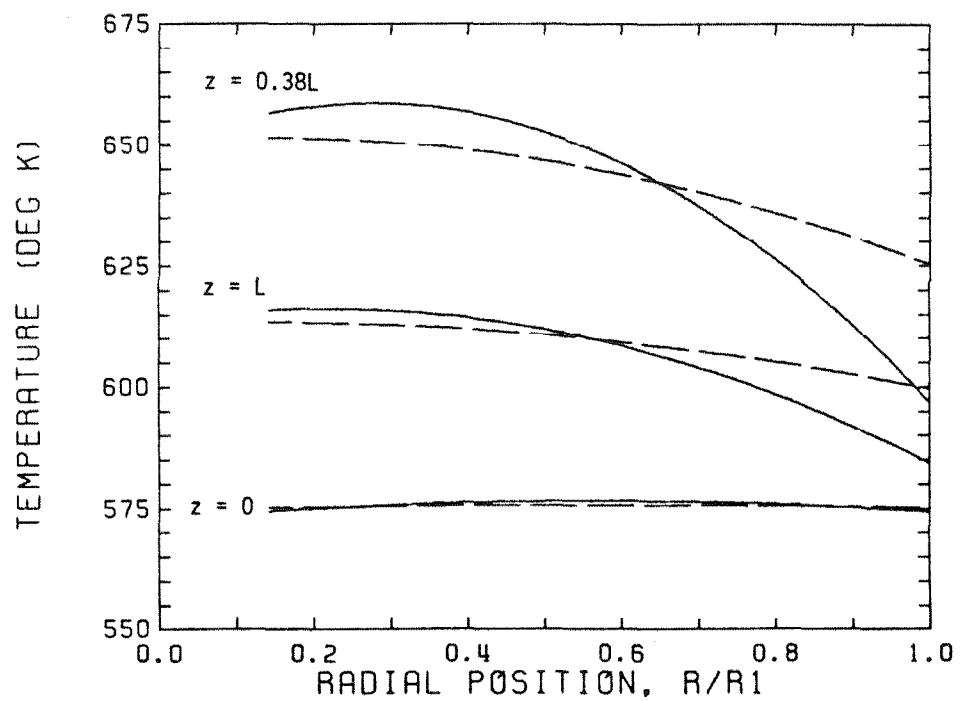


Figure 3.4-4
Steady State Radial Temperature Profiles
Standard Type I Operating Conditions

— Solid Phase - - - Gas Phase

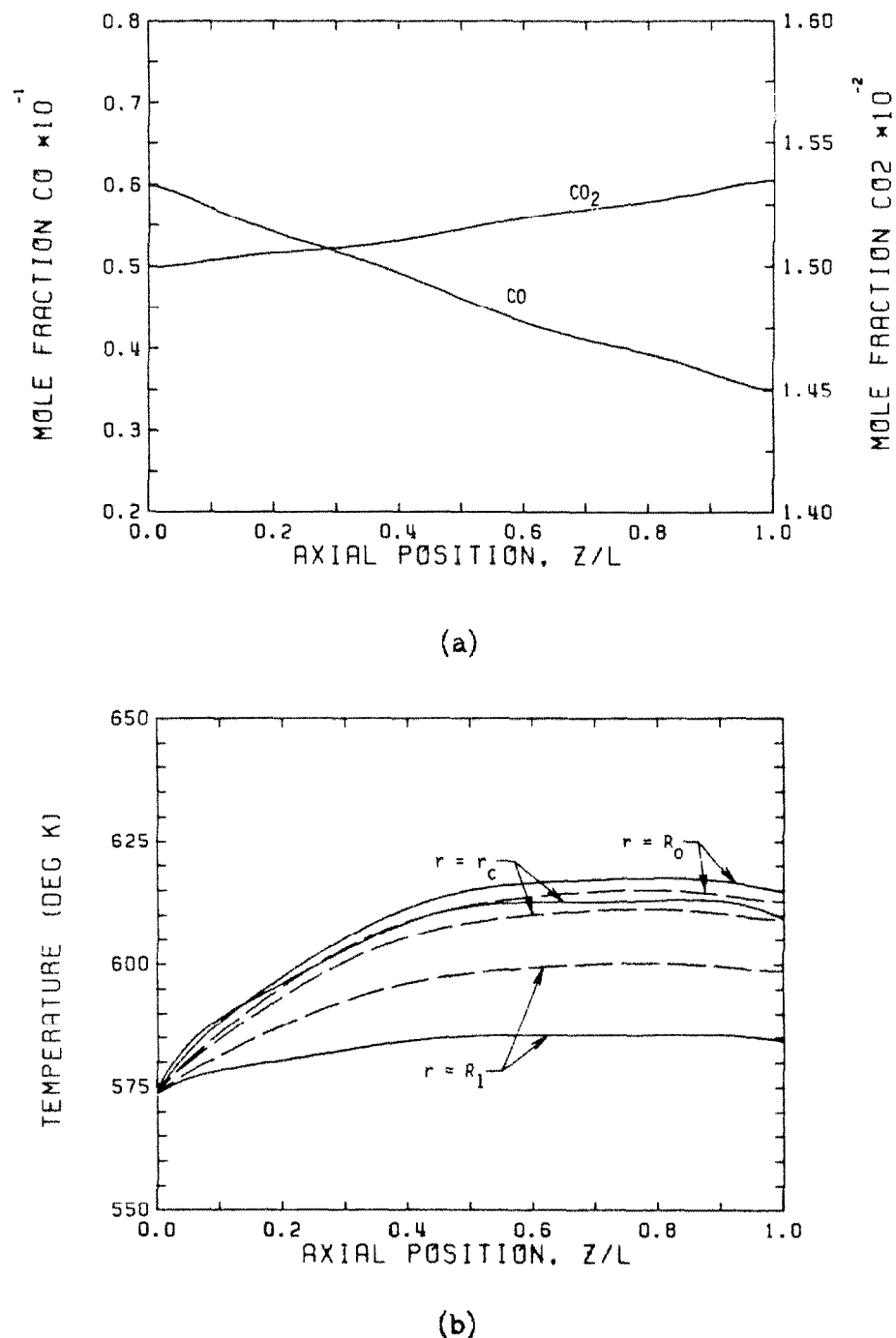


Figure 3.4-5
Steady State Axial Profiles
Standard Type II Operating Conditions

- a) Concentration Profiles Based on Inlet Total Moles
- b) Temperature Profiles at $r = R_0, r_c, R_1$

— Solid Phase - - - Gas Phase

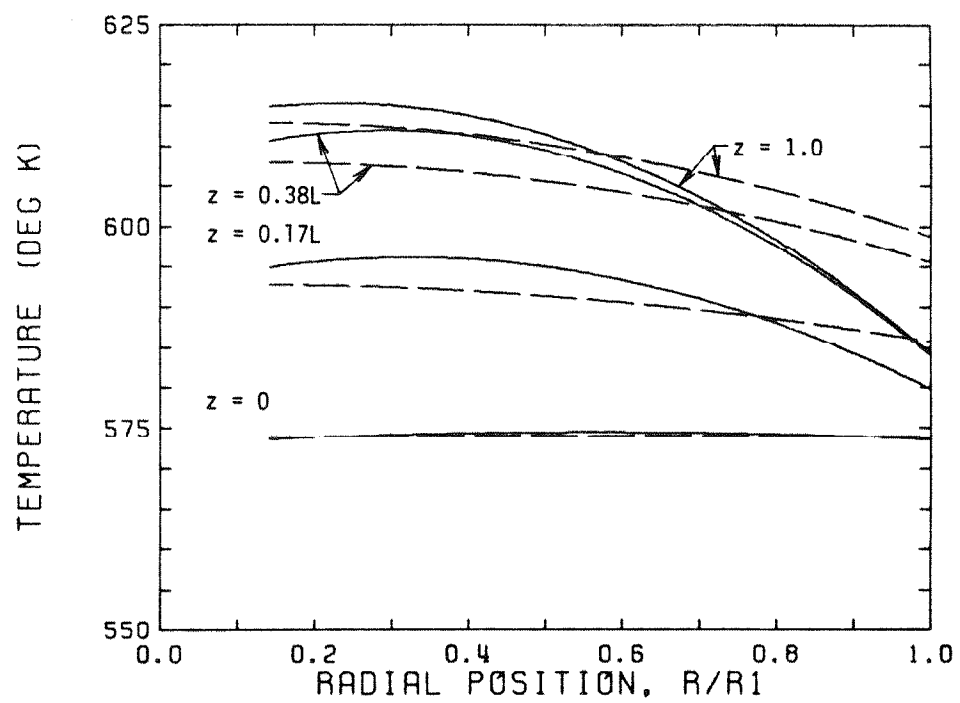


Figure 3.4-6
Steady State Radial Temperature Profiles
Standard Type II Operating Conditions

— Solid Phase - - - Gas Phase

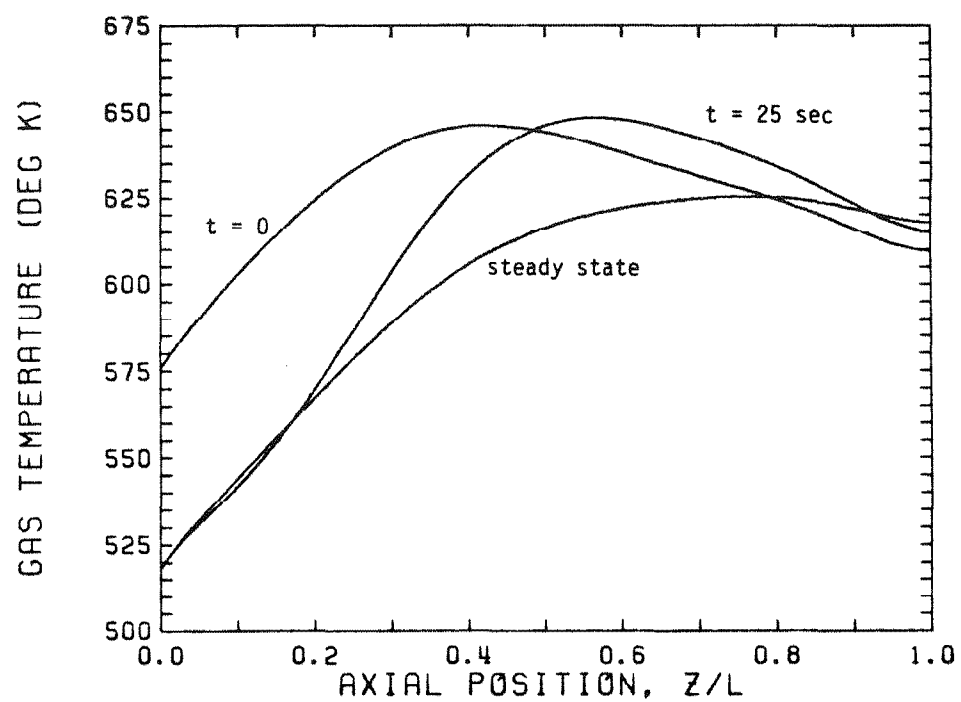


Figure 3.4-7
Disturbance (10% drop in Inlet Gas Temperature) Analysis
Transient Axial Temperature Profiles
Standard Type I Operating Conditions

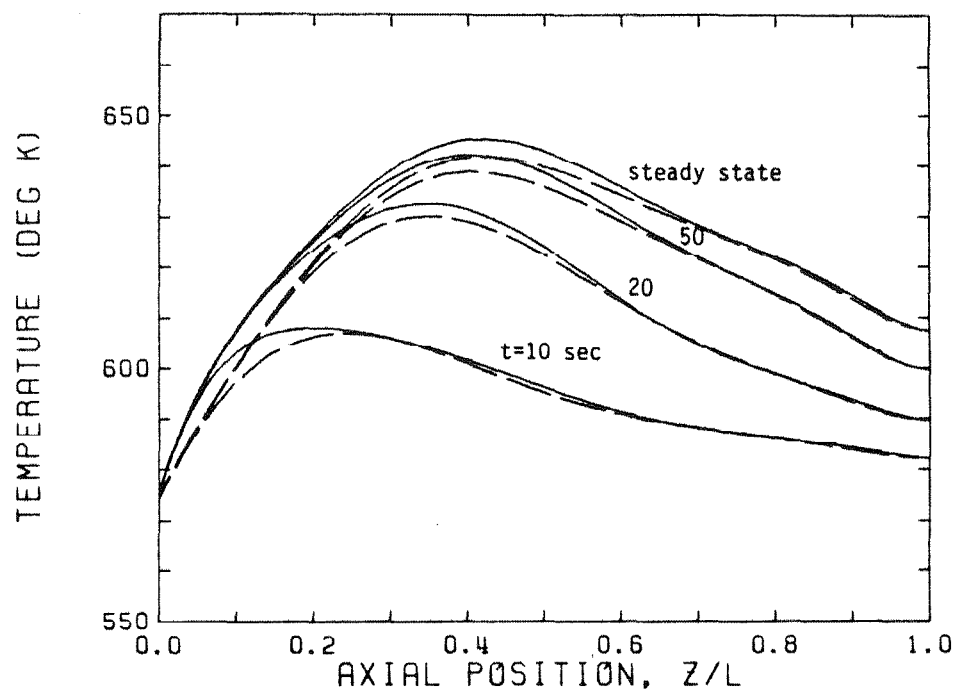


Figure 3.4-8
Axial Gas and Catalyst Temperatures during Start-up
Standard Type I Operating Conditions
— Solid Phase - - - Gas Phase

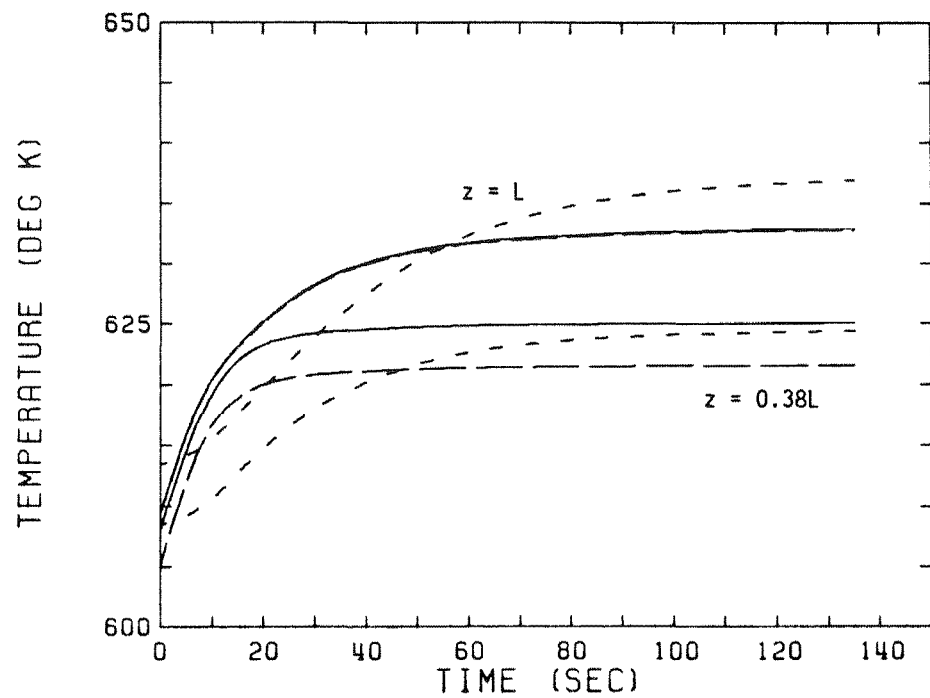


Figure 3.4-9
Temperatures After an Input Step Change
Standard Type II Operating Conditions
(T_w from 573° K to 593° K)

— Solid Phase - - - Gas Phase - - - - Thermal Well

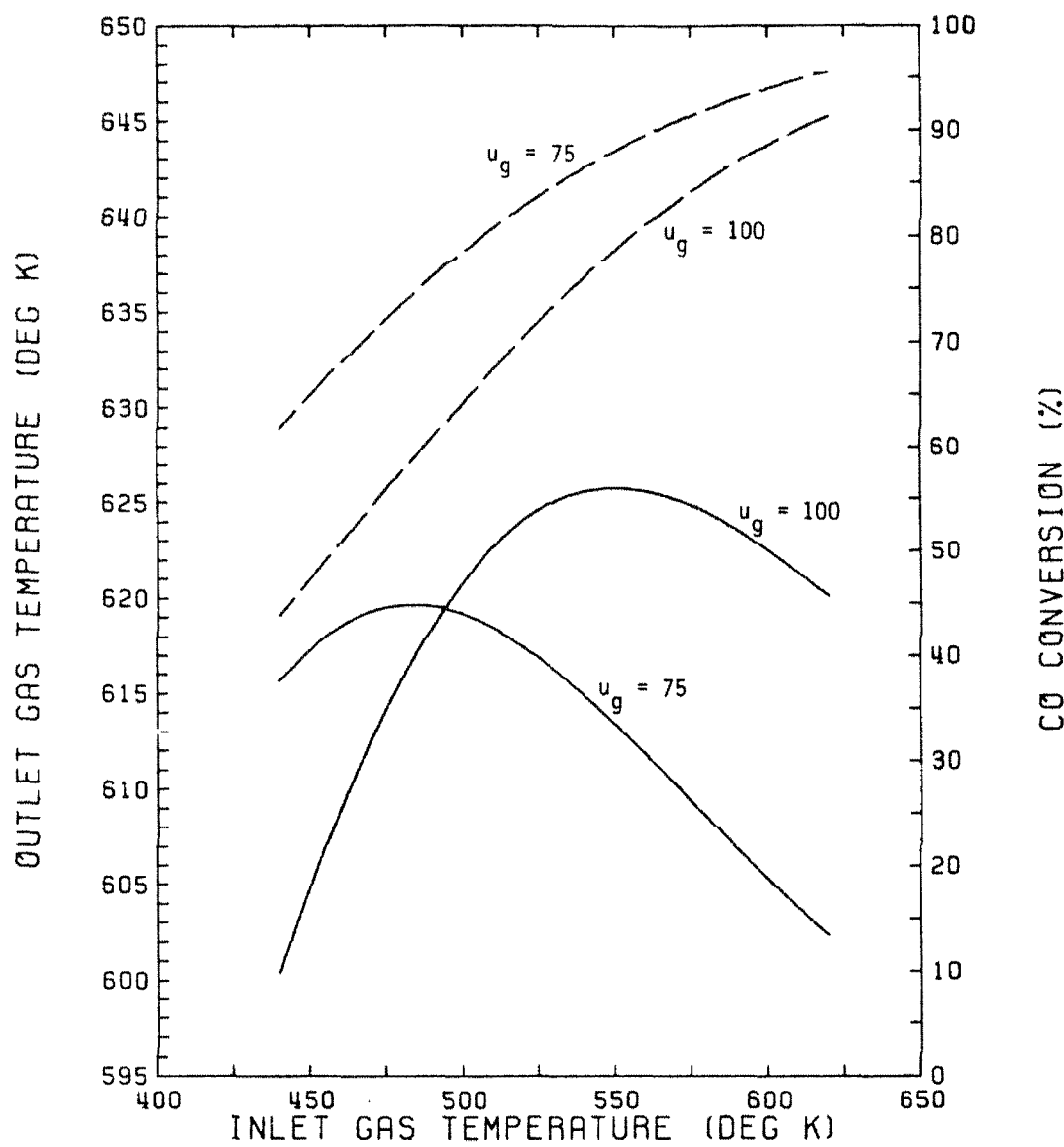


Figure 3.4-10
Effects of Inlet Gas Temperature
Standard Type I Operating Conditions

— Outlet Gas Temperature
- - - CO Conversion

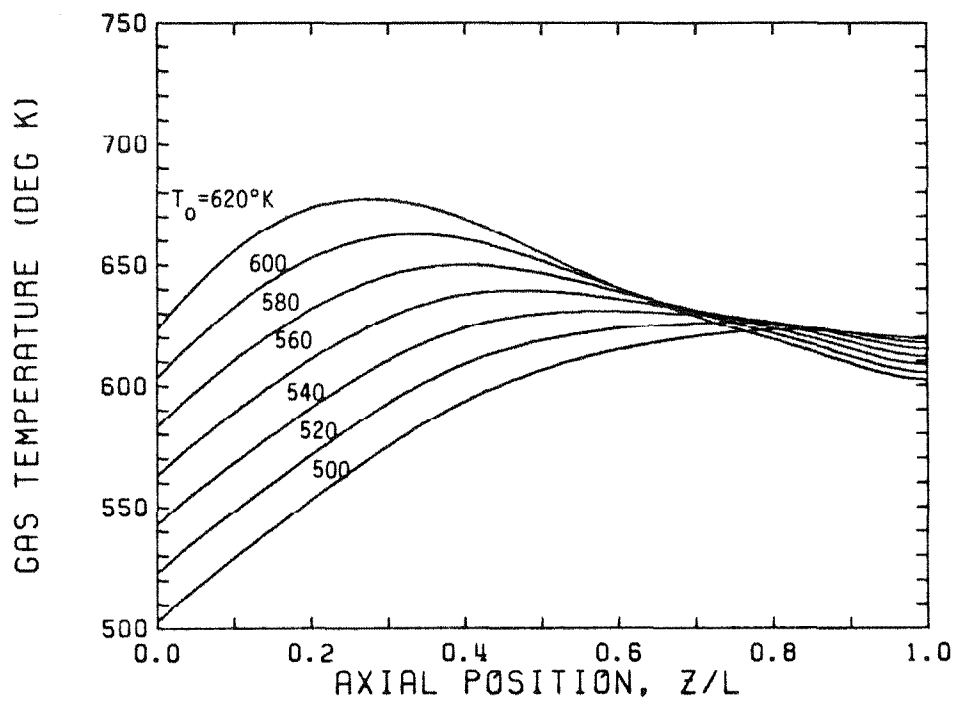


Figure 3.4-11
Effects of Inlet Gas Temperature
Steady State Axial Temperature Profiles
Standard Type I Operating Conditions

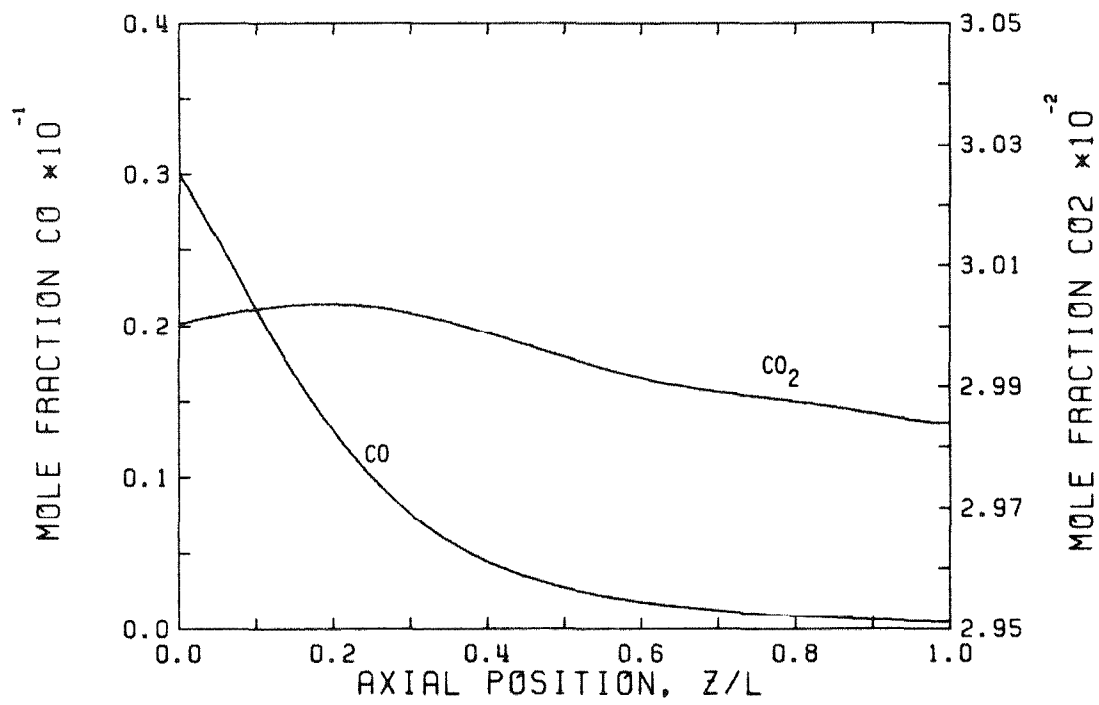


Figure 3.4-12
Axial Steady State Concentration Profiles for $T_o = 623^\circ \text{ K}$
Standard Type I Operating Conditions

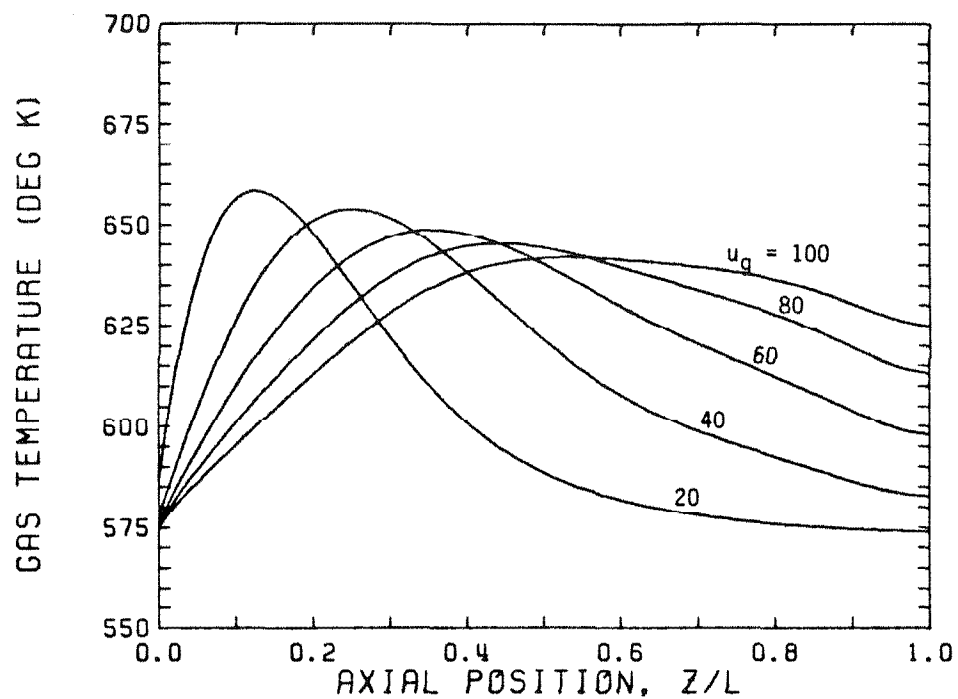


Figure 3.4-13
Effects of Inlet Gas Velocity
Steady State Axial Gas Temperature Profiles
Standard Type I Operating Conditions

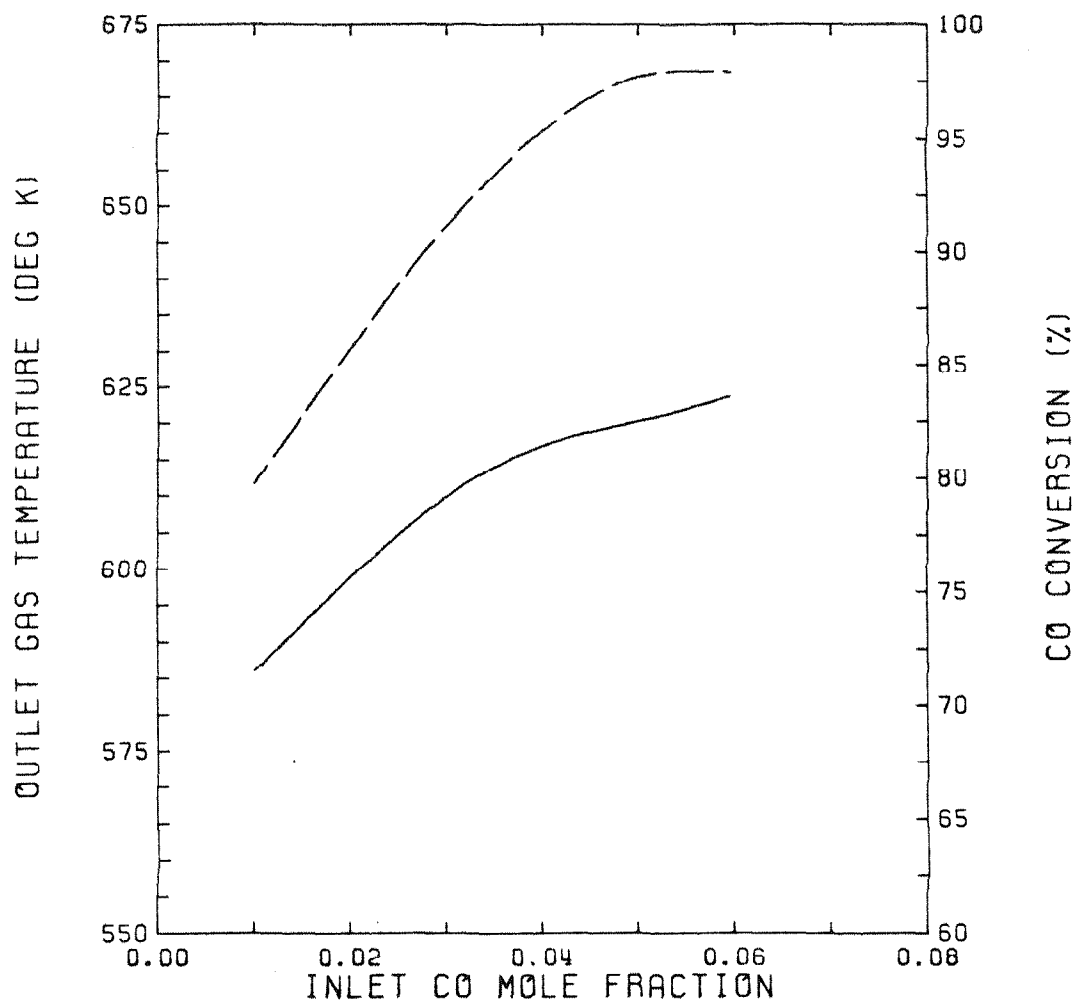


Figure 3.4-14
Effects of Inlet CO Concentration
Standard Type I Operating Conditions

— Outlet Gas Temperature
- - - CO Conversion

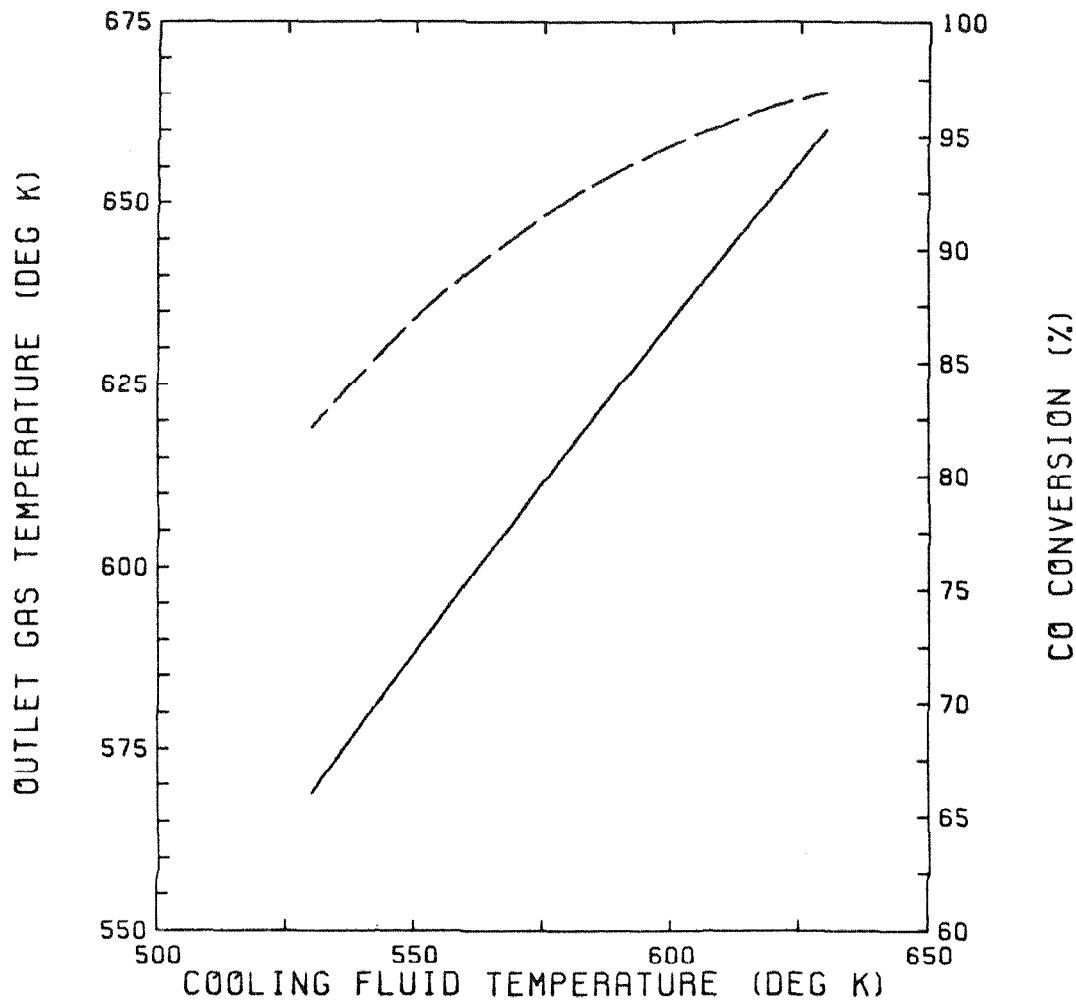
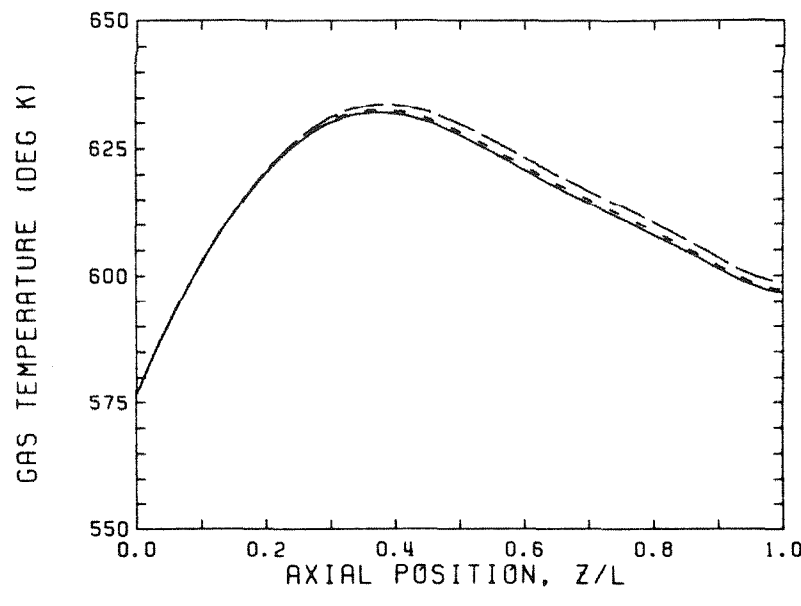
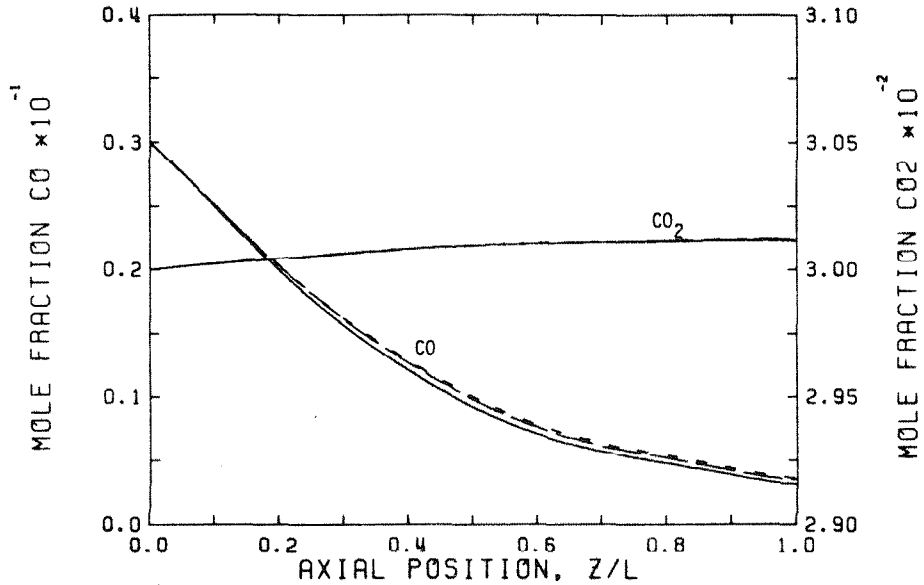


Figure 3.4-15
Effects of Cooling Fluid Temperature
Standard Type I Operating Conditions

— Outlet Gas Temperature
- - - CO Conversion



(a)



(b)

Figure 3.4-16
Multipoint Radial Concentration Collocation
Axial Gas Temperatures and Bulk Concentration Profiles
Standard Type I Operating Conditions

- Original Model - Infinite Radial Diffusion
- - - New Model - Radial Mass Peclet Number = 2.0
- - - New Model - Radial Mass Peclet Number = ∞

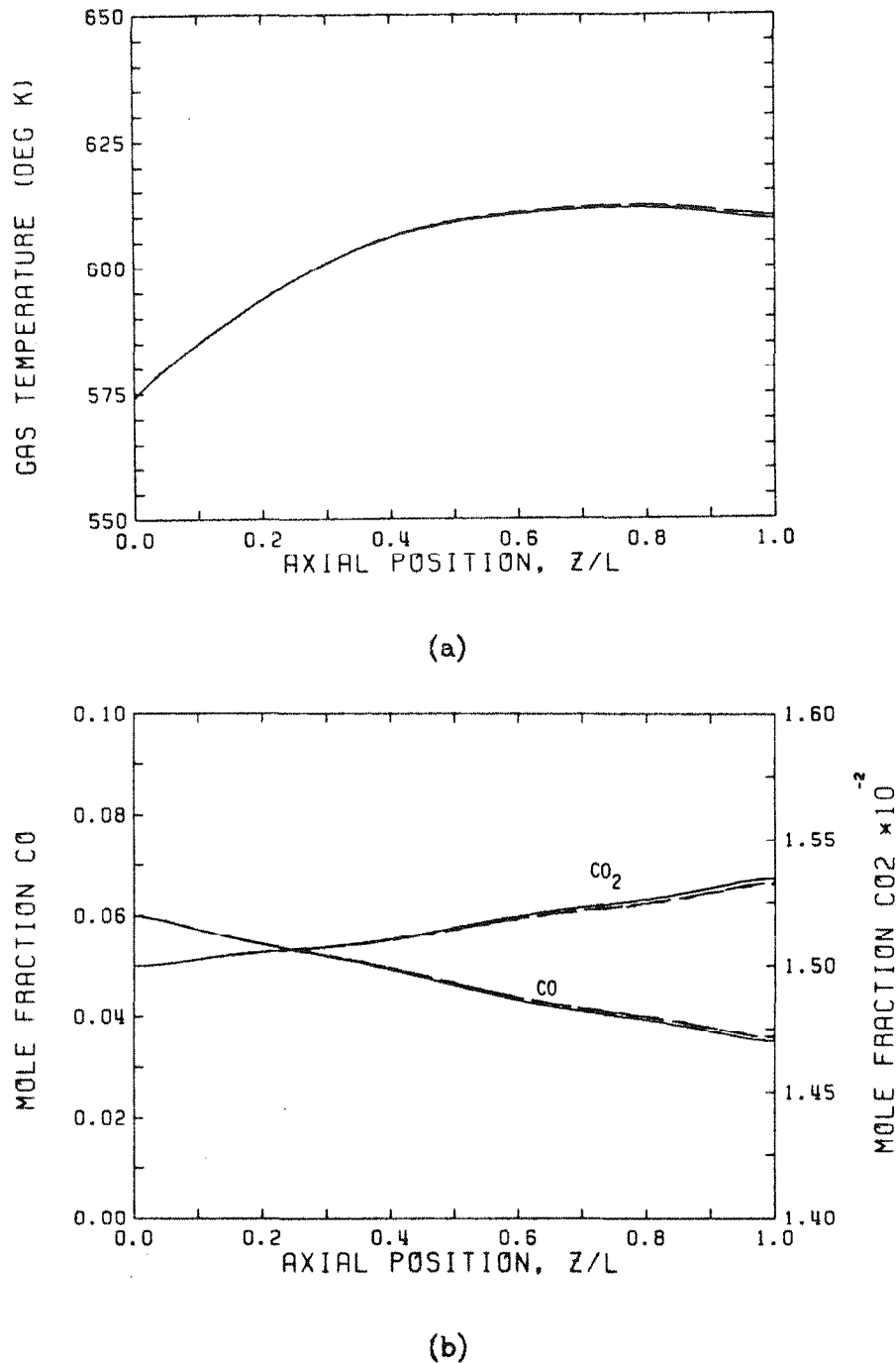


Figure 3.4-17
Multipoint Radial Concentration Collocation
Axial Gas Temperatures and Bulk Concentration Profiles
Standard Type II Operating Conditions

- Original Model - Infinite Radial Diffusion
- - - New Model - Radial Mass Peclet Number = 2.0
- - - New Model - Radial Mass Peclet Number = ∞

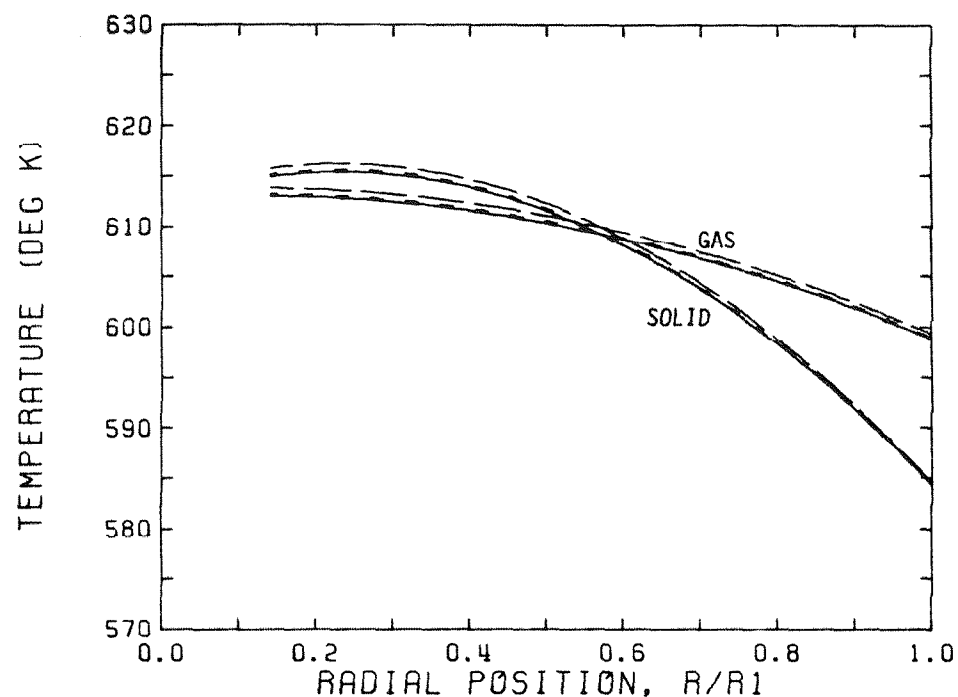


Figure 3.4-18
Multipoint Radial Concentration Collocation
Radial Gas and Catalyst Temperature Profiles at Reactor Outlet
Standard Type II Operating Conditions

- Original Model - Infinite Radial Diffusion
- - - New Model - Radial Mass Peclet Number = 2.0
- - - New Model - Radial Mass Peclet Number = ∞

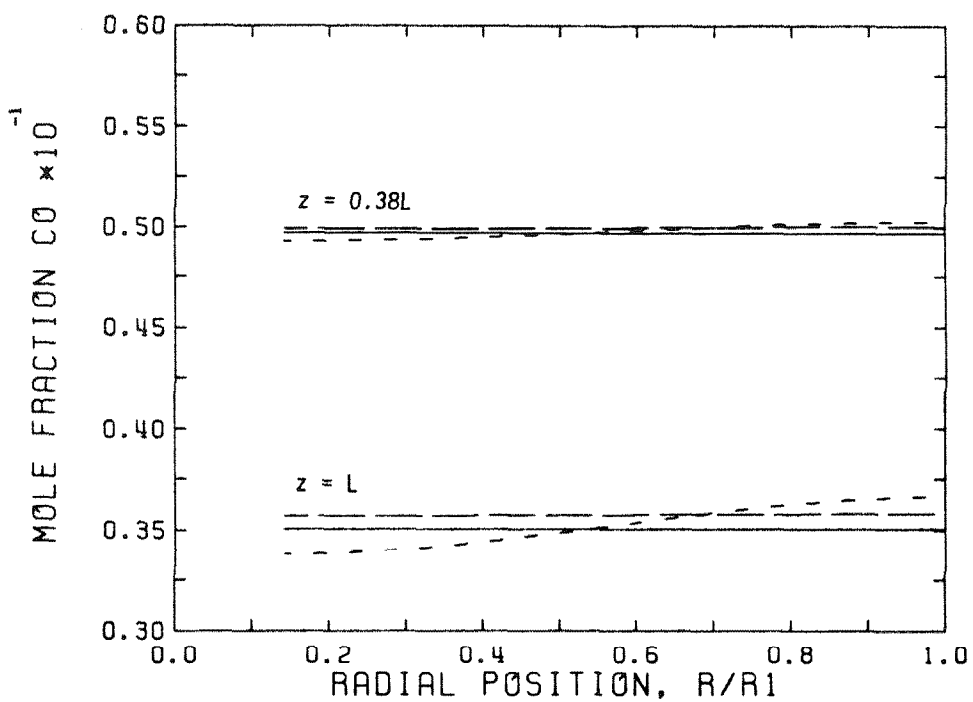
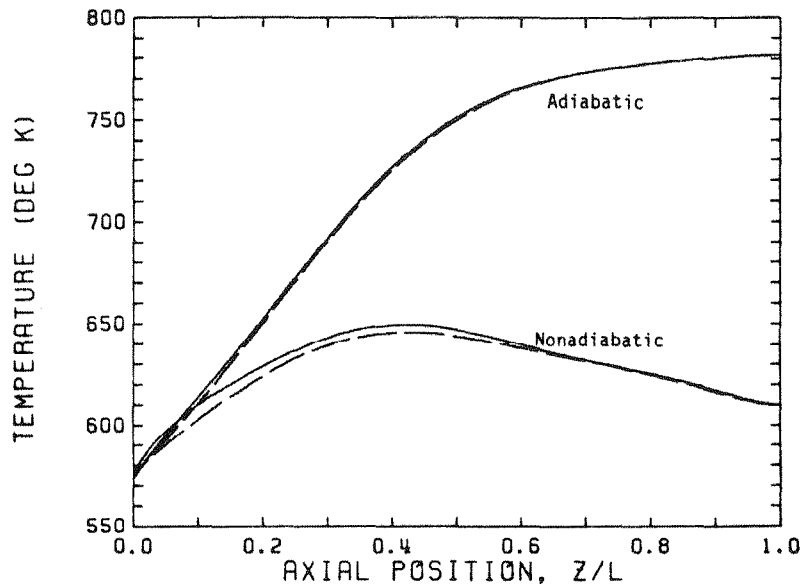
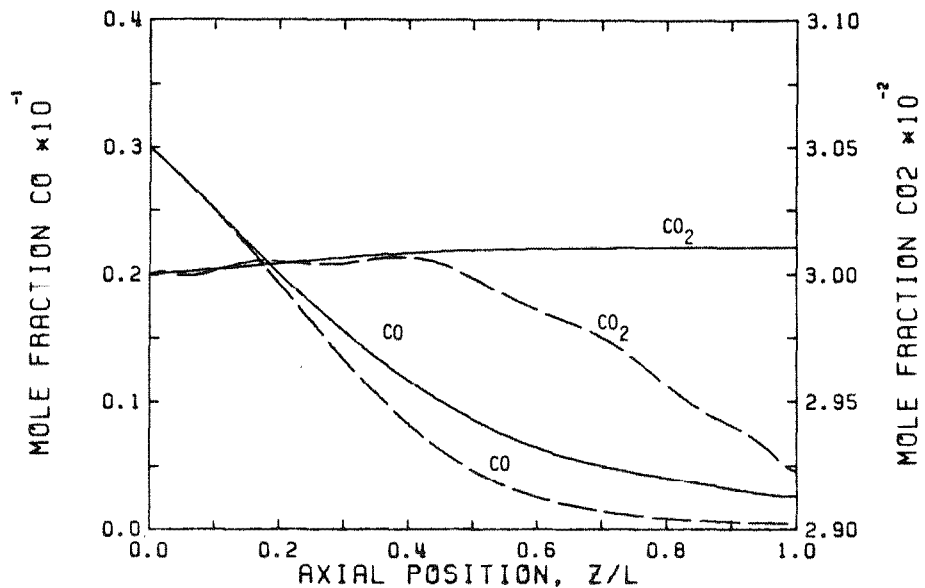


Figure 3.4-19
Multipoint Radial Concentration Collocation
Radial Concentration Profiles
Standard Type I Operating Conditions

— Original Model - Infinite Radial Diffusion
- - - New Model - Radial Mass Peclet Number = 2.0
- - - - New Model - Radial Mass Peclet Number = ∞



(a)



(b)

Figure 3.4-20
Adiabatic Steady State Axial Profiles
Standard Type I Operating Conditions

- a) Temperatures (— Catalyst —— Gas)
- b) CO and CO₂ Concentrations (— Nonadiabatic —— Adiabatic)

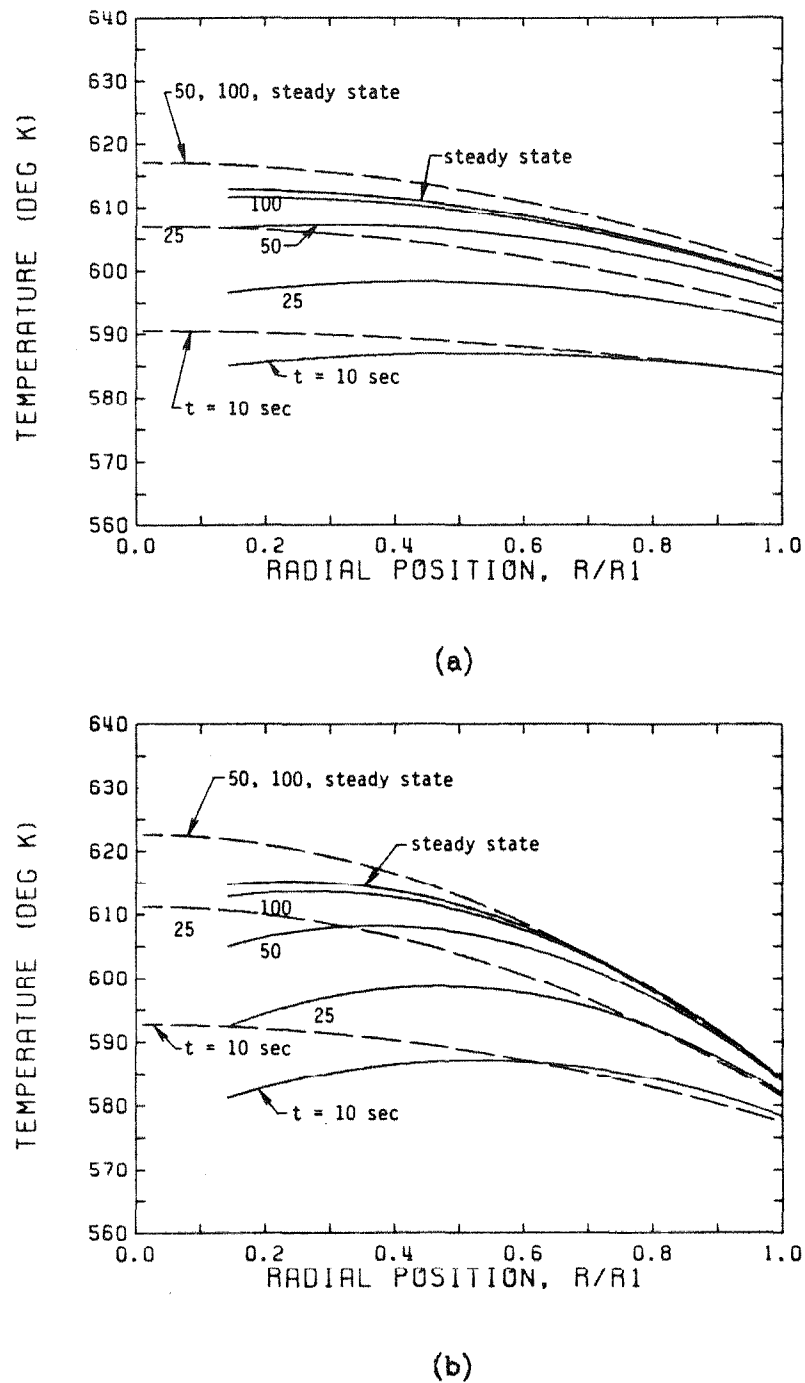
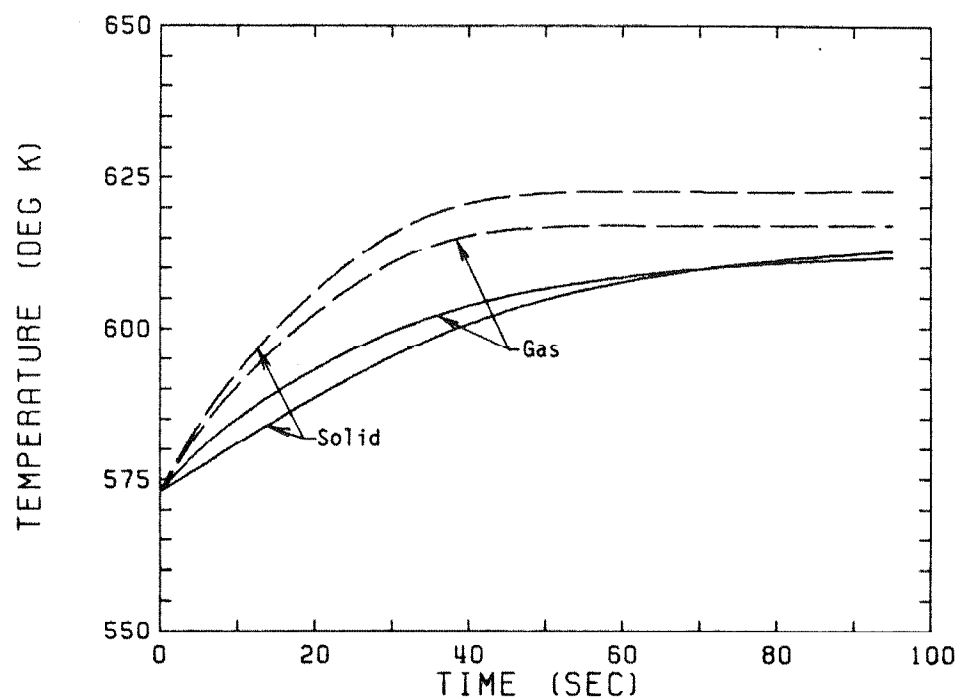


Figure 3.4-21
Effect of Thermal Well on Transient Radial Temperature Profiles
Standard Type II Operating Conditions

— 1/8" Thermal Well - - - No Thermal Well

- a) Gas Temperatures
- b) Solid Temperatures



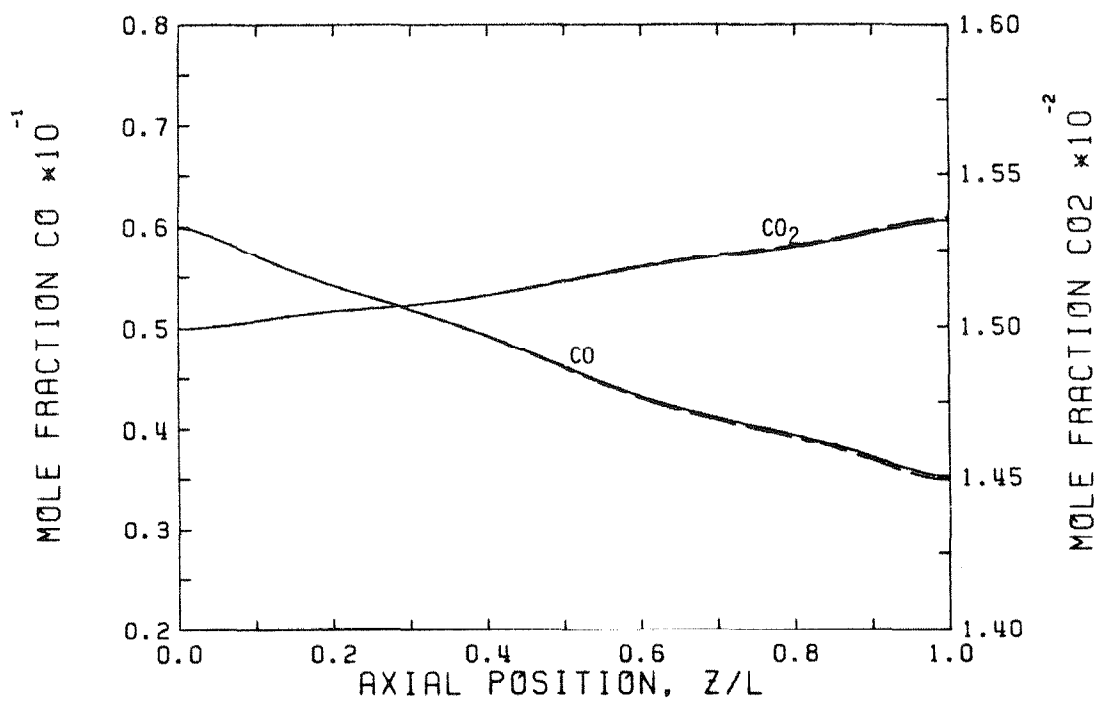


Figure 3.4-23
Steady State Axial Concentration Profiles
Standard Type II Operating Conditions

— 1/8" Thermal Well - - - No Thermal Well

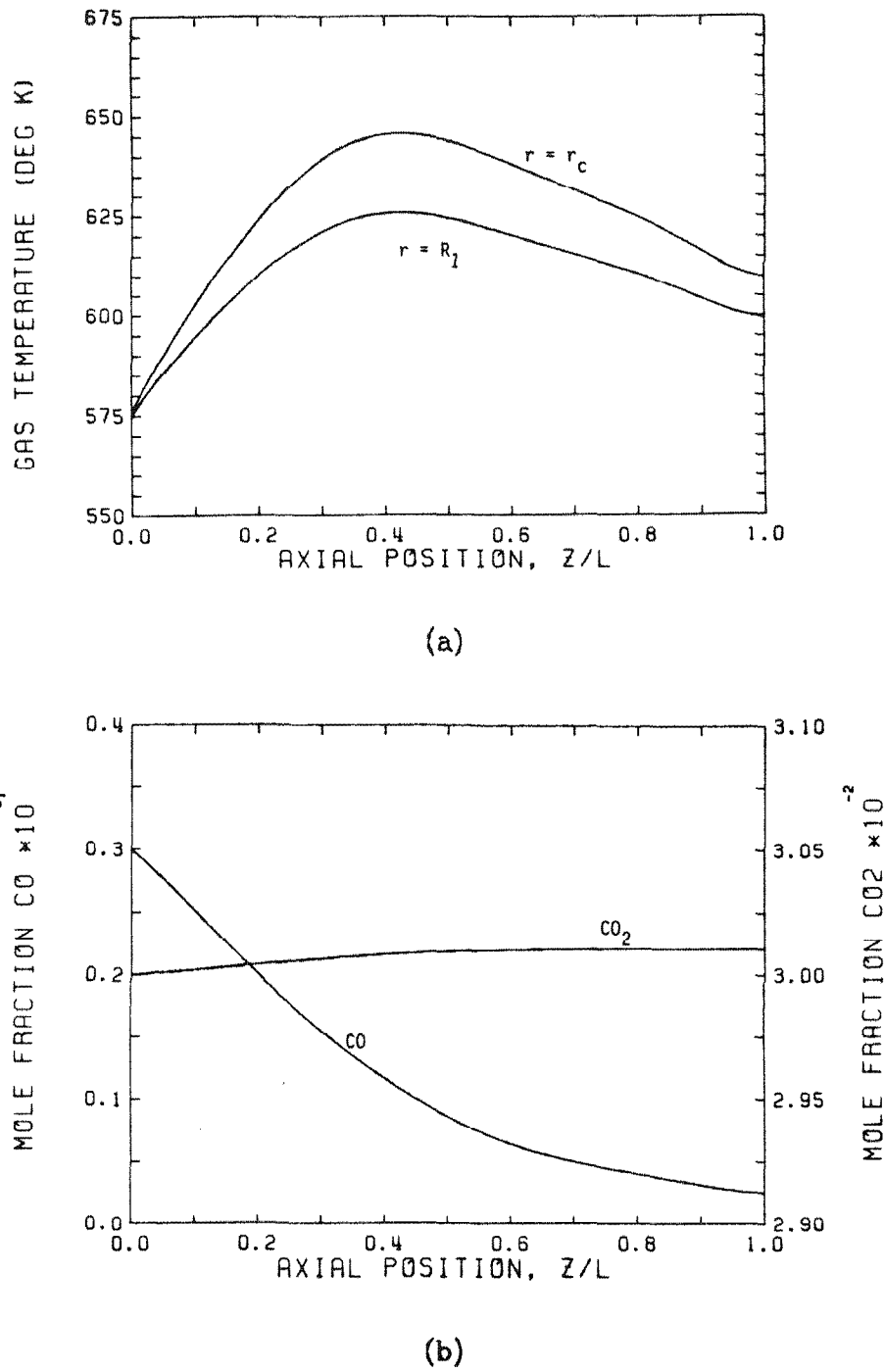
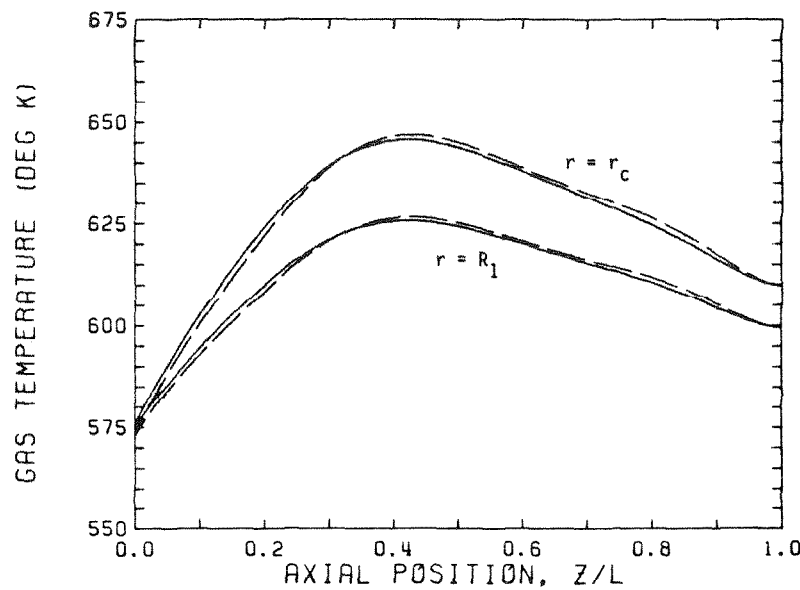


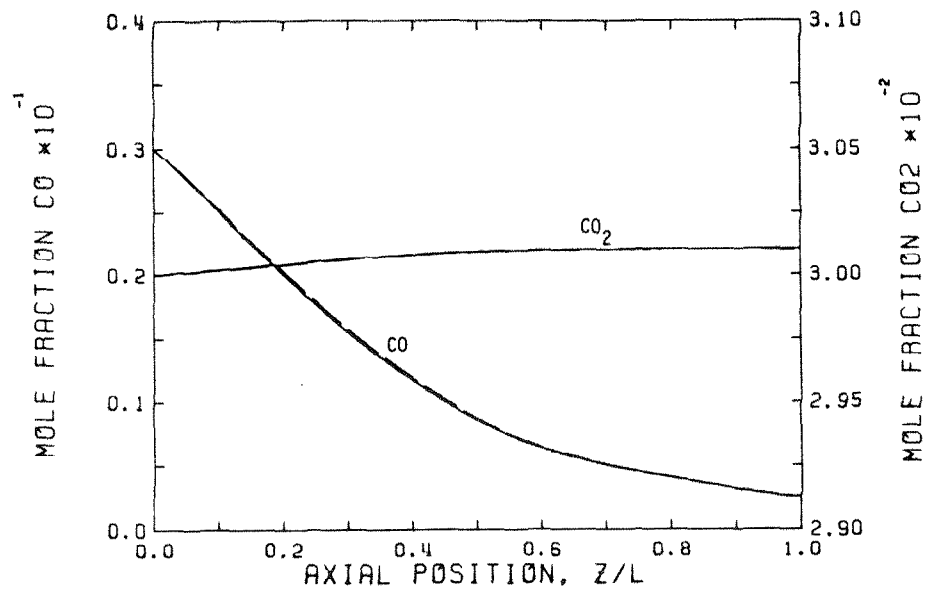
Figure 3.4-24
Steady State Axial Profiles - Neglecting Axial Mass Diffusion
Standard Type I Operating Conditions

— Original Model - - - No Axial Mass Diffusion

- a) Gas Temperature
- b) CO and CO_2 Concentrations



(a)



(b)

Figure 3.4-25
Steady State Axial Profiles - Neglecting Axial Heat Diffusion
Standard Type I Operating Conditions

— Original Model - - - No Axial Heat Diffusion

- a) Gas Temperature
- b) CO and CO₂ Concentrations

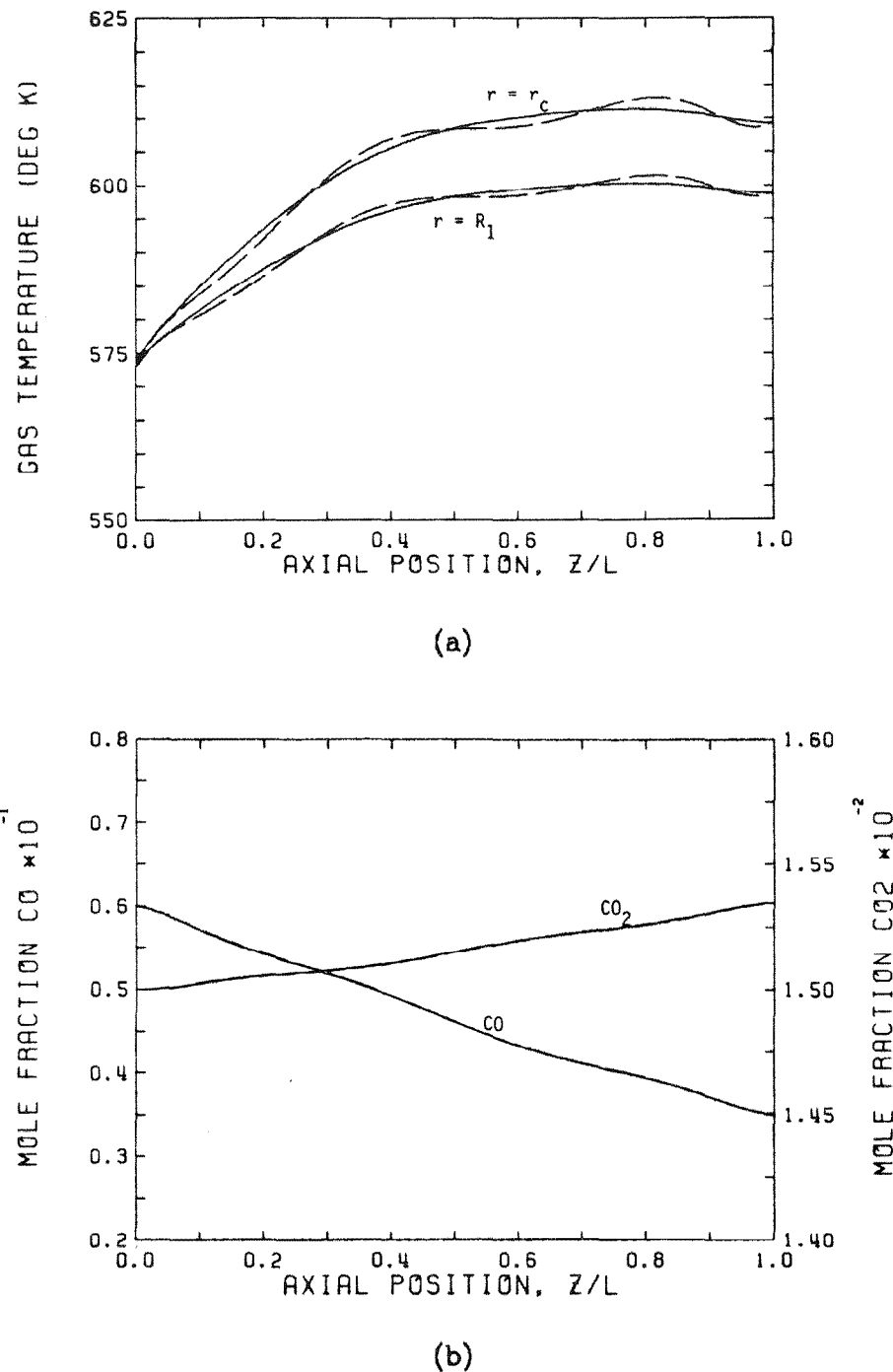


Figure 3.4-26
Steady State Axial Profiles - Neglecting Axial Heat Diffusion
Standard Type II Operating Conditions

— Original Model - - - No Axial Heat Diffusion

- a) Gas Temperature
- b) CO and CO₂ Concentrations

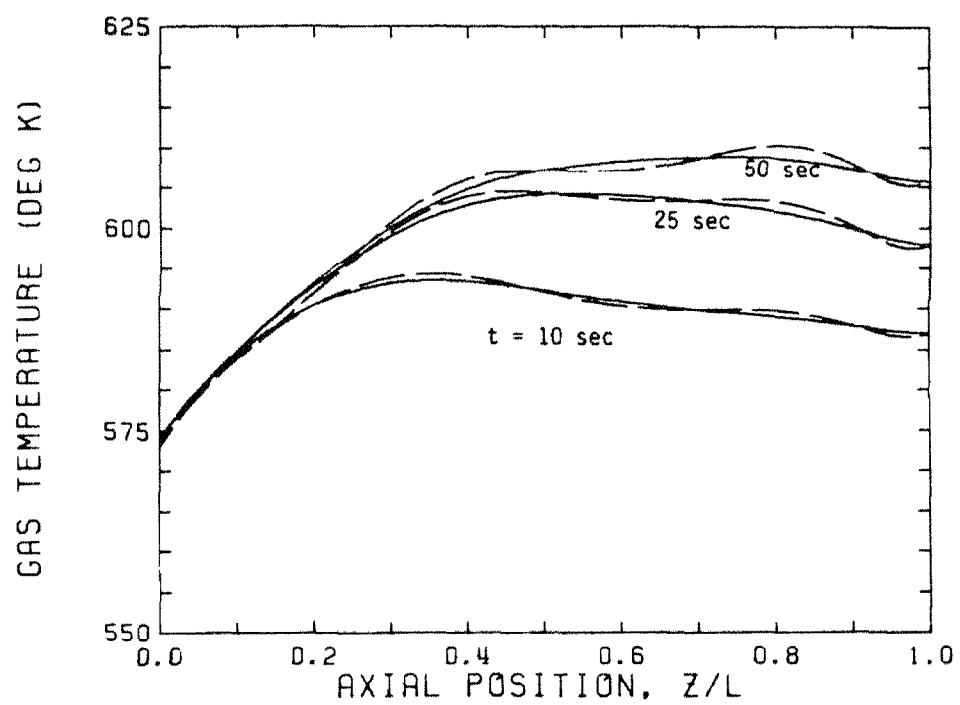


Figure 3.4-27
Dynamic Start-up Simulations - Neglecting Axial Heat Diffusion
Standard Type II Operating Conditions
— Original Model - - - No Axial Heat Diffusion

3.5 OCFE MODEL ANALYSIS

The reaction rate expression for the methanation reaction, Equation (3.3-1), used throughout much of this work is based on empirical work by Lee (1973) and Vatcha (1976). This expression, along with the rate equation, Equation (3.3-3), for the steam-shift reaction given by Moe (1962) provides valuable insight into the modeling of multiple reaction systems. Both reactions are reversible and are described by complex nonlinear rate expressions. Due to the reversibility of the reactions and the equilibrium constraints included in the rate expressions, severe temperature and concentration profiles are generally not observed. The orthogonal collocation procedure used for the numerical solution of the resulting mathematical model shows very little numerical instability and allows for rapid solution of even the most difficult profiles simply by increasing the number of collocation points.

However, in many chemical systems including packed bed reactors with rapid nonreversible kinetics, the interesting features of the solution are confined to a very small region where the solution profile changes rapidly. The orthogonal collocation method may become unwieldy because a large number of collocation points may be needed so that enough are placed within this region to provide an accurate representation of the solution.

A significant drawback of the orthogonal collocation technique is then its inability to accurately define profiles with very sharp gradients or abrupt changes, since the technique requires fitting a single polynomial to the entire profile. Under such cases, although the solution will be exact at the collocation points, significant oscillations in the profile are observed, and the obvious choice would be to resort to a finite difference procedure which considers each interval separately using first and second derivative matching conditions on the bound-

aries or to a finite element approach. Accurate representation of the solution is then possible even under extremely steep gradients simply by increasing the number of grid points. However, this technique can easily become numerically prohibitive due to the extremely high dimensionality of the resulting mathematical system. A compromise between the orthogonal collocation (OC) and finite difference techniques has been proposed by Carey and Finlayson (1975). This procedure is called Orthogonal Collocation on Finite Elements (OCFE).

3.5.1 Formulation of OCFE Technique

Although most of the preliminary analyses in this modeling work used the rate expressions by Lee (1973), Moe (1962), and Vatcha (1976), all significant conclusions were verified using the rate expression of Strand (1984) and ignoring the steam-shift reaction. An important difference between the two kinetic descriptions is the sharpness of the resulting profiles. The reaction kinetics determined by Strand (1984) are much faster than that proposed by Vatcha (1976) and can lead to rapid complete conversion within the reactor bed. For such kinetics, the numerical solution procedure described in Section 3.3.5 can have difficulties during solution of the steady state profiles.

Specifically, numerical solution of the expected steady state profiles with the new kinetics often requires excellent initial estimates, and in many cases even then has numerical convergence difficulties. This is often due to the rapid complete reaction of the carbon monoxide early in the reactor bed leading to steep temperature and concentration profiles, an abrupt change in the concentration profiles when the CO is depleted, and a linear concentration profile after complete conversion of the CO. The orthogonal collocation on finite elements procedure is then attempted to minimize the numerical difficulties associated

with orthogonal collocation.

Finlayson (1980) used the OCFE procedure for several examples with extremely sharp gradients, including diffusion and reaction in a porous catalyst pellet and transient convective diffusion. His analysis of the orthogonal collocation method, the finite difference method, and the orthogonal collocation on finite elements scheme for these and other chemical systems shows that the "orthogonal collocation method is by far and away the best method" except for systems with sharp profiles. The OCFE technique is then preferred. Finlayson points out that detailed, comparative studies of even simple two-dimensional problems using OCFE are rare, due to the complexity of the procedure. This section provides the first complete OCFE analysis of a packed bed reactor along with comparisons to simple orthogonal collocation results. This OCFE analysis is performed on the two-dimensional system resulting after the radial orthogonal collocation presented in Section 3.3.5.

The orthogonal collocation procedure uses a series of polynomials, each of which is defined over the entire range $0 \leq \zeta \leq 1$, as a trial function for the axial collocation. Complications with this global procedure arise in the presence of steep gradients or abrupt changes in the solution profile. In such situations, it may be advantageous to use trial functions that are defined over only part of the region and piece together adjacent functions to provide an approximation over the entire domain. Using such a procedure, smaller regions can be used near the location of the steep gradient. The OCFE technique involves using orthogonal collocation within each of these elements. A similar analysis can be performed using the Galerkin method within each element. However for non-linear problems, it may be necessary to use quadrature formulas to evaluate the integrals, resulting in lengthy calculations.

Two major forms of the OCFE procedure are common and differ only in the trial functions used. One uses the Lagrangian functions and adds conditions to make the first derivatives continuous across the element boundaries, and the other uses Hermite polynomials, which automatically have continuous first derivatives between elements. Difficulties in the numerical integration of the resulting system of equations occur using both types of trial functions, and personal preference must then dictate which is to be used. The final equations that need to be integrated after application of the OCFE method in the axial dimension to the reactor equations (radial collocation is performed using simple orthogonal collocation) can be expressed in the form

$$\mathbf{C} \frac{d\mathbf{a}}{dt} = \mathbf{Aa} - \mathbf{f(a)} \quad (3.5-1)$$

Using Hermite interpolation within the elements, the \mathbf{C} matrix is not diagonal. Explicit solution methods cannot be applied to this system of equations easily because of this nondiagonal matrix, and most integration packages are also not suitable for such a system. However using Lagrangian functions within the elements, the continuity and boundary conditions have no time derivatives, and the \mathbf{C} matrix in the above equation is diagonal with nonzero elements representing a residual and zero diagonal elements for the algebraic conditions. Most standard integration packages are also not suitable for mixed systems of algebraic and differential equations. However, our computer programs for the standard orthogonal collocation procedure (Appendix 4) are written for mixed systems. Thus the Lagrangian functions are used in this OCFE analysis.

The OCFE discretization analysis and computer programs developed in this work allow general specification of the number of finite elements and the degree of the collocation functions within each element. This is again an advancement over prior analyses where the same degree of collocation was often used within

each element. The entire domain is divided as shown in Figure 3.5-1. Within each of NE elements, we apply orthogonal collocation as usual using Lagrangian functions. The residual is evaluated at the internal collocation points. Using the Lagrangian polynomials, we need to guarantee continuity of the first derivatives or fluxes between elements. In our analysis, we use the continuity of the first derivative. We thus append $NE-1$ conditions at the element boundaries. Then the solution has continuous derivatives throughout the domain. With the additional two boundary conditions at $\zeta = 0$ and at $\zeta = 1$, there are a sufficient number of conditions to solve for the profile at all of the collocation points and at the element boundaries.

For the k th element, we define the transformation

$$u = \frac{z - z_{(k)}}{h_k} \quad h_k = z_{(k+1)} - z_{(k)} \quad (3.5-2)$$

so that the variable u is between zero and one in the element.¹ Redefining the differential equations in terms of the variable u allows the application of standard orthogonal collocation within each element. Figure 3.5-2 illustrates the local numbering system within each element. If we then define NE as the number of elements, N_k as the number of interior collocation points in element k , and M_k as $N_k + 2$, the relation between the global numbering i, j and the local numbering I, J is given by

$$i = \left[\sum_{j=1}^{k-1} (N_j + 1) \right] + I$$

$$z_i = z_{(k)} + u_I h_k \quad (3.5-3)$$

Then starting from the most general form of the dimensionless equations after the one point radial collocation, we can apply the OCFE procedure. As an example, let us consider the energy equation for the solid:

1. Note that z in this expression is the normalized axial coordinate (equivalent to ζ).

$$\frac{\partial \Theta_s}{\partial \vartheta} = \alpha_s \frac{\partial^2 \Theta_s}{\partial \zeta^2} + \omega_1 \Theta_s + \omega_2 \Theta_t + \gamma_s \Theta_g + \kappa_1 (1 + \varphi_1 \Theta_s) R'_M + \kappa_2 (1 + \varphi_2 \Theta_s) R'_S + \omega_3 \quad (3.5-4)$$

$$\begin{aligned} z=0 \quad \frac{\partial \Theta_s}{\partial \zeta} &= \lambda_{gzs} (\Theta_s - \Theta_g) \\ z=1 \quad \frac{\partial \Theta_s}{\partial \zeta} &= \lambda_{gzs} (\Theta_g - \Theta_s) \end{aligned}$$

All temperatures in this equation are in terms of the conditions at the radial collocation point.

Then for $k = 1$ to NE

$$z = z_{(k)} + uh_k \quad (3.5-5)$$

Thus within each element

$$\frac{\partial \Theta_s}{\partial \vartheta} = \frac{\alpha_s}{h_k^2} \frac{\partial^2 \Theta_s}{\partial u^2} + \omega_1 \Theta_s + \omega_2 \Theta_t + \gamma_s \Theta_g + \kappa_1 (1 + \varphi_1 \Theta_s) R'_M + \kappa_2 (1 + \varphi_2 \Theta_s) R'_S + \omega_3 \quad (3.5-6)$$

with the overall boundary conditions

$$\begin{aligned} \frac{1}{h_1} \frac{\partial \Theta_s}{\partial u} \Big|_{u=0} &= \lambda_{gzs} (\Theta_s - \Theta_g) \\ \frac{1}{h_{NE}} \frac{\partial \Theta_s}{\partial u} \Big|_{u=1} &= \lambda_{gzs} (\Theta_g - \Theta_s) \end{aligned}$$

If we assume axial profiles within each element $k = 1, \dots, NE$ of the form

$$\Theta_s(u, \vartheta) = \sum_{i=1}^{M_k} \Theta_{s_i}(\vartheta) L_i(u) \quad (3.5-7)$$

where as before L_i are Lagrangian interpolation polynomials, then as usual

$$\begin{aligned} A_{I,J} &= \left. \frac{dl_J(u)}{du} \right|_{z_i} \\ B_{I,J} &= \left. \frac{d^2 l_J(u)}{du^2} \right|_{z_i} \end{aligned} \quad (3.5-8)$$

After applying orthogonal collocation.

$$\frac{d\Theta_{s_i}}{d\vartheta} = \frac{\alpha_s}{h_k^2} \sum_{j=1}^{M_k} B_{i,j} \Theta_{s_j} + \omega_1 \Theta_{s_i} + \omega_2 \Theta_{g_i} + \gamma_s \Theta_{g_i} + \kappa_1 (1 + \varphi_1 \Theta_{s_i}) R'_M + \kappa_2 (1 + \varphi_2 \Theta_{s_i}) R'_S + \omega_3 \quad (3.3-9)$$

within element k for the interior collocation points $i = 2, \dots, N_k + 1$.

Then if we require the continuity of the first derivatives between the elements so that the first derivative of the solution is continuous in the entire domain $0 \leq \zeta \leq 1$:

$$\left[\frac{1}{h_{k-1}} \sum_{j=1}^{M_{k-1}} A_{M_{k-1},j} \Theta_{s_j} \right]_{\text{element } k-1} = \left[\frac{1}{h_k} \sum_{j=1}^{M_k} A_{1,j} \Theta_{s_j} \right]_{\text{element } k} \quad (3.5-10)$$

The system boundary conditions then only affect the first and last elements:

$$\begin{aligned} \frac{1}{h_1} \sum_{j=1}^{M_1} A_{1,j} \Theta_{s_j} &= \lambda_{gzs} (\Theta_{s_1} - \Theta_{g_1}) \\ \frac{1}{h_{NE}} \sum_{j=1}^{M_{NE}} A_{NE,j} \Theta_{s_j} &= \lambda_{gzs} (\Theta_{s_{M_{NE}}} - \Theta_{g_{M_{NE}}}) \end{aligned} \quad (3.5-11)$$

This same analysis is then performed for the energy balance for the gas, the energy balance for the thermal well, the two mass balances, and the continuity equation. The final coupled system of algebraic and differential equations is shown in Appendix 5, along with computer programs for steady state solution using this OCFE procedure. It consists of $5N$ ordinary differential equations and $N + 6(NE + 1)$ algebraic equations, where

$$N = \sum_{k=1}^{NE} N_k \quad (3.5-12)$$

The techniques used for the solution of this system are similar to those used previously with the orthogonal collocation analysis. The major complications are the potentially large number of resulting equations² and possible con-

2. Depending on the number of elements and number of interior collocation points per element.

fusion and errors in setting up the indexing in the computer algorithm. Extreme care must be taken in this last respect.

It should be pointed out that this approach using Lagrangian polynomials gives identical results to those that would be obtained using Hermite polynomials since on each element we use orthogonal polynomials of the same order, since the boundary conditions are satisfied by both solutions, since the residuals are evaluated at the same points, and since the first derivatives are continuous across the element boundaries. The only preference for one over the other is for convenience. The Lagrangian formulation, however, has the added advantage of being applicable in situations where the flux is continuous across the element boundaries but the the first derivative is discontinuous. This can occur if there is some type of physical change at the boundary.

A major advantage of the orthogonal collocation solution schemes is that the optimal location of the collocation points is automatically determined as the zeros of the orthogonal polynomial after specification of the number of collocation points. This point carries through to the OCFE technique; however, in this procedure, you must also specify the number and position of the elements. Several means for this are available. The simplest involves preliminary solutions using orthogonal collocation to provide reasonable estimates since, even though the OC solution may be numerically unsatisfactory due to oscillations in the profiles, it can give accurate indications of break points in the profiles.

If the OCFE solution procedure is to be used regularly for system analysis, a careful study of the problem of locating elements is necessary. Finlayson (1980) gives a basis for this study in a cursory examination of variable grid spacing and elements sizes, or 'adaptive meshes' as he calls them. The simplest procedure is based on physical information about the solution profile such as the point

where CO is depleted within the reactor bed. Several direct mathematical approaches are also discussed by Carey and Finlayson (1975) and Finlayson (1980). The first is based on the solution residuals. Although the residual is zero at the collocation points when using orthogonal collocation or OCFE, it can generally be nonzero elsewhere. After an approximate solution is calculated, the residual is evaluated throughout the interval $0 \leq \zeta \leq 1$. Ferguson and Finlayson (1972) and Carey and Finlayson (1975) show that the error in the solution is bounded by the mean square residual. Since we want the residual to be small everywhere, we can locate the elements to make the residuals approach zero everywhere. In particular, additional elements should be inserted at points where the residual is large. According to Carey and Finlayson (1975),

"in this way, as the number of elements is increased the solution should converge faster than for a uniform spacing of elements because the elements are placed where needed. ... However, the largest residual usually occurred at the endpoint of the element since a continuity condition is imposed there rather than setting a residual to zero. Thus in other calculations it would probably suffice to calculate the residual at the end points of the element and use that residual to determine the location of additional elements."

Other mathematical procedures are described by Finlayson (1980) based on extensions to Pearson's (1968) technique for finite difference methods and on work by Ascher et al. (1979) and Russel and Christiansen (1978). These are not discussed here since the above techniques are used in this thesis.

3.5.2 Model Comparisons

A large number of steady state simulations were performed using this OCFE procedure with various rate expressions to determine the applicability and necessity of the technique for packed bed reactor modeling. Using the original rate expressions of Lee (1973), Moe (1962), and Vatcha (1976), there is no major

necessity of the OCFE procedure since even for conditions with very steep profiles, an accurate, non-oscillating solution can usually be obtained simply by increasing the number of collocation points in the orthogonal collocation analysis.³ Due to the reversibility of the kinetics and the relatively low activation energy, the profiles remain relatively smooth without any abrupt changes or sharp transitions.

The importance of the orthogonal collocation on finite element approach is then considered using the single reaction non-reversible kinetics proposed by Strand (1984). Figure 3.5-3 shows the steady state axial gas temperatures using these kinetics with standard Type III (Table 3.4-5) operating conditions and with the parameters shown in Tables 3.4-1 and 3.3-4 along with the exceptions $U_{sg} = 8.50$, $k_{0M} = 25.1$, and $E_{aM} = 7000$. Figure 3.5-4 shows a comparison of the steady state axial temperature profiles using both orthogonal collocation (OC) and orthogonal collocation of finite elements (OCFE) for the same conditions. As shown, the numerical problems (oscillatory solution) exhibited in the orthogonal collocation solution with six collocation points are completely eliminated by increasing the number of collocation points or by using OCFE with appropriate selection of the elements and order of collocation within the elements. The major difference then between the OC solution with 12 interior collocation points and the OCFE solution with three elements and only 10 interior collocation points (plus two interior element boundaries) is the solution time. The OCFE steady state solution took almost exactly twice as long (123 seconds versus 59 seconds)! Thus if at all possible, the orthogonal collocation procedure is preferred, even at the expense of using additional interior collocation points.

Another major difficulty of the OCFE procedure is displayed in Figure 3.5-5.

3. Figures 3.4-26b and 3.4-20b show simulations using orthogonal collocation with possible numerical difficulties.

This is the non-trivial problem of optimal selection of the number and position of finite elements. Figure 3.5-5 shows a comparison of the OCFE steady state axial temperature profiles for the conditions of Figure 3.5-3 with three elements of length 0.15, 0.70, and 0.15 with $N_1 = 2$, $N_2 = 5$, and $N_3 = 3$ and with three elements of length 0.10, 0.80, and 0.10 with $N_1 = 1$, $N_2 = 5$, and $N_3 = 1$. Although these finite element schemes are only slightly different, the resulting solution is significantly affected and is nearly as bad as the orthogonal collocation solution with too few collocation points.

A final example shows the real power of the OCFE procedure. Figures 3.5-6 and 3.5-7 show 'best' solutions obtained using orthogonal collocation and OCFE for the steady state axial temperature and concentration profiles for the non-reversible kinetics where the reaction is extremely rapid with complete conversion early in the reactor bed. These conditions are identical to those in Figures 3.5-3 to 3.5-5 except that the reaction rate is twice as large ($k_{\text{on}} = 50.2$). As we would expect, the profiles are very sharp, and there is an abrupt change in the concentration profiles at the point of complete conversion. The 'best' solutions obtainable using orthogonal collocation require ten interior collocation points and still show significant numerical problems in both the temperature and concentration profiles. The use of more or less collocation points increases the oscillations in the profile, especially in the vicinity of zero concentration.

The solutions using the OCFE procedure show dramatic differences in the profiles. Based on an expected abrupt change in the concentration profile at about $\xi = 0.40$ (from the preliminary orthogonal collocation results), an OCFE solution was obtained using two elements of length 0.4 and 0.6 with $N_1 = 5$ and $N_2 = 1$ or a total of only six interior collocation points and one interior boundary point. These OCFE axial profiles are much sharper than those predicted by

the orthogonal collocation procedure simply because orthogonal collocation actually smooths the steep profiles by attempting to fit a single polynomial through the entire region. Figures 3.5-6 and 3.5-7 show the locations of the collocation points for both schemes. Grouping the collocation points around the region of sharp profile changes in the OCFE procedure allows more accurate representation of these changes. This is identical to the concept of increasing the number of grid points around a sharp transition when using standard finite element techniques.

As shown in Figure 3.5-7, the OCFE procedure is also capable of handling the abrupt concentration profile change where the reaction reaches completion with only a single collocation point being necessary in the final element, while the orthogonal collocation procedure shows significant error in the profiles even with additional collocation points. Increasing the number of collocation points in either element for the OCFE solution has no significant beneficial effect on the axial profiles and can introduce oscillations in the first element as shown in Figure 3.5-8. Increasing the number of elements without using sufficient interior collocation points or misplacing the elements can lead to very strange results (Figure 3.5-9 and 3.5-10) due to the individual polynomial representations and continuity conditions at the element boundaries.

Table 3.5-1 summarizes the steady state solution times and qualitative behavior of the resulting axial profiles for a variety of solution schemes. Notice that the solution times increase rapidly as the number of collocation points is increased with both solution techniques. The numerical computation times for the orthogonal collocation and OCFE solutions shown in Figures 3.5-6 and 3.5-7 are 11.3 minutes and 1.5 minutes, respectively, thus providing further evidence of the necessity of the OCFE procedure for these particular conditions.

Based on these and other simulations along with those by Finlayson (1974), we can conclude that, for chemical packed bed reactor modeling, orthogonal collocation is generally optimum in terms of accuracy and numerical solution times. However if steep gradients or abrupt profile changes occur within the reactor bed due to extremely fast kinetics or complete conversion of the limiting component, OCFE may be more accurate and faster than simple orthogonal collocation. It is then recommended that, if such conditions are expected, the modeling computer programs be written to allow either procedure to be used. Otherwise, the programs can be written only for orthogonal collocation. The computer programs in Appendix 5 are written for OCFE but allow orthogonal collocation simulation simply by letting NE equal one.

Procedure	h_i	N_i	Solution Time	Axial Profiles
OC		6	4:54	<i>Bad</i>
		7	5:28	Bad
		8	6:07	Bad
		10	11:20	Bad
		12	14:06	Bad
OCFE	0.4, 0.6	5, 1	1:33	Excellent
		6, 1	1:18	Slight Oscillation
		7, 1	2:16	Slight Oscillation
		5, 2	4:51	Excellent
		5, 3	6:27	Excellent
		5, 5	11:28	Excellent
		4, 3	5:44	Excellent
		3, 3	4:19	Bad
	0.15, 0.25, 0.60	1, 5, 1	2:15	Fair
		2, 5, 2	14:01	Fair
	0.15, 0.20, 0.65	3, 5, 2	17:04	Bad
	0.15, 0.15, 0.70	4, 5, 3	15:27	Bad

Table 3.5-1
OC and OCFE Solutions for Conditions in Figure 3.5-6

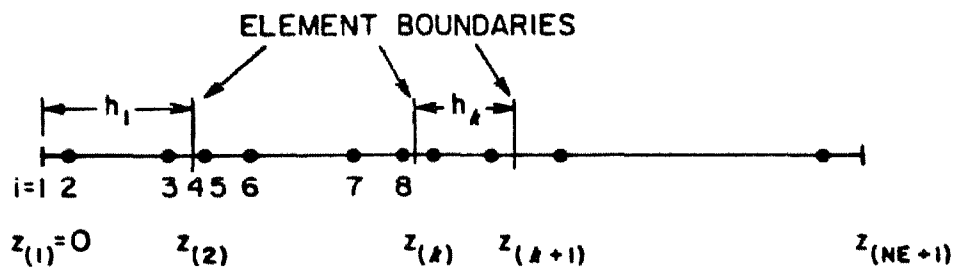


Figure 3.5-1
Orthogonal Collocation on Finite Elements
Global Numbering System

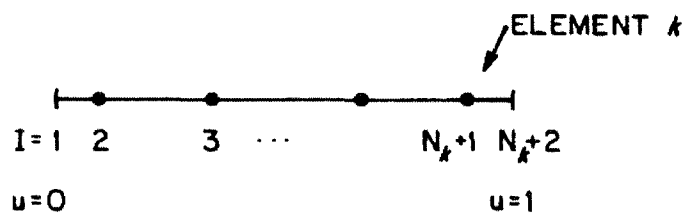


Figure 3.5-2
Orthogonal Collocation on Finite Elements
Local Numbering System

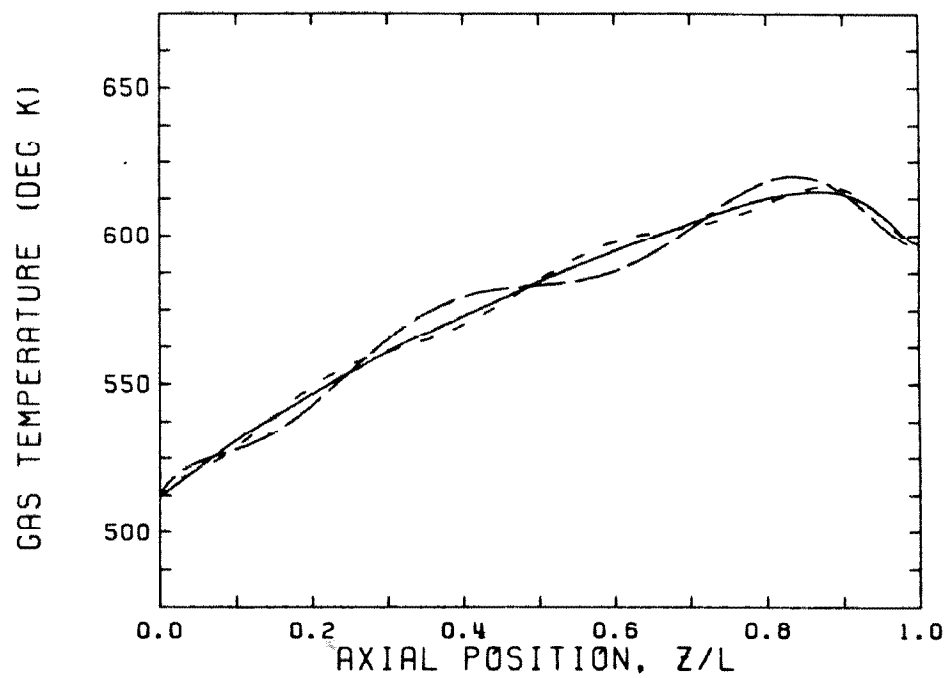


Figure 3.5-3
Orthogonal Collocation Axial Temperature Profiles
Standard Type III (Table 3.4-5) Conditions
Non-Reversible Kinetics ($U_{sg}=8.5$, $k_{0m}=25.1$, $E_{aM}=7000$)

— N = 12 - - - N = 8 - - - - N = 6

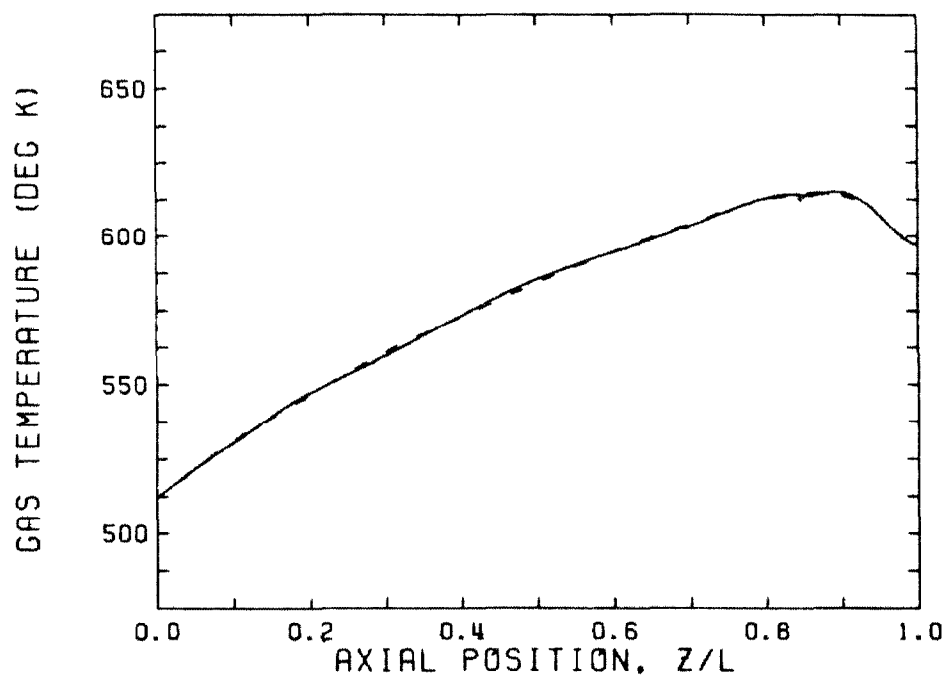


Figure 3.5-4
Axial Temperature Profiles
Same Conditions as Figure 3.5-3

— OCFE solution with 3 elements of length 0.15, 0.70, 0.15
 $N_1 = 2$, $N_2 = 5$, $N_3 = 3$
- - - OC solution with $N = 12$

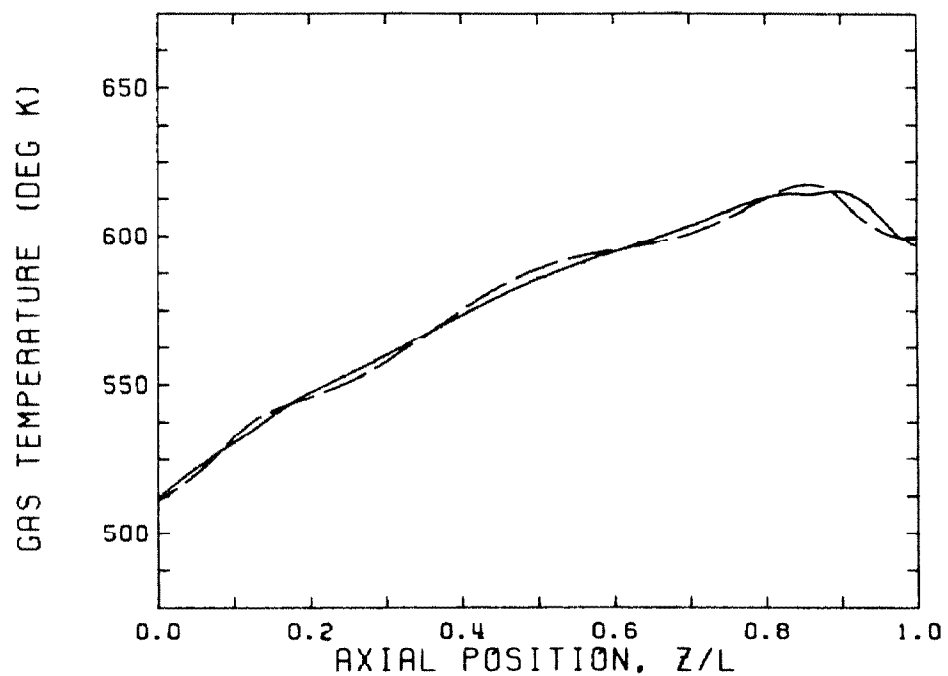
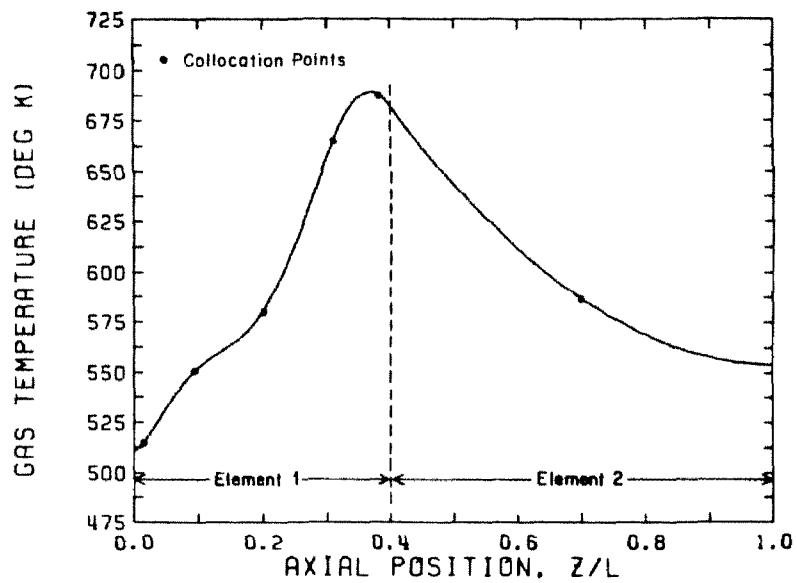
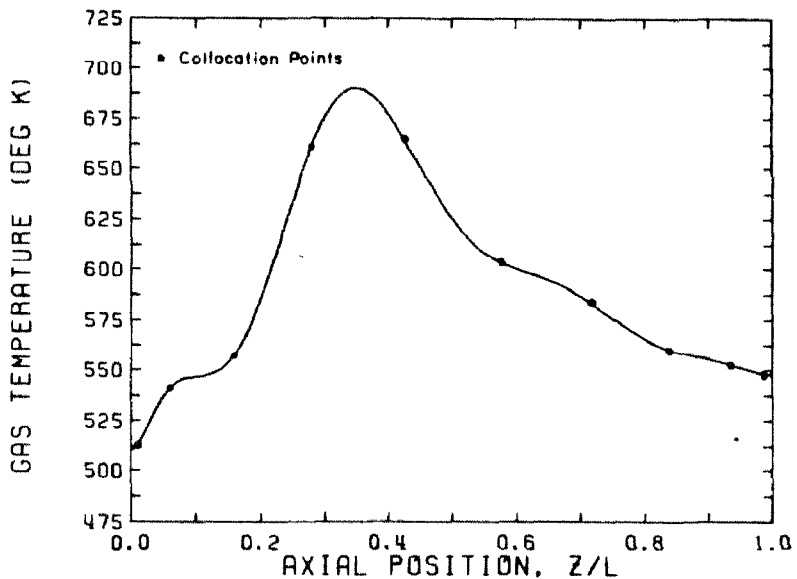


Figure 3.5-5
Axial Temperature Profiles
Same Conditions as Figure 3.5-3

- OCFE solution with 3 elements of length 0.15, 0.70, 0.15
 $N_1 = 2, N_2 = 5, N_3 = 3$
- - - OCFE solution with 3 elements of length 0.10, 0.80, 0.10
 $N_1 = 1, N_2 = 5, N_3 = 1$



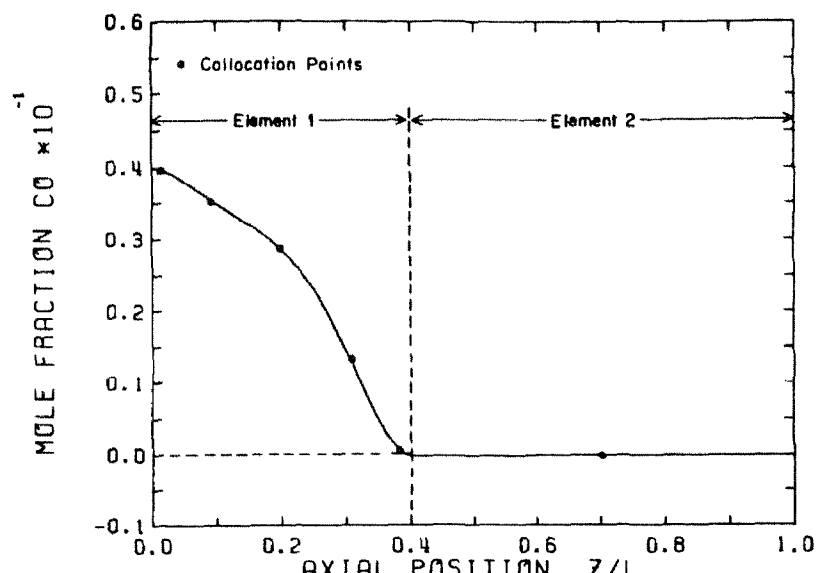
(a)



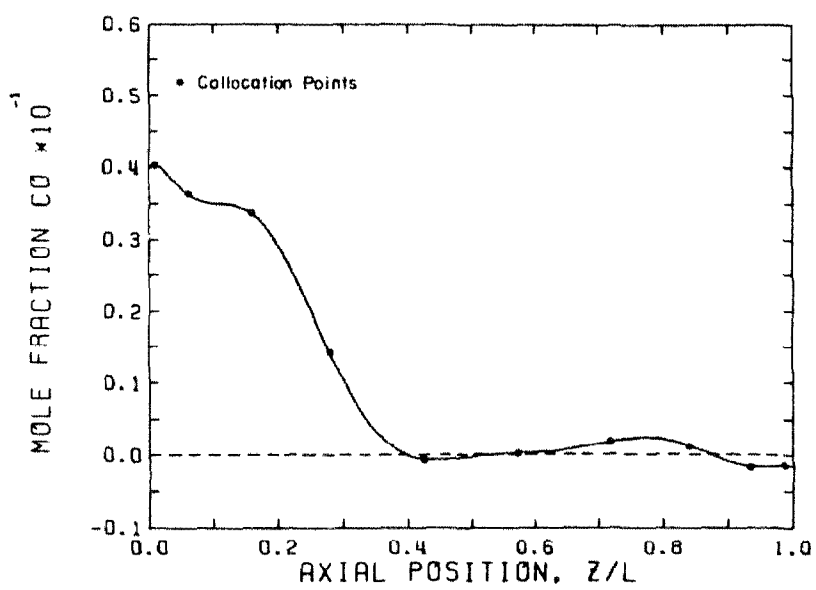
(b)

Figure 3.5-6
Axial Temperature Profiles
Same Conditions as Figure 3.5-5 except Double the Reaction Rate ($k_{0K}=50.2$)

- a) OCFE with 2 elements of length 0.4 and 0.6. $N_1=5$, $N_2=1$
- b) OC with $N=10$



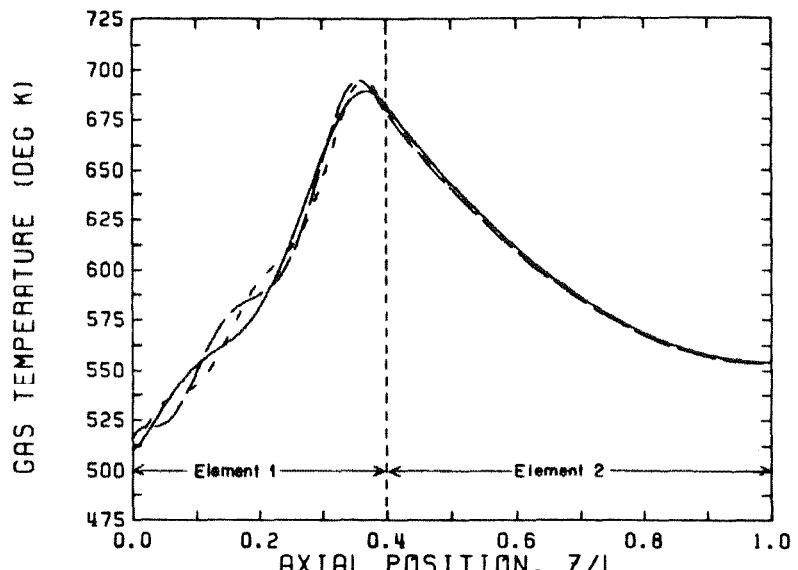
(a)



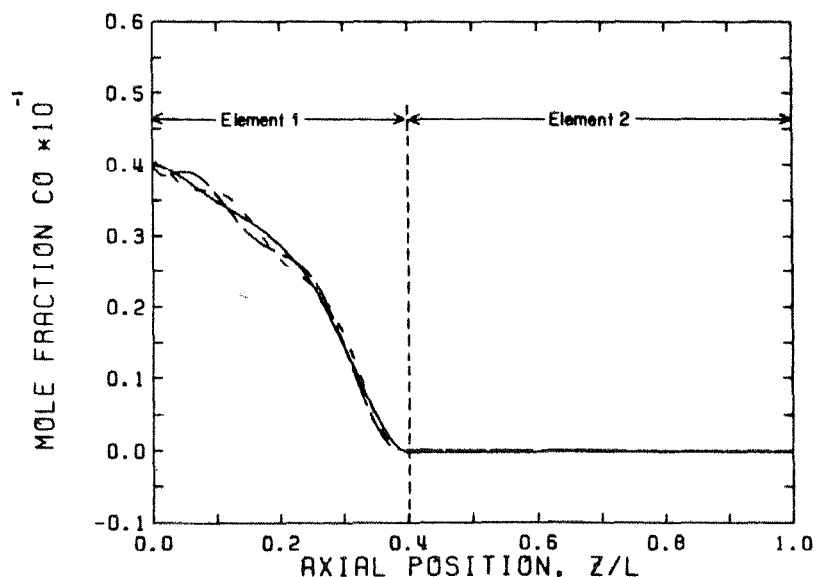
(b)

Figure 3.5-7
Axial Concentration Profiles
Same Conditions as Figure 3.5-6

- OCFE with 2 elements of length 0.4 and 0.6, $N_1=5$, $N_2=1$
- OC with $N=10$



(a)



(b)

Figure 3.5-8
Axial OCFE Temperature and Concentration Profiles
Two Elements of Length 0.4 and 0.6
Same Conditions as Figure 3.5-6

a. Gas Temperatures b. CO Concentrations

— $N_1 = 5, N_2 = 1$ - - - $N_1 = 6, N_2 = 1$ - - - $N_1 = 7, N_2 = 1$

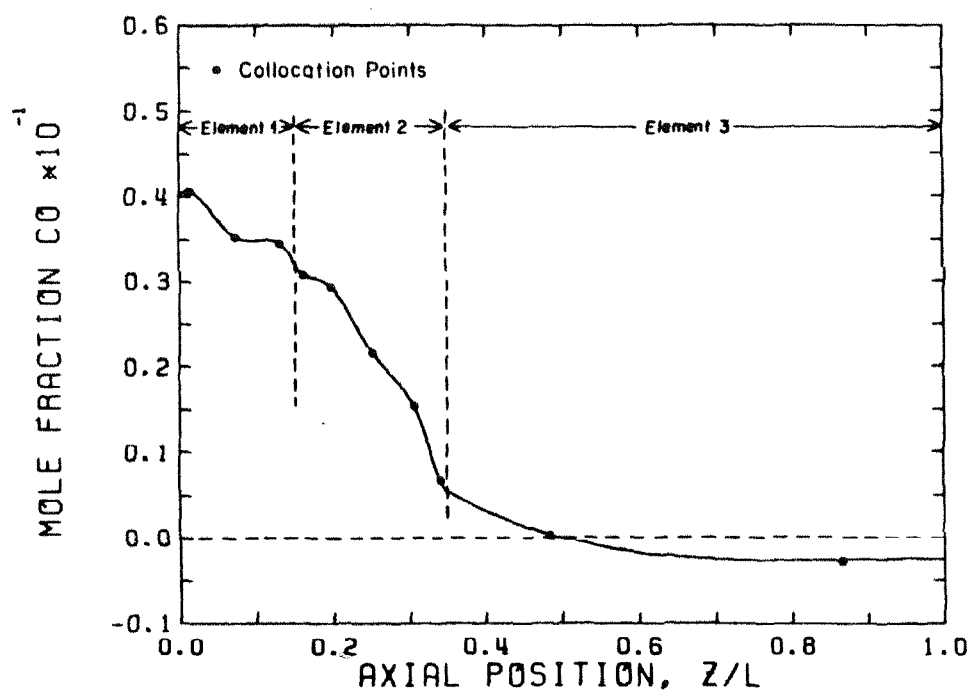


Figure 3.5-9
Axial OCFE Concentration Profiles
Same Conditions as Figure 3.5-6

$h_1=0.15, h_2=0.20, h_3=0.65; N_1=3, N_2=5, N_3=2$

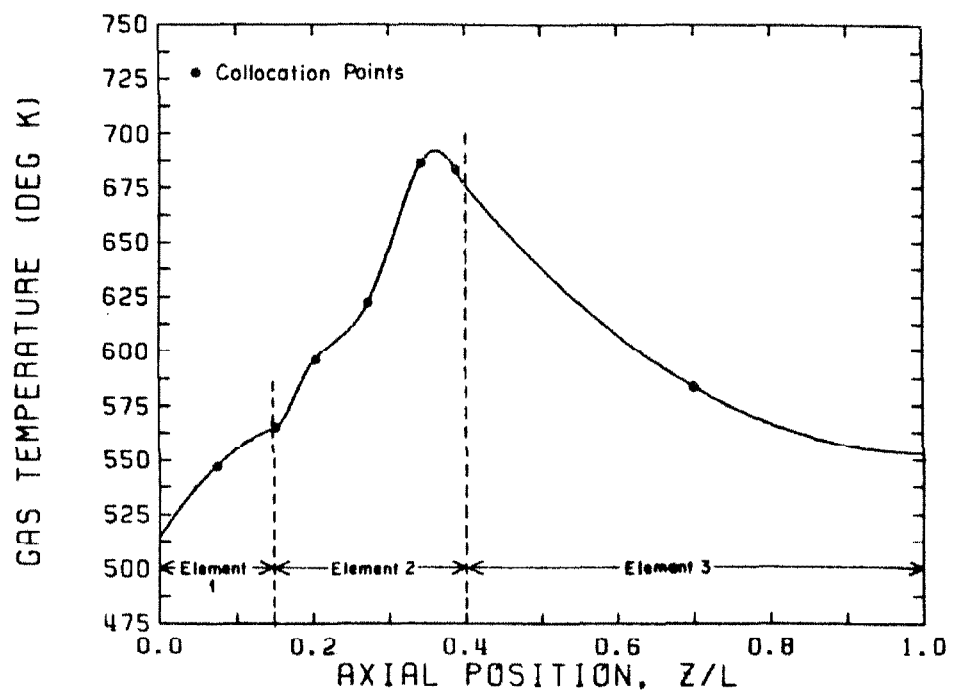


Figure 3.5-10
Axial OCFE Gas Temperature Profiles
Same Conditions as Figure 3.5-6

$h_1=0.15, h_2=0.25, h_3=0.60; N_1=1, N_2=5, N_3=1$

3.6 CONTROL MODEL DEVELOPMENT

As discussed by Ray (1981), the feedback control of distributed parameter systems requires a reduction of the distributed system to an appropriate lumped parameter model. Although this lumping can be performed prior to or subsequent to a control structure analysis, the modeling equations must be lumped for numerical integration during implementation. Our analysis of the mathematical relationships describing the chemical and physical processes within the reactor have used orthogonal collocation (OC) or orthogonal collocation on finite elements (OCFE) to replace the full distributed parameter system with a lumped approximation that allows simulation of the steady state and dynamic behavior of the packed bed catalytic reactor. Rather than making major simplifications *a priori*, the system analysis and numerical lumping used a detailed mathematical description of the reactor. However, computing facilities generally available for on-line control cannot currently perform the necessary calculations rapidly enough for practical control applications with the full, nonlinear model developed to this point. Furthermore, solution times for dynamic simulations with this model even make detailed parameter studies and process optimization impractical using the full model. Thus a simplified lower-order model is desired for on-line multivariable control and for process studies.

3.6.1 State-Space Representation

In simplifying the process model, it is advantageous if the equations can be reduced to fit into the framework of modern multivariable control theory, which usually requires a model expressed as a set of linear first-order ordinary differential equations in the state-space form:

$$\begin{aligned}\dot{\mathbf{x}}(t) &= \mathbf{A}\mathbf{x}(t) + \mathbf{B}\mathbf{u}(t) + \mathbf{D}\mathbf{d}(t) \\ \mathbf{y}(t) &= \mathbf{H}\mathbf{x}(t) + \mathbf{F}\mathbf{u}(t)\end{aligned}\quad (3.6-1)$$

where $\mathbf{x}(t)$, $\mathbf{u}(t)$, $\mathbf{d}(t)$, and $\mathbf{y}(t)$ are the state, control, disturbance, and measurement vectors, respectively.

Since the orthogonal collocation or OCFE procedure reduces the original model to a first-order ordinary differential equation system, linearization techniques can then be applied to obtain the necessary representation. A major advantage of the orthogonal collocation or OCFE procedure for the reduction of the partial differential equations over previous techniques such as finite differences or finite elements is that the size of the resulting ordinary differential equation system is inherently quite small. Further reduction may be desired and is discussed in Section 3.7. Once the dynamic equations have been transformed to the standard state-space form and the model parameters are estimated, various procedures can be used to design one or more multivariable control schemes, or the reduced model can be used for detailed process simulation and optimization.

However, real processes cannot accurately be described by the deterministic form of Equation (3.6-1). For control applications, modeling and measurement errors, reduction inaccuracies, and noise in the system may need to be accounted for by considering the addition of stochastic disturbance terms to the equations:

$$\begin{aligned}\dot{\mathbf{x}}(t) &= \mathbf{A}\mathbf{x}(t) + \mathbf{B}\mathbf{u}(t) + \mathbf{D}\mathbf{d}(t) + \psi(t) \\ \mathbf{y}(t) &= \mathbf{H}\mathbf{x}(t) + \mathbf{F}\mathbf{u}(t) + \eta(t)\end{aligned}\quad (3.6-2)$$

where $\psi(t)$ is a vector of random process noise and $\eta(t)$ is a vector of random measurement error. These can be thought of as representing the total effect of all of the disturbances or noises in the process not accounted for by the deterministic model. These stochastic disturbances can include uncontrolled or

unmodeled fluctuations in inlet concentrations or flow rates, in catalyst activity, in cooling wall temperature, and in heat transfer coefficients and can lead to suboptimal reactor performance or even system uncontrollability.

In developing a general state-space representation of the reactor, all possible control and expected disturbance variables need to be identified. In the following analysis, we will treat the control and disturbance variables identically to develop a model of the form

$$\begin{aligned}\dot{\mathbf{x}}(t) &= \mathbf{Ax}(t) + \mathbf{Ww}(t) \\ \mathbf{y}(t) &= \mathbf{Hx}(t) + \mathbf{Fw}(t)\end{aligned}\quad (3.6-3)$$

where $\mathbf{w}(t)$ now contains all control and disturbance terms, $\mathbf{Ww}(t) = \mathbf{Bu}(t) + \mathbf{Dd}(t)$. This model can then be used for process simulations. When specific control studies are desired, the $\mathbf{Ww}(t)$ term can simply be separated into the appropriate control term $\mathbf{Bu}(t)$ and disturbance term $\mathbf{Dd}(t)$, depending on the selected control configuration. Examples of this are shown in Section 4.3.

Consider the simplified flow diagram of the reactor system shown in Figure 3.6-1. The possible control variables or disturbances to the process are the flowrates of the input gases, the recycle ratio, the cooling jacket temperature, the heat load of the preheater, and the feed-effluent heat exchanger bypass. From the reactor's point of view (and thus the reactor model), the inlet gas temperature, the cooling wall temperature, the gas velocity, and the inlet gas concentration can be affected. We will thus consider the control and disturbance vector of the form

$$\mathbf{w} = \left[\Theta_w, v_{g_o}, \Theta_o, y_1^o, y_2^o, y_{H_2o}^o, y_{H_2}^o, y_{CH_4}^o \right]^T \quad (3.6-4)$$

where these variables are nondimensional and the superscript (o) or subscript (o) indicates inlet conditions.

3.6.2 Model Linearization

The major complication in the model after reduction of the original partial differential equations to ordinary differential equations is the nonlinearities that result from the nonlinear rate expressions and from the temperature, concentration, and velocity dependencies of the convective terms and of the gas and reaction properties. The reduction of the first-order ordinary differential equation model to the state-space representation involves linearization of the algebraic and differential equations about the steady state. The resulting mathematical description is then valid for small perturbations around this steady state.

This analytic linearization, although conceptually quite simple, is extremely tedious. Simple numerical linearization could be used during simulations and control through various readily available computer programs but does not provide a detailed analytical solution from which the effects of various parameters can be investigated.

Minor reduction of the nonlinear ordinary differential equation model developed using orthogonal collocation or OCFE first involved assuming constant heat capacity of the gas throughout the reactor bed¹ and neglecting the axial and radial mass diffusion terms, based on the results of the model analysis presented in Section 3.4. The resulting model was then linearized in three stages: linearization of the reaction rates, linearization of the algebraic equations and substitution into the differential equations, and linearization of the resulting ordinary differential equations.

1. Simulations showed no loss in accuracy by this assumption. Its only real benefit is a minor reduction in linearization effort.

3.6.2.1 Linearization of the Reaction Rates

The nondimensionalized reaction rate expressions

$$R'_S = (f_1 + f_2 P_{T_A} P_0) e^{-E_{aS}/R_s T_s} \left[y'_{CO} y'_{H_2} - \frac{K_{cS}}{K_{P_S}} y'_{CO} y'_{H_2} y'_{H_2O} \right] \quad (3.6-5)$$

$$R'_M = \frac{P_T^{1.5} e^{-E_{aM}/R_s T_s} (y_{H_2})^{0.5} (y_{CO}) (1 - v)}{1 + K'_2 P_T y_{H_2} + K'_3 P_T y_{CH_4}} \quad (3.6-6)$$

$$\text{where } y_i = y'_i (1 - 2\delta) \quad P_{T_A} = (1 - 2\delta) P_T \quad (3.6-7)$$

$$v = \frac{K_{cM}}{K_{P_M} P_0^2 P_T^2} \frac{y_{CH_4} y_{H_2O}}{y_{CO} (y_{H_2})^3} \quad (3.6-8)$$

$$K_{P_i} = e^{\left[K_{P_{i1}} + \frac{K_{P_{i2}}}{T_s T_0} \right]} \quad i = S, M \quad (3.6-9)$$

$$K_{cM} = \frac{\bar{x}_{CH_4}^0 \bar{x}_{H_2O}^0}{\bar{x}_{CO}^0 (\bar{x}_{H_2}^0)^3} \quad K_{cS} = \frac{\bar{x}_{CO}^0 \bar{x}_{H_2O}^0}{\bar{x}_{CO}^0 \bar{x}_{H_2}^0} \quad (3.6-10)$$

are first linearized about the steady state operating conditions (ss) using a Taylor series linearization approach. If we neglect the second and higher order terms in the Taylor series expansion, the linearization is of the form

$$R(\theta_s, y_1, y_2, y_{CH_4}^0, y_{H_2}^0, y_{H_2O}^0, y_1^0, y_2^0) \approx R_{ss} + \sum_s \left[\frac{\partial R}{\partial z} \right]_{ss} (z - \bar{z}) \quad (3.6-11)$$

$$\text{where } z = \theta_s, y_1, y_2, y_{CH_4}^0, y_{H_2}^0, y_{H_2O}^0, y_1^0, y_2^0$$

After lengthy analytic manipulation of the expressions, the resulting linearized rate expressions are of the form given in the equation above with the $\left[\frac{\partial R}{\partial z} \right]_{ss}$ terms defined in Appendix 6.

It is important to remember that the linearized expressions are only valid

in the vicinity of the specified steady state conditions. A comparison of the relative magnitudes of the linear and nonlinear reaction rates is presented in Table 3.6-1 for both Type I and Type II standard operating conditions defined in Table 3.4-5. These results are presented mainly to show the necessity for caution in using the linearized expressions since significant errors can occur away from the steady state. In general, although the rate expressions are highly nonlinear, the errors are relatively small even at considerable deviations from steady state. Although the errors in the steam-shift rate are quite large in several cases, the reaction rates in these cases are so small that the steam-shift reaction has insignificant effect on the reactor dynamics.

Type I Conditions						
	T _s	T _g	y ₁	y ₂	% Error	
					R _M	R _S
steady state	630	627	0.13	1.00		
	840	637	0.13	1.00	0.23	12.5
	650	647	0.13	1.00	0.85	25.1
	620	617	0.13	1.00	0.27	24.2
	630	627	0.25	0.99	0.27	7.5
	630	627	0.03	1.02	0.91	4.2
	640	637	0.25	0.99	4.03	2.5

Type II Conditions						
	T _s	T _g	y ₁	y ₂	% Error	
					R _M	R _S
steady state	613	610	0.71	1.01		
	603	600	0.71	1.01	0.31	0.57
	623	620	0.71	0.71	0.26	0.45
	613	610	0.82	1.01	0.15	2.60

Table 3.6-1
Nonlinear vs. Linearized Reaction Rates

3.6.2.2 Linearization of the Algebraic Equations

The algebraic equations for the orthogonal collocation model (shown in Section 3.3.5) consist of the axial boundary conditions along with the continuity

equation solved at the interior collocation points and at the end of the bed. This latter equation is algebraic since the time derivative for the gas temperature can be replaced with the algebraic expression obtained from the energy balance for the gas.

The boundary conditions for the mass balances and for the energy equation for the thermal well can be solved explicitly for the concentrations and thermal well temperatures at the axial boundary points as linear expressions of the conditions at the interior collocation points. The set of four boundary conditions for the gas and catalyst temperatures are coupled and are nonlinear due to the convective term in the inlet boundary condition for the gas phase. After a Taylor series linearization of this term around the steady state inlet gas temperature, gas velocity, and inlet concentrations, the system of four equations is solved for the gas and catalyst temperatures at the boundary points.

Linearization and solution of the continuity equation for the velocities at the interior collocation points and at the end of the reactor are somewhat more complex. Unfortunately, the time derivative of the gas temperature term adds significant complexity to these algebraic equations. Since the linearized model is expected to be valid over only a limited region around the steady state, and since a study of the magnitudes of the terms in this equation showed that this time derivative term is relatively small near the steady state, the term was neglected (equivalent to assuming $\frac{\partial \rho_g}{\partial t} = 0$). Simulations using the full, nonlinear model verified that negligible error resulted from dropping this term. The maximum error seen was during the first 10 seconds of a dynamic simulation and was generally less than 0.1% even during this period.

The resulting equation

$$\frac{\tau}{\tau z_i + 1} v_{g_i} \Theta_{g_i} + \sum_{j=0}^{N+1} A_{ij} [\Theta_{g_i} v_{g_j} - v_{g_i} \Theta_{g_j}] = 0 \quad (3.6-12)$$

for $i = 1, \dots, N+1$ was then linearized using the following relationship

$$\begin{aligned} v_{g_i} \Theta_{g_j} &\approx \bar{v}_i \bar{\Theta}_{g_j} + \bar{v}_{g_i} (\Theta_{g_j} - \bar{\Theta}_{g_j}) + \bar{\Theta}_{g_j} (v_{g_i} - \bar{v}_{g_i}) \\ &= \bar{v}_{g_i} \Theta_{g_j} + \bar{\Theta}_{g_j} v_{g_i} - \bar{v}_{g_i} \bar{\Theta}_{g_j} \end{aligned} \quad (3.6-13)$$

The algebraic equations for the endpoint gas temperatures were then substituted into the linearized continuity equations. These equations were then solved for the velocities. The results of this linearization of the algebraic equations is shown in Appendix 6.

3.6.2.3 Linearization of the Differential Equations

The linear reaction rate expressions and the linear expressions for the velocities and for the concentrations and temperatures at the axial boundary points were then substituted into the ordinary differential equations. Lengthy algebraic manipulation was necessary to linearize these equations due to extreme couplings between the different state variables. The linearization was completely analytical and retained all possible complications. The results of this analysis are shown in Appendix 6. Again great care must be exercised during this algebraic reduction due to the extreme complexity of the model. All results were verified through careful model simulations and finally by using the symbolic equation solver SMP available on the Caltech computer system.

The final linearized model is of the form

$$\dot{\mathbf{x}} = \mathbf{Ax} + \mathbf{Ww} + \mathbf{C} \quad (3.6-14)$$

where the state vector

$$\mathbf{x} = [\theta_{s_1}, \dots, \theta_{s_N}, \theta_{g_1}, \dots, \theta_{g_N}, \theta_{t_1}, \dots, \theta_{t_N}, y_{1_1}, \dots, y_{1_N}, y_{2_1}, \dots, y_{2_N}]^T \quad (3.6-15)$$

consists of the catalyst temperatures, the gas temperatures, the thermal well temperatures, the CO concentrations, and the CO₂ concentrations at the interior collocation points. The control and disturbance variables are

$$\mathbf{w} = [\theta_w, v_{g_0}, \theta_o, y_{CO}^0, y_{CO_2}^0, y_{H_2O}^0, y_{H_2}^0, y_{CH_4}^0]^T \quad (3.6-16)$$

This linear system is then of order 5N, where N is the number of interior collocation points. Analytical expressions for the elements of the matrices **A** and **W** are shown in Appendix 6. The constants **C** in the equations can be easily eliminated by using deviation variables about the steady state values. At steady state, $\dot{\mathbf{x}} = 0$ and thus

$$0 = \mathbf{Ax} + \mathbf{Ww} + \mathbf{C} \quad (3.6-17)$$

Subtracting this from the original equation,

$$\dot{\mathbf{x}} = \mathbf{A}(\mathbf{x} - \bar{\mathbf{x}}) + \mathbf{W}(\mathbf{w} - \bar{\mathbf{w}}) \quad (3.6-18)$$

Letting

$$\mathbf{x}' = \mathbf{x} - \bar{\mathbf{x}} \quad \text{and} \quad \mathbf{w}' = \mathbf{w} - \bar{\mathbf{w}} \quad (3.6-19)$$

the resulting equation is of the desired state-space representation:

$$\dot{\mathbf{x}}' = \mathbf{Ax}' + \mathbf{Ww}' \quad (3.6-20)$$

Note that in the remaining analyses, we will drop the ('). It should still be clear that deviation variables are being used. Then as per the previous discussion, this linear representation can easily be separated into the standard state-space representation shown in Equation (3.6-1) for any particular control configuration.

3.6.2.4 Numerical Solution of the Linearized Model

Numerical simulation of the behavior of the reactor using this linearized model is significantly simpler. The first step in the solution must be to solve the full, nonlinear model for the steady state profiles. This is accomplished using either the algorithm by Powell (Rabinowitz, 1970) or Brown (1967) discussed in Section 3.3.5. This first step is limiting in the sense that no further linearized analysis is possible without it. Due to the complexity of the nonlinear model, numerical convergence problems may be significant during this steady state solution. Obviously, the success of this solution is often based on the initial guesses for the steady state profile. Experience or empirical data can help in setting these values. Additionally, under extreme cases, the nonlinear dynamic simulation programs can be used to simulate the behavior of the system from specified profiles to the final steady state. As the dynamic solution approaches the steady state, the resulting profiles can be used as the initial guesses for the steady state solver so that the dynamic solution does not need to continue completely to steady state.

The steady state profiles are then used to calculate the matrices A and W . The Adams-Moulton predictor-corrector technique can again be used to numerically integrate the linear model for dynamic simulations. However, due to the linearity of the resulting mathematical system, an analytical solution of the differential equations is possible. The general solution of the differential system given by Equation (3.6-20) is

$$\mathbf{x}(t) = e^{(t-t_0)A} \mathbf{x}(t_0) + \int_{t_0}^t e^{(t-s)A} \mathbf{W} \mathbf{w}(s) ds \quad (3.6-21)$$

Then if we consider a time interval ($t \rightarrow t + dt$) over which w is constant,² this solution simplifies to

2. We can take very small time steps, dt , if needed.

$$\mathbf{x}'(t + dt) = e^{\mathbf{A}dt} \mathbf{x}'(t) + \mathbf{A}^{-1}(e^{\mathbf{A}dt} - \mathbf{I}) \mathbf{W} \mathbf{w}'(t) \quad (3.6-22)$$

The major complications in this analytical solution are obviously the matrix exponential and matrix inverse. If we let

$$\mathbf{A} = \mathbf{S} \mathbf{\Lambda} \mathbf{S}^{-1} \quad (3.6-23)$$

where $\mathbf{\Lambda}$ is a diagonal matrix of the eigenvalues of \mathbf{A} and \mathbf{S} is the corresponding matrix of eigenvectors, we then get

$$e^{\mathbf{A}dt} = \mathbf{S} e^{\mathbf{\Lambda}dt} \mathbf{S}^{-1} \quad \text{and} \quad \mathbf{A}^{-1} = \mathbf{S} \mathbf{\Lambda}^{-1} \mathbf{S}^{-1} \quad (3.6-24)$$

where $e^{\mathbf{A}dt}$ and $\mathbf{\Lambda}^{-1}$ are easily calculated since $\mathbf{\Lambda}$ is diagonal. Thus after the steady state is determined and the time steps (dt) are selected, we can calculate the eigenvalues and eigenvectors of the matrix \mathbf{A} and from these the values of \mathbf{A}^{-1} and $e^{\mathbf{A}dt}$. These lengthy calculations only need to be performed once for each steady state and selected time step! Of course these time steps can be quite large with the only restriction being that the control and disturbance variables are nearly constant during this period. If these variables are constant over more than one selected time step, even the value of $\mathbf{A}^{-1}(e^{\mathbf{A}dt} - \mathbf{I}) \mathbf{W} \mathbf{w}'$ will be constant and will not have to be recalculated between time steps.

Several computer programs have been written to simulate this linearized model of the reactor. These programs are discussed and listed in Appendix 4. Basically, two programs are used for the linear model. The first called LINMOD uses the Adams-Moulton predictor-corrector numerical integration of the linear differential equation system, including our variable time-step analysis. This program is similar in structure and operation to the nonlinear program NLNMOD. The second program written for the linear model simulation, ANAMOD, uses the analytical solution of the linear equations rather than performing a numerical solution. Thus it takes only a fraction of the solution time.

These programs are set up to automatically determine the steady state solution, to calculate the coefficient matrices for the linearized model, and to optimally perform the dynamic simulations for a large variety of step changes or disturbances or for start-up conditions. The program ANAMOD only performs the matrix inversions, exponentiations, and multiplications as necessary. The matrix inversion of the eigenvector matrix simply involves transforming the matrix into upper triangular form by successively multiplying it on the left by a transformation matrix that preserves the determinant of the original matrix. The triangular matrix is inverted by back substitution and finally the inverse of the original matrix is obtained by multiplying the inverse of the triangular matrix by the original transformations on the right.

The determination of eigenvalues and eigenvectors of the matrix A is based on a routine by Grad and Brebner (1968). The matrix is first scaled by a sequence of similarity transformations and then normalized to have the Euclidean norm equal to one. The matrix is reduced to an upper Hessenberg form by Householder's method. Then the QR double step iterative process is performed on the Hessenberg matrix to compute the eigenvalues. The eigenvectors are obtained by inverse iteration.

3.6.3 State-Space Simulations

Figure 3.6-2 shows the simulated dynamic behavior of the gas temperatures at various axial locations in the bed using both the linear and nonlinear simulation programs for a step change in the inlet CO concentration from a mole fraction of 0.06 to 0.07 and in the inlet gas temperature from 573° K to 593° K. Figure 3.6-3 shows the corresponding dynamic behavior of the CO and CO₂ concentrations at the reactor exit and at a point early in the reactor bed. The axial

concentration profiles at the initial conditions and at the final steady state using both the linear and nonlinear simulations are shown in Figure 3.6-4, and the axial gas temperature profiles are shown in Figure 3.6-5 at $t = 0$, 15 seconds, and 100 seconds (steady state). The temporal behavior of the profiles shows that the discrepancies between the linear and nonlinear results increase as the final steady state is approached. Even so, there are only slight discrepancies (less than 2% in concentrations and less than 0.5% in temperatures) in the profiles throughout the dynamic responses and at the final steady state even for this relatively major step input change.

Figure 3.6-6 shows dynamic linear and nonlinear simulations of the gas temperatures at $\zeta = 0.17$ and $\zeta = 0.38$ and Figure 3.6-7 shows the exit CO and CO_2 concentrations for a 50 second disturbance in the inlet gas temperature from 573° K to 601.65° K (a 5% increase) and in the inlet CO concentration from a mole fraction of 0.06 to 0.072 (a 20% increase). Again we find that only minor differences (less than 2%) are apparent between the two models and only then at conditions sufficiently far from the steady state. As expected, the models give identical results when the original steady state is reestablished after the disturbance.

Figure 3.6-8 shows the temporal behavior of the exit gas temperature and the gas temperature at $\zeta = 0.38$ under start-up operation using both the linear and nonlinear simulation programs. Figure 3.6-9 shows the axial temperature profiles at 15 seconds, 30 seconds, and at steady state. As expected, the major deviations between the models occur early in the simulation where the reactor conditions are relatively far from the steady state conditions around which the model is linearized. However, the magnitudes of the deviations are actually very small, thus verifying the ability of the linearized model to simulate reactor behavior even relatively far from steady state.

Thus the simulations show that the linear model is quite accurate even for relatively large deviations from the steady state. Of course, losses in accuracy are greater the larger the deviation. For start-up and disturbance simulations, the linearized model does predict an eventual return to the steady state around which the system was linearized. However for step input changes where the final steady state differed from the original, some minimal loss in accuracy is apparent in the final steady state reached using dynamic simulations of the linear model from the original steady state. This difficulty can easily be circumvented in the case of step changes by relinearizing about the new final steady state conditions somewhere during the simulation.

Table 3.6-2 shows a comparison of the solution times for the various dynamic simulations using the three models. As shown, the reduction in solution time is enormous using the linear model. Using numerical integration of the linear state-space model, simulation times are reduced by a factor of 10. The analytical solution reduces simulation times by another factor of up to 100 (to a point where real time solution is possible)! As expected, the results using both the numerical and analytic solutions of the linear model are identical.

Simulation	Model		
	NLNMOD	LINMOD	ANAMOD
Step $T_o \rightarrow 593^{\circ}\text{K}$ $x_{CO} \rightarrow 0.07$	2:54:24	12:54	00:36
Step $T_w \rightarrow 593^{\circ}\text{K}$	3:14:41	18:04	00:34
Start-up	4:43:26	28:39	00:29
Disturbance $T_o \rightarrow 602^{\circ}\text{K}$ (50 seconds) $x_{CO} \rightarrow 0.072$	4:58:42	23:10	00:31

Table 3.6-2
Comparison of Simulation Times

Thus the results of this investigation concerning locally linearized models along with the results of prior investigators (Hoiberg et al., 1971; Sinai and Foss,

1970) show that such models are quite descriptive of the overall system and are an extremely useful means of reducing model complexity. As pointed out by Hoiberg et al. (1971) and verified in this analysis, there is relatively little incentive for retaining the nonlinear representation in view of the large uncertainties in the numerical values of the physical and chemical parameters.

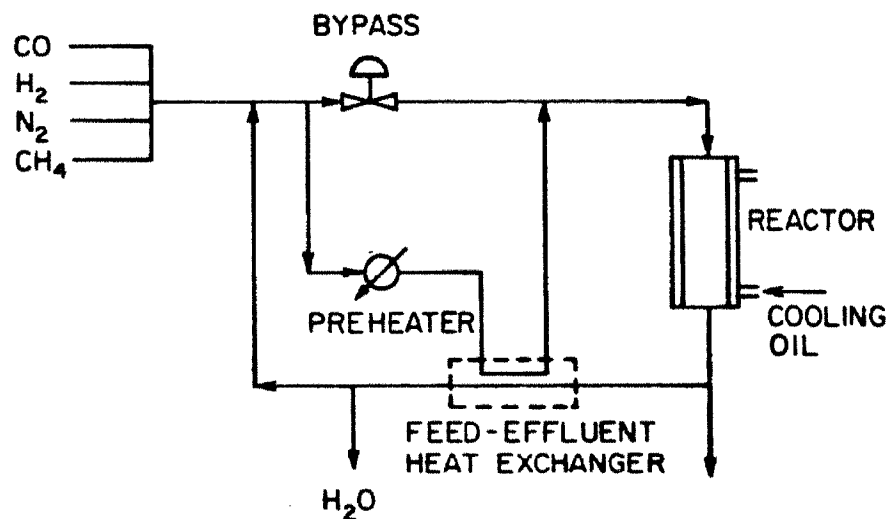


Figure 3.6-1
Simplified Reactor Flow Diagram

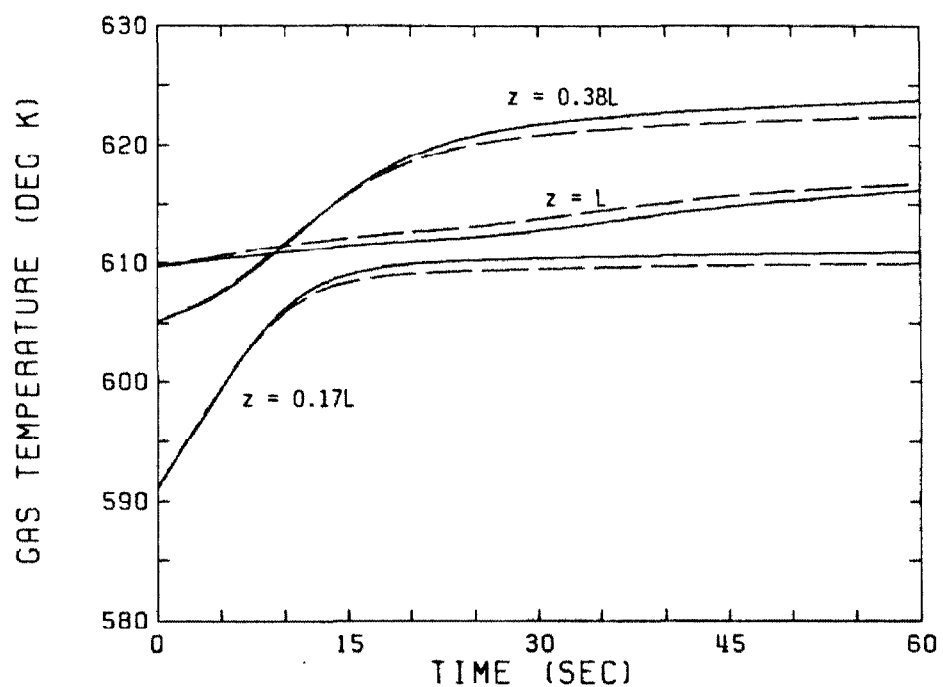


Figure 3.6-2
Gas Temperature During Step Input Change
Standard Type II (Table 3.4-5) Conditions
(T_0 from 573° K to 593° K, x_{CO} from 0.06 to 0.07)

— Nonlinear Model - - - Linear Model

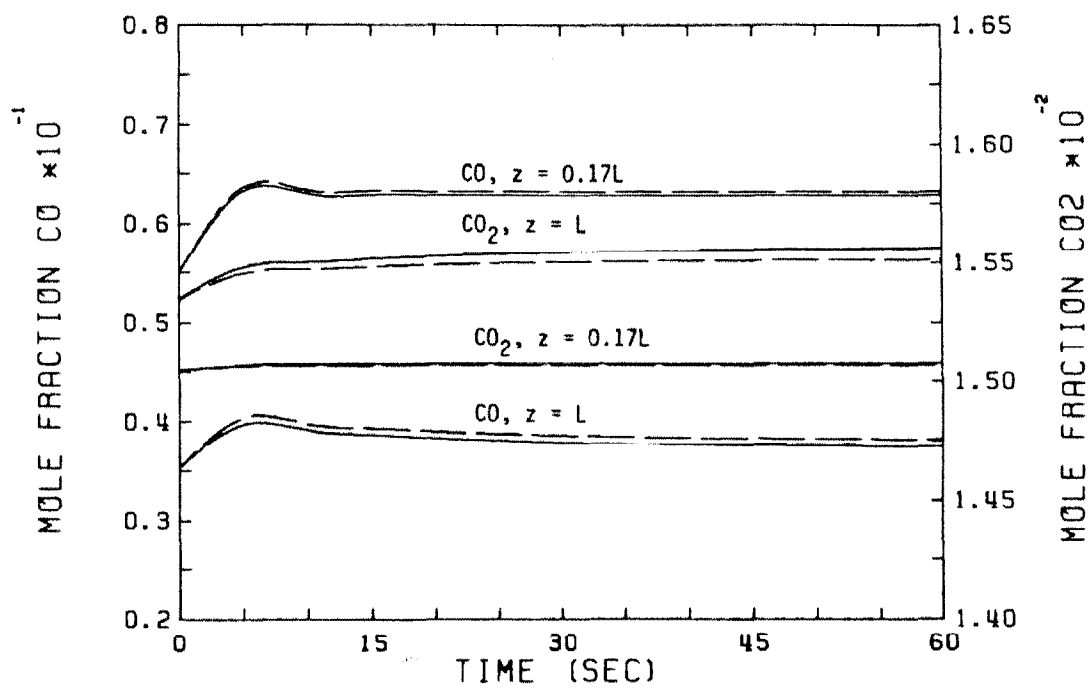


Figure 3.6-3
Concentrations During Step Input Change
Standard Type II (Table 3.4-5) Conditions
(T_0 from 573° K to 593° K, x_{CO} from 0.06 to 0.07)

— Nonlinear Model - - - Linear Model

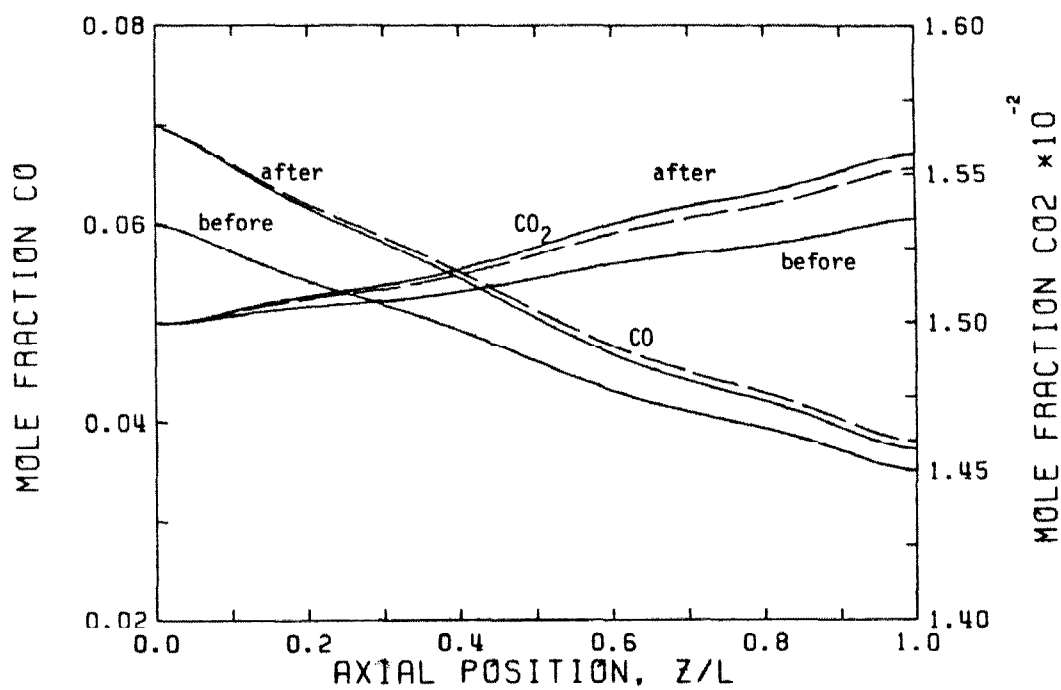


Figure 3.6-4
Axial Steady State Concentrations Before and After Step Change
Standard Type II (Table 3.4-5) Conditions
(T_0 from 573° K to 593° K, x_{CO} from 0.06 to 0.07)

— Nonlinear Model - - - Linear Model

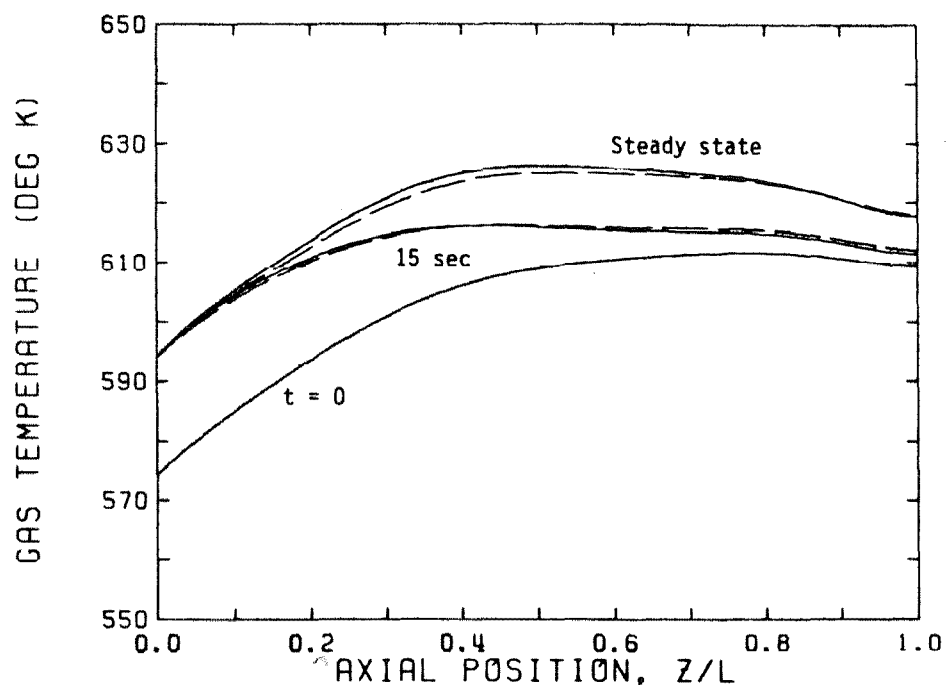


Figure 3.6-5
Axial Gas Temperature Profiles After Step Change
Standard Type II (Table 3.4-5) Conditions
(T_0 from 573° K to 593° K, x_{C0}^0 from 0.06 to 0.07)

— Nonlinear Model - - - - Linear Model

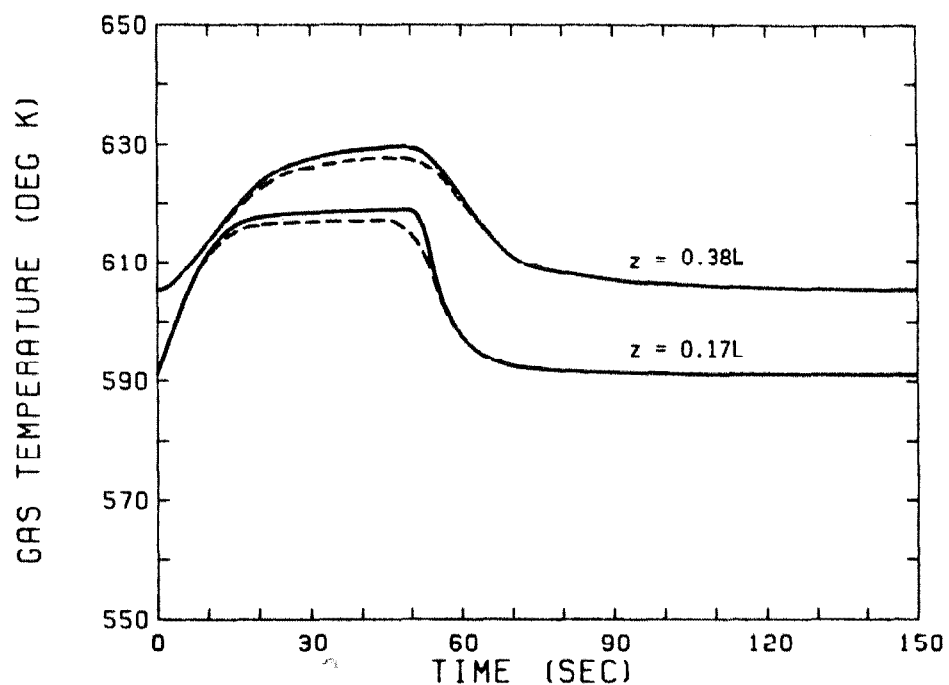


Figure 3.6-6
Gas Temperatures During 50 Second Disturbance
Standard Type II (Table 3.4-5) Conditions
(T_0 from 573° K to 602° K, x_{CO} from 0.06 to 0.072)

— Nonlinear Model - - - - Linear Model

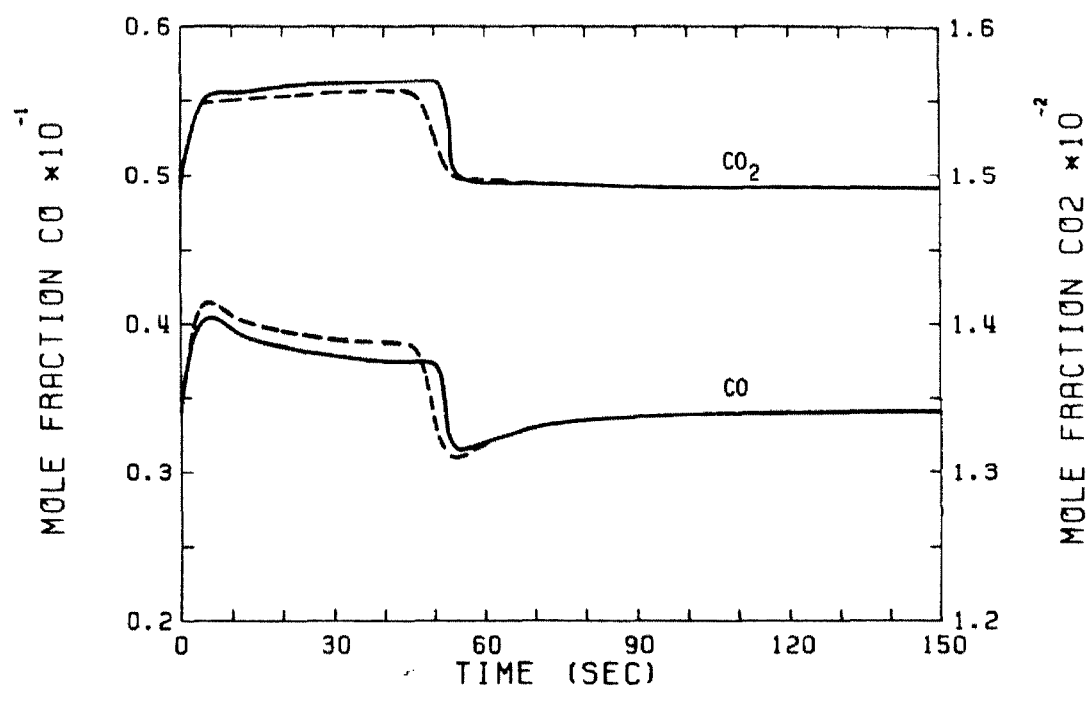


Figure 3.6-7
Exit Concentrations During 50 Second Disturbance
Standard Type II (Table 3.4-5) Conditions
(T_0 from 573° K to 602° K, x_{CO} from 0.06 to 0.072)

— Nonlinear Model - - - Linear Model

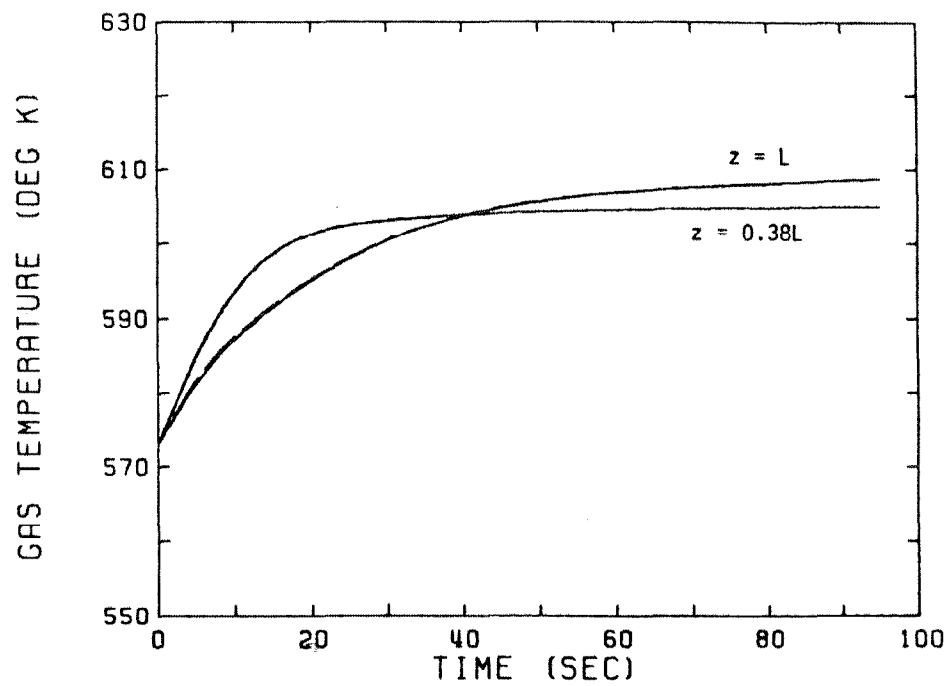


Figure 3.6-8
Temporal Behavior of Gas Temperatures during Start-Up
Standard Type II (Table 3.4-5) Conditions

— Nonlinear Model - - - - Linear Model

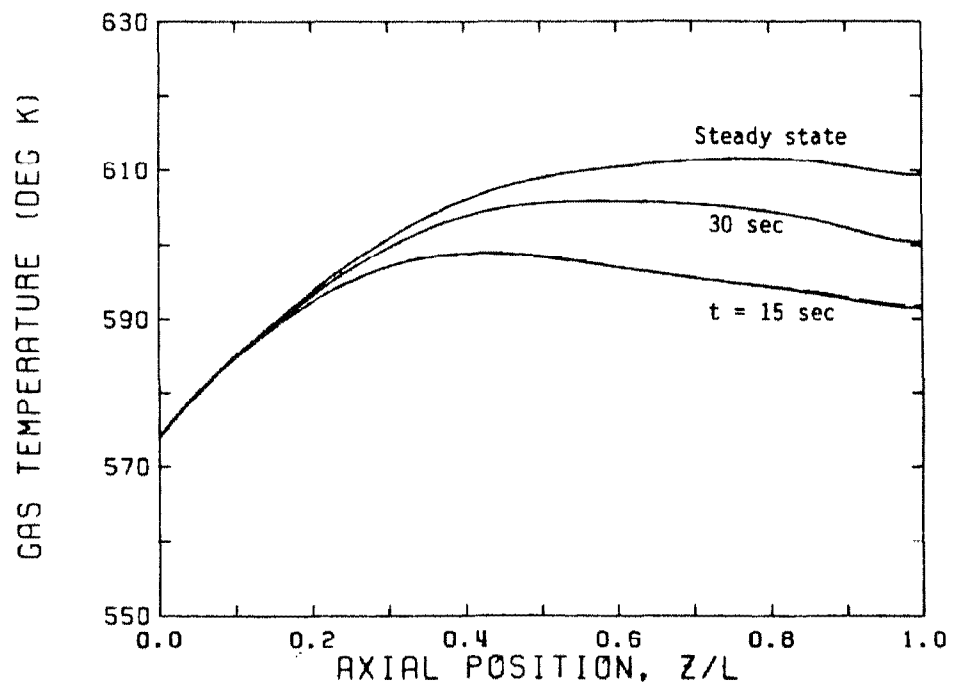


Figure 3.6-9
Axial Gas Temperature Profiles during Start-Up
Standard Type II (Table 3.4-5) Conditions

— Nonlinear Model - - - - Linear Model

3.7 MODEL DIMENSIONALITY

Mathematical models are widely used in the design, simulation, optimization, and control of chemical packed bed reactors. Although low-order models are often developed for control of simple chemical systems using statistical analysis of input/output data, these empirical models are generally inappropriate for complicated, highly nonlinear packed bed analyses where very low-order models are not sufficient and where operating conditions may vary greatly from the vicinity of the operating point for which the models were developed. For these systems, the mechanistic modeling approach presented in this thesis is necessary. In this mechanistic analysis, a detailed mathematical description of the physical and chemical phenomena in the system is solved directly. Although this generally provides a more detailed solution valid over a wider operating range and allows detailed investigation and prediction of the reactor behavior, the model even after linearization is often too complex for controller design or for implementation as part of the actual control system. Low-order models are thus required for on-line implementation of multivariable control strategies.

This section presents a dimensionality study of the model discretization and physical modeling assumptions for the mechanistic packed bed reactor model. A further discussion of model reduction to approximate the full system with one of moderate order (2Nth-order) is also presented. It is our opinion that further reduction probably is not needed or desired for control studies. If additional reduction is necessary, model reduction techniques such as those presented by Bonvin (1980) and Wilson et al. (1974) should be attempted.

3.7.1 Model Discretization

The model discretization or the number of collocation points necessary for

accurate representation of the profiles within the reactor bed has a major effect on the dimensionality and thus the solution time of the resulting model. As previously discussed, radial collocation with one interior collocation point generally adequately accounts for radial thermal gradients without increasing the dimensionality of the mathematical system. However, multipoint radial collocation may be necessary to describe radial concentration profiles. The analysis of Section 3.4.5 shows that even with very high radial mass Peclet numbers, the radial concentration is nearly uniform and that the axial bulk concentration and radial and axial temperatures are nearly unaffected by assuming uniform radial concentration. Thus model dimensionality can be kept to a minimum by also performing the radial concentration collocation with one interior collocation point.

In this section, the optimal choice for the number of axial collocation points is discussed. Obviously, if the number of axial collocation points is insufficient, the resulting axial solution for the temperature and concentration profiles will be incorrect. On the other hand, one of the problems with fitting high-order polynomials to the axial profiles is that the polynomials, if of sufficiently high order, may begin to ripple along the curve. As pointed out by Jutan et al. (1977), this rippling can be extremely detrimental since the collocation formulas are used to approximate derivatives. Since there is a tradeoff between lowering the number of collocation points to reduce model dimensionality and reduce profile rippling and increasing the number of collocation points to retain high simulation accuracy, extreme care is required in the selection of the number of axial collocation points.

The first attempts at determining the optimal number of axial collocation points simply involved repeating simulations with differing axial discretization to find conditions with minimum ripple and maximum accuracy. Figure 3.7-1

shows the steady state axial temperature profiles for standard Type I (Table 3.4-5) conditions as the number of axial collocation points is changed. Eight or more axial collocation points provide similar results, and even simulations with six collocation points show minimal inaccuracy. However, reducing the number of collocation points below this leads to major discrepancies in the axial profiles. These errors are even more important in the dynamic simulations shown in Figure 3.7-2.

Although this simulation procedure provides an optimal choice of the number of axial collocation points for steady state and can give an indication of the appropriate number of collocation points for dynamic simulations, Bonvin (1980) shows that the convergence pattern of the dominant eigenvalues of the model as the number of collocation points is increased can also be used as an important procedure for determining the optimal axial discretization. Since these dominant modes only describe the dynamic behavior of the linearized system, simulation of the full model should be used to verify the results for transient and steady state analyses.

If the axial discretization is fine enough, the dominant eigenvalues have converged to their true values. Figures 3.7-3 and 3.7-4 show the convergence of the dominant eigenvalues for the Type I and Type II (Table 3.4-5) operating conditions. The conditions for Figure 3.7-3 are the same as those used for Figures 3.7-1 and 3.7-2. The eigenvalue analysis shows that less than six collocation points will lead to significant errors in the dynamic simulations for these conditions since the dominant eigenvalues are far from their true values. Seven collocation points would seem to be sufficient and six may be satisfactory. These results verify those obtained above using simulations with differing discretization (Figure 3.7-1 and 3.7-2). With six interior axial collocation points, the full model would consist of 30 coupled, nonlinear ordinary differential equations

along with their algebraic boundary conditions. The linear model would be a 30th-order state-space representation!

Under conditions where very steep gradients exist within the reactor bed, collocation may lead to oscillatory axial profiles (rippling) due to the attempt to fit an Nth-order smooth polynomial function to the axial behavior. Although these oscillations can be often reduced by decreasing the number of collocation points, significant errors in the profiles can then result. Simple trial-and-error should be used to determine the best number of axial collocation points to reduce rippling and retain accuracy. In extreme cases with very steep axial profiles or abrupt changes in the profiles, the orthogonal collocation on finite element procedure explained in Section 3.5 may be necessary. Using this technique, not only the number of collocation points in each element needs to be specified but also the number and size of the elements.

3.7.2 Physical Modeling Simplifications

Due to the complexities of the full mathematical description of a packed bed reactor and the complications with numerical solution and analyses of such descriptions, the extensive use of physical modeling simplifications is common. Assumptions that reduce the complexity of the resulting mathematical model such as neglecting dispersion effects and radial gradients have been discussed elsewhere in this work. Basically, the common assumptions of neglecting radial temperature gradients, neglecting thermal dispersion, and neglecting the variation of physical properties significantly reduce the accuracy of the resulting model for numerical simulations and for further optimization or control studies without reducing the dimensionality of the resulting representation. In view of the advances in computational techniques over the past decade for the solution

of partial differential equation systems,¹ these simplifications are unnecessary and provide minimal, if any, reduction in solution effort. Transient reactor behavior can thus be simulated using accurate three-dimensional modeling with the inclusion of known dispersion effects and parameter variations.

To this point in the modeling analysis, we have tried to incorporate all of the mechanisms necessary for accurate description of the physical and chemical phenomena occurring in industrial reactors and to study the effects of various modeling simplifications. We continue this study by considering several major simplifications which do not simply reduce the structure of the partial differential equations but actually significantly reduce the number of necessary equations or the dimensionality of the process. These include the extensive use of pseudo-homogeneous models--those that do not distinguish between the conditions within the fluid and those on the solid catalyst--and the assumptions of quasi steady state for concentrations and negligible energy accumulation in the gas phase.

3.7.2.1 Homogeneous Analysis

The mathematical models of the heat and mass transfer processes in packed bed reactors are classified in two broad categories:

1. One-phase or pseudo-homogeneous models in which the reactor bed is approximated by a quasi-homogeneous medium.
2. Two-phase or heterogeneous models where the catalyst and fluid phases and the heat and mass transfer between phases are treated explicitly.

1. In particular, the collocation techniques.

Although the heterogeneous models are more realistic, they have been generally ignored until only recently due to difficulties with numerical solution and increased model dimensionality. Even several nonadiabatic packed bed reactor studies that begin with a two-phase analysis reduce the model to a pseudo-homogeneous form by assuming equal gas and catalyst temperatures for steady state and dynamic solution (Jutan et al., 1977) or at least for the steady state solution (Hoiberg et al., 1971). Some authors (Vortmeyer and Schaefer, 1974; Vortmeyer et al., 1974) have even considered the equivalence of the one- and two-phase approaches for one-dimensional or adiabatic studies. This thesis presents the first detailed two-dimensional heterogeneous dynamic and steady state packed bed reactor analysis.

However since it has been common practice to develop models for catalytic reactors that do not distinguish between thermal conditions within the fluid phase and those on the solid catalyst, a cursory examination of the homogeneous analysis is presented here. This assumption is generally justified by the expectations of small temperature differences between the solid and gas phases and results in a one-phase continuum representation of the actual reactor bed. As discussed by Jutan et al. (1977), the difference between gas and catalyst temperatures for fast flowing gas systems should be negligible. They further reference the work by Shaw (1974) that shows that there is ample driving force to remove the heat generated by reaction and that no temperature difference should exist between the gas and catalyst at steady state.

In our original system of partial differential equations, the two energy balances can be combined as proposed by Jutan et al. (1977) by eliminating the term, $\frac{U_{sg}}{V_b}(T_s - T_g)$, that describes the heat transfer between the solid and gas. If the gas and solid temperature are assumed equal ($T_s = T_g$), and the homogene-

ous gas/solid temperature is defined as T , the original combined energy balance for the gas and solid becomes

$$[\rho_s c_{p_s} (1-\varepsilon) + \rho_g c_{p_g} \varepsilon] \frac{\partial T}{\partial t} = -\rho_g c_{p_g} u_g \varepsilon \frac{\partial T}{\partial z} + k_z \frac{\partial^2 T}{\partial z^2} + k_r \left[\frac{\partial^2 T}{\partial r^2} + \frac{1}{r} \frac{\partial T}{\partial r} \right] + (-\Delta H_M) R_M + (-\Delta H_S) R_S \quad (3.7-1)$$

where k_z and k_r are effective conductivities for the combined gas/solid system. Additionally, since

$$\frac{\rho_g c_{p_g} \varepsilon}{\rho_s c_{p_s} (1-\varepsilon)} \approx 0.004 \quad (3.7-2)$$

the coefficient of the time derivative reduces to

$$[\rho_s c_{p_s} (1-\varepsilon) + \rho_g c_{p_g} \varepsilon] \approx \rho_s c_{p_s} (1-\varepsilon) \quad (3.7-3)$$

The boundary conditions are

$$\begin{aligned} z=0 \quad k_z \frac{\partial T}{\partial z} &= u_g c_{p_g} \rho_g \varepsilon (T - T_0) \\ z=L \quad \frac{\partial T}{\partial z} &= 0 \\ r=R_0 \quad k_r \frac{\partial T}{\partial r} &= h_t (T - T_t) \\ r=R_1 \quad -k_r \frac{\partial T}{\partial r} &= h_w (T - T_w) \end{aligned} \quad (3.7-4)$$

where h_t and h_w are effective heat transfer coefficients between the gas/solid medium and the thermal well and cooling wall, respectively.

This equation is solved with the continuity equation, the energy balance for the thermal well,² and the concentration equations using the same procedure as for the full system. The dimensionality of the model has now been reduced by N (i.e., the model now has order $4N$). Computer simulation programs were written

2. With an overall heat transfer coefficient being used rather than U_{tw} and U_{tg} .

for this homogeneous model. Unfortunately, no direct comparisons can be made between the simulations with the two-phase analysis and the homogeneous analysis since no direct mathematical relationship can be made between the effective and overall heat transfer coefficients of the homogeneous model (k_z , k_r , h_t , h_w , U_t) and the individual gas and solid coefficients of the two-phase model (k_{zs} , k_{zg} , k_{rs} , k_{rg} , h_{ts} , h_{ws} , h_{tg} , h_{wg} , U_{ts} , U_{tg}). Some attempts (Vortmeyer and Schaefer, 1974) have been made in this regard, but are not accurate enough for direct comparison of the simulations of the two models.

Solution times using the homogeneous model are 15% to 25% less than that for the full two-phase analysis, although the accuracy of the results may be somewhat in question. Figures 3.7-5 and 3.7-6 show the axial temperature and concentration profiles with Type I and II (Table 3.4-5) operating conditions and with realistic heat transfer parameters. Although these simulations appear similar to those obtained with the heterogeneous analysis, no direct comparison is possible as explained above.

However, simulations using the heterogeneous analysis even with high inlet velocities lead to steady state temperature profiles with differences of up to 10° K between the solid and gas phases and transient results with differences up to 20° K due to the high exothermicity of the methanation reaction on the catalyst surface. These temperature differences can lead to significant errors in the predicted reaction rates. Using the kinetics proposed by Strand (1984), the methanation reaction rate about doubles with every 10° K temperature rise over the normal operating region. Therefore although a homogeneous analysis may be adequate for reactions that are only slightly exothermic or simulations of steady state phenomena, a heterogeneous analysis is necessary for dynamic simulations of highly exothermic reaction processes.

The increased dimensionality of the heterogeneous system can be reduced using other techniques discussed in this section which require much milder assumptions. The assumption of negligible energy accumulation in the gas phase based on the approximation (Equation 3.7-3) provides the same reduction in system dimensionality as the homogeneous analysis but with a much less drastic assumption.

Measurement difficulties that arise in model verification of parameter estimation using a heterogeneous analysis are also often cited as reasons for a homogeneous analysis. Although theoretically it is possible to measure separately the gas and solid temperatures, in practice it is difficult without seriously affecting flow patterns within the reactor bed. These difficulties can be minimized by using an internal thermal well as is common in industrial systems and including this thermal well in the model development. This eliminates the concern over whether temperature measurements within the reactor bed are actually measuring gas or solid temperatures or a combination of both.

Another procedure often used with less severe assumptions than the equality of the gas and solid temperature is the pseudo-homogeneous analysis proposed by Vortmeyer and Schaefer (1974). This procedure has proven to be quite effective for simple adiabatic packed bed analyses and involves reducing the energy balances for the gas and catalyst to a single equation using the assumption

$$\frac{\partial^2 \Theta_g}{\partial z^2} = \frac{\partial^2 \Theta_s}{\partial z^2} \quad (3.7-5)$$

Although this assumption is often not too restrictive, additional more severe assumptions must be introduced to reduce our mathematical model to the pseudo-homogeneous form, since our reactor is nonadiabatic and requires radial temperature considerations. A literature search failed to find any

attempts of the Vortmeyer procedure for a nonadiabatic packed bed reactor. For the full mathematical model developed in Section 3.3, the following assumptions would be necessary in addition to the standard Vortmeyer assumption above:

1) Negligible energy accumulation in the gas phase.

2) No axial diffusion in the gas phase or

$$\frac{\partial}{\partial z} \left[\frac{\partial^2 T_g}{\partial z^2} \right] = 0$$

3)

$$\frac{\partial}{\partial r} \left[\frac{1}{r} \frac{\partial T_s}{\partial r} \right] = \frac{\partial}{\partial r} \left[\frac{1}{r} \frac{\partial T_g}{\partial r} \right]$$

4)

$$\frac{\partial (\rho_g u_g)}{\partial z} = 0$$

Obviously, these assumptions are too restrictive for standard nonadiabatic packed bed analyses.

3.7.2.2 Quasi Steady State Approximation

Transient analyses using the full, nonlinear model show that concentration profiles reach a quasi steady state quite rapidly (often within 3 to 5 seconds); whereas, the thermal response of the reactor bed is much slower³ due to the large heat capacity of the reactor bed and thermal well. An example of this phenomenon is shown in Figure 3.7-7, where the transient responses of the solid

3. Thermal time constants are about two orders of magnitude greater than the concentration time constants.

temperatures, thermal well temperatures, and concentrations are shown for a major step change in the inlet gas temperature and inlet CO concentration. In this example, the effect of the step change is nearly immediate on the concentration profiles with the major effect being within the first ten seconds. However, Figure 3.7-7a shows that the thermal well temperatures and the catalyst temperatures take up to ten times as long as the concentrations to approach the new steady state after the input step change. Note that the catalyst temperatures shown in the figure are at the radial collocation point $r = r_c$ and that the response of the catalyst temperatures near the center of the reactor (not shown) is very similar to the thermal well response.

Furthermore, comparison of the thermal (v_T) and the concentration (v_C) wave velocities as defined by Gould (1969)

$$v_T = \frac{\rho_g c_p g u_g \varepsilon}{\rho_s c_p s (1-\varepsilon)} \quad (3.7-6)$$
$$v_C = u_g$$

verify this quasi steady state for the concentration profiles. As in many solid catalyzed gas reactions, the ratio of the concentration wave velocity to the thermal wave velocity is quite large.⁴ This implies that the concentration profiles reach a quasi steady state rapidly and that this quasi steady state then follows the slowly changing temperature profile, thus providing theoretical backing for the transient behavior of the concentrations and temperatures in Figure 3.7-7. Packed bed studies by Jutan et al. (1977) have also shown that the concentration dynamics can be ignored in the packed bed modeling.

The quasi steady state approximation then allows the concentration time derivatives to be set equal to zero

4. About 250 for our reactor.

$$\frac{\partial \hat{x}_{CO}}{\partial t} \approx 0 \quad \frac{\partial \hat{x}_{CO_2}}{\partial t} \approx 0 \quad (3.7-7)$$

in the original partial differential equations or in the linearized model, thus reducing $2N$ of the discretized ordinary differential equations to algebraic equations. In the linear system, these algebraic equations can be solved directly for the concentrations and substituted into the differential equations. Computer programs (Appendix 4) were written to simulate the reactor using this assumption for both the full and linearized models. Although this approximation introduces considerable simplification in the nonlinear model, its effect on the linearized system is a simple reduction in system dimensionality, and it does not lead to any major reductions in analytic solution times.

Simulations show negligible differences in the transient temperature and concentrations profiles as a result of this approximation. Some of these simulations are shown in Section 3.7-4 where the model reduction procedures are compared. The major advantage of this assumption should be apparent in control system design where a reduction in the size of the state vector is computationally beneficial or in the time-consuming simulations of the full nonlinear model. It should be stressed that, although this quasi steady state approximation involves setting the time derivatives of the concentrations equal to zero, it does not imply that concentrations are independent of time, since concentrations are still coupled directly to temperatures, and temperatures are obviously time dependent.

3.7.2.3 Negligible Energy Accumulation in Gas

Another potential model simplification procedure involves assuming negligible energy accumulation in the gas phase as compared to that in the solid. This

is equivalent to the approximation above (Equation 3.7-3) based on the relative magnitude of the energy accumulation in the gas and solid. For our system, the accumulation of energy in the solid is approximately 250 to 300 times that in the gas phase due to the relative thermal capacitance of the gas (Equation 3.7-2) and the similarity of the temporal behavior of the gas and catalyst temperatures (e.g., Figure 3.7-8). Thus the accumulation term in the energy balance for the gas phase can be neglected:

$$\rho_g c_p \varepsilon \frac{\partial \theta_g}{\partial t} \approx 0 \quad (3.7-8)$$

in comparison to the energy accumulation in the catalyst and thermal well. This reduces N of the original ordinary differential equations (after orthogonal collocation) to algebraic equations. Again after linearization, these can be solved directly for the gas temperatures which can then be substituted into the remaining ordinary differential equations to eliminate the gas temperatures from the state vector. Simulation computer programs were again written (Appendix 4) and show negligible differences in the dynamic and steady state profiles, small reductions in solution times for the nonlinear model, and no major time reductions for the analytic solution. Some of these simulations are shown in Section 3.7-4.

3.6.1 Model Reduction

Regardless of whether orthogonal collocation or orthogonal collocation on finite elements is used for the discretization, the resulting linear state-space representation is of high order (30-40 states)¹ due to the original system of five coupled partial differential equations and the accurate treatment of the gas, catalyst and thermal well temperatures and concentrations. Although dynamic

1. This is actually of very low-order in comparison to traditional finite difference solutions.

simulations using the state-space representation are very fast, computational difficulties still exist in developing multivariable feedback control algorithms due to the relatively high order of the system. For such applications, an accurate reduced-order model is desired.

Significant reduction is possible through the introduction of the approximations of quasi steady state for the concentrations, negligible accumulation of energy in the gas phase, or pseudo-homogeneity of the system. Although these approximations could have been made in the original modeling, doing so without a careful analysis of their effects on the model behavior can be dangerous. The complete study of the mathematical modeling of a packed bed reactor allows careful investigation of the significance of these assumptions and the combined effects of several simplifications. Additionally, an analysis of the eigenstructure of the system shows that simple modal reduction techniques such as those presented by Bonvin (1980), Gould (1969), and Wilson et al. (1974) can lead to a low-order state-space model. This section considers explicit modal reduction approaches to model reduction that result in an explicit reduced model formulation without statistical analysis of input/output data.

Various model reduction approaches, or minor modifications to existing approaches, were proposed during the late 1960's and early 1970's. The basic strategy of these approaches is to retain certain modes of the high-order model in the low-order model. Wilson et al. (1974) summarized these techniques and showed that many of the published modal approaches are equivalent since they produce identical reduced models. They further considered the design of reduced-order control models by performing the model reduction on the high-order model and then designing a low-order controller and by designing a high-order controller and then reducing this to a low-order control law. Bonvin (1980) also provides a comparison of the various modal techniques with respect

to their steady state and dynamic accuracies as well as to the dependence of the reduced models on the retained state variables.

According to Gould (1969), the central theme in modal reduction and control is

"that the transient behavior of a process is predominantly determined by the modes associated with the smallest eigenvalues. If it is possible to approximate a high-order system by a lower-order system whose slow modes are the same as those of the original system, then attention can be focused on the attempt to alter the eigenvalues of the slow modes so as to increase the speed of recovery of the process from disturbances. It is essential to be aware of the fact that various disturbances excite the modes differently so that a scheme which is based on a lower-order model may be inappropriate if a disturbance injects most of its 'energy' in a fast mode which has been neglected."

This basic approach is really divided into several distinct categories. Two of these, Davison's method and Marshall's method, provide suitable model reduction for the state-space representation of the methanation reactor to a 12th-order model. Comparisons of the models and discussion of additional model reduction are presented in the next section.

3.7.3.1 *Davison's Method*

The principle of this method, proposed originally by Davison (1966), is to neglect eigenvalues of the original system which are farthest from the origin (the non-dominant modes) and retain only dominant eigenvalues and hence the dominant time constants of the system. If we consider the solution of the linearized model derived in Section 3.6,

$$\mathbf{x}(t+dt) = e^{\mathbf{A}dt} \mathbf{x}(t) + \mathbf{A}^{-1} (e^{\mathbf{A}dt} - I) \mathbf{Ww}(t) \quad (3.7-9)$$

and let

$$\mathbf{A} = \mathbf{S}\Lambda\mathbf{S}^{-1} \quad (3.7-10)$$

where Λ is the diagonal matrix of eigenvalues

$$\Lambda = \begin{bmatrix} \lambda_1 & 0 & \dots & 0 \\ 0 & \lambda_2 & & \cdot \\ \vdots & \vdots & \ddots & \vdots \\ \vdots & \vdots & & \vdots \\ 0 & 0 & \dots & \lambda_n \end{bmatrix} \quad (3.7-11)$$

and \mathbf{S} is the corresponding matrix of eigenvectors, the dynamic behavior of the system is governed by the term

$$\mathbf{A}^{-1}(e^{\mathbf{A}dt} - \mathbf{I})\mathbf{Ww}(t) = \mathbf{S}\Lambda^{-1}(e^{\mathbf{A}dt} - \mathbf{I})\mathbf{S}^{-1}\mathbf{Ww}(t)$$

$$= \mathbf{S} \begin{bmatrix} \frac{e^{\lambda_1 dt} - 1}{\lambda_1} & \dots & 0 \\ \vdots & \ddots & \vdots \\ \vdots & & \vdots \\ 0 & \dots & \frac{e^{\lambda_n dt} - 1}{\lambda_n} \end{bmatrix} \mathbf{S}^{-1}\mathbf{Ww}(t) \quad (3.7-12)$$

Obviously by neglecting the non-dominant eigenvalues, the dynamic behavior of the approximate system will be similar to the original system, since the contribution of the unretained modes will only be significant early in the dynamic response.

Table 3.7-1 shows the system eigenvalues for our full 30th-order linear state-space representation for Type II (Table 3.4-4) conditions. As shown, the eigenvalues can be grouped into five distinct groups based on the real parts of the eigenvalues:

Group	-(Real)
I	≈ 50
II	1 - 5
III	4 - 6
IV	0.06 - 0.08
V	0.01 - 0.03

Further analysis shows that the fastest modes (Group I) correspond directly to the gas temperatures at the interior collocation points and those of Groups II and III correspond to the concentrations. It is evident that, of the 30 modes of the full linear model (with $N = 6$), 18 are very fast in comparison to the remaining 12 (by two orders of magnitude or more). Thus direct modal reduction to a 12th-order model using Davison's method should provide good dynamic accuracy.

Group	Real Part	Imaginary Part
I	-53.49	± 1.93
	-52.93	± 6.31
	-51.98	± 10.48
II	- 5.03	± 5.76
	- 2.12	± 10.38
	- 1.37	± 10.35
III	- 6.27	± 1.89
	- 5.66	± 1.85
	- 4.34	± 5.68
IV	- 0.08	± 0.010
	- 0.07	± 0.035
	- 0.06	± 0.074
V	- 0.033	0.0000
	- 0.021	± 0.0011
	- 0.018	± 0.0009
	- 0.016	0.0000

Table 3.7-1
Eigenvalues of Full 30th-Order Linear Model

However by simply neglecting the non-dominant modes of the system, the

contribution of these modes is also absent at steady state, thus leading to possible (usually minor) steady state offset. Several identical modifications (Wilson et al., 1974) to Davison's original method have been proposed by Davison and Chidambara (Chidambara and Davison, 1967abc; Davison, 1968) and by Fossard (1970). In these methods, the states of the reduced model are artificially reconditioned to ensure desired steady state behavior.

3.7.3.2 Marshall's Method

Marshall's model reduction technique (Marshall, 1966) differs from Davison's in that the steady state characteristics of the original system are retained in the reduced model. Since the response of any element of the state vector associated with a large eigenvalue is much faster than that of elements associated with the smaller eigenvalues (or larger time constants), the dynamics of the non-dominant modes can simply be neglected.⁶ This is equivalent to approximating the response of the faster modes by an instantaneous step change. If the fast modes in the methanation model are taken as the gas temperatures and the CO and CO₂ concentrations, Marshall's procedure is a rigorous mathematical reduction identical to the assumptions of quasi steady state for the concentrations and negligible energy accumulation in the gas phase. An important advantage of Marshall's method over Davison's method is that the reduced-order model has the same steady state as the high-order model, since the time derivatives are identically zero for all state variables at steady state. However, the retained modes may no longer optimally represent the dynamic behavior.

Table 3.7-1 shows that, for the methanation reactor model, the dynamic

6. I.e., their time derivatives are set equal to zero.

response of the gas temperatures and CO and CO₂ concentrations should be much faster (by two orders of magnitude) than the response of the catalyst and thermal well temperatures. This prediction is verified in the dynamic responses shown in Figures 3.7-7 and 3.7-8 and the previous analysis of the thermal and concentration wave velocities.

Thus the state vector

$$\mathbf{x} = \left[\Theta_{g_i}, \Theta_{B_i}, \Theta_{t_i}, y_{1_i}, y_{2_i} \right]^T \quad i = 1, \dots, N \quad (3.7-13)$$

is partitioned into

$$\mathbf{x}_1 = \begin{bmatrix} \Theta_{g_i} \\ \Theta_{t_i} \end{bmatrix} \quad \mathbf{x}_2 = \begin{bmatrix} y_{1_i} \\ y_{2_i} \end{bmatrix} \quad (3.7-14)$$

The state-space representation

$$\dot{\mathbf{x}} = \mathbf{Ax} + \mathbf{Ww} \quad (3.7-15)$$

$$\text{where } \mathbf{A} = \begin{bmatrix} \mathbf{A}_{11} & \mathbf{A}_{12} & \mathbf{A}_{13} & \mathbf{A}_{14} & \mathbf{A}_{15} \\ \mathbf{A}_{21} & \mathbf{A}_{22} & \mathbf{A}_{23} & \mathbf{A}_{24} & \mathbf{A}_{25} \\ \mathbf{A}_{31} & \mathbf{A}_{32} & \mathbf{A}_{33} & \mathbf{A}_{34} & \mathbf{A}_{35} \\ \mathbf{A}_{41} & \mathbf{A}_{42} & \mathbf{A}_{43} & \mathbf{A}_{44} & \mathbf{A}_{45} \\ \mathbf{A}_{51} & \mathbf{A}_{52} & \mathbf{A}_{53} & \mathbf{A}_{54} & \mathbf{A}_{55} \end{bmatrix} \quad \text{and } \mathbf{W} = \begin{bmatrix} \mathbf{W}_1 \\ \mathbf{W}_2 \\ \mathbf{W}_3 \\ \mathbf{W}_4 \\ \mathbf{W}_5 \end{bmatrix} \quad (3.7-16)$$

can then be partitioned into two sets of equations:

$$\dot{\mathbf{x}}_1 = \begin{bmatrix} \mathbf{A}_{11} & \mathbf{A}_{13} \\ \mathbf{A}_{31} & \mathbf{A}_{33} \end{bmatrix} \mathbf{x}_1 + \begin{bmatrix} \mathbf{A}_{12} & \mathbf{A}_{14} & \mathbf{A}_{15} \\ \mathbf{A}_{32} & \mathbf{A}_{34} & \mathbf{A}_{35} \end{bmatrix} \mathbf{x}_2 + \begin{bmatrix} \mathbf{W}_1 \\ \mathbf{W}_3 \end{bmatrix} \mathbf{w} \quad (3.7-17)$$

$$\dot{\mathbf{x}}_2 = \begin{bmatrix} \mathbf{A}_{21} & \mathbf{A}_{23} \\ \mathbf{A}_{41} & \mathbf{A}_{43} \\ \mathbf{A}_{51} & \mathbf{A}_{53} \end{bmatrix} \mathbf{x}_1 + \begin{bmatrix} \mathbf{A}_{22} & \mathbf{A}_{24} & \mathbf{A}_{25} \\ \mathbf{A}_{42} & \mathbf{A}_{44} & \mathbf{A}_{45} \\ \mathbf{A}_{52} & \mathbf{A}_{54} & \mathbf{A}_{55} \end{bmatrix} \mathbf{x}_2 + \begin{bmatrix} \mathbf{W}_2 \\ \mathbf{W}_4 \\ \mathbf{W}_5 \end{bmatrix} \mathbf{w} \quad (3.7-18)$$

Then we can let $\dot{\mathbf{x}}_2 = 0$ in light of the quasi steady state approximation and the assumption of negligible energy accumulation in the gas or in light of the

significant differences in the magnitudes of the eigenvalues for the \mathbf{x}_1 and \mathbf{x}_2 states and solve for \mathbf{x}_2 as a function of \mathbf{x}_1 . Substituting this result into Equation (3.7-17) results in a reduced state-space model

$$\dot{\mathbf{x}}_1 = \mathbf{A}'\mathbf{x}_1 + \mathbf{W}'\mathbf{w} \quad (3.7-19)$$

where the state variables are now the catalyst and thermal well temperatures at the collocation points and the new matrices \mathbf{A}' and \mathbf{W}' are simply related to the original matrices:

$$\mathbf{A}' = \begin{bmatrix} \mathbf{A}_{11} & \mathbf{A}_{13} \\ \mathbf{A}_{31} & \mathbf{A}_{33} \end{bmatrix} - \begin{bmatrix} \mathbf{A}_{12} & \mathbf{A}_{14} & \mathbf{A}_{15} \\ \mathbf{A}_{32} & \mathbf{A}_{34} & \mathbf{A}_{35} \end{bmatrix} \mathbf{A}_c^{-1} \begin{bmatrix} \mathbf{A}_{21} & \mathbf{A}_{23} \\ \mathbf{A}_{41} & \mathbf{A}_{43} \\ \mathbf{A}_{61} & \mathbf{A}_{63} \end{bmatrix} \quad (3.7-20)$$

$$\mathbf{W}' = \begin{bmatrix} \mathbf{W}_1 \\ \mathbf{W}_3 \end{bmatrix} - \begin{bmatrix} \mathbf{A}_{12} & \mathbf{A}_{14} & \mathbf{A}_{15} \\ \mathbf{A}_{32} & \mathbf{A}_{34} & \mathbf{A}_{35} \end{bmatrix} \mathbf{A}_c^{-1} \begin{bmatrix} \mathbf{W}_2 \\ \mathbf{W}_4 \\ \mathbf{W}_5 \end{bmatrix} \quad (3.7-21)$$

$$\text{where } \mathbf{A}_c^{-1} = \begin{bmatrix} \mathbf{A}_{22} & \mathbf{A}_{24} & \mathbf{A}_{25} \\ \mathbf{A}_{42} & \mathbf{A}_{44} & \mathbf{A}_{45} \\ \mathbf{A}_{62} & \mathbf{A}_{64} & \mathbf{A}_{65} \end{bmatrix} \quad (3.7-22)$$

Of course, this technique does not actually eliminate the states Θ_{g_i} , y_{1_i} , and y_{2_i} . Instead it retains their steady state effects and relates their dynamic behaviour to the gas and thermal well temperatures. The reduced model is then of order $2N$, or of only 12th-order for $N=6$. Similarly, we could consider each assumption independently. If we retain the state variables Θ_{g_i} , the model is of $3N$ th-order.

3.7.4 Discussion of Reduced Model

The reduced-order model obtained using Marshall's method is an accurate $2N$ th-order approximation to the original $5N$ th-order model. Although the

resulting model is equivalent to simply making the common assumptions of negligible energy accumulation in the gas and quasi steady state for the concentrations, we have provided a rigorous mathematical approach to these assumptions based on the eigenstructure analysis and have provided an accurate means of evaluating their applicability. The steady state problems associated with Davison's method are eliminated, and the potential dynamic disagreement between the original and reduced models is minimal for the methanation reactor as verified by simulations.

Simulations using this reduced model show a reduction in computation time, along with storage space, without any significant loss in accuracy. Table 3.7-2 shows the simulation times for various simulations using various models and solution techniques with $N = 6$. All computer programs are documented in Appendix 4. The program RD1MOD simulates the $2N$ th-order model using analytic solution of the equations, and RD2MOD simulates an $3N$ th-order model where only the concentration dynamics have been neglected. Although the solution time advantages between the analytic solutions of the reduced models and the full linear model seem to be minimal, these analyses were conducted with a constant control and disturbance vector w over the periods of disturbance or simulation. If these values change frequently as may be the case in practice, the solution time savings for the reduced models will be increased.

Figures 3.7-9 and 3.7-10 show comparisons of the transient gas and solid axial temperature profiles for a step input change using the full model and the reduced models. The figures show negligible differences between the profiles at times as low as ten seconds. Concentration results (not shown) show even smaller discrepancies between the profiles. Additional simulations are not shown since all attempted simulations showed minimal differences between the solutions using the different linear models. Thus for the methanation system,

Simulation	Model				
	NLNMOD	LINMOD	ANAMOD	RD2MOD	RD1MOD
Step $T_o \rightarrow 593^{\circ}\text{K}$ $x_{CO} \rightarrow 0.07$	2:54:24	12:54	00:36	00:24	00:22
Step $T_w \rightarrow 593^{\circ}\text{K}$	3:14:41	18:04	00:34	00:22	00:20
Start-up	4:43:26	28:39	00:29	00:17	00:14
Disturbance $T_o \rightarrow 602^{\circ}\text{K}$ (50 seconds) $x_{CO} \rightarrow 0.072$	4:58:42	23:10	00:31	00:20	00:17

Table 3.7-2
Comparative Simulation Times of Models

Marshall's model reduction provides an accurate 2Nth-order reduced state-space representation of the original 5Nth-order linear model.

The excellent dynamic agreement between the original and reduced models (Figures 3.7-9 and 3.7-10) can be explained by the eigenstructure of the reduced system. As shown in Figure 3.7-11, the eigenvalues of the reduced model are nearly identical (within 1%) to the dominant eigenvalues of the original model. Thus the dynamic behavior is nearly identical to that which would result from modal reduction using Davison's method. The advantage then of Marshall's modal reduction for the methanation reactor model is that some contribution of the 'fast' modes is still retained in the algebraic equations that result from the assumptions. These contributions lead to small deviations in the remaining eigenvalues and eliminate steady state discrepancies without seriously affecting the dynamic responses.

Since the 2Nth-order reduced model based on Marshall's reduction procedure accurately simulates the performance of the full linear model for a large range of input changes and disturbances, there is little or no incentive to attempt other techniques. If however further model reduction is desired or necessary for control studies, more powerful reduction techniques would be needed since the eigenvalues of the 2Nth-order model are of similar magnitudes

and simple elimination of the larger ones may lead to major errors.

One possible procedure for further reduction would be Litz's modal reduction described in detail by Bonvin (1980). Litz proposed that the contribution of the non-dominant modes be taken as a linear combination of the dominant modes rather than simply being neglected. The appropriate linear combination is determined in order to minimize the error between the responses of the non-dominant modes in the original and in the reduced-order models. Bonvin (1980) further explains that the eigenvalues of the reduced model are identical to the dominant eigenvalues of the original model, but the eigenvectors are given a new optimal orientation. Bonvin uses this technique to reduce a 24th-order model for a tubular autothermal reactor to a 5th-order reduced model. He concludes that Litz's procedure is superior to all other modal approaches.

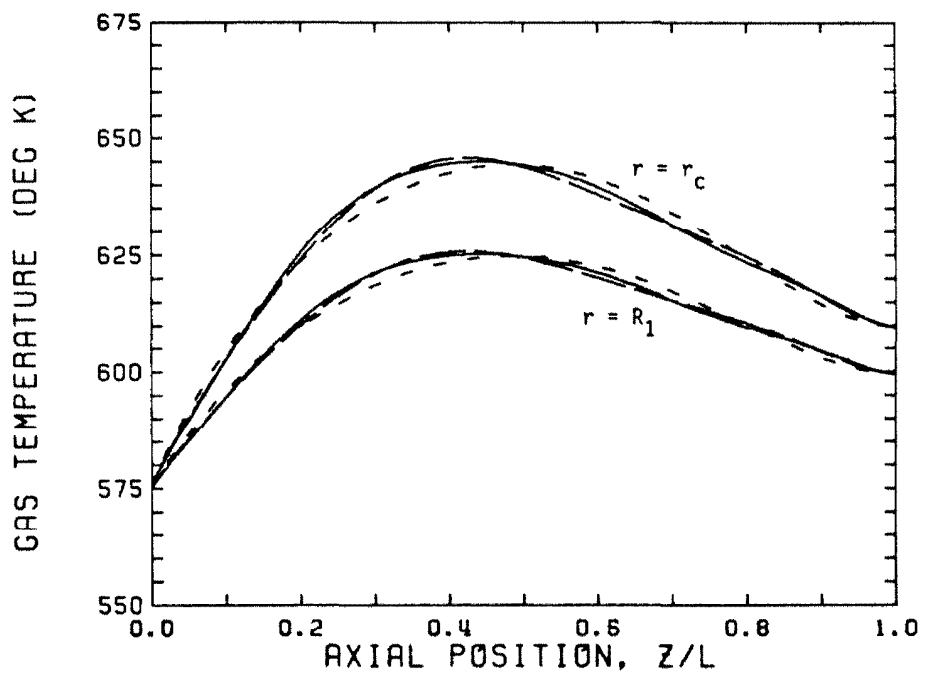


Figure 3.7-1
Steady State Axial Gas Temperature Profiles
Standard Type I (Table 3.4-5) Conditions
Varying Axial Discretization

— $N = 8, 10, 12$ - - - $N = 6$ - · - - $N = 4$

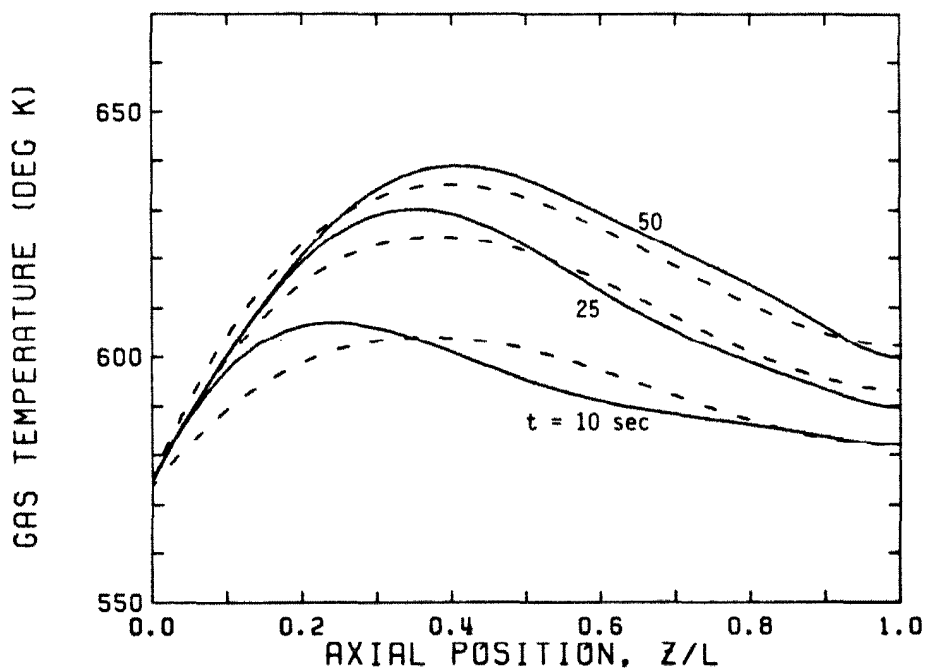


Figure 3.7-2
Dynamic Axial Gas Temperature Profiles
Standard Type I (Table 3.4-5) Conditions
Varying Axial Discretization

— $N = 8, 10, 12$ - - - $N = 4$

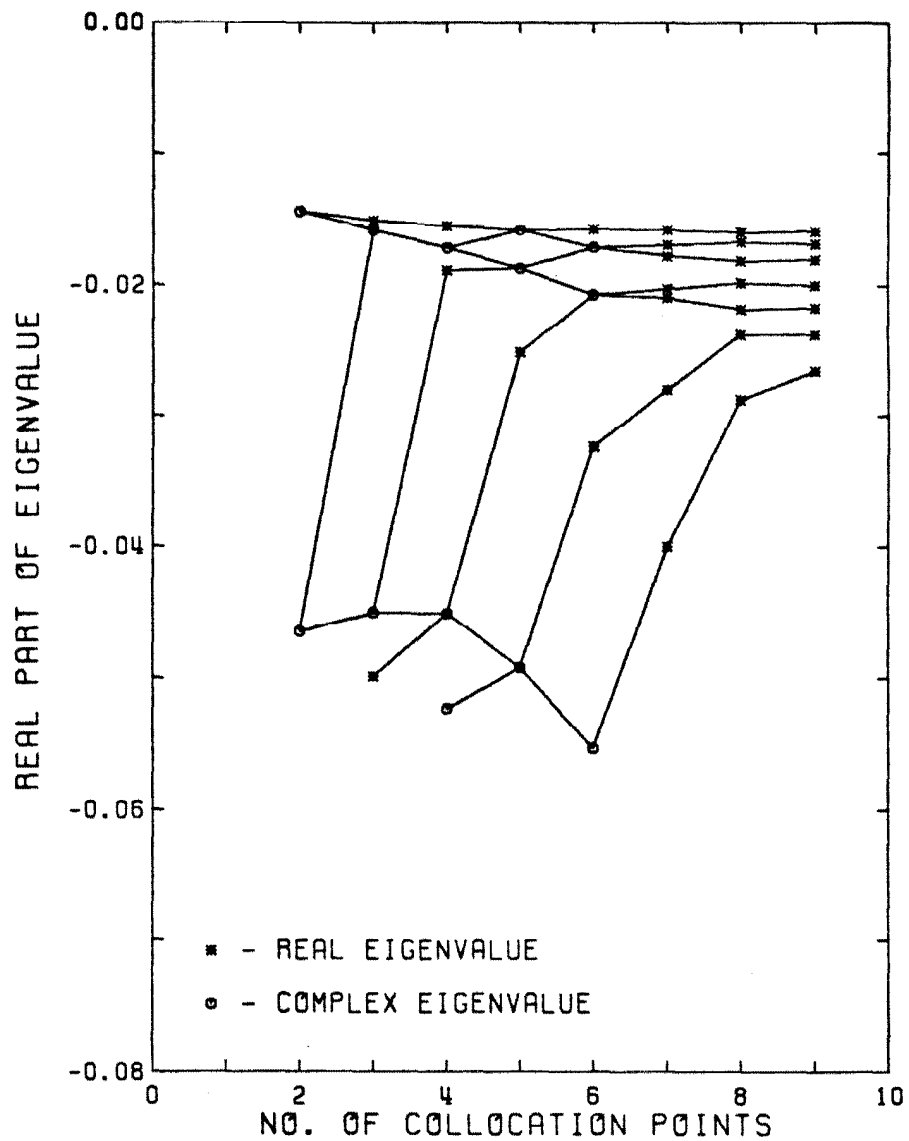


Figure 3.7-3
Convergence Pattern of Dominant Eigenvalues
Standard Type I (Table 3.4-5) Conditions

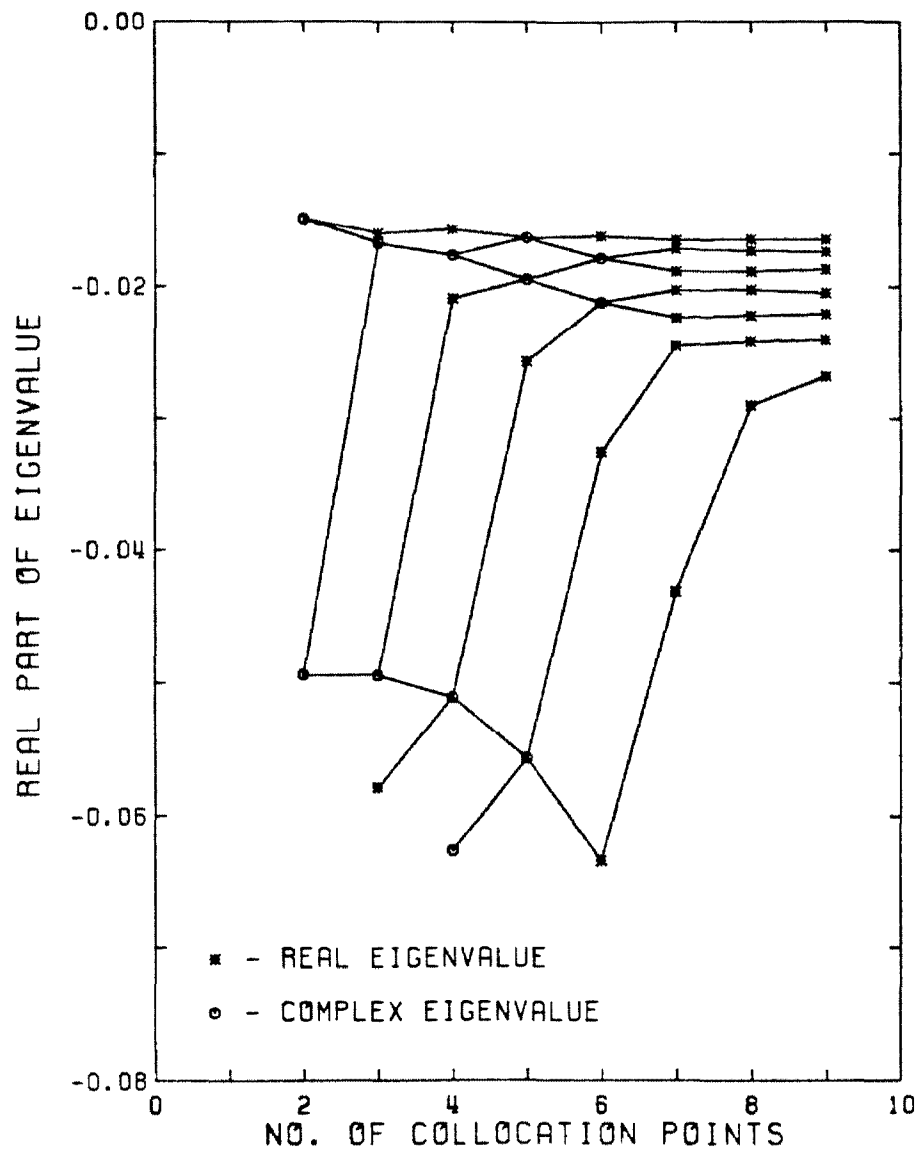
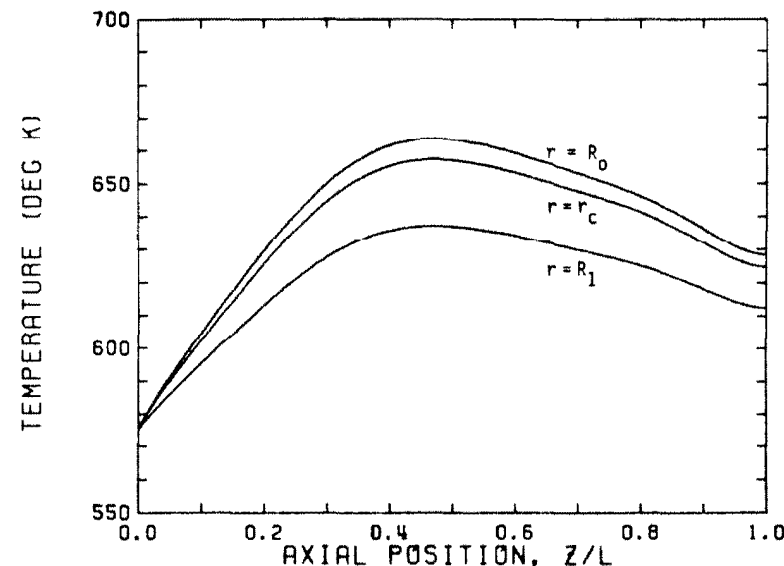
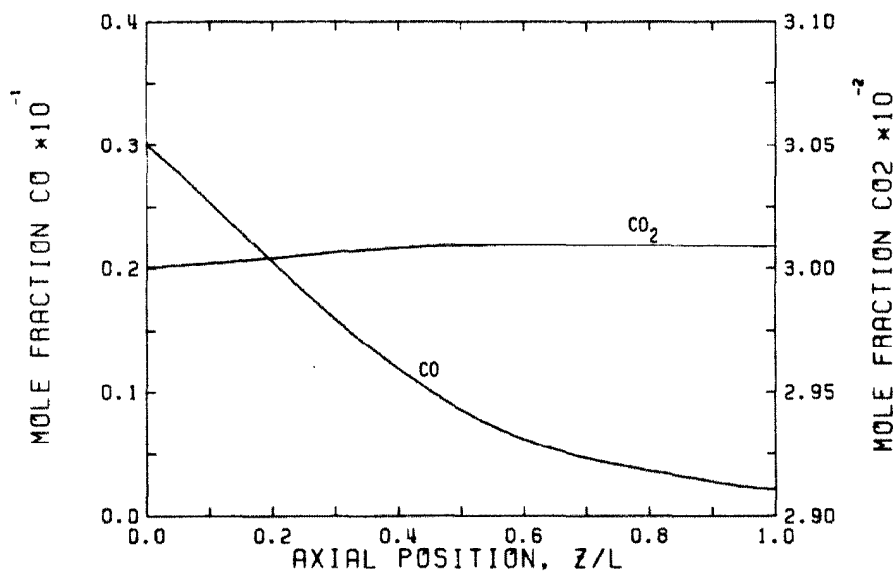


Figure 3.7-4
Convergence Pattern of Dominant Eigenvalues
Standard Type II (Table 3.4-5) Conditions



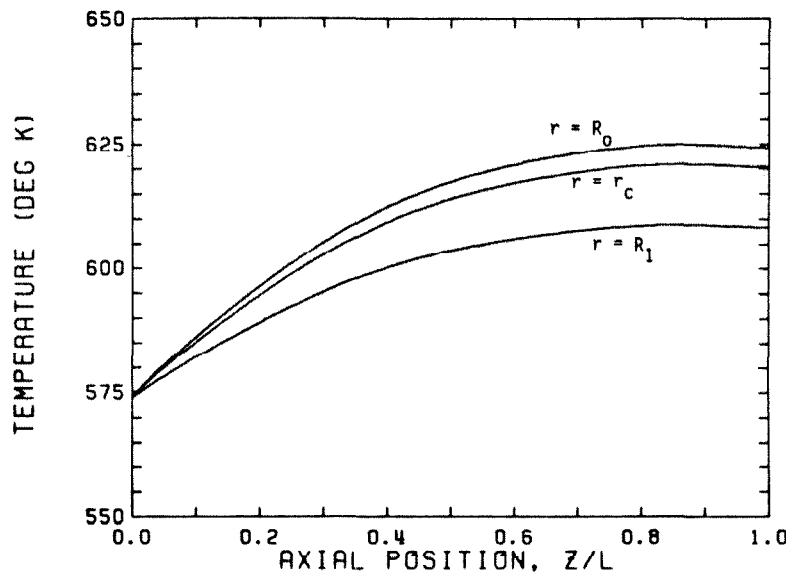
(a)



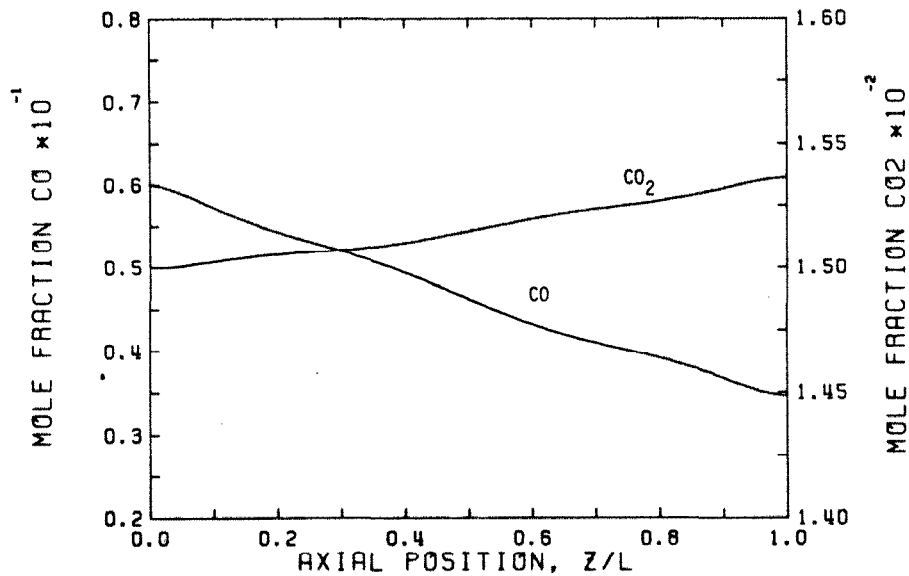
(b)

Figure 3.7-5
Axial Steady State Profiles - Homogeneous Model
Standard Type I (Table 3.4-5) Conditions

- a) Temperatures
- b) CO and CO₂ Concentrations



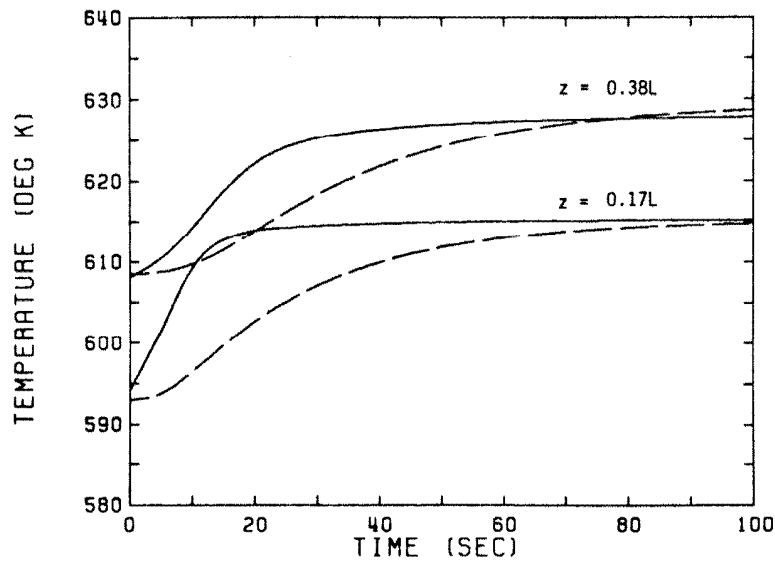
(a)



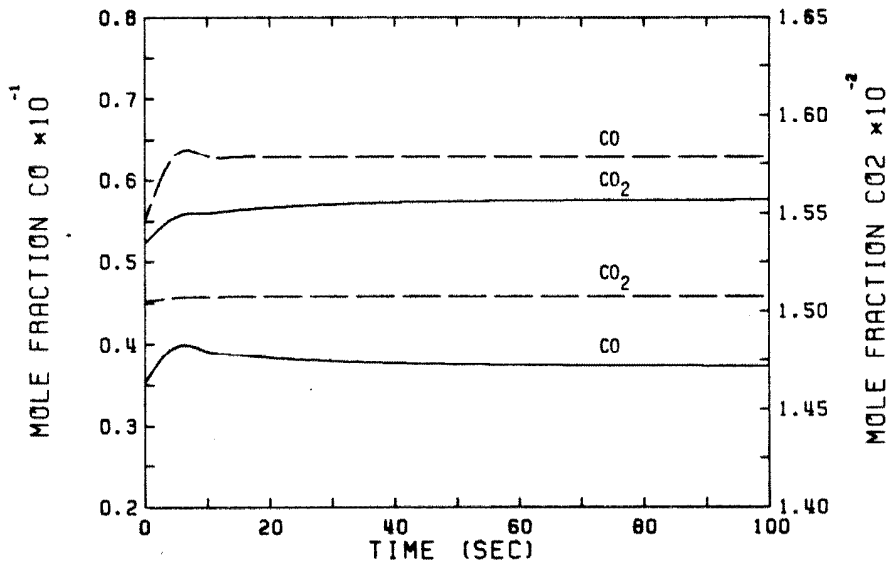
(b)

Figure 3.7-6
Axial Steady State Profiles - Homogeneous Model
Standard Type II (Table 3.4-5) Conditions

- a) Temperatures
- b) CO and CO_2 Concentrations



(a)



(b)

Figure 3.7-7
Transient Responses to Step Input Change
Standard Type II (Table 3.4-5) Conditions
(T_0 from 573° K to 593° K, x_{CO} from 0.06 to 0.07)

a) Temperature

— Catalyst - - - Thermal Well

b) CO and CO₂ Concentrations

— $z = 0.17L$ - - - $z = L$

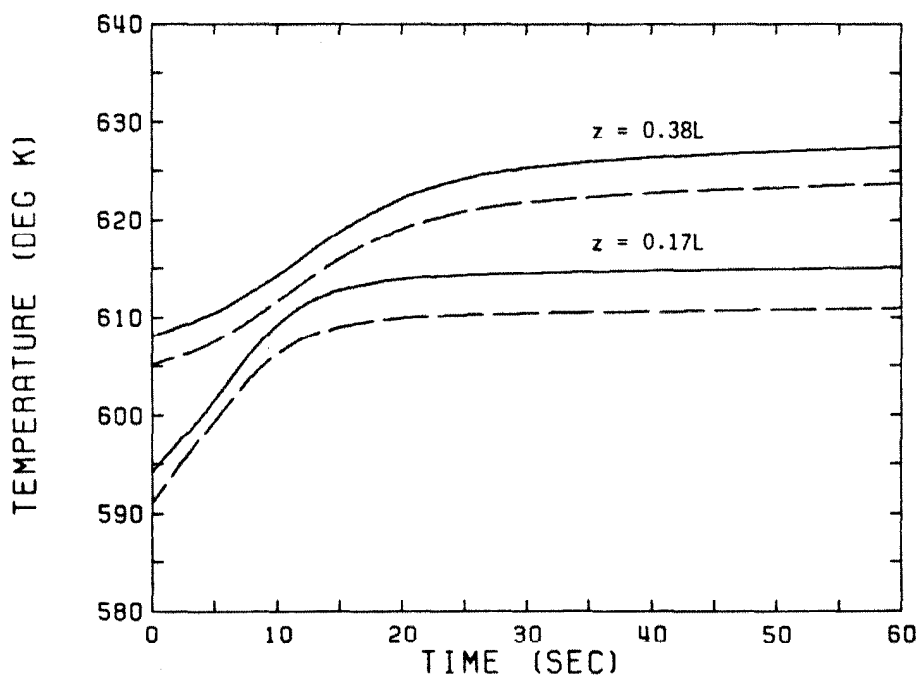
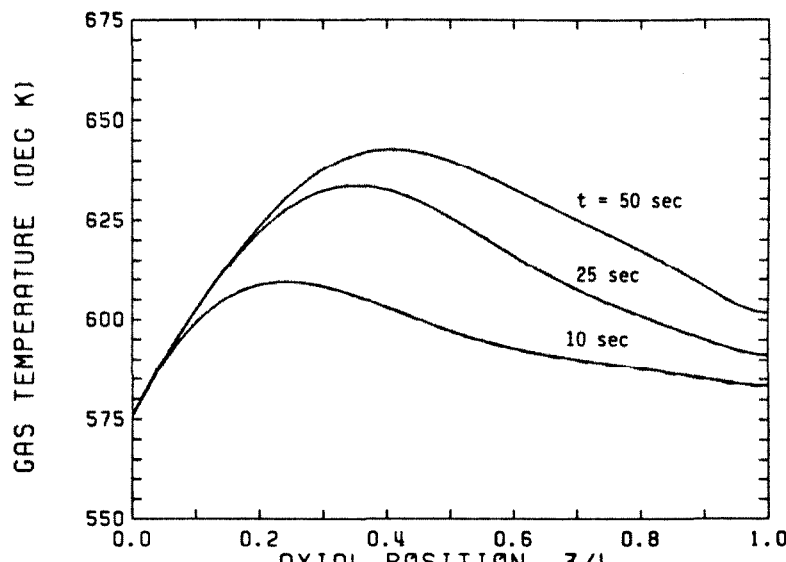
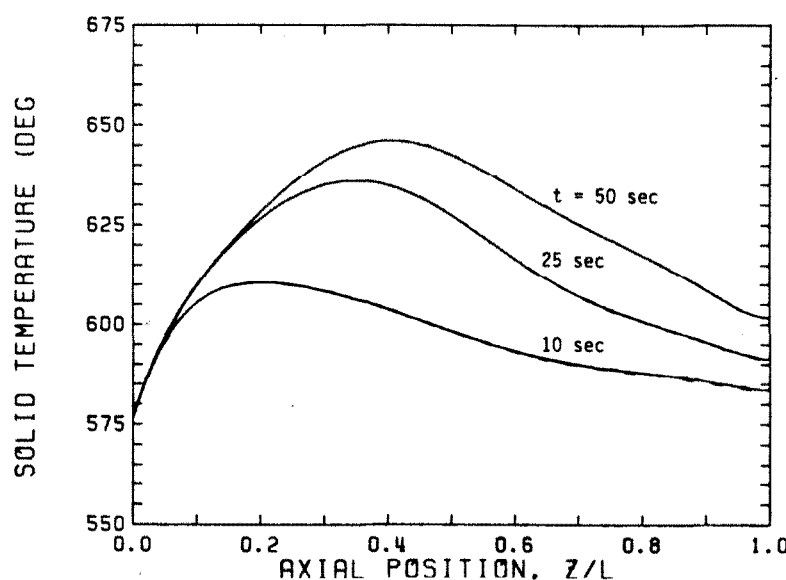


Figure 3.7-8
Transient Temperature Responses to Step Input Change
Standard Type II (Table 3.4-5) Conditions
(T_0 from 573° K to 593° K, x_{CO} from 0.06 to 0.07)

— Catalyst - - - Gas



(a)

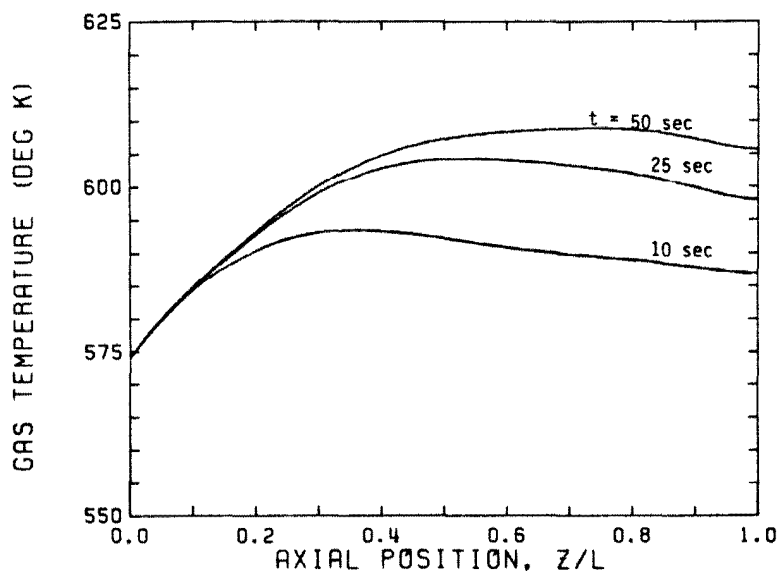


(b)

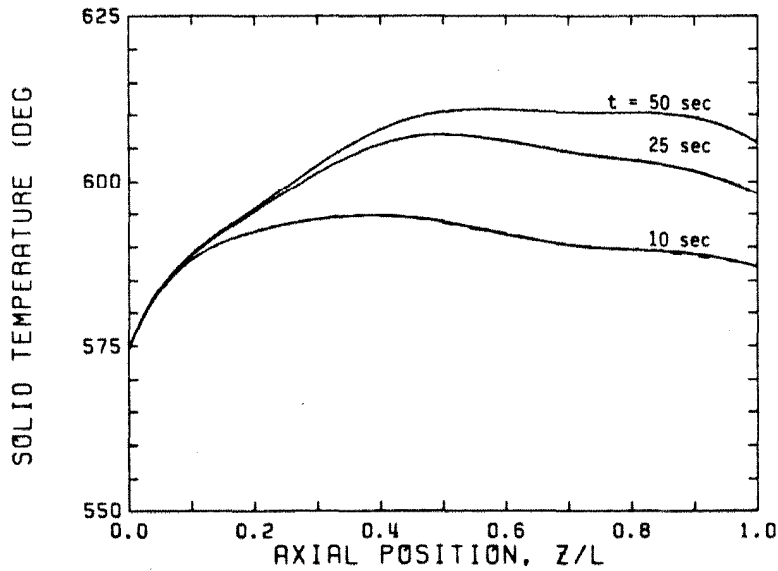
Figure 3.7-9
Transient Axial Temperature Profiles - Start-Up Simulation
Standard Type I (Table 3.4-5) Conditions

a. Gas Temperatures b. Solid Temperatures

- Full Linear Model
- - - Quasi Steady State for Concentration
- - - Negligible Accumulation of Energy in Gas



(a)



(b)

Figure 3.7- 10
Transient Axial Temperature Profiles - Start-Up Simulation
Standard Type II (Table 3.4-5) Conditions

a. Gas Temperatures b. Solid Temperatures

- Full Linear Model
- - - Quasi Steady State for Concentration
- - - Negligible Accumulation of Energy in Gas

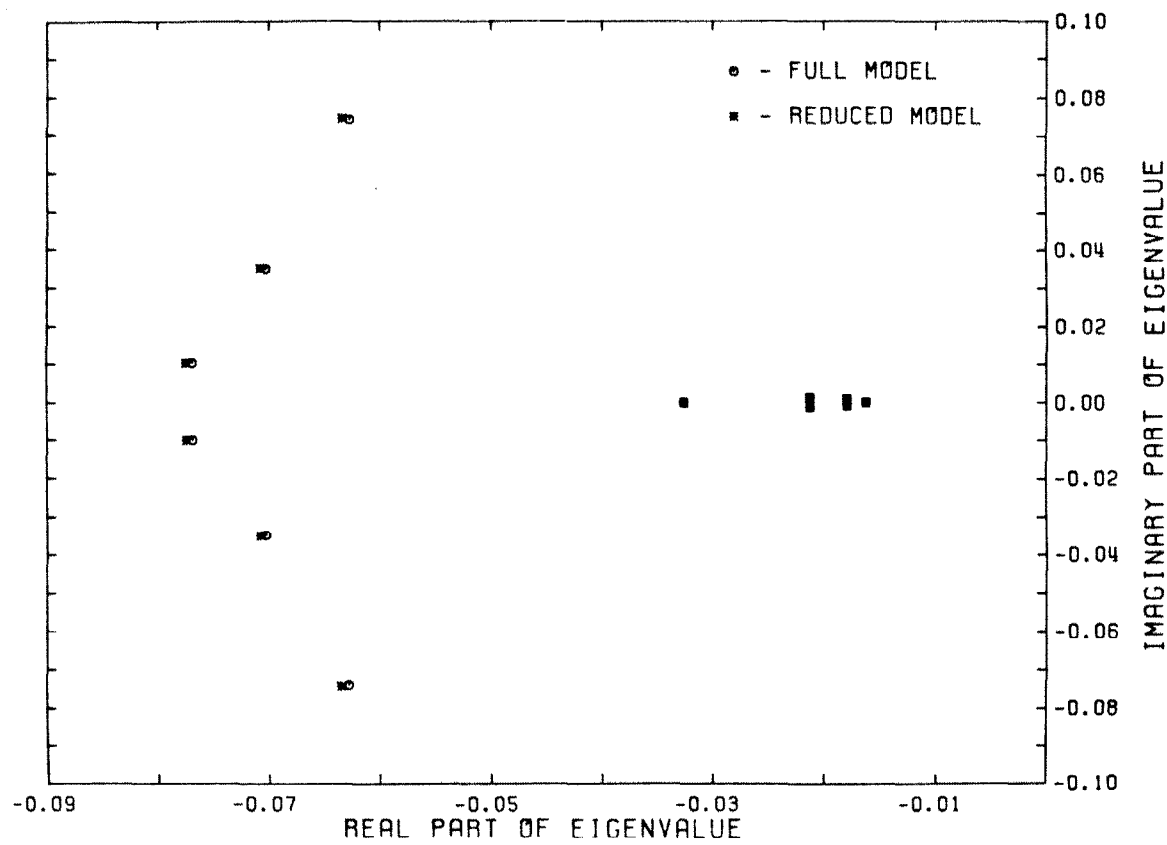


Figure 3.7-11
Dominant Eigenvalues of the Models
Standard Type II (Table 3.4-5) Conditions

Chapter 4

RESULTS AND DISCUSSION

OF FUTURE EXPERIMENTAL STUDIES

4.1 CONCLUSIONS OF CURRENT ANALYSIS

This thesis provides the basis for a concerted theoretical and experimental program in multivariable process control structure design for packed bed chemical reactors by presenting an in-depth control analysis of a practical, multivariable, distributed parameter system—the heat conduction problem defined by the simple diffusion equation—using both frequency-domain and time-domain analyses and the formulation, numerical solution, and analysis of a detailed model for packed bed reactors, along with reduction to a low-order state-space representation suitable for on-line process control.

The first portion of this work presented in Chapter 2 centers on the control aspects of a one-dimensional, two-input heat conduction system. In particular, an analysis of a number of multivariable process control strategies, including non-interacting control, optimal control, inverse Nyquist array, and characteristic locus techniques, is carried out theoretically. The significant results of this study are discussed in Section 2.8 and only the major conclusions are outlined here.

The study of the heat conduction system allowed for a careful study of various control design techniques. Of all of the ones considered, the characteristic locus procedure seems to have the most potential for this particular distributed parameter system. This scheme provides a systematic, computer-aided design strategy in terms of high and low frequency compensation that leads to an excellent, proportional-integral controller. The study also considers the relation between measurement structure and control system design. The choice of measurements and their locations significantly affects the optimal control design and the usefulness of the different design techniques. The importance of 'extra' measurements—those in excess of the number required in the feedback

loop—for improving the system response is also shown. The additional information on the process contained in these measurements can be used in a variety of ways, including reducing the interaction in the control system through the technique of inner-loop decoupling which is proposed in this work. Finally, the analysis of the heat conduction problem clearly shows the importance of an accurate process model and the necessity of model reduction to a low-order state-space representation for control structure design and implementation.

Based on these preliminary results, the second portion of this study provides a detailed mathematical modeling analysis of packed bed catalytic reactors that significantly extends previous studies in the detail of the model and in the consideration of all aspects of the model development and reduction to a state-space control representation. Explicit consideration of common simplifications is then presented, and the validity of these assumptions is assessed in light of their effects and overall benefits. The general view that modeling simplifications are desired since they lead to a reduction in numerical solution effort is contested, and it is shown that many simplifications are no longer necessary with today's advanced computational capabilities. A unified approach to dynamic reactor modeling is developed and its importance in the accurate description of dynamic and steady state reactor behavior, in the investigation of reactor start-up or the effects of process disturbances, and in the development of an accurate reduced state-space model for the design of control structures to stabilize the reactor under various disturbances or to provide optimal system recovery from input changes is shown.

The basic results from this modeling study can be broken down into four major classifications which are now discussed in detail.

Dynamic Modeling

A detailed two-dimensional, two-phase dynamic mathematical representation of packed bed chemical reactors is developed without any major *a priori* simplifications. The model accurately accounts for multiple chemical reactions, axial and radial diffusion of mass and energy, property variations due to temperature, pressure, and mole changes, and an axial thermal well. Detailed analysis shows the importance of the heterogeneous analysis for highly exothermic reaction systems, especially for control applications due to significant temperature differences between the gas and catalyst as a result of differences in the heat flow through each of the phases radially to the cooling jacket. Although a homogeneous analysis may be satisfactory for adiabatic or steady state analyses, the equivalent reduction in system dimensionality and thus solution time is available through other somewhat milder assumptions.

Radial temperature gradients were found to be important, although radial concentration gradients were shown to be quite small. Radial energy diffusion must be retained in the model since this is the basic mechanism for transfer of energy from the reactor bed to the outer cooling jacket. Although radial and axial mass diffusion are of minor importance if the aspect ratios for the reactor are sufficient, their inclusion in the detailed mathematical model does not increase its dimensionality. Finally, axial thermal diffusion should not be neglected since this assumption can lead to inaccuracies and since eliminating the axial thermal diffusion terms may significantly increase numerical solution time or may lead to instabilities in the solution procedure.

Numerical Solution

The orthogonal collocation technique of reducing the partial differential equations to ordinary differential equations is the best available method except for conditions with sharp profiles or abrupt profile changes. In such cases, the orthogonal collocation on finite elements procedure is recommended. This thesis provides the first analysis of a packed bed reactor using orthogonal collocation on finite elements. These techniques are far superior to finite difference procedures since only a fraction of the number of grid points is necessary, leading to a model of much smaller dimensionality. The number of collocation points necessary for accurate representation of the profiles has a major effect on the dimensionality of the resulting system of ordinary differential equations and thus on the numerical solution time. Simulations and eigenvalue analyses using the model developed in this work show that as few as six axial collocation points may be satisfactory for packed bed analyses. Further analysis shows that, if the order of the approximating polynomial is increased beyond that necessary for accurate representation of the solution, oscillations of the polynomials between the collocation points can become quite large. Since these polynomials are used for approximating derivatives in the partial differential equations, these oscillations or 'rippling' can be very detrimental to the solution.

Far fewer collocation points are required for the radial than for the axial profiles. The radial temperature profiles are accurately modeled by a quadratic function. Thus with the boundary points at the thermal well and the outer cooling wall, only one interior radial collocation point is needed for the thermal profiles. However, using one radial collocation point for the radial concentration profiles inherently assumes a uniform

radial concentration profile due to the zero flux boundary conditions. Although assuming a flat radial concentration profile is not identical to a cubic or quartic representation, differences are extremely small and definitely negligible in light of the increased system dimensionality of a higher-order representation.

In addition to the comparatively small dimensionality of the resulting ordinary differential equation system, other important benefits of the orthogonal collocation scheme are that the collocation points and trial functions are selected automatically and optimally and that the solutions are derived in terms of their values at the collocation points and at these points the solution is exact. One of the drawbacks of the orthogonal collocation on finite elements technique is the non-trivial problem of optimal selection of the number and position of the elements.

Control Model

An accurate state-space representation including all expected control and disturbance terms is obtained through analytic linearization of the reaction rate expressions, algebraic equations, and ordinary differential equations obtained from the original mathematical model of the packed bed reactor. Simple adjustments to this representation allow specific control considerations. Simulations of this linearized state-space model show it to be very accurate even at conditions relatively far from the steady state around which the linearization was performed. For sustained step input changes, relinearization around the new steady state is probably desired. With the accuracy of this linearized model and the significant reduction in solution time, there is relatively little incentive for retaining the nonlinear representation in most considerations.

Two techniques were found to be effective in reducing the dimensionality of the linear state-space representation for on-line control. Both procedures provided accurate model reduction to a $2N$ th-order model.¹ Direct modal reduction using Davison's (1966) procedure of retaining only the dominant modes is satisfactory for the packed bed model but can lead to possible steady state offset. Marshall's (1966) technique retains the steady state characteristics by neglecting the dynamics of the non-dominant modes. The $2N$ th-order model developed with this procedure retains the catalyst and thermal well dynamics and accurately simulates the performance of the full linear model for a large range of input changes and disturbances.

Packed Bed Reactor Behavior

The dynamic behavior of the packed bed reactor is dominated by the catalyst and thermal well due to their large thermal capacitance relative to the gas phase. The importance of the thermal well is minimal at steady state in terms of conversion within the reactor. Its significant effect is in the dynamics of the reactor. It does have a slight effect on the steady state temperature profiles by conducting heat axially.

Finally, simulations showed that radial temperature gradients are significant and that a 'hot spot' develops in the bed under conditions of rapid conversion. Furthermore, classical problems with 'wrong-way' behavior where increases in the inlet gas temperature produce a decrease in the outlet gas temperature are predicted. Obviously this can lead to significant control difficulties if the control design is based on the outlet gas temperature.

1. Where N is the number of axial collocation points.

Thus the major development effort in this work has been the careful mathematical modeling of the experimental reactor system and detailed analysis of modeling assumptions, numerical solution techniques, parameter sensitivity, model linearization, and model reduction using kinetic expressions based on literature studies and preliminary experimentation and heat transfer values obtained from standard correlations or published results. Other parameters are calculated directly from the physical properties of the gas and reactor system. Using these parameters, significant contributions in the area of packed bed reactor modeling and control model development have been possible, along with insight into expected operational and optimization difficulties of the laboratory experimental reactor system. The generality of the model developed in this analysis allows its use for various packed bed chemical reactors including those under adiabatic operation and those without an axial thermal well.

As mentioned previously, this study really provides a basis and a unified approach to packed bed modeling. An outline of this approach is as follows:

- The initial model development for dynamic and steady state analysis of packed bed reactors should include detailed consideration of all major physical and chemical phenomena within the system based on general mass and energy balances. With current numerical techniques, minimal *a priori* simplifications are needed. Include all dispersion effects, parameter variations due to temperature, pressure and mole changes, and axial variations in fluid velocity. The model should be heterogeneous and include both the radial and axial analysis. All potential reactions should be included in the model. If a thermal well is used for temperature measurements, its analysis should also be included.
- Nondimensionalize the equations with respect to the inlet steady state con-

ditions and the characteristic time for the reactor.

- Apply radial orthogonal collocation with one interior collocation point.

Then apply axial collocation using Lagrangian polynomials of degree N^2

- Use standard numerical techniques to simulate the behavior of this full nonlinear system of ordinary differential equations. Investigate the predicted behavior of the packed bed system. Check the applicability of the assumptions of negligible axial and radial mass diffusion.
- Linearize the reaction rate expressions, the algebraic equations, and the ordinary differential equations around the steady state. Replace all variables with deviation variables. This should result in a general state-space representation. Compare simulations of the linear model to the original nonlinear model.
- Consider the optimal model dimensionality by comparing simulations with differing number of axial collocation points and by plotting the behavior of the major eigenvalues as a function of the number of collocation points.
- Reduce the dimensionality of the model if necessary using Davison's (1966) or Marshall's (1966) modal technique.
- Finally, estimate the model parameters from experiments and compare the model simulations to empirical results. Incorporate nonuniform radial velocity profiles and more detailed pressure relations into the model if necessary.

In addition to the analyses of control model development, the current studies provide the mathematical tools necessary to develop and study control structures for the reactor system in our laboratory. These studies are currently

2. If sharp profiles or abrupt changes in the profiles are expected, use orthogonal collocation on finite elements instead.

in progress. The remainder of this chapter briefly outlines some of the experimental work in progress along with the applications for the models developed in this work.

4.2 PARAMETER ESTIMATION AND MODEL VERIFICATION

Before control studies can be performed using the control model developed in this work and before the implementation of these feedback control structures on the experimental reactor system, careful parameter estimation is necessary. Although many parameters necessary for the mathematical model can be calculated directly from physical considerations, the reaction and heat transfer parameters must be measured directly for the experimental system. If we neglect the radial and axial mass dispersion and the gas/solid heat transfer in the axial boundary conditions and assume similar heat transfer coefficients between the gas and solid and the reactor wall at both sides of the annulus ($r = R_0$ and $r = R_1$), the resulting dimensionless parameters in the model are shown in Table 4.2-1. We can then divide the necessary input parameters for the model into groups as shown in Table 4.2-2. Of course in addition to these parameters, we do need to specify the operating conditions such as inlet concentrations, pressures, cooling fluid temperature and inlet gas temperature.

The physical reactor parameters are measured for the experimental reaction system. The void fraction must be empirically determined for the specific catalyst used in the experiments due to differences in catalyst crushing. The catalyst for the preliminary experiments is standard Girdler G-65 methanation catalyst, and the thermal well is stainless steel (Type 304). Their physical properties are readily available as discussed in Section 3.4.1. Data are also available for the methanation and steam-shift reactions for heats of reaction and equilibrium constants. As discussed in Section 3.4.1, linear regression of the data is performed over the expected temperature ranges of operation to determine linear temperature relationships for the heats of reaction and relationships based on van't Hoff's equation for the equilibrium constants.

Aspect Ratios

$$\text{axial } n = L/d_p \quad \text{radial } m = R_1/d_p \quad \text{overall } a = L/R_1$$

Axial Dispersion

$$\alpha_s = \frac{k_{ss}}{\bar{u}_{g_0} c_{p_s} \rho_s (1-\varepsilon) L} \quad \alpha_g = (Pe_{zh} \varepsilon n)^{-1} \quad \alpha_t = \frac{k_t}{\rho_t c_{p_t} \bar{u}_{g_0} L}$$

Radial Dispersion

$$\beta_s = \frac{k_{rs}}{\rho_s c_{p_s} (1-\varepsilon) R_1^2 \bar{u}_{g_0}} \quad \beta_g = \frac{a}{Pe_{rh} \varepsilon m}$$

Heat Transfer

$$\gamma_s = \frac{U_{sg} L}{\bar{u}_{g_0} V_b \rho_s c_{p_s} (1-\varepsilon)} \quad \gamma_{ts} = \frac{U_{ts} L}{V_t \rho_t c_{p_t} \bar{u}_{g_0}} \\ \gamma_g = \frac{U_{sg} L}{\bar{u}_{g_0} V_b \bar{\rho}_{g_0} \bar{c}_{p_g} \varepsilon} \quad \gamma_{tg} = \frac{U_{tg} L}{V_t \rho_t c_{p_t} \bar{u}_{g_0}}$$

Heats of Reaction

$$\kappa_1 = \frac{L(-\Delta H_{M_2}) P_{t_0}^{1.5} (\bar{X}_{H_2}^0)^5 \bar{X}_{CO}^0 k_{o_M}}{\bar{u}_{g_0} c_{p_s} \bar{T}_0} \quad \kappa_2 = \frac{L(-\Delta H_{S_2}) \bar{X}_{CO_2}^0 \bar{X}_{H_2}^0 k_{o_S}}{\bar{u}_{g_0} c_{p_s} \bar{T}_0}$$

Reaction Coefficients

$$\sigma_1 = \frac{\bar{M}_{g_0} L \rho_s (1-\varepsilon) P_{t_0}^{1.5} (\bar{X}_{H_2}^0)^5 k_{o_M}}{\varepsilon \bar{\rho}_{g_0} \bar{u}_{g_0}} \quad \sigma_3 = \frac{\bar{M}_{g_0} L \rho_s (1-\varepsilon) \bar{X}_{H_2}^0 k_{o_S}}{\varepsilon \bar{\rho}_{g_0} \bar{u}_{g_0}} \\ \sigma_2 = \frac{\bar{M}_{g_0} L \rho_s (1-\varepsilon) \bar{X}_{H_2}^0 \bar{X}_{CO_2}^0 k_{o_S}}{\varepsilon \bar{\rho}_{g_0} \bar{u}_{g_0} \bar{X}_{CO}^0}$$

Biot Numbers

$$\lambda_{gzs} = \frac{h_{sg} L}{k_{ss}} \quad \lambda_{wrs} = \frac{h_{ws} R_1}{k_{rs}} \quad \lambda_{sgg} = \frac{h_{sg} L}{k_{sg}} \quad \lambda_{wrg} = \frac{h_{wg} R_1}{k_{rg}}$$

Table 4.2-1
Dimensionless Parameters

Reactor	ε	L	R_0	R_1
Catalyst	c_{p_s}	ρ_s	k_s	d_p
Thermal Well	c_{p_t}	ρ_t	k_t	
Heat Transfer	U_{ag} λ_{wrg}	U_{ws} λ_{gzs}	U_{wg} λ_{wts}	Pe_{rg} λ_{wrg}
Heat of Reaction	ΔH_{M_1}	ΔH_{M_2}	ΔH_{S_1}	ΔH_{S_2}
Equilibrium Constant	K_{PM_1}	K_{PM_2}	K_{PS_1}	K_{PS_2}
Reaction Kinetics	k_{o_M} k_{o_S}	E_{aM} E_{aS}	K_1 f_1	K_2 f_2

Table 4.2-2
Input Parameters for the Mathematical Model

The remaining parameters for the mathematical description of the experimental system are the heat transfer variables and the reaction kinetics. These remaining parameters need to be estimated from preliminary experiments for the specific catalyst and reactor bed. The strategy for this parameter estimation is shown in Figure 4.2-1. Due to the large number of parameters necessary for the mathematical description of the experimental system, simultaneous estimation of all parameters from preliminary experiments in the methanation reactor is not feasible. Instead the estimation is split into three stages. The

kinetic parameters (and the actual kinetic expression) are first estimated using a specially constructed kinetics reactor. This reactor system and the determination of the kinetic expression are discussed by Strand (1984). Preliminary results based on limited experiments were discussed earlier, along with their effect on the numerical solution of the mathematical model. The rate was found to be very fast and highly temperature dependent, leading to potential difficulties in numerical simulations due to very steep axial temperature and concentration profiles and complete conversion early in the reactor bed. These difficulties can be reduced by using the orthogonal collocation on finite elements solution technique rather than simple orthogonal collocation. Further experimentation is needed for accurate determination of the kinetics expressions, especially in terms of reaction reversibility, temperature dependence, and the importance of the steam-shift reaction.

The heat transfer parameters can first be estimated using experiments without reaction in the bed. These can be performed by measuring temperature responses in the thermal well, in the exit gas, and in the cooling fluid to input (inlet gas temperature, cooling fluid temperature, or gas velocity) disturbances or step changes.

Finally, all estimated parameters, except those that are found to be highly insensitive, can be updated from experiments in the methanation reactor operating under desired conditions. This parameter estimation is currently in progress.

A sensitivity analysis was also performed to evaluate how accurately some of the parameters must be determined. This analysis should be used in conjunction with a correlation analysis of the model parameters. The major heat transfer parameters were increased and decreased by twenty percent individu-

ally, and the kinetic parameters were changed by ten percent. The dynamic sensitivity is evaluated by the effect of the changes on the major eigenvalues; whereas, the steady state sensitivity is evaluated by the effect of the changes on the steady state profiles and the outlet temperatures and concentrations.

Table 4.2-3 shows results for the standard Type II (Table 3.4-5) conditions. The major parameters affecting the dynamic behavior of the system are those related to the thermal well, thus verifying earlier conclusions as to the importance of the well on the dynamics of the system. For steady state behavior, the methanation reaction parameters are of most importance.

	DYNAMIC				STEADY STATE			
	-Real λ_1		-Real λ_2		T_{out}		$x_{\text{CO}_{\text{out}}}$	
	+20%	-20%	+20%	-20%	+20%	-20%	+20%	-20%
U_{eg}	0.0165	0.0165	0.0172	0.0172	609	609	0.0370	0.0368
U_{ts}	0.0167	0.0164	0.0173	0.0170	609	609	0.0369	0.0369
U_{tg}		0.0133		0.0141	609.	609.	0.0369	0.0369
λ_{gzs}	0.0165	0.0165	0.0172	0.0172	609.	609.	0.0369	0.0369
λ_{sgz}	0.0165	0.0165	0.0172	0.0172	609.	609.	0.0369	0.0369
λ_{trz}	0.0164	0.0167	0.0170	0.0174	609.	610.	0.0369	0.0368
λ_{trg}	0.0155	0.0177	0.0162	0.0183	605.	615.	0.0373	0.0364
P_{ehz}	0.0166	0.0165	0.0172	0.0172	609.	609.	0.0369	0.0369
P_{ehr}	0.0167	0.0164	0.0173	0.0170	616.	602.	0.0363	0.0376
	+10%	-10%	+10%	-10%	+10%	-10%	+10%	-10%
k_{O_M}	0.0165	0.0165	0.0172	0.0172	609.	609.	0.0368	0.0369
k_{O_S}	0.0165	0.0165	0.0172	0.0172	612.	606.	0.0347	0.0392
K_1	0.0165	0.0165	0.0172	0.0172	609.	610.	0.0375	0.0362
K_2	0.0165	0.0165	0.0172	0.0172	608.	611.	0.0381	0.0355
E_{aM}	0.0166	0.0165	0.0173	0.0171	595.	622.	0.0473	0.0223
E_{aS}	0.0165	0.0165	0.0172	0.0172	609.	609.	0.0371	0.0358

Table 4.2-3
Parameter Sensitivity

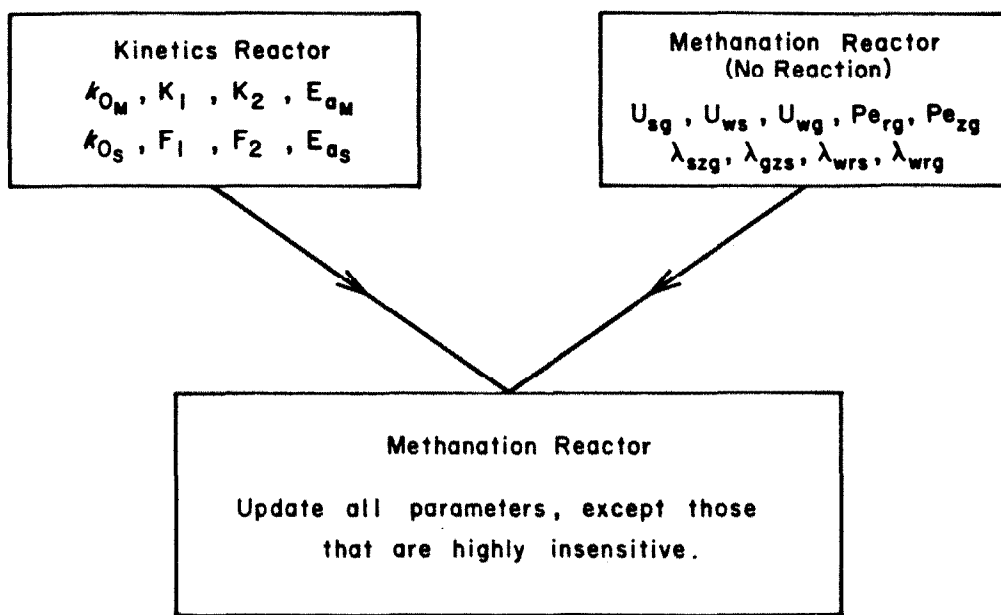


Figure 4.2-1
Parameter Estimation Strategy

4.3 CONTROL MODEL CONFIGURATION

In this section, we consider reconfiguring the general control model for a specific multivariable control structure. The control configuration shown in Figure 4.3-1 is studied for a single pass configuration of the reactor system. Note that we have also neglected the feed-effluent heat exchanger in this preliminary analysis. Temperature measurements are taken at M points within the reactor bed (using thermocouples within the thermal well). Let us consider the control of the gas temperature at the reactor outlet and at an internal point (possibly the 'hot spot') using the inlet process stream flowrate and the inlet gas temperature as the control variables and with expected disturbances in the inlet CO concentration and the cooling wall temperature. In our experimental system, the control of the process flowrate is really set point control of the three mass controllers with the ratio of hydrogen to carbon monoxide being kept nearly constant (at about 3 to 1). The control of the inlet gas temperature possibly involves a PID scheme with the overall control network controlling the inlet gas temperature setpoint and a local controller on the preheater controlling the actual gas temperature.

Consider the reduced state-space model developed earlier

$$\dot{\mathbf{x}}_1 = \mathbf{A}'\mathbf{x}_1 + \mathbf{W}'\mathbf{w} \quad (4.3-1)$$

where

$$\begin{aligned} \mathbf{x}_1 &= \left[\theta_{s_1}, \dots, \theta_{s_N}, \theta_{t_1}, \dots, \theta_{t_N} \right]^T \\ \mathbf{w} &= \left[\theta_w, v_{g_0}, \theta_o, y_1^0, y_2^0, y_{H_2O}^0, y_{H_2}^0, y_{CH_4}^0 \right]^T \end{aligned} \quad (4.3-2)$$

and the \mathbf{A} and \mathbf{W} matrices are defined as before, Equations (3.7-20) and (3.7-21), and all variables are deviation variables. The variables in the original control and disturbance vector \mathbf{w} then need to be related to the actual control or distur-

bance variables. Θ_w and y_i^o are disturbance variables, and $y_{H_2}^o$ is directly related to y_i^o by $y_{H_2}^o = \gamma y_i^o$ where γ usually equals about 3. This is analogous to a process where the CO/H₂ stream comes from some other process upstream and the ratio between the two remains nearly constant. The variables y_2^o , $y_{H_2O}^o$, and $y_{CH_4}^o$ are not used as either control or disturbance variables in this analysis. The inlet gas temperature Θ_0 is an input variable or is related to the heat to the preheater Q_p . Finally, the gas velocity u_{g_0} is directly related to the input flowrate and gas temperature:

$$u_{g_0} = \frac{F_p}{\rho_{g_0} \pi (R_1^2 - R_0^2) \varepsilon} \quad (4.3-3)$$

where the variables in this equation are dimensional. After nondimensionalization,

$$u_{g_0} = \frac{F_p}{\rho_{g_0}} \quad (4.3-4)$$

or in terms of the input variables

$$u_{g_0} = \frac{\bar{M}_{g_0} \Theta_0 F_p}{28 - 26\gamma \bar{x}_{CO}^o y_i^o} \quad (4.3-5)$$

and after linearization

$$u_{g_0} \approx \alpha F_p + \alpha \Theta_0 + \beta (26\gamma \bar{x}_{CO}^o) y_i^o - 28\beta \quad (4.3-6)$$

$$\text{where } \alpha = \frac{\bar{M}_{g_0}}{28 - 26\gamma \bar{x}_{CO}^o} \quad \beta = \frac{\bar{M}_{g_0}}{(28 - 26\gamma \bar{x}_{CO}^o)^2} \quad (4.3-7)$$

Thus the original state-space representation is reconfigured to the form

$$\dot{x} = Ax + Bu + Dd \quad (4.3-8)$$

$$\text{where } u = [F_p \quad \Theta_0]^T \quad d = [\Theta_w \quad y_i^o]^T \quad (4.3-9)$$

and all variables are nondimensional and are deviation variables. If the original control and disturbance matrix \mathbf{W} was defined as

$$\mathbf{W} = \begin{bmatrix} \mathbf{W}_1, \mathbf{W}_2, \mathbf{W}_3, \mathbf{W}_4, \mathbf{W}_5, \mathbf{W}_6, \mathbf{W}_7, \mathbf{W}_8 \end{bmatrix} \quad (4.3-10)$$

then the \mathbf{B} and \mathbf{D} matrices are given by

$$\begin{aligned} \mathbf{B} &= \begin{bmatrix} \alpha \mathbf{W}_2 & \alpha \mathbf{W}_2 + \mathbf{W}_3 \end{bmatrix} \\ \mathbf{D} &= \begin{bmatrix} \mathbf{W}_1 & \mathbf{W}_4 + \gamma \mathbf{W}_7 + \beta (26\gamma \bar{x}_{CO}) \mathbf{W}_2 \end{bmatrix} \end{aligned} \quad (4.3-11)$$

Finally we need to consider the measurement structure. For measurements at M points within the thermal well,

$$\mathbf{y} = \begin{bmatrix} \theta_1, \dots, \theta_M \end{bmatrix}^T \quad (4.3-12)$$

where θ_j is the dimensionless temperature of the thermal well at point z_j . Since

$$\theta_t(z_j, t) = \sum_{i=0}^{N+1} \theta_{t,i}(t) l_i(z_j) \quad (4.3-13)$$

and

$$\begin{aligned} \theta_{t,0} &= \theta_0 \\ \theta_{t,N+1} &= -\frac{1}{A_{N+1,N+1}} \left[\sum_{k=1}^N A_{N+1,k} \theta_{t,k} + A_{N+1,0} \theta_0 \right] \end{aligned} \quad (4.3-14)$$

if we let the temperature of the thermal well at $z = 0$ equal the inlet gas temperature, the measurement relationship in terms of deviation variables is

$$\mathbf{y} = \mathbf{Cx} + \mathbf{Fu} \quad (4.3-14)$$

where

$$\begin{aligned} \mathbf{C} &= \begin{bmatrix} \mathbf{0}_{M \times N} & \mathbf{I}_M \end{bmatrix} \\ \mathbf{D} &= \begin{bmatrix} \mathbf{0}_{M \times 1} & \mathbf{I}_M \end{bmatrix} \end{aligned} \quad (4.3-15)$$

$$\mathbf{L}_1 = \begin{bmatrix} l_1(z_1) - \frac{A_{N+1,1}}{A_{N+1,N+1}} l_{N+1}(z_1) & \dots & l_N(z_1) - \frac{A_{N+1,N}}{A_{N+1,N+1}} l_{N+1}(z_1) \\ \vdots & \ddots & \vdots \\ l_1(z_M) - \frac{A_{N+1,1}}{A_{N+1,N+1}} l_{N+1}(z_M) & \dots & l_N(z_M) - \frac{A_{N+1,N}}{A_{N+1,N+1}} l_{N+1}(z_M) \end{bmatrix} \quad (4.3-16)$$

$$\mathbf{L}_2 = \begin{bmatrix} l_0(z_1) - \frac{A_{N+1,0}}{A_{N+1,N+1}} l_{N+1}(z_1) \\ \vdots \\ l_0(z_M) - \frac{A_{N+1,0}}{A_{N+1,N+1}} l_{N+1}(z_M) \end{bmatrix}$$

Thus we have taken the general state-space representation described by Equation (4.3-1) and reconfigured it to the appropriate control model for the particular structure of interest. Consider the somewhat simpler control structure with only one manipulated variable, the inlet gas temperature, to simplify the following discussion. The reduction of the general state-space representation to the specific control model is similar to the above analysis. If we then consider one measurement at $\xi = 0.3$, the \mathbf{B} and \mathbf{C} matrices for standard Type II (Table 3.4-5) with $N = 7$ are

$$\mathbf{B} = \begin{bmatrix} 0.001 \\ -0.00008 \\ 0.00002 \\ -0.00001 \\ 0.000008 \\ -0.000009 \\ 0.000009 \\ 22.18 \\ -5.228 \\ 2.726 \\ -1.733 \\ 1.254 \\ -0.970 \\ 0.903 \end{bmatrix} \quad \mathbf{C} = \begin{bmatrix} 0 \\ 0 \\ 0 \\ 0 \\ 0 \\ 0 \\ 0 \\ 0.018 \\ -0.020 \\ 1.003 \\ 0.014 \\ -0.007 \\ 0.005 \\ -0.003 \end{bmatrix}^T$$

This example shows one of the potential drawbacks of the orthogonal collocation procedure for reducing the partial differential equations to ordinary differential equations. The input matrix \mathbf{B} multiplies the input by the appropriate proportionality constants to indicate the direct effect of an input change on the state variables. From physical considerations, it is known that the only temperatures within the reactor to be affected immediately by the inlet gas temperature are those at the bed entrance. However as shown by the above \mathbf{B} matrix, all state variables (catalyst bed and thermal well temperatures) are predicted by the model to be immediately affected as a consequence of the continuous nature of the polynomial approximations used along the length of the bed. Of course, the major effect of an input disturbance is still to the state variables closest to the bed entrance. Thus, instantaneous changes or sharp gradients moving through the bed cannot be adequately represented by these polynomial functions. Note that the effect on the thermal well temperatures is extremely high due to the assumption that the thermal well at the entrance of the bed is in equilibrium with the inlet gas temperature. A simple change in this boundary condition can reduce this effect if needed.

The **C** matrix further shows the relationship between the measurement at $\zeta = 0.3$ and the state variables. The coefficients in the **C** matrix show the relative effect of each state variable on the measurement. As expected, the dominant effect is of the thermal well temperature at the third collocation point (at $\zeta = 0.297$) since this is closest to the measurement location.

Although we have considered only two relatively simple examples, similar analysis on proposed control structures will be necessary to develop the appropriate control model. This analysis further provides some insight into the behavior of the experimental system and of the proposed control structure.

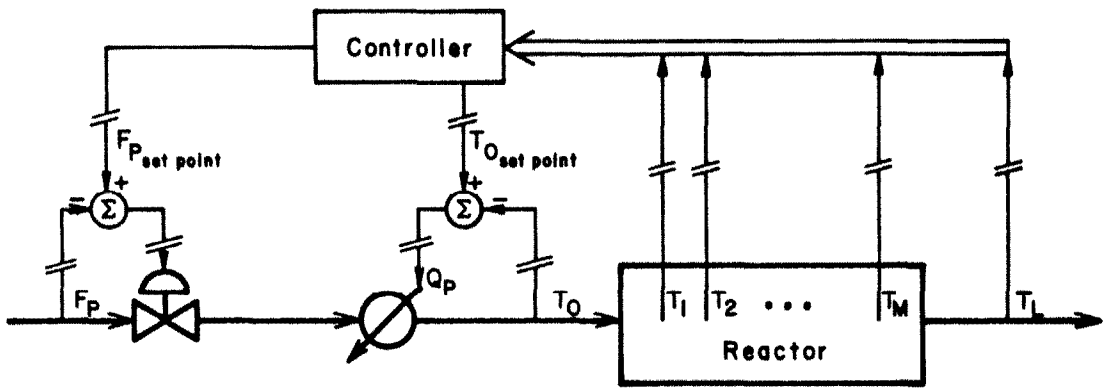


Figure 4.3-1
Control Configuration

4.4 CONTROL SYSTEM DESIGN

As discussed earlier, this thesis provides a basis for a concerted theoretical and experimental effort in multivariable process control structure design for packed bed chemical reactors. Such a control study must center around the basic elements of the control structure:

- the measured variables,
- the manipulated or control variables,
- the control configuration connecting the measured and manipulated variables, and
- the control logic determining the effects of the measurements on the values of the manipulated variables.

In an experimental system such as our methanation reactor, these decisions are by no means easy. It must be determined how to use the large number of potential measurements effectively. Are they all to be used? Or what subset is optimum? In our experimental system, the potential measurements include temperatures at up to 24 axial positions within the thermal well. Temperature measurements are also available elsewhere throughout the reactor system and within the cooling jacket and Dowtherm condenser. These latter measurements probably are not too useful for the control structure but do provide additional information on the operation of the process and can signal problems such as lack of effective flow through the cooling jacket. Another potentially important control measurement is the effluent CO, CO₂, and CH₄ concentrations. Currently these are only available using a gas chromatograph with a delay of up to three or four minutes. Since this is comparable to or slightly longer than the characteristic time constants of the reactor, these concentration measurements may be of little use in dynamic control but may be useful to update the model

parameters periodically. Because effluent concentration measurements are generally available in industrial processes and because they may significantly affect control performance, it is planned that an on-line CO/CO₂ analyzer will be added to the process.

The experimental system also has various possible control or manipulated variables. These include the heat to the preheater, the flowrate of the process stream, the bypass around the preheater and feed-effluent heat exchanger, the ratio of the H₂ to CO in the inlet process stream, and the recycle ratio. The inlet concentrations of other species and the cooling fluid temperature could also be manipulated if desired. Again a number of decisions must be made to select the optimal subset of manipulated variables.

Even after these questions have been answered, careful consideration of the control configuration and control logic is needed to design the control system to handle the large number of potential disturbances (e.g., inlet CO concentration, cooling fluid temperature, flowrates) and to meet the control objectives. For our experimental system, these objectives may include maintaining product quality, minimizing energy usage, minimizing hydrogen usage, and limiting temperature excursions within the bed.

The first step in any proposed control research on a new experimental system must be the application of existing control techniques to the system to assess their performance. Once this has been attempted, an important area of concern that should be studied is that of measurement structures in industrial systems. With all of the possible measured variables, decisions must be made as to the optimal measurement structure. However, since the measurements are such an important part of the overall control system, the measurement structure cannot be chosen independently but must depend on the choice of manipu-

lated variables, the control configuration, the control logic, and even the control objectives. Although various studies have been published on the measurement problem in an open-loop framework (Aidarous et al., 1975; Amouroux et al., 1976; Kumar and Seinfeld, 1978ab), the measurement location problem has been virtually ignored with respect to closed-loop behavior. Some of the work presented in Chapter 2 of this thesis provides a basis for research on the interaction between measurements and control structure. This analysis should be extended to the packed bed reactor with a detailed investigation of the approach to optimal measurement selection in a closed-loop control configuration.

Another potential control technique that should be considered is the evolutionary control structure. This should not be confused with the self-tuning regulator where the controller parameters are recomputed based on updated values of the model parameters. What is proposed here is an extension to the work by Alvarez et al. (1981). They investigated the feasibility of a variable measurement structure for a tubular reactor in which the best set of temperature sensors along the length of the reactor is selected in response to changes in the operating conditions. Moreover, the actual structure of the control system may need to be altered in response to changes in the characteristics of the process during operation. The packed bed reactor system developed by Strand (1984) and modeled in this thesis is an excellent system for the study of such evolutionary structures due to the large number of available measurements and controls, the fully automated nature of the system, and the substantial variance in the operating profiles. The mathematical model developed in this thesis should allow considerable study of the evolutionary control problem prior to actual experimental implementation.

Finally, the control of the packed bed reactor operating with energy and product recycle should be studied. Such systems are common in industry but have generally been neglected in dynamic and control analyses.

APPENDICES

APPENDIX 1

COMPUTER PROGRAMS FOR HEAT CONDUCTION PROBLEM

Many computer programs were written for the analysis of the heat conduction problem for determining root-loci, inverse Nyquist plots, and characteristic loci, for designing control strategies, for producing the necessary computer graphics, and for simulating the behavior of the heat conduction system. Since these programs are not unique but rather are based directly on published theoretical works by various authors, the computer programs are not all duplicated in this thesis. Rather they remain on the Caltech computer in the directory [RRK.HEAT].

However, two programs are presented in this appendix due to their importance in the characteristic locus control design for the heat conduction system. The first program performs the frame alignment for the design of the high frequency compensator. At high frequencies, it is desirable to reduce the misalignment angles between the compensated system's characteristic direction set and the standard basis vectors. This can be accomplished by designing a real compensator K_H that approximates the complex plane of $G_p^{-1}(j\omega)$ at some high frequency ω_h . Program ALIH, listed in Table A1-1, was written for this purpose and uses the routine ALIGN to perform the actual alignment.

At low frequencies, the encirclement criterion should be satisfied and the moduli of the characteristic loci should be large. This can be accomplished by manipulating the loci with an appropriate approximately commutative controller K_L , where $K_L = A\Gamma_k(s)B$ with A and B being the real frame matrices that approximate the complex frame of the eigenvector matrix and dual eigenvector matrix, respectively. Again the routine ALIGN is incorporated into a program.

ALL, for this purpose. This program is listed in Table A1-2. The elements of the diagonal matrix $\Gamma_k(s)$ are then chosen on the assumption that $q_i = g_i k_i$, where q_i and g_i are the eigenvalues of the compensated and uncompensated system and k_i are the elements of $\Gamma_k(s)$. The compensator K_L is thus used to insure stability and integrity and to adjust the gains at low frequency to reduce interaction.

```
C PERFORMS THE FRAME ALIGNMENT FOR DESIGN OF THE HIGH FREQUENCY COMPENSATOR
COMPLEX S,DEL,DET,B(5#,2),Q(5#,2)
DIMENSION Y(2,2),Z(2,2),EVI(2),EVR(2),IND(2),C(2,2),D(2,2)
DATA PI /3.141592654/
W=1000.
READ(5,3)XX1,XX2,W
SQ=SQRT(2.)
C SET UP Q(S)
AA=SQ*COS(PI*XX1)
BB=SQ*COS(2.*PI*XX1)
CC=SQ*COS(PI*XX2)
DD=SQ*COS(2.*PI*XX2)
S=CMPLX(B,B,W)
CALL QSET(S,Q,AA,BB,CC,DD)
CALL IDENT(B,5#,2,1,B)
CALL ALIGN(Q,Y,2)
PRINT 1, W,Y(1,1),Y(1,2),Y(2,1),Y(2,2)

DO 100 I=1,4
CALL ZERO1(EVR,2)
CALL ZERO1(EVI,2)
CALL ZERO1(IND,2)
CALL ZERO2(C,2,2)
CALL ZERO2(D,2,2)
Y1=1.
Y2=1.
IF(I .EQ. 2 .OR. I .EQ. 4)Y1=-Y1
IF(I .EQ. 3 .OR. I .EQ. 4)Y2=-Y2
Z(1,1)=Y1*((1.+SQ*AA+SQ*BB)*Y(1,1) + (1.-SQ*AA+SQ*BB)*Y(2,1))
Z(1,2)=Y2*((1.+SQ*AA+SQ*BB)*Y(1,2) + (1.-SQ*AA+SQ*BB)*Y(2,2))
Z(2,1)=Y1*((1.+SQ*CC+SQ*DD)*Y(1,1) + (1.-SQ*CC+SQ*DD)*Y(2,1))
Z(2,2)=Y2*((1.+SQ*CC+SQ*DD)*Y(1,2) + (1.-SQ*CC+SQ*DD)*Y(2,2))
CALL EIGENP(2,2,Z,EVR,EVI,C,D,IND)
PRINT 2, Y1,Y2,EVR(1),EVI(1),EVR(2),EVI(2)
100 CONTINUE
STOP
1 FORMAT(1H1, //5X,'FREQUENCY =',F18.4, //28X,'MATRIX KH',
      *      5X,E18.3,4X,E18.3/34X,E18.3,4X,E18.3, //5X)
2 FORMAT(18X,'Y1 =',F5.1,3X,'Y2 =',F5.1,6X,'EIGENVALUES OF CBKH',
      *      6X,E9.2,3X,E9.2/62X,E9.2,3X,E9.2//5X)
3 FORMAT(2X,3F5.1)
END

SUBROUTINE ALIGN(V,Y,M)
C THIS ROUTINE ALIGNS THE REAL AND COMPLEX EIGENFRAMES
COMPLEX V(5#,2)
DIMENSION Y(2,2),A(2,2),B(2,2),C(2,2),D(2,2),S(2,2),EVR(2),
      *      EVI(2),IND(2)
DATA EPS /1.0E-16/
DO 100 I=1,2
DO 100 J=1,2
IF(M .EQ. 2) A(I,J)=REAL(V(I,J))
IF(M .EQ. 2) B(I,J)=AIMAG(V(I,J))
IF(M .EQ. 1) A(I,J)=REAL(V(J,I))
IF(M .EQ. 1) B(I,J)=AIMAG(V(J,I))
100 CONTINUE
```

Table A1-1

Computer program ALIH

```

DO 1#4 I=1,2
L=3-I
CALL ZERO1(EVR,2)
CALL ZERO1(EVI,2)
CALL ZERO1(IND,2)
DO 1#1 J=1,2
DO 1#1 K=1,2
C(J,K)=A(I,J)*A(I,K) + B(I,J)*B(I,K)
D(J,K)=A(L,J)*A(L,K) + B(L,J)*B(L,K)
1#1 CONTINUE
DET=D(1,1)*D(2,2) - D(1,2)*D(2,1)
IF(ABS(DET) .LT. EPS)GO TO 5#8
S(1,1)=(C(1,1)*D(2,2) - C(2,1)*D(1,2))/DET
S(1,2)=(C(1,2)*D(2,2) - C(2,2)*D(1,2))/DET
S(2,1)=(C(2,1)*D(1,1) - C(1,1)*D(2,1))/DET
S(2,2)=(C(2,2)*D(1,1) - C(1,2)*D(2,1))/DET
CALL ZERO2(C,2,2)
CALL ZERO2(D,2,2)
CALL EIGENP12,2,S,EVR,EVI,C,D,IND)
IF(EVR(1) .GE. EVR(2))MM=1
IF(EVR(2) .GT. EVR(1))MM=2
IF(M .EQ. 2) Y(1,1)=C(1,MM)
IF(M .EQ. 2) Y(2,1)=C(2,MM)
IF(M .EQ. 1) Y(1,1)=C(1,MM)
IF(M .EQ. 1) Y(1,2)=C(2,MM)
1#4 CONTINUE
RETURN
5#8 PRINT 1#, DET
RETURN
1# FORMAT(1H1,3X,'MATRIX IS SINGULAR',5X,E1#4)
END

SUBROUTINE ZERO1(A,N)
DIMENSION A(N)
DO 1#9 I=1,N
A(I)=#.#
RETURN
END

SUBROUTINE ZERO2(A,N,M)
DIMENSION A(N,M)
DO 1#9 I=1,N
DO 1#9 J=1,M
A(I,J)=#.#
1#9 CONTINUE
RETURN
END

SUBROUTINE QSET(S,Q,A,B,C,D)
COMPLEX Q(5#,2),A1(5#,2),B1(5#,2),RK(2,2)
COMPLEX S,DET
DATA PI /3.141592654/
CALL IDENT(B1,5#,2,1,5)
Q(1,1)=1./S + SQRT(2.)*A/(S+PI**2) + SQRT(2.)*B/(S+4.*PI**2)
Q(1,2)=1./S - SQRT(2.)*A/(S+PI**2) + SQRT(2.)*B/(S+4.*PI**2)
Q(2,1)=1./S + SQRT(2.)*C/(S+PI**2) + SQRT(2.)*D/(S+4.*PI**2)
Q(2,2)=1./S - SQRT(2.)*C/(S+PI**2) + SQRT(2.)*D/(S+4.*PI**2)
RETURN
END

SUBROUTINE IDENT(A,N,M,Z)
COMPLEX A(N,M)
A(1,1)=CMPLX(Z,.#)
A(1,2)=CMPLX(.#,Z,.#)
A(2,1)=CMPLX(.#,Z,.#)
A(2,2)=CMPLX(Z,.#)
RETURN
END

SUBROUTINE MATMULT(A,B,M1,M1,M2,M2)
COMPLEX A(M1,M1),B(M2,M2),C1
C1=A(1,1)
A(1,1)=C1*B(1,1) + A(1,2)*B(2,1)
A(1,2)=C1*B(1,2) + A(1,2)*B(2,2)
C1=A(2,1)
A(2,1)=C1*B(1,1) + A(2,2)*B(2,1)
A(2,2)=C1*B(1,2) + A(2,2)*B(2,2)
RETURN
END

```

Table A1-1 Continued

```
C PERFORMS THE FRAME ALIGNMENT FOR DESIGN OF THE LOW FREQ. COMPENSATOR
COMPLEX S,DEL,DET,X(2,2),Q(2,2),B(5#,2),V(2),C(2,2),A(5#,2)
COMMON XX1,XX2,RH11,RH12,RH21,RH22,RL11,RL12,RL21,RL22,ALPHA
DIMENSION Y(2,2)
LOGICAL*4 WANTX

WANTX=.TRUE.
READ(5,4) IS,XX1,XX2,W,ALPHA,RH11,RH12,RH21,RH22,RL11,RL12,RL21,
1          RL22
PRINT 5,W,ALPHA,RL11,RL12,RH11,RH12,RL21,RL22,RH21,RH22
CALL IDENT (C,2,2,1,8)

C SET UP Q(S)
S=CMPLX(8,0,W)
CALL QSET(S,0)
CALL IDENT (8,5#,2,1,8)

C CALCULATE THE EIGENVALUES AND EIGENVECTORS
CALL EIGENC(2,2,Q,C,V,WANTX,X)
X1=CABS(V(1))
X2=CABS(V(2))
PRINT 1, V(1),X1,V(2),X2,X(1,1),X(1,2),X(2,1),X(2,2)
IF (IS .EQ. 1) STOP

C NORMALIZE EIGENVECTORS
DEL=CSQRT(X(1,1)**2 + X(2,1)**2)
DET=CSQRT(X(1,2)**2 + X(2,2)**2)
A(1,1)=X(1,1)/DEL
A(1,2)=X(1,2)/DET
A(2,1)=X(2,1)/DEL
A(2,2)=X(2,2)/DET

C ALIGN THE REAL AND COMPLEX EIGENFRAMES
CALL ALIGN (A,Y,1)
PRINT 2, Y(1,1),Y(1,2),Y(2,1),Y(2,2)
CALL CSLECD (A,2,B,2,DET,ILL)
CALL ALIGN(B,Y,2)
PRINT 3, Y(1,1),Y(1,2),Y(2,1),Y(2,2)

STOP
1 FORMAT(//////1BX,'EIGENVALUES:', 
*      2(/3BX,F8.2,' + ',F8.2,' I   ('',F7.2,''),///1BX,
*      'EIGENVECTORS:',2(/3BX,2(/3BX,2(F8.3,' + ',F8.3,' I',
*      3X)))
2 FORMAT(//////2BX,'MATRIX B',5X,E1#3.4X,E1#3.33X,E1#3.4X,E1#3.
3 FORMAT(//////2BX,'MATRIX A',5X,E1#3.4X,E1#3.33X,E1#3.4X,E1#3.
*      //////////////)
4 FORMAT(I2,3F5.1/9F8.3)
5 FORMAT(IH1,/////,5X,'FREQUENCY = ',F8.4///15X,'ALPHA = ',F5.1,
*      5X,'KL = ',2F9.3,5X,'KH = ',2F9.3/36X,2F9.3,9X,2F9.3)
END

SUBROUTINE ALIGN(V,Y,M)
C THIS ROUTINE ALIGNS THE REAL AND COMPLEX EIGENFRAMES
COMPLEX V(5#,2)
DIMENSION Y(2,2),A(2,2),B(2,2),C(2,2),D(2,2),S(2,2),EVR(2),
1          EVI(2),IND(2)
DATA EPS /1.0E-3#
DO 1#1 I=1,2
DO 1#2 J=1,2
IF(M .EQ. 2) A(I,J)=REAL(V(I,J))
IF(M .EQ. 2) B(I,J)=AIMAG(V(I,J))
IF(M .EQ. 1) A(I,J)=REAL(V(J,I))
IF(M .EQ. 1) B(I,J)=AIMAG(V(J,I))
1#1  CONTINUE

DO 1#3 I=1,2
L=3-I
CALL ZERO1(EVR,2)
CALL ZERO1(EVI,2)
CALL ZERO1(IND,2)
DO 1#4 J=1,2
DO 1#5 K=1,2
C(J,K)=A(I,J)*A(I,K) + B(I,J)*B(I,K)
D(J,K)=A(L,J)*A(L,K) + B(L,J)*B(L,K)
1#1  CONTINUE
```

Table A1-2

Computer program ALJL

```

DET=D(1,1)*D(2,2) - D(1,2)*D(2,1)
IF(ABS(DET) .LT. EPS)GO TO 555
S(1,1)=(C(1,1)*D(2,2) - C(2,1)*D(1,2))/DET
S(1,2)=(C(1,2)*D(2,2) - C(2,2)*D(1,2))/DET
S(2,1)=(C(2,1)*D(1,1) - C(1,1)*D(2,1))/DET
S(2,2)=(C(2,2)*D(1,1) - C(1,2)*D(2,1))/DET
CALL ZERO2(C,2,2)
CALL ZERO2(D,2,2)
CALL EIGENP(2,2,S,EVR,EV1,C,D,IND)
IF(EVR(1) .GE. EVR(2))MM=1
IF(EVR(2) .GT. EVR(1))MM=2
IF(M .EQ. 2) Y(1,1)=C(1,MM)
IF(M .EQ. 2) Y(2,1)=C(2,MM)
IF(M .EQ. 1) Y(1,1)=C(1,MM)
IF(M .EQ. 1) Y(1,2)=C(2,MM)
114  CONTINUE
RETURN
555  PRINT 10, DET
RETURN
10  FORMAT(////////,3X,'MATRIX IS SINGULAR',5X,E11.4)
END

SUBROUTINE ZERO1(A,N)
DIMENSION A(N)
DO 100 I=1,N
A(I)=0.0
100  RETURN
END

SUBROUTINE ZERO2(A,N,M)
DIMENSION A(N,M)
DO 100 I=1,N
DO 100 J=1,M
A(I,J)=0.0
100  CONTINUE
RETURN
END

SUBROUTINE QSET(S,Q)
COMPLEX Q(2,2),A1(50,2),B1(50,2),RK(2,2)
COMPLEX S,DET
COMMON XX1,XX2,RH11,RH12,RH21,RH22,RL11,RL12,RL21,RL22,ALPHA
DATA PI /3.141592654/

CALL IDENT(B1,50,2,1,0)
SQ=SQRT(2.)
RK(1,1)=ALPHA*RL11/S + RH11
RK(1,2)=ALPHA*RL12/S + RH12
RK(2,1)=ALPHA*RL21/S + RH21
RK(2,2)=ALPHA*RL22/S + RH22
AA=SQ*COS(PI*XX1)
BB=SQ*COS(2.*PI*XX1)
CC=SQ*COS(PI*XX2)
DD=SQ*COS(2.*PI*XX2)
Q(1,1)=1./S + SQ*AA/(S+PI**2) + SQ*BB/(S+4.*PI**2)
Q(1,2)=1./S - SQ*AA/(S+PI**2) + SQ*BB/(S+4.*PI**2)
Q(2,1)=1./S + SQ*CC/(S+PI**2) + SQ*DD/(S+4.*PI**2)
Q(2,2)=1./S - SQ*CC/(S+PI**2) + SQ*DD/(S+4.*PI**2)
CALL MATMULT(Q,RK,2,2,2,2)
RETURN
END

SUBROUTINE IDENT(A,N,M,Z)
COMPLEX A(N,M)
A(1,1)=CMPLX(Z,0.0)
A(1,2)=CMPLX(0.0,Z)
A(2,1)=CMPLX(Z,0.0)
A(2,2)=CMPLX(0.0,Z)
RETURN
END

SUBROUTINE MATMULT(A,B,M1,M1,M2,M2)
COMPLEX A(M1,M1),B(M2,M2),C1
C1=A(1,1)
A(1,1)=C1*B(1,1) + A(1,2)*B(2,1)
A(1,2)=C1*B(1,2) + A(1,2)*B(2,2)
C1=A(2,1)
A(2,1)=C1*B(1,1) + A(2,2)*B(2,1)
A(2,2)=C1*B(1,2) + A(2,2)*B(2,2)
RETURN
END

```

Table A1-2 Continued

APPENDIX 2

NORMALIZED PACKED BED REACTOR MODEL

The normalization of the original mathematical representation of the packed bed reactor is based on

$$\begin{aligned}
 \zeta &= \frac{z}{L} & \Theta &= \frac{T}{T_0} & \rho_g^* &= \frac{\rho_g}{\bar{\rho}_{g_0}} \\
 r &= \frac{r}{R_1} & y_t &= \frac{\hat{x}_t}{\bar{x}_{CO}} & c_{p_g}^* &= \frac{c_{p_g}}{\bar{c}_{p_g}} \\
 \vartheta &= \frac{t \bar{u}_{g_0}}{L} & v_g &= \frac{u_g}{\bar{u}_{g_0}} & \hat{M}_g^* &= \frac{\hat{M}_g}{\bar{M}_{g_0}}
 \end{aligned}$$

Note that in the following normalized equations the (*) is dropped from ρ_g^* , $c_{p_g}^*$, and \hat{M}_g^* and that

$$\begin{aligned}
 \varphi_0 &= \frac{R_0}{R_1} \\
 \rho_g &= \frac{M_g P}{R_g T_g} = \frac{\hat{M}_g \hat{P}}{R_g T_g} \rightarrow \rho_g^* = \frac{\hat{M}_g^* \hat{P}^*}{\Theta_g} \\
 \hat{P}^* &= \frac{\hat{P}}{P_{\zeta=0}} & \tau &= \frac{\hat{P}_{\zeta=1}}{\hat{P}_{\zeta=0}} - 1 \\
 c_{p_g} &= c_{p_{g_1}} T_0 + c_{p_{g_2}}
 \end{aligned}$$

Total mass conservation (continuity):

$$\frac{\partial \rho_g}{\partial \vartheta} + \frac{\partial (\rho_g v_g)}{\partial \zeta} = 0$$

$$\zeta = 0 \quad \rho_g v_g = \rho_{g_0} v_{g_0}$$

Energy balance for the gas:

$$\rho_g c_{p_g} \frac{\partial \Theta_g}{\partial \vartheta} = -\rho_g v_g c_{p_g} \frac{\partial \Theta_g}{\partial \zeta} + \alpha_g \frac{\partial^2 \Theta_g}{\partial \zeta^2} - \gamma_g (\Theta_g - \Theta_s) + \frac{\beta_g}{r} \frac{\partial}{\partial r} \left[r \frac{\partial \Theta_g}{\partial r} \right]$$

$$r = \varphi_0 \quad \frac{\partial \Theta_g}{\partial r} = \lambda_{rg} (\Theta_g - \Theta_t)$$

$$r = 1.0 \quad - \frac{\partial \Theta_g}{\partial r} = \lambda_{wrg} (\Theta_g - \Theta_w)$$

$$\zeta = 0 \quad \frac{\partial \Theta_g}{\partial \zeta} = \lambda_{szg} (\Theta_g - \Theta_s) - \frac{v_{g_0} c_{p_g} \rho_g}{\alpha_g} (\Theta_0 - \Theta_g)$$

$$\zeta = 1.0 \quad - \frac{\partial \Theta_g}{\partial \zeta} = \lambda_{szg} (\Theta_g - \Theta_s)$$

Note that the gas heat capacity, c_{p_g} , gas density, ρ_g , and gas velocity, v_g , are functions of position and time due to their dependence on mole changes, pressure, and temperature.

Energy balance for the catalyst:

Using a similar analysis to that for the energy balance of the gas and after assuming constant physical properties of the solid phase,

$$\frac{\partial \Theta_s}{\partial \vartheta} = \alpha_s \frac{\partial^2 \Theta_s}{\partial \zeta^2} + \frac{\beta_s}{r} \frac{\partial}{\partial r} \left[r \frac{\partial \Theta_s}{\partial r} \right] + \gamma_s (\Theta_g - \Theta_s)$$

$$+ \kappa_1 (1 + \varphi_1 \Theta_{s_1}) R'_M + \kappa_2 (1 + \varphi_2 \Theta_{s_2}) R'_S$$

$$\begin{aligned}
 r = \varphi_0 \quad & \frac{\partial \Theta_s}{\partial r} = \lambda_{trs} (\Theta_s - \Theta_t) \\
 r = 1.0 \quad & -\frac{\partial \Theta_s}{\partial r} = \lambda_{ws} (\Theta_s - \Theta_w) \\
 \zeta = 0 \quad & \frac{\partial \Theta_s}{\partial \zeta} = \lambda_{sg} (\Theta_s - \Theta_g) \\
 \zeta = 1.0 \quad & -\frac{\partial \Theta_s}{\partial \zeta} = \lambda_{sg} (\Theta_s - \Theta_g)
 \end{aligned}$$

Energy balance for the thermal well:

Assuming constant physical properties in the thermal well,

$$\frac{\partial \Theta_t}{\partial \vartheta} = \alpha_t \frac{\partial^2 \Theta_t}{\partial \zeta^2} + \gamma_{ts} (\Theta_{s,r=\varphi_0} - \Theta_t) + \gamma_{tg} (\Theta_{g,r=\varphi_0} - \Theta_t)$$

$$\begin{aligned}
 \zeta = 0 \quad & \Theta_t = \Theta_{t_0} \\
 \zeta = 1.0 \quad & \frac{\partial \Theta_t}{\partial \zeta} = 0
 \end{aligned}$$

Mass balance in the reactor section:

$$\begin{aligned}
 \frac{\partial y_i}{\partial \vartheta} = -v_g \frac{\partial y_i}{\partial \zeta} + \frac{\alpha_m}{\rho_g} \frac{\partial}{\partial \zeta} \left[\rho_g \frac{\partial y_i}{\partial \zeta} + \frac{2\rho_g y_i}{1-2\delta} \frac{\partial \delta}{\partial \zeta} \right] + \frac{\beta_m}{\rho_g r} \frac{\partial}{\partial r} \left[r \rho_g \frac{\partial y_i}{\partial r} + \frac{2\rho_g y_i r}{1-2\delta} \frac{\partial \delta}{\partial r} \right] \\
 + \begin{cases} -\sigma_1 \frac{\Theta_{g_t}}{\hat{P}} R'_M + \sigma_2 \frac{\Theta_{g_t}}{\hat{P}} R'_S & k = 1 \\ -\sigma_3 \frac{\Theta_{g_t}}{\hat{P}} R'_S & k = 2 \end{cases}
 \end{aligned}$$

where

$$\begin{aligned}
 \frac{\partial^2 \delta}{\partial \zeta^2} &= -\bar{x}_1^o \frac{\partial^2 y_1}{\partial \zeta^2} - \bar{x}_2^o \frac{\partial^2 y_2}{\partial \zeta^2} \\
 \frac{\partial \delta}{\partial \zeta} &= -\bar{x}_1^o \frac{\partial y_1}{\partial \zeta} - \bar{x}_2^o \frac{\partial y_2}{\partial \zeta}
 \end{aligned}$$

$$\begin{aligned}
 r = \varphi_0 \quad & \frac{\partial y_i}{\partial r} = 0 \\
 r = 1.0 \quad & \frac{\partial y_i}{\partial r} = 0 \\
 \xi = 0 \quad & \frac{\partial y_1}{\partial \xi} = \frac{v_g}{\alpha_m} (y_1 - y_1^o) \\
 \xi = 1.0 \quad & \frac{\partial y_1}{\partial \xi} = 0
 \end{aligned}$$

In these equations, the dimensionless quantities are defined as follows.

Aspect Ratios

$$\text{axial} \quad n = L/d_p \quad \text{radial} \quad m = R_1/d_p \quad \text{overall} \quad a = L/R_1$$

Axial Dispersion

$$\alpha_g = \frac{k_{zg}}{\bar{\rho}_{g_0} \varepsilon \bar{c}_{p_g} L \bar{u}_{g_0}} = (Pe_{zh} \varepsilon n)^{-1}$$

$$\alpha_s = \frac{k_{zs}}{\bar{u}_{g_0} c_{p_s} \rho_s (1-\varepsilon) L} \quad \alpha_t = \frac{k_t}{\rho_t c_{p_t} \bar{u}_{g_0} L}$$

$$\alpha_m = \frac{D_z}{L \bar{u}_{g_0}} = (Pe_{zm} n)^{-1}$$

Radial Dispersion

$$\beta_s = \frac{k_s}{\rho_s c_{p_s} (1-\varepsilon) R_1^2 \bar{u}_{g_0}} \quad \beta_g = \frac{k_{rg} L}{\bar{\rho}_{g_0} \bar{c}_{p_g} \varepsilon R_1^2 \bar{u}_{g_0}} = \frac{a}{Pe_{rg} \varepsilon m}$$

$$\beta_m = \frac{D_r L}{R_i^2 \bar{U}_{g_o}} = \frac{a}{P e_{rm} m}$$

Heat Transfer

$$\begin{aligned}\gamma_s &= \frac{U_{sg} L}{\bar{U}_{g_o} V_b \rho_s c_{p_s} (1-\varepsilon)} & \gamma_{ts} &= \frac{U_{ts} L}{V_t \rho_t c_{p_t} \bar{U}_{g_o}} \\ \gamma_g &= \frac{U_{tg} L}{\bar{U}_{g_o} V_b \bar{\rho}_{g_o} \bar{c}_{p_g} \varepsilon} & \gamma_{tg} &= \frac{U_{tg} L}{V_t \rho_t c_{p_t} \bar{U}_{g_o}}\end{aligned}$$

Heats of Reaction

$$\kappa_1 = \frac{L(-\Delta H_{M_2}) P_{T_o}^{1.5} (\bar{X}_{H_2}^o)^{.5} \bar{X}_{CO}^o k_{o_M}}{\bar{U}_{g_o} c_{p_s} \bar{T}_o} \quad \kappa_2 = \frac{L(-\Delta H_{S_2}) \bar{X}_{CO_2}^o \bar{X}_{H_2}^o k_{o_S}}{\bar{U}_{g_o} c_{p_s} \bar{T}_o}$$

$$\varphi_1 = \frac{\bar{T}_o (\Delta H_{M_1})}{\Delta H_{M_2}} \quad \varphi_2 = \frac{\bar{T}_o (\Delta H_{S_1})}{\Delta H_{S_2}}$$

Reaction Coefficients

$$\begin{aligned}\sigma_1 &= \frac{\bar{M}_{g_o} L \rho_s (1-\varepsilon) P_{T_o}^{1.5} (\bar{X}_{H_2}^o)^{.5} k_{o_M}}{\varepsilon \bar{\rho}_{g_o} \bar{U}_{g_o}} \\ \sigma_2 &= \frac{\bar{M}_{g_o} L \rho_s (1-\varepsilon) \bar{X}_{H_2}^o \bar{X}_{CO_2}^o k_{o_S}}{\varepsilon \bar{\rho}_{g_o} \bar{U}_{g_o} \bar{X}_{CO}^o} \\ \sigma_3 &= \frac{\bar{M}_{g_o} L \rho_s (1-\varepsilon) \bar{X}_{H_2}^o k_{o_S}}{\varepsilon \bar{\rho}_{g_o} \bar{U}_{g_o}}\end{aligned}$$

Biot Numbers

$$\lambda_{gss} = \frac{h_{sg} L}{k_{zs}} \quad \lambda_{sgs} = \frac{h_{sg} L}{k_{zg}}$$

$$\lambda_{ws} = \frac{h_{ws} R_1}{k_{rs}} \quad \lambda_{wrg} = \frac{h_{wg} R_1}{k_{rg}}$$

$$\lambda_{trs} = \frac{h_{ts}R_1}{k_{rs}} \quad \lambda_{trg} = \frac{h_{tg}R_1}{k_{rg}}$$

Reaction Rates

$$R_M = \rho_s(1-\varepsilon)P_{t_o}^{1.5}(\hat{x}_{H_2})^{.5}\hat{x}_{CO}k_{0_M}R'_M$$

$$R_S = \rho_s(1-\varepsilon)\hat{x}_{CO}\hat{x}_{H_2}k_{0_S}R'_S$$

APPENDIX 3

RADIAL COLLOCATION OF PACKED BED REACTOR MODEL

Gas Phase Radial Temperature Profile

At the three radial collocation points $r = \varphi_0$, r_c , and 1.0, let the gas temperatures be Θ_{g_0} , Θ_{g_r} , and Θ_{g_1} , and assume that the radial profile is quadratic:

$$\Theta_g(\vartheta, \zeta, r) = d_0(\vartheta, \zeta) + d_1(\vartheta, \zeta)r + d_2(\vartheta, \zeta)r^2$$

This profile must satisfy the boundary conditions

$$\begin{aligned}\frac{\partial \Theta_g}{\partial r} \Big|_{r=\varphi_0} &= \lambda_{trg}(\Theta_{g_{r=\varphi_0}} - \Theta_t) \\ \frac{\partial \Theta_g}{\partial r} \Big|_{r=1} &= -\lambda_{wrg}(\Theta_{g_{r=1}} - \Theta_w)\end{aligned}$$

where λ_{trg} and λ_{wrg} are the dimensionless radial Biot numbers at the thermal well and cooling wall, respectively. The profile must also be exact at the three collocation points:

$$\begin{aligned}\Theta_{g_0} &= d_0 + d_1\varphi_0 + d_2\varphi_0^2 \\ \Theta_{g_r} &= d_0 + d_1r_c + d_2r_c^2 \\ \Theta_{g_1} &= d_0 + d_1 + d_2\end{aligned}$$

After rearranging and eliminating Θ_{g_0} and Θ_{g_1} ,

$$\begin{bmatrix} 1 & r_c & r_c^2 \\ \lambda_{trg} & \varphi_0\lambda_{trg}-1 & \varphi_0^2\lambda_{trg}-2\varphi_0 \\ \lambda_{wrg} & \lambda_{wrg}+1 & \lambda_{wrg}+2 \end{bmatrix} \begin{bmatrix} d_0 \\ d_1 \\ d_2 \end{bmatrix} = \begin{bmatrix} \Theta_{g_r} \\ \lambda_{trg}\Theta_t \\ \lambda_{wrg}\Theta_w \end{bmatrix}$$

The expressions for $d_i(\vartheta, \zeta)$ in terms of Θ_{g_r} , Θ_t , and Θ_w can be simply obtained by applying Cramer's Rule. Let

$$\begin{aligned}
 \det &= (\varphi_0 \lambda_{\text{trg}} - 1)(\lambda_{\text{wrg}} + 2) + r_c \lambda_{\text{wrg}} (\varphi_0^2 \lambda_{\text{trg}} - 2\varphi_0) + r_c^2 \lambda_{\text{trg}} (\lambda_{\text{wrg}} + 1) \\
 &\quad - r_c^2 \lambda_{\text{wrg}} (\varphi_0 \lambda_{\text{trg}} - 1) - (\lambda_{\text{wrg}} + 1)(\varphi_0^2 \lambda_{\text{trg}} - 2\varphi_0) - r_c \lambda_{\text{trg}} (\lambda_{\text{wrg}} + 2)
 \end{aligned}$$

Then

$$\begin{aligned}
 d_0 &= w_1 \Theta_{g_r} + w_2 \Theta_t + w_3 \Theta_w \\
 d_1 &= w_4 \Theta_{g_r} + w_5 \Theta_t + w_6 \Theta_w \\
 d_2 &= w_7 \Theta_{g_r} + w_8 \Theta_t + w_9 \Theta_w
 \end{aligned}$$

where

$$\begin{aligned}
 w_1 &= \frac{(\varphi_0 \lambda_{\text{trg}} - 1)(\lambda_{\text{wrg}} + 2) - (\lambda_{\text{wrg}} + 1)(\varphi_0^2 \lambda_{\text{trg}} - 2\varphi_0)}{\det} \\
 w_2 &= \frac{\lambda_{\text{trg}}(\lambda_{\text{wrg}} + 1)r_c^2 - \lambda_{\text{trg}}r_c(\lambda_{\text{wrg}} + 2)}{\det} \\
 w_3 &= \frac{\lambda_{\text{wrg}}r_c(\varphi_0^2 \lambda_{\text{trg}} - 2\varphi_0) - \lambda_{\text{wrg}}(\varphi_0 \lambda_{\text{trg}} - 1)r_c^2}{\det} \\
 \\
 w_4 &= \frac{\lambda_{\text{wrg}}(\varphi_0^2 \lambda_{\text{trg}} - 2\varphi_0) - \lambda_{\text{trg}}(\lambda_{\text{wrg}} + 2)}{\det} \\
 w_5 &= \frac{\lambda_{\text{trg}}(\lambda_{\text{wrg}} + 2) - \lambda_{\text{trg}}\lambda_{\text{wrg}}r_c^2}{\det} \\
 w_6 &= \frac{\lambda_{\text{trg}}\lambda_{\text{wrg}}r_c^2 - \lambda_{\text{wrg}}(\varphi_0^2 \lambda_{\text{trg}} - 2\varphi_0)}{\det} \\
 \\
 w_7 &= \frac{\lambda_{\text{trg}}(\lambda_{\text{wrg}} + 1) - \lambda_{\text{wrg}}(\varphi_0 \lambda_{\text{trg}} - 1)}{\det} \\
 w_8 &= \frac{\lambda_{\text{trg}}\lambda_{\text{wrg}}r_c - \lambda_{\text{trg}}(\lambda_{\text{wrg}} + 1)}{\det} \\
 w_9 &= \frac{\lambda_{\text{wrg}}(\varphi_0 \lambda_{\text{trg}} - 1) - \lambda_{\text{trg}}\lambda_{\text{wrg}}r_c}{\det}
 \end{aligned}$$

Then based on the assumed quadratic profile

$$\frac{\partial \Theta_g}{\partial r} = d_1 + 2d_2 r$$

$$\frac{\partial^2 \Theta_g}{\partial r^2} = 2d_2$$

the dimensionless form of the energy equation for the gas becomes

$$\rho_g c_{p_g} \frac{\partial \Theta_g}{\partial \vartheta} = -\rho_g v_g c_{p_g} \frac{\partial \Theta_g}{\partial \zeta} + \alpha_g \frac{\partial^2 \Theta_g}{\partial \zeta^2} + \beta_g \left[4d_2 + \frac{d_1}{r_c} \right] + \gamma_g (\Theta_s - \Theta_g)$$

where Θ_g and Θ_s are now the temperatures at the radial collocation point r_c , and ρ_g and c_{p_g} are dimensionless parameters, normalized with respect to the inlet steady state values. Then if we let

$$\begin{aligned} \omega_4 &= 4\beta_g w_7 + \frac{\beta_g}{r_c} w_4 - \gamma_g \\ \omega_5 &= 4\beta_g w_8 + \frac{\beta_g}{r_c} w_5 \\ \omega_6 &= 4\beta_g \Theta_w w_9 + \frac{\beta_g}{r_c} \Theta_w w_6 \end{aligned}$$

the energy equation for the gas becomes

$$\rho_g c_{p_g} \frac{\partial \Theta_g}{\partial \vartheta} = -\rho_g v_g c_{p_g} \frac{\partial \Theta_g}{\partial \zeta} + \alpha_g \frac{\partial^2 \Theta_g}{\partial \zeta^2} + \omega_4 \Theta_g + \omega_5 \Theta_t + \gamma_g \Theta_s + \omega_6$$

Catalyst Phase Radial Temperature Collocation

Similar results are obtained for the energy balance of the catalyst using the expression

$$\Theta_s(\vartheta, \zeta, r) = d_0(\vartheta, \zeta) + d_1(\vartheta, \zeta)r + d_2(\vartheta, \zeta)r^2$$

The values for $d_i(\vartheta, \zeta)$ in terms of Θ_{s_r} , Θ_t , and Θ_w are derived as before. Let

$$\begin{aligned}
 \det &= (\varphi_0 \lambda_{trs} - 1)(\lambda_{wrs} + 2) + r_c \lambda_{wrs} (\varphi_0^2 \lambda_{trs} - 2\varphi_0) + r_c^2 \lambda_{trs} (\lambda_{wrs} + 1) \\
 &\quad - r_c^2 \lambda_{wrs} (\varphi_0 \lambda_{trs} - 1) - (\lambda_{wrs} + 1)(\varphi_0^2 \lambda_{trs} - 2\varphi_0) - r_c \lambda_{trs} (\lambda_{wrs} + 2)
 \end{aligned}$$

Then

$$\begin{aligned}
 d_0 &= w'_1 \Theta_{s_r} + w'_2 \Theta_t + w'_3 \Theta_w \\
 d_1 &= w'_4 \Theta_{s_r} + w'_5 \Theta_t + w'_6 \Theta_w \\
 d_2 &= w'_7 \Theta_{s_r} + w'_8 \Theta_t + w'_9 \Theta_w
 \end{aligned}$$

where

$$w'_1 = \frac{(\varphi_0 \lambda_{trs} - 1)(\lambda_{wrs} + 2) - (\lambda_{wrs} + 1)(\varphi_0^2 \lambda_{trs} - 2\varphi_0)}{\det}$$

$$w'_2 = \frac{\lambda_{trs}(\lambda_{wrs} + 1)r_c^2 - \lambda_{trs}r_c(\lambda_{wrs} + 2)}{\det}$$

$$w'_3 = \frac{\lambda_{wrs}r_c(\varphi_0^2 \lambda_{trs} - 2\varphi_0) - \lambda_{wrs}(\varphi_0 \lambda_{trs} - 1)r_c^2}{\det}$$

$$w'_4 = \frac{\lambda_{wrs}(\varphi_0^2 \lambda_{trs} - 2\varphi_0) - \lambda_{trs}(\lambda_{wrs} + 2)}{\det}$$

$$w'_5 = \frac{\lambda_{trs}(\lambda_{wrs} + 2) - \lambda_{trs}\lambda_{wrs}r_c^2}{\det}$$

$$w'_6 = \frac{\lambda_{trs}\lambda_{wrs}r_c^2 - \lambda_{wrs}(\varphi_0^2 \lambda_{trs} - 2\varphi_0)}{\det}$$

$$w'_7 = \frac{\lambda_{trs}(\lambda_{wrs} + 1) - \lambda_{wrs}(\varphi_0 \lambda_{trs} - 1)}{\det}$$

$$w'_8 = \frac{\lambda_{trs}\lambda_{wrs}r_c - \lambda_{trs}(\lambda_{wrs} + 1)}{\det}$$

$$w'_9 = \frac{\lambda_{wrs}(\varphi_0 \lambda_{trs} - 1) - \lambda_{trs}\lambda_{wrs}r_c}{\det}$$

$$\begin{aligned}\omega_1 &= 4\beta_s w'_7 + \frac{\beta_s}{r_c} w'_4 - \gamma_s \\ \omega_2 &= 4\beta_s w'_8 + \frac{\beta_s}{r_c} w'_5 \\ \omega_3 &= 4\beta_s \Theta_w w'_9 + \frac{\beta_s}{r_c} \Theta_w w'_6\end{aligned}$$

The energy equation for the catalyst becomes

$$\frac{\partial \Theta_s}{\partial \vartheta} = \alpha_s \frac{\partial \Theta_s}{\partial \zeta} + \omega_1 \Theta_s + \omega_2 \Theta_t + \gamma_s \Theta_g + \kappa_1 (1 + \varphi_1 \Theta_s) R'_M + \kappa_2 (1 + \varphi_2 \Theta_s) R'_S + \omega_3$$

Thermal Well Energy Balance

We can now relate $\Theta_{s_{r=\varphi_0}}$ and $\Theta_{g_{r=\varphi_0}}$ to the gas and catalyst temperatures at the radial collocation point. If we let

$$\begin{aligned}\omega_7 &= \gamma_{ts} (w'_1 + w'_4 \varphi_0 + w'_7 \varphi_0^2) \\ \omega_8 &= \gamma_{tg} (w_1 + w_4 \varphi_0 + w_7 \varphi_0^2) \\ \omega_9 &= \gamma_{ts} (w'_2 + w'_5 \varphi_0 + w'_8 \varphi_0^2 - 1) + \gamma_{tg} (w_2 + w_5 \varphi_0 + w_8 \varphi_0^2 - 1) \\ \omega_{10} &= \gamma_{ts} \Theta_w (w'_3 + w'_6 \varphi_0 + w'_9 \varphi_0^2) + \gamma_{tg} \Theta_w (w_3 + w_6 \varphi_0 + w_9 \varphi_0^2)\end{aligned}$$

the energy balance for the thermal well becomes

$$\frac{\partial \Theta_t}{\partial \vartheta} = \alpha_t \frac{\partial^2 \Theta_t}{\partial \zeta^2} + \omega_7 \Theta_s + \omega_8 \Theta_g + \omega_9 \Theta_t + \omega_{10}$$

Radial Concentration Collocation

For radial concentration profiles, a quadratic representation may not be adequate since application of the zero flux boundary conditions at $r = \varphi_0$ and $r = 1.0$ leads to $d_1 = d_2 = 0$. Thus a quadratic representation for the concentration profiles reduces to the assumption of uniform radial concentrations, which for a highly exothermic system may be significantly inaccurate. Although

additional radial collocation points greatly increase the dimensionality of the resulting model, they may be necessary to accurately express the radial concentration profiles. A detailed analysis of multipoint radial concentration collocation is presented in Section 3.4.5.

APPENDIX 4

DOCUMENTATION

COMPUTER MODEL OF THE PACKED BED REACTOR

A large variety of programs have been written to model the methanation packed bed reactor and to produce computer graphics of the various profiles on a Zeta plotter or on the Versatec. This documentation describes these programs, the necessary library routines and input data and the command sequences for operation of the programs. This description is complete only for the latest revision (version 4). All previous versions may have some major differences. This revision has been extensively tested under most expected operating conditions. The programs are located in directory [RRK.MOD4]. All important modeling programs are also included in this appendix.

Although the routines involve excellent numerical solution techniques, they may still experience numerical solution difficulties in some cases, due to the extreme complexity of the reactor model. Various parameters have been included so that the user can circumvent these numerical problems, but practice is necessary. In most cases, numerical difficulties will only occur during the steady state solutions due in large part to very bad input profiles for the initial guesses.

MODELING ROUTINES

A two-phase, two-dimensional dynamic model was employed in this analysis, with the assumption that the packed bed may be treated as a continuum insofar

as changes occur smoothly and continuously within each phase throughout the bed. This assumption should be valid under the conditions of the methanation reactor (Hlavacek, 1970) and allows for treating heat and mass fluxes in a form analogous to Fourier and Fick laws.

The original modeling analysis includes all major expected phenomena in the reactor bed. The model accounts for axial and radial dispersion of mass and energy, for mole changes that occur along the bed due to the methanation reaction, and for temperature, pressure, and mole dependencies of gas velocity, density, average molecular weight, and heat capacity, reaction rate constants, and heats of reaction. Additionally, a central axial thermal well is completely modeled, including axial conduction of energy along the well. Finally, the model is based on a three-dimensional (time, axial, and radial) heterogeneous analysis and incorporates the effects of axial pressure gradients.

The primary reaction in the analysis is the methanation reaction with the steam-shift reaction being the only significant side reaction. These reactions have been studied extensively and kinetic information is available. A rate expression for the methanation reaction for conditions similar to those in the present reactor is given by Lee(1973) and Vatcha (1976). A complete analysis of the steam-shift reaction is provided by Moe (1962). Although these rate expressions have been incorporated into the computer model of the system, the programs are written in such a way that the rate expressions can easily be changed simply by replacing one subroutine.

The only major assumptions underlying the original model are:

- Reactor wall temperature is equal to the cooling fluid temperature and is independent of length along the reactor.

- Gas properties are functions of temperature, pressure and total moles as dictated by the ideal gas law.
- There is no radial velocity.
- Global rate expressions are valid.
- Physical properties of the solid catalyst and thermal well are constant.
- Heats of reaction and gas heat capacities are described as linear functions of temperature.

This original model was coded into the programs **MODEL.FOR** and **DIST.FOR** (found in directory [RRK.MOD1] on the CHEMVAX). Further analysis using dynamic simulations to study the effect of making several major simplifications to the model structure are coded into the following programs (also in [RRK.MOD1]).

- a. Negligible energy accumulation in the gas. (**CMODEL1, CM1**)
- b. Quasi Steady state for concentration. (**CMODEL2, CM2**)
- c. Homogeneous analysis. (**CMODEL3, CM3**)

It was concluded from these analyses that the first two assumptions may be quite useful for later model reduction since they lead to minimal inaccuracies in the simulated profiles.

Considerable analysis using these complete modeling algorithms, led to the following conclusions.

- a. The temperature dependence of the heat capacity has very little effect on the simulations.
- b. Mass diffusion has little effect.

- c. The central axial thermal well has little effect on the concentration profiles but significantly alters the transient temperature responses.
- d. Numerical stability of the model solution is greatly enhanced by retaining the thermal dispersive effects.
- e. The assumption of pseudo homogeneity of the system leads to significant discrepancies in the dynamic and steady state profiles.

Finally, a very detailed and careful analysis was made concerning the radial concentration profile. The programs for this analysis are found in [RRK.CONC]. All of these programs use the full nonlinear model with no additional assumptions. A lengthy analysis concluded that the assumption of constant radial concentration profiles in the reactor bed leads to inconsequential differences in the axial bulk concentrations, radial temperatures and axial temperatures.

Thus the final models described in this report include the additional assumptions of constant heat capacity, negligible axial and radial mass diffusion and constant radial concentration profiles.

LA Solution Strategy

The basic relationships taken to describe the system are the continuity equation, the energy balance for the catalyst, the energy balance for the gas, the energy balance for the thermal well, mass balance for CO, mass balance for CO₂ and relationships for the density and pressure changes. These equations are first normalized with respect to the steady state inlet conditions.

The resulting system consists of six coupled, three-dimensional nonlinear partial differential equations, which must be solved to obtain the temperature profiles in the gas, catalyst and thermal well, the concentration profiles and the velocity profile. The technique of orthogonal collocation is used to reduce the

equations to a set of first-order ordinary differential equations in the time domain.

A one point radial collocation is performed. This is quite accurate for temperature profiles since it assumes a quadratic radial representation of the profile. Since the assumed quadratic profile must satisfy the boundary conditions and since the concentration boundary conditions are zero flux conditions, the use of one point radial collocation implicitly assumes constant radial concentration profiles.

Discretization of the resulting system is then performed by orthogonal collocation in the axial direction. Since the position and number of points are the only factors affecting the solution obtained by orthogonal collocation, any set of linearly independent polynomials may be used as trial functions. The Lagrangian polynomials of degree N based on the collocation points z_i are used in this analysis.

The resulting equations are a set of $6N+1$ ordinary differential equations along with eleven algebraic boundary relations, where N is the number of axial collocation points. The solution procedure is further simplified by solving the continuity equation for the velocities as a set of algebraic equations, using temperature values and temperature derivatives obtained from the solutions of the remaining differential equations. Additionally, simple algebraic manipulation allows for explicit solution of seven of the boundary variables. Thus the resulting dynamic model consists of a set of $5N$ coupled ordinary differential equations and $N+5$ coupled algebraic equations.

The solutions of the model are obtained using modified Caltech library routines. The system of ordinary differential equations is solved using a modification of the Caltech routine *MODDEQ* that uses an Adams-Moulton

predictor-corrector technique, with the method of Runge-Kutta-Gill being used to start the integration process. The nonlinear system of algebraic equations is solved using modifications of Caltech's routines *NSES1* and *NSES2*. The first of these uses the standard techniques of inverting the Jacobian matrix but calculates the Jacobian numerically rather than having it input by the user. The second uses Brown's (1967) quadratically convergent algorithm. *NSES1* is a faster routine but is not as numerically powerful as *NSES2*. The modeling programs are written to allow the user to specify which of the two routines to use to calculate the steady state solution. The dynamic solutions always use *NSES1*.

LB Modeling Programs

Several programs were written to perform various types of modeling analyses. All of the programs have been extensively tested and are completely compatible. I.e., they use the same data files, calling formats and library routines and have nearly identical output formats for easy comparison. All of the routines allow for completely arbitrary disturbances and step changes of the cooling wall temperature, linear gas velocity, inlet gas temperature and inlet concentrations of the methane, carbon monoxide, carbon dioxide, water and hydrogen. The routines are very modular, allowing for simple modifications and replacements of reaction equations, output formats, input formats, modeling equations and even solution strategies.

Difficulties may arise during some simulations due to very steep profiles or disturbances. The collocation solution technique has problems with these situations since it assumes a smooth continuous profile along the system. Sharp disturbances or steep-temperature profiles in the system can lead to oscillations in the calculated axial profiles. These problems can usually be reduced by increasing the number of collocation points.

The programs simulate the behavior of the model where the concentrations are normalized with respect only to the inlet steady state concentration of CO. This is better than normalizing with respect to the inlet steady state concentration of the individual species in case one or more of the other inlet steady state concentrations are zero.

a. **NLNMOD**

This program simulates the complete nonlinear solution of the system. The above techniques are combined with a variable time-step analysis to efficiently obtain the dynamic and steady state reactor responses. This variable time-step procedure is automatic and involves increasing the time steps as the system approaches steady state since the derivatives become smaller.

This program must be linked to **MLIB** and **LLIB**. A listing of this program is included in Table A4-1.

b. **LINMOD**

This program performs the simulation for the linearized version of the model, where the model is linearized about the steady state solution. The program thus first calculates the initial steady state solution, based on a user-defined initial guess. The program uses the standard numerical techniques used in **NLNMOD**, including the variable time-step analysis.

The linear system is of order $5N$ with the states being the solid temperatures, gas temperatures, thermal well temperatures, CO concentrations and CO_2 concentrations at the collocation points.

This program must be linked to **MLIB** and **LLIB**. A listing of this program is

included in Table A4-2.

c. **ANAMOD**

This program performs the same simulation as **LINMOD** except that it uses the analytical solution of the linear equations rather than performing a numerical solution. Thus it takes only a fraction of the solution time and does not need the variable time-step analysis. The solution of the equations can be obtained explicitly at any desired time.

This program must be linked to **MLIB**, **ELIB** and **LLIB**. A listing of this program is included in Table A4-3.

d. **RD1MOD**

This program performs the simulations for the reduced linear model using the analytical solution. The assumptions of negligible energy accumulation in the gas and quasi steady state for the concentrations are used to reduce the model to an order of $2N$. The retained states are the solid temperatures and thermal well temperatures at the collocation points.

This program must be linked to **MLIB**, **ELIB** and **LLIB**. A listing of this program is included in Table A4-4.

e. **RD2MOD**

This program performs the simulations for the reduced linear model using the analytical solution. The assumption of quasi steady state for concentration is used to reduce the order of the model to $3N$. The retained states are the solid temperatures, gas temperatures and thermal well temperatures

at the collocation points.

This program must be linked to **MLIB**, **ELIB** and **LLIB**. A listing of this program is included in Table A4-5.

LC Input Variables

The input variables are divided into groups and are described below. The group names given between slashes are the names of the COMMON arrays that the variables are stored in after they are read from the data file.

/REACP/ - REACTOR PARAMETERS

EPS	void fraction (cm**3 void/cm**3 bed)
L	length of reactor bed (cm)
R0	radius of thermal well (cm)
R1	radius of reactor bed (cm)

/CATLS/ - CATALYST PARAMETERS

CPS	heat capacity (cal/g °K)
PS	density (g/cm**3 catalyst)
TC	thermal conductivity (cal/sec cm °K)
DC	characteristic particle diameter (cm)

/THWEL/ - THERMAL WELL PARAMETERS

CPT	heat capacity (cal/g °K)
PT	density (g/cm**3)
KT	thermal conductivity (cal/sec cm °K)

/GASPA/ - GAS PARAMETERS

PTZ axial thermal Peclet number
PTR radial thermal Peclet number
UGS steady state inlet velocity (cm/sec)

/HEATT/ - HEAT TRANSFER PARAMETERS

OHSG heat transfer coefficient(solid-gas)(cal/sec °K)
OHTS heat transfer coefficient(wall-solid)(cal/sec °K)
OHTG heat transfer coefficient(wall-gas)(cal/sec °K)
BSG Biot number (solid-gas)
BGS Biot number (gas-solid)
BTS Biot number (wall-solid)
BTG Biot number (wall-gas)

/OPCON/ - OPERATING CONDITIONS

SCH4 steady state inlet methane mole fraction
SCO steady state inlet carbon monoxide mole fraction
SCO2 steady state inlet carbon dioxide mole fraction
SH2 steady state inlet hydrogen mole fraction
SH2O steady state inlet steam mole fraction
PT0 total inlet pressure (atm)
PT1 total outlet pressure (atm)
ST0 steady state inlet gas temperature (°K)

STW cooling wall temperature (°K)

/REAC1/ - REACTION PARAMETERS

DH1A heat of methanation constant, $DH1 = DH1A * T + DH1B$

DH1B heat of methanation constant (cal/mole)

DH2A heat of water-shift constant, $DH2 = DH2A * T + DH2B$

DH2B heat of water-shift constant (cal/mole)

KOP Arrhenius constant, methanation

K0 Arrhenius constant, water-gas shift

/REAC2/ - ADDITIONAL REACTOR PARAMETERS

KP1A equil constant, methanation, $\ln KP1 = KP1A + KP1B / T$

KP1B equil constant, methanation

KP2A equil constant, water-gas shift $\ln KP2 = KP2A + KP2B / T$

KP2B equil constant, water-gas shift

K2 constant for methanation reaction rate

K3 constant for methanation reaction rate

EA1 activation energy, methanation (cal/g mole)

EA2 activation energy, water-gas shift (cal/g mole)

OTHER INPUT PARAMETERS:

DT0 time step (sec)

N number of axial collocation points

TMAX maximum time (length of simulation) (sec)

RR radial collocation point with $0 < rr < 1$

NEP precision in numerical routines, 10^{**nep}

IFLAG type of initial profile guess

0 values input for const temps, conc, vel

1 entire profiles input

NFLAG steady state algebraic equation solver

1 - NSES1, 2 - NSES2

DL length of disturbance (sec)

IF max time step for variable time stepping is $DT0*4^{**}(IF-1)$

NP number of time steps between printing

These variables are read in under the following format:

READ 1, EPS,L,R0,R1

READ 1, CPS,PS,TC,DC

READ 1, CPT,PT,KT

READ 1, PTZ,PTR,UGS

READ 1, OHSG,OHTS,OHTG,BGS,BSG,BTS,BTG

READ 1, SCH4,SCO,SCO2,SH2,SH2O,PT0,PT1,ST0,STW

READ 1, DH1A,DH1B,DH2A,DH2B,K0,KOP

READ 1, KP1A,KP1B,KP2A,KP2B,K2,K3,EA1,EA2

READ 2, DT0,TMAX,RR,DL,N,NP,NEP,IFLAG,IF,NFLAG

where format 1 is (9f8.2) and format 2 is (4f8.2/6i8). All of these variables may not be necessary for all of the programs but to keep consistency in the input data files they are all included.

Note: Two of the variables change meanings in the different programs so that the values in the data file do not have to altered and so that the outputs of the programs will be identical. These are DTO and NP. In the programs that require numerical solution (**NLNMOD**, **LINMOD**), DTO must be taken very small (around 0.005 second) and then NP is set large so that the profiles are only printed out for every five or ten seconds during the simulation (i.e. NP=1000). However, in the programs that are based on analytical solutions, it is not necessary to take such small steps. If printouts of the solutions are desired for every 5 seconds, then the time steps should be set at 5 seconds. However, this would involve changing the data files if you wanted to run say **NLNMOD** and then compare it to **ANAMOD**. To eliminate this problem, the actual time steps used in the analytical programs are DTO*NP.

After this set of inputs, the user must specify the initial guesses for the steady state calculation as per the type specified by IFLAG:

IFLAG = 0

Input the constant gas temperature, solid temperature, thermal well temperature, CO concentration, CO₂ concentration and velocity under format (6f8.2).

IFLAG = 1

Input the gas temperature, solid temperature, thermal well temperature, CO concentration, CO₂ concentration and velocity at each collocation point under the format (6f8.2) and then the solid temperature at z=0 and z=1, the gas temperature at z=0 and z=1 and the velocity at z=0 under the format (5f8.2). The temperatures must be

entered in nondimensional terms (as is output by the programs) and the concentrations must be based on the inlet number of moles (as is the output). Thus these inputs can be directly taken from one of the output profiles.

Then finally, the type of simulation must be entered. The next input JFLAG tells what type of simulation is being run. This variable is entered under the format (i2).

JFLAG = 0 (step or disturbance)

The step or disturbance vector is then input. The inlet gas velocity, inlet gas temperature, CO concentration, CO₂ concentration, H₂O concentration, H₂ concentration, CH₄ concentration and cooling wall temperature are input under the format (8f8.2).

JFLAG = 1

This is to simulate the behavior of the system starting from any arbitrary profile to steady state. The entire profile should be input just as in IFLAG = 1 above.

A sample data file is shown below and is stored in [RRK.MOD4] as MOD4.DAT. This data file performs a simulation of the system with a step change in the inlet gas temperature from 573° K to 623° K. The simulation is for a step rather than a simple disturbance since DL is set to infinity. The output will show the simulated profiles at 10 second intervals from time 0 to 100 seconds.

0.57	30.0	0.1587	1.194
0.25	1.041	0.005	0.274437
0.12	8.02	0.039	

2.00 8.00 75.00
17.02 0.01795 0.1436 13.09 600.0 7.163 1.25
-6.144 -48350. -2.441 10760. 17.0 0.07524
-29.44 26340. 4.385 -4615. 1.470 0.7348 6950. 18900.
0.005 100.0 0.5 999999.
8 2000 -8 0 3 0
573.0 573.0 573.0 0.06 0.015 75.0
0
75.0 623.0 0.06 0.0150 0.02 0.19 0.60 573.0

LD Other Program Variables

Some of the other variables and arrays used throughout the routines are described below. The minimum dimensions of the arrays are based on the number of collocation points and are also described.

BWG = Biot number (wall-gas) - usually set equal to BTG
BWS = Biot number (wall-solid) - usually set equal to BTS
PGS = steady state inlet density (g/cm**3 gas)
ASG = heat transfer area, gas-catalyst (cm**2)
AST = heat transfer area, thermal well-catalyst (cm**2)
ATG = heat transfer area, thermal well-gas (cm**2)
VT = volume of thermal well (cm**3)
VB = volume of bed (cm**3)
RG = gas constant (cm**3 atm/gmole K)
RGP = gas constant (cal/gmole K)

CPG = heat capacity of gas (cal/g K**2)

MG = average molecular weight (g/g mole)

The following table describes the vectors and matrices used throughout the modeling programs.

NAME	MIN. DIMENSIONS	PURPOSE
A	N+2,N+2	first derivative collocation matrix
AA	5*N,5*N	state matrix 'A'
AI	5*N,5*N	inverse of the state matrix
B	N+2,N+2	second derivative collocation matrix
BB	5*N,8	control matrix 'B'
CC	5*N	AI*(EX-IDENTITY)*Q
DD	5*N	constant matrix 'D'
ET	5*N,5*N	AI*(EX-IDENTITY)
EVR	5*N	real part of eigenvalues
EVI	5*N	imag part of eigenvalues
EX	5*N,5*N	EXP(AA*DT)
R	N+2	vector containing collocation points
RL1	N,9	constants for linearized methanation rate
RL2	N,9	constants for linearized steam-shift rate
SR	5*N,5*N	real part of eigenvectors
SI	5*N,5*N	imag part of eigenvectors
SIR	5*N,5*N	real part of SR,SI inverse
SII	5*N,5*N	imag part of SR,SI inverse
U	8	disturbance or control vector
W	10	radial lumped coefficients
Y	6*N+5	state vector

YS 6*N+5 state vector

The structure of the state matrix (Y) and steady state state matrix (YS) is

1,...,N	Solid temperature at collocation pts
N+1,...,2*N	Gas temperature at collocation pts
2*N+1,...,3*N	Thermal well temperature at collocation pts
3*N+1,...,4*N	CO concentration at collocation pts
4*N+1,...,5*N	CO ₂ concentration at collocation pts
5*N+1,...,6*N+1	Velocities at collocation pts plus z=1
6N+2	Solid temperature at z=0
6N+3	Solid temperature at z=1
6N+4	Gas temperature at z=0
6N+5	Gas temperature at z=1

The structure of the control vector (U) is

- 1 cooling wall temperature
- 2 inlet velocity
- 3 inlet gas temperature
- 4 inlet CO concentration
- 5 inlet CO₂ concentration
- 6 inlet H₂O concentration
- 7 inlet H₂ concentration
- 8 inlet CH₄ concentration

All quantities in the programs except the inputs are nondimensional. However, the programs are not based on deviation variables. Thus the form of the linear model is

$$\dot{\mathbf{x}}(t) = \mathbf{A}\mathbf{x}(t) + \mathbf{B}\mathbf{u}(t) + \mathbf{D}$$

The analytic solution of this equation used by **ANAMOD**, **RD1MOD** and **RD2MOD** is :

$$\mathbf{x}(t_i) = e^{\mathbf{A}(t_i - t_0)} \mathbf{x}(t_0) + \mathbf{A}^{-1} [e^{\mathbf{A}(t_i - t_0)} - \mathbf{I}] [\mathbf{B}\mathbf{u} + \mathbf{D}]$$

This is valid for time t_0 to t_i during which the control is constant.

LE Program Outputs

The program output consists of displaying the input data, the program conditions, the steady state conditions, and the axial collocation points. The initial guess for the steady state solution is then shown with the calculated steady state solution.

The simulated profiles are then printed at the specified intervals up to the total time period. The final steady state, calculated by setting the time derivatives equal to zero in the original simulation and solving the resultant system of algebraic equations is printed. For the linearized cases, this steady state may be significantly in error since the model was linearized about the original steady state and since some of the variables such as MG and CPG are based on the steady state inputs. For this reason, the 'Actual Steady State' is also printed. This is the steady state based on the new conditions.

Table A4-6 show the output using the above data file with TMAX = 5 for an inlet gas temperature step change from 573° K to 623° K.

LIBRARY ROUTINES

Several sets of library routines have been written for the modeling and plotting programs. Some of these routines are modifications of Caltech library

routines. In these cases, the names are unchanged. The user may want to study the Caltech documentation that accompanies these programs. Although most have been changed to clean up portions of the routines not needed in this work, to reduce some of the restrictions, and to work in double precision, the basic techniques remain the same. These libraries are described below with brief descriptions of the various routines in each library. All of these are found in [RRKLIBR].

LLIB.FOR This library contains the many routines necessary for modeling the reactor. All of these routines have been written specifically for the packed bed model and are listed in Table A4-7.

DIMLES calculates the dimensionless parameters.

INITIAL sets up initial profiles.

SETUPS reads the input data, makes preliminary calculations and prints the inputs.

OUTPUT outputs the calculated profiles.

RADIAL calculates the constants for the radially lumped model.

COLLOC calculates the zeros of the orthogonal polynomial and sets up the axial collocation matrices.

INTLSS solves for the initial steady state profile.

FN1 defines the algebraic equations for use by *NSES1* when solving for the steady state.

FN2 identical to *FN1* but is written to be used with *NSES2*.

FN3 defines the steady state linearized equations for *NSES1*.

LREAC calculates the coefficients for the linearized rates.

ASETUP sets up the linearized model including the state matrix

ACTLSS calculates the final steady states.

INSIM initializes the simulation.

OUTCALC calculates the velocities and endpoint temperatures.

CPCALC calculates the gas heat capacity.

ENDPTS calculates the endpoint conditions.

REAC calculates the dimensionless rates.

ELJB.FOR This library is necessary for the calculation of the eigenproperties.

EIGENP calculates the eigenvalues and eigenvectors of a real matrix.

This routine uses the subprograms *SKALE*, *REALVE*, *HESQR*, *COMPVE* that are also included in this library.

MLJB.FOR This library includes various numerical and printing routines.

DFOPR evaluates the discretization matrices for collocation. This routine is from the text by Villadsen and Michelsen.

JCOBI evaluates the roots and derivatives of Jacobi polynomials. This subroutine is from the text by Villadsen and Michelsen.

MODDEQ may be used to solve a system of first-order differential equations.

This routine uses the subprograms *MADAM*, *MGILL*, *MREST*, *MSAVE* that are also included in this library.

NSE1 solves a system of algebraic equations by numerically calculat-

ing the Jacobian and using *MATINV* to invert it.

NSES2 solves a system of algebraic equations using Brown's quadratically convergent algorithm. This routine is slower than *NSES1* but is more powerful.

PRINTS prints the scalars $z(i)$, $i=1, \dots, 8$.

PRINTV prints the vector $z(m)$.

PRINTM prints the matrix $z(n,m)$.

ZEROV zeros the vector $z(m)$.

ZEROM zeros the matrix $z(n,m)$.

NEGCH checks a vector for any negative values, sets the negative value to zero and prints a warning message.

MATINV inverts a matrix.

BNDINV inverts a matrix.

CINVSE inverts a complex matrix.

MATCPY copies a portion of one matrix to another.

MATMULT multiplies two matrices.

ILA PLIB.FOR

This library of routines is necessary for the plotting routines. Several of the programs in this library are identical to those in *MLIB* except that they are written in single precision for the plotting.

JCOBI same as in *MLIB* but in single precision.

DFOPR same as in *MLIB* but in single precision.

INTRP evaluates the Lagrangian interpolation coefficients.

NAXS replaces the Caltech library routine for plotting the x axis.

NYAXIS replaces the Caltech library routine for plotting the y axis.

PLOTTING PROGRAMS

Several programs have been developed for plotting various types of profiles on the Zeta plotter. These programs all must be linked to **PLIB**. All of the routines have slightly differing input data structures. Thus it may be necessary to study the programs before attempting to use them the first time. Many of the variables used by the programs are defined below.

OX,OY - location of the origin on the page

XL,XY - length of the two axes

Y1,Y2 - starting and ending values for the y axis

X1,X2 - starting and ending values for the x axis

XT,YT - distance between tics on the two axes

ID - type of line drawn between the points

IST - 0 if the data is the last line for the plot, 1 if more lines follow

IS - speed of the plotter

N - number of collocation points

The following are the most useful programs. They are in [RRK.PLOT].

PGEN plots a completely general profile.

PLTA plots the axial temperature profiles, given the values at the collocation points.

PLTC plots the axial concentration profile, given the values at the collocation points.

PLTC1 is identical to *PLTC* except that the concentration that is plotted is that based on the inlet number of moles.

PLTCR plots the radial concentration profile.

PLTR plots the radial temperature profile given the values at the collocation points.

PLTT plots the time profiles of the temperature using the spline routines to fit the curve.

PLTTC plots the concentration time profiles using the spline routines to fit the curve.

```

THIS PROGRAM MODELS A NONISOTHERMAL, NONADIABATIC FIXED BED REACTOR
C WITH BOTH A COOLING JACKET AND A THERMAL WELL. THE ANALYSIS IS
C PERFORMED FOR A METHANATION OF CO SYSTEM.

C LINK TO MLIB.LLIBN

C THIS PROGRAMS SOLVES THE FULL NONLINEAR MODEL WITH THE CONCENTRATIONS
C NONDIMENSIONAL W.R.T. THE STEADY-STATE INLET CONC. OF CO

IMPLICIT REAL*8 (A-H,O-Z)
REAL*8 L,KT,MC,KB,KBP,KPIA,KP1B,KC1#,KP2A,KP2B,KC2#,K2P,K3P

COMMON /REACP/ EPS,L,R#,R1
* /CATLS/ CPS,PS,TC,DC
* /THWEL/ CPT,PT,KT
* /GASPA/ CPG,PTZ,PTR,MC,PGS,UGS,UM
* /HEATT/ OHSG,OHTS,ONTG,BGS,BSC,BTS,BTG,BWG,BWS
* /OPCON/ SCH4,SCO,SC02,SH2,SH2D,PTB,PT1,ST#,STW
* /REAC1/ DHIA,DH1B,DH2A,DH2B,K#,K#P
* /DIMLE/ ALS,ALG,ALT,BES,BEG,GAS,GAG,GTS,GTG,DE1,
* DE2,S11,S12,S13,PH12,PH13,PH1,PH2,PH3
* /RADIA/ W(1#),WP(9,2),DETA(2),RR
* /COMATA/ A(25,25),B(25,25),R(25),N
* /MISCI/ UU(1#)
* /REAC2/ KC1#,KPIA,KP1B,KC2#,KP2A,KP2B,K2P,K3P,EA1,EA2
* /LINEA/ AA(75,75),BB(75,8),DD(75),U(8)
* /STATE/ Y(1#),YDOT(1#),ST,DT

EXTERNAL DERIV.FN

C READ IN DATA AND CALCULATE CONSTANTS
  CALL SETUPS (DT#,TMAX,DL,M,RR,EP,IFLAG,NFLAG,NP,IF)

C CALCULATE THE DIMENSIONLESS PARAMETERS
  CALL DIMLES

C CALCULATE CONSTANTS FOR THE RADIAL LUMPED MODEL
  CALL RADIAL

C CALCULATE ZEROS OF THE ORTHOGONAL POLYNOMIAL AND SET UP AXIAL
C COLLOCATION MATRICES A AND B.
  CALL COLLOC

C SOLVE FOR THE STEADY STATE PROFILE
  CALL INTLSS(Y,U,IFLAG,NFLAG,L,UGS,PH1,N,EP)

C SPECIFY INITIAL CONDITIONS
  DT=DT#
  T#=D#
  CALL INSMINI(Y,U,UU,N,JFLAG)
  PRINT 1
  ST=UU(N+5)
  CALL MSES1(N+5,UU,EP,1##,B,FM)
  CALL OUTCALM (Y,UU,N)
  CALL OUTPUT (Y,U,T,L,UGS,PH1,B)

C INITIALIZE INTEGRATION ROUTINE MODDEQ
  LL=#
  JJI=2#
  NT=#
  K=1
  CALL MODDEQ (DERIV,K,B*N,T,Y,YDOT,DT,EP)

C SOLVE THE 5N O.D.E.'S FROM T TO T+DT
  NT=NT+1
  CALL MODDEQ (DERIV,K,B*N,T,Y,YDOT,DT,EP)
  IF (K .EQ. -1) PRINT 2
  IF (K .EQ. -1) STOP

C SOLVE THE N+5 ALGEBRAIC EQUATIONS AT TIME T+DT
  ST=UU(N+5)
  CALL MSES1(N+5,UU,EP,1##,B,FM)

C PRINT RESULTS AND CONTINUE PROCESS IF T IS LESS THAN TMAX
  IF (T .EQ. B .AND. T .GE. DL) GO TO 3##
  IF (T .NE. NP .AND. T .LT. TMAX) GO TO 2##
  CALL OUTCALN(Y,UU,N)
  CALL OUTPUT (Y,U,T,L,UGS,PH1,B)
  IF (T .GE. TMAX) GO TO 4##
  NT=#

```

Table A4-1
Computer Program **NLNMOD**

```
C ADJUST TIME STEP IF NECESSARY
RS=RFN (YDOT,Z*N)
JJ=IIDINT (RS) - 3
IF(JJ .EQ. 2) JJ=IIDINT(RS-.2D8) - 3
IF(JJ .LE. 1 .OR. JJ .GE. 1F) GO TO 288
DT1=DT8*4._SDB**JJ
IF((DT1-DT) .LE. .888108 .AND. (JJ1+3-RS) .LT. .18D8)GO TO 288
DT=DT1
JJ1=JJ
PRINT 4, (DT1/L/UGS)
GO TO 282

C ADJUST FOR END OF IMPULSE
288  LL=1
DO 281 I=2,8
U(I)=1.D8
U(I)=PH3
PRINT 3, (T=L/UGS)
DT=DT8
GO TO 282

C CALCULATE FINAL STEADY STATE
488  IF(LL.EQ.1 .OR. JFLAG.EQ.1)STOP
CALL ACTLSS(V,Y,EP,N)
PRINT 1
CALL OUTPUT(Y,U,E,DS,L,UGS,PH1,2)
STOP

1  FORMAT(1H1)
2  FORMAT(//,2X,'ERROR - MODDEQ COULD NOT CONVERGE',//)
3  FORMAT(////////,2X,'ACTUAL TIME OF IMPULSE END = ',F8.4,////////)
4  FORMAT(////////,2X,'NEW TIME STEP = ',F18.4////////)
END

SUBROUTINE INSMIM(Y,U,UU,N,JFLAG)
C THIS SUBROUTINE INITIALIZES THE SIMULATION.
IMPLICIT REAL*8 (A-H,O-Z)
REAL*8 MG,MG8
DIMENSION U(8),Y(188),UU(188)
COMMON /GASPA/ CFG,PTz,PTR,MG,PGS,UGS,UM
/OPCON/ SCH4,SCO,SC02,SH2,SH20,PT8,PT1,ST8,STW
READ(5,1) JFLAG
IF(JFLAG .EQ. 1)CALL INITIAL(Y,U,1)
IF(JFLAG .EQ. 1)GO TO 288

READ (5,2) UG8,T8,XCO,XC02,XH20,XH2,XCH4,TW
CALL CPCALC(XH2,XCO,XC02,XH20,XCH4,T8,MG8,CP,CP1,CP2)
UM=MG8/MG*(CP1*T8+CP2)/CPG
U(1)=TW/ST8
U(2)=UG8/UGS
U(3)=T8/ST8
U(4)=XCO/SCO
U(5)=XC02/SCO
U(6)=XH20/SCO
U(7)=XH2/SCO
U(8)=XCH4/SCO
PRINT 3, (U(I),I=1,8),UM

288  DO 388 I=1,N+5
UU(I)=Y(N+6+I)
RETURN

1  FORMAT(1H1)
2  FORMAT(9F8.2)
3  FORMAT(//,2X,'INITIAL CONTROL VECTOR:',//5X,'TW = ',F8.4,5X,
* 'UG8 = ',F8.4,5X,'T8 = ',F8.4,5X,'XCO = ',F8.4,5X,/5X,
* 'XC02 = ',F8.4,5X,'XH20 = ',F8.4,5X,'XH2 = ',F8.4,5X,'XCH4 = ',
* 'F8.4/5X,'UM = ',F8.4)
END

SUBROUTINE OUTCALM (Y,UU,N)
IMPLICIT REAL*8 (A-H,O-Z)
DIMENSION Y(188),UU(188)
DO 188 I=1,N+5
Y(5*N+1)=UU(I)
RETURN
END
```

Table A4-1 Continued

```

SUBROUTINE DERIV (NN,T,Y,YDOT)
C THIS SUBROUTINE DEFINES THE DIFFERENTIAL EQUATIONS FOR USE BY MODDEQ.
IMPLICIT REAL*8 (A-H,O-Z)
REAL*8 MG
DIMENSION Y(1#),YDOT(1#)
COMMON /DIMLE/ ALS,ALC,ALT,BES,BEG,GAS,GAG,GTS,GTG,DE1,
              DE2,S11,S12,S13,PH12,PH13,PH1,PH2,PH3
*          /RADIA/ W(1#),WP(9,21),DETA(2),RR
*          /COMAT/ A(25,25),B(25,25),R(25),N
*          /MISC1/ UU(1#)
*          /GASPA/ CPG,PTz,PTR,MG,PGS,UGS,UM
*          /LINEA/ AA(75,75),BB(75,8),DD(75),U(8)
NP2=NN+2
N2=N+2
N3=N+3
N4=N+4
TAU=PH2-1.D#
CALL ENDPTS (TT#,Y1#,Y1NP1,Y2#,Y2NP1,TTNP1,Y,PH1)
DO 1#1 I=1,N
IPI=I+1
PG=TAU*R(IPI)+1.D#
CALL REAC (Y(N3+2),Y(N4+I),Y(I),Y(N+I),PG,R1P,R2P)
S1=SUM(Y#,B,UU(N+2),UU(N+3),I,N)
S2=SUM(Y#,N,A,UU(N+4),UU(N+5),I,N)
S3=SUM(Y#,N,B,UU(N+4),UU(N+5),I,N)
S4=SUM(Y#,N3,A,Y1#,Y1NP1,I,N)
S6=SUM(Y#,N4,A,Y2#,Y2NP1,I,N)
S8=SUM(Y#,N2,B,TT#,TTNP1,I,N)
YDOT(I)= ALS*S1 + W(1)*Y(I) + W(2)*Y(N+I) + GAS*Y(N+I)
*          + DE1*R1P*(1.D#+PH12*Y(I)) + DE2*R2P*(1.D#+PH13*Y(I))
*          + W(3)*U(I)
YDOT(N+1)= -UU(I)*S2 + (ALC*S3 + W(4)*Y(N+I) + W(5)*Y(N+2+I)
*          + GAG*Y(I) + W(6)*U(I))/PG*Y(N+I)/UM
YDOT(N+2+I)= ALT*S8 + W(7)*Y(I) + W(8)*Y(N+I) + W(9)*Y(N+2+I)
*          + W(10)*U(I)
YDOT(N3+I)= -UU(I)*S4 + SI2*Y(N+I)*R2P/PG - S11*Y(N+I)*R1P/PG
YDOT(N4+I)= -UU(I)*S6 - S13*Y(N+I)*R2P/PG
CONTINUE
1#1
RETURN
END

SUBROUTINE FM (UU,V)
C THIS SUBROUTINE DEFINES THE ALGEBRAIC EQUATIONS FOR USE BY MSES2
IMPLICIT REAL*8 (A-H,O-Z)
REAL*8 MG
DIMENSION UU(1#),V(1)
COMMON /COMAT/ A(25,25),B(25,25),R(25),N
*          /DIMLE/ ALS,ALC,ALT,BES,BEG,GAS,GAG,GTS,GTG,DE1,
*          DE2,S11,S12,S13,PH12,PH13,PH1,PH2,PH3
*          /STATE/ Y(1#),YDOT(1#),ST,DT
*          /LINEA/ AA(75,75),BB(75,8),DD(75),U(8)
*          /GASPA/ CPG,PTz,PTR,MG,PGS,UGS,UM
*          /HEATT/ OHSG,OHTS,OHTG,BGS,BTG,BTG,BWS
NP2=NN+2
V(N+2)=SUM(Y#,B,A,UU(N+2),UU(N+3),B,N)+BGS*(UU(N+4)-UU(N+2))
V(N+3)=SUM(Y#,A,UU(N+2),UU(N+3),N+1,N)+BGS*(UU(N+3)-UU(N+5))
V(N+4)=SUM(Y#,N,A,UU(N+4),UU(N+5),B,N)+BGS*(UU(N+2)-UU(N+4))
*          +UM*U(2)*(U(3)-UU(N+4))/ALC/UU(N+4)
V(N+5)=SUM(Y#,N,A,UU(N+4),UU(N+5),N+1,N)+BGS*(UU(N+5)-UU(N+3))

TAU=PH2-1.D#
DO 2#1 K=1,N
V(K)=Y(N+K)+SUM(UU,B,A,U(2),UU(N+1),K,N)-UU(K)*SUM(Y,N,A,
              UU(N+4),UU(N+5),K,N)-YDOT(N+K)+UU(K)*Y(N+K)*TAU/
              (TAU*R(K+1)+1.D#)
V(N+1)=UU(N+6)+SUM(UU,B,A,U(2),UU(N+1),N+1,N)-UU(N+1)*SUM(Y,N,A,
              UU(N+4),UU(N+5),N+1,N)-(UU(N+5)-ST)/DT+UU(N+1)*UU(N+5)*TAU/
              (TAU+1.D#)
2#1
RETURN
END

```

Table A4-1 Continued

```
C THIS PROGRAM MODELS A NONISOTHERMAL, NONADIABATIC FIXED BED REACTOR
C . WITH BOTH A COOLING JACKET AND A THERMAL WELL. THE ANALYSIS IS
C . PERFORMED FOR A METHANATION OF CO SYSTEM.
C
C THIS PROGRAM PERFORMS THE SIMULATIONS FOR THE LINEARIZED MODEL
C USING THE NUMERICAL DIFFERENTIAL EQUATION SOLVER MODDEQ.
C
C LINK TO MLIB,LLIB
C
      IMPLICIT REAL*8 (A-H,O-Z)
      REAL*8 L,KT,MG,K0P,KP1A,KP1B,KC1B,KP2A,KP2B,KC2B,K2P,K3P
      DIMENSION YS(1#),RL1(15,9),RL2(15,9),Y(1#),YDOT(1#)
C
      COMMON /REACP/ EPS,L,RR,R1
      *      /CATLS/ CPS,PS,TC,DC
      *      /THWEL/ CPT,PT,KT
      *      /GASPA/ CPG,PTZ,PTR,MG,PGS,UGS,UM
      *      /HEATT/ OHSG,OHTG,BGS,BSG,BTS,BTG,BWG,BWS
      *      /OPCON/ SCH4,SCO,SCO2,SH2,SH20,PT#,PT1,ST#,STW
      *      /REAC1/ DH1A,DH1B,DH2A,DH2B,K0,K0P
      *      /DIMLE/ ALS,ALG,ALT,BES,BEG,GAS,GAG,GTS,GTG,DE1,
      *              DE2,S11,S12,S13,PH12,PH13,PH1,PH2,PH3
      *      /RADIA/ W(1#),WP(9,2),DETA(2),RR
      *      /COMAT/ A(25,25),B(25,25),R(25),N
      *      /REAC2/ KC1B,KP1A,KP1B,KC2B,KP2A,KP2B,K2P,K3P,EA1,EA2
      *      /LINEA/ AA(75,75),BB(75,8),DD(75),U(8)
      *      /LALGB/ S(4,4),H(2#,4#),RI(2#,4),AL(7)
C
      EXTERNAL FN3,DERIV
C
C READ IN DATA AND CALCULATE CONSTANTS
      CALL SETUPS (DT#,TMAX,DL,N,RR,EP,IFLAG,NFLAG,NP,IF)
C
C CALCULATE THE DIMENSIONLESS PARAMETERS
      CALL DIMLES
C
C CALCULATE CONSTANTS FOR THE RADIAL LUMPED MODEL
      CALL RADIAL
C
C CALCULATE ZEROS OF THE ORTHOGONAL POLYNOMIAL AND SET UP AXIAL
C   COLLOCATION MATRICIES A AND B.
      CALL COLLOC
C
C SOLVE FOR THE STEADY STATE PROFILES
      CALL INTLSS(YS,U,IFLAG,NFLAG,L,UGS,PH1,N,EP)
C
C CALCULATE THE COEFFICIENTS FOR THE LINEARIZED REACTION RATES
      CALL LREAC(YS,RL1,RL2)
      CALL ASETUP(YS,RL1,RL2)
C
C SPECIFY THE PROFILE AT T=#
      T=0.0#
      CALL INSIM(Y,YS,U,N,JFLAG)
      PRINT 1
      CALL OUTCALC(U,Y,YS(N*6+4),ALG)
      CALL OUTPUT(Y,U,T,L,UGS,PH1,B)
C
C INITIALIZE INTEGRATION ROUTINE MODDEQ
      LL=#
      J1=2#
      NT=#
      DT=DT#
      K=1
      2#2      CALL MODDEQ(DERIV,K,5*N,T,Y,YDOT,DT,EP)
C
C SOLVE THE 5N O.D.E.'S FROM T TO T+DT
      2#8      NT=NT+1
      CALL MODDEQ(DERIV,K,5*N,T,Y,YDOT,DT,EP)
      IF(K .EQ. -1) PRINT 2
      IF(K .EQ. -1) STOP
```

Table A4-2
Computer Program LINMOD

```
C PRINT RESULTS AND CONTINUE IF T < TMAX
  IF(LL.EQ.0 .AND. T.GE.DL) GO TO 388
  IF(NT.NE.NP .AND. T.LT.TMAX) GO TO 288
  CALL OUTCALC(U,Y,YS(N*6+4),ALG)
  CALL OUTPUT(Y,U,T,L,UGS,PH1,B)
  IF(T .GE. TMAX) GO TO 488
  NT=0

C ADJUST TIME STEP IF NECESSARY
  RS=RFDN (YDOT,2*N)
  JJ=IIDINT(RS)-3
  IF(JJ .EQ. 2) JJ=IIDINT(RS-.2D8) - 3
  IF((JJ.LE.8 .OR. JJ.GE.1F)GO TO 288
  DT1=DTB*4.D8**JJ
  IF((DT1-DT) .LE. .B881D8 .AND. (JJ1+3-RS) .LT. .1D8)GO TO 288
  DT=DT1
  JJ1=JJ
  PRINT 4, (DT*L/UGS)
  GO TO 282

C ADJUST FOR END OF IMPULSE
  388  LL=1
  DO 381 I=2,8
  U(I)=1.D8
  U(I)=PH3
  PRINT 3, (T*L/UGS)
  DT=DTB
  GO TO 282

C CALCULATE FINAL STEADY STATE
  488  IF(LL .EQ. 1 .OR. JFLAG .EQ. 1)STOP
  PRINT 1
  CALL NSESI(5*N,Y,EP*1.D-2,188,B,FN3)
  CALL OUTCALC(U,Y,YS(N*6+4),ALG)
  CALL OUTPUT(Y,U,B.D8,L,UGS,PH1,2)
  CALL ACTLSS(U,Y,EP,N)
  CALL OUTPUT (Y,U,B.D8,L,UGS,PH1,3)
  STOP

  1  FORMAT(1H1)
  2  FORMAT(//,2X,'ERROR - MODDEQ COULD NOT CONVERGE',//)
  3  FORMAT(////////,2X,'ACTUAL TIME OF IMPULSE END ',F8.4////////)
  4  FORMAT(////////,2X,'NEW TIME STEP ',F18.4////////)
  END

SUBROUTINE DERIV (N,T,Y,YDOT)
C THIS SUBROUTINE DEFINES THE DIFFERENTIAL EQUATIONS FOR USE BY MODDEQ
  IMPLICIT REAL*8 (A-H,O-Z)
  DIMENSION Y(188),YDOT(188)
  COMMON /LINEA/ AA(75,75),BB(75,8),DD(75),U(8)
  *           /LALGB/ S(4,4),H(28,48),RI(28,4),AL(7)

  DO 188 I=1,N
  YDOT(I)=DD(I)
  DO 181 J=1,N
  181 YDOT(I)=YDOT(I)+AA(I,J)*Y(J)
  DO 188 J=1,8
  188 YDOT(I)=YDOT(I)+BB(I,J)*U(J)
  RETURN
  END
```

Table A4-2 Continued

```
C THIS PROGRAM MODELS A MONISOTHERMAL, MONADIABATIC FIXED BED REACTOR
C WITH BOTH A COOLING JACKET AND A THERMAL WELL. THE ANALYSIS IS
C PERFORMED FOR A METHANATION OF CO SYSTEM.

C THIS PROGRAM PERFORMS THE SIMULATIONS FOR THE LINEARIZED MODEL
C USING THE ANALYTIC SOLUTION.

C LINK TO MLIB.LLIB.ELIB

      IMPLICIT REAL*8 (A-H,O-Z)
      REAL*8 L,KT,MG,KB,KP,KP1A,KP1B,KC1#,KP2A,KP2B,KC2#,K2P,K3P
      DIMENSION YS(1#),RL1(15,9),RL2(15,9),Y(1#),YDOT(1#)
      COMMON /REACP/ EPS,L,R#,R1
      *          /CATLS/ CPS,PS,TC,DC
      *          /TWELV/ CPT,PT,KT
      *          /GASPA/ CPG,PTZ,PTR,MG,PGS,UGS,UM
      *          /HEATT/ OHSG,OLHTS,OLHTG,BGS,BSG,BTS,BTG,BWG,BWS
      *          /OPCON/ SCH4,SCO,SC02,SH2,SH20,PT#,PT1,ST#,STW
      *          /REAC1/ DH1A,DH1B,DH2A,DH2B,KB,KP
      *          /DIMLE/ ALS,ALG,ALT,BES,BEG,GAS,GAG,GTS,GTG,DE1,
      *          DE2,S11,S12,S13,PH12,PH13,PH1,PH2,PH3
      *          /RADIA/ W(1#),WP(9,2),DETA(2),RR
      *          /COMAT/ A(25,25),B(25,25),R(25),N
      *          /REAC2/ KC1#,KP1A,KP1B,KC2#,KP2A,KP2B,K2P,K3P,EA1,EA2
      *          /LINEA/ AA(75,75),BB(75,8),DD(75),U(8)
      *          /LALGB/ S(4,4),H(2#,4#),R(2#,4),AL(7)
      *          /EIGEN/ EVR(75),EVI(75),SR(75,75),SI(75,75),SIR(75,75),
      *          SII(75,75)
      *          /ANLYT/ AI(75,75),EX(75,75),ET(75,75),CC(75)

      EXTERNAL FN3

C READ IN DATA AND CALCULATE CONSTANTS
      CALL SETUPS (DT,TMAX,DL,N,RR,EP,IFLAG,NFLAG,NP,IF)
      DT=DT*NP

C CALCULATE THE DIMENSIONLESS PARAMETERS
      CALL DIMLES

C CALCULATE CONSTANTS FOR THE RADIAL LUMPED MODEL
      CALL RADIAL

C CALCULATE ZEROS OF THE ORTHOGONAL POLYNOMIAL AND SET UP AXIAL
C COLLOCATION MATRICIES A AND B.
      CALL COLLOC

C SOLVE FOR THE STEADY STATE PROFILES
      CALL INTLSS(YS,U,IFLAG,NFLAG,L,UGS,PHI,N,EP)

C CALCULATE THE COEFFICIENTS FOR THE LINEARIZED REACTION RATES
      CALL LREAC(YS,RL1,RL2)
      CALL ASETUP(YS,RL1,RL2)

C SPECIFY THE PROFILE AT T=#
      T=#.D#
      CALL INSIM(Y,YS,U,N,JFLAG)
      PRINT 1
      CALL OUTCALC(U,Y,YS(N*6+4),ALG)
```

Table A4-3
Computer Program **ANAMOD**

```
      CALL OUTPUT(Y,U,T,L,UGS,PHI,B)
C  CALCULATE THE ANALYTIC CONSTANTS
      LL=B
      IN=B
2#2  CALL ANALYT(DT,N,IN)
C  SOLVE THE 5N O.D.E.'S FROM T TO T+DT
2#0  DO 2#3 I=1,5*N
      YDOT(I)=CC(I)
      DO 2#3 J=1,5*N
      YDOT(I)=YDOT(I)+EX(I,J)*Y(J)
      T=T+DT
      DO 2#1 I=1,5*N
2#1  Y(I)=YDOT(I)
C  PRINT RESULTS AND CONTINUE IF T < TMAX
      IF(LL.EQ.B .AND. T.GE.DL) GO TO 3#5
      CALL OUTCALC(U,Y,YS(N*6+4),ALG)
      CALL OUTPUT(Y,U,T,L,UGS,PHI,B)
      IF(T.GE.TMAX) GO TO 4#8
      GO TO 2#0
C  ADJUST FOR END OF IMPULSE
3#0  LL=1
      DO 3#1 I=2,B
3#1  U(I)=1.0B
      U(I)=PH3
      PRINT 2, (T*L/UGS)
      IN=2
      GO TO 2#2
C  CALCULATE FINAL STEADY STATE
4#5  IF(LL .EQ. 1 .OR. JFLAG .EQ. 1)STOP
      PRINT 1
      CALL NSES1(5*N,Y,EP*1.D-1,1#B,B,FN3)
      CALL OUTCALC(U,Y,YS(N*6+4),ALG)
      CALL OUTPUT(Y,U,B,D#,L,UGS,PHI,2)
      CALL ACTLSS(U,Y,EP,N)
      CALL OUTPUT(Y,U,B,D#,L,UGS,PHI,3)
      STOP
1  FORMAT(1H1)
2  FORMAT(/////////2X,'ACTUAL TIME OF IMPULSE END =',FB.4////////)
END
```

Table A4-3 Continued

```
SUBROUTINE ANALYT (DT,N,IN)
C THIS SUBROUTINE CALCULATES THE CONSTANTS NECESSARY FOR THE
C ANALYTICAL SOLUTION.
IMPLICIT REAL*8 (A-H,O-Z)
DIMENSION IND(75),Q(75)
COMMON /LINEA/ AA(75,75),BB(75,8),DD(75),U(8),
* /EIGEN/ EVR(75),EVI(75),SR(75,75),SI(75,75),SIR(75,75),
* SII(75,75)
* /ANLYT/ AI(75,75),EX(75,75),ET(75,75),CC(75)
IF(IN .EQ. 1) GO TO 288
IF(IN .EQ. 2) GO TO 388
C CALCULATE THE EIGENPROPERTIES
CALL ZEROM(SR,75,75)
CALL ZEROM(SI,75,75)
CALL ZEROV(EVR,75)
CALL ZEROV(EVI,75)
CALL MATCPY(AA,AI,75,75,75,75,75)
CALL EIGENP(S*N,75,AI,EVR,EVI,SR,SI,IND)
C CALCULATE S INVERSE AND A INVERSE
CALL ZEROM(SIR,75,75)
CALL ZEROM(SII,75,75)
CALL MATCPY(AA,AI,75,75,75,75,75,75)
DO 188 I=1,N*5
  SIR(I,I)=1.0E0
  CALL CINVSE(SR,SI,SIR,SII,75,5*N)
  CALL BNDINV(AI,5*N,ITEST)
C CALCULATE EXP(LAMBDA*DT)
288  DO 281 I=1,5*N
  CC(I)=DEXP(EVR(I)*DT)*DCOS(EVI(I)*DT)
281  Q(I)=DEXP(EVR(I)*DT)*DSIN(EVI(I)*DT)
  DO 283 I=1,5*N
  DO 283 J=1,5*N
  STR=0.0E0
  STI=0.0E0
  DO 282 K=1,5*N
  ST1=0.0E0
  ST2=0.0E0
  CALL CMULT(CC(K),DI(K),SIR(K,J),SII(K,J),ST1,ST2)
282  CALL CMULT(SR(I,K),SI(I,K),ST1,ST2,STR,STI)
283  EX(I,J)=STR
C CALCULATE ADDITIONAL CONSTANTS
DO 284 I=1,5*N
DO 284 J=1,5*N
ET(I,J)=0.0E0
DO 284 K=1,5*N
ALP=EX(K,J)
IF(K .EQ. J)ALP=ALP-1.0E0
ET(I,J)=ET(I,J)+AI(I,K)*ALP
284
388  DO 381 I=1,5*N
  Q(I)=0.0E0
  DO 381 J=1,8
  Q(I)=Q(I)+BB(I,J)*U(J)
  DO 382 I=1,5*N
  CC(I)=0.0E0
  DO 382 J=1,5*N
  CC(I)=CC(I)+ET(I,J)*Q(J)
382
RETURN
END
```

Table A4-3 Continued

```

C THIS PROGRAM MODELS A MONOTHERMAL, NONADIABATIC FIXED BED REACTOR
C WITH BOTH A COOLING JACKET AND A THERMAL WELL. THE ANALYSIS IS
C PERFORMED FOR A METHANATION OF CO SYSTEM.

C THIS PROGRAM PERFORMS THE SIMULATIONS FOR THE REDUCED LINEAR MODEL
C USING THE ANALYTIC SOLUTION. THE ASSUMPTION OF NEGLIGIBLE ENERGY
C ACCUMULATION IN THE GAS AND QUASI SS FOR CONCENTRATION ARE USED
C FOR THE MODEL REDUCTION.

C LINK TO MLIB,LLIB,ELIB

      IMPLICIT REAL*8 (A-H,O-Z)
      REAL*8 L,KT,MG,KP,KP1A,KP1B,KC1B,KP2A,KP2B,KC2B,K2P,K3P
      DIMENSION YS(1#8),RL1(15,8),RL2(15,8),Y(1#8),YDOT(1#8)
      COMMON /REACP/ EPS,L,RF,RL
      *          /CATLS/,CPS,PS,TC,DC
      *          /THVEL/,CPT,PT,KT
      *          /GASPA/,CPG,PTZ,PTR,MG,PGS,UGS,UM
      *          /HEAT/,OMSG,OMTS,OMTG,BGS,BSC,BTS,BTG,BVG,BVS
      *          /OPCON/,SC4,SC5,SC6,SC7,SH2,SH2,PT1,STB,STV
      *          /REAC1/,DH1A,DH1B,DH2A,DH2B,K1,KP
      *          /DIMLE/,ALS,ALG,ALT,BES,BEG,GAS,GAG,GTS,GTG,DE1,
      *          DE2,S11,S12,S13,PH12,PH1,PH2,PH3
      *          /RADIA/,W1B,W1B,W1B,W1B,W1B,W1B,W1B,W1B
      *          /COMAT/,KC1B,KP1A,KP1B,KC2B,KP2A,KP2B,K3P,EAI,EA2
      *          /LINEA/,A(75,75),B(75,8),D(75,8),U(8)
      *          /LALGB/,S(4,4),H(2B,4B),R(12B,4),AL(7)
      *          /EIGEN/,EV(75),EV(75),SR(75,75),SIR(75,75),
      *          SII(75,75)
      *          /ANLYT/,A(75,75),EX(75,75),ET(75,75),CC(75)
      *          /REDLN/,AC(75,75),AP(75,75),QP(75),C1(75,75),C2(75,1),
      *          AC1(75,75)

      EXTERNAL FN3

C READ IN DATA AND CALCULATE CONSTANTS
      CALL SETUPS (DT,TMAX,DL,N,RR,EP,IFLAG,NFLAG,MP,IF)
      DT=DT*MP

C CALCULATE THE DIMENSIONLESS PARAMETERS
      CALL DIMLES

C CALCULATE CONSTANTS FOR THE RADIAL LUMPED MODEL
      CALL RADIAL

C CALCULATE ZEROS OF THE ORTHOGONAL POLYNOMIAL AND SET UP AXIAL
C COLLOCATION MATRICES A AND B.
      CALL COLLOC

C SOLVE FOR THE STEADY STATE PROFILES
      CALL INTLSS(YS,U,IFLAG,NFLAG,L,UGS,PH1,N,EP)

C CALCULATE THE COEFFICIENTS FOR THE LINEARIZED REACTION RATES
      CALL LREAC(YS,RL1,RL2)
      CALL ASETUP(YS,RL1,RL2)

C SPECIFY THE PROFILE AT T=#
      T=#
      DT#
      CALL INSIM(Y,YS,U,N,JFLAG)
      PRINT 1
      CALL OUTCALC(U,Y,YS(N#6+4),ALC)
      CALL OUTPUT(Y,U,T,L,UGS,PH1,B)

C CALCULATE THE ANALYTIC CONSTANTS
      LL#
      IN#
      2#2  CALL REDUCE(N,IN)
      CALL ANALYT(DT,N,IN)

C SOLVE THE BN O.D.E.'S FROM T TO T+DT
      2#3  DO 2#3 I=1,M
      YDOT(1)=CC(1)
      YDOT(1+N)=CC(N+1)
      DO 2#3 J=1,N
      YDOT(N+I)=YDOT(N+I)+EX(I+N,J)*Y(J)+EX(I+N,J+N)*Y(2#N+J)
      2#3  YDOT(1)=YDOT(1)+EX(I,J)*Y(J)+EX(I,J+N)*Y(2#N+J)
      T=T+DT
      DO 2#1 I=1,N
      Y(2#N+I)=YDOT(N+I)
      2#1  Y(I)=YDOT(1)

C PRINT RESULTS AND CONTINUE IF T < TMAX
      IF(LL.EQ.B .AND. T.GE.DL) GO TO 3#8
      CALL OUTRA(Y,N)
      CALL OUTCALC(U,Y,YS(N#6+4),ALC)
      CALL OUTPUT(Y,U,T,L,UGS,PH1,B)
      IF(T.GE.TMAX) GO TO 4#8
      GO TO 2#3


```

Table A4-4
Computer Program RD1MOD

```

C ADJUST FOR END OF IMPULSE
388    LL=1
      DO 381 I=2,8
381    U(I)=1.0E0
      U(I)-PH3
      PRINT 1, (T=L/UGS)
      IN=2
      GO TO 282

C CALCULATE FINAL STEADY STATE
488    IF(LL .EQ. 1 .OR. JFLAG .EQ. 1)STOP
      PRINT 1
      CALL NSES1(5*N,Y,EP*1.0-2,1,LL,E,FN3)
      CALL OUTCALC(U,Y,YS(N*6+4),ALG)
      CALL OUTRA(Y,N)
      CALL OUTPUT(Y,U,E,DS,L,UGS,PH1,2)
      CALL ACTLSS(U,Y,EP,M)
      CALL OUTPUT(Y,U,E,DS,L,UGS,PH1,3)
      STOP

1    FORMAT(1X1)
2    FORMAT(/////////2X,'ACTUAL TIME OF IMPULSE END ',F8.4////////)
END

SUBROUTINE ANALYT (DT,N,IN)
C THIS SUBROUTINE CALCULATES THE CONSTANTS NECESSARY FOR THE
C ANALYTICAL SOLUTION.
      IMPLICIT REAL*8 (A-H,O-Z)
      DIMENSION IND(75),O(75)
      COMMON /LINEA/ AA(75,75),BB(75,8),DD(75),U(8)
      *          /EIGEN/ EVR(75),EVI(75),SR(75,75),SI(75,75),SIR(75,75),
      *          SII(75,75)
      *          /ANLYT/ AI(75,75),EX(75,75),ET(75,75),CC(75)
      *          /REDLN/ AP(75,75),QP(75),C1(75,75),C2(75,1),
      *          AC1(75,75)
      IF(IN .EQ. 1) GO TO 288
      IF(IN .EQ. 2) GO TO 388

C CALCULATE THE EIGENPROPERTIES
      CALL ZEROM(SR,75,75)
      CALL ZEROM(SI,75,75)
      CALL ZEROV(EVR,75)
      CALL ZEROV(EVI,75)
      CALL MATCPY(AP,AI,75,75,75,75,75)
      CALL EIGENP(2*N,75,AI,EVR,EVI,SR,SI,IND)

C CALCULATE S INVERSE AND A INVERSE
      CALL ZEROM(SIR,75,75)
      CALL ZEROM(SII,75,75)
      CALL MATCPY(AP,AI,75,75,75,75,75,75)
      DO 188 I=1,N*2
      SIR(I,I)=1.0E0
      CALL CINVSE(SR,SI,SIR,SII,75,2*N)
      CALL BNDINV(AI,2*N,ITEST)

C CALCULATE EXP(LAMBDA*DT)
288    DO 281 I=1,2*N
      CC(I)=DEXP(EVR(I)*DT)*DCOS(EVI(I)*DT)
      Q(I)=DEXP(EVR(I)*DT)*DSIN(EVI(I)*DT)
      DO 283 I=1,2*N
      DO 283 J=1,2*N
      STR=0.0E0
      STI=0.0E0
      DO 282 K=1,2*N
      ST1=0.0E0
      ST2=0.0E0
      CALL CHMULT(CC(K),Q(K),SIR(K,J),SII(K,J),ST1,ST2)
      CALL CHMULT(SR(I,K),SI(I,K),ST1,ST2,STR,STI)
      282   EXI(J)=STR
      283

C CALCULATE ADDITIONAL CONSTANTS
      DO 284 I=1,2*N
      DO 284 J=1,2*N
      ET(I,J)=0.0E0
      DO 284 K=1,2*N
      ALP=EXI(K,J)
      IF(K .EQ. J)ALP=ALP-1.0E0
      ET(I,J)=ET(I,J)+AI(I,K)*ALP
      284

388    DO 382 I=1,2*N
      CC(I)=0.0E0
      DO 382 J=1,2*N
      CC(I)=CC(I)+ET(I,J)*QP(J)
      382
      RETURN
END

```

Table A4-4 Continued

```

SUBROUTINE REDUCE(N,IN)
C THIS SUBROUTINE PERFORMS THE PHYSICAL MODEL REDUCTION FOR
C USE WITH THE ANALYTIC SOLUTION.
C
IMPLICIT REAL*8 (A-H,O-Z)
DIMENSION T1(58,58),T2(58,58)
COMMON /LINEA/ AA(75,75),BB(75,8),DD(75),U(8)
*      /REDLN/ AC(75,75),AP(75,75),QP(75),C1(75,75),C2(75,1),
          AC1(75,75)

IF(IN .EQ. 2) GO TO 2#B
N2=2*N
N3=3*N
N4=4*N
DO 1#B I=1,N
DO 1#B J=1,N
AC(I,J)=AA(N+I,N+J)
AC(I,N+J)=AA(N+I,N3+J)
AC(I,N2+J)=AA(N+I,N4+J)
AC(N+I,J)=AA(N3+I,N+J)
AC(N+I,N+J)=AA(N2+I,N3+J)
AC(N+I,N2+J)=AA(N3+I,N4+J)
AC(N2+I,J)=AA(N4+I,N+J)
AC(N2+I,N+J)=AA(N4+I,N3+J)
AC(N2+I,N2+J)=AA(N4+I,N4+J)
T1(I,J)=AA(I,N+J)
T1(I,N+J)=AA(I,N2+J)
T1(N+I,J)=AA(N2+I,N+J)
T1(N+I,N+J)=AA(N2+I,N3+J)
T1(N+I,N2+J)=AA(N2+I,N4+J)
T2(I,J)=AA(N+I,J)
T2(I,N+J)=AA(N3+I,N2+J)
T2(N+I,J)=AA(N3+I,J)
T2(N+I,N+J)=AA(N4+I,J)
T2(N+I,N2+J)=AA(N4+I,N2+J)
CALL MATCPY(T2,C1,58,58,75,75,N3,N2)
CALL BNDINV(AC,N3,ITEST)
CALL MATCPY(AC,AC1,75,75,75,75,N3,N3)
CALL MATMULT(AC,C1,75,75,75,75,N3,N2,N3)
CALL MATMULT(T1,AC,58,58,75,75,N2,N3,N3)
CALL MATMULT(AC,T2,75,75,58,58,N2,N2,N3)

DO 1#1 I=1,N
DO 1#1 J=1,N
AP(I,J)=AA(I,J)-T2(I,J)
AP(I,N+J)=AA(I,N2+J)-T2(I,N+J)
AP(N+I,J)=AA(N2+I,J)-T2(N+I,J)
AP(N+I,N+J)=AA(N2+I,N2+J)-T2(N+I,N+J)

1#1 DO 1#2 I=1,N
T2(I,1)=DD(N+I)
T2(N+1,1)=DD(N3+I)
T2(N2+1,1)=DD(N4+I)
T1(I,1)=DD(I)
T1(N+1,1)=DD(N2+I)
DO 1#2 J=1,8
T2(I,1)=T2(I,1)+BB(N+I,J)*U(J)
T2(N+1,1)=T2(N+1,1)+BB(N3+I,J)*U(J)
T2(N2+1,1)=T2(N2+1,1)+BB(N4+I,J)*U(J)
T1(I,1)=T1(I,1)+BB(I,J)*U(J)
T1(N+1,1)=T1(N+1,1)+BB(N2+I,J)*U(J)

1#2 CALL MATCPY(T2,C2,58,58,75,1,N3,1)
CALL MATMULT(AC1,C2,75,75,75,1,N3,1,N3)
CALL MATMULT(AC,T2,75,75,58,58,N2,1,N3)
DO 1#3 I=1,N2
QP(I)=T1(I,1)-T2(I,1)

1#3
RETURN
END

SUBROUTINE OUTRA(Y,N)
IMPLICIT REAL*8 (A-H,O-Z)
DIMENSION Y(1#B)
COMMON /REDLN/ AC(75,75),AP(75,75),QP(75),C1(75,75),C2(75,1),
          AC1(75,75)

N2=2*N
N3=3*N
N4=4*N
DO 1#B I=1,N
Y(I+N)=C2(I,1)
Y(I+N3)=C2(N+I,1)
Y(I+N4)=C2(N2+I,1)
DO 1#B J=1,N
Y(N+I)=Y(N+I)-C1(I,J)*Y(J)-C1(I,N+J)*Y(N2+J)
Y(N3+I)=Y(N3+I)-C1(N+I,J)*Y(J)-C1(N+I,N+J)*Y(N2+J)
Y(N4+I)=Y(N4+I)-C1(N2+I,J)*Y(J)-C1(N2+I,N+J)*Y(N2+J)
1#B
RETURN
END

```

Table A4-4 Continued

```
C THIS PROGRAM MODELS A NONISOTHERMAL, NONADIABATIC FIXED BED REACTOR
C WITH BOTH A COOLING JACKET AND A THERMAL WELL. THE ANALYSIS IS
C PERFORMED FOR A METHANATION OF CO SYSTEM.

C THIS PROGRAM PERFORMS THE SIMULATIONS FOR THE REDUCED LINEAR MODEL
C USING THE ANALYTIC SOLUTION. THE ASSUMPTION OF QUASI SS FOR
C CONCENTRATION IS USED FOR THE MODEL REDUCTION.

C LINK TO MLIB,LLIB,ELIB

      IMPLICIT REAL*8 (A-H,O-Z)
      REAL*8 L,KT,MG,KW,KP1,KP1A,KP1B,KC1#,KP2A,KP2B,KC2#,K2P,K3P
      DIMENSION VS(1#),RL1(15,9),RL2(15,9),Y(1#),YDOT(1#)
      COMMON /REACP/ EPS,L,R#,R1
      *          /CATIS/ CPS,L,PS,TC,DC
      *          /THVEL/ CPT,PT,KT
      *          /GASPA/ CPG,PTZ,PTR,MG,PGS,UGS,UM
      *          /HEATT/ OHSG,OHTS,OHTC,BGS,BSG,BTS,BTG,BWG,BWS
      *          /OPCON/ SCH4,SCO,SC02,SH2,SH20,PTF,PT1,ST#,STW
      *          /REAC1/ DH1A,DH1B,DH2A,DH2B,K#,KP#
      *          /DIMLE/ ALS,ALG,ALT,BES,BEG,GAS,GAG,GTS,GTG,DE1,
      *          DE2,S11,S12,S13,PH12,PH13,PH1,PH2,PH3
      *          /RADIA/ W(1#),UP(9,2),DETA(2),RR
      *          /COMAT/ A(25,25),B(25,25),R(25),N
      *          /REAC2/ KC1#,KP1A,KP1B,KC2#,KP2A,KP2B,K3P,EA1,EA2
      *          /LINEA/ AA(75,75),BB(75,75),DD(75),U(8)
      *          /LALGB/ S(4,4),H(2#,4#),R1(2#,4),AL(7)
      *          /EIGEN/ EVR(75),EV1(75),SR(75,75),SI(75,75),SIR(75,75),
      *          SII(75,75)
      *          /ANLYT/ A1(75,75),EX(75,75),ET(75,75),CC(75)
      *          /REDLN/ AC(75,75),AP(75,75),QP(75),C1(75,75),C2(75,1),
      *          AC1(75,75)

      EXTERNAL FN3

C READ IN DATA AND CALCULATE CONSTANTS
      CALL SETUPS (DT,TMAX,DL,N,RR,EP,IFLAG,MFLAG,NP,IF)
      DT=D*NP

C CALCULATE THE DIMENSIONLESS PARAMETERS
      CALL DIMLES

C CALCULATE CONSTANTS FOR THE RADIAL LUMPED MODEL
      CALL RADIAL

C CALCULATE ZEROS OF THE ORTHOGONAL POLYNOMIAL AND SET UP AXIAL
C   COLLOCATION MATRICES A AND B.
      CALL COLLOC

C SOLVE FOR THE STEADY STATE PROFILES
      CALL INTLSS(VS,U,IFLAG,MFLAG,L,UGS,PH1,N,EP)

C CALCULATE THE COEFFICIENTS FOR THE LINEARIZED REACTION RATES
      CALL LREAC(VS,RL1,RL2)
      CALL ASETPU(VS,RL1,RL2)

C SPECIFY THE PROFILE AT T=#
      T=#
      CALL INSIM(VS,U,N,JFLAG)
      PRINT 1
      CALL OUTCALC(U,V,VS(N#6+4),ALG)
      CALL OUTPUT(V,U,T,L,UGS,PH1,B)

C CALCULATE THE ANALYTIC CONSTANTS
      LL#
      IN#
      2#2  CALL REDUCE(N,IN)
      CALL ANALYT(DT,N,IN)

C SOLVE THE 5N O.D.E.'S FROM T TO T+DT
      2#8  DO 2#3 I=1,3*N
            YDOT(I)=CC(I)
      2#3  DO 2#3 J=1,3*N
            YDOT(I)=YDOT(I)+EX(I,J)*Y(J)
      2#1  T=T+DT
      2#1  DO 2#1 I=1,3*N
            Y(I)=YDOT(I)

C PRINT RESULTS AND CONTINUE IF T < TMAX
      IF(LL.EQ.# .AND. T.GE.DL) GO TO 3#8
      CALL OUTRA(V,N)
      CALL OUTCALC(U,V,VS(N#6+4),ALG)
      CALL OUTPUT(V,U,T,L,UGS,PH1,B)
      IF(T .GE. TMAX) GO TO 4#8
      GO TO 2#8
```

Table A4-5
Computer Program RD2MOD

```

C ADJUST FOR END OF IMPULSE
 388  LL=1
      DO 381 I=2,8
 381  U(I)=1.0#
      U(I)=PH3
      PRINT 2, (T=L/UGS)
      IN=2
      GO TO 2/2

C CALCULATE FINAL STEADY STATE
 488  IF(LL .EQ. 1 .OR. JFLAG .EQ. 1)STOP
      PRINT 1
      CALL NSESI(5*N,Y,EP*1.0-2,188,0,FN3)
      CALL OUTCALC(Y,YST(N-6+4),ALG)
      CALL OUTRA(Y,N)
      CALL OUTPUT(Y,U,0,D#,L,UGS,PH1,2)
      CALL ACTLSS(U,Y,EP,N)
      CALL OUTPUT(Y,U,0,D#,L,UGS,PH1,3)
      STOP

 1  FORMAT(1H1)
 2  FORMAT(////////,2X,'ACTUAL TIME OF IMPULSE END =',F0.4////////)
END

SUBROUTINE ANALYT (DT,N,IN)
C THIS SUBROUTINE CALCULATES THE CONSTANTS NECESSARY FOR THE
C ANALYTICAL SOLUTION.
      IMPLICIT REAL*8 (A-H,O-Z)
      DIMENSION IND(75),Q(75)
      COMMON /LINEA/ AA(75,75),BB(75,8),DD(75),U(8)
      *          /EIGEN/ EVR(75),EV1(75),SR(75,75),SI(75,75),SIR(75,75)
      *          SII(75,75)
      *          /ANLYT/ AI(75,75),EX(75,75),ET(75,75),CC(75)
      *          /REDLN/ AC(75,75),AP(75,75),QP(75),C1(75,75),C2(75,1),
      *          AC1(75,75)

      IF(IN .EQ. 1) GO TO 288
      IF(IN .EQ. 2) GO TO 388

C CALCULATE THE EIGENPROPERTIES
      CALL ZEROM(SR,75,75)
      CALL ZEROM(SI,75,75)
      CALL ZEROV(EVR,75)
      CALL ZEROV(EV1,75)
      CALL MATCPY(AP,AI,75,75,75,75,75,75)
      CALL EIGENP(3*N,75,AI,EVR,EV1,SR,SI,IND)

C CALCULATE S INVERSE AND A INVERSE
      CALL ZEROM(SIR,75,75)
      CALL ZEROM(SII,75,75)
      CALL MATCPY(AP,AI,75,75,75,75,75,75)
      DO 188 I=1,N**3
      SIR(I,I)=1.0#
      SII(I,I)=1.0#
      CALL CINVERSE(SR,SI,SIR,SII,75,3*N)
      CALL BNDINV(AI,3*N,1TEST)

C CALCULATE EXP(LAMBDA*DT)
 288  DO 281 I=1,3*N
      CC(I)=DEXP(EVR(I)*DT)*DCOS(EVI(I)*DT)
      Q(I)=DEXP(EVR(I)*DT)*DSIN(EVI(I)*DT)
      DO 283 I=1,3*N
      DO 283 J=1,3*N
      DO 283 K=1,3*N
      STR=0.0#
      STI=0.0#
      DO 282 K=1,3*N
      STI=0.0#
      ST2=0.0#
      CALL CMULT(CC(K),Q(K),SR(K,J),SII(K,J),ST1,ST2)
      CALL CMULT(SR(I,K),SI(I,K),ST1,ST2,STR,STI)
 282  EX(I,J)=STR

C CALCULATE ADDITIONAL CONSTANTS
 284  DO 284 I=1,3*N
      DO 284 J=1,3*N
      ET(I,J)=0.0#
      DO 284 K=1,3*N
      ALP=EX(K,J)
      IF(K .EQ. J)ALP=ALP-1.0#
      ET(I,J)=ET(I,J)+AI(I,K)*ALP
 284

 388  DO 382 I=1,3*N
      CC(I)=0.0#
      DO 382 J=1,3*N
 382  CC(I)=CC(I)+ET(I,J)*QP(J)

      RETURN
END

```

Table A4-5 Continued

```

SUBROUTINE REDUCE(N,IN)
C  THIS SUBROUTINE PERFORMS THE PHYSICAL MODEL REDUCTION FOR
C  USE WITH THE ANALYTIC SOLUTION.
      IMPLICIT REAL*8 (A-H,O-Z)
      DIMENSION T1(5#,5#),T2(5#,5#)
      COMMON /LINEA/ AA(75,75),BB(75,8),DD(75),U(8)
      *          /REDLN/ AC(75,75),AP(75,75),QP(75),C1(75,75),C2(75,1),
      *          AC1(75,75)
C
      IF(IN .EQ. 2) GO TO 288
      N2=2*N
      N3=3*N
      N4=4*N
      DO 188  I=1,N
      DO 188  J=1,N
      AC(I,J)=AA(N3+I,N3+J)
      AC(I,N+J)=AA(N3+I,N4+J)
      AC(N+I,J)=AA(N4+I,N3+J)
      AC(N+I,N+J)=AA(N4+I,N4+J)
      T1(I,J)=AA(I,N3+J)
      T1(I,N+J)=AA(I,N4+J)
      T1(N+I,J)=AA(N+I,N3+J)
      T1(N+I,N+J)=AA(N+I,N4+J)
      T1(N2+I,J)=AA(N2+I,N3+J)
      T1(N2+I,N+J)=AA(N2+I,N4+J)
      T2(I,J)=AA(N3+I,J)
      T2(I,N+J)=AA(N3+I,N+J)
      T2(I,N2+J)=AA(N3+I,N2+J)
      T2(N+I,J)=AA(N4+I,J)
      T2(N+I,N+J)=AA(N4+I,N+J)
      T2(N+I,N2+J)=AA(N4+I,N2+J)
      CALL MATCPY(T2,C1,5#,5#,75,75,N2,N3)
      CALL BNDINV(AC,N2,1TEST)
      CALL MATCPY(AC,AC1,75,75,75,75,N2,N2)
      CALL MATMULT(AC,C1,75,75,75,75,N2,N3,N2)
      CALL MATMULT(T1,AC,5#,5#,75,75,N3,N2,N2)
      CALL MATMULT(AC,T2,75,75,5#,5#,N3,N3,N2)
      DO 188  I=1,N3
      DO 188  J=1,N3
      188  AP(I,J)=AA(I,J)-T2(I,J)
      288  DO 188  I=1,N
      T2(I,1)=DD(N3+I)
      T2(N+1,1)=DD(N4+I)
      T1(I,1)=DD(I)
      T1(N+1,1)=DD(N+I)
      T1(N2+1,1)=DD(N2+I)
      DO 188  J=1,8
      T2(I,J)=T2(I,1)+BB(N3+I,J)*U(J)
      T2(N+1,J)=T2(N+1,1)+BB(N4+I,J)*U(J)
      T1(I,J)=T1(I,1)+BB(I,J)*U(J)
      T1(N+1,J)=T1(N+1,1)+BB(N+1,J)*U(J)
      T1(N2+1,J)=T1(N2+1,1)+BB(N2+1,J)*U(J)
      CALL MATCPY(T2,C2,5#,5#,75,1,N2,1)
      CALL MATMULT(AC1,C2,75,75,75,1,N2,1,N2)
      CALL MATMULT(AC,T2,75,75,5#,5#,N3,1,N2)
      DO 188  I=1,N3
      188  QP(I)=T1(I,1)-T2(I,1)
      RETURN
      END

SUBROUTINE OUTRA(Y,N)
      IMPLICIT REAL*8 (A-H,O-Z)
      DIMENSION Y(188)
      COMMON /REDLN/ AC(75,75),AP(75,75),QP(75),C1(75,75),C2(75,1),
      AC1(75,75)
      N2=2*N
      N3=3*N
      N4=4*N
      DO 188  I=1,N
      Y(I+N3)=-C2(I,1)
      Y(I+N4)=-C2(N+I,1)
      DO 188  J=1,N3
      Y(N3+I)=Y(N3+I)-C1(I,J)*Y(J)
      Y(N4+I)=Y(N4+I)-C1(N+I,J)*Y(J)
      RETURN
      END

```

Table A4-5 Continued

INPUT DATA:

REACTOR PARAMETERS	CATALYST PARAMETERS	THERMAL WELL PARAMETERS
EPS = 8.5700E+00	CPS = 8.2500E+00	CPT = 8.1200E+00
L = 8.3000E+02	PS = 8.1041E+01	PT = 8.8020E+01
R _B = 8.1587E+00	TC = 8.5000E-03	KT = 8.3900E-01
R _I = 8.1194E+01		

HEAT TRANSFER PARAMETERS

OHSG = 8.1702E+02	DH1A = -8.6144E+01
OHTS = 8.1795E-01	DH1B = -8.4835E+05
OHTG = 8.1436E+00	DH2A = -8.2441E+01
BGS = 8.6000E+03	DH2B = 8.1076E+05
BSG = 8.1389E+02	K _B = 8.1700E+02
BTS = 8.7163E+01	K _B P = 8.7524E-01
BTG = 8.1250E+01	
PTZ = 8.2000E+01	
PTR = 8.8000E+01	

REACTOR PARAMETERS

KP1A = -8.2944E+02
KP1B = 8.2634E+05
KP2A = 8.4385E+01
KP2B = -8.4615E+04
K2 = 8.1470E+01
K3 = 8.7348E+00
EA1 = 8.6950E+04
EA2 = 8.1890E+05

PROGRAM CONDITIONS:

TIME STEP = 8.0000
MAXIMUM TIME = 5.0000
DISTURBANCE LENGTH = 9999999.9999
RADIAL COLLOCATION POINT = 8.5000
NO. AXIAL COLLOC. POINTS = 8
ACCURACY OF CONVERGENCE = 8.1000E-08
INPUT FLAG = 5
NSES FLAG = 1
MAX VALUE OF DT = 8.5000

STEADY STATE CONDITIONS:

XCH4 = 8.6000E+00	TS = 8.5730E+03
XCO = 8.6000E-01	TW = 8.5730E+03
XCO2 = 8.1500E-01	PTB = 8.1000E+02
XH2 = 8.1900E+00	PT1 = 8.9000E+01
XH2O = 8.2000E-01	MG = 8.1593E+02
UGB = 8.7500E+02	CPG = 8.6572E+00

AXIAL COLLOCATION POINTS:

8.0000E+00 8.1986E-01 8.1017E+00 8.2372E+00
8.4883E+00 8.5917E+00 8.7628E+00 8.8983E+00
8.9851E+00 8.1000E+01

Table A4-6
Sample Output From Program NLNMOD

INITIAL GUESSES:

GAS TEMPERATURE			SOLID TEMPERATURE		
R = RS	R = RR	R = R1	R = RS	R = RR	R = R1
1.00000	1.00000	1.00000	1.00000	1.00000	1.00000
1.00000	1.00000	1.00000	1.00000	1.00000	1.00000
1.00000	1.00000	1.00000	1.00000	1.00000	1.00000
1.00000	1.00000	1.00000	1.00000	1.00000	1.00000
1.00000	1.00000	1.00000	1.00000	1.00000	1.00000
1.00000	1.00000	1.00000	1.00000	1.00000	1.00000
1.00000	1.00000	1.00000	1.00000	1.00000	1.00000
1.00000	1.00000	1.00000	1.00000	1.00000	1.00000
1.00000	1.00000	1.00000	1.00000	1.00000	1.00000
1.00000	1.00000	1.00000	1.00000	1.00000	1.00000
1.00000	1.00000	1.00000	1.00000	1.00000	1.00000
WELL TEMP.	CO CONC.	CO2 CONC.	VELOCITY		
1.00000	0.0000000	0.0150000	1.00000	1.00000	1.00000
1.00000	0.0000000	0.0150000	1.00199	1.00000	1.00000
1.00000	0.0000000	0.0150000	1.01027	1.00000	1.00000
1.00000	0.0000000	0.0150000	1.02438	1.00000	1.00000
1.00000	0.0000000	0.0150000	1.04257	1.00000	1.00000
1.00000	0.0000000	0.0150000	1.06289	1.00000	1.00000
1.00000	0.0000000	0.0150000	1.08258	1.00000	1.00000
1.00000	0.0000000	0.0150000	1.09878	1.00000	1.00000
1.00000	0.0000000	0.0150000	1.10867	1.00000	1.00000
1.00000	0.0000000	0.0150000	1.11111	1.00000	1.00000

STEADY STATE SOLUTION:

GAS TEMPERATURE			SOLID TEMPERATURE		
R = RS	R = RR	R = R1	R = RS	R = RR	R = R1
1.00150	1.00150	1.00150	1.00111	1.00283	1.00111
1.00635	1.00635	1.00642	1.00828	1.01156	1.00412
1.02313	1.02106	1.01496	1.02626	1.02654	1.00868
1.04569	1.04163	1.02958	1.04978	1.04786	1.01584
1.06272	1.05788	1.04895	1.06734	1.06208	1.01962
1.07254	1.06695	1.04693	1.07731	1.07842	1.02219
1.07361	1.06597	1.04757	1.07822	1.07863	1.02218
1.07227	1.06578	1.04673	1.07662	1.06985	1.02167
1.07811	1.06365	1.04518	1.07449	1.06668	1.02084
1.06991	1.06347	1.04505	1.07326	1.06377	1.01974
WELL TEMP.	CO CONC.	CO2 CONC.	VELOCITY		
1.00000	0.0000000	0.0150000	1.00000	1.00000	1.00000
1.00549	0.0056588	0.0150128	1.00621	1.00000	1.00000
1.02324	0.00573679	0.0151151	1.02955	1.00000	1.00000
1.04582	0.00543339	0.0152437	1.06494	1.00000	1.00000
1.05309	0.00494708	0.0154779	1.09995	1.00000	1.00000
1.07288	0.00455038	0.0156721	1.13896	1.00000	1.00000
1.07408	0.00411858	0.0159825	1.15287	1.00000	1.00000
1.07265	0.00389488	0.0160245	1.16875	1.00000	1.00000
1.07893	0.00370699	0.0161387	1.17699	1.00000	1.00000
1.07875	0.00368712	0.0161421	1.17939	1.00000	1.00000

INITIAL CONTROL VECTOR:

TW = 1.00000 UGS = 1.00000 TS = 1.0349 XCO = 1.00000
 XC02 = 0.25000 XH20 = 0.3333 XH2 = 3.1667 XCH4 = 10.00000
 UM = 1.0152

Table A4-6 Continued

TIME = 4.8888 SEC

GAS TEMPERATURE						SOLID TEMPERATURE					
R = RB	R = RR	R = R1	R = RB	R = RR	R = R1	R = RB	R = RR	R = R1	R = RB	R = RR	R = R1
1.82858	1.82378	1.81623	1.83254	1.82226	1.86613						
1.88635	1.88618	1.88442	1.88828	1.81156	1.88412						
1.82313	1.82186	1.81496	1.82626	1.82654	1.88868						
1.84569	1.84163	1.82958	1.84978	1.84786	1.81584						
1.86272	1.86788	1.84855	1.86734	1.86288	1.81962						
1.87254	1.86585	1.84693	1.87731	1.87842	1.82219						
1.87361	1.86697	1.84757	1.87822	1.87863	1.82218						
1.87227	1.86578	1.84673	1.87662	1.86985	1.82167						
1.87811	1.86365	1.84518	1.87449	1.86668	1.82884						
1.87828	1.86377	1.84525	1.87378	1.86487	1.81982						
WELL TEMP.			CO CONC.			CO2 CONC.			VELOCITY		
1.83498	8.8688888	8.8158888	1.88888			1.88888					
1.88549	8.8596588	8.8158128	8.98479								
1.82324	8.8573678	8.8151151	1.88768								
1.84582	8.8543335	8.8152437	1.84234								
1.86309	8.8494788	8.8154779	1.87639								
1.87288	8.84555038	8.8156721	1.87788								
1.87488	8.8411858	8.8159825	1.12886								
1.87265	8.8389488	8.8168245	1.14411								
1.87893	8.8378699	8.8161387	1.15173								
1.87123	8.8368712	8.8161421	1.15459								

TIME = 5.8888 SEC

GAS TEMPERATURE						SOLID TEMPERATURE					
R = RB	R = RR	R = R1	R = RB	R = RR	R = R1	R = RB	R = RR	R = R1	R = RB	R = RR	R = R1
1.83833	1.83619	1.82686	1.83838	1.83696	1.81189						
1.83576	1.83837	1.82883	1.83848	1.84325	1.81548						
1.83913	1.84861	1.83819	1.83439	1.84346	1.81514						
1.84915	1.84587	1.83289	1.85112	1.84994	1.81614						
1.86281	1.85728	1.84865	1.86731	1.86199	1.81961						
1.87227	1.86578	1.84666	1.87714	1.86999	1.82282						
1.87325	1.86656	1.84724	1.87799	1.87819	1.82282						
1.87198	1.86532	1.84637	1.87641	1.86855	1.82147						
1.86978	1.86317	1.84488	1.87422	1.86618	1.82865						
1.86955	1.86299	1.84466	1.87312	1.86329	1.81985						
WELL TEMP.			CO CONC.			CO2 CONC.			VELOCITY		
1.83498	8.8688888	8.8158888	1.88888			1.88888					
1.81973	8.8595398	8.8158172	1.88412								
1.82545	8.8568983	8.8151378	1.81461								
1.84625	8.8536898	8.8152788	1.83489								
1.86386	8.8486592	8.8155188	1.86394								
1.87287	8.8446432	8.8157174	1.89344								
1.87488	8.8403822	8.8159516	1.11454								
1.87264	8.8388558	8.8168755	1.12984								
1.87883	8.8361758	8.8161838	1.13778								
1.87883	8.8359769	8.8161945	1.14818								

Table A4-6 Continued

STEADY STATE SOLUTION:

GAS TEMPERATURE			SOLID TEMPERATURE		
R = RB	R = RR	R = RI	R = RB	R = RR	R = RI
1.03858	1.03651	1.02631	1.03849	1.03746	1.01279
1.04381	1.03991	1.02956	1.04614	1.04616	1.01584
1.05655	1.05149	1.03658	1.06133	1.05762	1.01836
1.07361	1.06704	1.04764	1.07894	1.07286	1.02387
1.08336	1.07585	1.05388	1.08998	1.08884	1.02546
1.08652	1.07678	1.05597	1.09183	1.08381	1.02688
1.08284	1.07463	1.05301	1.08693	1.07884	1.02446
1.07759	1.07863	1.05018	1.08246	1.07362	1.02386
1.07375	1.06688	1.04745	1.07831	1.06956	1.02171
1.07341	1.06656	1.04721	1.07784	1.06683	1.02066
WELL TEMP.	CO CONC.	CO2 CONC.	VELOCITY		
1.03498	1.0688888	1.0158888	1.0000000		
1.04112	1.0595295	1.0150176	1.00531		
1.05688	1.0567781	1.0151424	1.02483		
1.07387	1.0530768	1.0153843	1.05451		
1.08387	1.0476671	1.0155716	1.08211		
1.08692	1.0433679	1.0157988	1.10526		
1.08268	1.0389593	1.0160331	1.12238		
1.07888	1.0367156	1.0161596	1.13487		
1.07484	1.0348715	1.0162672	1.14115		
1.07454	1.0345773	1.0162787	1.14337		

Table A4-6 Continued

```

SUBROUTINE DIMLES

C THIS SUBROUTINE CALCULATES THE DIMENSIONLESS PARAMETERS

IMPLICIT REAL*8 (A-H,O-Z)
REAL*8 L,KT,MG,KB,KP,KC20,KP2A,KP2B,K1P,K2P
COMMON /REACP/ EPS,L,RB,R1
* /CATLS/ CPS,PS,TC,DC
* /THVEL/ CPT,PT,KT
* /GASPA/ CPG,PTZ,PTR,MG,PGS,UGS,UM
* /HEATT/ OHSG,OHTS,DHTG,BGS,BSG,BTS,BTG,BWG,BWS
* /OPCON/ SCH4,SCO,SCO2,SH2,SH20,PT#,PT1,ST#,STW
* /REAC1/ DH1A,DH1B,DH2A,DH2B,KB,KP
* /DIMLE/ ALS,ALG,ALT,BES,BEG,GAS,GAG,ETS,GTC,DE1,
* DE2,S11,S12,S13,PH12,PH13,PH2,PH3
* /REAC2/ EXPA,EXPB,EXPC,KC2#,KP2A,KP2B,K1P,K2P,EA1,EA2
DATA PI /3.14159265408/

VB=PI*R#**2*L
VB=PI*L*(R1**2-R#**2)
a=L/DC
AR=R1/DC
AO=L/R1
EM1=L*DB-EPS
ALS=TC/(PS*CPS*EM1*L*UGS)
ALG=L*DB/(PTZ*EPS*a)
ALT-KT/(PT*CP1*UGS)
BES=ALS*L**2/R1**2
BEG=AD/PTK/EPS/AR
GAS=OHSG*L/(VB*PS*CPS*EM1*UGS)
GAG=OHSG*L/(VB*PGS*CPG*EPS*UGS)
GTS=OHTS*L/(VT*PT*CP1*UGS)
GTC=OHTG*L/(VT*PT*CP1*UGS)
DE1=-L*DH1B*(PT#*SCO)**(EXPA+EXPB)*K#P/(UGS*CPS*ST#)
DE2=-L*DH2B*SCO**2*KB/(UGS*CPS*ST#)
S11=MG*PS*EM1*(PT#*SCO)**(EXPA+EXPB)*K#P*L/(EPS*UGS*PGS*SCO)
S12=MG*PS*EM1*SCO*KB*L/(EPS*UGS*PGS)
S13=S12
PH12=DH1A*ST#/DH1B
PH13=DH2A*ST#/DH2B
BWG=BTG
BWS=BTS
PH1=R2/R1
PH2=PT1/PT#
PH3=STW/ST#
RETURN
END

SUBROUTINE INITIAL (Y,U,IFLAG)

C THIS ROUTINE INITIALIZES THE SYSTEM

IMPLICIT REAL*8 (A-H,O-Z)
REAL*8 MG
DIMENSION Y(1#8),U(8)
COMMON /OPCON/ SCH4,SCO,SCO2,SH2,SH20,PT#,PT1,ST#,STW
* /GASPA/ CPG,PTZ,PTR,MG,PGS,UGS,UM
* /COMAT/ A(26,26),B(26,26),R(26),N

DO 388 I=2,4
388 U(I)=1,DB
U(1)=STW/ST#
U(5)=SCO2/SCO
U(6)=SH20/SCO
U(7)=SH2/SCO
U(8)=SCH4/SCO
UM=1,DB
IF(IFLAG .EQ. 1)GO TO 288
READ(5,1) TG,TS,TT,X1,X2,VEL
DO 188 I=1,N
Y(3*N+I)=X1/SCO
Y(4*N+I)=X2/SCO
Y(5*N+I)=VEL*PT#/((PT1-PT#)*R(I+1)+PT#)/UGS
Y(1)=TS/ST#
Y(1+N)=TG/ST#
Y(2+N)=TT/ST#
188 CONTINUE
Y(6*N+1)=VEL*PT#/PT1/UGS
Y(6*N+2)=TS/ST#
Y(6*N+3)=TS/ST#
Y(6*N+4)=TG/ST#
Y(6*N+5)=TT/ST#
Y(6*N+6)=X1/SCO
RETURN
288 DO 281 I=1,N
READ(5,1) Y(N+I),Y(1),Y(2*N+1),X1,X2,Y(5*N+1)
E=(SCO+SCO2-X1*X2)/(1,DB-2,DB*X1-2,DB*X2)
D=(SCO2-X2+2,DB*(SCO*X2-X1*SCO2))/(1,DB-2,DB*X1-2,DB*X2)
Y(3*N+I)=(SCO-E+D)/SCO
Y(4*N+I)=(SCO2-D)/SCO
281 CONTINUE
READ(5,1) Y(6*N+2),Y(6*N+3),Y(6*N+4),Y(6*N+5),Y(6*N+1)
RETURN
FORMAT(9FB.2)
END

```

Table A4-7

```

SUBROUTINE SETUPS (DT#,TMAX,DL,N,RR,EP,IFLAG,NFLAG,NP,IF)
C THIS SUBROUTINE READS IN THE INPUT DATA AND MAKES PRELIMINARY
C CALCULATIONS.

IMPLICIT REAL*8 (A-H,O-Z)
REAL*8 L,KT,NG,KB,KP,KP2B,KC2B,K1P,K2P,K2,K3
COMMON /REACP/ EPS,L,RF,RI
* /CATL5/ CPS,PS,TC,DC
* /THWEL/ CPT,PT,KT
* /GASPA/ CPG,PTZ,PTR,MG,PGS,UGS,UM
* /HEATT/ OHSG,OHTS,OHTG,BGS,BSG,BTS,BTG,BWS
* /OPCON/ SCH4,SCO,SCO2,SH2,SH20,PTB,PT1,ST#,STW
* /REAC1/ DH1A,DH1B,DH2A,DH2B,KB,KP
* /REAC2/ EXPX,EXPB,EXPC,KC2B,KP2A,KP2B,K1P,K2P,EA1,EA2
DATA RG,RGP,PI /B2.5440B,1.987D0,3.141592654D0/
READ(5,1) EPS,L,RF,RI
READ(5,1) CPS,PS,TC,DC
READ(5,1) CPT,PT,KT
READ(5,1) PTZ,PTR,UGS
READ(5,1) OHSG,OHTS,OHTG,BGS,BSG,BTS,BTG
READ(5,1) SCH4,SCO,SCO2,SH2,SH20,PTB,PT1,ST#,STW
READ(5,1) DH1A,DH1B,DH2A,DH2B,KB,KP
READ(5,1) EXPX,EXPB,EXPC,KP2A,KP2B,K2,K3,EA1,EA2
READ(5,2) DT#,TMAX,RR,DL,TS,N,EP,IFLAG,NFLAG,IF,NFLAG
DATA RG,RGP,PI /B2.5440B,1.987D0,3.141592654D0/
CALL CPCALC(SH2,SCO,SCO2,SH20,SCH4,ST#,NG,CPG,CPG1,CPG2)
PGS=MG*PT#/RG/ST#
K1P=K2*PT#/SCO
K2P=K3*PT#/SCO
KC2B=1.D0
EP1B,D0**NEP
KBP=KB*PT#/TS**(-.3)
PRINT 3,EPS,CPS,CPT,L,PS,PT,RF,TC,KT,R1,OHSG,DH1A,EXPX,
* OHTS,DH1B,EXPB,OHTG,DH2A,EXPC,BGS,DH2B,KP2A,BSG,KW,
* KP2B,BTS,KB,PTR,KT,PTZ,EA1,PTR,EA2
PRINT 4,DT#,TMAX,DL,RR,TS,N,EP,IFLAG,NFLAG,DT#*4,D0***(IF-1)
PRINT 5,SCH4,ST#,SCO,STW,SCO2,PTB,SH2,PT1,SH20,MG,UGS,CPG
DT#*=DT#/UGS/L
TMAX=TMAX*UGS/L
DL=DL*UGS/L
RR=(1.D0-R#/#1)*RR+R#/R1
EA1=EA1/RGP
EA2=EA2/RGP
RETURN
1 FORMAT(90B.2)
2 FORMAT(15F.2,/,6I8)
3 FORMAT(1H1,///,3X,'INPUT DATA',//,9X,'REACTOR PARAMETERS',/9X,
* 'CATALYST PARAMETERS',6X,'THERMAL WELL PARAMETERS',//,
* 9X,'EPS',E12.4,9X,'CPS',E12.4,9X,'CPT',E12.4,9X,
* 9X,'L',E12.4,9X,'PS',E12.4,9X,'PT',E12.4,9X,
* 9X,'TC',E12.4,9X,'KT',E12.4,9X,'RF',E12.4,9X,
* 9X,'RI',E12.4,9X,'K1P',E12.4,9X,'K2P',E12.4,9X,
* 9X,'KC2B',E12.4,9X,'KB',E12.4,9X,'KP',E12.4,9X,
* 9X,'K2',E12.4,9X,'K3',E12.4,9X,'K4',E12.4,9X,
* 9X,'K5',E12.4,9X,'K6',E12.4,9X,'K7',E12.4,9X,
* 9X,'K8',E12.4,9X,'K9',E12.4,9X,'K10',E12.4,9X,
* 9X,'K11',E12.4,9X,'K12',E12.4,9X,'K13',E12.4,9X,
* 9X,'K14',E12.4,9X,'K15',E12.4,9X,'K16',E12.4,9X,
* 9X,'K17',E12.4,9X,'K18',E12.4,9X,'K19',E12.4,9X,
* 9X,'K20',E12.4,9X,'K21',E12.4,9X,'K22',E12.4,9X,
* 9X,'K23',E12.4,9X,'K24',E12.4,9X,'K25',E12.4,9X,
* 9X,'K26',E12.4,9X,'K27',E12.4,9X,'K28',E12.4,9X,
* 9X,'K29',E12.4,9X,'K30',E12.4,9X,'K31',E12.4,9X,
* 9X,'K32',E12.4,9X,'K33',E12.4,9X,'K34',E12.4,9X,
* 9X,'K35',E12.4,9X,'K36',E12.4,9X,'K37',E12.4,9X,
* 9X,'K38',E12.4,9X,'K39',E12.4,9X,'K40',E12.4,9X,
* 9X,'K41',E12.4,9X,'K42',E12.4,9X,'K43',E12.4,9X,
* 9X,'K44',E12.4,9X,'K45',E12.4,9X,'K46',E12.4,9X,
* 9X,'K47',E12.4,9X,'K48',E12.4,9X,'K49',E12.4,9X,
* 9X,'K50',E12.4,9X,'K51',E12.4,9X,'K52',E12.4,9X,
* 9X,'K53',E12.4,9X,'K54',E12.4,9X,'K55',E12.4,9X,
* 9X,'K56',E12.4,9X,'K57',E12.4,9X,'K58',E12.4,9X,
* 9X,'K59',E12.4,9X,'K60',E12.4,9X,'K61',E12.4,9X,
* 9X,'K62',E12.4,9X,'K63',E12.4,9X,'K64',E12.4,9X,
* 9X,'K65',E12.4,9X,'K66',E12.4,9X,'K67',E12.4,9X,
* 9X,'K68',E12.4,9X,'K69',E12.4,9X,'K70',E12.4,9X,
* 9X,'K71',E12.4,9X,'K72',E12.4,9X,'K73',E12.4,9X,
* 9X,'K74',E12.4,9X,'K75',E12.4,9X,'K76',E12.4,9X,
* 9X,'K77',E12.4,9X,'K78',E12.4,9X,'K79',E12.4,9X,
* 9X,'K80',E12.4,9X,'K81',E12.4,9X,'K82',E12.4,9X,
* 9X,'K83',E12.4,9X,'K84',E12.4,9X,'K85',E12.4,9X,
* 9X,'K86',E12.4,9X,'K87',E12.4,9X,'K88',E12.4,9X,
* 9X,'K89',E12.4,9X,'K90',E12.4,9X,'K91',E12.4,9X,
* 9X,'K92',E12.4,9X,'K93',E12.4,9X,'K94',E12.4,9X,
* 9X,'K95',E12.4,9X,'K96',E12.4,9X,'K97',E12.4,9X,
* 9X,'K98',E12.4,9X,'K99',E12.4,9X,'K100',E12.4,9X,
* 9X,'K101',E12.4,9X,'K102',E12.4,9X,'K103',E12.4,9X,
* 9X,'K104',E12.4,9X,'K105',E12.4,9X,'K106',E12.4,9X,
* 9X,'K107',E12.4,9X,'K108',E12.4,9X,'K109',E12.4,9X,
* 9X,'K110',E12.4,9X,'K111',E12.4,9X,'K112',E12.4,9X,
* 9X,'K113',E12.4,9X,'K114',E12.4,9X,'K115',E12.4,9X,
* 9X,'K116',E12.4,9X,'K117',E12.4,9X,'K118',E12.4,9X,
* 9X,'K119',E12.4,9X,'K120',E12.4,9X,'K121',E12.4,9X,
* 9X,'K122',E12.4,9X,'K123',E12.4,9X,'K124',E12.4,9X,
* 9X,'K125',E12.4,9X,'K126',E12.4,9X,'K127',E12.4,9X,
* 9X,'K128',E12.4,9X,'K129',E12.4,9X,'K130',E12.4,9X,
* 9X,'K131',E12.4,9X,'K132',E12.4,9X,'K133',E12.4,9X,
* 9X,'K134',E12.4,9X,'K135',E12.4,9X,'K136',E12.4,9X,
* 9X,'K137',E12.4,9X,'K138',E12.4,9X,'K139',E12.4,9X,
* 9X,'K140',E12.4,9X,'K141',E12.4,9X,'K142',E12.4,9X,
* 9X,'K143',E12.4,9X,'K144',E12.4,9X,'K145',E12.4,9X,
* 9X,'K146',E12.4,9X,'K147',E12.4,9X,'K148',E12.4,9X,
* 9X,'K149',E12.4,9X,'K150',E12.4,9X,'K151',E12.4,9X,
* 9X,'K152',E12.4,9X,'K153',E12.4,9X,'K154',E12.4,9X,
* 9X,'K155',E12.4,9X,'K156',E12.4,9X,'K157',E12.4,9X,
* 9X,'K158',E12.4,9X,'K159',E12.4,9X,'K160',E12.4,9X,
* 9X,'K161',E12.4,9X,'K162',E12.4,9X,'K163',E12.4,9X,
* 9X,'K164',E12.4,9X,'K165',E12.4,9X,'K166',E12.4,9X,
* 9X,'K167',E12.4,9X,'K168',E12.4,9X,'K169',E12.4,9X,
* 9X,'K170',E12.4,9X,'K171',E12.4,9X,'K172',E12.4,9X,
* 9X,'K173',E12.4,9X,'K174',E12.4,9X,'K175',E12.4,9X,
* 9X,'K176',E12.4,9X,'K177',E12.4,9X,'K178',E12.4,9X,
* 9X,'K179',E12.4,9X,'K180',E12.4,9X,'K181',E12.4,9X,
* 9X,'K182',E12.4,9X,'K183',E12.4,9X,'K184',E12.4,9X,
* 9X,'K185',E12.4,9X,'K186',E12.4,9X,'K187',E12.4,9X,
* 9X,'K188',E12.4,9X,'K189',E12.4,9X,'K190',E12.4,9X,
* 9X,'K191',E12.4,9X,'K192',E12.4,9X,'K193',E12.4,9X,
* 9X,'K194',E12.4,9X,'K195',E12.4,9X,'K196',E12.4,9X,
* 9X,'K197',E12.4,9X,'K198',E12.4,9X,'K199',E12.4,9X,
* 9X,'K200',E12.4,9X,'K201',E12.4,9X,'K202',E12.4,9X,
* 9X,'K203',E12.4,9X,'K204',E12.4,9X,'K205',E12.4,9X,
* 9X,'K206',E12.4,9X,'K207',E12.4,9X,'K208',E12.4,9X,
* 9X,'K209',E12.4,9X,'K210',E12.4,9X,'K211',E12.4,9X,
* 9X,'K212',E12.4,9X,'K213',E12.4,9X,'K214',E12.4,9X,
* 9X,'K215',E12.4,9X,'K216',E12.4,9X,'K217',E12.4,9X,
* 9X,'K218',E12.4,9X,'K219',E12.4,9X,'K220',E12.4,9X,
* 9X,'K221',E12.4,9X,'K222',E12.4,9X,'K223',E12.4,9X,
* 9X,'K224',E12.4,9X,'K225',E12.4,9X,'K226',E12.4,9X,
* 9X,'K227',E12.4,9X,'K228',E12.4,9X,'K229',E12.4,9X,
* 9X,'K230',E12.4,9X,'K231',E12.4,9X,'K232',E12.4,9X,
* 9X,'K233',E12.4,9X,'K234',E12.4,9X,'K235',E12.4,9X,
* 9X,'K236',E12.4,9X,'K237',E12.4,9X,'K238',E12.4,9X,
* 9X,'K239',E12.4,9X,'K240',E12.4,9X,'K241',E12.4,9X,
* 9X,'K242',E12.4,9X,'K243',E12.4,9X,'K244',E12.4,9X,
* 9X,'K245',E12.4,9X,'K246',E12.4,9X,'K247',E12.4,9X,
* 9X,'K248',E12.4,9X,'K249',E12.4,9X,'K250',E12.4,9X,
* 9X,'K251',E12.4,9X,'K252',E12.4,9X,'K253',E12.4,9X,
* 9X,'K254',E12.4,9X,'K255',E12.4,9X,'K256',E12.4,9X,
* 9X,'K257',E12.4,9X,'K258',E12.4,9X,'K259',E12.4,9X,
* 9X,'K260',E12.4,9X,'K261',E12.4,9X,'K262',E12.4,9X,
* 9X,'K263',E12.4,9X,'K264',E12.4,9X,'K265',E12.4,9X,
* 9X,'K266',E12.4,9X,'K267',E12.4,9X,'K268',E12.4,9X,
* 9X,'K269',E12.4,9X,'K270',E12.4,9X,'K271',E12.4,9X,
* 9X,'K272',E12.4,9X,'K273',E12.4,9X,'K274',E12.4,9X,
* 9X,'K275',E12.4,9X,'K276',E12.4,9X,'K277',E12.4,9X,
* 9X,'K278',E12.4,9X,'K279',E12.4,9X,'K280',E12.4,9X,
* 9X,'K281',E12.4,9X,'K282',E12.4,9X,'K283',E12.4,9X,
* 9X,'K284',E12.4,9X,'K285',E12.4,9X,'K286',E12.4,9X,
* 9X,'K287',E12.4,9X,'K288',E12.4,9X,'K289',E12.4,9X,
* 9X,'K290',E12.4,9X,'K291',E12.4,9X,'K292',E12.4,9X,
* 9X,'K293',E12.4,9X,'K294',E12.4,9X,'K295',E12.4,9X,
* 9X,'K296',E12.4,9X,'K297',E12.4,9X,'K298',E12.4,9X,
* 9X,'K299',E12.4,9X,'K300',E12.4,9X,'K301',E12.4,9X,
* 9X,'K302',E12.4,9X,'K303',E12.4,9X,'K304',E12.4,9X,
* 9X,'K305',E12.4,9X,'K306',E12.4,9X,'K307',E12.4,9X,
* 9X,'K308',E12.4,9X,'K309',E12.4,9X,'K310',E12.4,9X,
* 9X,'K311',E12.4,9X,'K312',E12.4,9X,'K313',E12.4,9X,
* 9X,'K314',E12.4,9X,'K315',E12.4,9X,'K316',E12.4,9X,
* 9X,'K317',E12.4,9X,'K318',E12.4,9X,'K319',E12.4,9X,
* 9X,'K320',E12.4,9X,'K321',E12.4,9X,'K322',E12.4,9X,
* 9X,'K323',E12.4,9X,'K324',E12.4,9X,'K325',E12.4,9X,
* 9X,'K326',E12.4,9X,'K327',E12.4,9X,'K328',E12.4,9X,
* 9X,'K329',E12.4,9X,'K330',E12.4,9X,'K331',E12.4,9X,
* 9X,'K332',E12.4,9X,'K333',E12.4,9X,'K334',E12.4,9X,
* 9X,'K335',E12.4,9X,'K336',E12.4,9X,'K337',E12.4,9X,
* 9X,'K338',E12.4,9X,'K339',E12.4,9X,'K340',E12.4,9X,
* 9X,'K341',E12.4,9X,'K342',E12.4,9X,'K343',E12.4,9X,
* 9X,'K344',E12.4,9X,'K345',E12.4,9X,'K346',E12.4,9X,
* 9X,'K347',E12.4,9X,'K348',E12.4,9X,'K349',E12.4,9X,
* 9X,'K350',E12.4,9X,'K351',E12.4,9X,'K352',E12.4,9X,
* 9X,'K353',E12.4,9X,'K354',E12.4,9X,'K355',E12.4,9X,
* 9X,'K356',E12.4,9X,'K357',E12.4,9X,'K358',E12.4,9X,
* 9X,'K359',E12.4,9X,'K360',E12.4,9X,'K361',E12.4,9X,
* 9X,'K362',E12.4,9X,'K363',E12.4,9X,'K364',E12.4,9X,
* 9X,'K365',E12.4,9X,'K366',E12.4,9X,'K367',E12.4,9X,
* 9X,'K368',E12.4,9X,'K369',E12.4,9X,'K370',E12.4,9X,
* 9X,'K371',E12.4,9X,'K372',E12.4,9X,'K373',E12.4,9X,
* 9X,'K374',E12.4,9X,'K375',E12.4,9X,'K376',E12.4,9X,
* 9X,'K377',E12.4,9X,'K378',E12.4,9X,'K379',E12.4,9X,
* 9X,'K380',E12.4,9X,'K381',E12.4,9X,'K382',E12.4,9X,
* 9X,'K383',E12.4,9X,'K384',E12.4,9X,'K385',E12.4,9X,
* 9X,'K386',E12.4,9X,'K387',E12.4,9X,'K388',E12.4,9X,
* 9X,'K389',E12.4,9X,'K390',E12.4,9X,'K391',E12.4,9X,
* 9X,'K392',E12.4,9X,'K393',E12.4,9X,'K394',E12.4,9X,
* 9X,'K395',E12.4,9X,'K396',E12.4,9X,'K397',E12.4,9X,
* 9X,'K398',E12.4,9X,'K399',E12.4,9X,'K400',E12.4,9X,
* 9X,'K401',E12.4,9X,'K402',E12.4,9X,'K403',E12.4,9X,
* 9X,'K404',E12.4,9X,'K405',E12.4,9X,'K406',E12.4,9X,
* 9X,'K407',E12.4,9X,'K408',E12.4,9X,'K409',E12.4,9X,
* 9X,'K410',E12.4,9X,'K411',E12.4,9X,'K412',E12.4,9X,
* 9X,'K413',E12.4,9X,'K414',E12.4,9X,'K415',E12.4,9X,
* 9X,'K416',E12.4,9X,'K417',E12.4,9X,'K418',E12.4,9X,
* 9X,'K419',E12.4,9X,'K420',E12.4,9X,'K421',E12.4,9X,
* 9X,'K422',E12.4,9X,'K423',E12.4,9X,'K424',E12.4,9X,
* 9X,'K425',E12.4,9X,'K426',E12.4,9X,'K427',E12.4,9X,
* 9X,'K428',E12.4,9X,'K429',E12.4,9X,'K430',E12.4,9X,
* 9X,'K431',E12.4,9X,'K432',E12.4,9X,'K433',E12.4,9X,
* 9X,'K434',E12.4,9X,'K435',E12.4,9X,'K436',E12.4,9X,
* 9X,'K437',E12.4,9X,'K438',E12.4,9X,'K439',E12.4,9X,
* 9X,'K440',E12.4,9X,'K441',E12.4,9X,'K442',E12.4,9X,
* 9X,'K443',E12.4,9X,'K444',E12.4,9X,'K445',E12.4,9X,
* 9X,'K446',E12.4,9X,'K447',E12.4,9X,'K448',E12.4,9X,
* 9X,'K449',E12.4,9X,'K450',E12.4,9X,'K451',E12.4,9X,
* 9X,'K452',E12.4,9X,'K453',E12.4,9X,'K454',E12.4,9X,
* 9X,'K455',E12.4,9X,'K456',E12.4,9X,'K457',E12.4,9X,
* 9X,'K458',E12.4,9X,'K459',E12.4,9X,'K460',E12.4,9X,
* 9X,'K461',E12.4,9X,'K462',E12.4,9X,'K463',E12.4,9X,
* 9X,'K464',E12.4,9X,'K465',E12.4,9X,'K466',E12.4,9X,
* 9X,'K467',E12.4,9X,'K468',E12.4,9X,'K469',E12.4,9X,
* 9X,'K470',E12.4,9X,'K471',E12.4,9X,'K472',E12.4,9X,
* 9X,'K473',E12.4,9X,'K474',E12.4,9X,'K475',E12.4,9X,
* 9X,'K476',E12.4,9X,'K477',E12.4,9X,'K478',E12.4,9X,
* 9X,'K479',E12.4,9X,'K480',E12.4,9X,'K481',E12.4,9X,
* 9X,'K482',E12.4,9X,'K483',E12.4,9X,'K484',E12.4,9X,
* 9X,'K485',E12.4,9X,'K486',E12.4,9X,'K487',E12.4,9X,
* 9X,'K488',E12.4,9X,'K489',E12.4,9X,'K490',E12.4,9X,
* 9X,'K491',E12.4,9X,'K492',E12.4,9X,'K493',E12.4,9X,
* 9X,'K494',E12.4,9X,'K495',E12.4,9X,'K496',E12.4,9X,
* 9X,'K497',E12.4,9X,'K498',E12.4,9X,'K499',E12.4,9X,
* 9X,'K500',E12.4,9X,'K501',E12.4,9X,'K502',E12.4,9X,
* 9X,'K503',E12.4,9X,'K504',E12.4,9X,'K505',E12.4,9X,
* 9X,'K506',E12.4,9X,'K507',E12.4,9X,'K508',E12.4,9X,
* 9X,'K509',E12.4,9X,'K510',E12.4,9X,'K511',E12.4,9X,
* 9X,'K512',E12.4,9X,'K513',E12.4,9X,'K514',E12.4,9X,
* 9X,'K515',E12.4,9X,'K516',E12.4,9X,'K517',E12.4,9X,
* 9X,'K518',E12.4,9X,'K519',E12.4,9X,'K520',E12.4,9X,
* 9X,'K521',E12.4,9X,'K522',E12.4,9X,'K523',E12.4,9X,
* 9X,'K524',E12.4,9X,'K525',E12.4,9X,'K526',E12.4,9X,
* 9X,'K527',E12.4,9X,'K528',E12.4,9X,'K529',E12.4,9X,
* 9X,'K530',E12.4,9X,'K531',E12.4,9X,'K532',E12.4,9X,
* 9X,'K533',E12.4,9X,'K534',E12.4,9X,'K535',E12.4,9X,
* 9X,'K536',E12.4,9X,'K537',E12.4,9X,'K538',E12.4,9X,
* 9X,'K539',E12.4,9X,'K540',E12.4,9X,'K541',E12.4,9X,
* 9X,'K542',E12.4,9X,'K543',E12.4,9X,'K544',E12.4,9X,
* 9X,'K545',E12.4,9X,'K546',E12.4,9X,'K547',E12.4,9X,
* 9X,'K548',E12.4,9X,'K549',E12.4,9X,'K550',E12.4,9X,
* 9X,'K551',E12.4,9X,'K552',E12.4,9X,'K553',E12.4,9X,
* 9X,'K554',E12.4,9X,'K555',E12.4,9X,'K556',E12.4,9X,
* 9X,'K557',E12.4,9X,'K558',E12.4,9X,'K559',E12.4,9X,
* 9X,'K560',E12.4,9X,'K561',E12.4,9X,'K562',E12.4,9X,
* 9X,'K563',E12.4,9X,'K564',E12.4,9X,'K565',E12.4,9X,
* 9X,'K566',E12.4,9X,'K567',E12.4,9X,'K568',E12.4,9X,
* 9X,'K569',E12.4,9X,'K570',E12.4,9X,'K571',E12.4,9X,
* 9X,'K572',E12.4,9X,'K573',E12.4,9X,'K574',E12.4,9X,
* 9X,'K575',E12.4,9X,'K576',E12.4,9X,'K577',E12.4,9X,
* 9X,'K578',E12.4,9X,'K579',E12.4,9X,'K580',E12.4,9X,
* 9X,'K581',E12.4,9X,'K582',E12.4,9X,'K583',E12.4,9X,
* 9X,'K584',E12.4,9X,'K585',E12.4,9X,'K586',E12.4,9X,
* 9X,'K587',E12.4,9X,'K588',E12.4,9X,'K589',E12.4,9X,
* 9X,'K590',E12.4,9X,'K591',E12.4,9X,'K592',E12.4,9X,
* 9X,'K593',E12.4,9X,'K594',E12.4,9X,'K595',E12.4,9X,
* 9X,'K596',E12.4,9X,'K597',E12.4,9X,'K598',E12.4,9X,
* 9X,'K599',E12.4,9X,'K600',E12.4,9X,'K601',E12.4,9X,
* 9X,'K602',E12.4,9X,'K603',E12.4,9X,'K604',E12.4,9X,
* 9X,'K605',E12.4,9X,'K606',E12.4,9X,'K607',E12.4,9X,
* 9X,'K608',E12.4,9X,'K609',E12.4,9X,'K610',E12.4,9X,
* 9X,'K611',E12.4,9X,'K612',E12.4,9X,'K613',E12.4,9X,
* 9X,'K614',E12.4,9X,'K615',E12.4,9X,'K616',E12.4,9X,
* 9X,'K617',E12.4,9X,'K618',E12.4,9X,'K619',E12.4,9X,
* 9X,'K620',E12.4,9X,'K621',E12.4,9X,'K622',E12.4,9X,
* 9X,'K623',E12.4,9X,'K624',E12.4,9X,'K625',E12.4,9X,
* 9X,'K626',E12.4,9X,'K627',E12.4,9X,'K628',E12.4,9X,
* 9X,'K629',E12.4,9X,'K630',E12.4,9X,'K631',E12.4,9X,
* 9X,'K632',E12.4,9X,'K633',E12.4,9X,'K634',E12.4,9X,
* 9X,'K635',E12.4,9X,'K636',E12.4,9X,'K637',E12.4,9X,
* 9X,'K638',E12.4,9X,'K639',E12.4,9X,'K640',E12.4,9X,
* 9X,'K641',E12.4,9X,'K642',E12.4,9X,'K643',E12.4,9X,
* 9X,'K644',E12.4,9X,'K645',E12.4,9X,'K646',E12.4,9X,
* 9X,'K647',E12.4,9X,'K648',E12.4,9X,'K649',E12.4,9X,
* 9X,'K650',E12.4,9X,'K651',E12.4,9X,'K652',E12.4,9X,
* 9X,'K653',E12.4,9X,'K654',E12.4,9X,'K655',E12.4,9X,
* 9X,'K656',E12.4,9X,'K657',E12.4,9X,'K658',E12.
```

```

SUBROUTINE OUTPUT (Y,U,T,L,UGS,PH1,MM)
C THIS ROUTINE OUTPUTS THE CALCULATED RESULTS.

IMPLICIT REAL*8 (A-H,O-Z)
REAL*8 L
DIMENSION Y(1#MM),U(8)
COMMON /COMAT/ A(25,25),B(25,25),R(25),N
*      /OPCON/ SC1,SC0,SC02,SH2,SH0,PT#,PT1,ST#,STW
*      /RADIA/ W(1#),WP(9,2),DETA(2),RR
DATA RG /82.8544DB/
IF(MM .EQ. 1) PRINT 1
IF(MM .EQ. 2) PRINT 6
IF(MM .EQ. 3) PRINT 8
PH2=PT1/PT#
N2=2*N
N3=3*N
N4=4*N
N5=5*N
N6=6*N
N7=N+2
N8=N+2
TA=T#*UGS
IF(MM .EQ. 8)PRINT 7,TA
CALL ENDPTS (TT#,Y1#,Y1NP1,Y2#,Y2NP1,TTNP1,Y,UGS)
PRINT 2
PRINT 3, TR(Y(N6+4),TT#,2,PH1),Y(N6+4),TR(Y(N6+4),TT#,2,1,DB),
*      TR(Y(N6+2),TT#,1,PH1),Y(N6+2),TR(Y(N6+2),TT#,1,1,DB)
DO 1#1 I=1,N
1#1 PRINT 3, TR(Y(N+I),Y(N2+I),2,PH1),Y(N+I),TR(Y(N+I),Y(N2+I),2,
*      ,DB),TR(Y(I),Y(N2+I),1,PH1),Y(I),TR(Y(I),Y(N2+I),1,1,DB)
*      PRINT 3,TR(Y(N6+5),TTNP1,2,PH1),Y(N6+5),TR(Y(N6+5),TTNP1,2,1,DB),
*      ,TR(Y(N6+3),TTNP1,1,PH1),Y(N6+3),TR(Y(N6+3),TTNP1,1,1,DB)
PRINT 4
PRINT 5, TT#,Y1#*SCO,Y2#*SCO,UGS
DO 1#2 I=1,N
1#2 TH1=1,DB=2,DB*(SCO*(U(4)-Y(N3+I)+U(5)-Y(N4+I)))
PRINT 5,Y(N2+I),Y(N3+I)*SCO/TH1,Y(N4+I)*SCO/TH1,Y(N5+I)
TH1=1,DB=2,DB*(SCO*(U(4)-Y1NP1+U(5)-Y2NP1))
PRINT 5,TTNP1,Y1NP1*SCO/TH1,Y2NP1*SCO/TH1,Y(N6+1)
RETURN
1 FORMAT(1H1, //2X,'INITIAL GUESSES: ' //)
2 FORMAT(16X,'GAS TEMPERATURE',25X,
*      'SOLID TEMPERATURE',//8X,'R = RR',7X,'R = RR',7X,
*      'R = R1',9X,'R = RR',7X,'R = RR',7X,'R = R1')
3 FORMAT(5X,3(F9.5,4X),2X,3(F9.5,4X))
4 FORMAT(1/9X,'WELL TEMP.',5X,'CO CONC.',5X,'CO2 CONC.',4X,
*      'VELOCITY')
5 FORMAT(19X,F9.5,5X,F1#-7,3X,F1#-7,3X,F9.5,3X,F9.5)
6 FORMAT(//2X,'STEADY STATE SOLUTION', //)
7 FORMAT(//,2X,'TIME = ',F11.4,' SEC')
8 FORMAT(//,2X,'ACTUAL STEADY STATE SOLUTION: ',//)
END

SUBROUTINE RADIAL
C THIS SUBROUTINE CALCULATES THE CONSTANTS FOR THE RADIALLY LUMPED
C MODEL.

IMPLICIT REAL*8 (A-H,O-Z)
COMMON /DIMLE/ ALS,ALG,ALT,BES,BEG,GAS,GAG,GTS,GTG,DEI,
*      DE2,S11,S12,S13,PH12,PH13,PH1,PH2,PH3
*      /RADIA/ W(1#),WP(9,2),DETA(2),RR
*      /HEATT/ OHSG,OHTG,BG5,BSG,BTS,BTG,BWG,BWS
W(9)=#.DB#
W(1#)=#.DB#
I=1
S1=BTS
S2=BWS
S3=GAS
S4=BEG
S5=GTS
1#5 DETA(I)=(PH1+PH1)**2*(RR-1,DB)+RR**2*(1,DB-PH1)-RR)*S1*S2
*      +(2,DB*(PH1-RR)+RR**2*PH1**2)*S1
*      +(-1,DB+RR**2+2,DB*(PH1-PH1*RR))*S2+2,DB*PH1-2,DB
WP(1,I)=(PH1*S1-1,DB)*(S2+2,DB)*(PH1**2*S1-2,DB*PH1)
WP(2,I)=S1*(S2+1,DB)*RR**2*S1*RR*(S2+2,DB)
WP(3,I)=(S2*RR*(PH1**2*S1-2,DB*PH1)-S2*(PH1*S1-1,DB)*RR**2)
WP(4,I)=S2*(PH1**2*S1-2,DB*PH1)-S1*(S2+2,DB)
WP(5,I)=S1*(S2+2,DB)-S1*S2*RR**2
WP(6,I)=-(S1*S2*RR**2-S2*(PH1**2*S1-2,DB*PH1))
WP(7,I)=S1*(S2+1,DB)-S2*(PH1*S1-1,DB)
WP(8,I)=RR*S1*S2*(S2+1,DB)
WP(9,I)=(S2*(PH1*S1-1,DB)-RR*S1*S2)
W(1+I#3-3)=(4,DB*WP(7,I)+WP(4,I)/RR)*S4/DETA(I)-S3
W(2+I#3-3)=(4,DB*WP(8,I)+WP(5,I)/RR)*S4/DETA(I)
W(3+I#3-3)=(4,DB*WP(9,I)+WP(6,I)/RR)*S4/DETA(I)
W(7+I-1)=S5*(WP(1,I)+WP(4,I)*PH1+WP(7,I)*PH1**2)/DETA(I)
W(9)=W(9)+S5*(WP(2,I)+WP(5,I)*PH1+WP(8,I)*PH1**2)/DETA(I)-S5
W(1#)=W(1#)+S5*(WP(3,I)+WP(6,I)*PH1+WP(9,I)*PH1**2)/DETA(I)
IF(I .EQ. 2)RETURN
I=2
S1=BTG
S2=BWG
S3=GAG
S4=BEG
S5=GTG
GO TO 1#5
END

```

Table A4-7 Continued

```

SUBROUTINE FN1 (Y,V)
C THIS SUBROUTINE DEFINES THE ALGEBRAIC EQUATIONS FOR USE BY NSES1
IMPLICIT REAL*8 (A-H,O-Z)
DIMENSION Y(188),V(1)
COMMON /COMAT/ A(25,25),B(25,25),R(25),N
* /DIMLE/ ALS,ALG,ALT,BES,BEG,GAS,GAG,GTS,GTG,DE1,
* DE2,S11,S12,S13,PH12,PH13,PH1,PH2,PH3
* /RADIA/ W(18),WP(9,2),DETA(2),RR
* /HEATT/ OHSG,OHTS,OHTC,BGS,BSG,BTS,BTG,BWG,BVS
NP2=N+2
N2=N+2
N3=N+3
N4=N+4
N5=N+5
N6=N+6
TAU=PH2-1.0#
CALL ENDPTS (TT#,Y1#,Y1NP1,Y2#,Y2NP1,TTNP1,Y,UG#)
DO 1# I=1,N
IP1=I+1
PT=TAU*R(IP1)+1.0#
CALL REAC (Y(N3+I),Y(N4+I),Y(I),Y(N+I),PT,R1P,R2P)
S1=SUM(Y,B,B,Y(N6+2),Y(N5+3),I,N)
S2=SUM(Y,N,A,Y(N6+4),Y(N5+5),I,N)
S3=SUM(Y,N,B,Y(N6+4),Y(N5+5),I,N)
S4=SUM(Y,N3,A,Y1#,Y1NP1,I,N)
S5=SUM(Y,N4,A,Y2#,Y2NP1,I,N)
S6=SUM(Y,N2,B,I,RR,TTNP1,I,N)
S8=SUM(Y,N2,B,I,RR,TTNP1,I,N)
V(I) = ALS*S1 + W(1)*Y(I) + W(2)*Y(N2+I) + GAS*Y(N+I)
* + DE1*R1P*(1.0#+PH12*Y(I)) + DE2*R2P*(1.0#+PH13*Y(I))
* + W(3)*PH3
* V(I+N) = -Y(N5+I)*S2 + (ALG*S3 + W(4)*Y(N+I) + W(5)*Y(N2+I)
* + GAG*(Y(I) + W(6)*PH3))/PT*Y(N+I)
V(I+N2) = ALT*S8 - W(7)*Y(I) + W(8)*Y(N+I) + W(9)*Y(N2+I)
* + W(10)*PH3
V(I+N3) = -Y(N5+I)*S4 + S12*Y(N+I)*R2P/PT - S11*Y(N+I)*R1P/PT
V(I+N4) = -Y(N5+I)*S6 - S13*Y(N+I)*R2P/PT
CONTINUE
V(N6+2)=SUM(Y,B,A,Y(N6+2),Y(N6+3),B,N)+BGS*(Y(N6+4)-Y(N6+2))
V(N6+3)=SUM(Y,B,A,Y(N6+2),Y(N6+3),N+1,N)+BGS*(Y(N6+3)-Y(N6+5))
V(N6+4)=SUM(Y,N,A,Y(N6+4),Y(N6+5),B,N)+BGS*(Y(N6+2)-Y(N6+4))
* -(1.0#-1.0#/Y(N6+4))/ALG
V(N6+5)=SUM(Y,N,A,Y(N6+4),Y(N6+5),N+1,N)+BGS*(Y(N6+5)-Y(N6+3))
PT=PH2
CALL REAC(Y1NP1,Y2NP1,Y(N6+3),Y(N6+5),PT,R1P,R2P)
V(N6+6)=-Y(N6+1)*SUM(Y,N3,A,Y1#,Y1NP1,N+1,N)
* +S12*Y(N6+5)*R2P/PT - S11*Y(N6+5)*R1P/PT
DO 11# K=1,N
V(N5+K)=Y(N+K)*SUM(Y,N5,A,UG#,Y(N6+1),K,N)-Y(N5+K)*SUM(Y,N,A,
* Y(N6+4),Y(N6+5),K,N)+Y(N5+K)*Y(N+K)*TAU/(TAU*R(K-1)+1.0#)
V(N6+1)=Y(N6+5)*SUM(Y,N5,A,UG#,Y(N6+1),N+1,N)-Y(N6+1)*SUM(Y,N,A
* ,Y(N6+4),Y(N6+5),N+1,N)+Y(N6+1)*Y(N6+5)*TAU/(TAU+1.0#)
RETURN
END

SUBROUTINE FN2(KK,Y,V)
C THIS SUBROUTINE DEFINES THE ALGEBRAIC EQUATIONS FOR USE BY NSES2
IMPLICIT REAL*8 (A-H,O-Z)
DIMENSION Y(188)
COMMON /ALGEB/ A1(188),A2(4)
* /COMAT/ A(25,25),B(25,25),R(25),N,IB
* /DIMLE/ ALS,ALG,ALT,BES,BEG,GAS,GAG,GTS,GTG,DE1,
* DE2,S11,S12,S13,PH12,PH13,PH1,PH2,PH3
* /RADIA/ W(18),WP(9,2),DETA(2),RR
* /HEATT/ OHSG,OHTS,OHTC,BGS,BSG,BTS,BTG,BWG,BVS
NP2=N+2
N2=N+2
N3=N+3
N4=N+4
N5=N+5
N6=N+6
TAU=PH2-1.0#
CALL ENDPTS (TT#,Y1#,Y1NP1,Y2#,Y2NP1,TTNP1,Y,UG#)
V=B, DB
IF (KK .GT. N5) GO TO 2#
IF (KK .GT. N4) GO TO 11#
IF (KK .GT. N3) GO TO 12#
IF (KK .GT. N2) GO TO 13#
IF (KK .GT. N) GO TO 14#
I=KK
IP1=I+1
PT=TAU*R(IP1)+1.0#
CALL REAC (Y(N3+I),Y(N4+I),Y(I),Y(N+I),PT,R1P,R2P)
S1=SUM(Y,B,B,Y(N6+2),Y(N5+3),I,N)
V= ALS*S1 + W(1)*Y(I) + W(2)*Y(N2+I) + GAS*Y(N+I)
* + DE1*R1P*(1.0#+PH12*Y(I)) + DE2*R2P*(1.0#+PH13*Y(I))
* + W(3)*PH3
RETURN

```

Table A4-7 Continued

```

148  I=KK-N
1P1=I+1
PT=TAU*R(IP1)+1.D#
S2=SUM(Y,N,A,Y(N6+4),Y(N6+5),I,N)
S3=SUM(Y,N,B,Y(N6+4),Y(N6+5),I,N)
V= -Y(N5+1)*S2 + (ALG*S3 + W(4)*Y(N+I) + W(5)*Y(N2+I)
* + GAG*Y(I) + W(6)*PH3)/PT*Y(N+I)
RETURN

138  I=KK-N2
S8=SUM(Y,N2,B,1.D#,TTNP1,I,N)
V= ALT*SB + W(7)*Y(I) + W(8)*Y(N+I) + W(9)*Y(N2+I)
* + W(10)*PH3
RETURN

128  I=KK-N3
1P1=I+1
PT=TAU*R(IP1)+1.D#
CALL REAC_ (Y(N3+I),Y(N4+I),Y(I),Y(N+I),PT,R1P,R2P)
S4=SUM(Y,N3,A,Y1B,YINP1,I,N)
V= -Y(N5+1)*S4 + S12*Y(N+I)*R2P/PT - S11*Y(N+I)*R1P/PT
RETURN

118  I=KK-N4
1P1=I+1
PT=TAU*R(IP1)+1.D#
CALL REAC_ (Y(N3+I),Y(N4+I),Y(I),Y(N+I),PT,R1P,R2P)
S6=SUM(Y,N4,A,Y2B,Y2NP1,I,N)
RETURN

288  K=KK-N5
KPI=K+1
IF(K .LE. N+1) GO TO 188
L=K-M-1
IF (L .EQ. 1) V=SUM(Y,B,A,Y(N6+2),Y(N6+3),B,N)+BGS*(Y(N6+4)
* -Y(N6+2))
IF (L .EQ. 2) V=SUM(Y,B,A,Y(N6+2),Y(N6+3),N+1,N)+BGS*(Y(N6+3)
* -Y(N6+5))
IF (L .EQ. 3) V=SUM(Y,N,A,Y(N6+4),Y(N6+5),B,N)+BGS*(Y(N6+2)
* -Y(N6+4))- (1.D#-1.D#/Y(N6+4))/ALG
IF (L .EQ. 4) V=SUM(Y,N,A,Y(N6+4),Y(N6+5),N+1,N)+BGS*(Y(N6+5)
* -Y(N6+3))
RETURN

188  IF (K .EQ. N+1) V=Y(N5+K)*Y(N6+5)*TAU/(TAU+1.D#)+Y(N6+5)*
* SUM(Y,N5,A,UGB,Y(N5+1),K,N)-Y(N5+K)*
* SUM(Y,N,A,Y(N6+4),Y(N6+5),K,N)
IF (K .NE. N+1) V=Y(N5+K)*Y(N5+K)*TAU/(R(KP1)*TAU+1.D#)+Y(N+K)*
* SUM(Y,N5,A,UGB,Y(N5+1),K,N)-Y(N5+K)*
* SUM(Y,N,A,Y(N6+4),Y(N6+5),K,N)
RETURN
END

SUBROUTINE FN3 (Y,V)
IMPLICIT REAL*8 (A-H,O-Z)
DIMENSION Y(100),V(1)
COMMON /LINEA/ AA(75,75),BB(75,8),DD(75),U(8)
* /ALGB/ S(4,4),H(2B,4B),RI(2B,4),AL(7)
* /COMAT/ A(25,25),B(25,25),R(25),N
DO 188 I=1,N*5
V(I)=DD(I)
DO 181 J=1,N*5
V(I)=V(I)+AA(I,J)*Y(J)
DO 182 J=1,8
V(I)=V(I)+BB(I,J)*U(J)
182 CONTINUE
188 RETURN
END

```

Table A4-7 Continued

```

SUBROUTINE LREAC(VS,RL1,RL2)

C THIS SUBROUTINE CALCULATES THE COEFFICIENTS FOR THE
C LINEARIZED RATES.

IMPLICIT REAL*8 (A-H,O-Z)
REAL*8 KP2A,KP2B,KC2B,K1P,K2P,KP2
DIMENSION RL1(15,9),R(12,15,9),VS(1,9)
COMMON /OPCON/ SCH4,SCO,SC02,SH2,SH20,PTB,PT1,STB,STV
* /REAC2/, EXP4, EXPB, EXPc, KC2B, KP2A, KP2B, K1P, K2P, EA1, EA2
* /COMAT/, A(25,25), B(25,25), R(25), N
* /LINEA/, AA(75,75), BB(75,75), DD(75), U(8)
DATA F1,F2 /8.830E,8.170E/
DO 100 I=1,N
Y1=VS(3*N+I)
Y2=VS(4*N+I)
TS=VS(I)
TG=VS(N+I)
PT=(PT1/PTB-1.0E)=R(I+1)+1.0E
TT=STB*TS*TS
KP2=DEXP(KP2A+KP2B/TS/STB)
TH1=SCO*(U(4)-U(5))-Y1-Y2)
TH2=SCO*(U(5)-Y2)
TH3=1.0E-2.0E*TH1
YH2=(SH2-3.0E*TH1-TH2)/SCO
YH20=(SH20+TH1+TH2)/SCO
YCH4=(SCH4*TH1)/SCO
PA=PT*TH3
AAA=1.0E+K1P*PT*Y1+K2P*PT*YH2
RL1(I,1)=DEXP(-EA1/STB/TS)*PT***(EXP4+EXPB)*YH2**EXPB*Y1**EXP4
* /AAA**EXPc
RL1(I,2)=RL1(I,1)*EA1/TT
RL1(I,3)=RL1(I,1)*(2*EXPB/YH2+EXP4*Y1-EXPc*PT*(K1P+3*K2P)/AAA)
RL1(I,4)=RL1(I,1)*(4*EXPB/YH2-4*EXPc*K2P*PT/AAA)
RL1(I,5)=RL1(I,1)*(-3*EXPB/YH2-3*EXPc*K2P*PT/AAA)
RL1(I,6)=RL1(I,1)*(-4*EXPB/YH2-4*EXPc*K2P*PT/AAA)
RL1(I,7)=8.0E
RL1(I,8)=RL1(I,1)*(EXPB/YH2-EXPc*K2P*PT/AAA)
RL1(I,9)=8.0E
RL1(I,10)=CONTINUE
100
AAA=F1-F2*PA*PTB
CC=AAA*DEXP(-EA2/STB/TS)/TH3/TH3
DDD=3.0E*Y2+KC2B*Y1/KP2
EE=4.0E*Y2+2.0E*KC2B*Y1/KP2
RL2(I,1)=(Y2*YH2-KC2B/KP2*Y1*YH20)**CC
BBB=(2.0E*F2*PTB*PT/AAA-4.0E*TH3)*RL2(I,1)*SCO
RL2(I,2)=RL2(I,1)*EA2/TT-KC2B*Y1*YH20*KP2B*CC/KP2/TT
RL2(I,3)=BBB*CC*(DDD-KC2B*YH20/KP2)
RL2(I,4)=BBB*CC*(EE+YH2)
RL2(I,5)=-BBB-CC*DDD
RL2(I,6)=-BBB-CC*EE
RL2(I,7)=-CC*KC2B*Y1/KP2
RL2(I,8)=Y2*CC
RL2(I,9)=8.0E
RL2(I,10)=CONTINUE
RETURN
END

```

Table A4-7 Continued

```

SUBROUTINE ASETUP(Y,RL1,RL2)

C THIS SUBROUTINE SETS UP THE STATE MATRIX 'A', CONTROL MATRIX 'B' AND 'D'.

IMPLICIT REAL*8 (A-H,O-Z)
REAL*8 MG
DIMENSION Y(188),RL1(15,9),RL2(15,9),F(28,28),Q(4,28,28),P(28)
COMMON /LINEAR/ AA(75,75),BB(75,8),DD(75),U(8)
* /LALGB/ S(4,4),H(28,8),RI(28,4),AL(7)
* /DIMLE/ ALS,ALG,ALT,BES,BEG,GAS,GAG,GTS,GTG,DE1,
* DE2,ST1,S12,S13,PH12,PH13,PH1,PH2,PH3
* /RADIA/ W(18),WP(9,2),DETA(2),RR
* /COMAT/ A(25,25),B(25,25),R(25),N
* /GASPA/ CPG,PTZ,PTR,MG,POS,UGS,UM
* /OPCON/ SCH4,SCO,SCO2,SH2,SH20,PTB,PT1,STB,STW
* /HEATT/ OHSG,OHTS,OHTC,BGS,BSG,BTS,BTG,BWG,BWS

NP1=N+1
NP2=N+2
N2=N*2
N3=N*3
N4=N*4
N5=N*5
N6=N*6
TAU=PH2-1.0#
SCO28=SCO2/SCO
SCH48=SCH4/SCO
SH28=SH2/SCO
SH208=SH20/SCO
CALL CPCALC(SH2,SCO,SCO2,SH20,SCH4,STB,MG,CPG,CPG1,CPG2)

C CALCULATE THE S MATRIX
AA(1,1)=BGS-A(1,1)
AA(1,2)=A(1,NP2)
AA(1,3)=BGS
AA(1,4)=B,0#
AA(2,1)=A(NP2,1)
AA(2,2)=A(NP2,NP2)-BGS
AA(2,3)=B,0#
AA(2,4)=BGS
AA(3,1)=BGS
AA(3,2)=B,0#
AA(3,3)=1.0#/ALG/Y(N6+4)**2+BSG-A(1,1)
AA(3,4)=A(1,NP2)
AA(4,1)=B,0#
AA(4,2)=BSG
AA(4,3)=A(NP2,1)
AA(4,4)=A(NP2,NP2)-BSG
CALL BNDINV (AA,4,1TEST)
CALL MATCPY (AA,S,75,75,4,4,4,4)

C CALCULATE THE F AND H MATRICES, ALONG WITH MATRIX Q
DO 288 I=1,NP1
P(I)=TAU*R(I+1)+1.0#
ALL=TAU/P(NP1)*Y(N6+1)+SUM(Y,N5,A,UGS,Y(N6+1),NP1,N)
DO 188 J=1,N
JP1=J+1
S1=S(3,1)*A(1,JP1)+S(3,2)*A(NP2,JP1)
S2=S(4,1)*A(1,JP1)+S(4,2)*A(NP2,JP1)
S3=S(3,3)*A(1,JP1)+S(3,4)*A(NP2,JP1)
S4=S(4,3)*A(1,JP1)+S(4,4)*A(NP2,JP1)
DO 181 I=1,N
IP1=I+1
H(I,J)=(S1*A(IP1,1)+S2*A(IP1,NP2))*Y(N5+I)
H(I,N+J)=(A(IP1,JP1)+S3*A(IP1,1)+S4*A(IP1,NP2))*Y(N5+I)
Q(1,I,J)=ALG/P(I)*(B(IP1,1)*S1+B(IP1,NP2)*S2)
Q(2,I,J)=A(IP1,JP1)*S1-A(IP1,NP2)*S2
Q(3,I,J)=ALG/P(I)*(B(IP1,1)*S3+B(IP1,1)*S4+B(IP1,NP2)*S4)
Q(4,I,J)=A(IP1,JP1)-A(IP1,1)*S3-A(IP1,NP2)*S4
181 AA(I,J)=Y(N+I)*A(IP1,JP1)
AA(NP1,J)=Y(N6+5)*A(NP2,JP1)
AA(J,J)=A(A(J,J)+TAU/P(J))*Y(N+J)-SUM(Y,N,A,Y(N6+4),Y(N6+5),J,N)
H(J,N+J)=H(J,N+J)-TAU/P(J)*Y(N5+J)-SUM(Y,N5,A,UGS,Y(N6+1),J,N)
H(NP1,J)=(S1*A(NP2,1)+S2*A(NP2,NP2))*Y(N6+1)-ALL*S2
H(NP1,N+J)=(S3*A(NP2,1)+S4*A(NP2,NP2))*Y(N6+1)-ALL*S4
AA(J,NP1)=Y(N+J)*A(J,NP1)
CONTINUE
* AA(NP1,NP1)=Y(N6+5)*(A(NP2,NP2)+TAU/P(NP1))-SUM(Y,N,A,Y(N6+4),
* Y(N6+5),NP1,N)

CALL BNDINV (AA,NP1,1TEST)
CALL MATCPY (AA,F,75,75,28,28,NP1,NP1)
CALL MATMULT(F,H,28,28,28,48,NP1,N2,NP1)

```

Table A4-7 Continued

```

C CALCULATE THE I MATRIX
ST=(Y(N6+4)-1.0#)/ALG/Y(N6+4)
DO 118 I=1,N
  IPI=I+1
  ST1=Y(N5+I)*(A(IPI,1)*S(2,3)+A(IPI,NP2)*S(4,3))
  RI(I,1)=Y(N5+I)*SUM(Y,N,A,Y(N6+4),Y(N6+5),I,M)
  * +Y(N-1)*SUM(Y,N,A,Y(N6+4),Y(N6+5),I,N)+TAU/P(I)*
  * Y(N5+I)*Y(N-1)*ST1*ST
  RI(I,2)=-A(IPI,1)*Y(N+I)-ST1*ST
  RI(I,3)=-ST1*ST
  RI(I,4)=ST1/ALG/Y(N6+4)
118  CONTINUE
  ST1=Y(N6+1)*(A(NP2,1)*S(3,3)+A(NP2,NP2)*S(4,3))-ALL*S(4,3)
  RI(NP1,1)=-Y(N6+1)*SUM(Y,N,A,Y(N6+4),Y(N6+5),NP1,N)+Y(N6+5)*
  * SUM(Y,N5,A,UGB,Y(N6+1),NP1,N)+TAU/P(NP1)*Y(N6+1)*
  * Y(N6+5)*ST1*ST
  RI(NP1,2)=-A(NP2,1)*Y(N6+5)-ST1*ST
  RI(NP1,3)=-ST1*ST
  RI(NP1,4)=ST1/ALG/Y(N6+4)
  CALL MATMULT(F,RI,2#,2#,2#,4,NP1,4,NP1)

C FINALLY SET UP THE STATE MATRIX 'A'.
CALL ZERON(AA,75,75)
CALL ZERON(BB,75,75)
CALL ZEROD(UU,75)
AB=(2.0#-Y(N6+4))/ALG/Y(N6+4)

DO 25# I=1,N
  I1=I+1
  STT=AB*(S(1,3)*A(I1,1)*S(4,3)*A(I1,NP2))
  STI=A(I1,1)-A(NP2,1)*A(I1,NP2)/A(NP2,NP2)
  ST2=STI*SC028
  ST3=0.0#
  DO 199 K=1,N
    STT=STT+Q(2,I,K)*Y(K)+Q(4,I,K)*Y(N+K)
    STI=STI+(A(I1,K+1)-A(I1,NP2)*A(NP2,K+1)/A(NP2,NP2))*Y(N3+K)
    ST2=ST2+(A(I1,K+1)-A(I1,NP2)*A(NP2,K+1)/A(NP2,NP2))*Y(N4+K)
    ST3=ST3+Q(1,I,K)*Y(K)+Q(3,I,K)*Y(N+K)
199  CONTINUE
  DO 2#1 J=1,N
    J1=J+1
    AA(I,J)=ALS*(B(I1,J1)+B(I1,1)*(S(1,1)*A(1,J1)+S(1,2)*A(NP2,J1))
    * +B(I1,NP2)*(S(2,1)*A(1,J1)+S(2,2)*A(NP2,J1)))
    AA(I,J+M)=ALS*(B(I1,J1)*(S(1,3)*A(1,J1)+S(1,4)*A(NP2,J1))
    * +B(I1,NP2)*(S(2,3)*A(1,J1)+S(2,4)*A(NP2,J1)))
    AA(N+I,J)=AA(N+I,J)*Y(N+I)+Q(2,I,J)*Y(N5+I)+H(I,J)*STT
    AA(N+I,N+J)=Q(3,I,J)*Y(N+I)+Q(4,I,J)*Y(N5+I)+H(I,N+J)*STT
    AA(N2+I,N+J)=ALG*(B(I1,J1)-B(I1,NP2)*A(NP2,J1)/A(NP2,NP2))
    AA(N3+I,J)=-H(I,J)*ST1
    AA(N3+I,N+J)=-H(I,J)*ST1
    AA(N4+I,J)=-Y(N5+I)*(A(I1,J1)-A(NP2,J1)*A(I1,NP2)/A(NP2,NP2))
    AA(N4+I,N+J)=-H(I,N+J)*ST2
    AA(N4+I,N+J)=AA(N3+I,N+J)
2#1  CONTINUE
  S1=1.0#+PHI2*Y(I)
  S2=1.0#+PHI3*Y(I)
  S3=B(I1,1)*S(1,3)+B(I1,NP2)*S(2,3)
  S4=B(I1,1)*S(3,3)+B(I1,NP2)*S(4,3)
  S5=A(I1,1)*S(3,3)+A(I1,NP2)*S(4,3)
  S6=Y(N+I)/P(I)
  AA(I,I)=AA(I,I)+W(I)+DE1*(RL1(I,2)*S1+PHI2*RL1(I,1))+DE2*
  * (RL2(I,1)*S2+PHI3*RL2(I,1))
  AA(I,N+I)=AA(I,N+I)+CAS
  AA(I,N2+I)=W(I)
  AA(I,N3+I)=DE1*RL1(I,4)*S1+DE2*RL2(I,4)*S2
  AA(N+I,I)=AA(N+I,I)+GAG*S5
  AA(N+I,N+I)=AA(N+I,N+I)+ST3*(S(3,3)*B(I1,1)+S(4,3)*B(I1,NP2))
  * +AB*ALG*W(6)*PH3+GAG*Y(I)+W(5)*Y(N2+I)+2.0#*W(4)*Y(N+I))/P(I)
  AA(N+I,N2+I)=W(7)
  AA(N2+I,N+I)=W(8)
  AA(N2+I,N2+I)=AA(N2+I,N2+I)+W(9)
  AA(N3+I,I)=AA(N3+I,I)+(S12*RL2(I,2)-S11*RL1(I,2))*S6
  AA(N3+I,N+I)=AA(N3+I,N+I)+(S12*RL2(I,1)-S11*RL1(I,1))/P(I)
  AA(N3+I,N2+I)=AA(N3+I,N2+I)+(S12*RL2(I,3)-S11*RL1(I,3))*S6
  AA(N3+I,N3+I)=(S12*RL2(I,4)-S11*RL1(I,4))*S6
  AA(N4+I,I)=AA(N4+I,I)-S13*RL2(I,2)*S6
  AA(N4+I,N+I)=AA(N4+I,N+I)-S13*RL2(I,1)/P(I)
  AA(N4+I,N3+I)=S13*RL2(I,3)*S6
  AA(N4+I,N4+I)=AA(N4+I,N4+I)-S13*RL2(I,4)*S6

```

Table A4-7 Continued

```

      BB(I,1)=-ST*ALS*S3
      BB(I,2)=BB(I,1)
      BB(I,3)=ALS*S3/ALG/Y(N6+4)
      DO 358 J=4,8
      BB(I,J)=DE1*RL1(I,J+1)*S1+DE2*RL2(I,J+1)*S2
      BB(N3+I,J)=(S1*RL2(I,J+1)-S1*RL1(I,J+1))*S6
      BB(N4+I,J)=-S1*RL2(I,J+1)*S6
      BB(N-1,1)=-Y(N-1)*ST3-(W(4)*Y(N+1)+W(5)*Y(N2+I)+GAG*Y(I)+W(6)*
      * PH3+(AB-ST)*ALG*S4)*S6+ST*Y(N5+I)*S5+R(I,3)*ST
      BB(N-1,2)=R(I,2)*STT-ST*S6*ALG*S4+ST*Y(N5+I)*S5
      BB(N-1,3)=(S4*S6-Y(N5+I)*S5/ALG)/Y(N6+4)+R(I,4)*STT
      BB(N2+I,3)=ALT*(B(I,1)-B(I,NP2)*A(NP2,1)/A(NP2,NP2))
      BB(N3+I,1)=-R(I,1)*ST1
      BB(N3+I,2)=-R(I,2)*ST1
      BB(N3+I,3)=-R(I,3)*ST1
      BB(N3+I,4)=BB(N3+I,4)-Y(N5+I)*(A(I1,1)-A(NP2,1)*A(I1,NP2)/
      * A(NP2,NP2))
      BB(N4+I,1)=-R(I,2)*ST2
      BB(N4+I,2)=-R(I,3)*ST2
      BB(N4+I,3)=-R(I,4)*ST2
      BB(N4+I,5)=BB(N4+I,5)-Y(N5+I)*(A(I1,1)-A(NP2,1)*A(I1,NP2)/
      * A(NP2,NP2))

      AL(1)=(-CPG1*MG*ST#+(-.7757D-3)*ST#/6.775)/MG/CPG
      AL(2)=CPG1*ST#/CPG
      AL(3)=SC0*(ST#*(.4243D-3)-.175D#)/MG/CPG
      AL(4)=SC0*(ST#*(3.44D3D-3)+1.27626D#)/MG/CPG
      AL(5)=SC0*(ST#*(6.3943D-3)+4.425D#)/MG/CPG
      AL(6)=SC0*(ST#*(.8343D-3)-.155D#)/MG/CPG
      AL(7)=SC0*(ST#*(11.6525D-3)-1.5742D#)/MG/CPG

      ST4=RL1(I,2)*Y(I)+RL1(I,3)*Y(N3+I)+RL1(I,4)*Y(N4+I)+RL1(I,5)
      * +RL1(I,6)*SC02B+RL1(I,7)*SH20B+RL1(I,8)*SH2B+RL1(I,9)
      * *SCH4B
      ST5=RL2(I,1)*Y(I)+RL2(I,3)*Y(N3+I)+RL2(I,4)*Y(N4+I)+RL2(I,5)
      * +RL2(I,6)*SC02B+RL2(I,7)*SH20B+RL2(I,8)*SH2B
      DD(I)=DE1*S1*(RL1(I,1)-STA)-DE1*RL1(I,1)*PH12*Y(I)
      * +DE2*S2*(RL2(I,1)-ST5)-DE2*RL2(I,1)*PH13*Y(I)+ST*ALS*S3
      * +AL(I)*BB(I,1)
      DD(N+1)=STT*(R(I,1)-Y(N5+I))+ST*(ALG*S6*S4-S5*Y(N5+I))
      * +AL(I)*BB(N+I,1)
      DD(N2+I)=B.D#
      DD(N3+I)=(Y(N5+I)-R(I,1))*ST1+SI1*S6*ST4-S12*S6*ST5+
      * +AL(I)*BB(N3+I,1)
      DD(N4+I)=(Y(N5+I)-R(I,1))*ST2+SI3*S6*ST5+AL(I)*BB(N4+I,1)
      CONTINUE

      DO 358 I=1,N5
      DO 358 J=3,8
      BB(I,J)=BB(I,J)+AL(J-1)*BB(I,1)
      DO 408 I=1,7
      BB(I,1)=V(I,3)
      BB(N-1,1)=W(6)*Y(N+I)/P(I)
      BB(N2+I,1)=W(1,D#)
      BB(N3+I,1)=B.D#
      BB(N4+I,1)=B.D#
      408
      BB(N4+I,1)=B.D#
      RETURN
      END

```

Table A4-7 Continued

```

SUBROUTINE ACTLSS(U,V,EP,W)
C THIS SUBROUTINE CALCULATES THE FINAL STEADY STATE
IMPLICIT REAL*8 (A-H,O-Z)
REAL*8 MG,KC2B,KP2A,KP2B,K1P,K2P
DIMENSION U(8),V(25),Y(1#)
COMMON /GASPA/ CPG,PTZ,PTR,NG,PGS,UGS,UM
*          /OPCON/ SCH4,SCO,SCO2,SH2,SH20,PTB,PT1,STS,STW
*          /REAC2/ EXPAC,EXPB,EXPC,KC2B,KP2A,KP2B,K1P,K2P,EA1,EA
EXTERNAL FN1

ST=MG
V(1#)=STW
STW=U(1)*STB
UGS=U(2)*UGS
STB=U(3)*STB
SCO=U(4)*SCO
SCO2=U(5)*SCO
SH20=U(6)*SCO
SH2=U(7)*SCO
SH4=U(8)*SCO
CALL CPCALC(SH2,SCO,SCO2,SH20,SH4,STB,MG,CPG,CPG1,CPG2)
PGS=PGS*MG/ST*U(3)
K1P=K1P*U(4)
K2P=K2P*U(4)

DO 1# I=1,8
V(1)=U(I)
U(1)=1.0#
U(1)=STW/STB
U(5)=SCO2/SCO
U(6)=SH20/SCO
U(7)=SH2/SCO
U(8)=SH4/SCO
V(9)=UM
UM=1.0#
CALL DIMLES
CALL RADIAL

CALL MSES1(6*N+5,Y,EP,1#,#,FN1)

DO 1# I=1,8
U(I)=V(I)
UM=V(9)
DO 1# I=1,N
Y(1)=Y(I)*U(3)
Y(N+1)=Y(N+1)*U(3)
Y(2*N+1)=Y(2*N+1)*U(3)
Y(3*N+1)=Y(3*N+1)*U(4)
Y(4*N+1)=Y(4*N+1)*U(4)
Y(5*N+1)=Y(5*N+1)*U(2)
Y(6*N+1)=Y(6*N+1)*U(2)
Y(6*N+2)=Y(6*N+2)*U(3)
Y(6*N+3)=Y(6*N+3)*U(3)
Y(6*N+4)=Y(6*N+4)*U(3)
Y(6*N+5)=Y(6*N+5)*U(3)
ST=MG
STW=V(1#)
UGS=UGS/U(2)
STB=STB/U(3)
SCO=SCO/U(4)
SCO2=SCO/U(5)
SH20=SCO/U(6)
SH2=SCO/U(7)
SH4=SCO/U(8)
CALL CPCALC(SH2,SCO,SCO2,SH20,SH4,STB,MG,CPG,CPG1,CPG2)
PGS=PGS*MG/ST*U(3)
K1P=K1P/U(4)
K2P=K2P/U(4)
CALL DIMLES
CALL RADIAL
RETURN
END

```

Table A4-7 Continued

```

SUBROUTINE INSIM(Y,VS,U,N,JFLAG)
C THIS SUBROUTINE INITIALIZES THE SIMULATION.
IMPLICIT REAL*8 (A-H,O-Z)
REAL*8 MG,MGB
DIMENSION U(8),Y(188),VS(188)
COMMON /GASPA/ CPG,PTZ,PTR,MG,PGS,UGS,UM
* /OPCON/ SCH4,SCO,SCO2,SH2,SH20,PT#,PT1,ST#,STW
* /LALGB/ S(4,4),H(28,48),R(28,4),AL(7)
READ(5,1) JFLAG
IF(JFLAG .EQ. 1)CALL INITIAL(Y,U,VS)
IF(JFLAG .EQ. 1)RETURN
DO 188 I=1,5*N
Y(I)=VS(I)
188
READ (5,2) UGB,TB,XCO,XCO2,XH20,XH2,XCH4,TW
U(1)=TW/ST#
U(2)=UGB/UGS
U(3)=TB/ST#
U(4)=XCO/SCO
U(5)=XCO2/SCO
U(6)=XH20/SCO
U(7)=XH2/SCO
U(8)=XCH4/SCO
UM=AL(1)+AL(2)*U(3)+AL(3)*U(4)+AL(4)*U(5)+AL(5)*U(6)+AL(6)
* U(7)+AL(7)*U(8)
PRINT 3, (U(I),I=1,8),UM
RETURN
1 FORMAT(12)
2 FORMAT(9F.2)
3 FORMAT(//,2X,'INITIAL CONTROL VECTOR:',//5X,'TW  ',F8.4,5X,
* 'UGB  ',F8.4,5X,'TB  ',F8.4,5X,'XCO  ',F8.4,5X,'/5X,
* 'XCO2  ',F8.4,5X,'XH20  ',F8.4,5X,'XH2  ',F8.4,5X,'XCH4=',
* F8.4/5X,'UM  ',F8.4)
END

SUBROUTINE OUTCALC(U,Y,VS,ALG)
C THIS SUBROUTINE CALCULATES THE VELOCITIES AND ENDT TEMPERATURES
IMPLICIT REAL*8 (A-H,O-Z)
REAL*8 MG
DIMENSION Y(188),SA(4),U(8)
COMMON /LALGB/ S(4,4),H(28,48),R(28,4),AL(7)
* /COMAT/ A(25,25),B(25,25),R(25),N
* /GASPA/ CPG,PTZ,PTR,MG,PGS,UGS,UM

NP2=N+2
N5=N*5
N61=N*6+1
CALL ENOPTS (TT#,Y18,YINP1,YZB,Y2NP1,TTNP1,Y,UGB)
DO 188 I=1,N+1
Y(N5+I)=R(I,1)+R(I,2)*UGB+R(I,3)*UM+R(I,4)*U(3)
DO 188 J=1,N
Y(N5+I)=Y(N5+I)+H(I,J)*Y(J)+H(I,J+N)*Y(N+J)
188
CONTINUE
CALL ZEROV(SA,4)
DO 182 J=1,N
J1=J+1
SA(1)=SA(1)+A(1,J1)*Y(J)
SA(2)=SA(2)+A(NP2,J1)*Y(J)
SA(3)=SA(3)+A(1,J1)*Y(N+J)
SA(4)=SA(4)+A(NP2,J1)*Y(N+J)
182 ST=(YS-1.D8)/ALG/VS
SA(3)=ST-ST*UM-ST*UGB+U(3)/ALE/YS+SA(3)
DO 183 I=1,4
Y(N61+I)=B(1,0)
DO 183 J=1,4
183 Y(N61+I)=Y(N61+I)+S(I,J)*SA(J)
183
RETURN
END

```

Table A4-7 Continued

```

SUBROUTINE CPCALC(SH2,SCO,SCO2,SH20,SC4,ST#,MG,CPG,CPG1,CPG2)
C THIS SUBROUTINE CALCS THE HEAT CAPACITY
IMPLICIT REAL*8 (A-H,O-Z)
REAL*8 MG
SN2=1.0#-SH2-SCO-SCO2-SH20-SC4
MG=SC4*16.0#430#*SCO*28.0#1#40#*SCO2*44.0#980#*SH2*2.0#160#
* SH20*18.0#1540#*SCO*28.0#1#340#*SCO2*44.0#980#*SH2*2.0#160#
* CPG1=(SH2*.010-3*SN2*.77570-3*SCO*1.2D-3*SCO2*4.216D-3
* +SH20*7.170-3*SC4*12.42B2D-3)/MG
* CPG2=(SH2*.620#*SCO*6.775D#*SCO*6.6D#*SCO2*8.0#5126D#)
* +SH20*11.2D#*SC4*5.2B#8D#)/MG
CPG=CPG1*ST#*CPG2
RETURN
END

SUBROUTINE ENDPTS (TT#,Y1#,Y1NP1,Y2#,Y2NP1,TTNP1,Y,UG#)
C THIS ROUTINE CALCULATES THE ENDPOINT CONDITIONS.
IMPLICIT REAL*8 (A-H,O-Z)
DIMENSION Y(1#)
COMMON /COMAT/ A(25,25),B(25,25),R(25),N
* /LINEA/ AA(75,75),BB(75,8),DD(75),U(8)
* /DIMLE/ ALS,ALG,ALT,BES,BEG,GAS,GAG,GTS,GTG,DE1,
DE2,S11,S12,S13,PH12,PH13,PH1,PH2,PH3
NP2=N+2
N2=2*N
N3=3*N
N4=4*N
UG#=U(2)*Y(N*6+4)/U(3)
Y1#=U(4)
Y2#=U(5)
Y1NP1=Y(N*6+5)
Y2NP1=A(NP2,1)/A(NP2,NP2)*U(5)
TTNP1=0.0#
TT#*U(3)
DO 1# I=1,N
IP1=I+1
Y2NP1=Y2NP1-A(NP2,IP1)/A(NP2,NP2)*Y(N4+I)
TTNP1=TTNP1+A(NP2,IP1)*Y(N2+I)
CONTINUE
1# TTNP1=-(TTNP1+A(NP2,1)*TT#)/A(NP2,NP2)
RETURN
END

FUNCTION SUM(Y,NN,AA,X1,X2,I,N)
IMPLICIT REAL*8 (A-H,O-Z)
DIMENSION Y(1#),AA(25,25)
SUM=0.0#
IP1=I+1
DO 1# J=1,N
JP1=J+1
SUM=SUM+AA(IP1,JP1)*Y(J+NN)
SUM=SUM+AA(IP1,1)*X1+AA(IP1,N+2)*X2
RETURN
END

SUBROUTINE REAC (Y1,Y2,TS,TG,PT,R1P,R2P)
C THIS SUBROUTINE CALCULATES THE DIMENSIONLESS RATES
IMPLICIT REAL*8 (A-H,O-Z)
REAL*8 MG,KP2A,KP2B,KC2#,K1P,K2P,KP2
COMMON /OPCON/ SC4,SCO,SCO2,SH2,SH20,PT#,PT1,ST#,STW
* /REAC2/ EXP4,EXP8,EXP4,EXP8,EXP4,EXP8,EXP4,EXP8
* /LINEA/ AA(75,75),BB(75,8),DD(75),U(8)

GA=0.0#
TT=ST#/TS
KP2=DEXP(KP2A+KP2B/TT)
TH1=SCO*(U(4))-Y1+U(5)-Y2
TH2=SCO*(U(5))-Y2
TH3=1.0#-2.0#*TH1
YH2=(SCO*U(7))-3.0#*TH1-TH2)/SCO/TH3
YH20=(SCO*U(6))-TH1+TH2)/SCO/TH3
YCHA=(SCO*U(8)+TH1)/SCO/TH3
YCO=Y1/TH3
YCO2=Y2/TH3
PA=PT#/TH3
IF(YH2 .LT. 0.0#)YH2=1.0#-1#
IF(YCO .LT. 0.0#)YCO=1.0#-1#
R1P=DEXP(-EA1/TT)*PA**((expa+expb)*YH2**expb*YCO**expa/
(1.0#+K1P*PA*YCO+K2P*PA*YH2)**expc
* R2P=DEXP(-EA2/TT)*(.83D#+.17D#*PA*PT#)*(YCO2-YH2-YCO*YH20/
* KP2*KC2#)
RETURN
END

```

Table A4-7 Continued

```

FUNCTION TR(T,TT,L,R)
IMPLICIT REAL*8 (A-H,O-Z)
COMMON /RADIA/ W(18),WP(9,2),DETA(2),RR
/LINEA/ AA(75,75),BB(75,8),DD(75),U(8)
*
TR=((WP(1,L)+WP(4,L)*R+WP(7,L)*R**2)*T
* + (WP(2,L)+WP(5,L)*R+WP(8,L)*R**2)*TT
* +WP(3,L)*U(1)+WP(6,L)*U(1)*R+WP(9,L)*U(1)*R**2)/DETA(L)
RETURN
END

FUNCTION REN (AA,NN)
IMPLICIT REAL*8 (A-H,O-Z)
DIMENSION AA(188)
ST#D8
DO 188 I=1,NN
IF(DABS(AA(I)) .GE. ST) ST=AA(I)
RFN=-DLOG10(DABS(ST))
RETURN
END

SUBROUTINE COLLOC
C THIS ROUTINE CALCULATES THE ZEROS OF THE ORTHOGONAL POLYNOMIAL AND
C SETS UP THE AXIAL COLLOCATION MATRICES A AND B
IMPLICIT REAL*8 (A-H,O-Z)
DIMENSION D1(25),D2(25),D3(25),V1(25),V2(25)
COMMON /COMAT/ A(25,25),B(25,25),R(25),N
CALL JCOBI(25,N,1,1,8,D8,8,D8,D1,D2,D3,R)
PRINT 1, (R(J),J=1,N+2)
DO 181 I=1,N+2
CALL DFOPR(25,N,1,1,1,1,D1,D2,D3,R,V1)
CALL DFOPR(25,N,1,1,1,2,D1,D2,D3,R,V2)
DO 182 J=1,N+2
A(I,J)=V1(J)
B(I,J)=V2(J)
CONTINUE
181 CONTINUE
182 CONTINUE
RETURN
1 FORMAT(//,3X,'AXIAL COLLOCATION POINTS:',//,3(18X,4(E12.4)))
END

SUBROUTINE INTLSS(Y,U,IFLAG,NFLAG,L,UGS,PH1,N,EP)
C THIS ROUTINE CALCULATES THE INITIAL STEADY STATE PROFILE
IMPLICIT REAL*8 (A-H,O-Z)
real*8 1
DIMENSION Y(188),U(8)
EXTERNAL FM1,FM2
CALL INITIAL (Y,U,IFLAG)
CALL OUTPUT(Y,U,8,D8,L,UGS,PH1,1)
IF(NFLAG .EQ. 1)CALL NSES1(6*N+6,Y,EP,2888,8,FM1)
IF(NFLAG .EQ. 2)CALL NSES2(6*N+5,Y,EP,588,1T,FM2)
IF(1T .EQ. 588) PRINT 1
CALL OUTPUT(Y,U,8,D8,L,UGS,PH1,2)
RETURN
1 FORMAT(//,2X,'REACHED MAXIT IN NSES2'//)
END

```

Table A4-7 Continued

APPENDIX 5

ORTHOGONAL COLLOCATION ON FINITE ELEMENTS MODEL

The technique and application of orthogonal collocation on finite elements is described in detail in Section 3.5. This appendix presents a summary of the final coupled system of algebraic and differential equations. Computer programs for solution of the packed bed reactor model using orthogonal collocation on finite elements are presented in Tables A5-1 and A5-2 and are stored in directory [RRK.OCFE]. These are very similar in structure and operation to those in Appendix 4.

After applying orthogonal collocation on finite elements, the packed bed reactor model becomes

Catalyst Energy Balance

For elements $k = 1, \dots, NE$,

$$\frac{d\Theta_{s_I}}{d\vartheta} = \frac{\alpha_s}{h_k^2} \sum_{j=1}^{M_k} B_{I,j} \Theta_{s_j} + \omega_1 \Theta_{s_I} + \omega_2 \Theta_{t_I} + \gamma_s \Theta_{g_I} + \kappa_1 (1 + \varphi_1 \Theta_{s_I}) R'_M + \kappa_2 (1 + \varphi_2 \Theta_{s_I}) R'_S + \omega_S$$

within each element k for the interior collocation points $I = 2, \dots, N_k + 1$. For elements $k = 2, \dots, NE$,

$$\left(\frac{1}{h_{k-1}} \sum_{j=1}^{M_{k-1}} A_{M_{k-1},j} \Theta_{s_j} \right)_{element \ k-1} = \left(\frac{1}{h_k} \sum_{j=1}^{M_k} A_{1,j} \Theta_{s_j} \right)_{element \ k}$$

and for the first ($k=1$) and last ($k=NE$) elements:

$$\frac{1}{h_1} \sum_{J=1}^{M_1} A_{1,J} \Theta_{g_J} = \lambda_{gzs} (\Theta_{g_1} - \Theta_{g_1})$$

$$\frac{1}{h_{NE}} \sum_{J=1}^{M_{NE}} A_{M_{NE},J} \Theta_{g_J} = \lambda_{gzs} (\Theta_{g_{M_{NE}}} - \Theta_{g_{M_{NE}}})$$

Gas Energy Balance

For elements $k = 1, \dots, NE$,

$$\frac{(\tau\zeta_i+1)\hat{M}_g c_{p_g}}{\Theta_{g_I}} \frac{d\Theta_{g_I}}{d\vartheta} = \frac{-(\tau\zeta_i+1)v_{g_I} \hat{M}_g c_{p_g}}{h_k \Theta_{g_I}} \sum_{J=1}^{M_k} A_{I,J} \Theta_{g_J}$$

$$+ \frac{\alpha_g}{h_k^2} \sum_{J=1}^{M_k} B_{I,J} \Theta_{g_J} + \omega_4 \Theta_{g_I} + \omega_5 \Theta_{t_I} + \gamma_g \Theta_{s_I} + \omega_6$$

within each element k for the interior collocation points $I = 2, \dots, N_k+1$. For elements $k = 2, \dots, NE$,

$$\left[\frac{1}{h_{k-1}} \sum_{J=1}^{M_{k-1}} A_{M_{k-1},J} \Theta_{g_J} \right]_{element \ k-1} = \left[\frac{1}{h_k} \sum_{J=1}^{M_k} A_{1,J} \Theta_{g_J} \right]_{element \ k}$$

and for the first ($k=1$) and last ($k=NE$) elements:

$$\frac{1}{h_1} \sum_{J=1}^{M_1} A_{1,J} \Theta_{g_J} = -\lambda_{gzs} (\Theta_{g_1} - \Theta_{g_1}) + \frac{v_{g_0} \hat{M}_{g_0} c_{p_{g_0}}}{\alpha_g \Theta_{g_1}} (\Theta_{g_1} - \Theta_0)$$

$$\frac{1}{h_{NE}} \sum_{J=1}^{M_{NE}} A_{M_{NE},J} \Theta_{g_J} = \lambda_{gzs} (\Theta_{g_{M_{NE}}} - \Theta_{g_{M_{NE}}})$$

Mass Balances

For elements $k = 1, \dots, NE$,

$$\begin{aligned} \frac{dy_l}{d\vartheta} &= -\frac{v_g}{h_k} \sum_{j=1}^M A_{I,j} y_l + \frac{\alpha_m}{h_k} \left\{ \sum_{j=1}^M B_{I,j} y_l + \left(\sum_{j=1}^M A_{I,j} y_l \right) \left[\frac{\tau h_k}{\tau \zeta_i + 1} - \frac{1}{\theta_g} \sum_{j=1}^M A_{I,j} \theta_{g_j} \right] \right\} \\ &- \frac{2y_l}{1-2\delta} \frac{\partial^2 \delta}{\partial \zeta^2} - \frac{2}{1-2\delta} \left(\sum_{j=1}^M A_{I,j} y_{l,j} \right) \frac{\partial \delta}{\partial \zeta} - \frac{2y_l}{1-2\delta} \left[\frac{\tau h_k}{\tau \zeta_i + 1} - \frac{1}{\theta_g} \sum_{j=1}^M A_{I,j} \theta_{g_j} \right] \frac{\partial \delta}{\partial \zeta} \\ &+ \frac{4y_l}{(1-2\delta)^2} \left(\frac{\partial \delta}{\partial \zeta} \right)^2 \end{aligned}$$

$$+ \begin{cases} -\sigma_1 \frac{\theta_{g_i}}{\hat{P}} R'_M + \sigma_2 \frac{\theta_{g_i}}{\hat{P}} R'_S & l = 1 \\ -\sigma_3 \frac{\theta_{g_i}}{\hat{P}} R'_S & l = 2 \end{cases}$$

where

$$\begin{aligned} \frac{\partial^2 \delta}{\partial \zeta^2} &= - \left[\bar{x}_1^0 \sum_{j=1}^M B_{I,j} y_{1,j} + \bar{x}_2^0 \sum_{j=1}^M B_{I,j} y_{2,j} \right] \\ \frac{\partial \delta}{\partial \zeta} &= - \left[\bar{x}_1^0 \sum_{j=1}^M A_{I,j} y_{1,j} + \bar{x}_2^0 \sum_{j=1}^M A_{I,j} y_{2,j} \right] \end{aligned}$$

within each element k for the interior collocation points $I = 2, \dots, N_k + 1$. For elements $k = 2, \dots, NE$,

$$\left(\frac{1}{h_{k-1}} \sum_{j=1}^{M_{k-1}} A_{M_{k-1},j} y_{l,j} \right)_{\text{element } k-1} = \left(\frac{1}{h_k} \sum_{j=1}^{M_k} A_{1,j} y_{l,j} \right)_{\text{element } k}$$

and for the first ($k=1$) and last ($k=NE$) elements:

$$\begin{aligned} \frac{1}{h_1} \sum_{j=1}^{M_1} A_{1,j} y_{l,j} &= \frac{v_{g_0}}{\alpha_m} (y_{l_1} - y_{l_0}^0) \\ \sum_{j=1}^{M_{NE}} A_{M_{NE},j} y_{l,j} &= 0 \end{aligned}$$

Thermal Well Energy Balance

For elements $k = 1, \dots, NE$,

$$\frac{d\Theta_{t_I}}{d\vartheta} = \frac{\alpha_t}{h_k} \sum_{J=1}^{M_k} B_{I,J} \Theta_{t_J} + \omega_7 \Theta_{s_I} + \omega_8 \Theta_{g_I} + \omega_9 \Theta_{t_I} + \omega_{10}$$

within each element k for the interior collocation points

$I = 2, \dots, N_k + 1$. For elements $k = 2, \dots, NE$,

$$\left(\frac{1}{h_{k-1}} \sum_{J=1}^{M_{k-1}} A_{M_{k-1},J} \Theta_{t_J} \right)_{\text{element } k-1} = \left(\frac{1}{h_k} \sum_{J=1}^{M_k} A_{1,J} \Theta_{t_J} \right)_{\text{element } k}$$

and for the first ($k=1$) and last ($k=NE$) elements:

$$\Theta_{t_1} = \Theta_{t_0}$$

$$\sum_{J=1}^{M_{NE}} A_{M_{NE},J} \Theta_{t_J} = 0$$

Overall Continuity

For $I = 2, \dots, N_k + 1$ for each element $k = 1, \dots, NE-1$ and for $I = 2, \dots, N_{NE} + 2$

for $k = NE$:

$$\frac{\Theta_{g_I}}{h_k} \sum_{J=1}^{M_k} A_{I,J} v_{g_J} + \frac{v_{g_I} \tau \Theta_{g_J}}{\tau \zeta_i + 1} + \frac{1}{\rho_g c_{p_g}} \left[\frac{\alpha_g}{h_k^2} \sum_{J=1}^{M_k} B_{I,J} \Theta_{g_J} + \omega_1 \Theta_{g_I} + \omega_5 \Theta_{t_I} + \gamma_g \Theta_{s_I} + \omega_9 \right] = 0$$

For elements $k = 2, \dots, NE$,

$$\left(\frac{1}{h_{k-1}} \sum_{J=1}^{M_{k-1}} A_{M_{k-1},J} v_{g_J} \right)_{\text{element } k-1} = \left(\frac{1}{h_k} \sum_{J=1}^{M_k} A_{1,J} v_{g_J} \right)_{\text{element } k}$$

and for $k = 1$

$$v_{g_1} \rho_{g_1} = v_{g_0} \rho_{g_0}$$

```
C THIS PROGRAM MODELS A NONISOTHERMAL, NONADIABATIC FIXED BED REACTOR
C WITH BOTH A COOLING JACKET AND A THERMAL WELL. THE ANALYSIS IS
C PERFORMED FOR A METHANATION OF CO SYSTEM.
C THIS PROGRAM USES THE ORTHOGONAL COLLOCATION OF FINITE ELEMENTS METHOD
C LINK TO MLIB,OCFELIB
C THIS PROGRAMS SOLVES THE FULL NONLINEAR MODEL WITH THE CONCENTRATIONS
C NONDIMENSIONAL W.R.T. THE STEADY-STATE INLET CONC. OF CO

IMPLICIT REAL*8 (A-H,O-Z)
REAL*8 L,KT,MG,K0,K0P,KP1A,KP1B,KC10,KP2A,KP2B,KC20,K2P,K3P

COMMON /REACP/ EPS,L,R0,R1
* /CATLS/ CPS,PS,TC,DC
* /THWEL/ CPT,PT,KT
* /GASPA/ CPG,PTZ,PTR,MG,PGS,UGS,UM
* /HEATT/ OHSG,OHTS,OHTG,BGS,BSG,BTS,BTG,BWG,BWS
* /OPCON/ SCH4,SCO,SCO2,SH2,SH20,PT0,PT1,ST0,STW
* /REAC1/ DH1A,DH1B,DH2A,DH2B,K0,K0P
* /DIMLE/ ALS,ALG,ALT,BES,BEG,GAS,GAG,GTS,GTG,DE1,
* DE2,SI1,SI2,SI3,PHI2,PHI3,PH1,PH2,PH3
* /RADIA/ W(10),WP(9,2),DETA(2),RR
* /COMAT/ NE,N(5),H(5),ZI(6),NS(6),Z(5,25),A(5,25,25),
* B(5,25,25)
* /INDEX/ NSE,NTS,NTT,NTG,NCO,NC2,NUG,NNE,NE1
* /MISCI/ UU(100)
* /REAC2/ KC10,KP1A,KP1B,KC20,KP2A,KP2B,K2P,K3P,EA1,EA2
* /LINEA/ AA(75,75),BB(75,8),DD(75),U(8)
* /STATE/ Y(100),YDOT(100),ST,DT
```

EXTERNAL DERIV,FN

```
C READ IN DATA AND CALCULATE CONSTANTS
CALL SETUPS (DT0,TMAX,DL,RR,EP,NP,IF,IFLAG)
C CALCULATE THE DIMENSIONLESS PARAMETERS
CALL DIMLES
C CALCULATE CONSTANTS FOR THE RADIAL LUMPED MODEL
CALL RADIAL
C CALCULATE ZEROS OF THE ORTHOGONAL POLYNOMIAL AND SET UP AXIAL
C COLLOCATION MATRICIES A AND B.
CALL COLLOC
C SOLVE FOR THE STEADY STATE PROFILE
CALL INTLSS(Y,U,EP,IFLAG)
STOP
END
```

Table A5-1
Computer Program OCFE

SUBROUTINE DIMLES

C THIS SUBROUTINE CALCULATES THE DIMENSIONLESS PARAMETERS

```
IMPLICIT REAL*8 (A-H,O-Z)
REAL*8 L,KT,MG,KB,KP,KC20,KP2A,KP2B,K1P,K2P
COMMON /REACP/ EPS,L,RB,R1
*          /CATLS/ CPS,PS,TC,DC
*          /THWEL/ CPT,PT,KT
*          /GASPA/ CPG,PTZ,PTR,MG,PGS,UGS,UM
*          /HEATT/ OHSG,OHTS,OHTC,BGS,BSC,BTS,BTG,BWG,BWS
*          /OPCON/ SCH4,SCO,SCO2,SH2,SH2O,PTB,PT1,STB,STW
*          /REAC1/ DH1A,DH1B,DH2A,DH2B,KB,KP
*          /DIMLE/ ALS,ALG,ALT,BES,BEG,GAS,GAG,GTS,GTG,DE1,
*                   DE2,SI1,SI2,SI3,PHI2,PHI3,PH1,PH2,PH3
*          /REAC2/ EXPA,EXPB,EXPC,KC2B,KP2A,KP2B,K1P,K2P,EA1,EA2
DATA PI /3.141592654D/
VT=PI*RB**2*L
VB=PI*L*(R1**2-RB**2)
AZ=L/DC
AR=R1/DC
AO=L/R1
EM1=1.0D0-EPS
ALS=TC/(PS*CPS*EM1*L*UGS)
ALG=1.0D0/(PTZ*EPS*AZ)
ALT=KT/(PT*CPT*L*UGS)
BES=ALS*L**2/R1**2
BEG=AO/PTR/EPS/AR
GAS=OHSG*L/(VB*PS*CPS*EM1*UGS)
GAG=OHSG*L/(VB*PGS*CPG*EPS*UGS)
GTS=OHTS*L/(VT*PT*CPT*UGS)
GTG=OHTG*L/(VT*PT*CPT*UGS)
DE1=-L*DHI1B*(PTB*SCO)***(EXPA+EXPB)*KB/P/(UGS*CPS*STB)
DE2=-L*DHI2B*SCO**2*KB/(UGS*CPS*STB)
SI1=MG*PS*EM1*(PTB*SCO)***(EXPA+EXPB)*KB/P/L/(EPS*UGS*PGS*SCO)
SI2=MG*PS*EM1*SCO*KB*L/(EPS*UGS*PGS)
SI3=SI2
PHI2=DH1A*STB/DH1B
PHI3=DH2A*STB/DH2B
BWG=BTG
BWS=BTS
PH1=RB/R1
PH2=PT1/PTB
PH3=STW/STB
RETURN
END
```

Table A5-2
Computer Program OCFELIB

```
SUBROUTINE INITIAL (Y,U)

C THIS ROUTINE INITIALIZES THE SYSTEM

IMPLICIT REAL*8 (A-H,O-Z)
REAL*8 MG
DIMENSION Y(100),U(8)
COMMON /OPCON/ SCH4,SCO,SCO2,SH2,SH20,PT#,PT1,ST#,STW
*           /GASPA/ CPG,PTZ,PTR,MG,PGS,UGS,UM
*           /COMAT/ NE,N(5),H(5),Z(6),NS(6),Z(6,25),A(5,25,25),
*           B(5,25,25)
*           /INDEX/ NSE,NTS,NTT,NTG,NCO,NC2,NUC,NNE,NE1

DO 300 I=2,4
300  U(I)=1.0#
U(1)=STW/ST#
U(5)=SCO2/SCO
U(6)=SH20/SCO
U(7)=SH2/SCO
U(8)=SCH4/SCO
UM=1.0#
READ(5,1) TG,TS,TT,X1,X2,VEL
DO 100 K=1,NE
CALL INDICES(K,NK,N1,N2,N3,N4,N5,N6)
DO 100 I=1,NK
Y(N1+I)=TS/ST#
Y(N2+I)=TT/ST#
Y(N3+I)=TG/ST#
Y(N4+I)=X1/SCO
Y(N5+I)=X2/SCO
Y(N6+I)=VEL/PRES(I,K)/UGS
100  CONTINUE

DO 200 J=1,NE1
Y(NTS+J)=TS/ST#
Y(NTT+J)=TT/ST#
Y(NTG+J)=TG/ST#
Y(NCO+J)=X1/SCO
Y(NC2+J)=X2/SCO
IF(J .NE. NE1)Y(NUG+J)=VEL/PRES(0,J)/UGS
IF(J .EQ. NE1)Y(NUG+J)=VEL*PT#/PT1/UGS
200  CONTINUE

      RETURN
1      FORMAT(9F8.2)
END
```

Table A5-2 Continued

SUBROUTINE SETUPS (DTB,TMAX,DL,RR,EP,MP,IF)

C THIS SUBROUTINE READS IN THE INPUT DATA AND MAKES PRELIMINARY CALCULATIONS.

```

IMPLICIT REAL*8 (A-H,O-Z)
REAL*8 L,KT,MG,KB,KP,KP2A,KP2B,KC2#,K1P,K2P,K2,K3
COMMON /REACP/ EPS,L,RT#,R1
*          /CATLS/ CPS,PS,TC,DC
*          /THWEL/ CPT,PT,KT
*          /GASPA/ CPG,PTZ,PTR,MG,PGS,UGS,UM
*          /HEATT/ OHSG,OHTS,OHTG,BGS,BSG,BTS,BTG,BWG,BWS
*          /OPCON/ SCH4,SCO,SCO2,SH2,SH20,PT#,PT1,ST#,STW
*          /REAC1/ DH1A,DH1B,DH2A,DH2B,KB,KP
*          /REAC2/ EXPA,EXPB,EXPC,KP2A,KP2B,K1P,K2P,EA1,EA2
*          /COMAT/ NE,N(5),H(5),ZI(6),NS(6),Z(5,25),A(5,25,25),
*          B(5,25,25)
DATA RG,RGP,PI /82.0544D#,.1.987D#,3.141592654D#/
```

```

READ(5,1) EPS,L,RT#,R1
READ(5,1) CPS,PS,TC,DC
READ(5,1) CPT,PT,KT
READ(5,1) PTZ,PTR,UGS
READ(5,1) OHSG,OHTS,OHTG,BGS,BSG,BTS,BTG
READ(5,1) SCH4,SCO,SCO2,SH2,SH20,PT#,PT1,ST#,STW
READ(5,1) DH1A,DH1B,DH2A,DH2B,KB,KP
READ(5,1) EXPA,EXPB,EXPC,KP2A,KP2B,K2,K3,EA1,EA2
READ(5,2) DTB,TMAX,RR,DL,TS,NE,NP,NEP,IFLAG,IF
READ(5,6) (N(J),J=1,5),(H(J),J=1,6)
```

```

CALL CPCALC(SH2,SCO,SCO2,SH20,SCH4,ST#,MG,CPG,CPG1,CPG2)
PGS=MG*PT#/RG/ST#
K1P=K2*PT#/SCO
K2P=K3*PT#/SCO
KC2#=1.D#
EP=1E.D#**NEP
KB=KP*TS**(-.3)
```

```

* PRINT 3,EPS,CPS,CPT,L,PS,PT,RT#,TC,KT,R1,OHSG,DH1A,EXPA,
*          OHTS,DH1B,EXPB,OHTG,DH2A,EXPC,BGS,DH2B,KP2A,BSG,KB,
*          KP2B,BTS,KB,P,K2,BTG,K3,PTZ,EA1,PTR,EA2
* PRINT 4,DTB,TMAX,DL,RR,TS,EP,DTB**4.D#***(IF-1)
* PRINT 5,SCH4,ST#.SCO,STW,SCO2,PT#,SH2,PT1,SH20,MG,UGS,CPG
```

```

DTB=DTB*UGS/L
TMAX=TMAX*UGS/L
DL=DL*UGS/L
RR=(1.D#-RB/R1)*RR+RB/R1
EA1=EA1/RGP
EA2=EA2/RGP
```

```

RETURN
1 FORMAT(9D8.2)
2 FORMAT(5F8.2,/6I8)
3 FORMAT(1H1.//,.3X,'INPUT DATA:',//,9X,'REACTOR PARAMETERS',9X,
*          'CATALYST PARAMETERS',6X,'THERMAL WELL PARAMETERS',//,
*          9X,'EPS =',E12.4,9X,'CPS =',E12.4,9X,'CPT =',E12.4/
*          9X,'L =',E12.4,9X,'PS =',E12.4,9X,'PT =',E12.4/
*          9X,'RT# =',E12.4,9X,'TC =',E12.4,9X,'KT =',E12.4/
*          9X,'R1 =',E12.4//,6X,
*          'HEAT TRANSFER PARAMETERS',19X,'REACTOR PARAMETERS'//,
*          9X,'OHSG ',E12.4,9X,'DH1A =',E12.4,9X,'EXPA =',E12.4/
*          9X,'OHTS =',E12.4,9X,'DH1B =',E12.4,9X,'EXPB =',E12.4/
*          9X,'OHTG =',E12.4,9X,'DH2A =',E12.4,9X,'EXPC =',E12.4/
*          9X,'BGS =',E12.4,9X,'DH2B =',E12.4,9X,'KP2A =',E12.4/
*          9X,'BSG =',E12.4,9X,'K2 =',E12.4,9X,'KP2B =',E12.4/
*          9X,'BTS =',E12.4,9X,'KB =',E12.4,9X,'K2 =',E12.4/
*          9X,'BTG =',E12.4,36X,'K3 =',E12.4/
*          9X,'PTZ =',E12.4,36X,'EA1 =',E12.4/
*          9X,'PTR =',E12.4,36X,'EA2 =',E12.4)
4 FORMAT(//,.3X,'PROGRAM CONDITIONS',//,9X,
*          'TIME STEP =',F8.4,/9X,'MAXIMUM TIME =',F8.4,/9X,
*          'DISTURBANCE LENGTH =',F15.4,/9X,
*          'RADIAL COLLOCATION POINT =',F8.4,/9X,
*          'START TIME (HRS) =',F15.4,/9X,
*          'ACCURACY OF CONVERGENCE =',E18.3,/9X,
*          'MAX VALUE OF DT =',F8.4)
5 FORMAT(//,.3X,'STEADY STATE CONDITIONS:',//,9X,'XCH4 =',
*          E12.4,9X,'TB =',E12.4,/9X,'XCO =',E12.4,9X,'TW =',
*          E12.4,/9X,'XCO2 =',E12.4,9X,'PT# =',E12.4,/9X,'XH2 =',
*          E12.4,9X,'PT1 =',E12.4,/9X,'XH20 =',E12.4,9X,'MG =',
*          E12.4,/9X,'UG# =',E12.4,9X,'CPG =',E12.4)
6 FORMAT(5I4/5F8.2)
END
```

Table A5-2 Continued

```
SUBROUTINE OUTPUT (Y,U,T,MM)

C THIS ROUTINE OUTPUTS THE CALCULATED RESULTS.

IMPLICIT REAL*8 (A-H,O-Z)
REAL*8 L, MG
DIMENSION Y(100), U(8)
COMMON /COMAT/ NE, N(5), H(5), ZI(6), NS(6), Z(5,25), A(5,25,25),
* B(5,25,25)
* /OPCON/ SCH4, SCO, SC02, SH2, SH20, PT0, PT1, ST0, STW
* /RADIA/ W(10), WP(9,2), DETA(2), RR
* /GASPA/ CPG, PTZ, PTR, MG, PGS, UGS, UM
* /REACP/ EPS, L, R0, RI
* /INDEX/ NSE, NTS, NTT, NTG, NCO, NC2, NUG, NNE, NE1
DATA RG /82.544D0/
IF(MM .EQ. 1) PRINT 1
IF(MM .EQ. 2) PRINT 6
IF(MM .EQ. 3) PRINT 8
PH2=PT1/PT0
PH1=R0/R1
TA=T*L/UGS
IF(MM .EQ. 8)PRINT 7,TA

PRINT 2
DO 100 K=1,NE
CALL INDICES(K,NK,N1,N2,N3,N4,N5,N6)
PRINT 3, TR(Y(NTG+K),Y(NTT+K),2,PH1),Y(NTG+K),
* TR(Y(NTG+K),Y(NTT+K),2,1,D0),TR(Y(NTS+K),Y(NTT+K),1,PH1),
* Y(NTS+K),TR(Y(NTS+K),Y(NTT+K),1,1,D0)
DO 100 I=1,NK
100 PRINT 3, TR(Y(N3+I),Y(N2+I),2,PH1),Y(N3+I),TR(Y(N3+I),Y(N2+I),2,
* 1,D0),TR(Y(N1+I),Y(N2+I),1,PH1),Y(N1+I),TR(Y(N1+I),Y(N2+I),
* 1,1,D0)

PRINT 3, TR(Y(NTG+NE1),Y(NTT+NE1),2,PH1),Y(NTG+NE1),
* TR(Y(NTG+NE1),Y(NTT+NE1),2,1,D0),TR(Y(NTS+NE1),Y(NTT+NE1),
* 1,PH1),Y(NTS+NE1),TR(Y(NTS+NE1),Y(NTT+NE1),1,1,D0)

PRINT 4
DO 200 K=1,NE
CALL INDICES(K,NK,N1,N2,N3,N4,N5,N6)
CALL ACTCONC(Y(NCO+K),Y(NC2+K),X1,X2)
PRINT 5, Y(NTT+K),X1,X2,Y(NUG+K)
DO 200 I=1,NK
200 CALL ACTCONC(Y(N4+I),Y(N5+I),X1,X2)
PRINT 5,Y(N2+I),X1,X2,Y(N6+I)

CALL ACTCONC(Y(NCO+NE1),Y(NTC+NE1),X1,X2)
PRINT 5,Y(NTT+NE1),X1,X2,Y(NUG+NE1)
RETURN

1  FORMAT(1H1, //2X, 'INITIAL GUESSES: ', //)
2  FORMAT(16X, 'GAS TEMPERATURE', 25X,
* 'SOLID TEMPERATURE', //8X, 'R = R0', 7X, 'R = RR', 7X,
* 'R = R1', 9X, 'R = R0', 7X, 'R = RR', 7X, 'R = R1')
3  FORMAT(5X, 3(F9.5,4X), 2X, 3(F9.5,4X))
4  FORMAT(1/9X, 'WELL TEMP.', 5X, 'CO CONC.', 5X, 'CO2 CONC.', 4X,
* 'VELOCITY')
5  FORMAT(19X, F9.5, 5X, F10.7, 3X, F10.7, 3X, F9.5, 3X, F9.5)
6  FORMAT(//2X, 'STEADY STATE SOLUTION: ', //)
7  FORMAT(//, 2X, 'TIME = ', F11.4, ' SEC')
8  FORMAT(//, 2X, 'ACTUAL STEADY STATE SOLUTION: ', //)
END
```

Table A5-2 Continued

```
SUBROUTINE RADIAL
C  THIS SUBROUTINE CALCULATES THE CONSTANTS FOR THE RADIALLY LUMPED
C  MODEL.
      IMPLICIT REAL*8 (A-H,O-Z)
      COMMON /DIMLE/ ALS,ALG,ALT,BES,BEG,GAS,GAG,GTS,GTG,DEI,
      *                   DE2,S11,S12,S13,PHI2,PHI3,PH1,PH2,PH3
      *                   /RADIA/ W(18),WP(9,2),DETA(2),RR
      *                   /HEATT/ OHSG,OHTS,OHTG,BGS,BSG,BTS,BTG,BWG,BWS
      W(9)=B.DB
      W(18)=B.DB
      I=1
      S1=BTS
      S2=BWS
      S3=GAS
      S4=BES
      S5=GTS
 188  DETA(I)=(PH1+PHI**2*(RR-1.DB)+RR**2*(1.DB-PH1)-RR)*S1*S2
      *           +(2.DB*(PH1-RR)+RR**2-PH1**2)*S1
      *           +(-1.DB+RR**2+2.DB*(PH1-PH1*RR))*S2+2.DB*PH1-2.DB
      WP(1,I)=(PH1*S1-1.DB)*(S2+2.DB)-(S2+1.DB)*(PH1**2*S1-2.DB*PH1)
      WP(2,I)=S1*(S2+1.DB)*RR**2-S1*RR*(S2+2.DB)
      WP(3,I)=(S2*RR*(PH1**2*S1-2.DB*PH1)-S2*(PH1*S1-1.DB)*RR**2)
      WP(4,I)=S2*(PH1**2*S1-2.DB*PH1)-S1*(S2+2.DB)
      WP(5,I)=S1*(S2+2.DB)-S1*S2*RR**2
      WP(6,I)=(S1*S2*RR**2-S2*(PH1**2*S1-2.DB*PH1))
      WP(7,I)=S1*(S2+1.DB)-S2*(PH1*S1-1.DB)
      WP(8,I)=RR*S1*S2-S1*(S2+1.DB)
      WP(9,I)=S2*(PH1*S1-1.DB)-RR*S1*S2
      W1+I*3-3)=(4.DB*WP(7,I)+WP(4,I))/RR)*S4/DETA(I)-S3
      W12+I*3-3)=(4.DB*WP(8,I)+WP(5,I))/RR)*S4/DETA(I)
      W(3+I*3-3)=(4.DB*WP(9,I)+WP(6,I))/RR)*S4/DETA(I)
      W(7+I-1)=S5*(WP(1,I)+WP(4,I)*PH1+WP(7,I)*PH1**2)/DETA(I)
      W(9)=W(9)+S5*(WP(2,I)+WP(5,I)*PH1+WP(8,I)*PH1**2)/DETA(I)-S5
      W(18)=W(18)+S5*(WP(3,I)+WP(6,I)*PH1+WP(9,I)*PH1**2)/DETA(I)
      IF(I .EQ. 2)RETURN
      I=2
      S1=BTG
      S2=BWG
      S3=GAG
      S4=BEG
      S5=GTG
      GO TO 188
      END
```

Table A5-2 Continued

```

SUBROUTINE FN1 (Y,V)
C THIS SUBROUTINE DEFINES THE ALGEBRAIC EQUATIONS FOR USE BY NSES1
IMPLICIT REAL*8 (A-H,O-Z)
REAL *8 MG
DIMENSION Y(100),V(1)
COMMON /COMAT/ NE,N(5),H(5),Z(6),NS(6),Z(5,25),A(5,25,25),
B(5,25,25)
* /DIMLE/ ALS,ALG,ALT,BES,BEG,GAS,GAG,GTS,GTG,DE1,
* DE2,SI1,SI2,SI3,PH12,PH13,PH1,PH2,PH3
* /LINEA/ AA(75,75),BB(75,8),DD(75),U(8)
* /RADIA/ W(18),WP(9,2),DETA(2),RR
* /HEATT/ OHSG,OHTS,OHTG,BGS,BSG,BTS,BTG,BWG,BWS
* /INDEX/ NSE,NTS,NTT,NTG,NCO,NC2,NUG,NNE,NE1
* /GASPA/ CFG,PTZ,PTR,MG,PGS,UGS,UM
DO 188 K=1,NE
CALL INDICES(K,NK,N1,N2,N3,N4,N5,N6)
DO 188 I=1,NK
PT=PRES(I,K)
CALL REAC (Y(N4+I),Y(N5+I),Y(N1+I),Y(N2+I),PT,R1P,R2P)
V(I+N1) = ALS*SUM(Y,I,K,1,2) + W(1)*Y(N1+I) + W(2)*Y(N2+I)
* + GAS*Y(N3+I) + DE1*PR1P*(1.0#+PH12*Y(N1+I))
* + DE2*R2P*(1.0#+PH13*Y(N1+I)) + W(3)*PH3
V(I+N2) = ALT*SUM(Y,I,K,2,2) + W(7)*Y(N1+I) + W(8)*Y(N3+I)
* + W(9)*Y(N2+I) + W(18)*PH3
V(I+N3) = -Y(N6+I)*SUM(Y,I,K,3,1) + (ALG*SUM(Y,I,K,3,2)
* + W(4)*Y(N3+I) + W(5)*Y(N2+I) + GAG*Y(N1+I)
* + W(6)*PH3)/PT*Y(N3+I)
V(I+N4) = -Y(N6+I)*SUM(Y,I,K,4,1) + SI2*Y(N3+I)*R2P/PT
* - SI1*Y(N3+I)*R1P/PT
V(I+N5) = -Y(N6+I)*SUM(Y,I,K,5,1) - SI3*Y(N3+I)*R2P/PT
V(I+N6) = Y(N3+I)*SUM(Y,I,K,6,1) + Y(N3+I)*Y(N6+I)*
(PH2-1.0#)/PT - Y(N6+I)*SUM(Y,I,K,3,1)
188  CONTINUE
DO 388 L=1,6
N7=6*NSE+(L-1)*NE1
DO 388 K=2,NE
V(N7+K) = SUM(Y,N(K-1)+1,K-1,L,1) - SUM(Y,B,K,L,1)
V(NTS+1) = SUM(Y,B,1,1,1) - BGS*(Y(NTS+1)-Y(NTG+1))
V(NTS+NE1) = SUM(Y,NNE,NE,1,1) - BGS*(Y(NTG+NE1)-Y(NTS+NE1))
V(NTT+1) = Y(NTT+1) - U(3)
V(NTT+NE1) = SUM(Y,NNE,NE,2,1)
V(NTG+1) = SUM(Y,B,1,3,1) + BSG*(Y(NTS+1)-Y(NTG+1))
* - (1.0#-1.0#/(Y(NTG+1)))/ALG
V(NTG+NE1) = SUM(Y,NNE,NE,3,1) - BSG*(Y(NTS+NE1)-Y(NTG+NE1))
V(NCO+1) = Y(NCO+1)-U(4)
V(NCO+NE1) = SUM(Y,NNE,NE,4,1)
V(NC2+1) = Y(NC2+1)-U(5)
V(NC2+NE1) = SUM(Y,NNE,NE,5,1)
V(NUG+1) = Y(NUG+1)-U(2)
V(NUG+NE1) = Y(NTG+NE1)*SUM(Y,NNE,NE,6,1) + Y(NUG+NE1)*
Y(NTG+NE1)*(PH2-1.0#)/PH2 - Y(NUG+NE1)*
SUM(Y,NNE,NE,3,1)
388  RETURN
END

```

Table A5-2 Continued

```

SUBROUTINE CPCALC(SH2,SCO,SCO2,SH20,SCH4,ST#,MG,CPG,CPG1,CPG2)
C THIS SUBROUTINE CALCS THE HEAT CAPACITY
IMPLICIT REAL*8(A-H,O-Z)
REAL*8 MG
SN2=1.D0-SH2-SCO-SCO2-SH20-SCH4
* MG=SCH4*16.43D#*SCO*28.81D#*SCO2*44.889D#*SH2*2.816D#
* +SH20*18.8154D#*SN2*28.8134D#
* CPG1=(SH2*.81D-3*SN2*.7757D-3+SCO*1.2D-3+SCO2*4.216D-3
* +SH20*7.17D-3*SCH4*12.4282D-3)/MG
* CPG2=(SH2*6.62D#*SN2*6.775D#*SCO*6.6D#*SCO2*8.85126D#
* +SH20*11.2D#*SCH4*5.288D#)/MG
CPG=CPG1*ST#+CPG2
RETURN
END

FUNCTION SUM(Y,I,K,L,M)
IMPLICIT REAL*8 (A-H,O-Z)
DIMENSION Y(100)
COMMON /COMAT/ NE,N(5),H(5),ZI(6),NS(6),Z(5,25),A(5,25,25),
* B(5,25,25)
SUM=0.D#
IP1=1+1
NN=(L-1)*NS(NE+1)+NS(K)
N7=6*NS(NE+1)+(L-1)*(NE+1)
IF(M .EQ. 2) GO TO 200
DO 100 J=1,N(K)
JP1=J+1
100 SUM=SUM+A(K,IP1,JP1)*Y(J+NN)
SUM=SUM+A(K,IP1,1)*Y(N7+K)+A(K,IP1,N(K)+2)*Y(N7+K+1)
SUM=SUM/H(K)
RETURN

200 DO 201 J=1,N(K)
JP1=J+1
201 SUM=SUM+B(K,IP1,JP1)*Y(J+NN)
SUM=SUM+B(K,IP1,1)*Y(N7+K)+B(K,IP1,N(K)+2)*Y(N7+K+1)
SUM=SUM/H(K)/H(K)
RETURN
END

SUBROUTINE REAC (Y1,Y2,TS,TG,PT,R1P,R2P)
C THIS SUBROUTINE CALCULATES THE DIMENSIONLESS RATES
IMPLICIT REAL*8 (A-H,O-Z)
REAL*8 MG,KP2A,KP2B,KC2#,K1P,K2P,KP2
COMMON /OPCON/ SCH4,SCO,SCO2,SH2,SH20,PT#,PT1,ST#,STW
* /REAC2/ EXP4,EXP8,EXPc,KC2#,KP2A,KP2B,K1P,K2P,EA1,EA2
* /LINEA/ AA(75,75),BB(75,8),DD(75),U(B)

GA=0.D#
TT=ST#+TS
KP2=DEXP(KP2A+KP2B/TT)
TH1=SCO*(U(4)-Y1+U(5)-Y2)
TH2=SCO*(U(5)-Y2)
TH3=1.D#-2.D#*TH1
YH2=(SCO*U(7)-3.D#*TH1-TH2)/SCO/TH3
YH20=(SCO*U(6)+TH1+TH2)/SCO/TH3
YCH4=(SCO*U(8)+TH1)/SCO/TH3
YCO=Y1/TH3
YCO2=Y2/TH3
PA=PT#*TH3
IF(YH2 .LT. 0.D#) YH2=1.D-1#
IF(yco .LT. 0.d#) yco=1.d-1#
R1P=DEXP(-EA1/TT)*PA**((expa+expb)*YH2**expb*YCO**expa/
* (1.D#+K1P*PA*YCO+K2P*PA*YH2)**expc
* R2P=DEXP(-EA2/TT)*(.83D#+.17D#*PA*PT#)*(YCO2*YH2-YCO*YH20/
* KP2*KC2#)

RETURN
END

```

Table A5-2 Continued

```
FUNCTION TR(T,TT,L,R)
IMPLICIT REAL*8 (A-H,O-Z)
COMMON /RADIA/ W1(B),WP(9,2),DETA(2),RR
/LINEA/ AA(75,75),BB(75,8),DD(75),U(8)
* TR=((WP(1,L)+WP(4,L)*R+WP(7,L)*R**2)*T
* +(WP(2,L)+WP(5,L)*R+WP(8,L)*R**2)*TT
* +WP(3,L)*U(1)+WP(6,L)*U(1)*R+WP(9,L)*U(1)*R**2)/DETA(L)
RETURN
END

FUNCTION RFN (AA,NN)
IMPLICIT REAL*8 (A-H,O-Z)
DIMENSION AA(100)
ST=0.0B
DO 100 I=1,NN
IF(DABS(AA(I)) .GE. ST) ST=AA(I)
RFN=DLOG10(DABS(ST))
RETURN
END

SUBROUTINE ACTCONC(Y1,Y2,X1,X2)
IMPLICIT REAL*8 (A-H,O-Z)
COMMON /OPCON/ SCH4,SCO,SCO2,SH2,SH20,PTB,PT1,STB,STW
/LINEA/ AA(75,75),BB(75,8),DD(75),U(8)
TH1=1.0B-2.0B*(SCO*(U(4)-Y1+U(5)-Y2))
X1=Y1*SCO/TH1
X2=Y2*SCO/TH1
RETURN
END

FUNCTION PRES(I,K)
IMPLICIT REAL*8 (A-H,O-Z)
COMMON /OPCON/ SCH4,SCO,SCO2,SH2,SH20,PTB,PT1,STB,STW
* /COMAT/ NE,N(5),H(5),ZI(6),NS(6),Z(5,25),A(5,25,25),
* B(5,25,25)
* PRES=((PT1-PTB)*(ZI(K)+H(K)*Z(K,I+1))+PTB)/PTB
RETURN
END

SUBROUTINE INDICES (K,NK,N1,N2,N3,N4,N5,N6)
IMPLICIT REAL*8 (A-H,O-Z)
COMMON /COMAT/ NE,N(5),H(5),ZI(6),NS(6),Z(5,25),A(5,25,25),
* B(5,25,25)
NSE=NS(NE+1)
NK=N(K)
N1=NS(K)
N2=NSE+NS(K)
N3=2*NSE+NS(K)
N4=3*NSE+NS(K)
N5=4*NSE+NS(K)
N6=5*NSE+NS(K)
RETURN
END
```

Table A5-2 Continued

```
SUBROUTINE COLLOC

C THIS ROUTINE CALCULATES THE ZEROS OF THE ORTHOGONAL POLYNOMIAL AND
C SETS UP THE AXIAL COLLOCATION MATRICES A AND B

IMPLICIT REAL*8 (A-H,O-Z)
DIMENSION D1(25),D2(25),D3(25),V1(25),V2(25),R(25)
COMMON /COMAT/ NE,N(5),H(5),ZI(6),NS(6),Z(5,25),A(5,25,25),
* B(5,25,25)
* /INDEX/ NSE,NTS,NTT,NTG,NCO,NC2,NUG,NNE,NE1

PRINT 1
DO 100 K=1,NE
NK=N(K)
CALL JCOBI(25,NK,1,1,B,D8,B,D8,D1,D2,D3,R)
PRINT 2, K,H(K),(R(J),J=1,NK+2)
DO 100 I=1,NK+2
CALL DFOPR(25,NK,1,1,I,1,D1,D2,D3,R,V1)
CALL DFOPR(25,NK,1,1,I,2,D1,D2,D3,R,V2)
DO 102 J=1,NK+2
A(K,I,J)=V1(J)
B(K,I,J)=V2(J)
102 CONTINUE
Z(K,I)=R(I)
100 CONTINUE

NS(1)=B
ZI(1)=B,D8
DO 200 K=1,NE
NS(K+1)=NS(K)+N(K)
ZI(K+1)=ZI(K)+H(K)
200 PRINT 3,((ZI(K)+H(K)*Z(K,J)),J=1,N(K)+1),K=1,NE),1.D8

NE1=NE+1
NSE=NS(NE1)
NNE=N(NE)+1
NTS=6*NSE
NTT=6*NSE+NE1
NTG=6*NSE+2*NE1
NCO=6*NSE+3*NE1
NC2=6*NSE+4*NE1
NUG=6*NSE+5*NE1

RETURN
1 FORMAT(1H1,/,3X,'ORTHOGONAL COLLOCATION OF FINITE ELEMENTS')
2 * FORMAT(//2X,'ELEMENT #',I3,5X,'LENGTH = ',F5.3,/,7X,
* 'COLLOCATION POINTS: ',//,3(1BX,6F8.4/))
3 FORMAT(//2X,'COLLOCATION POINT SUMMARY:',//,6(1BX,6F8.4/))
END

SUBROUTINE INTLSS(Y,U,EP)

C THIS ROUTINE CALCULATES THE INITIAL STEADY STATE PROFILE

IMPLICIT REAL*8 (A-H,O-Z)
DIMENSION Y(100),U(8)
COMMON /INDEX/ NSE,NTS,NTT,NTG,NCO,NC2,NUG,NNE,NE1
EXTERNAL FN1

CALL INITIAL (Y,U)
CALL OUTPUT(Y,U,B,D8,1)
CALL NSES1(6*(NSE+NE1),Y,EP,2000,B,FN1)
CALL OUTPUT(Y,U,B,D8,2)
RETURN

END
```

Table A5-2 Continued

APPENDIX 6

LINEAR PACKED BED REACTOR MODEL

Linearization of Reaction Rates

Methanation

$$R'_M = \frac{P_T^{1.5} e^{-E_{aM}/RT_o\Theta_s} (y_{H_2})^{0.5} (y_{CO})(1-\nu)}{1 + K'_1 P_T y_{H_2} + K'_2 P_T y_{CH_4}}$$

If we neglect the second and higher order terms in a Taylor series expansion, the linearized rate is of the form

$$R'_M \approx R_{M_{ss}} + R_{M_{\Theta_s}} (\Theta_s - \bar{\Theta}_s) + R_{M_{y_{CO}}} (y_{CO} - \bar{y}_{CO}) + R_{M_{y_{CO_2}}} (y_{CO_2} - \bar{y}_{CO_2}) + R_{M_{y_{CO_2}^0}} (y_{CO_2}^0 - 1.0)$$

$$+ R_{M_{y_{CO_2}^0}} (y_{CO_2}^0 - \bar{y}_{CO_2}^0) + R_{M_{y_{H_2}^0}} (y_{H_2}^0 - \bar{y}_{H_2}^0) + R_{M_{y_{CH_4}^0}} (y_{CH_4}^0 - \bar{y}_{CH_4}^0) + R_{M_{y_{H_2}^0}} (y_{H_2}^0 - \bar{y}_{H_2}^0)$$

where

$$R_{M_z} = \left[\frac{\partial R_M}{\partial z} \right]_{ss}$$

After performing the differentiation

$$R_{M_{ss}} = \frac{P_T^{1.5} e^{-E_{aM}/RT_o\bar{\Theta}_s} (\bar{y}_{H_2})^{0.5} \bar{y}_{CO} (1-\bar{\nu})}{1 + K'_1 P_T \bar{y}_{H_2} + K'_2 P_T \bar{y}_{CH_4}}$$

$$R_{M_{\Theta_s}} = \left[\frac{E_{aM}}{R_g \bar{T}_o \bar{\Theta}_s^2} - \frac{K_{P_{M2}} \bar{\nu}}{\bar{T}_o \bar{\Theta}_s^2 (1-\bar{\nu})} \right] R_{M_{ss}}$$

$$R_{M_{y_{CO}}} = \left[\frac{1}{\bar{y}_{CO}} + \frac{\bar{\nu}}{1-\bar{\nu}} \left(\frac{1}{\bar{y}_{H_2O}} + \frac{1}{\bar{y}_{CH_4}} + \frac{1}{\bar{y}_{CO}} + \frac{9}{\bar{y}_{H_2}} \right) + \frac{1.5}{\bar{y}_{H_2}} \right.$$

$$\left. - \frac{3K'_1 P_T - K'_2 P_T}{1 + K'_1 P_T \bar{y}_{H_2} + K'_2 P_T \bar{y}_{CH_4}} \right] R_{M_{ss}}$$

$$R_{M_{y_{CO_2}}} = \left[\frac{\bar{\nu}}{1-\bar{\nu}} \left(\frac{2}{\bar{y}_{H_2O}} + \frac{1}{\bar{y}_{CH_4}} + \frac{12}{\bar{y}_{H_2}} \right) + \frac{2}{\bar{y}_{H_2}} - \frac{4K'_1 P_T - K'_2 P_T}{1 + K'_1 P_T \bar{y}_{H_2} + K'_2 P_T \bar{y}_{CH_4}} \right] R_{M_{ss}}$$

$$R_{M_{y_{CO}}} = - \left[\frac{\bar{\nu}}{1-\bar{\nu}} \left(\frac{1}{\bar{y}_{H_2O}} + \frac{1}{\bar{y}_{CH_4}} + \frac{9}{\bar{y}_{H_2}} \right) + \frac{1.5}{\bar{y}_{H_2}} - \frac{3K'_1 P_T - K'_2 P_T}{1 + K'_1 P_T \bar{y}_{H_2} + K'_2 P_T \bar{y}_{CH_4}} \right] R_{M_{ss}}$$

$$R_{M_{y_{CO_2}^0}} = -R_{M_{y_{CO_2}}}$$

$$R_{M_{y_{H_2O}^0}} = - \left[\frac{\bar{\nu}}{(1-\bar{\nu}) \bar{y}_{H_2O}} \right] R_{M_{ss}}$$

$$R_{M_{y_{H_2}^0}} = \left[\frac{3\bar{\nu}}{\bar{y}_{H_2}(1-\bar{\nu})} + \frac{1}{2\bar{y}_{H_2}} - \frac{K'_1 P_T}{1 + K'_1 P_T \bar{y}_{H_2} + K'_2 P_T \bar{y}_{CH_4}} \right] R_{M_{ss}}$$

$$R_{M_{y_{CH_4}^0}} = - \left[\frac{\bar{\nu}}{(1-\bar{\nu}) \bar{y}_{CH_4}} + \frac{K'_2 P_T}{1 + K'_1 P_T \bar{y}_{H_2} + K'_2 P_T \bar{y}_{CH_4}} \right] R_{M_{ss}}$$

Steam-Shift

$$R'_s = \frac{(f_1 + f_2 \bar{P}_{T_A} P_0) e^{-E_{as}/R_g T_o \bar{\theta}_s}}{(1-2\delta)^2} \left[y_{CO_2} y_{H_2} - \frac{K_{c_s}}{K_{P_s}} y_{CO} y_{H_2O} \right]$$

$$\text{where } \bar{P}_{T_A} = (1-2\delta)P_T$$

If we neglect the second and higher order terms in a Taylor series expansion, the linearized rate is of the form

$$\begin{aligned} R'_s \approx & R_{s_{ss}} + R_{s_{\bar{\theta}_s}} (\bar{\theta}_s - \bar{\theta}_s) + R_{s_{y_{CO}}} (y_{CO} - \bar{y}_{CO}) + R_{s_{y_{CO_2}}} (y_{CO_2} - \bar{y}_{CO_2}) + R_{s_{y_{H_2O}}} (y_{H_2O} - 1.0) \\ & + R_{s_{y_{CO_2}}} (y_{CO_2} - \bar{y}_{CO_2}) + R_{s_{y_{H_2O}}} (y_{H_2O} - \bar{y}_{H_2O}) + R_{s_{y_{CH_4}}} (y_{CH_4} - \bar{y}_{CH_4}) + R_{s_{y_{H_2}}} (y_{H_2} - \bar{y}_{H_2}) \end{aligned}$$

where

$$R_{s_z} = \left[\frac{\partial R_s}{\partial z} \right]_{ss}$$

Then after differentiation

$$R_{s_{ss}} = \frac{(f_1 + f_2 \bar{P}_{T_A} P_0) e^{-E_{as}/R_g T_o \bar{\theta}_s}}{(1-2\delta)^2} \left[\bar{y}_{CO_2} \bar{y}_{H_2} - \frac{K_{c_s}}{K_{P_s}} \bar{y}_{CO} \bar{y}_{H_2O} \right]$$

$$R_{s_{\bar{\theta}_s}} = \frac{E_{as}}{R_g \bar{T}_o \bar{\theta}_s^2} R_{s_{ss}} - \frac{(f_1 + f_2 \bar{P}_{T_A} P_0) e^{-E_{as}/R_g T_o \bar{\theta}_s} K_{c_s} \bar{y}_{CO} \bar{y}_{H_2O} K_{P_s}}{\bar{K}_{P_s} \bar{T}_o \bar{\theta}_s^2 (1-2\delta)^2}$$

$$R_{S_{y_{CO}}} = \left[\frac{2f_2 P_0 P_T \bar{x}_{CO}^0}{f_1 + f_2 \bar{P}_{T_A} P_0} - \frac{4\bar{x}_{CO}^0}{1-2\delta} \right] R_{S_{\infty}} + \frac{(f_1 + f_2 \bar{P}_{T_A} P_0) e^{-E_{as}/R_g T_o \bar{E}_s}}{(1-2\delta)^2} \left[3\bar{y}_{CO_2} + \frac{K_{cs}(\bar{y}_{CO} - \bar{y}_{H_2} O)}{\bar{K}_{ps}} \right]$$

$$R_{S_{y_{CO_2}}} = \left[\frac{2f_2 P_0 P_T \bar{x}_{CO}^0}{f_1 + f_2 \bar{P}_{T_A} P_0} - \frac{4\bar{x}_{CO}^0}{1-2\delta} \right] R_{S_{\infty}} + \frac{(f_1 + f_2 \bar{P}_{T_A} P_0) e^{-E_{as}/R_g T_o \bar{E}_s}}{(1-2\delta)^2} \left[4\bar{y}_{CO_2} + \bar{y}_{H_2} + \frac{2K_{cs}\bar{y}_{CO}}{\bar{K}_{ps}} \right]$$

$$R_{S_{y_{CH_4}^0}} = 0$$

$$R_{S_{y_{H_2}^0}} = - \frac{K_{cs}\bar{y}_{CO}(f_1 + f_2 \bar{P}_{T_A} P_0) e^{-E_{as}/R_g T_o \bar{E}_s}}{\bar{K}_{ps}(1-2\delta)^2}$$

$$R_{S_{y_{H_2}^0}} = - \frac{\bar{y}_{CO_2}(f_1 + f_2 \bar{P}_{T_A} P_0) e^{-E_{as}/R_g T_o \bar{E}_s}}{(1-2\delta)^2}$$

$$R_{S_{y_{CO}^0}} = \left[\frac{4\bar{x}_{CO}^0}{1-2\delta} - \frac{2f_2 P_0 P_T \bar{x}_{CO}^0}{f_1 + f_2 \bar{P}_{T_A} P_0} \right] R_{S_{\infty}} - \frac{(f_1 + f_2 \bar{P}_{T_A} P_0) e^{-E_{as}/R_g T_o \bar{E}_s}}{(1-2\delta)^2} \left[3\bar{y}_{CO_2} + \frac{K_{cs}\bar{y}_{CO}}{\bar{K}_{ps}} \right]$$

$$R_{S_{y_{CO_2}^0}} = \left[\frac{4\bar{x}_{CO}^0}{1-2\delta} - \frac{2f_2 P_0 P_T \bar{x}_{CO}^0}{f_1 + f_2 \bar{P}_{T_A} P_0} \right] R_{S_{\infty}} - \frac{(f_1 + f_2 \bar{P}_{T_A} P_0) e^{-E_{as}/R_g T_o \bar{E}_s}}{(1-2\delta)^2} \left[4\bar{y}_{CO_2} + \frac{2K_{cs}\bar{y}_{CO}}{\bar{K}_{ps}} \right]$$

Linearization of Algebraic Equations

The boundary conditions for the mass balances and for the energy equation for the thermal well can be solved explicitly for the concentrations and thermal well temperatures at the axial boundary points as linear expressions of the conditions at the interior collocation points. However, the set of four boundary conditions for the gas and catalyst temperatures are coupled and are nonlinear as a result of the convective term in the inlet boundary condition for the gas. After a Taylor series linearization of this term around the steady state inlet gas temperature, gas velocity, and inlet concentrations, the system of four equations is solved for the gas and catalyst temperatures at the boundary points:

$$\begin{bmatrix} \Theta_{s_0} \\ \Theta_{s_{N+1}} \\ \Theta_{g_0} \\ \Theta_{g_{N+1}} \end{bmatrix} = S \begin{bmatrix} \sum_{j=1}^N A_{0,j} \Theta_{s_j} \\ \sum_{j=1}^N A_{N+1,j} \Theta_{s_j} \\ \sum_{j=1}^N A_{0,j} \Theta_{g_j} + \Gamma \\ \sum_{j=1}^N A_{N+1,j} \Theta_{g_j} \end{bmatrix}$$

with

$$\begin{aligned} \Gamma &= \left(\frac{\bar{\Theta}_o - \bar{\Theta}_{g_o}}{\alpha_g \bar{\Theta}_{g_o}} \right) M_g c_{p_g} + \left(\frac{\bar{\Theta}_o - \bar{\Theta}_{g_o}}{\alpha_g \bar{\Theta}_{g_o}} \right) u_{g_o} + \left(\frac{1}{\alpha_g \bar{\Theta}_{g_o}} \right) \Theta_o + \frac{\bar{\Theta}_{g_o} + 1 - 2\bar{\Theta}_o}{\alpha_g \bar{\Theta}_{g_o}} \\ \Omega &= \frac{1}{\alpha_g \bar{\Theta}_{g_o}^2} \end{aligned}$$

and

$$S = - \begin{bmatrix} (A_{0,0} - \lambda_{gzs}) & A_{0,N+1} & \lambda_{gzs} & 0 \\ A_{N+1,0} & (A_{N+1,N+1} + \lambda_{gzs}) & 0 & -\lambda_{gzs} \\ \lambda_{sg} & 0 & (A_{0,0} - \lambda_{sg} - \Omega) & A_{0,N+1} \\ 0 & -\lambda_{sg} & A_{N+1,0} & (A_{N+1,N+1} + \lambda_{sg}) \end{bmatrix}^{-1}$$

Linearization and solution of the continuity equation for the velocities at the interior collocation points and at the end of the reactor are somewhat more complex. After linearization as described in Section 3.6 and after substitution of the linearized equations above for the endpoint temperatures, the continuity equation was solved for the velocities:

$$v_{g_i} = \sum_{j=1}^N H_{i,j} \Theta_{g_j} + \sum_{j=1}^N H_{i,N+j} \Theta_{g_j} + I_i$$

where

$$\begin{aligned} H &= F^{-1}G \\ I &= F^{-1}E \end{aligned}$$

The matrices **E**, **F**, and **G** have the following elements¹

$$F_{ij} = \begin{cases} \bar{\Theta}_{g_i} A_{ii} + P_i \bar{\Theta}_{g_i} - \sum_{k=0}^{N+1} A_{ik} \bar{\Theta}_{g_k} & i=j \\ \bar{\Theta}_{g_i} A_{ij} & i \neq j \end{cases} \quad \text{for } i, j = 1, \dots, N+1$$

For $i, j = 1, \dots, N$:

$$G_{i,j} = (A_{i,0}S_{31}A_{0,j} + A_{i,0}S_{32}A_{N+1,j} + A_{i,N+1}S_{41}A_{0,j} + A_{i,N+1}S_{42}A_{N+1,j})\bar{v}_{g_i}$$

$$G_{i,N+j} = (A_{i,j} + A_{i,0}S_{33}A_{0,j} + A_{i,0}S_{34}A_{N+1,j} + A_{i,N+1}S_{43}A_{0,j} + A_{i,N+1}S_{44}A_{N+1,j})\bar{v}_{g_i}$$

$$G_{i,N+i} = (A_{i,i} + A_{i,0}S_{33}A_{0,i} + A_{i,0}S_{34}A_{N+1,i} + A_{i,N+1}S_{43}A_{0,i} + A_{i,N+1}S_{44}A_{N+1,i})\bar{v}_{g_i}$$

$$- P_i \bar{v}_{g_i} - \sum_{k=0}^{N+1} A_{i,k} \bar{v}_{g_k}$$

1. Note that S_{ij} are the elements of the above **S** matrix.

$$E_i = - \sum_{j=0}^{N+1} A_{i,j} (\bar{v}_{g_i} \bar{\Theta}_{g_j} - \bar{v}_{g_j} \bar{\Theta}_{g_i}) + P_i \bar{v}_{g_i} \bar{\Theta}_{g_i} - A_{i,0} \bar{\Theta}_{g_i} v_{g_0} + \bar{v}_{g_i} (A_{i,0} S_{33} + A_{i,N+1} S_{43}) \Gamma$$

For $i = N+1, j = 1, \dots, N$:

$$G_{i,j} = (A_{i,0} S_{31} A_{0,j} + A_{i,0} S_{32} A_{N+1,j} + A_{i,N+1} S_{41} A_{0,j} + A_{i,N+1} S_{42} A_{N+1,j}) \bar{v}_{g_i}$$

$$- \left[P_i \bar{v}_{g_i} + \sum_{k=0}^{N+1} A_{i,k} \bar{v}_{g_k} \right] (S_{41} A_{0,j} + S_{42} A_{N+1,j})$$

$$G_{i,N+1} = (A_{i,j} + A_{i,0} S_{33} A_{0,j} + A_{i,0} S_{34} A_{N+1,j} + A_{i,N+1} S_{43} A_{0,j} + A_{i,N+1} S_{44} A_{N+1,j}) \bar{v}_{g_i}$$

$$- \left[P_i \bar{v}_{g_i} + \sum_{k=0}^{N+1} A_{i,k} \bar{v}_{g_k} \right] (S_{43} A_{0,j} + S_{44} A_{N+1,j})$$

$$E_i = - \sum_{j=0}^{N+1} A_{i,j} (\bar{v}_{g_i} \bar{\Theta}_{g_j} - \bar{v}_{g_j} \bar{\Theta}_{g_i}) + P_i \bar{v}_{g_i} \bar{\Theta}_{g_i} - A_{i,0} \bar{\Theta}_{g_i} v_{g_0} + \bar{v}_{g_i} (A_{i,0} S_{33} + A_{i,N+1} S_{43}) \Gamma$$

$$- \left[P_i \bar{v}_{g_i} + \sum_{k=0}^{N+1} A_{i,k} \bar{v}_{g_k} \right] S_{43} \Gamma$$

Linearization of the Differential Equations

The linear reaction rate expressions and the linear expressions for the velocities and for the concentrations and temperatures at the axial boundary points are then substituted into the differential equations. Due to extreme coupling between the state variables, lengthy manipulation is necessary to linearize the resulting equations. The linearization is completely analytic and the resulting

model is²

$$\dot{\mathbf{x}} = \mathbf{Ax} + \mathbf{Ww}$$

where

$$\mathbf{x} = \left[\theta_{s_1}, \dots, \theta_{s_N}, \theta_{g_1}, \dots, \theta_{g_N}, \theta_{t_1}, \dots, \theta_{t_N}, y_{1_1}, \dots, y_{1_N}, y_{2_1}, \dots, y_{2_N} \right]^T$$

$$\mathbf{w} = \left[\theta_w, v_{g_0}, \theta_o, y_{CO}, y_{CO_2}, y_{H_2O}, y_{H_2}, y_{CH_4} \right]^T$$

The elements of the state and control matrices \mathbf{A} and \mathbf{B} are as follows.³

Elements of the State Matrix

For $i, j = 1, \dots, N$ ($i \neq j$)

$$A_{i,j} = \alpha_s B_{i,j} + \alpha_s B_{i,0} (S_{11} A_{0,j} + S_{12} A_{N+1,j}) + \alpha_s B_{i,N+1} (S_{21} A_{0,j} + S_{22} A_{N+1,j})$$

$$A_{i,i} = \alpha_s B_{i,i} + \alpha_s B_{i,0} (S_{11} A_{0,i} + S_{12} A_{N+1,i}) + \alpha_s B_{i,N+1} (S_{21} A_{0,i} + S_{22} A_{N+1,i})$$

$$+ \omega_1 + \kappa_1 (1 + \varphi_1 \bar{\theta}_{s_i}) R_{M_{\theta_{s_i}}} + \varphi_1 R_{M_{\theta_{s_i}}} + \kappa_2 (1 + \varphi_2 \bar{\theta}_{s_i}) R_{S_{\theta_{s_i}}} + \varphi_2 R_{S_{\theta_{s_i}}}$$

$$A_{i,N+j} = \alpha_s B_{i,0} (S_{13} A_{0,j} + S_{14} A_{N+1,j}) + \alpha_s B_{i,N+1} (S_{23} A_{0,j} + S_{24} A_{N+1,j})$$

$$A_{i,N+i} = \alpha_s B_{i,0} (S_{13} A_{0,i} + S_{14} A_{N+1,i}) + \alpha_s B_{i,N+1} (S_{23} A_{0,i} + S_{24} A_{N+1,i}) + \gamma_s$$

2. In terms of deviation variables.

3. Note that the $A_{i,j}$ and $B_{i,j}$ terms on the left of the equalities correspond to the elements of the state and control matrices \mathbf{A} and \mathbf{B} , whereas those on the right of the equalities correspond to Lagrangian derivatives as given by Equation (3.3-43). The terms $H_{i,j}$ correspond to elements of the above \mathbf{H} matrix.

$$A_{i,2N+j} = 0 \quad A_{i,2N+i} = \omega_2$$

$$A_{i,3N+j} = 0 \quad A_{i,3N+i} = \kappa_1(1+\varphi_1\bar{\Theta}_{g_i})R_{M_{y_{CO_i}}} + \kappa_2(1+\varphi_2\bar{\Theta}_{g_i})R_{S_{y_{CO_i}}}$$

$$A_{i,4N+j} = 0 \quad A_{i,4N+i} = \kappa_1(1+\varphi_1\bar{\Theta}_{g_i})R_{M_{y_{CO_{g_i}}}} + \kappa_2(1+\varphi_2\bar{\Theta}_{g_i})R_{S_{y_{CO_{g_i}}}}$$

$$A_{N+i,j} = Q_{1_{i,j}}\bar{\Theta}_{g_i} + Q_{2_{i,j}}\bar{v}_{g_i} + H_{i,j} \left[\sum_{k=1}^N (Q_{2_{i,k}}\bar{\Theta}_{g_k} + Q_{4_{i,k}}\bar{\Theta}_{g_k}) - (S_{33}A_{i,0} + S_{43}A_{i,N+1})\bar{\Gamma} \right]$$

$$A_{N+i,i} = Q_{1_{i,i}}\bar{\Theta}_{g_i} + Q_{2_{i,i}}\bar{v}_{g_i} + H_{i,i} \left[\sum_{k=1}^N (Q_{2_{i,k}}\bar{\Theta}_{g_k} + Q_{4_{i,k}}\bar{\Theta}_{g_k}) - (S_{33}A_{i,0} + S_{43}A_{i,N+1})\bar{\Gamma} \right]$$

$$- \frac{\gamma_g \bar{\Theta}_{g_i}}{\tau \zeta_i + 1}$$

$$A_{N+i,N+j} = Q_{3_{i,j}}\bar{\Theta}_{g_i} + Q_{4_{i,j}}\bar{v}_{g_i} + H_{i,N+j} \left[\sum_{k=1}^N (Q_{2_{i,k}}\bar{\Theta}_{g_k} + Q_{4_{i,k}}\bar{\Theta}_{g_k}) - (S_{33}A_{i,0} + S_{43}A_{i,N+1})\bar{\Gamma} \right]$$

$$A_{N+i,N+i} = Q_{3_{i,i}}\bar{\Theta}_{g_i} + Q_{4_{i,i}}\bar{v}_{g_i} + H_{i,N+i} \left[\sum_{k=1}^N (Q_{2_{i,k}}\bar{\Theta}_{g_k} + Q_{4_{i,k}}\bar{\Theta}_{g_k}) - (S_{33}A_{i,0} + S_{43}A_{i,N+1})\bar{\Gamma} \right]$$

$$+ \frac{1}{\tau \zeta_i + 1} \left[(S_{33}B_{i,0} + S_{43}B_{i,N+1})\bar{\Gamma} \alpha_g + 4\beta_g w_g + \frac{\beta_g}{r_c} w_g + \gamma_g \bar{\Theta}_{g_i} \right.$$

$$\left. + \omega_5 \bar{\Theta}_{g_i} + 2\omega_4 \bar{\Theta}_{g_i} \right] + \sum_{k=1}^N (Q_{1_{i,k}}\bar{\Theta}_{g_k} + Q_{3_{i,k}}\bar{\Theta}_{g_k})$$

$$A_{N+i,2N+j} = 0 \quad A_{N+i,2N+i} = \frac{\omega_5 \bar{\Theta}_{g_i}}{\tau \zeta_i + 1}$$

$$A_{N+i,3N+j} = A_{N+i,3N+i} = A_{N+i,4N+j} = A_{N+i,4N+i} = 0$$

$$A_{2N+i,j} = 0 \quad A_{2N+i,i} = \omega_7$$

$$A_{2N+i,N+j} = 0 \quad A_{2N+i,N+i} = \omega_8$$

$$A_{2N+i,2N+j} = \alpha_i \left[B_{i,j} - \frac{B_{i,N+1}A_{N+1,j}}{A_{N+1,N+1}} \right]$$

$$A_{2N+i,2N+i} = \alpha_i \left[B_{i,i} - \frac{B_{i,N+1}A_{N+1,i}}{A_{N+1,N+1}} \right] + \omega_9$$

$$A_{2N+i,3N+j} = A_{2N+i,3N+i} = A_{2N+i,4N+j} = A_{2N+i,4N+i} = 0$$

$$A_{3N+i,j} = -H_{i,j} \left[\sum_{k=1}^N \left[A_{i,k} - \frac{A_{N+1,k}A_{i,N+1}}{A_{N+1,N+1}} \right] \bar{y}_{CO_k} + A_{i,0} - \frac{A_{N+1,0}A_{i,N+1}}{A_{N+1,N+1}} \right]$$

$$A_{3N+i,i} = -H_{i,i} \left[\sum_{k=1}^N \left[A_{i,k} - \frac{A_{N+1,k}A_{i,N+1}}{A_{N+1,N+1}} \right] \bar{y}_{CO_k} + A_{i,0} - \frac{A_{N+1,0}A_{i,N+1}}{A_{N+1,N+1}} \right]$$

$$+ \sigma_2 \frac{\bar{\Theta}_{S_i}}{P_{T_i}} R_{S_{\Theta_{S_i}}} - \sigma_1 \frac{\bar{\Theta}_{M_i}}{P_{T_i}} R_{M_{\Theta_{M_i}}}$$

$$A_{3N+i,N+j} = -H_{i,N+j} \left[\sum_{k=1}^N \left[A_{i,k} - \frac{A_{N+1,k}A_{i,N+1}}{A_{N+1,N+1}} \right] \bar{y}_{CO_k} + A_{i,0} - \frac{A_{N+1,0}A_{i,N+1}}{A_{N+1,N+1}} \right]$$

$$A_{3N+i,N+i} = -H_{i,N+i} \left[\sum_{k=1}^N \left[A_{i,k} - \frac{A_{N+1,k}A_{i,N+1}}{A_{N+1,N+1}} \right] \bar{y}_{CO_k} + A_{i,0} - \frac{A_{N+1,0}A_{i,N+1}}{A_{N+1,N+1}} \right]$$

$$+ \sigma_2 \frac{R_{S_{\Theta_{S_i}}}}{P_T} - \sigma_1 \frac{R_{M_{\Theta_{M_i}}}}{P_T}$$

$$A_{3N+i,2N+j} = A_{3N+i,2N+i} = 0$$

$$A_{3N+i,3N+j} = -\bar{v}_{g_i} \left[A_{i,j} - \frac{A_{N+1,j} A_{i,N+1}}{A_{N+1,N+1}} \right]$$

$$A_{3N+i,3N+i} = -\bar{v}_{g_i} \left[A_{i,i} - \frac{A_{N+1,i} A_{i,N+1}}{A_{N+1,N+1}} \right] + \sigma_2 \frac{\bar{\Theta}_{g_i}}{P_{T_i}} R_{S_{y_{CO_2}}} - \sigma_1 \frac{\bar{\Theta}_{g_i}}{P_{T_i}} R_{M_{y_{CO_2}}}$$

$$A_{3N+i,4N+j} = 0 \quad A_{3N+i,4N+i} = \sigma_2 \frac{\bar{\Theta}_{g_i}}{P_{T_i}} R_{S_{y_{CO_2}}} - \sigma_1 \frac{\bar{\Theta}_{g_i}}{P_{T_i}} R_{M_{y_{CO_2}}}$$

$$A_{4N+i,j} = -H_{i,j} \left[\sum_{k=1}^N \left[A_{i,k} - \frac{A_{N+1,k} A_{i,N+1}}{A_{N+1,N+1}} \right] \bar{y}_{CO_2}^k + A_{i,0} \bar{y}_{CO_2}^0 - \frac{A_{N+1,0} A_{i,N+1}}{A_{N+1,N+1}} \bar{y}_{CO_2}^0 \right]$$

$$A_{4N+i,i} = -H_{i,i} \left[\sum_{k=1}^N \left[A_{i,k} - \frac{A_{N+1,k} A_{i,N+1}}{A_{N+1,N+1}} \right] \bar{y}_{CO_2}^k + A_{i,0} \bar{y}_{CO_2}^0 - \frac{A_{N+1,0} A_{i,N+1}}{A_{N+1,N+1}} \bar{y}_{CO_2}^0 \right]$$

$$- \sigma_3 \frac{\bar{\Theta}_{g_i}}{P_{T_i}} R_{S_{y_{CO_2}}}$$

$$A_{4N+i,N+j} = -H_{i,N+j} \left[\sum_{k=1}^N \left[A_{i,k} - \frac{A_{N+1,k} A_{i,N+1}}{A_{N+1,N+1}} \right] \bar{y}_{CO_2}^k + A_{i,0} \bar{y}_{CO_2}^0 - \frac{A_{N+1,0} A_{i,N+1}}{A_{N+1,N+1}} \bar{y}_{CO_2}^0 \right]$$

$$A_{4N+i,N+i} = -H_{i,N+i} \left[\sum_{k=1}^N \left[A_{i,k} - \frac{A_{N+1,k} A_{i,N+1}}{A_{N+1,N+1}} \right] \bar{y}_{CO_2}^k + A_{i,0} \bar{y}_{CO_2}^0 - \frac{A_{N+1,0} A_{i,N+1}}{A_{N+1,N+1}} \bar{y}_{CO_2}^0 \right]$$

$$- \sigma_3 \frac{R_{S_{y_{CO_2}}}}{P_T}$$

$$A_{4N+i,2N+j} = A_{4N+i,2N+i} = 0$$

$$A_{4N+i,3N+j} = 0 \quad A_{4N+i,3N+i} = -\sigma_3 \frac{\bar{\Theta}_{g_i}}{P_T} R_{S_{y_{CO_2}}}$$

$$A_{4N+i,4N+j} = -\bar{v}_{g_i} \left[A_{i,j} - \frac{A_{N+1,j} A_{i,N+1}}{A_{N+1,N+1}} \right]$$

$$A_{4N+i,4N+i} = -\bar{v}_{g_i} \left[A_{i,i} - \frac{A_{N+1,i} A_{i,N+1}}{A_{N+1,N+1}} \right] - \sigma_S \frac{\bar{\Theta}_{g_i}}{P_{T_i}} R_{Sco_{g_i}}$$

where

$$Q_{1_{i,j}} = \frac{\alpha_g}{\tau\zeta_i + 1} \left[B_{i,0} (S_{31} A_{0,j} + S_{32} A_{N+1,j}) + B_{i,N+1} (S_{41} A_{0,j} + S_{42} A_{N+1,j}) \right]$$

$$Q_{2_{i,j}} = - \left[A_{i,0} (S_{31} A_{0,j} + S_{32} A_{N+1,j}) + A_{i,N+1} (S_{41} A_{0,j} + S_{42} A_{N+1,j}) \right]$$

$$Q_{3_{i,j}} = \frac{\alpha_g}{\tau\zeta_i + 1} \left[B_{i,j} + B_{i,0} (S_{33} A_{0,j} + S_{34} A_{N+1,j}) + B_{i,N+1} (S_{43} A_{0,j} + S_{44} A_{N+1,j}) \right]$$

$$Q_{4_{i,j}} = - \left[A_{i,j} + A_{i,0} (S_{33} A_{0,j} + S_{34} A_{N+1,j}) + A_{i,N+1} (S_{43} A_{0,j} + S_{44} A_{N+1,j}) \right]$$

Elements of Control Matrix

To define the elements of the matrix \mathbf{B} , the following definitions are needed. For the methanation system,

$$c_{p_g} = c_{p_{g_1}} \bar{T}_o \Theta_o + c_{p_{g_2}}$$

where after substituting for the concentration of nitrogen in terms of the other chemical species

$$c_{p_{g_1}} = \frac{1}{M_{g_0}} \left[\alpha_{1_c} + \bar{x}_{CO}^o (\alpha_{1_{H_2}} y_{H_2}^o + \alpha_{1_{CO}} y_{CO}^o + \alpha_{1_{CO_2}} y_{CO_2}^o + \alpha_{1_{H_2O}} y_{H_2O}^o + \alpha_{1_{CH_4}} y_{CH_4}^o) \right]$$

$$c_{p_{g_2}} = \frac{1}{M_{g_0}} \left[\alpha_{2_c} + \bar{x}_{CO}^o (\alpha_{2_{H_2}} y_{H_2}^o + \alpha_{2_{CO}} y_{CO}^o + \alpha_{2_{CO_2}} y_{CO_2}^o + \alpha_{2_{H_2O}} y_{H_2O}^o + \alpha_{2_{CH_4}} y_{CH_4}^o) \right]$$

Based on readily available data for the heat capacities of the gases,

α_{1_c}	0.000776	α_{2_c}	6.775
$\alpha_{1_{H_2}}$	0.000034	$\alpha_{2_{H_2}}$	-0.155
$\alpha_{1_{CO}}$	0.000424	$\alpha_{2_{CO}}$	-0.175
$\alpha_{1_{CO_2}}$	0.003440	$\alpha_{2_{CO_2}}$	1.276
$\alpha_{1_{H_2O}}$	0.006394	$\alpha_{2_{H_2O}}$	4.425
$\alpha_{1_{CH_4}}$	0.011653	$\alpha_{2_{CH_4}}$	-1.574

Then let us define

$$\alpha_1 = \frac{\bar{c}_{p_{g_1}} \bar{T}_o}{\bar{c}_{p_g}}$$

$$\alpha_2 = \frac{\bar{x}_{CO}^o (\bar{T}_o \alpha_{1_{CO}} + \alpha_{2_{CO}})}{\bar{M}_{g_0} \bar{c}_{p_g}}$$

$$\alpha_3 = \frac{\bar{x}_{CO}^o (\bar{T}_o \alpha_{1_{CO_2}} + \alpha_{2_{CO_2}})}{\bar{M}_{g_0} \bar{c}_{p_g}}$$

$$\alpha_4 = \frac{\bar{x}_{CO}^o(\bar{T}_o \alpha_{1_{H_2O}} + \alpha_{2_{H_2O}})}{\bar{M}_{g_o} \bar{c}_{p_g}}$$

$$\alpha_5 = \frac{\bar{x}_{CO}^o(\bar{T}_o \alpha_{1_{H_2}} + \alpha_{2_{H_2}})}{\bar{M}_{g_o} \bar{c}_{p_g}}$$

$$\alpha_6 = \frac{\bar{x}_{CO}^o(\bar{T}_o \alpha_{1_{CH_4}} + \alpha_{2_{CH_4}})}{\bar{M}_{g_o} \bar{c}_{p_g}}$$

Then if we define

$$\gamma_1 = \left(\frac{\bar{\Theta}_{g_o} - \bar{\Theta}_o}{\alpha_g \bar{\Theta}_{g_o}} \right) \quad \gamma_2 = \frac{1}{\alpha_g \bar{\Theta}_{g_o}} \quad \gamma_3 = \frac{\bar{\Theta}_{g_o} + 1 - 2\bar{\Theta}_o}{\alpha_g \bar{\Theta}_{g_o}}$$

the original definition for the constant Γ becomes

$$\Gamma = \gamma_3 - \gamma_1 M_g c_{p_g} - \gamma_1 v_{g_o} + \gamma_2 \Theta_o$$

The matrix I can then be partitioned using the definition of vector E

$$E = [E_1 \quad E_2 \quad E_3 \quad E_4] \begin{pmatrix} 1 \\ v_{g_o} \\ M_g c_{p_g} \\ \Theta_o \end{pmatrix}$$

where for $i = 1, \dots, N$

$$E_{1_i} = - \sum_{j=0}^{N+1} A_{i,j} (\bar{v}_{g_i} \bar{\Theta}_{g_j} - \bar{v}_{g_j} \bar{\Theta}_{g_i}) + P_i \bar{v}_{g_i} \bar{\Theta}_{g_i} + \bar{v}_{g_i} (A_{i,0} S_{33} + A_{i,N+1} S_{43}) \gamma_3$$

$$E_{2_i} = -A_{i,0} \bar{\Theta}_{g_i} - \bar{v}_{g_i} (A_{i,0} S_{33} + A_{i,N+1} S_{43}) \gamma_1$$

$$E_{S_i} = -\bar{v}_{g_i}(A_{i,0}S_{33} + A_{i,N+1}S_{43})\gamma_1$$

$$E_{4_i} = \bar{v}_{g_i}(A_{i,0}S_{33} + A_{i,N+1}S_{43})\gamma_2$$

and for $i = N+1$

$$E_{1_i} = -\sum_{j=0}^{N+1} A_{i,j}(\bar{v}_{g_i}\bar{\Theta}_{g_j} - \bar{v}_{g_j}\bar{\Theta}_{g_i}) + P_i \bar{v}_{g_i}\bar{\Theta}_{g_i} + \bar{v}_{g_i}(A_{i,0}S_{33} + A_{i,N+1}S_{43})\gamma_3$$

$$- \left[P_i \bar{v}_{g_i} + \sum_{k=0}^{N+1} A_{i,k} \bar{v}_{g_k} \right] S_{43}\gamma_3$$

$$E_{2_i} = -A_{i,0}\bar{\Theta}_{g_i} - \bar{v}_{g_i}(A_{i,0}S_{33} + A_{i,N+1}S_{43})\gamma_1 + \left[P_i \bar{v}_{g_i} + \sum_{k=0}^{N+1} A_{i,k} \bar{v}_{g_k} \right] S_{43}\gamma_1$$

$$E_{3_i} = -\bar{v}_{g_i}(A_{i,0}S_{33} + A_{i,N+1}S_{43})\gamma_1 + \left[P_i \bar{v}_{g_i} + \sum_{k=0}^{N+1} A_{i,k} \bar{v}_{g_k} \right] S_{43}\gamma_1$$

$$E_{4_i} = \bar{v}_{g_i}(A_{i,0}S_{33} + A_{i,N+1}S_{43})\gamma_2 - \left[P_i \bar{v}_{g_i} + \sum_{k=0}^{N+1} A_{i,k} \bar{v}_{g_k} \right] S_{43}\gamma_2$$

Thus we get

$$I = I_1 + I_2 v_{g_0} + I_3 M_g c_{p_i} + I_4 \Theta_0$$

Also if we define

$$X_i = -\sum_{j=1}^N (Q_{1_{i,j}}\bar{\Theta}_{g_j}\bar{\Theta}_{g_i} + Q_{3_{i,j}}\bar{\Theta}_{g_i}\bar{\Theta}_{g_j}) - \frac{1}{\tau\zeta_i + 1} \left[\omega_4 \bar{\Theta}_{g_i}^2 + \omega_5 \bar{\Theta}_{g_i}\bar{\Theta}_{g_i} + \gamma_6 \bar{\Theta}_{g_i}\bar{\Theta}_{g_i} \right]$$

$$+ \bar{\Theta}_{g_i} \bar{\Theta}_{w_i} (4\beta_g w_0 + \frac{\beta_g}{r_c} w_0) + (\bar{\Gamma} + \gamma_1) \bar{\Theta}_{g_i} \alpha_g (S_{33} B_{i,0} + S_{43} B_{i,N+1}) \Big]$$

$$+ \gamma_1 \bar{v}_{g_i} (S_{33} A_{i,0} + S_{43} A_{i,N+1}) + I_{S_i} \left[\sum_{j=1}^N (Q_{2_{i,j}} \bar{\Theta}_{s_j} + Q_{4_{i,j}} \bar{\Theta}_{s_j}) - (S_{33} A_{i,0} - S_{43} A_{i,N+1}) \bar{\Gamma} \right]$$

$$Z_{1_i} = -I_{S_i} \left[A_{i,0} - \frac{A_{N+1,0} A_{i,N+1}}{A_{N+1,N+1}} + \sum_{k=1}^N (A_{i,k} - \frac{A_{i,N+1} A_{N+1,k}}{A_{N+1,N+1}}) \bar{y}_{CO_k} \right]$$

$$Z_{2_i} = -I_{S_i} \left[A_{i,0} \bar{y}_{CO_2}^o - \frac{A_{N+1,0} A_{i,N+1}}{A_{N+1,N+1}} \bar{y}_{CO_2}^o + \sum_{k=1}^N (A_{i,k} - \frac{A_{i,N+1} A_{N+1,k}}{A_{N+1,N+1}}) \bar{y}_{CO_{p_k}} \right]$$

Then the elements of the control matrix B are

$$B_{i,1} = 4\beta_g w_0 + \frac{\beta_g}{r_c} w_0 \quad B_{i,2} = -\gamma_1 \alpha_g (B_{i,0} S_{13} + B_{i,N+1} S_{23})$$

$$B_{i,3} = \alpha_s (\gamma_2 - \alpha_1 \gamma_1) (B_{i,0} S_{13} + B_{i,N+1} S_{23})$$

$$B_{i,4} = \kappa_1 (1 + \varphi_1 \bar{\Theta}_s) R_{M_{\bar{y}_{CO_i}^o}} + \kappa_2 (1 + \varphi_2 \bar{\Theta}_s) R_{M_{\bar{y}_{CO_i}^o}} - \alpha_2 \gamma_1 \alpha_s (B_{i,0} S_{13} + B_{i,N+1} S_{23})$$

$$B_{i,5} = \kappa_1 (1 + \varphi_1 \bar{\Theta}_s) R_{M_{\bar{y}_{CO_{p_i}}^o}} + \kappa_2 (1 + \varphi_2 \bar{\Theta}_s) R_{M_{\bar{y}_{CO_{p_i}}^o}} - \alpha_3 \gamma_1 \alpha_s (B_{i,0} S_{13} + B_{i,N+1} S_{23})$$

$$B_{i,6} = \kappa_1 (1 + \varphi_1 \bar{\Theta}_s) R_{M_{\bar{y}_{H_2O_i}^o}} + \kappa_2 (1 + \varphi_2 \bar{\Theta}_s) R_{M_{\bar{y}_{H_2O_i}^o}} - \alpha_4 \gamma_1 \alpha_s (B_{i,0} S_{13} + B_{i,N+1} S_{23})$$

$$B_{i,7} = \kappa_1 (1 + \varphi_1 \bar{\Theta}_s) R_{M_{\bar{y}_{H_2O_i}^o}} + \kappa_2 (1 + \varphi_2 \bar{\Theta}_s) R_{M_{\bar{y}_{H_2O_i}^o}} - \alpha_5 \gamma_1 \alpha_s (B_{i,0} S_{13} + B_{i,N+1} S_{23})$$

$$B_{i,8} = \kappa_1 (1 + \varphi_1 \bar{\Theta}_s) R_{M_{\bar{y}_{CH_4_i}^o}} - \alpha_6 \gamma_1 \alpha_s (B_{i,0} S_{13} + B_{i,N+1} S_{23})$$

$$B_{N+i,1} = \frac{\bar{\Theta}_{g_i}}{\tau\zeta_i + 1} (4\beta_g w_g + \frac{\beta_g}{r_c} w_g)$$

$$B_{N+i,2} = -\frac{\gamma_1 \bar{\Theta}_{g_i} \alpha_g}{\tau\zeta_i + 1} (S_{33} B_{i,0} + S_{43} B_{i,N+1}) + \gamma_1 \bar{v}_{g_i} (S_{33} A_{i,0} + S_{43} A_{i,N+1})$$

$$+ I_{2_i} \left[\sum_{j=1}^N (Q_{2_{i,j}} \bar{\Theta}_{g_j} + Q_{4_{i,j}} \bar{\Theta}_{g_j}) - (S_{33} A_{i,0} - S_{43} A_{i,N+1}) \bar{\Gamma} \right]$$

$$B_{N+i,3} = \frac{\gamma_2 \bar{\Theta}_{g_i} \alpha_g}{\tau\zeta_i + 1} (S_{33} B_{i,0} + S_{43} B_{i,N+1}) - \gamma_2 \bar{v}_{g_i} (S_{33} A_{i,0} + S_{43} A_{i,N+1})$$

$$+ I_{4_i} \left[\sum_{j=1}^N (Q_{2_{i,j}} \bar{\Theta}_{g_j} + Q_{4_{i,j}} \bar{\Theta}_{g_j}) - (S_{33} A_{i,0} - S_{43} A_{i,N+1}) \bar{\Gamma} \right] + \alpha_1 X_i$$

$$B_{N+i,4} = \alpha_2 X_i \quad B_{N+i,5} = \alpha_3 X_i \quad B_{N+i,6} = \alpha_4 X_i$$

$$B_{N+i,7} = \alpha_5 X_i \quad B_{N+i,8} = \alpha_6 X_i$$

$$B_{2N+i,1} = \gamma_{ts} (w'_3 + w'_8 \varphi_0 + w'_9 \varphi_0^2) + \gamma_{tg} (w_3 + w_8 \varphi_0 + w_9 \varphi_0^2)$$

$$B_{2N+i,2} = 0 \quad B_{2N+i,3} = \alpha_t B_{i,0} - \frac{\alpha_t B_{i,N+1} A_{N+1,0}}{A_{N+1,N+1}}$$

$$B_{2N+i,4} = B_{2N+i,5} = B_{2N+i,6} = B_{2N+i,7} = B_{2N+i,8} = B_{3N+i,1} = 0$$

$$B_{3N+i,2} = -I_{2_i} \left[A_{i,0} - \frac{A_{N+1,0} A_{i,N+1}}{A_{N+1,N+1}} + \sum_{k=1}^N (A_{i,k} - \frac{A_{i,N+1} A_{N+1,k}}{A_{N+1,N+1}}) \bar{y}_{CO_k} \right]$$

$$B_{3N+i,3} = -I_{4i} \left[A_{i,0} - \frac{A_{N+1,0}A_{i,N+1}}{A_{N+1,N+1}} + \sum_{k=1}^N (A_{i,k} - \frac{A_{i,N+1}A_{N+1,k}}{A_{N+1,N+1}}) \bar{y}_{CO_k} \right] + \alpha_1 Z_{1i}$$

$$B_{3N+i,4} = -A_{i,0} \bar{v}_{g_i} - \sigma_1 \frac{\bar{\Theta}_{g_i}}{P_T} R_M \bar{y}_{CO_i}^o + \sigma_2 \frac{\bar{\Theta}_{g_i}}{P_T} R_S \bar{y}_{CO_i}^o - \frac{A_{i,N+1}A_{N+1,0}}{A_{N+1,N+1}} \bar{v}_{g_i} + \alpha_2 Z_{1i}$$

$$B_{3N+i,5} = -\sigma_1 \frac{\bar{\Theta}_{g_i}}{P_T} R_M \bar{y}_{CO_{2i}}^o + \sigma_2 \frac{\bar{\Theta}_{g_i}}{P_T} R_S \bar{y}_{CO_{2i}}^o + \alpha_3 Z_{1i}$$

$$B_{3N+i,6} = -\sigma_1 \frac{\bar{\Theta}_{g_i}}{P_T} R_M \bar{y}_{H_2O_i}^o + \sigma_2 \frac{\bar{\Theta}_{g_i}}{P_T} R_S \bar{y}_{H_2O_i}^o + \alpha_4 Z_{1i}$$

$$B_{3N+i,7} = -\sigma_1 \frac{\bar{\Theta}_{g_i}}{P_T} R_M \bar{y}_{H_2_i}^o + \sigma_2 \frac{\bar{\Theta}_{g_i}}{P_T} R_S \bar{y}_{H_2_i}^o + \alpha_5 Z_{1i}$$

$$B_{3N+i,8} = -\sigma_1 \frac{\bar{\Theta}_{g_i}}{P_T} R_M \bar{y}_{CH_4_i}^o + \alpha_6 Z_{1i}$$

$$B_{4N+i,1} = 0$$

$$B_{4N+i,2} = -I_{2i} \left[A_{i,0} \bar{y}_{CO_2}^o - \frac{A_{N+1,0}A_{i,N+1}}{A_{N+1,N+1}} \bar{y}_{CO_2}^o + \sum_{k=1}^N (A_{i,k} - \frac{A_{i,N+1}A_{N+1,k}}{A_{N+1,N+1}}) \bar{y}_{CO_{2k}} \right]$$

$$B_{4N+i,3} = -I_{4i} \left[A_{i,0} \bar{y}_{CO_2}^o - \frac{A_{N+1,0}A_{i,N+1}}{A_{N+1,N+1}} \bar{y}_{CO_2}^o + \sum_{k=1}^N (A_{i,k} - \frac{A_{i,N+1}A_{N+1,k}}{A_{N+1,N+1}}) \bar{y}_{CO_{2k}} \right] + \alpha_1 Z_{2i}$$

$$B_{4N+i,4} = -\sigma_3 \frac{\bar{\Theta}_{g_i}}{P_T} R_S \bar{y}_{CO_4}^o + \alpha_2 Z_{2i}$$

$$B_{4N+i,5} = -A_{i,0}\bar{v}_{g_i} + \frac{A_{i,N+1}A_{N+1,0}}{A_{N+1,N+1}}\bar{v}_{g_i}\bar{y}_{CO_2}^o - \sigma_3 \frac{\bar{\Theta}_{g_i}}{P_T} R_{S_{y_{CO_2}^o}} + \alpha_3 Z_{2_i}$$

$$B_{4N+i,6} = -\sigma_3 \frac{\bar{\Theta}_{g_i}}{P_T} R_{S_{y_{H_2O_i}^o}} + \alpha_4 Z_{2_i}$$

$$B_{4N+i,7} = -\sigma_3 \frac{\bar{\Theta}_{g_i}}{P_T} R_{S_{y_{H_2O_i}^o}} + \alpha_5 Z_{2_i} \quad B_{4N+i,8} = \alpha_6 Z_{1_i}$$

REFERENCES

Ahmed, N.U., and K.L. Teo, *Optimal Control of Distributed Parameter Systems*, North Holland, New York (1981).

Aidarous, S.E., M.R. Gevers and M.J. Installe, *Int. J. Control.*, **22**, 197-212 (1975).

Alvarez, J., J.A. Romagnoli and G. Stephanopoulos, *Chem. Eng. Sci.*, **36**, 1695-1712 (1981).

Amouroux, M., G. DiPillo and L. Grippo, *Richerche di Automatica*, **7**, 92 (1976).

Ascher, U., J. Christiansen and R.D. Russell, *Math. Comp.*, **33**, 659-679 (1979).

Balas, M.J., *Int. J. Control.*, **29**, 3, 523-538 (1979).

Beek, J., *Advances in Chemical Engineering*, Vol. 3, Academic Press, New York (1962).

Belletrutti, J., and A.G.J. MacFarlane, *Proc. IEE*, **118**, 1291-1297 (1971).

Betts, J.T., and S.J. Citron, *AIAA Journal*, **10**, 1, 19-23 (1972).

Bird, R.B., W.E. Stewart and E.N. Lightfoot, *Transport Phenomena*, John Wiley & Sons, New York (1960).

Bonvin, D., 'Dynamic Modeling and Control Structures for a Tubular Autothermal Reactor at an Unstable State,' Ph.D. Thesis, University of California, Santa Barbara, CA (1980).

Bonvin, D., R.G. Rinker and D.A. Mellichamp, 'Tubular Autothermal Reactors: Dynamic Modeling in the Region of Multiple Steady States,' presented at AIChE Meeting, San Francisco (1979).

Bonvin, D., R.G. Rinker and D.A. Mellichamp, *Chem. Eng. Sci.*, **35**, 603-612 (1980).

Bradshaw, A., and B. Porter, *Int. J. Control.*, **16**, 2, 277-285 (1972).

Bristol, E.H., *Instrumentation in the Chemical and Petroleum Industries*, **16**, 151-158 (1980).

Brockett, R.W., *Finite Dimensional Linear Systems*, John Wiley & Sons, New York (1970).

Brown, K.M., *Comm. ACM*, **10**, 11, 728-729 (1967).

Bryson, A.E., and Y-C Ho, *Applied Optimal Control*, Blaisdell, Waltham, Mass. (1969).

Carberry, J.J., *Chemical and Catalytic Reactor Engineering*, McGraw-Hill, New York (1976).

Carberry, J.J., and J.B. Butt, *Catal. Rev.*, **10**, 221 (1975).

Carberry, J.J., and M. Wendel, *AICHE J.*, **9**, 129-133 (1963).

Carberry, J.J., and D. White, *Ind & Eng Chem.*, **61**, 27-35 (1969).

Carey, G.F., and B.A. Finlayson, *Chem. Eng. Sci.*, **30**, 587-596 (1975).

Chidambara, M.R., and E.J. Davison, *IEEE Trans. Auto. Control*, **AC-12**, 119-121 (1967a).

Chidambara, M.R., and E.J. Davison, *IEEE Trans. Auto. Control*, **AC-12**, 213-215 (1967b).

Chidambara, M.R., and E.J. Davison, *IEEE Trans. Auto. Control*, **AC-12**, 799-800 (1967c).

Clement, K., and S.B. Jorgensen, 8th IFAC World Congress, Kyoto, Japan, Aug 24-28 (1981).

Clement, K., S.B. Jorgensen and J.P. Sorensen, *Chem. Eng. Sci.*, **35**, 1231-1236 (1980).

Dahlquist, G., and A. Björke, translated by N. Anderson, *Numerical Analysis*, Prentice-Hall, Englewood Cliffs, New Jersey (1974).

Davis, M.E., *Numerical Methods and Modeling for Chemical Engineers*, John Wiley & Sons, New York (1984).

Davison, E.J., *IEEE Trans. Auto. Control*, **AC-11**, 93-101 (1966).

Davison, E.J., *IEEE Trans. Auto. Control*, **AC-13**, 214-215 (1968).

Davison, E.J., *IEEE Trans. Auto. Control*, **AC-15**, 348-350 (1970).

Davison, E.J., and K.J. Chadha, *Automatica*, **8**, 263-273 (1972).

De Wasch, A.P., and G.F. Froment, *Chem. Eng. Sci.*, **26**, 5, 629-634 (1971).

Douglas, J.M., *Process Dynamics and Control*, Vol. 2, *Control System Synthesis*, Prentice-Hall, Englewood Cliffs, New Jersey (1972).

Edmunds, J., and B. Kouvaritakis, *Int. J. Control.*, **29**, 5, 787-796 (1979).

Ellis, J.K., and G.W.T. White, *Control*, **9**, 82, 193-197 (1965a).

Ellis, J.K., and G.W.T. White, *Control*, **9**, 83, 252-256 (1965b).

Ellis, J.K., and G.W.T. White, *Control*, **9**, 84, 317-321 (1965c).

Fahien, R.W., and I.M. Stankovic, *Chem. Eng. Sci.*, **34**, 1350 (1979).

Fan, L.T., K.C. Chen and L.E. Erickson, *Chem. Eng. Sci.*, **26**, 379-387 (1971).

Ferguson, N.B., and B.A. Finlayson, *Chem. Eng. J.*, **1**, 327-335 (1970).

Ferguson, N.B., and B.A. Finlayson, *AIChE J.*, **18**, 1053-1059 (1972).

Finlayson, B.A., *Chem. Eng. Sci.*, **26**, 1081-1091 (1971).

Finlayson, B.A., *The Method of Weighted Residuals and Variational Principles*, Academic Press, New York (1972).

Finlayson, B.A., *Cat. Rev. Sci. Engng.*, **10**, 1, 69-138 (1974).

Finlayson, B.A., *Nonlinear Analysis in Chemical Engineering*, McGraw-Hill, New York (1980).

Fisher, R.J., and M.M. Denn, *AIChE J.*, **24**, 3, 519-523 (1978).

Foss, A.S., *AIChE J.*, **19**, 2, 209-214 (1973).

Foss, A.S., J.M. Edmunds and B. Kouvaritakis, *I&EC Fundamentals*, **19**, 109-117 (1980).

Fossard, A., *IEEE Trans. Auto. Control*, **AC-15**, 261-262 (1970).

Froment, G.F., *Adv. Chem. Ser.*, **109**, 1-34 (1972).

Froment, G.F., *Chem. Eng. Tech.*, **46**, 9, 381 (1974).

Gould, L.A., *Chemical Process Control: Theory and Applications*, Addison Wesley, Reading, Massachusetts (1969).

Gould, L., and M.A. Murray-Lasso, *IEEE Trans. Auto. Control*, **AC-11**, 4, 729-737 (1966).

Grad, J., and M.A. Brebner, *Comm. ACM*, **11**, 12 (1968).

Hallager, L., and S.B. Jorgensen, 8th IFAC World Congress, Kyoto, Japan, Aug 24-28 (1981).

Hansen, K.W., and S.B. Jorgensen, *Adv. Chem. Ser.*, **133**, 505 (1974).

Hansen, K.W., and S.B. Jorgensen, *Chem. Eng. Sci.*, **31**, 579-586 (1976a).

Hansen, K.W., and S.B. Jorgensen, *Chem. Eng. Sci.*, **31**, 587-598 (1976b).

Hlavacek, V., *Ind. Eng. Chem.*, **62**, 7, 8-26 (1970).

Hlavacek, V., and M. Marek, *Chem. Eng. Sci.*, **21**, 501 (1966).

Hoiberg, J.A., B.C. Lyche and A.S. Foss, *AIChE J.*, **17**, 6, 1434-1447 (1971).

Hsu, C.H., and C.T. Chen, *Proc. IEEE*, **56**, 2061-2062 (1968).

Jutan, A., J.P. Tremblay, J.F. MacGregor and J.D. Wright, *AIChE J.*, **23**, 5, 732-742 (1977).

Karanth, N.G., and R. Hughes, *Cat Rev Sci Eng*, **9**, 169 (1974a).

Karanth, N.G., and R. Hughes, *Chem. Eng. Sci.*, **29**, 197-205 (1974b).

Khanna, R., and J.H. Seinfeld, *Int. J. Control.*, **36**, 1, 1-24 (1982).

Kouvaritakis, B., *Int. J. Control.*, **27**, 5, 705-724 (1978).

Kouvaritakis, B., and A.G.J. MacFarlane, *Int. J. Control.*, **23**, 2, 149-166 (1976a).

Kouvaritakis, B., and A.G.J. MacFarlane, *Int. J. Control.*, **23**, 2, 167-181 (1976b).

Kouvaritakis, B., W. Murray and A.G.J. MacFarlane, *Int. J. Control.*, **29**, 2, 325-358 (1979).

Kouvaritakis, B., and U. Shaked, *Int. J. Control.*, **23**, 3, 297-340 (1976).

Kumar, S., and J.H. Seinfeld, *IEEE Trans. Auto. Control*, **AC-23**, 690 (1978a).

Kumar, S., and J.H. Seinfeld, *Chem. Eng. Sci.*, **33**, 11, 1507-1516 (1978b).

Leden, B., *IEEE Trans. Auto. Control*, **AC-21**, 3, 408-410 (1976).

Lee, A.L., "Methanation for Coal Gasification," Symp. on Clean Fuels from Coal, Chicago, Sept. 1973.

Lee, E.B., and L. Marcus, *Foundations of Optimal Control*, Wiley, New York (1967).

Lynn, L.L., and R.L. Zahradnik, *Int. J. Control.*, **12**, 1079-1087 (1970).

MacFarlane, A.G.J., *Automatica*, **8**, 455-492 (1972).

MacFarlane, A.G.J., and J.J. Bellettrutti, *Automatica*, **9**, 575-588 (1973).

MacFarlane, A.G.J., and B. Kouvaritakis, *Int. J. Control.*, **25**, 6, 837-874 (1977).

MacFarlane, A.G.J., and I. Postlethwaite, *Int. J. Control.*, **25**, 1, 81-127 (1977).

MacGregor, J.F., and A.L.K. Wong, "Identification and Stochastic Control of a Packed Bed Reactor," presented at AIChE Symposium, Miami (1978).

Mahapatra, G.B., *IEEE Trans. Auto. Control*, **AC-22**, 3, 481-482 (1977).

Marshall, S.A., *Control*, **10**, 642-643 (1966).

Matsumoto, J., and K. Ito, *Int. J. Control*, **12**, 3, 401-419 (1970).

McCausland, I., *Proc. IEE*, **112**, 3, 543-548 (1970).

McGlothin, G.E., *Int. J. Control*, **20**, 3, 417-432 (1974).

McGowin, C.R., and D.D. Perlmutter, *Chem. Eng. J.*, **2**, 125-131 (1971).

Mears, D.E., *Ind. Eng. Chem. Fundam.*, **15**, 1, 20-23 (1976).

Michelsen, M.L., H.B. Vakil and A.S. Foss, *I&EC Fundamentals*, **12**, 3, 323-328 (1973).

Moe, J.M., *CEP*, **58**, 3, 33-36 (1962).

Newman, C.P., and A. Sen, *Int. J. Control*, **16**, 539-548 (1972).

Norrie, D.H., and G. DeVries, *The Finite Element Method*, Academic Press, New York (1973).

Ogunnaike, B.A., and W.H. Ray, *AIChE J.*, **25**, 6, 1043-1057 (1979).

Paris, J.R., and W.F. Stevens, *The Canadian Journal of Chemical Engineering*, **48**, 2 (1970).

Pearson, C., *J. Math. Phys.*, **47**, 351-358 (1968).

Perry, R.H., and C.H. Chilton, *Chemical Engineers' Handbook*, McGraw-Hill, New York (1973).

Porter, B., and A. Bradshaw, *Int. J. Control*, **15**, 4, 673-681 (1972).

Prabhu, S.S., and I. McCausland, *Proc. IEE*, **117**, 7, 1398-1403 (1970).

Rabinowitz, P., ed., *Numerical Methods for Nonlinear Algebraic Equations*, Gordon & Breach, New York (1970).

Ray, W.H., *Advanced Process Control*, McGraw-Hill, New York (1981).

Rosenbrock, H.H., *CEP*, **58**, 9, 43-50 (1962).

Rosenbrock, H.H., *Proc. IEE*, **116**, 11, 1929-1936 (1969).

Russel, R.D., and J. Christiansen, *SIAM J. Num. Anal.*, **15**, 59-80 (1978).

Sakawa, Y., *IEEE Trans. Auto. Control*, **AC-9**, 4, 420-426 (1964).

Schwartz, C.E., and J.M. Smith, *Ind. Eng. Chem.*, **45**, 1209 (1953).

Seborg, D.E., and T.F. Edgar, eds., *Chemical Process Control 2*, United Engineering Trustees, New York (1982).

Shaw, I.D., 'Modeling and Discrimination Studies in a Catalytic Fluidized Bed Reactor,' Ph.D. Thesis, McMaster University, Hamilton, Canada (1974).

Sheirah, M.A., and M.H. Hamza, *Int. J. Control.*, **19**, 5, 891-902 (1974).

Silva, J.M., 'Multi-Bed Catalytic Reactor Control Systems: Configuration, Development and Experimental Testing,' Ph.D. Thesis, University of California, Berkeley (1978).

Silva, J.M., H. Wallman and A.S. Foss, *I&EC Fundamentals*, **18**, 4, 383-391 (1979).

Sinai, J., and A.S. Foss, *AIChE J.*, **16**, 4, 658-669 (1970).

Smith, J.M., *Chemical Engineering Kinetics*, McGraw-Hill, New York (1970).

Sorensen, J.P., *Chem. Eng. Sci.*, **31**, 719-725 (1976).

Sorensen, J.P., *Chem. Eng. Sci.*, **32**, 763-774 (1977).

Sorensen, J.P., S.B. Jorgensen and K. Clement, *Chem. Eng. Sci.*, **35**, 1223-1230 (1980).

Stewart, W.E., *Chem. Eng. Progr. Symp. Ser.*, **61**, 58, 61 (1967).

Stewart, W.E., and J.V. Villadsen, *AIChE J.*, **15**, 28 (1969).

Strand, D.M., 'Design and Construction of a Fixed Bed, Non-Adiabatic Methanator for Multivariable Computer Control Studies,' Ph.D. Thesis, California Institute of Technology, Pasadena, CA (1984).

Vakil, H.B., M.L. Michelsen and A.S. Foss, *I&EC Fundamentals*, **12**, 3, 328-335 (1973).

Valstar, J.M., P.J. Van Den Berg and J. Oyserman, *Chem. Eng. Sci.*, **30**, 7, 723-728 (1975).

Vatcha, S.R., 'Analysis and Design of Methanation Processes in the Production of Substitute Natural Gas from Coal,' Ph.D. Thesis, California Institute of Technology, Pasadena, CA (1976).

Villadsen, J.V., and M.L. Michelsen, *Solution of Differential Equation Models by Polynomial Approximation*, Prentice-Hall, Englewood Cliffs, New Jersey (1978).

Villadsen, J.V., and W.E. Stewart, *Chem. Eng. Sci.*, **22**, 1483-1501 (1967).

Vortmeyer, D., K.J. Dietrich and K.O. Ring, *Chemical Reaction Engineering II*, 588-599 (1974).

Vortmeyer, D., and R.J. Schaefer, *Chem. Eng. Sci.*, **29**, 485-491 (1974).

Wallman, H., J.M. Silva and A.S. Foss, *I&EC Fundamentals*, **18**, 4 (1979).

Wang, P.K.C., *IEEE Trans. Auto. Control.*, **AC-17**, 4, 552-553 (1972).

Wang, P.K.C., *Siam. J. Control*, **13**, 2, 274-293 (1975).

Weast, R.C., ed., *CRC Handbook of Chemistry and Physics*, CRC Press, Cleveland, Ohio (1976).

Wilson, R.G., D.G. Fisher and D.E. Seborg, *AIChE J.*, **20**, 6, 1131-1140 (1974).

Wright, J.D., and L. Schryer, "An Application of Multivariable Model Reference Adaptive Control to a Pilot Scale Catalytic Reactor," presented at AIChE Symposium, Miami (1978).

Young, L.C., and B.A. Finlayson, *I&EC Fundamentals*, **12**, 4, 412-422 (1973).